JANUARY 1973

VOLUME 70

NUMBER 1

PROCEEDINGS OF THE

National Academy of Sciences

OF THE UNITED STATES OF AMERICA

THE PROCEEDINGS OF THE
National Academy of Sciences
OF THE UNITED STATES OF AMERICA

Officers of the Academy

PHILIP HANDLER *President*
G. B. KISTIAKOWSKY *Vice President*
ALAN V. ASTIN *Home Secretary*
HARRISON BROWN *Foreign Secretary*
E. R. PIORE *Treasurer*

Editorial Board of the Proceedings

ROBERT L. SINSHEIMER *Chairman*
ROBERT M. SOLOW *Vice Chairman*
MICHAEL KASHA *Vice Chairman*
ALAN V. ASTIN *Home Secretary*
HARRISON BROWN *Foreign Secretary*
E. R. PIORE *Treasurer*

C. B. ANFINSEN
ALEXANDER G. BEARN
BERNARD D. DAVIS
KINGSLEY DAVIS
HERMAN EISEN
LOUIS B. FLEXNER
ROBERT A. GOOD
MARK KAC
MARTIN D. KAMEN
SEYMOUR S. KETY
MACLYN MCCARTY
EUGENE P. ODOM
ARTHUR B. PARDEE
ALEXANDER RICH
PAUL A. SAMUELSON
EMIL L. SMITH

Managing Editor: JEROLD A. LAST
Senior Associate Managing Editor: THEODORE P. ZACHARIA
Associate Managing Editor: MURRIE W. BURGAN

Editorial correspondence: PROCEEDINGS OF THE NATIONAL ACADEMY OF SCIENCES, 2101 Constitution Avenue, Washington, D.C. 20418.

Business correspondence: Printing and Publishing Office, National Academy of Sciences, 2101 Constitution Avenue, Washington, D.C. 20418.

Subscriptions are entered on a calendar-year basis only. The current subscription rate is $35. The price of a single issue is $4. Volumes 1 through 58 are available from Johnson Reprint Corporation, 111 Fifth Avenue, New York, N.Y. 10003; prices are available from that organization upon request.

Subscribers are requested to notify the Printing and Publishing Office of any change of address; also the local postmaster. The Academy is not responsible for nonreceipt of issues because of improper address unless a change of address is on file. The notice of address change should list both the old and new addresses.

Claims for replacement copies will not be honored more than 60 days after the mailing date for domestic subscribers and not more than 90 days after the mailing date for foreign subscribers.

Microfilms of complete volumes are available to regular subscribers only and may be obtained from University Microfilms, Xerox Corporation, Ann Arbor, Michigan 48103.

Second-class postage paid at Washington, D.C. and at additional mailing offices PRINTED IN THE USA

THE PROCEEDINGS OF THE NATIONAL ACADEMY OF SCIENCES U.S.A. *is published monthly by*

THE NATIONAL ACADEMY OF SCIENCES, *2101 Constitution Avenue, Washington, D.C. 20418*

INFORMATION TO CONTRIBUTORS

(January 1973)

Purpose and scope

The *Proc. Nat. Acad. Sci. USA* publishes brief reports (not previously published) of the results of original research by members of the Academy or by others if the communication is sponsored by an Academy member. Articles should be as brief as adequate presentation allows, and may not exceed five printed pages. Since the PROCEEDINGS publishes papers in all branches of science represented in the Academy, it is desirable, whenever possible, for articles to be written so as to be intelligible to a wide scientific audience. Both because of the space limitations and the broad scientific audience of the PROCEEDINGS, detailed scientific papers may often be more appropriately submitted to more specialized journals.

Sometimes, preliminary findings of major importance are published in the PROCEEDINGS without full documentation; authors must indicate that the paper is a preliminary one, and that a detailed report will be published elsewhere.

Upon invitation from the Editorial Board, some papers presented at Academy symposia, special Academy lectures, or papers on subjects of general interest to scientists are also published in the PROCEEDINGS.

Conditions for submission

Manuscripts will be accepted only from members of the Academy, who will assume responsibility for their propriety and scientific standards. In communicating an article on behalf of a nonmember, an Academy member should explicitly state that it contains findings of more than ordinary importance to investigators working on related problems, or of particularly broad interest to diverse groups of scientists. No Academy member may sponsor more than 10 papers in any annual volume.

Before submitting an article on behalf of a nonmember, an Academy member must also obtain a written opinion on it by a qualified referee. For maximal objectivity in the reviewing process, it is highly desirable that the member select the referee himself and that he not divulge the referee's identity to the author, at least until the member receives the comments. Ordinarily, the referee should not be a close colleague or former mentor of the author or a member of the Academy member's department. Forms on which the referee's comments should be submitted are provided on request by the PROCEEDINGS Office. The Academy member must enclose a copy of the referee's report with his letter of transmittal. He retains the privilege of communicating the paper if the referee's report is unfavorable, but in that case he should state in his letter of transmittal his reasons for disagreeing with the referee.

Papers are generally processed rapidly for publication; however, the Editorial Board reserves the right to subject manuscripts to further review when this seems desirable and to reject papers if they do not meet the general criteria for publication, as defined by the By-Laws of the Academy.

No person may be author or coauthor of papers totaling more than five pages in any one issue.

Manuscripts reporting experiments with humans should be accompanied by a copy of the document authorizing the proposed research by the responsible institutional committee. Authors are referred to the Declaration of Helsinki for further guidance.

Page charges are assessed for all communicated papers. A member of the Academy who communicates an article on behalf of a nonmember author is responsible for the costs of publishing the paper; if a nonmember author is to be billed for the page charges, the member communicating the paper should make sure that there is a clear understanding to this effect with the author before the paper is communicated. Members may not use the annual publishing allowances extended them by the Academy for the payment of the costs of publishing papers by other authors. The standard charge is now $75 per printed page; in addition, authors may be billed for the costs of extensive changes made in proof, and for other items of special cost.

Manuscripts are to be submitted in duplicate to the PROCEEDINGS OF THE NATIONAL ACADEMY OF SCIENCES, Room 253, 2101 Constitution Avenue, Washington, D.C. 20418. Those that are in good form can usually be published 8–13 weeks later. If articles are to be published on schedule, it is essential that communicated manuscripts are in the form in which authors wish their papers to appear and that their length be appropriate for the PROCEEDINGS.

Length

Five printed pages will accommodate about 5500 words. The title and the heading material usually occupy space equivalent to about 600 words. Appropriate allowance should be made for the space occupied by references, footnotes, tables, and figures with their legends. Figures will be scaled to one- or two-column width according to the size of the lettering (see *Illustrations* below).

Articles estimated on first receipt as longer than five pages will be returned to authors for shortening without further editorial consideration.

Illustrations

Present only such illustrative material as is essential for the point being made. Drawings made for slide projection are rarely suitable for publication. Design line drawings to fit into one- or two-column width with minimum wasted space. *Thin-stroke* lettering should be used in sizes such that *after reduction* the smallest letter or numeral will not be less than 1.5 mm in height. Avoid extraneous detail in figures; use the legends for details as to cell type used, identification of symbols, etc.

All figures should be identified on the back with a soft pencil and the orientation should, if necessary, be indicated by means of an arrow and the word "top". Do not mount figures unless a composite figure is desired. Indicate the magnification of photomicrographs in the legend, or include a bar indicating scale in the figure (or both).

Legends to figures should be typed double-spaced, in numerical order, on a separate page.

Tables

Tables should be typed double-spaced *throughout*, numbered with arabic numerals, and provided with titles (above the table). A list of footnotes to a table must be typed *doubled-spaced*, on a separate page if necessary. Reference to the footnotes should be made by means of the symbols *, †, ‡, §, ¶, ||, in that order, followed by doubled symbols if necessary. A lengthy list of footnotes is better keyed with lowercase superscript letters or, in exceptional cases where this would be confusing, with superscript numbers.

Title page

Provide a separate title page, containing the following items:

Classification. Give any one of the sciences named in the

titles of the sections of the Academy, or Immunology, Pathology, Cell Biology, or Statistics.

Title. This should be brief, specific, and rich in informative words. Add up to five *amplifying key terms* to alert readers, and computers, to subjects in the article *not* referred to in the title. The PROCEEDINGS discourages the use of uninformative serial titles such as *On Steroids*, XIX. If a paper is part of a series, indicate this by a symboled footnote on the first page, and include a reference to the immediately preceding paper of the series.

By-line. If there are several authors with different affiliations, key authors to institutions by means of symbols *, †, ‡, §, ¶. If reprint requests are to be addressed to any but the first author, indicate this by a footnote.

From-line. List the institutions and provide Zip Codes.

Running Title. Provide a running title of not more than 50 characters, including spaces.

Footnotes. Give, as first unsymboled footnote, a list of nonstandard abbreviations (see below, under *Abbreviations*), if any, that have been used in the paper. Other title-page footnotes may indicate present addresses of the authors or address(es) to which reprint requests are to be sent. Do *not* include acknowledgments of grant support here.

Abstract

Every paper must begin with an abstract, typed on a separate page. This should state the subject and main conclusions of the article in generally intelligible terms. Avoid abbreviations. The abstract must be intelligible to a reader before he reads the paper, and suitable for reproduction by abstracting services without rewriting. It should usually not exceed 250 words.

Nomenclature

The PROCEEDINGS strives for the greatest possible conformity with international standards on nomenclature. Guides and special considerations in different disciplines are listed below.

Mathematics. Notations that are expensive to typeset should be avoided by use of the devices given on p. 7 of the American Mathematical Society's *Manual for Authors* (1970): for example, replace $\frac{a}{b}$ by a/b, e^{x^2} by $\exp(x^2)$, $\vec{r}$ by $\mathbf{r}$ (denoted in manuscript by a wavy underline). Manuscripts in which this has not been done may be returned to the author.

Provide a list of special characters used in the paper for the printer's guidance, and identify all Greek, Hebrew, or script letters by means of marginal notes at their first appearance.

Physics. Use the American Institute of Physics' *Style Guide* (revised 1969).

Chemistry. Use the American Chemical Society's *Handbook for Authors* (1967).

Life Sciences. Use the Conference of Biology Editors' *Style Manual* (1972) (American Institute of Biological Sciences, Washington, D.C.). Some of their recommendations are expanded by the *Handbook of Biochemistry (with Selected Data for Molecular Biology)* (1970), ed. Sober, H. A. (Chemical Rubber Company, Cleveland, Ohio), 2nd ed. This book contains the International Union of Biochemistry rules of nomenclature for vitamins, enzymes, synthetic polypeptides, carbohydrates, lipids, and polynucleotides. Further guidance on nomenclature can be obtained from the NAS-NRC Office of Biochemical Nomenclature (Dr. Waldo E. Cohn), Oak Ridge National Laboratory, P.O. Box Y, Oak Ridge, Tennessee 37830. For bacterial genetics, follow the recommendations of Demerec, M., Adelberg, E. A., Clark, A. J. & Hartman, P. E. (1966) *Genetics* **54,** 61–76. For human immunoglobulins and their genetic factors, follow the World Health Organization rules (see, for example, section A of *Handbook of Biochemistry*).

Enzymes should be given their recommended names on first mention, together with the Enzyme Commission (EC) number when this has been assigned.

Abbreviations

Standard Abbreviations for units of measure and for certain substances (e.g., DNA) are listed in the style manuals and handbooks named above. These need not be spelled out. Some standard abbreviations and symbols whose correct form is not familiar to all authors are listed on the following pages. Rules of the IUPAC–IUB Commission on Biochemical Nomenclature are followed [see *J. Biol. Chem.* (1966) **241,** 527 and *J. Mol. Biol.* (1971) **55,** 299, for example, for guidance].

Nonstandard Abbreviations are defined as those not given in the handbooks' lists, even if they may be familiar to those in the field. (*a*) Keep them to a minimum, and only for cumbersome words that *must* be used more than five times in the paper. (*b*) Spell out nonstandard abbreviations at their first appearance in the text. (*c*) If possible, avoid them completely in the Abstract. (*d*) List them on the title page for inclusion as a footnote on the first printed page of the article.

References

Cite references in order throughout the text by means of arabic numerals (not superscript) between parentheses (in mathematical papers, square brackets may be used to avoid confusion with numbered equations, or the reference number may be preceded by "ref."). Citations are to be made in this way *only* to papers already published or "in press" in a stated journal or other publication. Any reference to unpublished work should be made *in the text* or, rarely, in the form of a symboled footnote. Reference to "personal communication" should also be made in the text; *written approval by the person cited should accompany the manuscript.*

We encourage the provision of titles and require inclusive pagination for articles cited. References must be typed *double-spaced* in the style used by the PROCEEDINGS, thus (for journal articles):

10. Smith, A. B., Jones, C. D. & Robinson, E. F. (1969) "Conformational changes in ribosomes during protein synthesis," *Proc. Nat. Acad. Sci. USA* **64,** 191–195.

Titles of journals should be abbreviated according to the American National Standard for the Abbreviation of Titles of Periodicals (see *ACCESS* or *BIOSIS List of Periodicals*).

For references to articles in books, the following sequence should be maintained: author(s), year of publication in *complete title of book*, names of editors (if applicable), (name of publishers, place of publication), page numbers if necessary, thus:

11. Jones, C. D. & Shapiro, L. M. (1966) in *Enzyme Reactions in Protozoa*, ed. Smith, T. G. & Williams, H. I. (Universal Press, New Brunswick, N.J.), pp. 646–672.

It is extremely important that the final typed list of references be checked for accuracy against the original articles or photocopies of them.

Acknowledgments

Keep acknowledgments brief. Acknowledgments to persons usually precede those for grant support. They should be typed double-spaced.

SOME STANDARD AND RECOMMENDED ABBREVIATIONS AND SYMBOLS

For simplicity, one preferred abbreviation or symbol has been adopted in most cases, even though the handbooks listed below may give equally favored alternatives.

absorbance	*A* (*not* OD)
N-acetylglucosamine	GlcNAc
asparaginyl	Asn
aspartyl	Asp
asparaginyl *or* aspartyl	Asx
5-bromodeoxyuridine	BrdU (*not* BUdR)*
5-bromouracil	BrUra (*not* BU)
cyclic AMP (3′:5′)	cAMP
cysteinyl	Cys
deoxy (carbohydrates and nucleotides)	d
deoxyribonuclease	DNase
deoxyribonucleic acids	DNAs
2,4-dinitrophenyl	Dnp-
formylmethionyl	fMet
glucose	G or Glc†
guanosine	G or Guo†
gluconic acid	GlcA
glucosamine	GlcN
glucuronic acid	GlcUA
glutamyl	Glu
glutaminyl	Gln
glutamyl *or* glutaminyl	Glx
hemoglobin	Hb
immunoglobulin G(M)	IgG(IgM)
isoleucyl	Ile
methemoglobin	MetHb
methionyl	Met
micromicro	*use* pico (p)
micron	*use* micrometer (μm)
millimicro	*use* nano (n)
millimicron	*use* nanometer (nm)
mole(s)	mol
mitochondrial DNA	mtDNA
myoglobin	Mb
nucleotide (unknown)	N (*not* X)
optical density	OD ‡
phosphate (in compounds)	*P* or p
phosphate, inorganic	P_i
plaque-forming units	PFU
ribonuclease	RNase
ribonucleic acids	RNAs
ribosomal RNA	rRNA
ribosyl	r (only if needed to distinguish from d)
ribosylthymine	rT
thymidine	dT
2,4,6-trinitrophenyl	Tnp-
tryptophanyl	Trp
uracil	Ura (*not* U)
uridine	U

* Similarly for other halogenated nucleosides.
† Use 3-letter abbreviation when G can be ambiguous.

‡ Use only for reduced light (or UV) transmission through turbid suspensions; for light (or UV) absorption by solutions, use absorbance, *A*.

Isotopes. The mass number of an atom should be written as a superior prefix: ^{14}C, not C^{14}; ^{35}S, not S^{35}. Enclose the symbol for the isotope in *square brackets* placed immediately before the name or abbreviation of the compound: [^{32}P]CMP (not CM^{32}P); [^{14}C]urea; [α-^{14}C]leucine; [*carboxy*-^{14}C]leucine; ($\alpha\beta$-$^{14}C_2$]maleic anhydride; L-[*methyl*-^{14}C]methionine. The symbol *U* denotes uniform labeling, e.g., [*U*-^{14}C]glucose. With chemical formulas, use $^{14}CO_2$, $H_2{}^{35}S^{18}O_4$, etc. (no square brackets). For fully deuterated solvents use, for example, [*U*-^{2}H]pyridine or $C_5{}^2H_5N$.

Peptide Symbols. For peptides of known sequence, represent the CO–NH bonds by hyphens, as in Gly-Tyr-Ala. Groups of residues of unknown sequence are enclosed in parentheses and separated by commas.

Nucleoside Symbols. Use A, C, G, I, ψ, T, U, X, for *residues* of adenosine, cytidine, guanidine, inosine, pseudouridine, ribosylthymine, uridine, or xanthosine (N, *not* X, for unknown nucleotide) in 3′-5′ linkages; dA, dC, etc., for corresponding deoxy compounds. End phosphoric residues are specified by p, internal (phosphodiester) phosphoric residues by a hyphen. Synthetic polynucleotides: poly is *always* to be followed by parentheses, without intervening space, *thus* poly(A). Phosphodiester bonds are denoted by hyphens, *thus* poly(dA-dT) for a polymer of alternating adenosine and thymidine residues. Random or unknown order is denoted by commas, *thus* poly(dA, dT). Indicate noncovalent associations by a center dot, *thus* poly(I)·poly(C), RNA·DNA hybrids.

Transfer RNAs that accept specific amino acids are designated thus: $tRNA^{Ala}$ ("alanine tRNA"). When the tRNA is bound to an amino-acid residue, use alanyl-tRNA (alanyl-$tRNA^{Ala}$ if necessary) or, e.g., fMet-$tRNA_f$.

HANDBOOKS AND STYLE MANUALS

American Mathematical Society. *A Manual for Authors of Mathematical Papers (1970)*. AMS, 321 South Main Street, P.O. Box 6248, Providence, R.I. 02904.

American Chemical Society. *Handbook for Authors of Papers in the Journals of the American Chemical Society (1967)*. ACS Publications, 1155 Sixteenth Street, N.W., Washington, D.C. 20036.

American Institute of Physics, Publication Board. *Style Manual for Guidance in the Preparation of Papers Published by the American Institute of Physics (1959, rev. 1969)*. AIP, 335 East 45th Street, New York, N.Y. 10017.

Conference of Biological Editors, Committee on Form and Style. *Style Manual for Biological Journals (1972), 3rd ed.* American Institute of Biological Sciences, 3900 Wisconsin Avenue, N.W., Washington, D.C. 20016.

Handbook of Biochemistry (with Selected Data for Molecular Biology) (1970), ed. Sober, H. A. (Chemical Rubber Company, Cleveland, Ohio), 2nd ed.

American Psychological Association. *Publication Manual of the American Psychological Association (1967)*. APA, 1200 Seventeenth Street, N.W., Washington, D.C. 20036.

Abbreviations of Units of Measurement and of Physical and Chemical Quantities

(These abbreviations may be used without definition. They are not normally followed by periods except as shown.)

Prefixes to the Names of Units

giga	10^9	G	micro	10^{-6}	μ
mega	10^6	M	nano	10^{-9}	n
kilo	10^3	k	pico	10^{-12}	p
centi	10^{-2}	c	femto	10^{-15}	f
milli	10^{-3}	m	atto	10^{-18}	a

*Units of Concentration**

molar (mol/liter)	M†
millimolar (mmol/liter)	mM (rather than 10^{-3} M)
micromolar (μmol/liter)	μM (rather than 10^{-6} M)
nanomolar	nM (not mμM)
picomolar	pM (not $\mu\mu$M)

Other Words

logarithm (Briggsian)	log
logarithm (natural)	ln
standard deviation of series	SD
standard error of mean	SEM

Physical and Chemical Quantities

meter	m
centimeter	cm
millimeter	mm
micrometer (not micron)	μm (not μ)
nanometer	nm (not mμ)
picometer	pm
Angstrom (0.1 nm)‡	Å
square centimeter	cm^2
cubic centimeter	cm^3
milliliter	ml
microliter	μl (not λ)
gram	g
milligram	mg
microgram	μg (not γ)
second	sec
minute	min
counts per minute	cpm
revolutions per minute	rpm
curie(s)	Ci
equivalent	eq
Svedberg unit of sedimentation coefficient (10^{-13} S) with numeral	S
mol	not abbreviated further
cycle per second (Hertz)	Hz
retardation factor	R_F
acceleration of gravity	g
specific rotation	$[\alpha]_\lambda^t$
sedimentation coefficient	s
sedimentation coefficient in water at 20°, extrapolated to zero concentration	$s^0_{20,w}$
diffusion coefficient (usually given in $cm^2\ s^{-1}$)	D
degree Centigrade or Celsius	°§
degree absolute (Kelvin)	°K
equilibrium constant	K
Michaelis constant	K_m
calorie¶	cal
kilocalorie¶	kcal
joule¶	J

* Term such as milligram percent (mg%) should not be used. Weight concentrations should be given as g per ml, g per 100 ml, g per liter, etc.

† The letter M is not an abbreviation for mole; it is reserved for molar. Use mM for 10^{-3} M and μM for 10^{-6}. Avoid designating concentrations as μmol per ml, for example. The designation should, in this case, properly be mM (i.e., millimolar). Maintain consistency in the use of units in situations where they are to be compared (e.g., do not juxtapose 10^{-4} M and 10^{-6} M).

‡ The PROCEEDINGS will continue to accept certain units as listed (e.g., Angstrom, calorie, minute) even though they are not part of the Système Internationale. Note that nanometer is preferred instead of millimicron or Angstrom units.

§ Use °C abbreviation if ° could be ambiguous.

¶ The Système Internationale (SI) recommends joules. When calories are used the equivalent value in joules should be given (1 calorie = 4.184 joules).

Proc. Nat. Acad. Sci. USA
Vol. 70, No. 1, pp. 1–4, January 1973

The Contribution of the α and β Chains to the Kinetics of Oxygen Binding to and Dissociation from Hemoglobin

(heme proteins/ligand binding/protein chemistry)

QUENTIN H. GIBSON

Department of Biochemistry and Molecular Biology, Wing Hall, Cornell University, Ithaca, New York 14850

Communicated by Leon A. Heppel, October 20, 1972

ABSTRACT **A new type of experiment in which hemoglobin is exposed briefly to oxygen has shown that the half-time of dissociation of oxygen from some partly oxygenated intermediates is about 1 msec at 20° and 10 msec at 2°. The rapid dissociation occurs selectively from one type of chain, provisionally identified as the β-chain. Chains that show the rapid rate of dissociation of oxygen also bind rapidly. It follows that the kinetic equivalent of the Adair equation and the Monod–Wyman–Changeux model are quite unsuited to represent the kinetics of the oxygen–hemoglobin reaction. The reaction of oxygen with hemoglobin closely resembles that of the alkyl isocyanides and differs radically from that of carbon monoxide.**

When the velocity of dissociation of the first oxygen molecule from sheep oxyhemoglobin was measured by Gibson and Roughton (1), and compared with the overall rate of oxygen dissociation in the presence of dithionite, it became clear that the rate of dissociation of oxygen from partly saturated intermediates must be greater than the rate of dissociation from fully liganded hemoglobin. Attempts to fit the time course of the oxygen-binding reaction to an elementary kinetic scheme equivalent to the Adair equation (3), as set out in Eq. **1**, have suggested that the ratio of the rates might be of the order of 100:1 (4), but such estimates are subject to the major uncertainties associated with curve-fitting methods.

$$\mathrm{Hb_4(O_2)_{n-1}} + \mathrm{O_2} \underset{k_n}{\overset{k_n'}{\rightleftharpoons}} \mathrm{Hb_4(O_2)_n},\ n = 1,4. \qquad [1]$$

This paper gives a preliminary account of results with a new type of experiment, which will be called the oxygen-pulse technique, that allows the dissociation of oxygen from intermediates to be observed directly. It has been found for human hemoglobin that the ratio of the rates of dissociation of the first and fourth molecules of oxygen is about 1:60. This ratio, however, applies only to one type of chain, tentatively identified as the β-chain. Corresponding figures for the α-chains are not yet available, but the ratio for them must be much smaller. The discovery of a substantial difference between the chains came as a surprise, since although large differences between chains have been demonstrated for the bulky ligand *n*-butyl isocyanide (5), it has been rather generally believed that there is little functional difference between them in their reactions with oxygen. In the only individual reaction so far investigated, the ratio k_4^α/k_4^β was only about 1:2 (6). Investigation of the oxygen–deoxyhemoglobin reaction under chosen conditions has now shown very significant differences between the chains. These differences are great enough to make the use of Eq. **1** in representing oxygen–hemoglobin kinetics physically meaningless. Similar considerations apply, of course, to special forms of Eq. **1** such as the Monod–Wyman–Changeux model, recently applied by Hopfield *et al.* (7) to interpret a wide range of kinetic experiments with hemoglobin.

MATERIALS AND METHODS

Hemoglobin was prepared as described (4) and stripped before use (8). The stopped-flow apparatus and data collection system were as described by DeSa and Gibson (9). Gases and other materials were obtained from the sources specified in (4).

RESULTS

Oxygen dissociation from intermediates

Oxygen pulse experiments were performed by mixing deoxyhemoglobin solutions containing dithionite with solutions of oxygen in the stopped-flow apparatus. On mixing, oxygen begins to disappear from the solution by reaction with dithionite in a zero-order reaction (2) and at the same time reacts with deoxyhemoglobin. The oxygen binding is quickly terminated by the disappearance of free oxygen from the solution, the time required depending on the concentrations of oxygen and of dithionite (typically 1–10 msec.). In these circumstances the population of partially oxygenated intermediates formed, from which oxygen subsequently dissociates, is determined primarily by the kinetic constants for binding the first one or two molecules of oxygen. Such populations differ widely from those established at equilibrium, where, as a result of cooperativity, the species $\mathrm{Hb_4}$ and $\mathrm{Hb_4(O_2)_4}$ are heavily represented. The kinetically determined populations, thus, permit the behavior of the partially oxygenated intermediates to be examined. The results of an experiment performed at 2° in 0.05 M phosphate buffer, pH 7.0, are shown plotted in semi-logarithmic form in Fig. 1. The rapid binding reaction, much of which occurs in the dead time of the stopped-flow apparatus, is followed by a deoxygenation reaction, which consists of two clearly separated phases differing in rate by about 20-fold. The relative amplitude of these phases is a function of the peak saturation reached, the proportion of rapid reaction increasing as the peak saturation declines, and approaching 100% below a peak saturation of 0.1. The reaction can be satisfactorily represented by two rates only, of about 100/sec and 6/sec.

The two distinct phases in Fig. 1 might represent the effects of heme–heme interaction upon functionally similar hemes, as

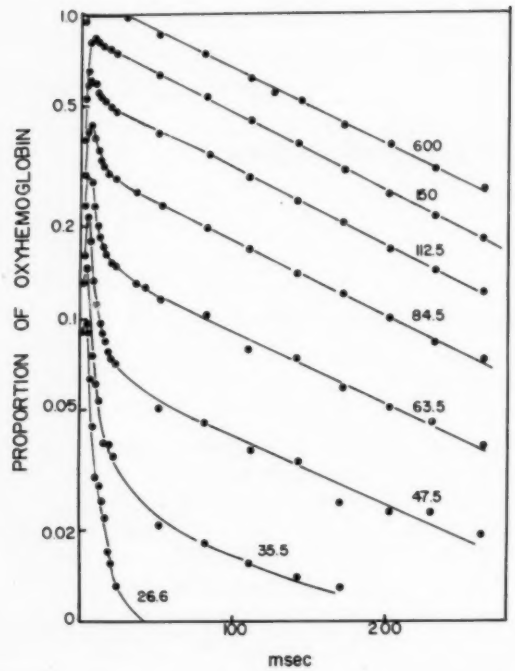

FIG. 1. The time course of the absorbance change at 438 nm in an oxygen pulse experiment performed at 2°. The concentration of hemoglobin was 17 μM (heme basis) after mixing. Hemoglobin was dissolved in 0.05 M phosphate buffer, pH 7.0, containing 0.1% sodium dithionite (before mixing). This solution was mixed with buffers containing oxygen to give the concentrations of oxygen (μM) shown opposite each curve (after mixing).

assumed in the Adair equation and in the Monod–Wyman–Changeux model, or they might be due to interactive effects superimposed upon intrinsically different α and β chains. This point has been investigated by examination of the wavelength dependence of the time course of the deoxygenation reaction. In the neighborhood of suitable isosbestic points there is a well-marked dependence of the apparent rate of deoxygenation upon wavelength; an example is given in Fig. 2. It follows that the biphasic behavior shown in Fig. 1 arises in a large measure from the presence of two chemically distinct species having widely separated rates of oxygen dissociation. By analogy with *n*-butyl isocyanide (5), the more rapid rates may be assigned to the β chains. An additional check on this assignment is possible by use of the effects of inositol hexaphosphate. As shown by Gray and Gibson (10), this compound increases the rate of oxygen dissociation from the β chains, which can be identified spectrophotometrically as shown by Olson *et al.* (6). When inositol hexaphosphate is added to oxyhemoglobin and the overall deoxygenation reaction in the presence of dithionite is examined, a biphasic reaction is observed with a wavelength dependence similar to that exemplified in Fig. 2.

Effect of pH, temperature, and anions on oxygen dissociation from intermediates

Oxygen pulse experiments have been performed under conditions other than those of Fig. 1. At 20° and in 0.05 M phosphate, pH 7.0, the general pattern of Fig. 1 is maintained, but the proportion of the rapid phase is less at any given peak saturation. The rate of the rapid phase is about 1100/sec. The results at pH 6 are closely similar to those obtained at pH 7. In 0.05 M borate buffer, pH 9.0, the proportion of the rapid phase is smaller than at pH 7, and the rate drops to about 500/sec. In 0.05 M Bis-Tris buffer, pH 6 and pH 7, the amplitude of the rapid phase is similar to that seen in borate pH 9, but the rate is about 1000/sec. The addition of 50 μM inositol hexaphosphate greatly increases the amplitude of the rapid phase at pH 6 and pH 7 when added either to Bis-Tris or phosphate buffers. There may be a small increase in the rapid rate also.

Oxygen-binding experiments

In view of the oxygen dissociation behavior just described, wavelength dependence was looked for in the oxygen-binding reaction. The results obtained in the region of the isosbestic point at 585 nm are illustrated in Fig. 3. It is clear that the time course of the absorbance change is a function of the observed wavelength, with fast and slow components disposed as in the case of the oxygen pulse experiments. An approximate analysis of a series of experiments performed with different concentrations of oxygen is presented in Fig. 4, which gives the rates obtained if it is assumed that the time course of the absorbance change may be represented by the sum of two exponentials. The results suggest a rate of about 2.5×10^6 $M^{-1}sec^{-1}$ for binding to the fast component (β-chains), and a dissociation rate of about 100/sec, similar to that observed directly in the oxygen-pulse experiments. The slow component has a nonlinear dependence on oxygen concentration, and a much lower dissociation velocity. The results shown in Fig. 4 exactly parallel those reported by Olson and Gibson (5) for *n*-butyl isocyanide.

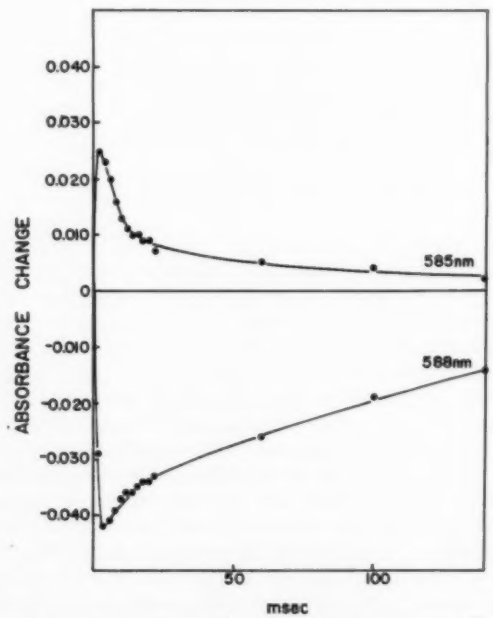

FIG. 2. The time course of the absorbance changes at 585 and 588 nm in an oxygen pulse experiment. Conditions are as for Fig. 1, but hemoglobin concentration was 35 μM, optical path 2 cm, oxygen concentration 124 μM after mixing, dithionite 0.4%.

DISCUSSION

The results just presented show that there are large and hitherto unsuspected differences between the α and β chains in their reaction with oxygen. It follows that Eq. **1**, which assumes chain equivalence, cannot be used to represent the kinetics of the oxygen-binding reaction. The Monod–Wyman–Changeux model, as recently applied by Hopfield *et al.* (7) for this purpose, is equally inapplicable, and constants derived from either scheme are without physical meaning. The simplest realistic scheme, which incorporates chain differences, appears to be that used by Olson and Gibson (5) for *n*-butyl isocyanide, but even this scheme requires that nine equilibrium constants be assigned. Preliminary examination of the oxygen data suggests that there may be appreciable α–β interactions, as well as the major change in the tetramer that occurs when an organic anion is released. As compared with *n*-butyl isocyanide and carbon monoxide, extra data can be obtained for oxygen by use of the dithionite reactions, and it is hoped that these extra data may permit at least a plausible determination of the rate constants in the scheme used by Olson and Gibson (5).

Brunori *et al.* (11) have recently deduced from comparisons of the carbon monoxide equilibrium curve of hemoglobin in the light and in the dark that the dissociation velocity constants for carbon monoxide from partly liganded intermediates cannot be much greater than those from fully liganded carbon monoxide–hemoglobin. Their result is widely different from those with oxygen and *n*-butyl isocyanide. It is interesting to note that the absolute rate of dissociation of the fourth molecule of carbon monoxide (i.e. the rate of dissociation from Hb_4CO) would be about 30,000 times less than the rate of dissociation of oxygen from $Hb_4(O_2)\beta$, and it may be that the rate-limiting step in the dissociation process is different for the two types of ligand. Taken together, the present results and those of Brunori *et al.* (11) strongly support the conclusion of Roughton (12) that the equilibrium curves for oxygen and carbon monoxide cannot be superimposed by application of a scale factor.

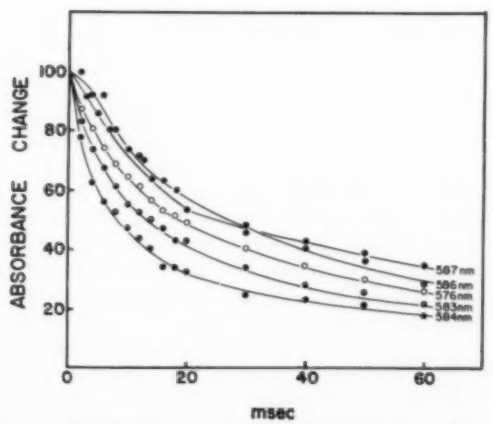

FIG. 3. The time course of the absorbance change observed on oxygen binding at wavelengths near the 585-nm isosbestic point. Conditions: 0.05 M phosphate buffer, pH 7.0, 2°, 2-cm optical path, hemoglobin 30 μM, oxygen 31 μM. The excursions have been normalized to permit ready comparisons. Data obtained at 576 nm, remote from the isosbestic point, have been included.

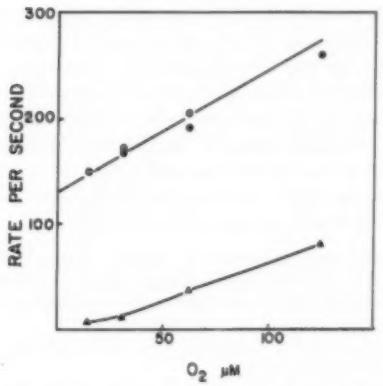

FIG. 4. Rates of absorbance change observed during oxygen binding. The time course was treated graphically to yield two rates for each oxygen concentration used. The *open circles* are for data at 576 nm, the *filled circles* are for data at 585 nm. The *crosses* were derived from data at 576 nm. The experimental conditions were those of Fig. 3, with oxygen concentrations as shown on the abscissa.

The oxygen pulse experiments show beyond reasonable doubt that the large values of the oxygen-dissociation velocity constants suggested as a result of curve-fitting work have a real physical existence even though they were derived from an unsuitable model. This not only complicates kinetic work, but if the kinetic differences carry over to the equilibria, modifies the interpretation of equilibrium constants derived from the extremes of the equilibrium curve. At low saturation the higher affinity chain will be examined, and at high saturation the lower affinity chain will be examined. The apparent interaction energy derived from Hill plots may, therefore, be modified appreciably. Since $K_1 = 2(A_1 + B_1)$, where $K_1 = k_1'/k_1$ of Eq. **1** and A_1 and B_1 are the intrinsic equilibrium constants for binding of the first ligand molecules to α and β chains, respectively, it is possible to estimate, very roughly, the relative affinities of the two types of chain. Roughton and Lyster (15) have given K_1 at 20° in 0.6 M phosphate, pH 7, as 0.049/mm of Hg for human hemoglobin, but in a personal communication made several years later Prof. F. J. W. Roughton informed the author that experiments with more dilute hemoglobin in 0.1 M phosphate had given a value of 0.1/mm of Hg for K_1. Adoption of the latter value, and application of the only temperature coefficient for K_1 available, that of Paul and Roughton (13) for sheep hemoglobin, gives K_1 at 2° as 0.18/μM (converting into concentrations). If B_1 is about 0.025/μM, A_1 would be about 0.065/μM. Clearly a direct determination of K_1 under the conditions of the kinetic experiment would be desirable, but it seems likely, nevertheless, that the α chains may have a higher affinity for oxygen than the β chains at low fractional saturations.

The new experiments explain clearly why K_1 calculated from kinetic data by Gibson (4) was substantially smaller than that observed by Roughton. The kinetic constants necessarily took into account the high rate of dissociation of the β chain, whereas Roughton was primarily studying the α chain, which has a higher affinity. The new experiments, however, do

nothing to account for the discrepancy between the kinetic results of Berger *et al.* (14) and those of Gibson (4) for the oxygen-binding reaction. Berger *et al.* observed a lag at the beginning of the oxygen-binding reaction that was reproduced in some measure by the Monod–Wyman–Changeux model as applied by Hopfield *et al.* (7). The new results indicate clearly that there can be no such lag, and suggest that the observations of Berger *et al.* (14) may have included an instrumental artifact in the earliest stages of the reaction.

This work was supported by United States Public Health Services Grant GM 14276-07. I thank Drs. S. J. Edelstein and J. K. Moffat for helpful discussions, and for reading the draft of this paper.

1. Gibson, Q. H. & Roughton, F. J. W. (1955) *Proc. Roy. Soc. Ser. B* **143**, 310–334.
2. Hartridge, H. & Roughton, F. J. W. (1925) *Proc. Roy. Soc. Ser. B* **107**, 395–429.
3. Adair, G. S. (1925) *J. Biol. Chem.* **63**, 529–545.
4. Gibson, Q. H. (1970) *J. Biol. Chem.* **245**, 3285–3288.
5. Olson, J. S. & Gibson, Q. H. (1972) *J. Biol. Chem.* **247**, 1713–1726.
6. Olson, J. S., Andersen, M. E. & Gibson, Q. H. (1971) *J. Biol. Chem.* **246**, 5919–5923.
7. Hopfield, J. J., Shulman, R. G. & Ogawa, S. (1971) *J. Mol. Biol.* **61**, 425–443.
8. Benesch, R., Benesch, R. E. & Yu, C. I. (1968) *Proc. Nat. Acad. Sci. USA*, **59**, 526–530.
9. DeSa, R. J. & Gibson, Q. H. (1969) *Comput. Biomed. Res.* **2**, 494–505.
10. Gray, R. D. & Gibson, Q. H. (1971) *J. Biol. Chem.* **246**, 7168–7174.
11. Brunori, M., Bonaventura, J., Bonaventura, C., Antonini, E. & Wyman, J. (1972) *Proc. Nat. Acad. Sci. USA* **69**, 868–871.
12. Roughton, F. J. W. (1972) in *Oxygen Affinity of Hemoglobin and Red Cell Acid Base Status*, eds. Rorth, M & Astrup, P. (Munksgaard, Copenhagen), pp. 84–92.
13. Paul, W. & Roughton, F. J. W. (1951) *J. Physiol.* **113**, 23–35.
14. Berger, R. L., Antonini, E., Brunori, M., Wyman, J. & Rossi-Fanelli, A. (1967) *J. Biol. Chem.* **242**, 4841–4843.
15. Roughton, F. J. W. & Lyster, R. L. J. (1965) *Hvalradets Skr.* **48**, 185–198.

Proc. Nat. Acad. Sci. USA
Vol. 70, No. 1, pp. 5–9, January 1973

RNA Related to That of a Murine Leukemia Virus in Burkitt's Tumors and Nasopharyngeal Carcinomas

D. KUFE, R. HEHLMANN, AND S. SPIEGELMAN

Institute of Cancer Research and Department of Human Genetics and Development, College of Physicians and Surgeons, Columbia University, New York, N.Y. 10032

Contributed by S. Spiegelman, September 18, 1972.

ABSTRACT **RNA homologous to that of the Rauscher leukemia virus has been detected in Burkitt's lymphomas and nasopharyngeal carcinomas. Earlier excellent experimental evidence has linked these two human tumors with the Epstein–Barr virus, a DNA-containing agent.**

The detection of viral-specific RNA in tumors (1) by molecular hybridization (2) has revealed that certain human neoplasias exhibit a specific pattern of viral-related RNAs remarkably similar to that observed in the corresponding viral-induced tumors of mice. Thus, human breast carcinomas contain an RNA possessing homology to that of the mouse mammary tumor virus. The breast tumor RNA exhibited no sequence relatedness to RNA of the Rauscher leukemia virus, an agent possessing no homology to mouse mammary tumor virus (manuscript in preparation). On the other hand, RNAs from human leukemic cells (3), human sarcomas (4), Hodgkins' disease, and other human lymphomas (5) were all unrelated to that of the breast tumor virus, showing instead unique homology to the RNA of the leukemogenic Rauscher virus.

The pattern of specificities exhibited by the human tumors examined are in accord with the experience accumulated with the mouse experimental system. It was of obvious interest to subject this intriguing parallelism to further scrutiny by a similar analysis of Burkitt's lymphoma and nasopharyngeal carcinoma, both of which have been experimentally related to the DNA-containing Epstein–Barr virus.

Burkitt's disease, a malignant lymphoma, is the most common cancer found in children living in a geographical belt extending across Central Africa. Epidemiological (6, 7), serological (7, 8), and nucleic acid hybridization (9) studies have linked this disease to the herpes-like Epstein–Barr virus detected in (10) and isolated (11) from Burkitt's lymphoma cells grown in culture. Nasopharyngeal carcinoma, a tumor containing both epithelial and lymphoid elements (12), is prevalent in certain groups in the Far East. Serological (8, 13) and hybridization (9) evidence has similarly implicated the Epstein–Barr virus in this disease.

Though arresting, such correlative data cannot by themselves permit a definitive decision on whether Epstein–Barr virus is causative or contributory in these diseases (14). Even finding sequences from this virus in the relevant human cancer cells is not conclusive, and particularly so until other types of "oncogenic" information have been sought for and eliminated as possible participants in the carcinogenic process. To shed light on these and related issues, we address ourselves to the following question: Do Burkitt's lymphomas and nasopharyngeal carcinomas contain RNA homologous to that of the RNA tumor viruses found in our studies (1–5) of human lymphomas and other neoplasias?

The data obtained establish that African Burkitt's tumors and nasopharyngeal carcinomas do contain RNA homologous to that of the Rauscher leukemia virus.

METHODS AND RESULTS

Annealing reactions between [^{3}H]DNA of Rauscher virus and RNA from polysomes of tumors and normal tissues were performed in 0.4 M NaCl–50% formamide at 37° for 18 hr. These conditions were chosen because they (unpublished observations) minimize thermal degradation of RNA during the incubation. Although initial rates of hybridizations can be increased by elevation of the temperature, the extent of hybridization reached at 37° after 18 hr was the same as at higher temperatures.

Annealing reactions were analyzed in Cs_2SO_4 gradients. This method was chosen because of its low background and superior sensitivity to other methods—such as hydroxylapatite chromatography and the use of nucleases specific for single-stranded nucleic acid. The specificity of positive reactions in Cs_2SO_4 gradients with tumor RNA was internally monitored by parallel tests with RNA from normal tissues, as well as by challenging positive tumor RNA with DNA homologous to unrelated RNA from mouse mammary tumor virus and avian myeloblastosis virus.

Annealing reactions with RNA from tumors

Fig. 1 shows Cs_2SO_4 gradient profiles that result from annealing reactions between [^{3}H]DNA from Rauscher virus and polysomal RNA isolated from several Burkitt's lymphomas and a nasopharyngeal carcinoma. The responses seen are comparable in magnitude to those obtained with the same [^{3}H]DNA annealed to polysomal RNA preparations derived from human sarcomas and leukemic cells. In general, 1–5% of the input [^{3}H]DNA is hybridized to the polysomal RNA from the Burkitt and nasopharyngeal carcinoma tumors. Their position in the density gradient implies that RNA in the complexes is much larger than the DNA in the complexes and, therefore, determines the density of the DNA·RNA hybrid structure.

A more extensive examination of the annealing reaction is shown in Fig. 2, in which a fixed amount of [^{3}H]DNA from Rauscher virus is annealed to different concentrations of polysomal RNA, and the % of [^{3}H]DNA hybridized is determined by isopycnic separation in Cs_2SO_4 gradients. The Burkitt's

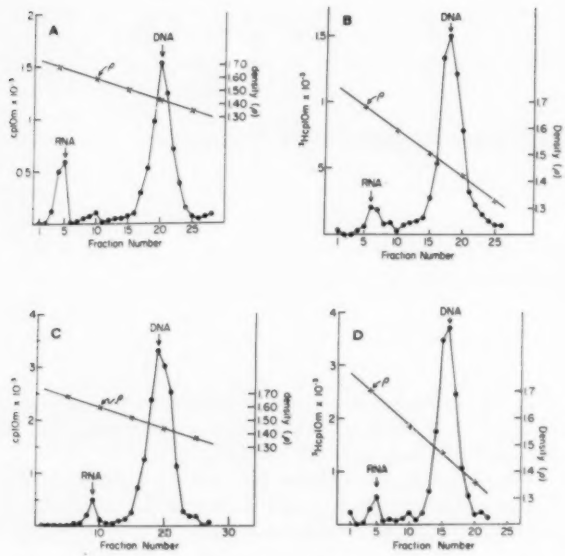

FIG. 1. Cs_2SO_4 density profiles of Rauscher leukemia virus [^{3}H]DNA hybridized to polysomal RNA obtained from Burkitt's tumors NA, 11719, and 12079 (*A,C,D*) and from nasopharyngeal carcinoma 15903 (*B*). [^{3}H]DNA was synthesized as follows: A 1-ml reaction mixture, containing 100 μg of viral protein purified from plasma, 50 μmol of Tris·HCl (pH 8.3), 40 μmol of KCl, 6 μmol of $MgCl_2$, 2.5 μmol of S_2 threitol, 0.00125% NP-40 (Shell Chemical Co.), 0.8 μmol of dGTP, dATP, and dCTP, and 50 nmol of [^{3}H]TTP (8000 cpm per pmol), was incubated at 37° for 180 min. After addition of 0.5% Na dodecylSO_4 and extraction with an equal volume of phenol–cresol, the [^{3}H]DNA product was purified by Sephadex G-50 chromatography and treated with 0.5 M NaOH at 43° for 24 hr to hydrolize any viral RNA present.

In studies such as those contemplated here, it must be shown before use that the radioactive DNA product bands solely in the DNA density region of a Cs_2SO_4 gradient and that it hybridizes with homologous RNA, and not to normal cellular RNA.

The RNA (designated as polysomal RNA) used in the hybridizations is derived from a cytoplasmic pellet consisting of a mixture of monosomes and polysomes. Suitable care must be exercised to insure the complete removal of protein contaminants. For the preparation of polysomal RNA, the tumors were disrupted by a Silverson homogenizer at 4° in two volumes of 5% sucrose in TNM buffer [0.01 M Tris·HCl (pH 7.4)–0.15 M NaCl–2 mM $MgCl_2$]. The suspension was centrifuged at 20,000 × *g* for 15 min at 0°. The supernatant fluid was then layered on 20 ml of 25% sucrose in TNM buffer containing 200 μg of polyvinyl sulfate per ml and spun for 180 min at 180,000 × *g* in a 60 Ti rotor (Spinco). The pellet was resuspended in TNM buffer with 0.5% Na dodecylSO_4 and the RNA was extracted twice with an equal volume of cresol–phenol (pH 8.0). Nucleic acid was precipitated from the aqueous phase by addition of two volumes of ethanol and 0.1 volume of 4 M NaCl. The polysomal RNA was redissolved in 50% formamide—50% 5 mM EDTA. The [^{3}H]DNA was denatured by incubation at 80° for 15 min in 70% formamide and subsequent quick chilling. An average of 350 μg of polysomal RNA was hybridized to 2000 cpm of Rauscher virus-[^{3}H]DNA in 60 μl (0.4 M NaCl–50% formamide). The reaction was incubated for 18 hr at 37°, mixed with 11 ml of half-saturated Cs_2SO_4 (starting density 1.52), and centrifuged at 44,000 rpm for 60 hr at 15° in a 50 Ti rotor (Spinco), and 0.4-ml (8-drop) fractions were collected through an 18-gauge needle from the bottom of the tube and assayed for Cl_3CCOOH-precipitable radioactivity.

lymphoma polysomal RNA (Fig. 2*A*) shows no evidence of saturation at 5.8 mg/ml, at which point 4.75% of the [^{3}H]-DNA from Rauscher virus has been involved in the complex. Similarly, the nasopharyngeal carcinoma polysomal RNA has not reached saturation at 11.3 mg/ml when 2% of the [^{3}H]-DNA has been hybridized.

As in previous studies, a method of recording our findings has been adopted that avoids the inconvenience of presenting the Cs_2SO_4 gradient of every tissue examined. After correction for background counts, the sum of the tritium counts in the RNA density region (density 1.62–1.69 g/ml) was used to measure the amount of DNA complexed to RNA. To achieve the accuracy desired, 10-min counts (cp10m) were taken on each sample. An operational mean background and its standard deviation (*S*) were empirically determined for individual machines from the total cp10m of three tubes in the negative region (i.e., tubes 2, 3, and 4) of each of 60 gradients. The convention was adopted that specimens showing a cp10m of less than three standard deviations of the background mean were considered negative.

Tables 1 and 2 record the outcomes of the annealing reactions with polysomal RNA from Burkitt's lymphomas and nasopharyngeal carcinomas. The results are recorded as the total cp10m (corrected for background) in the RNA density region, and as multiples of the mean background standard deviation. Not detailed in either table, but included in the graphical summary of Fig. 3, are the control hybridizations with polysomal RNA from various normal adult and fetal tissues. Of the 21 Burkitt's lymphomas examined, 76% yielded positive responses with Rauscher virus [^{3}H]DNA, whereas 50% of the 20 nasopharyngeal carcinomas were positive. In contrast, none of the polysomal RNA preparations from the 52 normal adult and fetal tissues responded with a reaction that was unambiguously positive. The Burkitt's lymphoma clinical data presented in Table 1 demonstrate that positive

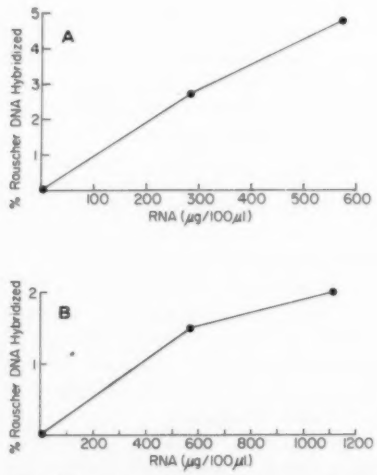

FIG. 2. Hybridization reactions between Rauscher virus-[^{3}H]DNA and polysomal RNA from Burkitt's tumor 11719 (*A*) and from nasopharyngeal carcinoma 15505 (*B*) at different RNA concentrations. The individual annealing reactions were analyzed by Cs_2SO_4 density centrifugation, and the % DNA hybridized determined by the number of [^{3}H]DNA-cp10m (corrected for background) banded in the RNA region (density 1.62–1.68) of the gradients.

responses were obtained in primary cases, as well as recurrences, and that prior therapy did not significantly influence the results.

The strikingly different response of the malignant and normal samples of Rauscher virus-[^{3}H]DNA argues strongly for the specificity of the positive reactions observed with the polysomal RNAs from lymphomas and carcinomas. Nevertheless, as in our previous studies (3–5), it is desirable to offer further support for this conclusion by use of [^{3}H]DNA complementary to the RNA of unrelated oncogenic viruses. This is particularly relevant in view of the recent findings (15–17) that the RNAs of tumor viruses contain extensive stretches of poly(A). Preferential complexing to Rauscher virus-RNA might then be explained by the presence of poly(T) stretches in the synthetic DNA probe. However, if the annealing reaction is specific for the overall sequence, one would not expect Burkitt's lymphoma or nasopharyngeal carcinoma polysomal RNA, positive for a reaction with Rauscher virus-[^{3}H]DNA, to show the ability to hybridize with unrelated DNAs. Tables 3 and 4, as well as Fig. 4, show

TABLE 1. *Test for viral-specific RNA in Burkitt's lymphomas*

Number	RNA cp10m	RNA cp10m/*S*	Reaction	Recurrence*	Previous treatment
10438	397	4.61	+	+	+
11719	850	9.90	+	+	+
12079	821	9.54	+	+	+
14858	544	6.30	+	+	−
11392	391	4.55	+	+	+
12078	606	7.05	+	−	−
14857	271	3.15	+	−	−
15043	590	6.86	+	+	+
15976	541	6.29	+	+	+
697	292	3.40	+	−	−
1143	428	4.98	+	−	−
LU	463	5.38	+	−	−
NA	1211	14.08	+	−	−
AN	682	7.93	+	−	−
NK	371	4.31	+	+	+
P_3HR-1†	524	6.10	+		
16253	238	2.77	−	−	−
9471	31	0.36	−	−	−
6606	59	0.69	−	−	−
8176	179	2.08	−	−	−
6613	34	0.40	−	+	+

Results of hybridization reactions between Raucher virus-[^{3}H]DNA and polysomal RNA isolated from Burkitt's tumors. Between 200 and 600 μg of polysomal RNA of each sample were hybridized to 2000 cpm of Rauscher virus-[^{3}H]DNA, and the reactions were analyzed by Cs_2SO_4 equilibrium centrifugation. The amount of DNA banding in the RNA region of the gradient (density 1.62–1.69) was determined. The results are expressed as cp10m (corrected for background) banding in the RNA region for each RNA sample tested, and as multiples of *S*, the operational standard deviation (see text and legend to Fig. 3). The annealing reaction is considered positive only if the cp10m per RNA region is greater than 3*S*, thus providing 99.9% confidence. Columns *5* and *6* refer to clinical data.

21 tested, 16 positive; 76%.

* (+) indicates a recurrent tumor and (−) indicates a primary tumor.

† Tissue culture line.

TABLE 2. *Test for viral-specific RNA in nasopharyngeal carcinomas*

Number	RNA cp10m	RNA cp10m/*S*	Reaction
12707	386	4.48	+
6720	403	4.69	+
13030	302	3.51	+
10924	535	6.22	+
13092	374	4.34	+
8507	297	3.45	+
15903	615	7.15	+
15803	324	3.76	+
7820	432	5.02	+
15505	559	6.50	+
13337	207	2.40	−
9423	26	0.30	−
8778	225	2.61	−
11682	228	2.65	−
9857	57	0.66	−
15434	171	1.98	−
2782	174	2.02	−
2723	136	1.58	−
719	143	1.66	−
16304	175	2.03	−

Results of hybridization reactions between Rauscher virus-[^{3}H]DNA and polysomal RNA isolated from nasopharyngeal carcinomas. (See Table 1 for details.)

that these expectations are realized. None of the Rauscher virus-positive lymphoma or nasopharyngeal carcinoma polysomal RNAs annealed significantly to either unrelated viral DNA tested.

DISCUSSION

Of the 21 African Burkitt's lymphomas, 76% were positive, as were 50% of 20 nasopharyngeal carcinomas. The absence of positive reactions with some of the tumors examined may raise questions of universality in the minds of some. However, there are various reasons why a negative outcome cannot be accepted as definitive evidence for the complete absence of

TABLE 3

Viral [^{3}H]DNA	Burkitt's tumor no.	RNA cp10m	RNA cp10m/*S*	Reaction
Avian myeloblastosis	11719	52	0.60	−
Avian myeloblastosis	10438	153	1.77	−
Mouse mammary tumor	11719	138	1.60	−
Mouse mammary tumor	10438	236	2.74	−
Mouse mammary tumor	14857	3	0.04	−

Results of hybridization reactions between avian myeloblastosis virus and mouse mammary tumor virus [^{3}H]DNA and polysomal RNA isolated from Burkitt's tumors. Between 200 and 600 μg of polysomal RNA of each sample were annealed to 2000 cpm of [^{3}H]DNA, and the reactions were subjected to Cs_2SO_4 equilibrium centrifugation. The data are expressed on cp10m (corrected for background) banding in the RNA region of the gradient, and as multiples of the standard deviation (*S*) (as described in the legends to Table 1 and Fig. 3.)

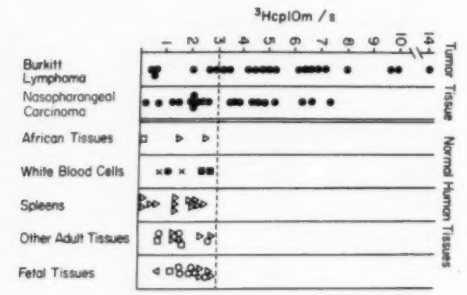

FIG. 3. Results of hybridization reactions with Rauscher virus-[³H]DNA and polysomal RNA from Burkitt's tumors, nasopharyngeal carcinomas, and normal human cells. The polysomal RNAs of normal tissues were derived from normal leukocytes (×), PHA-stimulated lymphocytes (⊠), a human lymphocyte cell line, NC37 (⊗), spleens, other adult tissues: liver (△), intestine (○), striated muscle (□), fetal tissues: liver (△), lung (▽), limbs (○), placenta (□), and African control tissues: tonsillitis (△), benign mandibular cyst (□). The reactions were then subjected to Cs_2SO_4 equilibrium density centrifugation as described under Fig. 1. The amount of [³H]DNA, expressed as cp10m corrected for background banding in the density region of RNA (density 1.62–1.69), was determined for each reaction. An operational mean and standard deviation (S) were then determined for each counter by the total cp10m of three tubes (i.e., 2,3,4) of each of 60 gradients. The number of [³H]DNA cp10m corrected for background banding in the RNA region of the gradient was then divided by the appropriate operational standard deviation. Any reaction with cp10m in the RNA region less than $3S$ is considered negative, thus providing 99.9% confidence that those reactions retained as positive (greater than $3S$) are significant.

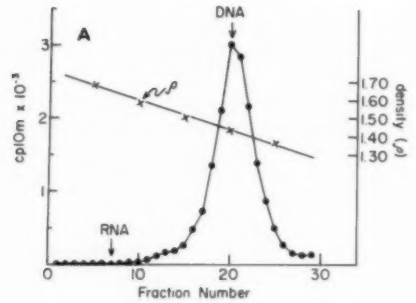

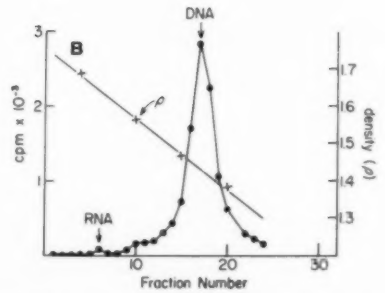

FIG. 4. Cs_2SO_4 density profiles of avian myeloblastosis virus [³H]DNA hybridized to polysomal RNA obtained from Burkitt's tumor 11719 positive in a reaction with Rauscher virus-[³H]DNA (A) and of mouse mammary tumor virus [³H]DNA hybridized to polysomal RNA from nasopharyngeal carcinoma 15903 positive with [³H]DNA from Rauscher virus (B). The annealing reactions were analyzed by Cs_2SO_4 density centrifugation as described in Fig. 1.

the relevant RNA, whether the tissue being tested is neoplastic or normal. In the first place, all of the samples tested in the present series were collected in laboratories remote from our own. Any significant delay between removal and freezing of the sample, or if it suffers more than one freezing and thawing, can lead to loss of the relevant RNA by nucleolytic degradation. The sensitivity of detection of complementary RNA is limited by the amount of polysomal RNA that can be dissolved in the annealing mixture, a difficulty that will be obviated by the development of a suitable enrichment procedure for the pertinent RNA fraction. Finally, it may be worth explicitly noting an inherent difficulty in the kinds of hybridizations we can perform. The DNA probes generated by RNA-directed DNA polymerase do not constitute complete copies of the viral RNAs used as templates. Both of these features diminish the effectiveness of these probes as detecting devices. The eventual availability of proper DNA transcripts of the appropriate viral RNA will greatly improve the sensitivity and certainty of the annealing reactions. Until this result is achieved, and the other technical difficulties noted are overcome, negative outcomes must remain uninterpretable.

TABLE 4

Viral [³H]DNA product	Nasopharyngeal carcinoma	RNA cp10m	RNA cp10m/S	Reaction
Avian myeloblastosis	15505	146	1.69	–
Avian myeloblastosis	6720	149	1.73	–
Mouse mammary tumor	15903	175	2.03	–
Mouse mammary tumor	15505	226	2.62	–
Mouse mammary tumor	15803	207	2.40	–

Results of hybridization reactions between avian myeloblastosis virus and mouse mammary tumor virus [³H]DNA and polysomal RNA obtained from nasopharyngeal carcinomas.

The fact that we find RNA that is related to Rauscher virus-RNA does not of course establish the presence of tumor viruses in these human malignancies. One must now perform experiments designed to answer the following two questions: (*i*) How large is the RNA in question? and (*ii*) Is it associated physically with a reverse transcriptase in structures characteristic of complete or incomplete virus particles? The requisite techniques to answer these questions have been developed (18, 19).

It is obviously desirable and necessary to perform similar studies on those animal neoplasias in which a DNA virus has been implicated, including the Lucké tumor of the frog, tumors induced by polyoma, and by SV-40 viruses. Even the avian Marek's disease, where the evidence for involvement of a herpes-like virus as the causative agent is impressive (20), could conceivably yield unexpected information of value.

Of particular interest is infectious mononucleosis in

humans, a self-limiting non-neoplastic condition in which prospective studies (21, 22) have strongly implicated the Epstein–Barr virus. This benign disease may well provide the opportunity to identify the type of viral-related information that is unique to malignant tissues.

Finally, we want to emphasize that we draw no conclusions on the etiology of Burkitt's lymphoma and nasopharyngeal carcinoma from the experiments described here. The presence of RNA homologous to that of Rauscher virus is obviously an observation worthy of note to those who wish to understand the biology of these tumors. The etiologic questions and implications generated by these findings will be resolved only by further investigation. There also remains the question of a possible homology between Epstein–Barr virus-DNA and Rauscher virus-RNA.

This investigation owes much to Dr. George Klein of the Karolinska Institute, Department of Tumor Biology, Stockholm, Sweden, who encouraged its initiation and helped with a generous supply of tumor material, along with relevant clinical information. DNA-directed DNA polymerase was a gift from O. Nussbaum, Hoffman La Roche, Nutley, N.J. Highly purified Epstein–Barr virus DNA was the gift of H. zur Hausen, Institute for Virology, Würzburg, Germany. We thank Dr. J. Ziegler, Uganda Cancer Institute, Uganda, Africa, for supplying several of the Burkitt's tumors, and E. Gordon, J. Myers, and L. Hindin for excellent technical assistance. This research was supported by the National Institutes of Health, National Cancer Institute, Special Virus Cancer Program Contract 70-2049, and by Research Grant CA-02332.

1. Axel, R., Schlom, J. & Spiegelman, S. (1972) *Proc. Nat. Acad. Sci. USA* **69,** 535–538.
2. Axel, R., Schlom, J. & Spiegelman, S. (1972) *Nature* **235,** 32–36.
3. Hehlmann, R., Kufe, D. & Spiegelman, S. (1972) *Proc. Nat. Acad. Sci. USA* **69,** 435–439.
4. Kufe, D., Hehlmann, R. & Spiegelman, S. (1972) *Science* **175,** 182–185.
5. Hehlmann, R., Kufe, D. & Spiegelman, S. (1972) *Proc. Nat. Acad. Sci. USA* **69,** 1727–1731.
6. Wright, D. H. (1967) *Cancer Res.* **27,** 2424–2438.
7. Henle, G., Henle, W., Clifford, P., Diehl, V., Kafuko, G. W., Kirya, B. G., Klein, G., Morrow, R. H., Munube, G. M. R., Pike, P., Tukel, P. M. & Ziegler, J. L. (1969) *J. Nat. Cancer Inst.* **43,** 1147–1157.
8. Gunven, P., Klein, G., Henle, G., Henle, W. & Clifford, P. (1970) *Nature* **228,** 1053–1055.
9. zur Hausen, H., Schulte-Holthausen, H., Klein, G., Henle, W., Henle, G., Clifford, P. & Santesson, L. (1970) *Nature* **228,** 1056–1058.
10. Epstein, M. A., Achong, B. G. & Barr, Y. M. (1964) *Lancet* **i,** 702–703.
11. Epstein, M. A., Henle, G., Achong, B. G. & Barr, Y. M. (1965) *J. Exp. Med.* **121,** 761–770.
12. Gazzolo, L., de-Thé, G., Vuillaume, M. & Ho, H. C. (1972) *J. Nat. Cancer Inst.* **48,** 73–86.
13. Henle, W., Henle, G., Ho, H. C., Burtin, P., Cachin, Y., Clifford, P., de Schryver, A., de-Thé, G., Diehl, V. & Klein, G. (1970) *J. Nat. Cancer Inst.* **44,** 225–231.
14. Klein, G. (1972) *Proc. Nat. Acad. Sci. USA* **69,** 1056–1064.
15. Lai, M. M. C. & Duesberg, P. H. (1972) *Nature* **235,** 383–386.
16. Gillespie, D., Marshall, S. & Gallo, R. C. (1972) *Nature New Biol.* **236,** 227–231.
17. Green, M. & Cartas, M. (1972) *Proc. Nat. Acad. Sci. USA* **69,** 791–794.
18. Gulati, S. C., Axel, R. & Spiegelman, S. (1972) *Proc. Nat. Acad. Sci. USA* **69,** 2020–2024.
19. Baxt, W., Hehlmann, R. & Spiegelman, S. (1972) *Nature,* in press.
20. Okazaki, W., Purchase, H. & Burmester, B. (1970) *Avian Dis.* **14,** 413–429.
21. Henle, G., Henle, W. & Diehl, V. (1967) *Proc. Nat. Acad. Sci. USA* **59,** 94–101.
22. Niederman, J. C., Evans, A. S., Subrahmanyan, L. & McCollum, R. W. (1970) *N. Engl. J. Med.* **282,** 361–365.

Proc. Nat. Acad. Sci. USA
Vol. 70, No. 1, p. 10, January 1973

Methadone Plasma Level: Sustained by a Reservoir of Drug in Tissue

(heroin/humans/opiate/maintenance treatment/addiction)

VINCENT P. DOLE AND MARY JEANNE KREEK

Rockefeller University, New York, N.Y. 10021

Contributed by Vincent P. Dole, October 24, 1972

ABSTRACT **Binding of methadone in body tissues limits the rise in plasma concentration and prolongs the pharmacological action in patients receiving a daily maintenance dose. An opiate with equal intrinsic activity but greater binding affinity would, therefore, be a better drug than methadone for maintenance treatment; it would be safer when taken in a single dose and longer in its duration of action when taken on a regular schedule.**

In maintenance treatment of narcotic addicts, methadone is administered as a single daily dose of constant magnitude (1). On this schedule the patients remain functionally normal (2), without symptoms of abstinence, during the 24-hr span between doses. If a single dose is omitted, they generally experience only minor discomfort (some nausea and grippe-like aching) during the subsequent 24-hr period without medication.

On the other hand, quantitative studies of the analgesic effect of methadone in acute experiments have shown that the duration of the drug effect is only about 6 hr, no greater than that of morphine (3). There is thus a significant difference between the periods of action of the drug on acute and chronic administration. Paradoxically, the effect of methadone persists longer in the patients who have become refractory to the narcotic action of the drug (the maintenance patients) than in subjects who have not received previous doses of methadone and, therefore, are more sensitive to it.

The explanation suggested by recent studies of maintenance patients in this laboratory is that methadone accumulates in tissue when given repeatedly. Bound methadone, equilibrated with drug circulating in plasma, sustains a pharmacologically effective plasma level for 24 hr or longer. Since a single dose is rapidly cleared from the plasma, this dose, in the absence of tissue stores, soon loses its effect. On the other hand, a daily dose of methadone, given to a maintenance patient, stabilizes him pharmacologically by maintaining a reservoir of drug in tissue; this reservoir, in turn, holds the plasma level within narrow limits. This buffering action makes short-term fluctuations in dosage unimportant. In any 24-hr period, the dose taken by a maintenance patient may be halved or doubled without significant effect, whereas a change of this magnitude if continued over several days would be felt by the patient.

The approximate capacity of the methadone reservoir and the rate of elimination of drug from the body can be estimated from data recently obtained by us (M. J. K., manuscript in preparation) and other investigators (4, 5). In our study, nine patients who had been maintained on methadone for 1–5 years prior to the study, and known to be reliable (urines consistently free of other drugs, steady employment, good reputations), were stabilized on a daily dose of 100 mg for a period of 8 weeks. At 2-week intervals, each patient spent a day in the clinic during which time blood samples were taken before ingestion of the daily dose of methadone, and at intervals of 2 and 6 hr afterwards. Urine samples were also taken for analysis of methadone and routine monitoring for drugs of abuse (none were found). Plasma methadone concentrations were determined by isotope dilution and gas–liquid chromatography (manuscript in preparation). The recovery of methadone added to plasma was 97.6 ± 7.5%, over a concentration range from 0.3 to 2.0 μg/ml.

Plasma concentrations before ingestion of the morning dose (i.e., 24 hr since the last dose) averaged 0.58 μg/ml. Analysis of variance showed no significant trend in these levels over the 8-week period of observation, and no consistent difference between the two values obtained from the samples taken 2 and 6 hr after the dose—the latter result presumably reflecting variations in the time that the plasma maximum occurred after ingestion. The average increment in plasma level (difference between the zero-time level and the greater of the two values after ingestion) was 0.33 μg/ml; thus, only about 1 mg (assumed plasma volumes of 3500 ml) of the 100 mg administered was recovered in circulating plasma.

The ratio between the maximal observed concentration of methadone in plasma and the level 18–22 hr later was 1.6. Therefore, the half-time of excretion has a magnitude of the order of 24 hr, and the average rate of clearance of drug from plasma is about 140 ml/min. These values are only preliminary estimates, but the magnitude of these parameters is not in doubt. A large reservoir outside of plasma must exist to account both for the limitation of plasma concentration to a low level after absorption of a large dose, and for maintenance of a relatively high plasma concentration 24 hr later.

The concept of a tissue reservoir as the determinant of plasma level suggests a direction in which to search for a better drug than methadone—one that is both safer if taken by a nontolerant subject and longer in duration of action when used for maintenance treatment. If an opiate could be found with intrinsic activity equal to that of methadone, but with a tissue-binding affinity ten times greater, it would be almost devoid of narcotic effect in a single oral dose, yet when it was given repeatedly this hypothetical drug would establish a tissue reservoir that could be maintained by doses spaced at intervals of 2 weeks.

1. Dole, V. P., Nyswander, M. E. & Kreek, M. J. (1966) "Narcotic blockade," *Arch. Intern. Med.* 118, 304–309.
2. Gordon, N. B. (1973) "The functional status of the methadone maintained person," in *Discrimination and the Addict*, eds., Simmons, L. R. & Gold, M. B. (Sage Publications, Beverly Hills, Calif.), in press.
3. Houde, R. W., Wallenstein, S. L. & Rogers, A. (1971) Reported to the Committee on Problems of Drug Dependence, Thirty third Annual Scientific Meeting, p. 199.
4. Inturrisi, C. E. & Verebely, K. (1972) "A gas-liquid chromatographic method for the quantitative determination of methadone in human plasma and urine," *J. Chromatogr.* 65, 361–369.
5. Sullivan, H. R. & Blake, D. A. (1972) "Quantitative determination of methadone concentrations in human blood, plasma and urine by gas chromatography," *Chem. Pathol. Pharmacol.* 3, 467–478.

Proc. Nat. Acad. Sci. USA
Vol. 70, No. 1, pp. 11–14, January 1973

In Situ Hybridization of RD114-Virus RNA with Human Metaphase Chromosomes

(density gradient centrifugation/karyotype/RNA-dependent DNA polymerase)

PETER M. PRICE*, KURT HIRSCHHORN*, NORMAN GABELMAN†, AND SAMUEL WAXMAN†

* Division of Human Genetics, Department of Pediatrics; and † Cancer Chemotherapy Laboratory, Department of Medicine, Mount Sinai School of Medicine of the City University of New York, N.Y. 10029

Communicated by Robert J. Huebner, October 17, 1972

ABSTRACT ***In situ* hybridization was used to detect regions of human metaphase chromosomes exhibiting complementarity with radioactively-labeled RNA isolated from RD114-virus. The region of homology, as identified by autoradiography, was confined to one D-group chromosome.**

In a previous paper (1), we reported the probable localization of hemoglobin genes on human chromosomes. Hemoglobin structural genes were tentatively identified by autoradiographic detection of molecular hybrids formed *in situ* between purified, radiolabeled hemoglobin message and the DNA of metaphase chromosomes.

The present communication reports the detection of regions of homology between the RNA extracted from RD114-virus (2), isolated from a serially cultured line of human rhabdomyosarcoma cells (3), and a group-D chromosome from a human lymphoid cell line cultured serially. Methods were as described (2, 3).

MATERIALS AND METHODS

Virus and Cells. RNA was isolated from virus released into the culture medium from RD114 cells (RD114-virus). The RD114 cell line (gift from Dr. Aaron Freeman) was grown in 75-cm² tissue culture flasks (Falcon Plastics) or in roller bottles (670-cm² surface area, Bellco) in complete medium [medium RPMI-1640 (GIBCO) supplemented with 10% fetal-calf serum, containing 4 mM glutamine and 50 μg of gentamycin per ml]. Cells were fed with fresh complete medium every fourth day and subcultured every eighth day.

Morphology and growth characteristics of RD114 cells appeared to be similar to those reported by McAllister *et al.* (3). The cells extruded virus into the culture medium that incorporated [³H]U, demonstrated RNA-directed DNA polymerase (reverse transcriptase) activity (4, 5), and had a buoyant density of about 1.16 g/ml in a 15–65% sucrose gradient (Fig. 1). These findings are similar to those reported by McAllister *et al.* (2).

Radioactive virus was prepared (6) in complete medium containing 20 μCi/ml of [³H]U (28 Ci/mmol). The purified, labeled virus was isolated from supernatant tissue-culture fluid clarified and pooled as follows: An equal volume of saturated ammonium sulfate was added and the precipitate was collected by centrifugation (30,000 × *g*, 5 min at 4°) and dissolved in 5 ml of NTE (100 mM NaCl–10 mM Tris·HCl–1 mM Na_2EDTA, pH 7.4). The dissolved ammonium sulfate precipitate was then layered over a discontinuous gradient containing 0.7 ml of 65% sucrose and 3 ml of 20% sucrose in NTE and centrifuged in a Spinco SW39 rotor for 2 hr at 32,000 rpm. The interphase was collected, diluted 10–20 times, and centrifuged (37,000 × *g*, 120 min at 4°). The pellet was then dissolved in 0.4 ml of NTE, layered onto a 5-ml 20–65% sucrose gradient, and spun in an SW39 rotor (37,500 rpm, 120 min at 4°). 0.3-ml Fractions were collected from the bottom of the tube. Each fraction was assayed for density, radioactivity, and RNA-directed DNA polymerase activity (3, 5, 6).

Isolation of RD114 [³H] RNA. Fractions of the sucrose gradient with a density between 1.13 and 1.19 and demonstrating incorporation of [³H]U and/or RNA-directed DNA polymerase activity (fractions 3–7, Fig. 1) were pooled and diluted with an equal volume of NTE. To this were added 2-mercaptoethanol (final concentration 0.01 M) and sodium dodecyl sulfate (final concentration 1%) with stirring (15 min at 4°). The labeled RNA was then extracted by stirring the virus solution with 0.5 volume of phenol–cresol for 30 min at 25°. The resulting emulsion was then centrifuged (18,000 × *g*, 20 min at 4°) and the aqueous phase was retained. The phenol layer was

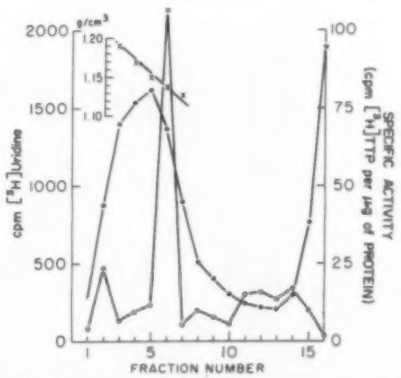

FIG. 1. Equilibrium sucrose density gradient centrifugation of [³H]U-labeled RD114 virus. Centrifugation was for 2 hr at 37,500 rpm and 4° in a Spinco SW39 rotor after the virus was layered over a 5-ml sucrose gradient (20–65%) in NTE buffer. A 0.01-ml aliquot of each fraction was assayed for radioactivity and a 0.1-ml aliquot of each fraction was assayed for RNA-directed DNA polymerase activity. Radioactivity, cpm of [³H]U, ●——●; RNA-dependent DNA polymerase, [³H]TTP incorporation/μg of protein, O——O; solution density, ×——×.

Abbreviation: SSC, 0.15 M NaCl–0.015 M Na-acetate.

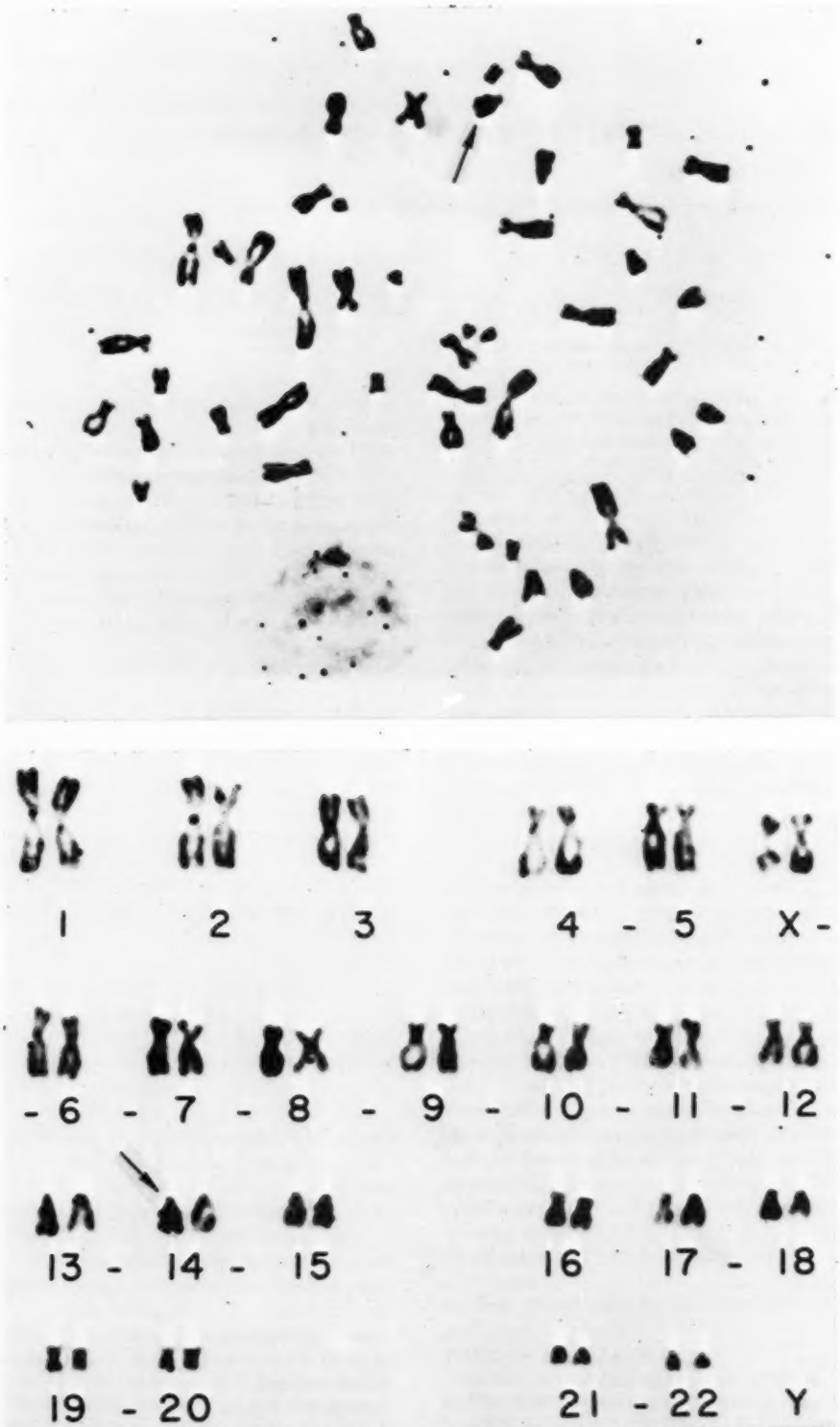

FIG. 2. Karyotype and chromosome spread showing significant label on both long arms of D-group chromosome (*arrow*). Silver grains on the labeled D chromosomes were so dense as to make accurate grain counts impossible. For this reason the statistical analysis is based on whether or not a millimeter segment of a chromosome has grains. *Dashes* between numbers under chromosomes indicate inability to distinguish individual chromosome groups on the basis of morphology alone.

then shaken with an equal volume of 0.1 M sodium acetate made pH 5.0 with acetic acid and recentrifuged. The aqueous phases were pooled and sodium acetate (final concentration 2%) and two volumes of ethanol were added. The precipitated RD114[^{3}H] RNA was collected by centrifugation (18,000 × *g*, 20 min at 4°), dissolved in 0.1 ml of 0.01 × SSC (SSC = 0.15 M NaCl–0.015 M sodium acetate, pH 7.4) ([^{3}H]RNA concentration, 1.4 μg/ml; specific activity, 695 cpm/μg), and frozen at −20°.

In Situ Hybridization. Human metaphase chromosomes were prepared from long-term lymphoid cultures (7) on glass slides, initially incubated for 10 min at 100°, and plunged immediately into ice-water. The slides were then dehydrated with 70, 90, and 100% ethanol. 0.05 ml of RD114-RNA solution previously adjusted to 2 × SSC with 10 × SSC was placed on each slide. A siliconized coverslip was placed on top of each slide and sealed to it with rubber cement. The slides were incukated, first at 100° for 10 min and then at 65° for 20 min, and plunged into ice–water immediately after each incubation. The coverslips were removed and the slides were washed three times with a solution containing 100 mM NaCl–1 mM EDTA. The slides were then incubated with RNase (Sigma, 1 μg/ml in NaCl–EDTA) boiled for 5 min to destroy DNase activity, in order to remove nonhybridized RNA, again washed three times with NaCl–EDTA, dehydrated with ethanol as before, and stained with 2% acetoorcein. Autoradiography was performed with AR10 stripping film and, after 6 days of incubation at 4°, the slides were developed and photographed.

RESULTS

Among over 1000 metaphase chromosomes sufficiently spread to allow the assignment of silver grains associated with the chromosomes, only eight (including one tetraploid) showed association greater than background. Statistical analysis of the grain distribution (Table 1) indicates that a D-group chromosome displays a region in its distal half (Figs. 2 and 3) that is significantly labeled ($P \leq 0.000027\%$). These data indicate that a D-group chromosome in apparently uninfected human lymphoid cells contains stretches of DNA that exhibit sequence homology with RNA isolated fron RD114-virus.

DISCUSSION

It is statistically highly likely that one of the D-group chromosomes of human lymphoid cells not known to be infected with RD114-virus contains informational sequences related to those involved in the production of RD114-virus. The presence of virus-related DNA sequences in cells not actively producing virus has been detected by other techniques (8–10).

FIG. 3. D chromosomes exhibiting radioactive label. Note continuity of grains.

This study has obvious relevance to the oncogene hypothesis (11) in that our findings indicate that a DNA replica of part or all of an oncogenic RNA virus genome appears to be resident in a highly restricted region of the hereditary material of human lymphoid cells. Our finding is in contrast to those reported for potentially oncogenic DNA viruses, such as

TABLE 1. *Significance of radioactive labeling of chromosomes**

Chromosome no.†	mm labeled‡	No. of times mm labeled§	P (%)¶
B	0–1	1	>99
	1–2	1	>99
	2–3	1	>99
	3–4	1	>99
	4–5	1	>99
	5–6	1	>99
	10–11	1	>99
	11–12	1	>99
	12–13	1	>99
	13–14	1	>99
D	0–1	1	>99
	1–2	1	>99
	2–3	2	13.4
	3–4	3	0.97
	4–5	6	0.000027
	5–6	7	0.00000044
	6–7	6	0.000027
	7–8	6	0.000027
		42	

* Karyotypes = 8 (with 1 tetraploid).

† All B chromosomes were adjusted to 15 mm. All D-group chromosomes were adjusted to 8 mm. Total length per karyotype (46 chromosomes) = 500 mm (all adjustments were based on average chromosome length in karyotypes). All measurements were made from the top of a chromosome; only millimeter segments that have label are considered in this table.

‡ Areas were considered labeled when grains were found in any two consecutive millimeter segments of the chromosome. Any noncontiguous label was considered to be background. The first millimeter segment from the distal end of the short arm of the chromosome was considered as segment 0–1.

§ Number of chromosomes in which this millimeter segment is labeled, according to the above consideration.

¶ The probability that label in a specific millimeter segment is random was computed from the following (*Documenta Geigy*. 7th Ed., p. 189, formula 805b): probability of labeling any millimeter segment of a chromosome of the 8 karyotypes = 1.0 (100%).

Probability of labeling any labeled millimeter segment =

$$\frac{d!}{(d-e)!e!}\,\frac{(a-d)!}{a!}\,\frac{b!}{(b-e)!}\,\frac{c!}{(c-d+e)!}$$

Where a = total millimeters remaining = 4500 − 1 = 4499; b = total millimeters remaining that are identical to one labeled = (18 − 1 = 17); c = total other millimeters remaining = 4482; d = *total remaining millimeters to label* = *42* − *1* = *41* (*42* = *total millimeters labeled*); e = frequency of labeling any millimeter segment homologous to a labeled millimeter segment (so that if a millimeter segment is labeled five times, e = 4). Only 4 or more "hits" in any particular millimeter segment are considered significant, because only then is P below the 0.01% level.

Adenovirus-12 (12, 13), in which hybridization of viral DNA was found to occur on multiple sites in the human karyotype.

We are fully aware that the localization demonstrated in our study does not yet prove the specificity of the site on the D chromosome exlcusively for RD114 RNA. If the specificity of this phenomenon is proven, these experiments are of potential significance in the understanding of the relationship of virus infection to human neoplasia and of the role of the human genome in the expression of malignant transformation.

We thank Stephanie Berman for excellent technical assistance and Dr. Ezra M. Greenspan for his encouragement and advice. This work was supported by grants from the Chemotherapy Foundation of New York, The Damon Runyon Fund (DRG 1117), the National Institutes of Health (HD 02552 and Genetic Center Grant GM 19443). P. M. P. is a USPHS pre-doctoral trainee (HD 00210), K. H. is a career scientist of the Health Research Council of New York City (I-513), and N. G. is an NIH post-doctoral fellow (FO2-CA-52230-01).

1. Price, P. M., Conover, J. H. & Hirschhorn, K. (1972) *Nature* **237**, 340–342.
2. McAllister, R. M., Nicholson, M., Gardner, M. B., Rongey, R. W., Rasheed, S., Sarma, P. G., Huebner, R. J., Hatanaka, M., Oroszlan, S., Gilden, R. V., Kabigting, A. & Vernon, L. (1972) *Nature New Biol.* **235**, 3–6.
3. McAllister, R. M., Nelson-Rees, W. A., Johnson, E. Y., Rongey, R. W. & Gardner, M. B. (1971) *J. Nat. Cancer Inst.* **47**, 603–607.
4. Temin, H. M. & Mizutani, S. (1970) *Nature* **226**, 1211–1213.
5. Spiegelman, S., Burny, A., Das, M. R., Keydar, J., Schlom, J., Travincek, M. & Watson, K. (1970) *Nature* **227**, 563–567.
6. Oroszlan, S., Fisher, C. L., Stanley, T. B. & Gilden, R. V. (1970) *J. Gen. Virol.* **8**, 1–10.
7. Broder, S. W., Glade, P. R. & Hirschhorn, K. (1970) *Blood* **35**, 539–542.
8. Green, M. (1972) *Proc. Nat. Acad. Sci. USA* **69**, 1036–1041.
9. Lowy, D. R., Rowe, W. P., Teich, N. & Hartley, J. W. (1971) *Science* **174**, 155–156.
10. Gilden, R. V. & Oroszlan, S. (1972) *Proc. Nat. Acad. Sci. USA* **69**, 1021–1025.
11. Todaro, G. J. & Huebner, R. J. (1972) *Proc. Nat. Acad. Sci. USA* **69**, 1009–1015.
12. Zur Hausen, H. (1967) *J. Virol.* **1**, 1174–1185.
13. McDougall, J. K., Dunn, A. R. & Jones, K. W. (1972) *Nature* **236**, 346–348.

Proc. Nat. Acad. Sci., USA
Vol. 70, No. 1, pp. 15–17, January 1973

Malignant Lymphomas of African Children

(lymphoblastic leukemia/Burkitt lymphoma/malaria/(Epstein–Barr virus/cancer survey)

ALICE STEWART*, J. N. P. DAVIES†, GILBERT DALLDORF‡, AND FRANCES E. BARNHART‡

* Department of Social Medicine, University of Oxford, Oxford, England; † Department of Pathology, Albany Medical College, Albany, New York 12208; and ‡ Oxford, Maryland 21654

Contributed by Gilbert Dalldorf, October 17, 1972

ABSTRACT **Clinical, pathologic, and epidemiologic observations of malignant tumors of children in sub-Sahara Africa suggest alternative theories of causation, and give insight into environmental influences that may play a large role in the etiology and form of malignant lymphatic tumors and cerebral neoplasms of infants.**

Malignant lymphomas account for nearly half of the cancers of young children, but there are striking geographic differences among the several types. In northern hemispheres the malignant lymphomas are commonly lymphoblastic leukemias, but in central, sub-Sahara Africa and in New Guinea they are almost always solid, multicentric tumors, the so-called Burkitt type of lymphoma. In Brazil, and probably in South Africa as well, the ratios are intermediate, and in both areas hybrid forms have been conspicuous. Indeed, the pattern of Burkitt tumor in North America is notably different from that in Africa as, for example, in the frequency of leukemia and of jaw tumors.

The Burkitt tumor has been intensively investigated (1) during the past dozen years, largely because its distribution in Africa resembles the geographic pattern of arbovirus infections; these studies led to the suggestion that the tumor might be caused by a mosquito-borne virus (2). A miscellany of agents have since been recovered from African tumors and one, a herpes virus, is still being exhaustively studied because of its intimate association with the tumor. Whatever the role of this virus may prove to be, it is now quite evident that it is just as intimately associated with various other diseases, which include infectious mononucleosis, cancers of the postnasal space, and Hodgkin's disease. The elevated antibody levels to the virus, which attracted much attention when they were first associated with the Burkitt tumor, are also present in these and other circumstances; elevated antibody levels are now thought to be an expression of impaired cellular immunity, rather than indicative of a casual relationship (3).

Furthermore, the Epstein–Barr (EB) virus is distributed worldwide and, therefore, offers no explanation of the uneven distribution of the Burkitt tumors. In addition there is little in the known natural history of EB virus infection to distinguish it from other herpes viruses, especially the cytomegalo viruses and virus III, which is a passenger of the Brown–Pearce tumor of rabbits. On the other hand, a herpes virus is believed to be the cause of a lymphatic malignancy in primates, and herpes viruses have been related to cancers of the cervix and uterus; continued exploration of the role of all these agents is surely in order.

An environmental factor that plays a significant role in determining the geographic pattern of the lymphomas is tropical malaria—holo- or hyper-endemic malaria. The association of malaria of this kind, in which repeated infections during the first year of life induce a severe and uninterrupted struggle with the parasite was originally recognized epidemiologically (4) and has been repeatedly confirmed. Initially, it was simply postulated that the pre-existing malaria transformed acute leukemia into a restricted, localized, subacute, or chronic disease. Both processes, the malaria and the leukemia, compete within the reticuloendothelial system; it was presumed that the leukemia cell is greatly disadvantaged by the malaria and survives and grows only in distant loci, such as the jaw bones and ovaries, the favorite sites of the African tumors. This view of pathogenesis also provided an explanation of the somewhat later peak-age incidence of the Burkitt tumor and its greater response to chemotherapy. The concept was further reinforced by the observation that myeloid leukemia at times behaves in a more chronic fashion in Africa than in European children, and that chloromatous deposits are more frequently seen in Africa than elsewhere (5).

If the Burkitt tumor bears such a relationship to acute, lymphoblastic leukemia, then the reciprocal ratios of the two are easily understood and the lessons of the Oxford survey, which revealed that childhood leukemia is initiated during gestation and that its prolonged latency is characterized by extreme susceptibility to various infections (6), may be pertinent to the Burkitt tumor as well. The first of these two observations, the origin during gestation, is critical to the proposition that the Burkitt lymphoma is caused by a postnatal virus infection, such as that associated with EB virus. The second observation is a reminder of deficiencies in the developing countries of adequate vital statistics. We cannot measure the mortality among the young that is due to holoendemic malaria, or measure the relationship between deaths during infancy that are caused by malaria and by leukemia.

We found no answers to these questions during a recent survey that spanned central Africa, but we did benefit from the firmly established and expertly directed cancer registries in Ibadan, Kampala, and Nairobi. Selected, combined notifications from these three registries are shown in Table 1 in parallel with the 1962–1965 notifications from England and Wales. Table 1 (which assumes the population at risk is unknown for the African series) recognizes two types of lymphatic neoplasm, two types of solid tumors, and three age

TABLE 1. *The relative frequency of different types of cancer in African and European children*

	Age at notification, years							
	0–4		5–9		10–14		All ages	
Diagnosis	*A*	*B*	*A*	*B*	*A*	*B*	*A*	*B*
Leukemia	23 (7)	671	37 (19)	375	38 (29)	258	98 (15)	1304
Lymphomas	131 (186)	137	493 (614)	156	288 (253)	221	912 (345)	514
Neural tumors	36 (10)	629	27 (13)	404	16 (10)	314	75 (11)	1347
Other cancers	302 (92)	640	142 (119)	231	185 (102)	352	629 (100)	1223
Leukemia + lymphomas	154 (37)	808	530 (194)	531	326 (132)	479	1010 (108)	1810
Neural and others	334 (51)	1269	169 (52)	635	201 (59)	666	704 (53)	2570
Total	488 (46)	2077	699 (117)	1166	527 (89)	1145	1714 (76)	4388

A, a consecutive series of cancer notifications from Ibadan, Kampala, and Nairobi Cancer Registries (1966–1969).

B, cancer notifications, England and Wales. The Registrar General's Cancer Supplement 1962–1965.

The Standardized Incidence Ratios are shown in parentheses. Standard equals 100.

groups. The numbers of leukemias, solid lymphomas, neural tumors, and other cancers are shown in the upper lines and immediately beneath (in parentheses) the incidence ratios when the 1852 solid tumors, other than neuroblastomas, are allowed to set the standard of comparison (i.e., when the A:B ratio for solid tumors other than neuroblastomas equals 100).

For all forms of cancer the A:B ratio was 76, and for the lymphatic neoplasms and solid tumors the ratios were 108 and 53, respectively. The slight excess (8%) of lymphatic tumors in Series A was accompanied by an 85% deficit of leukemia and a 89% deficit of neural tumors. For children under 5 years of age the corresponding figures were 93 and 90%, respectively, and for children over 10 years they were 71 and 90%, respectively.

These observations suggest that the central African environment, perhaps due to the repeated attacks of malaria during infancy that are characteristic of the regions in question, have several consequences for children who are incubating malignant diseases: (*i*) the malaria may make survival difficult, hence the relative deficit in the youngest age group, (*ii*) the masking effect of true incidence may be disproportionately large on cancers with short latent periods, such as leukemia and neuroblastoma, (*iii*) the acquisition of resistance to malaria among the survivors may determine the switch from leukemia to the multifocal form of lymphoma.

The problem of underreporting has long been recognized as a worrisome aspect of the leukemia problem in Africa; during our recent survey, special attention was given to the evidence regarding leukemia. It seems more and more certain that the acute forms of lymphoblastic leukemia are seldom seen among young children in the countries we visited. The deficiency of acute leukemias of all forms is most marked among the youngest age groups. Thus, Essien (7) provided convincing evidence in Ibadan—where interest is high and pediatric hematologic consultations are commonplace. Of the 91 cases of acute leukemia Doctor Essien had personally studied, 37 were younger than 15 years, but only 5 of these were below 10 years of age. Essien calculated the incidence of acute leukemia in Ibadan to be 0.35/100,000 per annum, but only 0.19/100,000 in children younger than 15 years (7). Equally thorough studies in Kampala (8) provided similar evidence.

Of special interest to us during the 1972 survey were clues in Kampala and Nairobi that acute lymphoblastic leukemia may now be emerging as a more common disease among young children than was true even a few years ago. The Kampala evidence is based on an intensive, 11-month search for instances of acute leukemia among clinic patients that revealed eight cases, of which three were lymphoblastic (9). The authors also reviewed recent hospital records; they concluded that underreporting had occurred. The possibility of increasing incidence due to environmental changes and the relationship of leukemia to the solid lymphatic tumors was not discussed.

In Nairobi, 13 cases of acute, lymphoblastic leukemia alone had been observed during the past 2 years, a striking increase over our experience in the same community 12 years before, when such illnesses were rarely seen in young children. Some of the evidence was found in the cancer registry, but others were brought to our attention by Dr. R. B. Barr, who had personally documented the nature of many of the illnesses.

The records of the Nairobi patients were searched for evidence of malarial infection, along with the records of an equal number of patients of similar ages who were currently being treated for Burkitt lymphomas in the same hospital. All but one of the Burkitt's lymphoma patients in whose records malaria was mentioned was infected, but evidence of malaria was completely lacking in those who were leukemic; nine of the leukemic patients had laboratory notations of the absence of plasmodia, or malarial pigment, or both. Unfortunately, the comparison of the two groups could not be extended to their geographic origins since the Burkitt patients had been drawn from all parts of Kenya to the Kenyatta National Hospital, which has long been a study center of such tumors, while the leukemia patients had largely lived in or near Nairobi.

Both Kampala and Nairobi are in the midst of striking social changes, and there was evidence in both places of increasing control of malaria. In Nairobi the use of malarial prophylactics has increased, and improvements in housing, sanitation, and nutrition are conspicuous. The situation in Kampala is believed to be similar, and the leukemias that occur there will hopefully be critically examined for evidence of malaria. Much more detailed evidence will be needed to determine whether tropical malaria alters the pattern of the malignant lymphomas of young children, and to explore the mechanisms that may be involved, but the experience of the past decade is testimony to the value of clinical epidemiologic studies of the natural history of malignant diseases.

Tumors resembling the African variety occasionally occur in many places where malaria is rarely or never seen. They are less frequent and often less distinct, but it is clear that other environmental influences than malaria need to be considered.

Research Corporation provided the funds that enabled us to visit and interview faculty in the medical schools in Ghana, Nigeria, Uganda, and Kenya. These colleagues generously shared their observations and assisted us with great patience and kindness.

1. Burkitt, D. P. & Wright, D. H. (1970) "Burkitt's Lymphoma" (Livingstone, Edinburgh and London).
2. Burkitt, D. P. & Davies, J. N. P. (1961) "The lymphoma syndrome in Uganda and tropical Africa," *Med. Press* **245**, 367–369.
3. Evans, A. S. (1971) "The spectrum of infections with Epstein–Barr virus: A hypothesis," *J. Infect. Dis.* **124**, 330–337.
4. Dalldorf, G., Linsell, C. A., Barnhart, F. E. & Martyn, R. (1964) "An epidemiological approach to the lymphomas of African children and Burkitt's sarcoma of the jaws," *Perspect. Biol. Med.* **7**, 435–449.
5. Davies, J. N. P. (1968) *Tumours of Childhood*, (eds. Marsden, H. B. & Stewart, J. K. Springer-Verlag, Heidelberg).
6. Stewart, A. & Kneale, G. W. (1970) "Age distribution of cancers caused by obstetric x-rays and their relevance to cancer latent periods," *Lancet* **1**, 4–8, and (1969) "The role of local infections in the recognition of hemopoetic neoplasms," *Nature* **223**, 741.
7. Essien, E. M. (1972) "The acute leukemias," *Afr. J. Med. Sci.*, in press.
8. Templeton, A. C. & Viegas, O. A. C. (1970) "Racial variations in tumour incidence in Uganda," *Trop. Geogr. Med.* **22**, 431–438.
9. Vanier, T. M. & Pike, M. C. (1967) "Leukemia incidence in tropical Africa," *Lancet* **1**, 512–513.

Proc. Nat. Acad. Sci. USA
Vol. 70, No. 1, pp. 18–21, January 1973

Translational Control of Specific Uterine Protein Synthesis After Estrogen Induction

(rat/gel electrophoresis/actinomycin D/17β-estradiol)

ANTHONY B. DEANGELO* AND GEORGE I. FUJIMOTO†

Department of Biochemistry, Albert Einstein College of Medicine, Bronx, New York 10461

Communicated by Alfred Gilman, October 17, 1972

ABSTRACT **The rate of leucine incorporation into a specific estrogen-induced protein of immature rat isolated by gel electrophoresis declines rapidly between 2–4 hr after estrogen stimulation *in vivo* followed by incubation *in vitro*. Actinomycin D present during the *in vitro* phase prevents this decline, and elicits a "superinduction" effect at 2 hr. Labeled induced protein remains stable during this time period, indicating that its decline is due to a reduction in synthesis capacity for the inducible protein, rather than to its degradation. A second injection of hormone at 3 hr has no effect on the reduced level of synthesis capacity for induced protein noted at 4 hr in the rat uterus.**

Specific protein synthesis has long been implicated in development of the estrogen response of the uterus (1). Recently, increased incorporation of labeled amino acids into a distinct, induced-protein (IP) band after estrogen treatment has been observed upon analysis of soluble uterine proteins by gel electrophoresis (2). IP synthesis, demonstrable by both *in vivo* and *in vitro* hormone stimulation (3, 4), begins after a lag period of 45–60 min (5). Since actinomycin D blocks this induction, IP synthesis is dependent upon RNA synthesis (6). The accumulation of IP-synthesizing capacity, which is a reflection of the amount of mRNA for IP, however, is independent of concurrent protein synthesis, since neither puromycin nor cycloheximide is effective in preventing this response; accumulation of synthesis capacity precedes IP synthesis by 30 min. No measurable lag period of accumulation of IP RNA after estrogen administration is observed. In the *in vivo* studies reported, both the rate and absolute amount of IP synthesis decline sharply by 4 hr after hormone injection, from a peak at 1–2 hr (2, 5, 6). This decline is in sharp contrast to the relative stability of IP RNA, for which a half-life of 3–4 hr has been measured (7).

In this paper, we present data that demonstrate both an inhibition of the temporal decline of IP synthesis and a "superinduction" effect during the time of maximum synthesis when surviving uteri from estrogen-stimulated rats are incubated with actinomycin D. That the decline of IP synthesis appears to be due to a reduction in IP-synthesizing capacity, rather than to a degradation of IP, is shown by the stability of synthesized IP throughout this time period. Furthermore, a second injection of hormone at 3 hr cannot reverse the lowered IP-synthesizing capacity previously noted at 4 hr.

Abbreviation: IP, induced protein.

* Present Address; Department of Biochemistry, Northwestern University School of Medicine, Chicago, Ill. 60611.
† Reprint requests may be sent to this author.

MATERIALS AND METHODS

Immature Sprague–Dawley rats between 21 and 25 days of age were purchased from Carworth Farms, Long Island City, N.Y. The experimental design of these studies was a modification of that reported (6). Experimental animals (3 per group) were injected intraperitoneally with 5 μg of 17β-estradiol in 0.15 M saline. Control animals (3 per group) received saline alone. After 1 hr, animals were decapitated and their uteri, with all adhering fat removed, were transferred to flasks containing 2 ml of Eagle's HeLa medium (Difco), with or without 10 μg/ml of actinomycin D. After incubation for 2, 3, or 4 hr, uteri were transferred to fresh medium containing 10 μg/ml of actinomycin D and radioactive leucine. Proteins were labeled with either 20 μCi of L-[^{3}H]leucine (*experimental;* 52 Ci/mmol, Schwarz) or 5 μCi of L-[^{14}C]leucine (*control;* 310 Ci/mol, Schwarz) for 2 hr. All incubations were at 37° under a 95% O_2–5% CO_2 atmosphere. At the termination of the incubation period, control and treated uteri were combined, rinsed with cold 0.05% Na_2ETDA, and homogenized in 0.8 ml of this solution. Homogenates were centrifuged for 30 min at 27,000 × *g* in a Sorvall refrigerated centrifuge, and the resulting supernatant fraction (uterine supernatant proteins) was frozen at −14° until use.

Proteins were separated by acrylamide gel electrophoresis (6). At the termination of an electrophoretic run, the gels were stained in 0.2% Coomassie blue. Destained gels were frozen over solid CO_2, sectioned into 2-mm slices, and prepared for scintillation counting. Each slice was placed into a mini-vial (Nuclear Associates), dried at 55° for 3 hr, and incubated in 0.4 ml of Protosol solution (New England Nuclear; Protosol–toluene–H_2O, 6:3.5:0.5). The vials were capped and incubation was continued for 5 hr; the vials then were kept at room temperature overnight. After 5 ml of toluene scintillant (0.5% PPO–0.03% POPOP) was added, samples were counted in a Packard Tri-Carb scintillation spectrometer. Counting efficiencies were 18% for ^{3}H and 50% for ^{14}C. Relative IP synthesis was calculated by averaging the percent increase in the ^{3}H/^{14}C ratio observed under the IP peak on the acrylamide gels.

In IP stability experiments, the rats were administered 17β-estradiol or saline at zero time and killed 45 min later. Excised uteri were placed into 2 ml of HeLa medium and incubated with [^{3}H]leucine (*experimental;* 40 μCi) or [^{14}C]-leucine (*control;* 10 μCi) for 75 min. The tissues were rinsed and transferred into a chase medium containing 8 mM unlabeled leucine, with or without 10 μg/ml of actinomycin D. Incubations were terminated after 210 or 300 min. The uteri were

processed and IP was measured. To determine the effectiveness of the chase, uteri (2 per point) were incubated with labeled leucine for 30, 60, 90, and 120 min. Isotope uptake was terminated with cold 10% trichloroacetic acid. Another group of uteri, after labeling for 60 min, was transferred into the chase medium and incubated (2 uteri per point) until 70, 90, or 120 min had elapsed. Total protein was extracted and its specific activity was measured (8).

RESULTS

Fig. 1 shows electrophoretic patterns of labeled, uterine supernatant proteins exposed for 2 or 3 hr to combined *in vivo–in vitro* estrogen stimulation. Inspection of both the tritium counts incorporated into the IP band and the corresponding ratio changes shows that IP synthesis at 3 hr declined from the 2-hr value. This IP decline, which has been consistently observed, becomes even more pronounced at 4 hr. The curves in Fig. 2 are obtained from electrophoretic profiles, examples of which are shown in Fig. 1. Each point is a measure of accumulated IP-RNA translation (IP-synthesizing capacity) during the isotope uptake period. In each case actinomycin D has been either present or absent during the *in vitro* incubation preceding isotope uptake. The control curve (minus inhibitor) shows maximal IP synthesis between 1 and 2 hr rapidly declining to one-third of this value by 4 hr. With inhibitor present during the incubation before uptake, decline of IP synthesis is effectively blocked. When the 2, 3, and 4 hr time points from each of the two curves are drawn on a semilogarithmic plot, the translational capacity (IP-RNA half-life) is seen to decline with a half-life of 1.5 hr when actinomycin D is excluded, while remaining more stable (half-life = 3.5 hr) with the inhibitor present. This 3.5-hr value is in close agreement to that reported earlier (7). It may further be noted from Fig. 2 that the relative amount of IP synthesized at 2 hr in the presence of the inhibitor is greater than the corresponding amount synthesized at 2 hr without inhibitor. Thus, we have a superinduction effect similar to that observed in other hormone systems (9, 10).

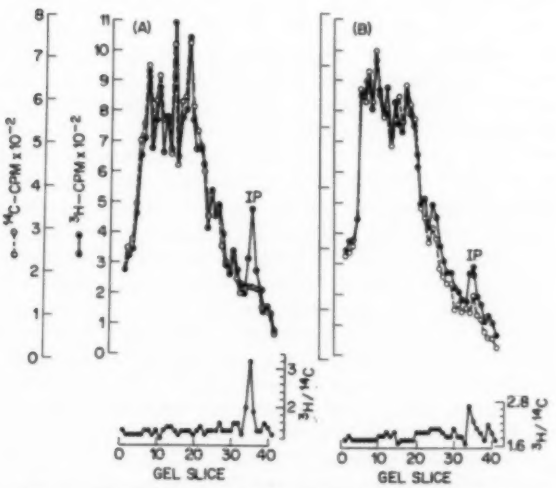

FIG. 1. IP synthesis after 2 hr (*A*) and 3 hr (*B*) of *in vivo–in vitro* estrogen stimulation. Immature rats (3 per group) were given 17β-estradiol (5 μg per rat) or saline and killed 1 hr later. The uteri were incubated in 2 ml of HeLa medium for either 1 or 2 additional hr. At the end of each incubation period, uteri were transferred to fresh medium containing 10 μg/ml of actinomycin D and either 20 μCi of [^{3}H]leucine (●——●) or 5 μCi of [^{14}C]-leucine (○- - -○). Isotope uptake was allowed for 2 hr, after which uteri were combined and homogenized. Soluble proteins were obtained and separated on 6% acrylamide gels, which were stained and sectioned. Radioactivity and ^{3}H/^{14}C ratios in each slice were measured.

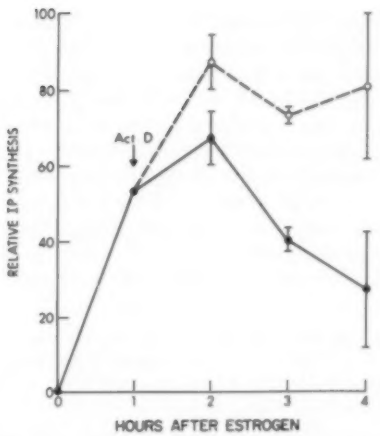

FIG. 2. IP synthesis after *in vivo–in vitro* estrogen stimulation. Relative IP synthesis was determined from experiments similar to those shown in Fig. 1. All groups of rats received 17β-estradiol at zero time, and were killed at 1 hr. The uteri were transferred into incubation media for time up to 2, 3, or 4 hr after hormone administration. The 1-hr groups were transferred directly into incubation medium containing labeled leucine. Actinomycin D (10 μg/ml) was either present (○- - -○) or absent (●——●) during the incubation periods before addition of isotope. At the end of each time period, all uteri were transferred to fresh medium containing the inhibitor and radioactive leucine (see Fig. 1 and *Methods* for details). Each time point is the average of three group determinations (±SEM).

Protein synthesis in both untreated and inhibitor-treated uteri after exposure to hormone for 2 and 3 hr remains similar when assessed by summation of the tritium counts incorporated into total protein subjected to electrophoresis. A tendency to a lower mean value is noted with increased inhibitor exposure, but is not statistically significant. These values, expressed as cpm $\times 10^{-2}$ per gel are: 2 hr, 16.5 ± 2.9; 3 hr, 15.1 ± 3.1; 2 hr + actinomycin D, 14.4 ± 3.7; 3 hr + actinomycin D, 12.9 ± 1.8. Only after exposure to hormone for 4 hr is there an increase in isotope incorporation into total protein on the gel (21.5 ± 1.8), or a decrease when inhibitor is present before isotope uptake (8.6 ± 1.1). Therefore, it is highly unlikely that the observed drop in IP-synthesizing capacity is due solely to a relative increase of total protein synthesis in the cytosol fraction.

While the preceding data agrees with the belief that IP-synthesizing capacity (IP-RNA translation) in a uterus declines sharply 2–4 hr after the initiation of estrogen action, the possibility that IP degradation is responsible for the decline during this time period is not excluded. In the experiments shown in Fig. 3, uterine proteins labeled during the first 2 hr of estrogen stimulation are chased in [^{1}H]leucine for 3.5 and 5 hr. Actinomycin D is either present during, or excluded from, the chase. If the synthesis or activation of any specific

proteolytic enzyme occurred, [^{3}H]IP content would decline as the chase progressed. Presumably, actinomycin D would prevent a decline only if the appearance of the enzyme required prior RNA synthesis. IP, however, persists throughout the chase period, which covers the time when IP-synthesizing capacity sharply declines. The greater amounts of IP remaining at 3.5 and 5 hr relative to that present at the end of the isotope incorporation period (2 hr) are not readily explained. These higher values (the increase is probably not significant) cannot be the result of continued ^{3}H uptake during the chase, since the concentration of unlabeled leucine is effective (Fig. 3, *insert*). Still, it is important to note that (*i*) previously synthesized IP remains stable over the 5-hr period after the initiation of estrogen action and (*ii*) no difference is observed between the two curves when the inhibitor is either present during or absent from the chase.

Finally, the effectiveness of an additional hormone injection at 3 hr in reversing the decline of IP-synthesizing capacity was tested. The experiment was done at two doses of hormone (0.5 or 5 μg per rat). Three groups of animals were injected at time zero. One group was killed at 2 hr and another at 4 hr. The third received an additional hormone injection 1 hr before death at 4 hr. Fig. 4 shows that the second hormone injection at 3 hr is ineffective in restoring 4-hr synthesis of IP to the 2-hr value. This result is obtained at either of the two doses used.

DISCUSSION

The accumulation of a specific RNA (IP-synthesizing capacity) detectable within minutes after estrogen administration is one of the earliest synthetic responses of uterine cells (6). Whether this induction occurs according to the Jacob–Monod scheme (11), or to a modified hypothesis proposed by Tomkins (9) for adrenal steroid induction of liver cell enzymes, is not clear. In the former scheme, control of IP-RNA synthesis would be placed at the transcriptional level, with IP-RNA accumulation resulting from an increase in its rate of synthesis. According to the latter hypothesis, the nuclear-bound hormone would inhibit the production of a repressor that inactivates IP RNA. The RNA for the repressor protein would have a shorter half-life than IP RNA. Experimental data accumulated thus far, and our results as well, support this second mechanism. More recent data are pertinent to these considerations. Actinomycin D given concomitantly with estrogen maintains IP synthesis at a basal level (6). The present study indicates that when the inhibitor is administered several hours after the hormone, both synthesis of the short-lived repressor message and IP RNA are blocked; because of the relative stability of the IP RNA, a superinduction effect occurs. Synthesis of IP continues at a higher rate than without actinomycin D present. Superinduction by actinomycin D would appear to be a general phenomenon, having been observed in such diverse systems as tyrosine aminotransferase induction by glucocorticoids (12), avidin induction by progesterone (10), somatotropic hormone induction of gulonolactone hydroxylase (13), retinal pigment cell modulation (14), and substrate-inducible microsomal aryl hydroxylase (15).

The rate of increase of IP-synthesizing capacity accumulated *in vitro* or *in vivo* falls off rapidly by 30 min after estrogen administration (7). A simple feedback mechanism by which newly synthesized IP would inhibit further accumulation during this step has been discounted, because IP synthesis does not begin until at least 45 min after the hormone is given. It may be that after estrogen treatment a lowered steady-state for IP-RNA repressor synthesis is reached, giving rise to the elevated IP-synthesizing capacity at 2 hr. Subsequent treatment with actinomycin D would result in the superinduction effect by further reducing the synthesis of the rapidly metabolized repressor message. Between 2 and 3 hr, in the absence of actinomycin D, repressor message steady-state would be

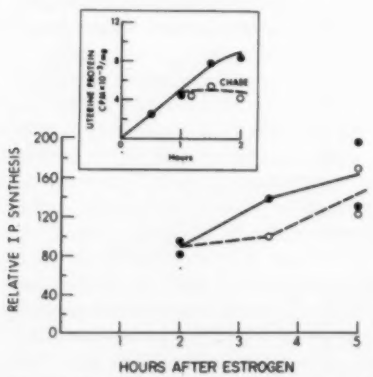

FIG. 3. IP stability. Immature rats (3 per group) were given 17β-estradiol (5 μg per rat) or saline and killed 45 min later. Excised uteri were labeled with 40 μCi of [^{3}H]leucine (treated) or 10 μCi of [^{14}C]leucine (control). After the isotope uptake period (75 min), the uteri were transferred into fresh medium containing 8 mM leucine with (O– – –O) or without (●——●) actinomycin D (10 μg/ml). The experiments were terminated 3.5 or 5 hr after hormone injection. Uteri were processed and IP was measured as outlined in Fig. 1 and *Methods*. Each point represents an individual determination. *Inset*, Specific activity of uterine proteins after the isotope uptake period (●——●) and after the chase (O– – –O) (see *Methods*). Each point is the average of two determinations.

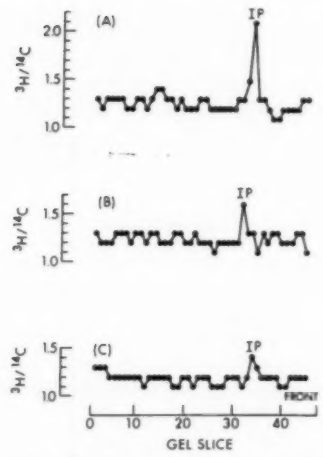

FIG. 4. Effect of a second 17β-estradiol treatment after 3 hr on IP synthesis at 4 hr. Three groups of rats were injected with 5 μg of 17β-estradiol per rat (controls received saline). One group each was killed at 2 hr (*A*) and at 4 hr (*B*) after treatment. The third received an additional injection (5 μg per rat) or 17β-estradiol 1 hr before death at 4 hr (*C*). Uterine protein labeling, tissue processing, and IP measurement were as outlined in Fig. 1 and *Methods*. ^{3}H/^{14}C ratios from one experiment are shown.

returned close to the preinduction level, resulting in increased repressor synthesis. Consequently, IP synthesis declines at 4 hr to about one-third of the value observed at 2 hr.

Some insight into the basis of the drop in IP-synthesizing capacity at 4 hr can be gained from the results in Fig. 4, in which an additional injection of hormone at 3 hr does not restore IP synthesis to the 2-hr value. The decrease in IP-synthesizing capacity has been consistently observed only in studies in which the hormone has been administered *in vivo* (2, 5, 6). It is not clear whether *in vitro* estrogen stimulation elicits accumulation of IP-synthesizing capacity that decreases with time (4). Estrogen is present during the entire incubation before the isotope-uptake period‡. Studies with tritiated estradiol, under either *in vivo* or *in vitro* conditions, appear to suggest a correlation between 17β-estradiol binding to nuclei and IP-synthesizing capacity. During incubation of surviving uteri with hormone, nuclear binding of 17β-estradiol reaches a peak at 1–2 hr, and remains at that level throughout an experiment (8–24 hr) (16, 17). After a single *in vivo* injection of the labeled hormone, radioactivity in the nuclear fraction falls off rapidly to a 4-hr level nearly half that at 2 hr. In addition, an understanding of the restoration of IP-synthesizing capacity should consider the state of the 8S cytoplasmic estrogen receptor during the decline. The estrogen-binding capacity of the cytoplasmic receptor decreases by only 50% after a single *in vivo* administration of 0.1 μg of 17β-estradiol (16). *In vitro* hormone stimulation of surviving whole uteri results in a 2-hr cytoplasmic binding capacity of only 20%, which remains at this low level for as long as 24 hr. However, the inability of a second estrogen exposure at 3 hr to restore IP-synthesizing capacity to the 2-hr induced value might indicate that this early accumulation of IP-synthesizing capacity is a time-specific cyclic response of uterine cells to the nuclear-bound hormone. IP-synthesizing capacity may be entering a refractory period to estrogen stimulation, such as observed for mitotic activity in mice (18), after a short interval. A second injection of estrogen failed to stimulate stromal cell division in the mouse uterus to any greater extent for a period up to 36 hr after the first treatment.

Decline of IP synthesis 3–4 hr after the initiation of estrogen action appears to be due to inhibition of the capacity to synthesize IP, rather than to degradation of protein molecules formed either before or during this time period. The lack of degradation is seen when IP labeled with radioactive leucine continues to be present, even when actinomycin D is excluded from the chase incubation. These data do not support a mechanism in which accumulation of a specific protein occurs due to inhibition of its breakdown (19).

Finally, we reiterate that these studies based on use of inhibitors constitute indirect evidence for the involvement of mRNAs and repressor proteins. Direct proof can be gained only by isolating and measuring the specific IP and its corresponding IP RNA. Recent isolation of messenger RNA regulated by a specific steroid (20) indicates that such proof may be secured.

‡ In one extensively studied system, the induced level of tyrosine amino-transferase in cultured rat hepatoma cells depended on the continuous presence of steroid inducer (12).

This work was supported by Contract no. 69-2216 with the National Institutes of Health.

1. Gorski, J., Noteboom, W. D. & Nicolette, J. (1965) *J. Cell. Comp. Physiol.* **66**, Suppl., 1, 91–110.
2. Notides, A. & Gorski, J. (1966) *Proc. Nat. Acad. Sci. USA* **56**, 230–235.
3. Mayol, R. F. & Thayer, S. A. (1970) *Biochemistry* **9**, 2484–2489.
4. Katzenellenbogen, B. S. & Gorski, J. (1972) *J. Biol. Chem.* **247**, 1299–1305.
5. Barnea, A. & Gorski, J. (1970) *Biochemistry* **9**, 1899–1904.
6. DeAngelo, A. B. & Gorski, J. (1970) *Proc. Nat. Acad. Sci. USA* **66**, 693–700.
7. Gorski, J., Katzenellenbogen, B. & DeAngelo, A. (1972) *4th Int. Congr. Endocrinol. Proc.*, Washington, D.C., 1972, (Exerpta Medica Fdn., Amsterdam), in press.
8. Noteboom, W. D. & Gorski, J. (1963) *Proc. Nat. Acad. Sci. USA* **50**, 250–255.
9. Tomkins, G. M., Gelehrter, T. D., Granner, D., Martin, D. Jr., Samuels, H. H. & Thompson, E. B. (1969) *Science* **166**, 1474–1480.
10. O'Malley, B. W. (1967) *Biochemistry* **6**, 2546–2551.
11. Jacob, F. & Monod, J. (1961) *J. Mol. Biol.* **3**, 318–356.
12. Tomkins, G. M., Thompson, E. B., Hayashi, S., Gelehrter, T. D., Granner, D. K. & Peterkofsky, B. (1966) *Cold Spring Harbor Symp. Quant. Biol.* **31**, 349–360.
13. Stubbs, D. W. & Haufrect, D. B. (1968) *Arch. Biochem. Biophys.* **124**, 365–371.
14. Whittaker, J. R. (1968) *J. Exp. Zool.* **169**, 143–159.
15. Nebert, D. W. & Gelboin, H. V. (1968) *J. Biol. Chem.* **243**, 6250–6261.
16. Sarff, M. & Gorski, J. (1971) *Biochemistry* **10**, 2557–2563.
17. Giannopoulos, G. & Gorski, J. (1971) *J. Biol. Chem.* **246**, 2524–2529.
18. Finn, C. A., Martin, L. & Carter, J. (1969) *J. Endocrinol.* **44**, 121–126.
19. Reel, J. R. & Kenney, F. T. (1968) *Proc. Nat. Acad. Sci. USA* **61**, 200–206.
20. Rosenfield, G., Comstock, J., Miller, D., Means, A. & O'Malley, B. (1972) 4th Int. Congr. *Endocrinol.*, Washington, D.C., 1972, Abstracts.

Proc. Nat. Acad. Sci. USA
Vol. 70, No. 1, pp. 22–26, January 1973

Inhibition of Reticulocyte Peptide-Chain Initiation by Pactamycin: Accumulation of Inactive Ribosomal Initiation Complexes

(methionyl-puromycin/methionyl-tRNA$_f$/initiation factors/Mg^{2+} concentration)

LIZZY S. KAPPEN, HIDEO SUZUKI, AND IRVING H. GOLDBERG

Department of Pharmacology, Harvard Medical School, Boston, Massachusetts 02115

Communicated by Paul C. Zamecnik, October 24, 1972

ABSTRACT **Pactamycin does not inhibit the overall initiation factor- and GTP-dependent binding of [^{35}S]Met-tRNA$_f$ to rabbit reticulocyte ribosomes but does prevent the formation of Met-puromycin, provided that the antibiotic is present during the course of the binding reaction. These data indicate that pactamycin blocks the synthesis of a functional peptide-chain initiation complex. Sucrose density gradient centrifugation analysis of binding reactions shows that pactamycin causes the accumulation of an initiation complex on the smaller ribosomal subunit (smaller initiation complex), to which the 60S ribosomal subunit either cannot join or with which it forms a larger inactive 80S initiation complex that falls apart under the conditions used for isolation. The smaller initiation complex formed in the presence of pactamycin differs from the normal intermediate in peptide-chain initiation in being much more resistant to degradation by pancreatic RNase. In the presence of pactamycin, the inactive smaller complex can also form on mRNA to which an unaffected ribosomal couple is already attached, forming an oligoribosome lacking a larger ribosomal subunit or a "1.5 mer." These effects of pactamycin can be overcome to a considerable degree by elevation of the Mg^{2+} concentration.**

Low concentrations of the antibiotic pactamycin selectively inhibit the initiation of polypeptide synthesis in intact cells and ribosome-containing extracts of eukaryotes (1–3). Thus, we have shown that pactamycin binds to the smaller subunit of rabbit reticulocyte ribosomes and blocks the formation of new polypeptide chains, while allowing the completion of globin chains already started on polyribosomes (1, 2). In reticulocyte lysates, pactamycin permits the orderly decay of polyribosomes to single ribosomes, while blocking the formation of new polyribosomal structures (2–4). Further, we have found that globin synthesis dependent on the addition of initiation factors to salt-washed ribosomes is sensitive to the antibiotic, whereas synthesis not requiring the starting of new polypeptide chains is resistant (5).

Although pactamycin, as an inhibitor of polypeptide chain initiation, has already proved to be a useful tool in determining the gene order of certain RNA viruses infecting animal cells (6–8), the precise mechanism by which the antibiotic interferes with initiation is not known. Several lines of evidence have suggested that the antibiotic produces an inactive initiation complex (2, 5, 9). In this paper we show that in the presence of pactamycin, the smaller initation complex (40S ribosomal subunit–mRNA–Met-tRNA$_f$) is formed at 2 mM Mg^{2+}, but it is unable to join with the 60S ribosomal subunit to form a functional, stable larger initiation complex. At higher Mg^{2+} concentrations, however, a functional larger initiation complex is formed despite the presence of pactamycin. The smaller initiation complex that accumulates with pactamycin at low Mg^{2+} concentrations is more resistant to pancreatic RNase than is the smaller initiation complex that is a normal intermediate in polypeptide chain initiation.

MATERIALS AND METHODS

Preparation of 0.5 M KCl-washed reticulocyte ribosomes and KCl wash (crude initiation factors) was as described by Gilbert and Anderson (10). Ribosomes were washed for only 10 min. The ribosomal salt-wash was treated with DEAE-cellulose, dialyzed, concentrated by the method of Gupta *et al.* (11), and stored in liquid nitrogen in small aliquots. Rabbit liver tRNA (General Biochemicals) was charged with [^{35}S]-methionine (160 Ci/mmol) (New England Nuclear) with *E. coli* synthetase, which acylates only the formylatable species (12).

Met-tRNA$_f$ Binding Assay and Met-Puromycin Synthesis. The endogenous mRNA-dependent binding of Met-tRNA$_f$ was measured by Millipore filtration, essentially as described by Crystal and Anderson (13). For Met-puromycin synthesis, 0.5 mM (neutralized) puromycin dihydrochloride was added after binding had taken place, and incubation was continued for the time indicated in the legends at 30°. The reaction was terminated by the addition of 1 ml of 0.1 M potassium phosphate buffer (pH 8.0), and Met-puromycin was extracted with 3 ml of ethylacetate; 2 ml of the extract was counted in Bray's solution (14).

Sucrose Density Gradient Centrifugation of Met-tRNA$_f$ Bound to Ribosomes Bearing Endogenous mRNA. The binding of Met-tRNA to ribosomes was analyzed on 15–30% linear sucrose gradients containing 100 mM KCl–2 mM $MgCl_2$–1 mM dithiothreitol–0.1 mM potassium cacodylate (pH 5.5) by the procedure of Crystal and Anderson (13), except that the Mg^{2+} concentration in the incubation mixture and in the gradient was 2 mM. After centrifugation in a Beckman SW41 rotor at 41,000 rpm at 2° for 3 hr, the tubes were pierced through the bottom and the samples were displaced from the top through a Beckman fraction recovery system. A Gilford spectrophotometer equipped with an 2-mm path flow cell from International Equipment was used to follow the absorbance of the fractions at 260 nm, except in Fig. 2 where each fraction was measured in a Zeiss spectrophotometer.

Pancreatic RNase (Worthington Biochemical Corp.) activity was assayed by measurement of the trichloroacetic acid-soluble nucleotides produced from [^{14}C]RNA (isolated from Erlich ascites tumor cells grown in the presence of [^{14}C]-

formate) after incubation at 37° for 10 min with 0.4 μg/ml of RNase.

RESULTS

The total binding of [^{35}S]Met-tRNA$_f$ to reticulocyte ribosomes bearing endogenous mRNA is not significantly affected by pactamycin or NaF, but is inhibited by aurintricarboxylic acid (Table 1). The synthesis of a functional initiation complex, as judged by its ability to form [^{35}S]Met-puromycin, however, is impaired by both pactamycin and NaF, provided that these agents are present during complex formation. If it is added after most of the active complex has been formed, pactamycin is not able to interfere significantly with the puromycin reaction (Table 1 and Fig. 1). These results are in agreement with those found with wheat-embryo ribosomes and tobacco mosaic virus RNA as messenger (9).

The formation of an active 80S initiation complex proceeds via a 40S ribosomal subunit–mRNA-Met-tRNA$_f$ intermediate to which a 60S ribosomal subunit joins (15, 16). The overall process requires initiation factors and GTP. The analysis of binding reactions similar to those described in Table 1 by sucrose density gradient centrifugation shows that formation of the puromycin-reactive 80S initiation complex (Fig. 2*A*, and *D*) is prevented by pactamycin (Fig. 2*B* and *E*), and that this activity of the drug is associated with a pronounced increase in the amount of [^{35}S]Met-tRNA$_f$ bound to the smaller initiation complex, which sediments slightly further down the gradient (about 50S) than the 40S ribosomal subunit. On the other hand, if the addition of pactamycin is delayed until after most of the active 80S complex has been formed, there is only a slight inhibition of [^{35}S]Met-puromycin formation (Fig. 2*C* and *F*). It should be noted, however, that the small amount

TABLE 1. *Effect of pactamycin and other agents on Met-tRNA$_f$ binding to reticulocyte ribosomes and on Met-puromycin formation*

Inhibitor	[^{35}S]Met-tRNA$_f$ binding	Met-puromycin formation
	cpm bound (% inhibition)	Met-puromycin, cpm (% inhibition)
None	7823 (—)	3433 (—)
Pactamycin (1 μM)	— —	766 (78)
Pactamycin (1 μM) at 7 min	— —	2952 (14)
Pactamycin (2 μM)	7791 (0)	665 (81)
Pactamycin (2 μM) at 7 min	— —	2495 (27)
Pactamycin (10 μM)	7190 (8)	267 (92)
NaF (10 mM)	5602 (28)	852 (75)
ATA (0.2 mM)	2347 (70)	— —

Binding incubations (7 min, 23°) in a total volume of 0.1 ml contained 20 mM Tris·HCl (pH 7.5), 1 mM dithiothreitol, 0.5 mM GTP, 100 mM KCl, 2 mM $MgCl_2$, 2.2A_{260} units of 0.5 M KCl-washed ribosomes, 0.17 A_{260} units of [^{35}S]Met-tRNA (46,000 cpm), and 278 μg of ribosomal wash protein. For Met-puromycin synthesis, 0.5 mM puromycin was added to the binding incubation at 7 min, and incubation was continued for 10 min at 30°. Pactamycin, NaF, and aurintricarboxylic acid (*ATA*) were present from the start of the reaction unless otherwise indicated.

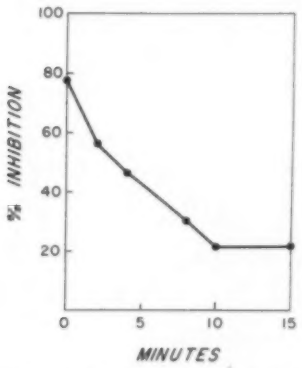

FIG. 1. Inhibition of Met-puromycin synthesis by pactamycin added at different times. Binding incubations (15 min, 30°) similar to those described in the legend for Table 1 contained 2.4 A_{260} units of ribosomes, 600 μg of ribosomal wash protein, and 0.156 A_{260} units of [^{35}S]Met-tRNA (70,000 cpm). Pactamycin (1 μM) was added at the indicated times. At 15 min, 0.5 mM puromycin was added to all the tubes and incubation was continued for 8 min. In the absence of pactamycin, 3418 cpm was incorporated into Met-puromycin.

of [^{35}S]Met-tRNA$_f$ bound to the 80S initiation complex in the presence of pactamycin (Fig. 2*B*) is poorly releasable by puromycin (Fig. 2*E*). Pactamycin does not in itself cause the 80S complex to dissociate, since the pattern of binding found in Fig. 2*C* is identical to that in a reaction lacking pactamycin (not shown) that was stopped at the time the antibiotic was added in Fig. 2*C*.

Although in the control incubation a small peak of [^{35}S]Met-tRNA$_f$ is found in an area on the gradient corresponding to the dimer region (Fig. 2*A*), in the presence of pactamycin the predominant fast-moving radioactive peak is neither in the monomer or the dimer region, but is between the two regions (about 95 S) (Fig. 2*B*). While the amount of this particle varies in different experiments for unexplained reasons, its location 3–4 fractions earlier on the gradient than the dimer region is highly reproducible. This material is not produced when pactamycin is added late in the binding reaction (Fig. 2*C*). Its position on the sucrose gradient suggests that it represents a hybrid ("1.5 mer") between a monosome (ribosome couple on a strand of mRNA) and a pactamycin-inactivated 40S ribosomal subunit bearing [^{35}S]Met-tRNA$_f$ located on the initiation site of the mRNA. Such ribosomal structures have been found under various conditions (15, 17), especially in the presence of NaF (17). Additional support for the notion that pactamycin produces initiation-inactivated 1.5 mers to which the 60S ribosomal subunit fails to join comes from experiments with puromycin or pancreatic RNase. The addition of puromycin to the reaction after binding results in the disappearance of radioactivity (about 2500 cpm) from the putative 1.5 mer region of the gradient, and a comcomittant increase (about 2500 cpm) in the amount of radioactivity found in the smaller initiation complex (Fig. 2*E*). This result is the expected one, since puromycin should lead to the release of the uninvolved ribosomal couple from the mRNA, while the inactivated ribosomal subunit with its [^{35}S]Met-tRNA$_f$ remains attached. By contrast, [^{35}S]methionine associated with ribosome monomers and dimers is released to the top

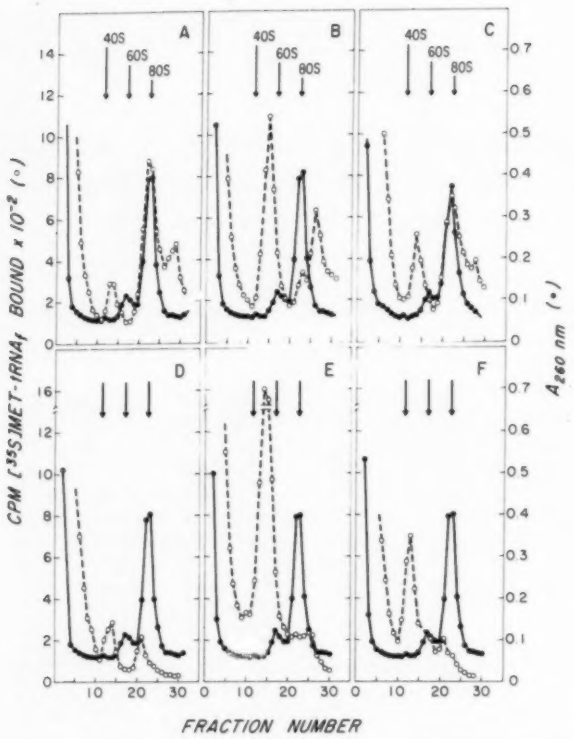

FIG. 2. Sucrose gradient centrifugation of [^{35}S]Met-tRNA$_f$ bound to washed reticulocyte ribosomes, and the effect of pactamycin. Reaction mixtures (0.1 ml) containing 20 mM Tris·HCl (pH 7.5), 1 mM dithiothreitol, 1 mM GTP, 100 mM KCl, 2 mM $MgCl_2$, 2.9 A_{260} units of ribosomes, 400 μg of ribosomal wash protein, and 0.39 A_{260} units of [^{35}S]Met-tRNA (61,400 cpm) were incubated for 14 min at 30° in the presence or absence of pactamycin (1 μM), and layered onto sucrose gradients. After centrifugation, the gradients were fractionated; the fractions were diluted to 1 ml with the gradient buffer before absorbance at 260 nm was measured in a Zeiss spectrophotometer. Centrifugation was from *left* to *right*. (*A*) Control without pactamycin. (*B*) Pactamycin present from the beginning. (*C*) Pactamycin added at 7 min. (*D*, *E*, and *F*) 0.5 mM puromycin was added at 7 min to incubations identical to *A*, *B*, *C*, respectively.

of the gradient as [^{35}S]Met-puromycin (Fig. 2*D* and *F*). Furthermore, RNase treatment of binding reactions results in disappearance of the putative radioactive 1.5 mer, with little change or a small increase in the radioactivity associated with the 80S complex (Fig. 3). Because there is a large amount of radioactivity in the region of the smaller initiation complex in incubations containing pactamycin, compared with the small peak of the putative 1.5 mer, it has not been possible to consistently account for the counts lost in the putative 1.5 mer region as appearing in the smaller complex region. Therefore, several attempts have been made to isolate the putative 1.5 mer by centrifugation, and to treat it with RNase before further centrifugation on a sucrose gradient. Although we have been able to demonstrate the unequivocal formation of radioactive smaller initiation complexes by this procedure, the recoveries have been repeatedly low, on the order of 20–30%. On the other hand, treatment of labeled 80S complexes with RNase does not decrease their radioactivity, and no labeled smaller initiation complexes are produced.

We have obtained evidence that pactamycin alters the structure of the smaller initiation complex. Such structures are considerably more resistant to degradation by pancreatic RNase than are similarly sedimenting particles that form at early times in the absence of pactamycin (Fig. 3*B* and *D*). This protective action of pactamycin is not due to inhibition of RNase itself, as shown in experiments with [^{14}C]RNA derived from ascites tumor cells.

The sensitivity of Met-puromycin formation to pactamycin depends on the concentration of Mg^{2+} (Fig. 4). When the binding reaction takes place at higher Mg^{2+} concentrations, the pactamycin effect is considerably decreased. Sucrose gradients (Fig. 5) confirm that formation of the functional 80S initiation complex at 5 mM Mg^{2+} is inhibited to the same small extent as is the synthesis of Met-puromycin. If the Mg^{2+} concentration is increased to 5 mM after binding in the presence of pactamycin is over, there is a partial reversal of inhibition of the puromycin reaction and formation of the 80S initiation complex.

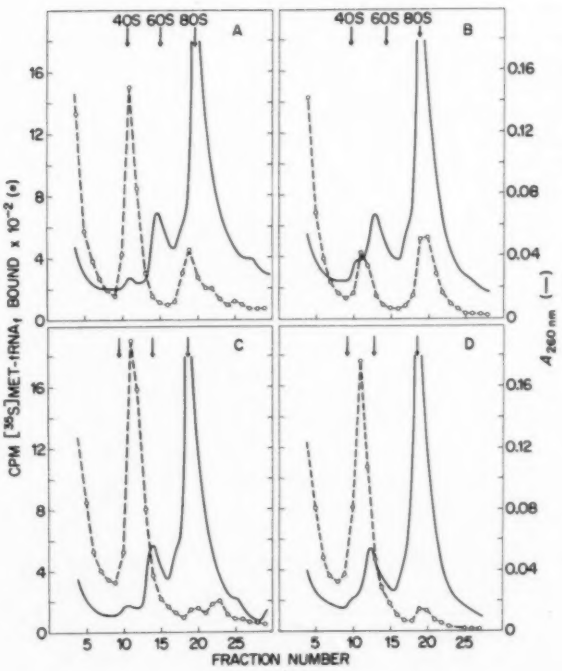

FIG. 3. Effect of RNase treatment on [^{35}S]Met-tRNA$_f$ bound at 4 min to reticulocyte ribosomes. Incubation mixture, in a total volume of 0.1 ml, contained 2.5 A_{260} units of ribosomes, 600 μg of ribosomal wash protein, and 0.29 A_{260} units of [^{35}S]Met-tRNA (63,000 cpm). Other conditions are similar to those in Fig. 2. The tubes were incubated for 4 min at 30° and chilled to 0°; RNase (1 μg/ml) was added as indicated. After standing at 0° for 15 min, the mixture (90 μl) was layered on the sucrose gradient. (*A*) Control. (*B*) Control after treatment with RNase. (*C*) Binding in the presence of pactamycin (2 μM) from the start of the incubation. (*D*) *C* after RNase treatment.

DISCUSSION

These experiments provide additional support for the concept that pactamycin produces a nonfunctional initiation complex with reticulocyte ribosomes bearing endogenous mRNA (2, 5). A similar conclusion has been reached from experiments with wheat embryo ribosomes and tobacco mosaic virus RNA as messenger (9). Our results on sucrose density gradients, however, differ from those reported by Seal and Marcus (9) and Weeks and Baxter (17) with wheat embryo ribosomes and viral mRNA. These workers report that pactamycin does not lead to the accumulation of the smaller ribosomal initiation complex. In the only sucrose gradient data actually presented from the wheat embryo system, the Mg^{2+} concentration in the binding reaction was relatively high, 3.6 mM (17). It is not clear, however, whether the difference in results is due to differences in reaction conditions, or to basic differences between reticulocyte and wheat embryo ribosomes, mRNA, or initiation factors. The data from Fig. 2*B* and *E* are compatible with the formation of an inactive 80S complex in the presence of pactamycin in the reticulocyte system but, in contrast to the results in the wheat embryo system, the altered larger initiation complex readily dissociates into its subunit components.

It is clear that pactamycin, which binds only to the smaller ribosomal subunit (1), alters the structure of the smaller initiation complex in such a way that it is resistant to the action of pancreatic RNase. Whether antibiotic bound to the 40S ribosomal subunit induces a structural change in the complex that affords greater protection to the attached mRNA or tRNA is not known. Furthermore, it is of interest that the smaller initiation complex, which is a normal intermediate in peptide-chain initiation, is sensitive to mild RNase treatment, whereas the larger initiation complex, like the pactamycin-modified smaller initiation complex, is resistant (Fig. 3). This finding raises the possibility that the protective phenomena due to the attachment of the 60S ribosomal subunit or to the binding of the antibiotic have a common structural basis, an induced change in the conformation of the smaller initiation complex.

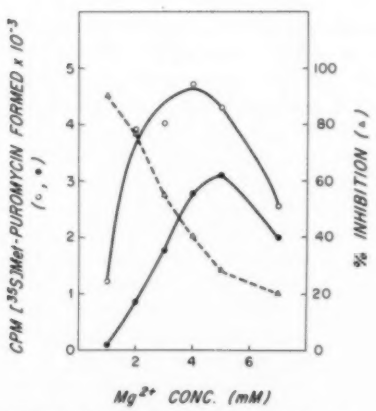

FIG. 4. Effect of magnesium concentration on pactamycin inhibition of Met-puromycin synthesis. The reaction conditions are similar to those described in the legend for Fig. 1, except that the concentration of the initiation factors was 400 μg and puromycin (0.5 mM) and pactamycin (1 μM) were present from the start of the reaction. ○, Control; ●, with pactamycin; △, % inhibition by pactamycin.

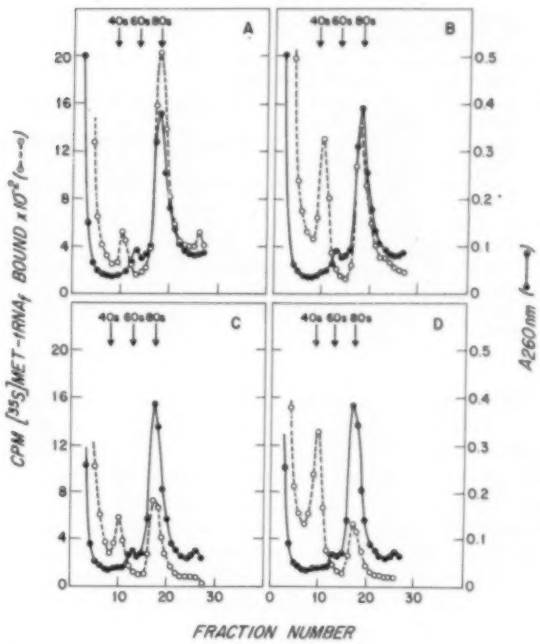

FIG. 5. Effect of pactamycin on puromycin-sensitive initiation complex formation at 5 mM magnesium. Incubation conditions and centrifugation analysis were the same as in Fig. 2, except that 0.29 A_{260} units of [^{35}S]Met-tRNA (63,000 cpm) was used. (*A*) Control. (*B*) Pactamycin (1 μM). (*C*) Puromycin (0.5 mM) added to control at 7 min. (*D*) Puromycin (0.5 mM) added to *B* at 7 min.

The lack of puromycin-reactivity of ribosome-bound Met-tRNA$_f$ found at 2 mM Mg^{2+} in the presence of pactamycin in the system used in this paper can be accounted for by the accumulation of smaller initiation complexes (either free or as oligoribosomes). What, if any, relation these phenomena have to the inhibition of peptide chain initiation found in more complex systems such as reticulocytes and their lysates remains to be elucidated. The specificity of pactamycin for initiation may rest rather on the fact that the antibiotic binds to free 40S ribosomal subunits or run-off ribosomes, but not to ribosomes (in polysomes) already engaged in chain elongation (1). In this way the step in the protein synthesis sequence blocked by pactamycin need not be one peculiar to initiation but may be one involved in elongation, such as translocation or acceptor site binding. Thus, only the last ribosome to join a polysome structure would be unable to move down the mRNA. Such an effect would be viewed grossly (as measured by polysome degradation and globin chain completion) as one on "initiation," even though it is actually "elongation" that is being affected. We are studying the effect of pactamycin on the formation of the initial di- and tripeptides of globin in an effort to settle these points.

This work was supported by grants GM 12573 and Ca 10736 from the National Institutes of Health, United States Public Health Service.

1. Macdonald, J. S. & Goldberg, I. H. (1970) *Biochem. Biophys. Res. Commun.* **41**, 1–8.
2. Stewart-Blair, M. L., Yanowitz, I. S. & Goldberg, I. H. (1971) *Biochemistry* **10**, 4198–4206.
3. Lodish, H. F., Housman, D. & Jacobsen, M. (1971) *Biochemistry* **10**, 2348–2356.
4. Colombo, B., Felicetti, L. & Baglioni, C. (1966) *Biochim. Biophys. Acta* **119**, 109–119.
5. Goldberg, I. H., Stewart, M. L., Ayuso, M. & Kappen, L. S. (1972) *Fed. Proc.*, in press.
6. Summers, D. F. & Maizel, J. V. (1971) *Proc. Nat. Acad. Sci. USA* **68**, 2852–2856.
7. Taber, R., Rekosh, D. & Baltimore, D. (1971) *J. Virol.* **8**, 395–401.
8. Butterworth, B. E. & Rueckert, R. R. (1972) *Fed. Proc.* **31**, 407.
9. Seal, S. N. & Marcus, A. (1972) *Biochem. Biophys. Res. Commun.* **46**, 1895–1902.
10. Gilbert, J. M. & Anderson, W. F. (1970) *J. Biol. Chem.* **245**, 2342–2349.
11. Gupta, N. K., Chatterjee, N. K., Woodley, C. L. & Bose, K. K. (1971) *J. Biol. Chem.* **246**, 7460–7469.
12. Gupta, N. K., Chatterjee, N. K., Bose, K. K., Bhaduri, S. & Chung, A. (1970) *J. Mol. Biol.* **54**, 145–154.
13. Crystal, R. G. & Anderson, W. F. (1972) *Proc. Nat. Acad. Sci. USA* **69**, 706–711.
14. Bray, G. A. (1960) *Anal. Biochem.* **1**, 279–285.
15. Crystal, R. G., Shafritz, D. A., Prichard, P. M. & Anderson, W. F. (1971) *Proc. Nat. Acad. Sci. USA* **68**, 1810–1814.
16. Weeks, D. P., Verma, D. P. S., Seal, S. N. & Marcus, A. (1972) *Nature* **236**, 167–168.
17. Weeks, D. P. & Baxter, R. (1972) *Biochemistry* **11**, 3060–3064.

Proc. Nat. Acad. Sci. USA
Vol. 70, No. 1, pp. 27–30, January 1973

Human Lymphotoxin: Purification and Some Properties

(phytohemagglutinin/human lymphocytes)

G. A. GRANGER*, E. C. LASERNA, W. P. KOLB†, AND F. CHAPMAN

*Department of Molecular Biology and Biochemistry, University of California, Irvine, Calif. 92664; and †Scripps Clinic and Research Foundation, La Jolla, Calif. 92037

Communicated by R. W. Gerard, September 25, 1972

ABSTRACT **Lymphotoxin is secreted by human lymphocytes stimulated with phytohemagglutinin *in vitro*. Combinations of DEAE-cellulose and Sephadex chromatography, acrylamide gel electrophoresis, and isoelectric focusing were used to purify lymphotoxin 2000- to 4000-fold; 15–25% of the activity has been recovered. Lymphotoxin appears to be a weakly charged molecule(s) of molecular weight about 90,000–100,000 that migrates in Pevikon block electrophoresis as a β- or α_2 globulin. It is a discrete molecule(s), because it is completely separable from medium serum proteins and carrier and phytohemagglutinin proteins. Isoelectric-focusing studies indicate that there may be a limited heterogeneity among lymphotoxin molecules.**

Lymphoid cells are central effectors in such important immunologic reactions as graft rejection (1), tumor immunity (2), and delayed hypersensitivity (3). All of these reactions appear to share at least two common steps: (*a*) a recognition step, which requires the interaction of the foreign tissue or graft cell with hypothetical lymphocyte-membrane receptor sites (4, 5) and (*b*) an effector step, which involves active cellular metabolism and biosynthesis (5). These events lead, by some unknown mechanism, to the destruction of the foreign cell.

Lymphoid cells from experimental animals and man can be activated *in vitro* specifically with antigens (6), or nonspecifically with mitogens, e.g. phytohemagglutinin (PHA) (7), to release various soluble molecules into the cell culture medium. These soluble molecules have been proposed to be effector substances associated with cellular immunity (6, 7). The treatments and agents that trigger the release of these factors are very broad and unrelated, yet they all induce similar changes in lymphocytes, namely, activation of RNA and protein synthesis and morphologic changes associated with transformation (8). One of these factors is a cell toxin termed lymphotoxin (LT). A few of the physical properties of a cell toxin released by normal human lymphocytes stimulated with PHA *in vitro* were reported (9). The toxin appeared to be a protein of molecular weight about 80,000 (9). This is a brief description of the methods for purification and some physical properties of LT released by human lymphocytes stimulated with PHA *in vitro*.

MATERIALS AND METHODS

Production of Human Lymphotoxin and Control Media. The details of these methods have been published (10). Cells were maintained in medium RPMI 1640 (from GIBCO), containing 0.1% bovine-serum albumin, at a density of 5×10^5 cells per ml, in 32-oz prescription bottles, 200 ml per bottle, then 20 μg of PHA-P (Difco, Detroit, Mich., Lot no. 561822) per ml was added. After 5 days, the medium was collected, pooled, then cleared of cells and debris by centrifugation. Controls consisted of either lymphocytes cultured under identical conditions without the addition of PHA, or heat-killed lymphocytes (56° for 30 min) with 20 μg of PHA added at the time the cultures were established. After collection, the medium was concentrated twentyfold by ultrafiltration.

DEAE-Cellulose Column Chromatography. Previously washed Whatman DE-11 resin was poured into a 3.4×60-cm column and pressure packed (10 lb/in^2) to a bed height of 30 cm. The columns were equilibrated with 10 mM Tris·HCl, (pH 8.0)–25 mM NaCl–0.1 mM EDTA buffer (low salt buffer). 100 ml (2 grams of protein) of concentrated toxic or control medium, previously dialyzed against low salt buffer and clarified by centrifugation, was applied to the column. Proteins were eluted from the column in a linear salt gradient from 25 mM to 350 mM NaCl in 10 mM Tris·HCl (pH 8.0)–0.1 mM EDTA buffer. 12-ml Fractions were collected, and the conductivity and absorbance at 280 nm of every fraction was measured.

Sephadex Chromatography. A 2.5×120-cm siliclad-coated column (Chromatronix, Berkeley, Calif.) was packed with Sephadex G-100 or G-150 to a bed height of 100 cm. Each column was pretested with molecular weight markers (blue dextran; molecular weight 2×10^6), human IgG (150,000), bovine-serum albumin (67,000), and hemoglobin (68,000). Cytotoxic and control fractions from DEAE-cellulose columns were then pooled, lyophilized, solubilized in 5 ml of sterile distilled water, applied to the column, and eluted with 10 mM Tris·HCl (pH 8.0)–150 mM NaCl–0.1 mM EDTA buffer. 200-Drop (3.2-ml) fractions were collected, and their absorbance was monitored at 280 nm.

Density Gradient Centrifugation. Linear sucrose gradients (10–30%) were prepared in 5-ml cellulose nitrate tubes (11). Fractions from DEAE-cellulose columns (0.4 mg of protein) and 0.8 mg of bovine-serum albumin marker were layered on separate gradients and centrifuged at 35,000 rpm in a Beckman L3-40 ultracentrifuge for 45 hr. Absorbance at 280 nm of each of the 0.9-ml fractions was determined. The sucrose was removed by dialysis of the fractions against 4 liters of 10 mM Tris·HCl (pH 7.0)–150 mM NaCl–0.1 mM EDTA (physiologic dialysis buffer).

Abbreviations: LT, lymphotoxin; PHA, phytohemagglutinin.

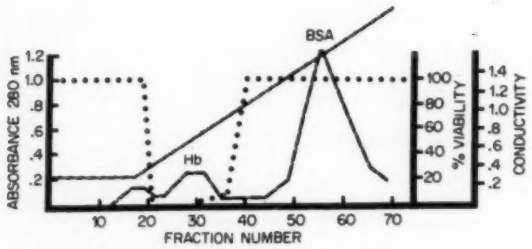

FIG. 1. Elution of LT from DEAE-cellulose with a linear NaCl gradient. Concentrated LT medium containing hemoglobin (Hb) and bovine-serum albumin (BSA) carriers was eluted from DEAE-cellulose columns as described in *text*. The *dotted line* indicates the toxic activity of each fraction, the *double slashed line* represents the conductivity of each fraction, and the *single slashed line* is absorbance at 280 nm.

Pevikon Block Electrophoresis. Zone electrophoresis was performed as described by Müller–Eberhard and Osterlund (12). 60 mg or 3 ml of 20-times concentrated crude LT or control medium was loaded 5 inches from the cathode on a 5 × 17 × ½-inch Pevikon block. Electrophoresis was performed at 4° in barbitol buffer (pH 8.6) for about 20 hr at 400 V and 60 mA until the bromphenol blue marker had migrated 15 inches from the origin. The block was then cut into 0.5-inch strips, and the sample was eluted with 0.15 M NaCl solution. The absorbance of each fraction was measured at 280 nm and, in addition, the amount of protein in each fraction was determined by the Folin–Lowry method (13). Fractions containing each peak were dialyzed against low salt buffer, pooled, lyophilized, and reconstituted in distilled water. Then, each sample was subjected to immunoelectrophoresis (14).

Preparative Polyacrylamide Disc Electrophoresis. Test and control DEAE-cellulose fractions were subjected to preparative polyacrylamide gel electrophoresis in our modification of the apparatus designed by Furlong *et al.* (15). A 6-cm layer of 7% polyacrylamide was first allowed to gel in a 1.5 × 12-cm glass column. Then, a 1-cm stacking gel was polymerized on top. A glass column of 1.5 × 2 cm was completely filled with a solution of 7% acrylamide. After polymerization, one end was covered with a piece of dialysis tubing. The short and long units were then joined together with a sleeve containing two elution ports, one on each side. 15 mg of LT containing the DEAE-cellulose fraction in 30% glycerol was added to the top of the column and covered with buffer. Electrophoresis was performed at 4° with a constant current of 7 mA in glycine buffer (pH 9), and fractions were eluted at a constant flow rate of one drop every 11 sec. 0.5-ml Fractions were collected, and absorbance was determined at 280 nm.

Isoelectric Focusing. These experiments were performed in 1% ampholine (pH 3–10) (16). Control and cytotoxic fractions were electrofocussed for 48 hr. After equilibration, 50-drop fractions (0.8 ml) were collected in an ISCO fraction collector at a constant flow rate of 1 drop per sec. The absorbance at 280 nm and pH of the fractions were measured, then fractions were dialyzed against 8 liters of physiologic dialysis buffer for 18 hr with four changes to remove the ampholine.

Assay for Cytotoxicity. After test and control media had been subjected to the various physical separation techniques, the residual buffers and salts were removed by dialysis against low salt buffer, physiologic dialysis buffer, or distilled water. Fractions dialyzed against hypotonic physiologic salt concentrations were reconstituted to physiologic tissue culture conditions by addition of a concentrated additive (9), or were added at 1:10 or 1:20 dilution directly to complete cell culture media. The medium was tested for cytotoxicity on cultures in tubes (17), or in microplates (18). Degree of cytotoxicity in microplates was determined by direct cell counts. In tubes, it was determined from the average of results of two different methods, a direct cell count made in a Coulter Counter, or the capacity of the remaining cells to incorporate [^{14}C]aminoacids into cellular protein after 48 hr of exposure to the test or control medium. The amount of LT activity in a sample was determined by testing the effect of doubling dilutions of test and control media on target cells. One unit of LT activity was defined as the amount that destroyed 50% of the target culture.

RESULTS

DEAE-cellulose column chromatography

Studies with protein-free and protein-containing media revealed that addition of bovine-serum albumin carrier (0.1%) to the initial culture medium helped protect the LT during the initial harvesting, storage, and concentration steps.

DEAE-cellulose is an ion-exchange resin that binds proteins with an overall negative charge. The proteins can then be differentially eluted from the column with an increasing gradient of cations. The location of LT activity after fractionation on DEAE-cellulose is shown in Fig. 1. LT activity eluted from the column with hemoglobin and before the bovine-serum albumin carrier. Fig. 1 is typical of over 30 separate column separations. When dilutions of the pooled LT-containing fractions were tested, 25–50% of the original activity was not recovered. A series of experiments in which all fractions eluted from the column were pooled and tested for activity revealed that this loss was irreversible. In later experiments, 20 mg of purified human hemoglobin was added to each sample to serve as a visible marker, because it was eluted with LT. Concentrated LT loaded on the column had from 1.5 to 2.5 units of activity per mg of protein. Pooled, concentrated fractions eluted from the column had from 35 to 110 units of activity per mg. Analysis of the DEAE-cellulose samples by acrylamide gel electrophoresis and immunodiffusion revealed 9–12 separate proteins. Control preparations had almost identical elution profiles, but little or no toxicity.

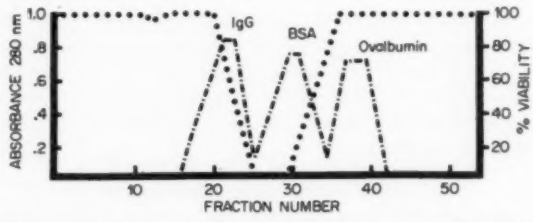

FIG. 2. Elution of LT activity from Sephadex. DEAE-cellulose and crude LT fractions were loaded and eluted from a Sephadex G-150 column. The *dotted line* indicates the toxic activity of each fraction and the *dashed line* indicates absorbance at 280 nm of the protein markers.

Sephadex column chromatography

Sephadex separates molecules according to their size, with the largest molecules eluting first. A typical Sephadex G-150 run containing LT with the marker proteins is shown in Fig. 2. The elution profile of LT from the columns was essentially the same, whether the original sample was crude medium or fractionated on DEAE-cellulose. This figure is representative of some 25–30 different column runs. LT activity eluted behind the IgG marker and in front of the bovine-serum albumin marker. When DEAE-cellulose fractions were applied to the column, LT fractions were collected with 320–1200 units of LT activity per mg of protein. Control runs had little or no toxicity. Recovery of LT activity was almost 100% in these columns. To see if LT was a small molecule, noncovalently linked to larger molecules, samples fractionated on DEAE-cellulose and crude samples were passed through the same columns in buffers containing various concentrations of NaCl, from 0.025 to 4.0 M. While there were various degrees of aggregation in 0.025 M and above 0.8 M NaCl, little or no aggregation occurred at 0.15 M NaCl. However, there was no major shift of the LT-elution pattern to regions containing smaller molecules during any of these studies. Analysis of the LT fractions on analytical polyacrylamide gels stained by Coomassie blue revealed several major and one minor protein bands.

Velocity sedimentation studies

Sedimentation of samples in sucrose gradients is a common method for obtaining an approximate value of the molecular weight of a macromolecule. DEAE-cellulose fractions were loaded on 5-ml linear 10–30% sucrose gradients. In each centrifuge run, one tube in the head contained a bovine-serum albumin marker, and the other tubes contained the LT samples. Typical results of these studies are shown in Fig. 3. It is clear that LT sediments just in front of the albumin marker.

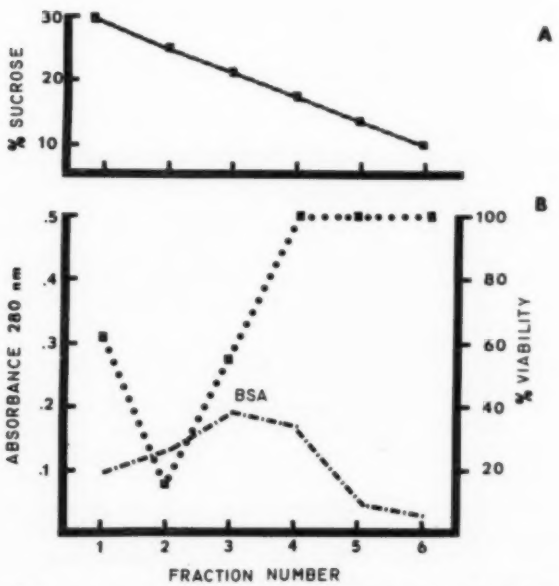

FIG. 3. Sucrose gradient centrifugation. DEAE-cellulose fractions and a BSA marker were sedimented through 10–30% (W/V) sucrose gradients. Sedimentation is from right to left. (*A*) Illustrates linearity of the gradient. (*B*) The *dotted line* indicates the toxicity of each fraction and the *dashed line* indicates absorbance at 280 nm of BSA marker.

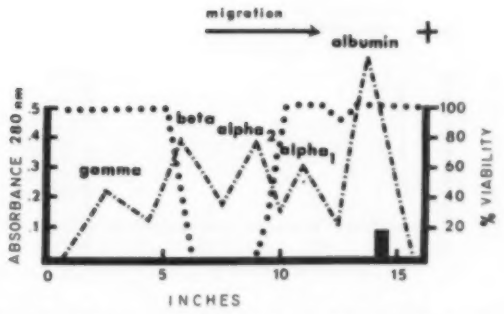

FIG. 4. Migration of LT activity in Pevikon block electrophoresis. Concentrated crude LT medium and human serum markers were electrophoresed. Peaks of absorbance at 280 nm were identified by immunoelectrophoresis. *Dotted lines* indicate the toxic activity of each fraction. The *dashed line* indicates absorbance at 280 nm.

Block electrophoresis

This is a method for separation or comparison of materials by observation of their migration in an electric field. The electrophoretic mobility of human LT was determined; the well-known migration pattern of human serum proteins was used as reference. 20-Times concentrated crude medium was used in both test and control separations. A typical result representative of nine separate tests is shown in Fig. 4. Each of the 280-nm absorbance peaks were identified in agar-slide immunoelectrophoresis, with rabbit antiserum directed against specific human serum proteins. LT activity migrated as a broad band, which localized in the region of the β- and α_2 globulins. Although the total protein recovery was good, there was only a 25–50% recovery of LT activity. Moreover, when all fractions were pooled, concentrated, and tested, original activity was not regained.

Preparative polyacrylamide gel electrophoresis

This is a technique that simultaneously separates materials by charge and size. To further purify LT, DEAE-cellulose fractionated samples were separated on polyacrylamide gel columns. A typical result of one of these separations, containing phenol red, bovine-serum albumin and hemoglobin markers, is shown in Fig. 5. LT eluted behind, and was separable from, the hemoglobin marker. This is representative of 10 separate experiments. Recovery of LT ranges from 25–60%. In the most recent experiments, reduced glutathione (100 mM) was added; it improved recovery of LT activity by 15–25%. When DEAE-cellulose fractions containing LT were separated on the preparative column, they were found to contain very low concentrations of protein. Because of this, specific LT activity per mg of protein is difficult to calculate. However, it ranges from about 2000–4000 units/mg. Analytical polyacrylamide gels of concentrated LT fractions stained with Coomassie blue revealed one minor protein band in the area of LT activity in one of four experiments. However, these samples contain so little protein that we usually are unable to detect any bands.

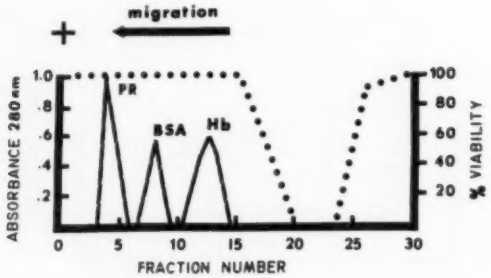

FIG. 5. Migration of LT in preparative polyacrylamide gel electrophoresis. DEAE-cellulose fractions were separated on 1.4 × 6-cm polyacrylamide gel columns. *Dotted lines* indicate toxic activity of each fraction; the *slashed line* indicates absorbance at 280 nm. Phenol red and BSA were added to this particular run to provide markers.

Isoelectric focusing

Samples are electrophoresed in a sucrose and pH gradient until they reach their isoelectric point, when they cease to migrate. Resolution of closely related proteins is possible by this highly sensitive technique. Crude LT, DEAE-cellulose fractions, and samples that had been run through DEAE-cellulose and Sephadex G-150 columns were separated by isoelectric focusing. In all cases, LT activity was localized in the pH range between 6.8 and 8.0 in a pH gradient of 3–10. Control samples had little or no toxic activity. Final analyses of these fractions are, however, not yet completed.

DISCUSSION

We used two protein carriers, bovine-serum albumin, which stabilized human LT during the collection, storage, and concentration steps, and human hemoglobin, which served as a carrier and visible marker for LT through DEAE-cellulose and Sephadex.

Human LT is a macromolecule that has a molecular weight of about 85–100 × 10^3 or 3.2–4 S, as evidence by molecular sieving on Sephadex G-150 and velocity sedimentation through 10–30% sucrose gradients. The present studies suggest that it is not a small molecular complexed to a larger molecule by noncovalent bonds. Human LT is not a highly charged molecule, as evidenced by its early elution from DEAE-cellulose and slow migration rate in Pevikon and acrylamide gel electrophoresis.

Human LT is either a single molecule or several very closely related materials. We were unable to separate LT activity into multiple components. Also, the loss of activity seen in the various separations was attributed to inactivation, because it could not be recovered. However, there may be some heterogeneity among molecules with LT activity, because elution patterns were sometimes broad. This is supported by the broad spread of LT activity (pH 6.8–8.0) observed in isoelectric focusing experiments. Human LT is clearly separable from all carriers, serum proteins, and medium factors. With the combinations of DEAE-cellulose, Sephadex, and, finally, either the acrylamide gel electrophoresis or isoelectric focusing, degrees of purification in excess of 2000- to 4000-fold have been achieved, with 15–25% recovery of the original activity.

The role of factors released by lymphocytes in cell-mediated immune reactions *in vivo* and *in vitro* is still unclear. Purification and characterization of LT will greatly facilitate our ability to (*a*) determine the relationship of LT to the other lymphocyte effector molecules and (*b*) prepare specific blocking agents to provide the means whereby we can begin to elucidate the actual role assignable to this factor in cell-mediated reactions.

This research was supported by Grant AI 09460-3, from the Institute of Allergy and Infectious Diseases, NIH, and a grant from the Cancer Research Co-ordinating Committee of the University of California. G.A.G. is supported by a career award from N.I.A.I.D. of the NIH.

1. Weaver, J. G., Algire, G. & Prehn, R. T. (1955) *J. Nat. Cancer Inst.* **15,** 1737–1746.
2. Gorer, P. A. (1956) *Advan. Cancer Res.* **4,** 149–156.
3. Landsteiner, K. & Chase, M. W. (1942) *Proc. Soc. Exp. Biol. Med.* **49,** 688–698.
4. Rosenau, W. & Moon, H. D. (1961) *J. Nat. Cancer Inst.* **27,** 471–481.
5. Holm, G. (1969) *Advan. Immunol.* **11,** 117–157.
6. Lawrence, H. S. & Landy, M. (1969) *Mediators of Cellular Immunity* (Academic Press, New York).
7. Bloom, B. & Glade, P. (1971) *In Vitro Methods in Cell-mediated Immunity* (Academic Press, New York).
8. Ling, N. R. (1968) *Lymphocyte Stimulation* (John Wiley & Sons, New York).
9. Kolb, W. P. & Granger, G. A. (1968) *Proc. Nat. Acad. Sci. USA* **61,** 1250–1255.
10. Kolb, W. P., Williams, T. W. & Granger, G. A. (1971) in *In Vitro Methods in Cell-mediated Immunity* (Academic Press, New York), p. 333.
11. Martin, R. G. & Ames, B. N. (1961) *J. Biol. Chem.* **263,** 1372–1380.
12. Muller-Eberhard, H. J. & Osterland, C. K. (1968) in *Methods in Immunology,* eds. Williams, C. A. & Chase, M. W. (Academic Press, New York) Vol. 2, p. 57.
13. Lowry, O. H., Rosebrough, N. J., Farr, A. L. & Randall, R. J. (1951) *J. Biol. Chem.* **193,** 265–275.
14. Ouchterlony, O. (1967) in *Handbook of Experimental Immunology* (Blackwell Scientific Publications, Oxford), p. 655.
15. Furlong, C. E., Willis, R., Cirakoglu, C. & Santy, P. (1972) *Anal. Biochem.,* in press.
16. LKB Instruction Manual, No. 8100.
17. Granger, G. A., & Kolb, W. P. (1968) *J. Immunol.* **101,** 111–120.
18. Kramer, J. J. & Granger, G. A. (1972) *Cell. Immunol.* **3,** 144–154.

Proc. Nat. Acad. Sci. USA
Vol. 70, No. 1, pp. 31–35, January 1973

Mechanism of Protein Chain Termination: Further Characterization of a Mutant Defective in a New Protein Synthesis Factor

(ribosomes/f2 bacteriophage/coding/peptidyl-tRNA/thermolabile proteins)

M.C. GANOZA*‡, J. VANDERMEER*, N. DEBRECENI*, AND S. L. PHILLIPS†

* Banting and Best Department of Medical Research, University of Toronto, Toronto 101, Canada; and
† Department of Biochemistry, University of Pittsburgh, Pittsburgh, Pennsylvania 15200

Communicated by Edward L. Tatum, October 24, 1972

ABSTRACT **Mutant N4316 is conditionally lethal at 43°. At 36° it suppresses the termination codons UGA and UAA, but not the UAG codon or a missense mutant of T4 bacteriophage. *In vitro*, a factor rescues protein synthesis from a temperature-dependent arrest when N4316 extracts are used with RNA from bacteriophage f2. Analyses of the substrate in the arrested synthesis and of the product of the rescue reaction indicate that the factor works at the level of coat protein termination, and that it also affects the synthesis of noncoat protein products. The rescue factor is different from the release factors RF-1, RF-2, and RF-3. Model systems previously used to study release fail to score for at least one vital function in protein chain termination.**

One of the principal assumptions about translation of the genetic code is that triplets are read in phase, one at a time, and that the response of the translation machinery to each codon is not affected by the neighboring triplets (1). Although this process may indeed be inevitable in protein chain elongation, recent data suggest that the proper recognition of AUG and GUG as initiator codons may depend on the sequence of the nucleotides surrounding them (2). In protein chain termination, similar considerations may be applicable. For example, there is evidence that suppression of nonsense codons may be drastically affected by the composition of the nucleotides adjacent to the termination triplets (3). This evidence invites speculation that the signal for termination of proteins that occurs in the intercistronic stretches (2, 4), and closely precedes initiation signals, may also be influenced by adjacent bases. In fact, the close proximity of the two markers may imply a coupling of the two biochemical events.

One of the *in vitro* experiments described here with a mutant (N4316) (5–7), reported to be temperature sensitive in polypeptide chain termination, suggests that under nonpermissive conditions when termination of f2 coat protein is impaired the reading of other cistrons may also be affected.

The *in vitro* defect in coat protein release is reversed by a factor isolated from the parental strain. This factor unlike RF-1, RF-2, and RF-3, is not required in the model *in vitro* termination assays that respond to the simple addition of the single nonsense codons UAA, UAG, or UGA (8). This protein also appears to be unrelated to the factors IF-1, IF-2, and IF-3 that are needed for proper initiation of the coat protein cistron *in vitro* (9).

Abbreviations: sus_3RNA, mutant of bacteriophage f2 with an amber codon at the 7th amino acid in its coat protein; su_{III}^{+} tRNA, suppressor tyrosine-accepting tRNA.

‡ Address reprint requests to: Dr. M. C. Ganoza, 112 College St., C. H. Best Institute, University of Toronto, Toronto 101, Ontario, Canada.

RESULTS AND DISCUSSION

Certain Properties of the N4316 Mutation. The isolation and several properties of strain N4316 have been described (5–7). The parental strain of N4316 is *E. coli* strain D_{10} Met^- Thy^- $RNase_I^-$ (10, 11). The mutant, N4316, belongs to a class designated *sts* (starvation temperature sensitive) that is conditionally lethal at 43° (10). At 36°, strain N4316 suppresses UAA and UGA codons, but not UAG or a missense mutant of T4 bacteriophage (5). These two properties, thermolethality and suppression of nonsense codons, transduce together and revert to the parental phenotype together, suggesting that a single mutation is responsible for both effects (5).

In vitro, N4316 extracts programmed with f2 or R17 RNA are impaired in protein synthesis at nonpermissive temperatures (5–7). The extent of impairment is 2- to 3-fold compared to synthesis at permissive temperatures with N4316, or parental (D_{10}) extracts at either temperature. The defect in protein synthesis is not due to a mutation in any of the 20 aminoacid activating enzymes (6). When programmed with poly(U), (A), (AU, 3:1), (UG, 5:1), or (UC, 1:1), synthesis is the same at the higher or lower temperatures (ref. 7 and unpublished data). Furthermore, the formation of the initiation complex of R17 with fMet-tRNA is not affected (6).

Peptides accumulate on 70S ribosomes at nonpermissive temperatures (5, 6). This result, and the temperature-dependent suppression of nonsense codons *in vivo*, suggested that the strain might be defective in protein chain termination.

Table 1 shows our attempt to detect temperature sensitivity with *N*-acetylmethionine release as a model system (8). This assay responds to the release factor RF-1 with UAA or UAG, or to RF-2 when UAA or UGA are included (8). Treatment of parental or mutant extracts at 43° reduced synthesis with phage f2 RNA irreversibly, but it did not affect the nonsense codon-dependent release of *N*-acetylmethionine stimulated by UAA, UAG, or UGA.

Since release of *N*-acetylmethionine is stable to heat, another termination assay was tried, namely, the release of polypeptides from ribosomal-bound polypeptidyl-tRNA. Fig 1 shows that the percent free peptides released with poly(A_3U), a message that contains a high frequency of UAA codons (12,

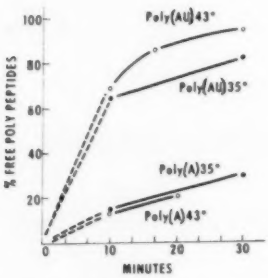

FIG. 1. Free polypeptides synthesized by N4316 ribosomes and soluble proteins. Analysis of total and free peptides was as described (12, 13) except that incubations (0.155 ml) containing 150 μg of ribosomes and 6.3 μg of soluble protein were heated for 5 min at 43° (where indicated). The reaction was run at 35° for 15 min. Counts incorporated without added polynucleotides (less than 10% of the incorporation) were subtracted from each value. With parental extracts, the incorporation with poly(A) or poly(AU) was slightly higher after 43° treatment, but the percent release was identical at all temperatures.

13), is normal in a thermally inactivated extract of N4316. We conclude that the mutation does not affect any of the soluble or ribosomal factors needed in release that are scored by this assay (14). In addition, all other attempts to show thermolability of release in these assays by variation of reaction conditions failed. Taken together, these results suggested that the defect with f2 RNA observed *in vitro* is not scored by the model systems commonly used to study release.

TABLE 1.

Extract	Prior treatment at 43°	*N*-acetyl-[^{3}H]methionine released, pmol		
		UAA	UAG	UGA
D_{10}	−	1.27	0.19	2.60
D_{10}	+	1.02	0.19	2.15
N4316	−	1.10	0.16	1.37
N4316	+	0.98	0.19	2.20

Trinucleotide-dependent release was assayed as described by Caskey *et al.* (28), except that *N*-acetylmethionyl-tRNA was used (18) instead of *N*-formylmethionyl-tRNA. Reactions (45 μl) contained 2.6 pmol of *N*-acetyl-[^{3}H]methionyl-tRNA$_f^{Met}$–AUG ribosome complex, 5 nmol of UAG, UAA, or UGA, and 5 μl of crude extract from N4316 or D_{10}. Since this assay cannot be performed at 43° (25), portions of each extract were heated for 5 min at 43° before assay at 24°. Reactions containing UAA or UAG were incubated for 15 min, those containing UGA for 60 min. Counts released without added triplets (0.15 pmol for 15 min and about 0.3 pmol for 60 min) were subtracted. Values are the average of triplicates, which were within 10% of each other. Purification of the extracts did not elevate the activity of RF-1. Unheated parental extracts incorporated 85,000 cpm of [^{3}H]lysine (see Fig. 2 for description of assay) in response to f2 RNA, and 75,000 cpm after heat treatment. Mutant extracts incorporated 78,000 cpm before heat treatment and 39,000 cpm of [^{3}H]lysine after heat treatment. After they were heated at 43°, extracts were exposed to 24° for 60 min without change in the incorporation values.

Analysis of Products Synthesized under Nonpermissive Conditions. We have analyzed the products of synthesis after separation of peptidyl-tRNA from free protein by means of sucrose density gradients containing dodecyl sulfate (13). The separated peptidyl-tRNA and free peptides were concentrated by ethanol precipitation, and were further analyzed by electrophoresis in polyacrylamide gels containing Na dodecyl sulfate.

Fig. 2 shows the separation in sucrose gradients of peptidyl-tRNA (peak I) and free protein (peak II) made at nonpermissive temperatures with either strain D_{10} or strain N4316. 90% of the total peptides made by the parental extract were released at 47°, whereas the mutant always released significantly less of the protein it synthesized, e.g., 70% in the experiment of Fig. 2 and as much as 50% in other experi-

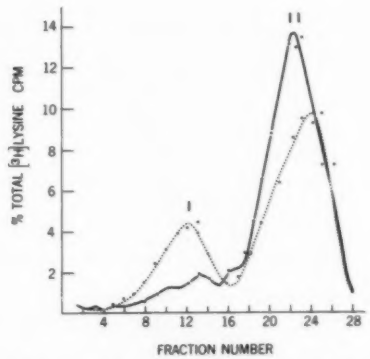

FIG. 2. Dodecyl sulfate–sucrose density gradient centrifugation of f2 RNA products made with N4316 or D_{10} extracts at 47°. Cells were grown at 33° to a density of 5×10^8 viable cells per ml. Thermostable revertants were routinely less than 0.1%. Before analysis, cell extracts were prepared (26) and assayed for incorporation of amino acids into protein (18) at several temperatures; the temperature at which maximum relative inactivation of N4316 extracts occurred varied and had to be determined for each new pair of mutant and wild-type extracts made. Routinely, D_{10} extracts lost less than 10% activity at the higher temperatures (here, 47°). The standard assay (60 μl) contained: 10 μl of incubated S-30 extract, 10 mM $MgCl_2$, 30 mM NH_4Cl, 30 mM Tris·HCl (pH 7.4), 5.3 mM P-enolpyruvate, 3.3 mM ATP, 0.4 mM GTP, 8 mM dithiothreitol, 2.5 μCi [^{3}H]lysine, 0.1 mM (each) of a mixture of 19 [^{12}C]aminoacids lacking lysine, 7.5 μg of calcium leucovorin, 5 μg of pyruvate kinase, and 10 μg of f2 RNA. Extracts of D_{10} and N4316 were incubated for 10 min at the permissive or nonpermissive temperatures. f2 RNA was added, and incubation was continued for 15 min at 47°. The first incubation destroyed completely the activity of a partially purified rescue factor (see below) isolated from N4316. An aliquot (60 μl) of the incubation mixture was layered on a sucrose gradient (5–12% sucrose, 3 ml total volume) containing 0.5% dodecyl sulfate and 0.1 M LiCl (13). Sedimentation was at 12° for 17 hr at 40,000 rpm in an SW56 Beckman rotor. Fractions were collected, precipitated with 15% Cl_3CCOOH, heated for 15 min at 90°, and filtered on Millipore filters (18, 26). Recoveries of radioactivity from the gradients were 12,000 cpm (D_{10} reaction) or 6800 cpm (N4316 reaction); 80–90% recovery of the total acid-insoluble counts analyzed. Parallel gradients of reaction mixtures without f2 RNA did not contain significant radioactivity in the region of peak I, but 2900 cpm or 3200 cpm were recovered in peak II when D_{10} or N4316 were analyzed. These counts were subtracted from the experimental values.

ments. The smaller extent of release observed with the mutant must be related to the temperature lesion, since less than 5% of the products synthesized at permissive temperatures were found attached to tRNA with extracts of either D_{10} or N4316.

Electrophoretic analysis of the free peptides made at nonpermissive temperatures with D_{10} or N4316 are shown in Fig. 3*a–c*. The major product released at 47° with D_{10} or N4316 corresponds in size to coat protein. The conclusion that the major peak observed in Fig. 3*a–c* is coat protein rests on the position of this product on polyacrylamide gels. In addition, we show in Fig. 3*c* that this major product is eliminated when synthesis is programmed by an amber mutant (sus_3RNA) (15) that cannot make coat protein. Under conditions shown to eliminate polarity effects of this mutation *in vitro* (16), addition of a purified suppressor tRNA (17, 18) restores synthesis of this major product.

The lack of extensive release of noncoat products (Fig. 3*d–f*) occurred at permissive temperatures with both D_{10} and N4316, indicating that this effect is unrelated to the mutation.

Since no qualitative differences could be observed in the peptides released by N4316 and D_{10}, we examined the size distribution of the nascent peptides made by both strains. Fig. 3*d* and *e* show electropherograms of the nascent peptides

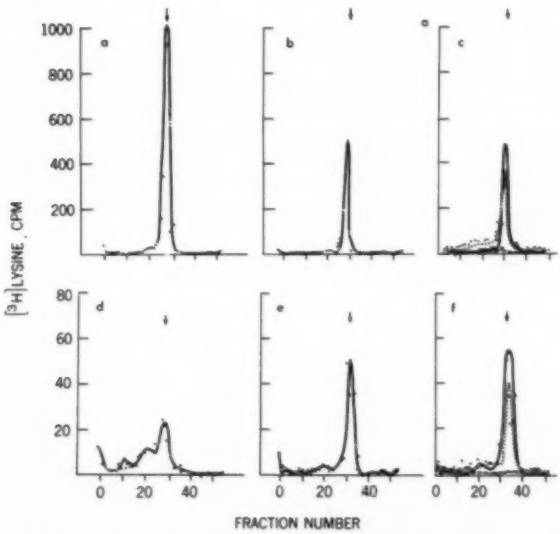

FIG. 3. Released peptides (*a–c*) or nascent peptides (*d–f*) synthesized with D_{10} (*a*, *d*) and N4316 (*b*, *c*, *e*, and *f*) at 47°. Incorporation of labeled lysine (3×10^3 Ci/mol) was described in Fig. 2. Conditions for suppression of coat protein and purification of su_{III}^+ tRNA were described (18). Incubations (0.10 ml) were layered and centrifuged on sucrose containing dodecyl sulfate and LiCl (see Fig. 2). After addition of carrier S-100 and two volumes of ethanol, fractions I and II were concentrated by centrifugation. The pellets were suspended in 0.01 M Tris·HCl (pH 7.4) and were treated with 10 μg of RNase at 35° for 10 min. Each sample was made 1% in dodecyl SO_4, 50% in glycerol and 0.1 M in 2-mercaptoethanol. Polyacrylamide gel electrophoresis was for 3.5 hr at 8 V/cm, and 4 A per gel (27). Fractions were cut, digested, and counted for 50 min (18). Recovery of added radioactivity was 80–100%. Each gel contained, as markers, f2 coat and maturation proteins (26). Peptides of small size are not seen because they are soluble in ethanol.

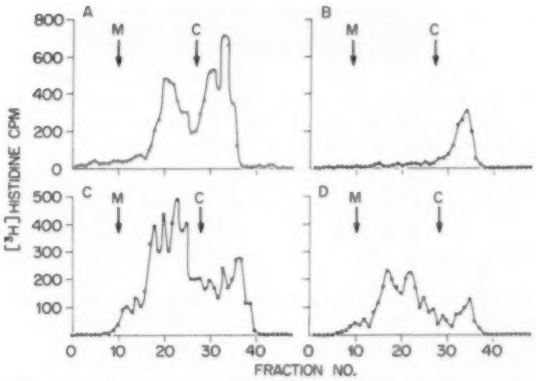

FIG. 4. Nascent peptides containing [^{3}H]histidine (4×10^4 Ci/mol) made with D_{10} extracts at 46° (*A*) or at 35° (*C*) or with N4316 extracts at 46° (*B*) or at 35° (*D*). Conditions of synthesis and analysis of products as in Figs. 2 and 3. The position of the coat (C) and maturation proteins (M) are indicated by the *arrows*.

made by D_{10} or N4316 at 47°. N4316 makes only one major product attached to tRNA; it corresponds in molecular weight to coat protein. In contrast, D_{10} makes nascent peptides larger than coat protein, as well as some peptides that correspond in size to the coat. The major product made by N4316 is eliminated when synthesis is programmed by sus_3-RNA (Fig. 3*f*). Addition of a purified suppressor tRNA also restores synthesis of this major product. The data in Fig. 3*d–f* show that release of coat protein is affected in the mutant strain. Furthermore, at permissive temperatures, both D_{10} and the mutant made and released the same amount and type of peptides. At nonpermissive temperatures, however, synthesis by N4316 is lowered, more nascent coat protein molecules accumulate on ribosomes, and fewer larger nascent peptides are observed.

To gain some insight into the nature of the nascent peptides that were larger than the coat, the products were labeled with histidine, an amino acid that does not occur in the coat protein (19). Fig. 4 shows analyses of nascent peptides labeled with histidin At permissive temperatures, the bulk of thee. histidine-containing nascent peptides in both D_{10} and N4316 are larger than the coat protein. A striking lack of synthesis of histidine-labeled larger noncoat products occurs only in N4316, and not in the parental strain; this lack may be due to faulty initiation of other cistrons.

At nonpermissive temperatures, both D_{10} and the mutant make more peptides that are slightly smaller than coat protein. These peptides do not appear to be precursors of the larger products, because their mobility was unaltered in pulse–chase experiments of the sort reported in Fig. 5.

Site of Action and Characteristics of the Rescue Factor. When thermally inactivated extracts are included at saturating levels, addition of increasing amounts of similarly heated parental extracts increased the rate of protein synthesis by about 3-fold (data not shown). There is a similar dependence on the amount of parental "rescue" factor added that can be used as an assay to purify the relevant factor [previously designated Z (6, 7)]. Our partially purified factor gives three bands on dodecyl sulfate–polyacrylamide electrophoresis (manuscript in preparation).

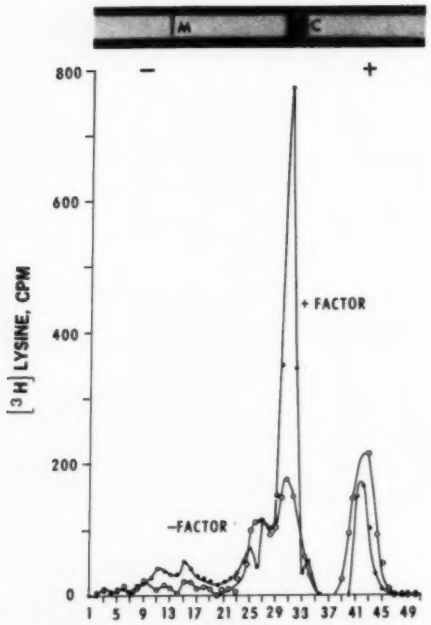

FIG. 5. Effect of factor on release of coat protein. Incorporation of amino acids into protein was as described in Fig. 2 and refs. 18 and 26: crude ribosomes and soluble protein from heat-inactivated N4316 extracts were used. Incubation was for 5 min at 35°. Then 17 mM [^{12}C]lysine was added and incubation was continued for 10 min at 35°. Products were isolated on sucrose gradients (26), and the ribosome-free fraction was concentrated by addition of cold 5% Cl_3CCOOH. The pellets were suspended in buffer, extracted with ether, and analyzed on dodecyl SO_4–polyacrylamide gels (see Fig. 3). The coat (*C*) and maturation protein (*M*) used as internal markers are shown. Reactions without f2 RNA were also electrophoresed, and the small amounts of radioactivity observed in the regions of small peptides were subtracted from the above profiles. Complete system minus rescue factor (○——○); complete system, with 5 μl of partially purified rescue factor (●——●). The presence of small peptides in this experiment may be due to the fact that the products were concentrated with Cl_3CCOOH rather than ethanol.

The component that reverses the N4316 lesion purifies as a protein; its activity can be destroyed by trypsin, elevated temperatures, or reagents that block sulfhydryl groups (6, 7), but treatment with pancreatic RNase is ineffective. The factor has a molecular weight of about 96,000, as determined by both sucrose density gradient analysis and chromatography on Sephadex columns. Thus, we clearly are not dealing with a temperature-sensitive suppressor tRNA of the sort reported by Smith *et al.* (20).

The rescue factor is separable from the termination factors RF-1, RF-2, and RF-3 (8) by partition on DEAE-Sephadex and alumina C_γ. In Table 2 we show that the rescue factor preparation does not contain any of the other known release factors. We also find (data not shown) that the rescue factor is free of the initiation proteins IF-1, IF-2, and IF-3. The factor that rescues synthesis, seemingly unlike the initiation factors, is found in ribosome-free cytoplasm.

The assay for rescue of synthesis from the thermal defect of N4316 extracts by parental extracts is nonspecific, since it only measures incorporation of amino acids into acid-insoluble precipitates. We can obtain some idea regarding the mechanism of this rescue by examining the products of the rescue assay. Fig. 5 shows an analysis by dodecyl sulfate–polyacrylamide gel electrophoresis of the peptides released from ribosomes before and after addition of rescue factor. In these experiments, synthesis with f2 RNA was performed for 5 min with thermally inactivated extracts of the mutant; then, further incorporation of amino acids into protein was blocked by addition of a 1000-fold excess of [^{12}C]lysine. After 30 sec, rescue factor was added and synthesis was allowed to continue for another 10 min. As shown in Fig. 5, some release of coat protein does occur without added rescue factor. Addition of the factor results in an about doubled release of coat protein free of tRNA, leading to the disappearance of ribosomal-bound coat protein tRNA (data not shown). The experiment strongly suggests that the rescue factor participates in release when a natural messenger RNA programs synthesis. If labeled histidine is added at the same time as the rescue factor, nascent peptides larger than coat protein (see Fig. 4*A–D*) are observed, supporting the notion that this protein affects the initiation of noncoat protein products.

The Possible Role of the Rescue Factor. This factor rescues protein synthesis *in vitro* from a temperature-dependent arrest when N4316 extracts are used with f2 RNA as messenger. Analysis of the substrate in the arrested synthesis and of the products of the rescue reaction indicate that the factor works at the level of chain termination when a natural messenger RNA programs synthesis. This factor is different from the known termination proteins RF-1, RF-2, and RF-3 that stimulate release in response to single nonsense codons.

RF-1 and RF-2, which participate at least indirectly in recognition of single nonsense codons (21–23), are required for release of the coat protein and the replicase of R17 bac-

TABLE 2.

Factor added	*N*-Acetyl-[^{3}H]methionine released, pmol			
	Exp. 1			Exp. 2
	UAA	UAG	UGA	UAA
None	1.35	1.35	1.35	0.96
RF-1 + RF-2	5.37	7.50	1.93	3.00
Rescue	1.05	0.88	1.15	1.02
RF-1 + RF-2 + Rescue	3.69	4.86	2.05	2.24
RF-1 + RF-2 + RF-3	—	—	—	9.77

Release of formylmethionine was assayed (28) with fraction 3 (21) as a source of RF-1 and RF-2. In Exp. 1, reaction mixtures (45 μl) contained 22 pmol of [^{3}H]acetylmethionyl-tRNA$_f^{Met}$–AUG–ribosome complex (18) and, where indicated, 6.3 nmol of UAG, 2.5 nmol of UAA, 4.0 nmol of UGA, 80 μg of RF-1 and RF-2 or 2 μg of rescue factor (fraction 5). Incubation was for 30 min at 24°. In Exp. 2, reaction mixtures contained 2.5 nmol of UAA and, where indicated, 5 μl of an ammonium sulfate fraction of RF-3 (25) or 2 μg of rescue factor (fraction 5). The inhibition of release observed with rescue factor added to RF-1 and RF-2 occurred also when a purified rescue factor from N4316 was thermally inactivated. Variation of triplet concentration, inclusion of 0.1 mM GTP, increase in rescue factor levels, or alteration of salt concentration did not alter the lack of effect of rescue factor in this assay; 0.1–2 μg of the rescue factor restored synthesis completely in the rescue assay.

teriophage (24). However, participation of the rescue protein in recognition of the normal signal for release is not excluded by these observations.

Since we find that the mutation also affects the synthesis of noncoat products, we do not know whether the rescue protein affects termination directly or indirectly. The lack of synthesis of noncoat products could, for example, occur if arrested ribosomes, bearing coat-protein tRNA, prevented initiation of the contiguous cistron. By the same token, the impaired termination could result from a fault in the initiation of the replicase cistron.

We acknowledge the MRC of Canada and NSF grant GB 26315X1 to S.P. for financial support. We thank Miss Anne Tirpak and Mrs. Nada Barraclough for technical help, and Dr. A. Becker for help in writing this manuscript.

1. Crick, F. H. C., Barnett, L., Brenner, S. & Watts-Tobin, J. R. (1961) *Nature* **192,** 1227–1232.
2. Steitz, J. A. (1969) *Nature* **224,** 957–964.
3. Salzer, W., Fluck, M. & Epstein, R. (1969) *Cold Spring Harb. Symp. Quant. Biol.* **34,** 513–520.
4. Nichols, J. L. (1970) *Nature* **225,** 147–151.
5. Phillips, S. L., Schlessinger, D. & Apirion, D. (1969) *Cold Spring Harb. Symp. Quant. Biol.* **34,** 499–503.
6. Phillips, S. L. (1971) *J. Mol. Biol.* **59,** 461–472.
7. Ganoza, C. & Phillips, S. (1971) *Fed. Proc.* **30,** 1382.
8. Caskey, T., Scolnick, E., Tompkins, R., Goldstein, J. & Milman, G. (1969) *Cold Spring Harb. Symp. Quant. Biol.* **34,** 479–491.
9. Wahba, A. J., Iwasaki, K., Miller, M. J., Sabol, S., Sillero, M. A. G. & Vasquez, C. (1969) *Cold Spring Harb. Symp. Quant. Biol.* **34,** 291–299.
10. Phillips, S. L., Schlessinger, D. & Apirion, D. (1969) *Proc. Nat. Acad. Sci. USA* **62,** 772–777.
11. Apirion, D., Phillips, S. L. & Schlessinger, D. (1969) *Cold Spring Harb. Symp. Quant. Biol.* **34,** 117–128.
12. Ganoza, M. C. & Nakamoto, T. (1966) *Proc. Nat. Acad. Sci. USA*, **55,** 162–169.
13. Bretscher, M. S., Goodman, H. M., Menninger, J. R. & Smith, J. D. (1965) *J. Mol. Biol.* **14,** 634–639.
14. Ganoza, M. C. & Thach, R. (1969) *Cold Spring Harb. Symp. Quant. Biol.* **34,** 488–489.
15. Englehardt, D. L., Webster, R. E., Wilhelm, R. C. & Zinder, N. D. (1965) *Proc. Nat. Acad. Sci. USA* **54,** 1791–1797.
16. Capecchi, M. R. (1967) *J. Mol. Biol.* **30,** 213–217.
17. Gefter, M. L. & Russell, R. L. (1969) *J. Mol. Biol.* **39,** 145–157.
18. Ghosh, H. P., Ghosh, K. & Ganoza, M. C. (1972) *J. Biol. Chem.*, **24,** 5322–5326.
19. Weber, K. & Konigsberg, W. J. (1967) *J. Biol. Chem.* **242,** 3563–3578.
20. Smith, J. D., Barnett, L., Brenner, S. & Russell, R. L. (1970) *J. Mol. Biol.* **54,** 1–14.
21. Ganoza, M. C. & Tompkins, J. K. (1970) *Biochem. Biophys. Res. Commun.* **40,** 1455–1463.
22. Beaudet, A. L. & Caskey, C. T. (1970) *Nature* **227,** 38–40.
23. Scolnick, E. & Caskey, C. T. (1969) *Proc. Nat. Acad. Sci. USA* **64,** 1235–1241.
24. Capecchi, M. & Klein, H. A. (1970) *Nature* **226,** 1029–1033.
25. Milman, G., Goldstein, J., Scolnick, E. & Caskey, T. (1969) *Proc. Nat. Acad. Sci. USA* **63,** 183–190.
26. Webster, R. E. & Zinder, N. D. (1969) *J. Mol. Biol.* **42,** 425–439.
27. Weber, K. & Osborn, M. (1969) *J. Biol. Chem.* **244,** 4406–4412.
28. Caskey, C. T., Tompkins, R., Scolnick, E., Caryk, T. & Nirenberg, M. (1968) *Science* **162,** 135–138.
29. Salas, M., Hille, M. B., Last, J. A., Wahba, A. J. & Ochoa, S. (1967) *Proc. Nat. Acad. Sci. USA* **57,** 387–394.
30. Nirenberg, M. & Leder, P. (1964) *Science* **145,** 1399–1407.

Proc. Nat. Acad. Sci. USA
Vol. 70, No. 1, pp. 36–40, January 1973

Structural Characteristics of Some Murine RNA Tumor Viruses Studied by Lactoperoxidase Iodination

(radiation leukemia virus/Moloney leukemia virus/mouse mammary tumor virus/gel electrophoresis)

OWEN N. WITTE, IRVING L. WEISSMAN, AND HENRY S. KAPLAN

Departments of Pathology and Radiology, Stanford University School of Medicine, Stanford, California 94305

Contributed by Henry S. Kaplan, October 15, 1972

ABSTRACT **Iodination by the noninvasive enzymatic lactoperoxidase technique has been used to study the enzyme-accessible and enzyme-inaccessible proteins of three oncorna viruses (radiation leukemia virus, Moloney leukemia virus, and mouse mammary tumor virus).**

The number and relative molecular weight of proteins associated with virion preparations purified on sucrose gradients were characterized by scans of Coomassie blue-stained bands after dodecyl sulfate-polyacrylamide gel electrophoresis. Gel scans from the leukemia viruses are similar, each showing six distinct major protein bands on stained gels. The mammary tumor virus proteins by this analysis are not similar to those of the leukemia viruses.

Enzymatic iodination of intact virion preparations led to the solitary labeling of one of the major proteins of each virus—the 80,000-dalton protein of the leukemia viruses and the 52,500-dalton protein of the mammary tumor virus. These are tentatively positioned as surface (enzyme-accessible) moieties in the virions. Disruption of each virus with a nonionic detergent before enzymatic iodination led to the labeling of the remaining stainable bands. The four lower molecular weight bands of the leukemia viruses are tentatively positioned as internal (enzyme-inaccessible) components.

The structural proteins of RNA oncogenic viruses of mice have been studied by various techniques, including gel filtration, isoelectric focusing, and polyacrylamide gel electrophoresis (1–3). Major proteins commonly defined include a high molecular weight (80,000) glycoprotein, presumably present on the viral membrane, and a lower molecular weight (30,000) protein that may possess both intraspecies and interspecies antigenic reactivities (4). The relationship between individual proteins and their location in the virion is of interest, both for the study of viral assembly and to elucidate interrelationships of tumor cell-surface antigens and virion antigens. Electron microscopic analysis has been combined with the isolation of subviral particles to generate tentative models of virion structure (5, 6).

The purposes of this study were:

(*i*) To determine the virion-associated proteins of radiation leukemia virus (RadLV), (a naturally occurring C-type virus consistently recoverable from radiation-induced leukemias and lymphomas of strain C57BL mice (7, 8), now propagated in tissue culture), and to compare it to Moloney leukemia virus (MLV) and mouse mammary tumor virus (MTV).

(*ii*) To use the noninvasive and nondestructive lactoperoxidase iodination technique to label intact virions in order to distinguish enzyme-accessible (external) proteins from enzyme-inaccessible (internal) ones.

Abbreviations; RadLV, Radiation leukemia virus: MLV, Moloney leukemia virus: MTV, mouse mammary tumor virus: PBS, phosphate-buffered saline, pH 7.4.

MATERIALS AND METHODS

RadLV. Supernatant fluids from a RadLV-infected C57BL/Ka embryo fibroblast line, BL-5 (RadLV), were provided by Mr. O. Niwa and Dr. A. Declève of the Department of Radiology. Supernatant fluid from the uninfected BL-5 line of C57BL/Ka fibroblasts was used as a control. All of the BL-5 (RadLV) cells carry RadLV, as determined by immunofluorescence for group-specific antigen and by infectious center counts by the XC plaque assay (9). BL-5 (RadLV) supernatant fluid contains about 5×10^7 focus-forming units/ml, as monitored by the XC assay with newly infected mouse-embryo fibroblasts. BL-5 cells are completely virus-negative when examined by either assay (O. Niwa, A. Declève, and H. S. Kaplan, manuscript in preparation).

MLV was purified from the ascitic fluid of Balb/c mice carrying the transplantable LSTRA Moloney lymphoma (10). These cell-free ascitic supernatants (at dilutions up to 1:1000) were capable of inducing infectious-center plaques on XC cells with primarily infected mouse-embryo fibroblasts (assayed by Dr. A. Declève). Because this source of MLV might well be contaminated with other macromolecular aggregates of similar density, we felt this would be an interesting test of the resolving power of dodecyl sulfate–gel electrophoresis.

MTV was purified from chelated milk of lactating Balb/c mice fostered on strain C3H, and was a gift from Dr. P. Blair, Cancer Research and Genetics Laboratory, University of California, Berkeley.

Virus Purification—RadLV. After clarification of supernatants at 4° (Sorvall RC2B centrifuge, GSA rotor, 11,000 rpm, 15 min) virus was pelleted in a Beckman L3-50 ultracentrifuge, T-15 rotor (14,000 rpm, 2.5 hr). Virus pellets were resuspended in phosphate-buffered saline, 0.15 M NaCl–15 mM NaH_2PO_4–K_2HPO_4 containing 1 mM EDTA (pH 7.4) and spun through discontinuous 45–25% (w/w) sucrose (Swartz–Mann, ultrapure) gradients in PBS–EDTA in a Beckman SW27 rotor at 26,000 rpm for 2 hr. Material sedimenting to the interphase was slowly diluted and layered over 10-ml preformed (45–25%) continuous sucrose gradients and spun for 17 hr at 26,000 rpm in a SW27 rotor. A Hoffer gradient-collecting device was used to separate 0.4-ml fractions. Sucrose densities were measured with a Bausch

and Lomb Abbe 3L refractometer. Protein was monitored by its adsorbance at 280 nm with a Zeiss PMQ II spectrophotometer. Ratios of *A* 280/260 were taken for each gradient fraction to monitor the relative concentrations of protein and nucleic acids.

MLV. After cell removal and clarification, virus was purified by the two sucrose gradient steps described above.

MTV. Infected milk was chelated and skimmed as described by Nowinski *et al.* (11), then processed in sucrose gradients as above.

Concentrates containing each of these viruses shall hereafter be referred to as RadLV, MLV, and MTV, although there is no evidence that these preparations consist exclusively of biologically homogeneous virus particles.

Iodination. Lactoperoxidase iodination (12) was done at room temperature. About 0.4 ml of a sucrose-banded virus preparation was labeled either intact or with prior disruption with 0.2% (v/v) Triton X-100 (Rohm and Haas Chemical Corp.) at 37° for 30 min. $Na^{125}I$ in 0.1 N NaOH (New England Nuclear) was added, to a final concentration of 70–100 μCi/sample. Lactoperoxidase grade B (Calbiochem) was used at 15 μg/ml. Three to four additions of freshly prepared H_2O_2 (10 μl of a 6 μM solution in deionized–distilled H_2O) were made at 10-min intervals. The reaction mixture was extensively dialyzed at 4° to remove free iodide.

Gel Electrophoresis was performed as described by Hung *et al.* (13). Samples were pelleted and resuspended or dialyzed into 0.01 M NaH_2PO_4–Na_2HPO_4 (pH 7.2) buffer containing 1% dodecyl sulfate, 1% 2-mercaptoethanol, and 1 mM EDTA. 50-μl Aliquots were made 6 M with urea (Swartz-Mann, Ultrapure), heated at 37° for 0.5 hr, and then at 100° for 5 min before they were loaded onto gels. 3 μl of 0.05% Bromphenol blue was used as a tracking dye.

Gels were 5-mm diameter, 7% acrylamide (Biorad, electrophoresis purity grade) crosslinked with *N,N'*-methylene bisacrylamide (Eastman Kodak, recrystallized from chloroform), *N,N,N',N'*-tetramethylethylenediamine, and ammonium persulfate. The gel buffer, as well as the upper and lower tank buffer, was 0.1 M NaH_2PO_4–Na_2HPO_4 (pH 7.2) with 0.1% dodecyl sulfate. In two experiments, 10% acrylamide gels with proportional crosslinking were used.

Samples were electrophoresed at 10 mA/gel until the tracking dye had migrated about 8 cm. Gels were stained with Coomassie Brilliant Blue R (Sigma Chemicals), as described by Weber and Osborn (14), and destained at 37° with shaking against 7.5% acetic acid–5% methanol. Gel patterns were recorded with a Gilford model 2000 spectrophotometer equipped with a linear gel-transport system.

Gels containing iodinated proteins were frozen and cut into 1-mm slices with a Hoffer gel fractionator and counted in a Packard model 578 Autogamma spectrophotometer.

Incorporation of [^{3}H]Uridine into RadLV. Both BL-5 and BL-5(RadLV) cell lines were seeded at 2×10^6 cells per 75-cm² flask (Falcon Plastics), and fed with 1 mCi of [^{3}H]-uridine (New England Nuclear) in 20 ml of Minimal Essential Medium (Gibco) with added glutamine and antibiotics. Supernatants were harvested after 3 days and clarified; 5-ml aliquots were analyzed directly on 10-ml preformed linear 60–20% (w/w) sucrose–PBS–EDTA gradients in a SW27 rotor at 26,000 rpm for 3 hr. 10 μl of 0.3-ml fractions were dried on Whatman GF/C filter papers and counted in a toluene-based scintillation fluid.

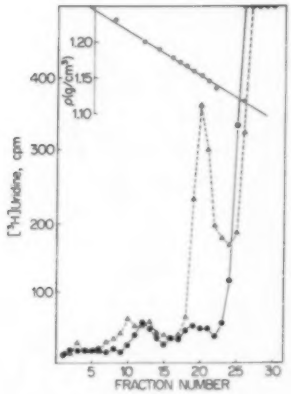

FIG. 1. 5-ml Aliquots of BL-5(RadLV) (△) and BL-5 line (●) culture supernatants labeled with [^{3}H]uridine were centrifuged onto 60–20% sucrose–PBS–EDTA gradients (SW 27 rotor, 26,000, rpm, 3 hr). 10 μl of each 0.3-ml fraction was counted. Sucrose densities were measured with a Bausch and Lomb refractometer.

RESULTS

Internal labeling of RadLV

Labeling with [^{3}H]uridine of a particulate fraction with a density of 1.14–1.15 g/cm³ was demonstrated in supernatant fluids from the BL-5(RadLV) cell line, but not in those from the control BL-5 line, analyzed on continuous sucrose gradients (Fig. 1). Although incorporation is evident, the total number of counts available were not sufficient to use such internally labeled preparations for radioimmune assays or *in vivo* localization studies. Instead, the labeled BL-5(RadLV) supernatant was used as a tracer in the development of a purification scheme for RadLV from large volumes of BL-5(RadLV) culture supernatants and from the *in vivo* virus sources.

Virus purification

Viruses pelleted from large volumes of tissue culture fluid and viruses from *in vivo* sources were first banded on discontinuous sucrose gradients. They were further purified on 45–25% (w/w) continuous sucrose gradients with isopycnic banding to select out a very narrow density range for further structural studies. The results of three such gradients are shown in Fig. 2*a* for RadLV, MLV, and MTV. Sucrose density determinations for all three gradients were the same. Peak densities were: RadLV = 1.145 g/cm³, MLV = 1.154 g/cm³, and MTV = 1.174 g/cm³. Only material from such peak fractions was used for iodination procedures or gel analysis.

Iodination of standard proteins, and both intact and disrupted virus preparations, was performed at room temperature. It was not necessary to remove sucrose or Triton X-100 from reaction mixtures before labeling. Concentrations of up to 1% Triton X-100 did not significantly change the efficiency of labeling of serum albumin by lactoperoxidase iodination. The reaction is specific for tyrosine and histidine residues (12). Self-labeling by lactoperoxidase was not detectable in the presence of substrate protein (unpublished

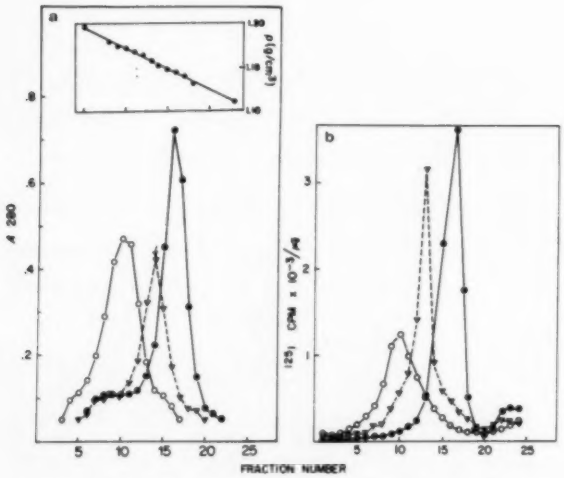

FIG. 2. (*a*) MTV (○), MLV (▽), and RadLV (●) purified on discontinuous 45–25% sucrose gradients were slowly diluted and centrifuged onto linear 45–25% continuous gradients for 17 hr (SW27 rotor, 26,000 rpm). 0.4-ml Fractions were monitored for A_{280}, with no correction for the effects of light scattering. Sucrose density determinations were nearly identical for all six gradients. Average values are shown. (*b*) Aliquots of MTV, MLV, and RadLV from peak fractions (shown above) were labeled with ^{125}I by the lactoperoxidase method, then rebanded as in (*a*). cpm normalized per μg of protein, estimated from *A* 280/260 ratio, with correction for light scattering.

observations, and ref. 15). The reaction is sensitive to changes in available tyrosine and histidine residues, free ^{125}I, enzyme concentration, and—especially—to the concentration of peroxide. To prevent the deleterious oxidizing effects of excess H_2O_2, several additions of a dilute solution were used (see *Methods*). The conditions of reaction and specific activities of protein standards and virus preparations are shown in Table 1.

TABLE 1. *Properties of iodinated protein standards and viral preparations*

	Substrate	μg*	Total cpm-($\times 10^{-6}$) after dialysis	cpm-($\times 10^{-6}$) per 100 μg
1.	Cytochrome *c*	800	7.2	0.9
2.	Bovine 7S Globulin	3000	41.0	1.4
3.	Ovalbumin	250	6.1	2.4
4.	Human serum albumin	770	63.0	8.2
5.	RadLV (intact)	175	2.5	1.4
6.	RadLV (disrupted)	175	6.6	3.8
7.	MLV (intact)	100	3.1	3.1
8.	MLV (disrupted)	100	4.3	4.3
9.	MTV (intact)	200	1.5	0.8
10.	MTV (disrupted)	200	12.3	6.1

The noted amounts of protein standards and virus preparations were reacted with 70 μCi of ^{125}I for protein standards and 100 μCi for each virus preparation, in 0.4 ml of PBS–EDTA buffer with 6 μg of lactoperoxidase. All reaction mixtures received three additions of 10 μl of 6 μM H_2O_2 at 10-min intervals, except MLV preparations, which received four.

* 1–4 by weight, 5–10 from *A* 280/260 after correction for light scattering (24).

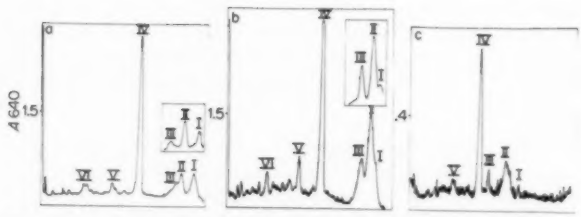

FIG. 3. (*a*) RadLV from peak fraction of a gradient as shown in Fig. 2 disrupted with dodecyl sulfate–urea–mercaptoethanol, then analyzed on a 7% acrylamide gel, stained with Coomassie blue, and scanned with a Gilford model 2000 spectrophotometer with a linear gel transport. Molecular weight estimates for the numbered peaks are given in Table 2. Electrophoresis is from *left* to *right*. *Inset:* scan of the low molecular weight region analyzed on a 10% acrylamide gel. (*b*) MLV prepared as above. (*c*) MTV prepared as above.

Both RadLV and MLV could be labeled to high specific activities by the lactoperoxidase method and still remain intact. Such preparations, rebanded on sucrose gradients, retain the density characteristics of untreated virus (Fig. 2*b*). Rebanded iodinated virus fixed on carbon-coated grids and stained with uranyl acetate (5) showed dense nucleoids enclosed by membrane-like structures. These images were indistinguishable from unlabeled virus (unpublished observations). Prior disruption with a nonionic detergent exposed additional proteins to the labeling process and increased the relative specific activity. MTV was not labeled as well as the other two viruses while it was intact (see below).

Dodecyl sulfate–acrylamide gel electrophoresis

Preparations of RadLV, MLV, and MTV showed distinctive protein spectra when analyzed on 7% acrylamide gels stained with Coomassie blue (Fig. 3). 10% gels were needed to resolve the low molecular weight bands (10,000–15,000) found in the leukemia viruses. Molecular weight estimates for the major proteins shown in Table 2 are the average of at least three determinations, relative to the standard curve plotted in Fig. 4. Many very faint bands, that do not appear on the densitometer scans, were present on all gels, especially in the high molecular weight range above 50,000. These bands may represent aggregates of lower molecular weight forms or specific macromolecules present in virus preparations in very low concentrations.

RadLV and MLV were similar in that most of the Coomassie blue-positive material present was found in four lower molecular weight (10,000–30,000) proteins, generally referred to as those bearing the group-specific antigens (1). However, the relative concentrations and molecular weights of these four macromolecules from RadLV and MLV differ significantly. In the higher molecular weight range, MLV has two major bands, of molecular weights 44,000 and 80,000. These correspond to the glycoproteins reported by other workers (2). The higher molecular weight glycoprotein is believed to be the major protein of the viral membrane (16). RadLV

TABLE 2. *Molecular weight estimates of major viral proteins*

Band no.	MW × 10^{-3}		
	RadLV	MLV	MTV
I	10.5	10.7	26.0
II	13.0	12.0	32.0
III	15.0	14.0	43.0
IV	29.5	29.5	52.5
V	47.0–51.0*	44.0	85.0
VI	77.0–89.0†	80.0	—

* Two close bands.
† Three close bands.

has a doublet in the range 47,000–51,000, and a triplet between 77,000 and 89,000. Preparations of MTV showed one large peak at 52,500, other major bands at 26,000, 32,000, 43,000, and 85,000, and many minor bands in the higher molecular weight region.

Differential enzymatic iodination

A striking difference is seen in the iodination patterns of intact and disrupted virus preparations. Both leukemia viruses label in a very restricted fashion. MLV labels primarily over peak VI, while RadLV labels over the area of the three stained bands at peak VI.

When MLV and RadLV are disrupted before enzymatic iodination with a nonionic detergent known to release internal proteins (17), the iodine label is found on the low molecular weight (10,000–30,000) proteins, as well as the high molecular weight proteins labeled under intact conditions (Fig. 5). The coincidence of radioiodinated peaks and Coomassie blue peaks strengthens the interpretation that these are, in fact, structural proteins; however, Coomassie blue stains molecules other than proteins under certain conditions (18).

Intact preparations of MTV did not label as well as intact leukemia viruses. A comparison of iodinated intact MTV with iodinated disrupted MTV indicates that there may be few available tyrosine residues on the membrane protein. Labeling of the major polypeptide of MTV (52,500) generally

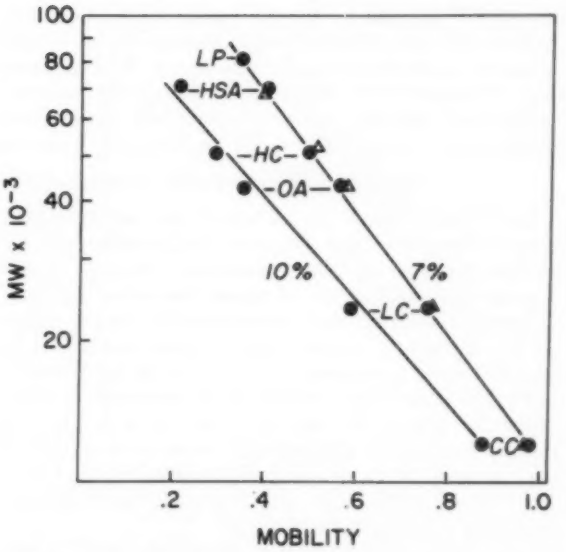

FIG. 4. Semilogarithmic plot of molecular weight (*MW*) against mobility of protein standards on 7 and 10% acrylamide gels, calculated relative to bromphenol blue by the method of Weber and Osborn (14), where:

$$\text{Mobility} = \frac{\text{distance of protein migration}}{\text{length after destaining}} \times \frac{\text{length before staining}}{\text{distance of dye migration}}$$

Abbreviations; Cytochrome *c* (*CC*), Bovine 7S gammaglobulin, light and heavy chains (*LC*, *HC*), ovalbumin (*OA*), human serum albumin (*HSA*), and lactoperoxidase (*LP*). Analyzed from stained gels (●). Analyzed with iodinated proteins (△).

associated with the nucleoid (11) under intact conditions was unexpected, and the presence of disrupted virions was excluded by first rebanding the iodinated virus, followed by analysis of the peak fraction by gel electrophoresis. The result was the same as shown in Fig. 5*c*. Other proteins of

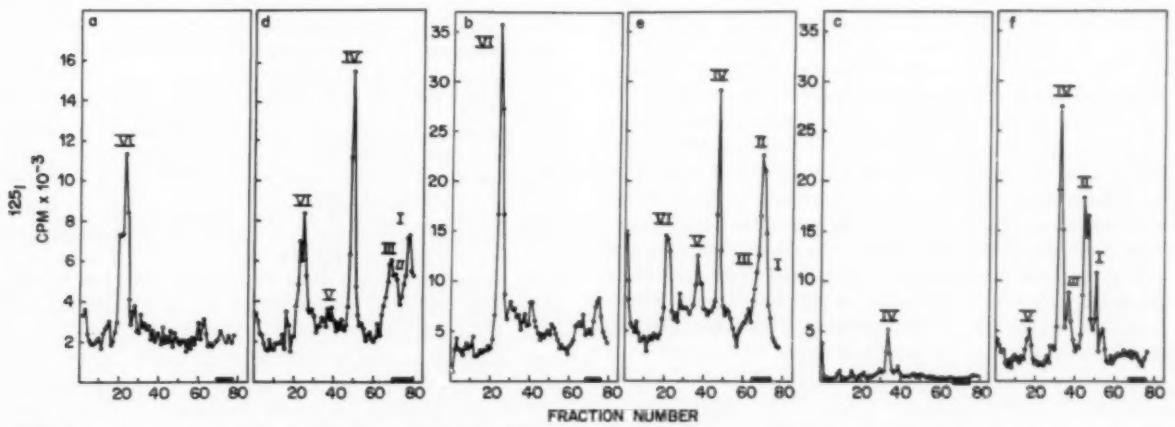

FIG. 5. Isopycnically-banded RadLV iodinated intact (*a*) or after disruption with Triton X-100 (*d*) analyzed on 7% gels after treatment with dodecyl sulfate, mercaptoethanol, and urea. Frozen gels were sliced into 1-mm pieces and counted in a Packard autogamma spectrophotometer. Numbered positions I to VI correspond to those in Fig. 3. Position of bromphenol blue tracking dye is indicated by the *bar*. (*b* and *e*) MLV treated as above. (*c* and *f*) MTV treated as above.

intact MTV (III and V) may be exposed to the iodination reaction, but were not clearly demonstrated in our experiments due to the lower specific activities of these preparations. Disrupted MTV labels comparably to the leukemia viruses, and iodinated peaks correspond well with stained preparations.

DISCUSSION

When studying viruses isolated from *in vivo* sources or from tissue culture, where high precursor labeling efficiency is not possible, one must use an exogenous label. Although various reagents are available (19), enzymatic iodination has many advantages. Reactions may be performed in neutral buffers in the presence of sucrose and nonionic detergents. ^{125}I may be counted in a gamma-ray counter or by liquid scintillation, and is useful as a marker in autoradiographic experiments (20). Due to the large size of lactoperoxidase and its site-specific catalysis, this method is noninvasive and may be used to study topographical characteristics of cell surfaces (21). Stanley and Haslam (22) have also used iodination techniques to study influenza virus.

Preparations of RadLV (tissue culture), MLV (ascitic fluid), and MTV (milk) all contained a limited number of major polypeptides, as evidenced by gels stained with Coomassie blue or iodinated, after disruption with Triton X-100. In all stained preparations there were numerous faint bands, especially in the higher molecular weight region. These may represent aggregates of lower molecular weight forms, since large amounts of virus (25–50 μg per gel) must be analyzed due to the preponderance of one major polypeptide in all three viruses (see Fig. 3). Gel electrophoresis of iodinated viruses showed a significant level of counts throughout the length of the gel (Fig. 5) when viruses were labeled under disrupted, as well as intact, conditions. This uniform distribution of label may represent contamination carried through the purification scheme, host-cell proteins carried by the virus, or virus-specific proteins present in low concentrations (such as viral enzymes).

Enzymatic iodination of intact MTV labeled the major polypeptide (molecular weight 52,500), which has been suggested to be a component of the viral nucleoid (11). This result strongly suggests that portions of at least some copies of this protein are at or near the surface of the virion. The failure to label the putative membrane protein of intact MTV (11) could relate to a lack of available tyrosine residues. Other aminoacid-specific reagents may prove more useful.

Although many similarities among the murine C-type viruses have been described (23), differences within the group have not been extensively studied. RadLV and MLV have quite distinctive protein distributions on stained gels and on unstained gels analyzed for iodinated proteins (see Figs. 3 and 5). Slight differences in the reported number and size of virion-associated proteins reported here and elsewhere are most likely due to differences in viral sources and separation techniques. The solitary labeling of the high molecular weight species (80,000), which coincides with the major glycoprotein reported by other workers (2), gives physical-chemical data to support its electron-microscopic and antigenic role as the major surface protein in the leukemia viruses. The inability to label low molecular weight proteins (10,000–30,000) of RadLV and MLV unless the virions are first disrupted with Triton X-100 presumably places them at internal (core) positions.

We thank O. Niwa and Dr. A. Declève for their performance of virus assays, their help with internal labeling of tissue-culture virus, and for their supplying tissue-culture supernatants for analysis. We thank Drs. D. Sedwick, G. Stark, and W. Robinson for helpful discussions during the course of this study. Supported by Grants IC-63A and IN-32M from the American Cancer Society, CA-03352 and CA-10372 from the National Cancer Institute, and AI-09072 from the National Institutes of Health. O.N.W. is a predoctoral fellow, Medical Scientist Training Program, National Institutes of Health-GM1922. I.L.W. is a Senior Dernham Fellow in Oncology, California Division, American Cancer Society.

1. Nowinski, R. C., Fleissner, E., Sarkar, N. H. & Aoki, T. (1972) *J. Virol.* **9**, 359–366.
2. Moroni, C. (1972) *Virology* **47**, 1–7.
3. Oroszlan, S., Foreman, C., Kelloff, G. & Gilden, R. V. (1971) *Virology* **43**, 665–674.
4. Parks, W. P. & Scolnick, E. M. (1972) *Proc. Nat. Acad. Sci. USA* **69**, 1766–1770.
5. Luftig, R. B. & Kilham, S. S. (1971) *Virology* **46**, 277–297.
6. Sarkar, N. H., Nowinski, R. C. & Moore, D. H. (1971) *J. Virol.* **8**, 564–572.
7. Lieberman, M. & Kaplan, H. S. (1959) *Science* **130**, 387–388.
8. Kaplan, H. S. (1967) *Cancer Res.* **27**, 1325–1340.
9. Rowe, W. P., Pugh, W. E. & Hartley, J. W. (1970) *Virology* **42**, 1136–1139.
10. Fefer, A., McCoy, J. L. & Glynn, J. P. (1967) *Cancer Res.* **27**, 962–967.
11. Nowinski, R. C., Sarkar, N. H., Old, L. J., Moore, D. H., Scheer, D. I. & Hilgers, J. (1971) *Virology* **46**, 21–38.
12. Morrison, M., Bayse, G. & Danner, D. J. (1970) in *Biochemistry of the phagocytic process*, ed. Schultz, J. (North-Holland Publ. Co., Amsterdam), pp. 51–66.
13. Hung, P. P., Robinson, H. L. & Robinson, W. S. (1971) *Virology* **43**, 251–266.
14. Weber, K. & Osborn, M. (1969) *J. Biol. Chem.* **244**, 4406–4412.
15. Marchalonis, J. J. (1969) *Biochem. J.* **113**, 299–305.
16. Duesberg, P. H., Martin, G. S. & Vogt, P. K. (1970) *Virology* **41**, 631–646.
17. Gerwin, B. I., Todaro, G. J., Zeve, V., Scolnick, E. M. & Aaronson, S. A. (1970) *Nature* **228**, 435–438.
18. Dreyer, W. J., Papermaster, D. S. & Kühn, H. (1972) *Ann N.Y. Acad Sci.* **195**, 61–74.
19. Hoelzl Wallach, D. F. (1972) *Biochim. Biophys. Acta* **265**, 61–83.
20. Perkins, W. D., Karnovsky, M. J. & Unanue, E. R. (1972) *J. Exp. Med.* **135**, 267–276.
21. Poduslo, J. F., Greenberg, C. S. & Glick, M. C. (1972) *Biochemistry* **11**, 2616–2621.
22. Stanley, P. & Haslam, E. (1971) *Virology* **46**, 764–773.
23. Nowinski, R. C., Old, L. J., Sarkar, N. H. & Moore, D. H. (1970) *Virology* **42**, 764–773.
24. Layne, E. (1957) in *Methods in Enzymology*, eds. Colowick, S. & Kaplan, N. O. (Academic Press, New York), Vol. III, pp. 447–553.

Proc. Nat. Acad. Sci. USA
Vol. 70, No. 1, pp. 41–45, January 1973

Protein Initiation in Eukaryotes: Formation and Function of a Ternary Complex Composed of a Partially Purified Ribosomal Factor, Methionyl Transfer RNA$_f$, and Guanosine Triphosphate

(binding assay/L-cells/ribosome subunits/protein inhibitors)

DANIEL H. LEVIN, DAVID KYNER, AND GEORGE ACS

Institute for Muscle Disease, Inc., 515 East 71st Street, New York, N.Y. 10021

Communicated by Norton D. Zinder, August 10, 1972

ABSTRACT **A protein factor contained in a 1 M KCl extract of L-cell ribosomes and partially purified by chromatography on DEAE-cellulose forms a specific ternary complex with rat-liver Met-tRNA$_f$ and GTP. The complex is measured by its quantitative retention on nitrocellulose membranes. Complex assembly is optimal at 100 mM KCl and 0.2 mM $MgCl_2$, and is independent of mRNA and of ribosomes. The GTP requirement can be replaced over 65% by its methylene analogue GDPCH$_2$P, indicating that GTP hydrolysis is not involved. Complex formation is inhibited by 10 μM aurintricarboxylic acid, but is unaffected by 100 μM pactamycin, 100 μM fusidic acid, or by excess uncharged methionine tRNA$_f$. The ternary complex is relatively stable and appears at the void volume during filtration on Sephadex G-100. At 1–3 mM $MgCl_2$ and in the presence of other factors, the ternary complex is implicated in protein initiation by (*i*) its capacity to bind to the 40S ribosomal subunit to form a 48S complex; and (*ii*) the subsequent association of the 48S complex with a 60S subunit to form a functional "80S complex."**

There is considerable evidence to suggest that in eukaryotes, the rate-determining step in protein synthesis occurs during the initiation phase of translation. Such a rate-limiting step has been observed in such diverse tissues as cells in mitosis (1), muscles of diabetic animals (2), livers of fasted animals (3, 4), as well as in cell cultures exposed to aminoacid-deficient medium (5, 6), temperature changes (7), and alterations in sodium–potassium ratios (8). Other studies in both prokaryotes and eukaryotes indicate that the sequence of events leading to the formation of an 80S initiation complex is mediated by the stepwise participation of specific ribosome factors (9–14). Consequently, the first steps in the initiation sequence are of particular importance if it is assumed that they represent logical sites for the operation of regulatory controls. Recent studies in prokaryotic systems have reported that one of the earliest steps in the initiation sequence is the formation of a ternary complex containing the ribosome initiation factor IF-2, fMet-tRNA$_f$, and GTP (15, 16).

In this report, we describe the *in vitro* formation of a eukaryotic ternary complex with similar properties, composed of a partially purified ribosome factor from L-929 mouse fibroblasts (L-cells), rat-liver Met-tRNA$_f$, and GTP. Preliminary data were presented in a previous communication (17). Complex formation is specific for initiator Met-tRNA$_f$ and GTP, and is independent of mRNA and ribosomes. The complex is implicated in the initiation process by its capacity to bind 40S ribosomal subunits, which in turn are incorporated into functional 80S complexes.

METHODS

Chromatography of a Ribosomal Extract on DEAE-Cellulose. A post-mitochondrial extract of L-cells was centrifuged overnight at 0° through a deep cushion of 68% sucrose in TKM buffer (18). The pellet was suspended in 10 mM Tris·HCl (pH 7.5)–250 mM sucrose–0.1 mM EDTA–1 mM dithiothreitol to 5 mg/ml of ribosomes and brought to 1 M KCl. The suspension was slowly stirred for 1 hr at 13°, then centrifuged at 0° for 1 hr at 180,000 × *g*. The top three-fourths of the supernate was dialyzed at 4° for 2 hr against 30 mM Tris·HCl (pH 7.5)–100 mM KCl–1 mM $MgCl_2$–2 mM dithiothreitol (TKMD buffer). Debris was removed by low-speed centrifugation. About 10 mg of dialyzed protein was applied to a DEAE-cellulose column (0.9 cm × 20 cm) previously equilibrated in the same buffer, but containing 50 mM KCl. Four protein fractions were eluted by a discontinuous gradient in TKMD buffer with KCl concentrations of 0.05 M (*A*), 0.1 M (*B*), 0.2 M (*C*), and 0.3 M (*D*). Effluent fractions were monitored at 280 nm to insure separation. Peak fractions were pooled and concentrated by ammonium sulfate precipitation; protein was dissolved in TKMD buffer containing 0.2 M KCl and dialyzed at 4° for 90 min against the same buffer–KCl. Debris was removed as before and the extract was stored at −80° in small aliquots. Under these conditions, fraction *C* maintained its activity for several months without significant loss.

Treatment of Ribosomal Subunits with 1 M KCl. The isolation and separation of L-cell 40S and 60S subunits in 0.5 M KCl have been described (18). For treatment of these particles with 1 M KCl, 20 A_{260} units of each subunit were diluted to 1 ml in 50 mM triethanolamine·HCl (pH 7.6)–1 M KCl–1.8 mM $MgCl_2$ (increased to 3 mM for 60S subunits). The 40S suspension was incubated at 27° for 40 min and the 60S suspension at 18° for 5 min. Each suspension was then centrifuged at 18° through separate 30-ml 10–30% sucrose density gradients in 50 mM triethanolamine·HCl (pH 7.6)–500 mM KCl–5 mM $MgCl_2$ for 5 hr at 64,000 × *g* (18, 19). The subunit peaks were collected and stored as described for the 0.5 M KCl subunits (18).

Preparation of Labeled Aminoacyl-tRNAs. Rat-liver tRNA$_f^{Met}$ and tRNA$_m^{Met}$ were separated by chromatography of bulk tRNA on benzoylated DEAE (BD)-cellulose (18, 20). tRNA$_f^{Met}$ was charged with [^{3}H]methionine (4 Ci/mmol) or [^{35}S]methionine (8 Ci/mmol) with S100 extracts free of

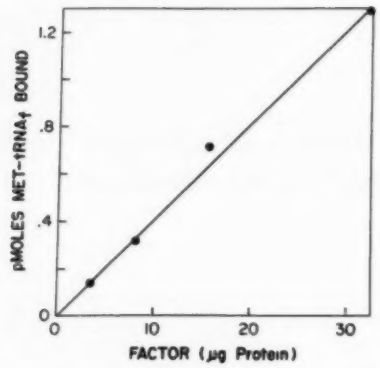

FIG. 1. Dependence of ternary complex formation on factor *C* concentration. Reaction mixtures and assay conditions are as described in Table 1, except that 7 pmol of [^{3}H]Met-tRNA$_f$ (1200 cpm/pmol) was present in all incubations. Factor *C* was added as indicated. Each value on the curve is an average of two determinations, and is corrected for the amount of label (0.03 pmol) bound in the absence of *C*.

endogenous tRNA from *Escherichia coli* strain MRE; tRNA$_m^{Met}$ and purified rat-liver tRNA^{Phe} were charged with [^{3}H]methionine (4 Ci/mmol) and [^{3}H]phenylalanine (11 Ci/mmol), respectively, by crude L-cell synthetases free of endogenous tRNA.

MATERIALS

Reticulocyte supernatant factors EF-T$_1$ and EF-T$_2$ were gifts of Drs. I. Krisco and D. Richter, Rockefeller University (New York, N.Y.). Fusidic acid was a gift of Drs. A. L. Haenni and F. Lipmann of Rockefeller University. Bulk rat-liver tRNA and purified rat-liver tRNA^{Phe} were gifts of Drs. D. Grünberger and I. B. Weinstein of Columbia University (New York, N.Y.). Pactamycin was donated by the National Products Section of the National Cancer Institute (Bethesda, Md.). Aurintricarboxylic acid was obtained from Sigma Chemical Co. (St. Louis, Mo.). [^{3}H]Methionine and [^{3}H]-phenylalanine were purchased from New England Nuclear Corp. (Boston, Mass.), and [^{35}S]methionine was from Amersham/Searle (London).

TABLE 1. *Specific binding of Met-tRNA$_f$ to a ribosomal protein fraction*

Fraction	pmol of aminoacyl-tRNA bound		
	Met-tRNA$_f$	Met-tRNA$_m$	Phe-tRNA
A	0.03	0.03	1.31
B	0.05	0.09	0.33
C	0.92	0.17	0.26
D	0.10	0.04	0.19
Unfractionated	0.22	0.45	4.51

Incubations contained the following components in a final volume of 50 μl: 20 mM Tris·HCl (pH 7.5), 100 mM KCl, 0.2 mM $MgCl_2$, 0.1 mM GTP, 1 mM dithiothreitol, and—where indicated—5 pmol of [^{3}H]Met-tRNA$_f$ (1200 cpm/pmol), [^{3}H]-Met-tRNA$_m$ (1200 cpm/pmol), or 5 pmol of [^{3}H]Phe-tRNA (2900 cpm/pmol). Ribosomal protein fractions obtained by DEAE-cellulose fractionation (*Methods*) were added (where indicated) as follows: 14 μg of fraction *A*, 12 μg of fraction *B*, 17 μg of fraction *C*, 14 μg of fraction *D*, and 27 μg of unfractionated extract. Incubation was at 37° for 5 min. The reaction was stopped by dilution with 3 ml of cold 20 mM Tris·HCl (pH 7.5)–100 mM KCl–0.2 mM $MgCl_2$, and immediately collected on a nitrocellulose membrane (0.45 μm, Millipore Filter Corp.) followed by three rinses of 3 ml each; only the binding complexes were retained. The membrane was dried and counted in Liquiflor (New England Nuclear Corp.) in a Nuclear–Chicago scintillation counter.

RESULTS

Specific Binding of Met-tRNA$_f$ to a Ribosomal Protein Factor. A crude 1 M KCl extract of L-cell ribosomes (see *Methods*) was fractionated on DEAE-cellulose into four protein fractions by a discontinuous gradient with different concentrations of KCl (Table 1). Each protein fraction was tested for its ability to bind rat-liver Met-tRNA$_f$, Met-tRNA$_m$, and Phe-tRNA. The extent of binding was measured by the quantitative retention of the binding complex on nitrocellulose membranes. Fraction *C*, which eluted at 0.2 M KCl, displayed a selective affinity for Met-tRNA$_f$ compared to Met-tRNA$_m$ and Phe-tRNA (Table 1). Assembly of the complex was dependent upon GTP; on that basis, it was designated a ternary complex with the tentative composition [*C*–Met-tRNA$_f$–GTP]. Optimal binding of Met-tRNA$_f$ was obtained at 150 mM KCl and 0.2 mM $MgCl_2$, a concentration that contrasts with the high $MgCl_2$ concentration (5 mM) used for the homologous prokaryotic ternary complex (15, 16). The efficient binding of Phe-tRNA by the unfractionated extract may have been due to Phe-tRNA synthetase, which is present in high concentration in the preparation and is eluted primarily in fraction *A* (Table 1). In this regard, it should be noted that fraction *C*, which binds Met-tRNA$_f$, was free of Met-tRNA synthetase activity. The amount of ternary complex formed was proportional to the concentration of fraction *C* (Fig. 1). At limiting Met-tRNA$_f$ concentrations, all of the substrate was bound.

Effect of Inhibitors and Specificity of GTP. The addition of excess uncharged tRNA$_f^{Met}$ or tRNA$_m^{Met}$ did not interfere with the binding of Met-tRNA$_f$, indicating that the methionyl moiety is required for recognition by fraction *C* (Table 2). Complex formation was essentially unaffected by 0.1 mM fusidic acid or 0.1 mM pactamycin, but was 80%

TABLE 2. *Effect of uncharged tRNA and inhibitors on ternary complex formation*

Additions	pmol Met-tRNA$_f$ bound
—	1.71
tRNA$_f^{Met}$	1.69
tRNA$_m^{Met}$	1.65
ATA (0.1 mM)	0.06
ATA (0.01 mM)	0.32
Pactamycin (0.1 mM)	1.80
Fusidic acid (0.1 mM)	1.58

Incubation conditions and components are as described in Table 1, except that 7 pmol of [^{3}H]Met-tRNA$_f$ (1200 cpm/pmol) and 27 μg of fraction *C* were present in all incubations. In addition, uncharged tRNA$_f^{Met}$ (0.1 A_{260} units), uncharged tRNA$_m^{Met}$ (0.1 A_{260} units), aurintricarboxylic acid (*ATA*), pactamycin, and fusidic acid were added as indicated.

inhibited by 0.01 mM aurintricarboxylic acid emphasizing the selectivity of aurintricarboxylate inhibition in this step (Table 2). Examination of the GTP requirement revealed that neither ATP nor GDP could substitute for GTP; however, the methylene analogue of GTP, $GDPCH_2P$, was 65% effective in replacing GTP, indicating that complex assembly did not involve GTP hydrolysis (Table 3).

Inactivity of Supernatant Elongation Factors. Fraction *C* also contained traces of the supernatant elongation factors, EF-T_1 and EF-T_2, which were contaminants of the 1 M KCl extract of the ribosomes. In order to eliminate the possibility that complex formation was due to the elongation factors, we examined the effect of highly purified EF-T_1 and EF-T_2 on Met-$tRNA_f$ binding to fraction *C* (Table 4). Alone or in combination, the eukaryotic supernatant factors did not replace fraction *C*, nor did they interfere with ternary complex formation (Table 4). Consequently, the complex is unrelated to the ternary complexes containing supernatant elongation factors derived from bacteria (21–23) and calf brain (24).

Molecular Sieve Filtration of the Ternary Complex. Analysis by gel filtration on Sephadex G-100 of the ternary complex prepared with [^{3}H]Met-$tRNA_f$ and [γ-^{32}P]GTP revealed a profile with a peak at the void volume that contained both labeled components (Fig. 2). The position of the complex indicated a molecular weight of at least 100,000. In the absence of either GTP or fraction *C*, no complex was formed. The impurity of fraction *C* and a low level binding of [γ-^{32}P]-GTP in the absence of Met-$tRNA_f$ (not shown) does not permit a stoichiometric analysis of the reaction components. The appearance of [γ-^{32}P]GTP in the complex (Fig. 2) is in accord with the observation that GTP is not hydrolyzed during complex formation (see Table 3). Similar results were reported for the prokaryotic ternary complex (15, 16).

Binding of Ternary Complex to Ribosomes. In the course of studies on a possible functional role for the ternary complex during protein initiation, we found that at 1.5 mM $MgCl_2$, the labeled complex binds to 40S ribosomal subunits previously stripped of initiation factors with 1 M KCl; the new complex sediments to the 48S region in sucrose density gradients (Fig. 3*b*). Binding does not occur with similarly-treated 60S subunits alone (Fig. 3*c*). However, addition of 60S ribosomal subunits to the 48S assembly at 3 mM $MgCl_2$ produces a further shift of label to the 80S region (Fig. 3*d*). No binding of label or subsequent shifts take place if the first incubation for ternary complex formation is omitted. The two stepwise shifts are dependent upon the presence of additional ribosomal factors, but are independent of mRNA. This phenomenon resembles an mRNA-independent binding of Met-

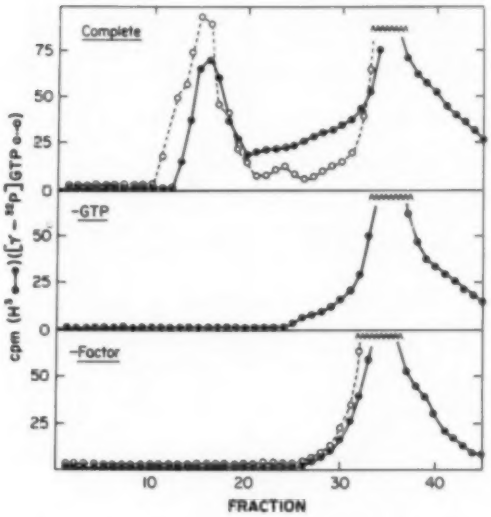

FIG. 2. Profile of ternary complex on Sephadex G-100. Three 50-μl reaction mixtures were prepared as described in Table 1, except that all three contained 5 pmol of [^{3}H]Met-$tRNA_f$ (1200 cpm/pmol). In addition, two incubations contained 0.1 mM [γ-^{32}P]GTP (1800 cpm/pmol) (*top*, *bottom* panels), and in one incubation GTP was omitted (*middle*); 27 μg of fraction *C* was present in two incubations (*top*, *middle*) and omitted in one incubation (*bottom*). After 5 min at 37°, the incubations were diluted to 1 ml with cold 20 mM Tris·HCl (pH 7.5)–100 mM KCl–0.2 mM $MgCl_2$, loaded on separate columns of Sephadex G-100 (0.9 cm × 24 cm), and collected in 0.4-ml fractions during filtration in the same buffer. Aliquots were counted directly in Bray's scintillation solution (27) in a Nuclear-Chicago scintillation counter with voltage settings adjusted for double-label counting [^{3}H/^{32}P] where required (*top* and *bottom*). The intact ternary complex eluted at the void volume (*top*). [^{3}H]Met-$tRNA_f$ (●——●); [γ-^{32}P]GTP (O- - -O).

TABLE 3. *Dependence of ternary complex formation on GTP*

Nucleotide	pmol Met-$tRNA_f$ bound
—	0.04
GTP	0.97
GDP	0.04
$GDPCH_2P$*	0.63
ATP	0.12
GTP + $GDPCH_2P$	0.98

Incubation conditions and components are as described in Table 1, except that 5 pmol of [^{3}H]Met-$tRNA_f$ (1200 cpm/pmol) and 17 μg of fraction *C* were present in all reaction mixtures. In addition, 0.3 mM GDP, 0.3 mM $GDPCH_2P$, and 0.5 mM ATP were added where indicated.

* β,γ-methylene guanosine triphosphate.

TABLE 4. *Comparison of ribosome factor with EF-T_1 and EF-T_2*

Enzyme fraction	pmol Met-$tRNA_f$ bound
C	2.01
EF-T_1	0.03
EF-T_2	0.13
EF-T_1 + EF-T_2	0.12
C + EF-T_1	2.03
C + EF-T_2	1.96
C + EF-T_1 + EF-T_2	2.00

Incubation conditions and components are as described in Table 1, except that 7 pmol of [^{3}H]Met-$tRNA_f$ (1200 cpm/pmol) was present in all of the incubations. In addition, 27 μg of fraction *C*, 2.1 μg of reticulocyte EF-T_1, and 3.2 μg of reticulocyte EF-T_2 were added as indicated.

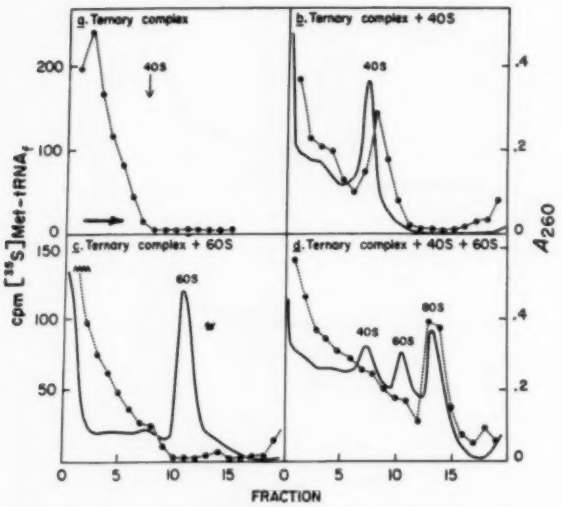

FIG. 3. Sucrose density gradient profiles of initiation complexes. Formation of the ternary complex and binding to ribosomes were performed in three consecutive incubation steps; all contained 20 mM Tris·HCl (pH 7.5), 0.4 mM GTP, and 1 mM dithiothreitol throughout. *Step 1:* additions for ternary complex formation in 25 μl were 4 pmol of [^{35}S]Met-tRNA$_f$ (5900 cpm/pmol), 100 mM KCl, 12 μg of fraction *C*, incubation was at 37° for 5 min (*a*). *Step 2:* additions and changes were 0.25 A_{260} units of 40S subunits (or 0.5 units of 60S subunits), 1.5 mM $MgCl_2$, 80 mM KCl, and 15 μg of unfractionated ribosomal extract in a final volume of 35 μl, incubation was 5 min at 37° (*b*, *c*). *Step 3:* additions and changes were 0.5 A_{260} units of 60S subunits, 3 mM $MgCl_2$, 52 mM KCl in a final volume of 50 μl, incubation was 5 min at 37°. The sedimentation profile of each incubation stage was determined in 5-ml sucrose gradients (5–20%) in the same buffer–salt mixtures used in the corresponding incubation. Centrifugation was at 130,000 × *g* for 55 min at 14°. The gradients were monitored at A_{260} in an ISCO fractionator, and fractions were collected dropwise. Each fraction of each gradient was diluted in the corresponding buffer–salt mixture, collected on nitrocellulose membranes, and counted as described in Table 1. [^{35}S]Met-tRNA$_f$ (●– – –●); A_{260} (——).

tRNA$_f$ at elevated $MgCl_2$ concentrations (8–16 mM) that was observed (18) with untreated subunits that retained their initiation factors. Although active in protein synthesis, such subunits imposed obvious restrictions upon detailed studies of the initiation sequence *in vitro*. From the current studies, it is apparent that stripped subunits, which depend on exogenous factors and are effective at low $MgCl_2$ concentrations, permit a stepwise analysis of the initiation process.

DISCUSSION

In the studies presented here, a partially purified ribosome factor, designated *C*, is implicated in eukaryotic protein initiation by its ability to specifically bind Met-tRNA$_f$ in a ternary complex with GTP. The possibility that factor *C* represents a ribosomal binding site for initiator Met-tRNA is supported by stepwise formation of 48S and 80S complexes that are dependent upon prior assembly of the ternary complex [*C*–Met-tRNA$_f$–GTP] as follows:

(*a*) C + Met-tRNA$_f$ + GTP → [*C*–Met-tRNA$_f$–GTP].

(*b*) [*C*–Met-tRNA$_f$–GTP] + 40S + factor(s) + GTP → (48S complex).

(*c*) (48S complex) + 60S + factor(s) + GTP → (80S complex).

The 80S complex formed by this sequence is functional to the extent that in the presence of puromycin, the methionyl moiety is quantitatively released to form methionyl-puromycin. The specific nature of the factor and GTP requirements in the proposed scheme is still under investigation. Preliminary data indicate that each step in the sequence is mediated by separate factors; in addition, the GTP requirement in reactions (*b*) and (*c*), which has been demonstrated to some extent in other eukaryotic systems (10–12, 25, 26), has also been confirmed (unpublished data).

An interesting anomaly of the above scheme is the apparent absence of an mRNA requirement in the sequential formation of the 80S complex. Since mRNA is an essential component of the true 80S initiation complex, the possibility cannot be excluded that the factor or subunit preparations contain trace amounts of mRNA fragments. However, preliminary data from studies in progress indicate that a factor-dependent addition of exogenous viral mRNA to the sequence considerably augments binding of Met-tRNA$_f$ in an [80S–Met-tRNA$_f$–mRNA] initiation complex. An analysis of the sequence to determine in which step mRNA was inserted revealed two essential features that support the contention that the ternary complex is involved in protein initiation: (*i*) in the stepwise sequence leading to the formation of the 80S initiation complex, no assembly of ribosomal complexes occurred without the prior formation of the ternary complex; and, (*ii*) the binding of the ternary complex to the 40S subunit preceded the incorporation of mRNA (unpublished data).

It is not clear if the entire ternary complex binds to the 40S subunit in reaction (*b*), or if the complex acts primarily as a carrier for initiator Met-tRNA$_f$. However, the similarity of the eukaryotic complex to the prokaryotic ternary complex [IF-2–fMET-tRNA$_f$–GTP] of Rudland *et al.* (15) and of Lockwood *et al.* (16) is manifest. If a mechanism analogous to the prokaryotic complex is assumed to occur in eukaryotes, it is probable that the eukaryotic ternary complex binds intact to the 40S subunit.

Addendum. After submission of this manuscript for publication, evidence for a similar eukaryotic ternary complex [factor–Met-tRNA$_f$–GTP] with a factor derived from reticulocyte ribosomes was published by Chen, Y. C., Woodley, C. L., Bose, K. K., & Gupta, N. K. (1972) *Biochem. Biophys. Res. Commun.* **48,** 1–9.

We thank Miss Gilda Castillo for excellent technical assistance. These studies were supported by the National Institutes of Health (CA-08751), the American Cancer Society (NP-36 I), and the Muscular Dystrophy Associations of America.

1. Fan, H. & Penman, S. (1970) *J. Mol. Biol.* **50,** 655–670.
2. Stirewalt, W. S., Wool, I. G. & Cavicchi, P. (1967) *Proc. Nat. Acad. Sci. USA* **57,** 1885–1892.
3. Fleck, A., Shepherd, J. & Munro, H. N. (1965) *Science* **150,** 628–629.
4. Wilson, S. H. & Hoagland, M. B. (1967) *Biochem. J.* **103,** 556–566.
5. Vaughan, M. A., Pawlowski, P. J. & Forchhammer, J. (1971) *Proc. Nat. Acad. Sci. USA* **68,** 2057–2061.

6. Van Venrooij, W. J. W., Henshaw, E. C. & Hirsh, C. A. (1972) *Biochim. Biophys. Acta* **259**, 127–137.
7. McCormick, W. & Penman, S. (1969) *J. Mol. Biol.* **39**, 315–333.
8. Christman, J. K., Reiss, B., Levin, D. & Kyner, D. (1972) *Fed. Proc.* **31**, 849.
9. Wahba, A. J., Iwasaki, K., Miller, M. J., Sabol, S., Sillers, M. A. G., & Vasquez, C. E. (1969) *Cold Spring Harbor Symp. Quant. Biol.* **34**, 291–300.
10. Heywood, S. M. & Thompson, W. C. (1971) *Biochem. Biophys. Res. Commun.* **43**, 470–475.
11. Weeks, D. P., Verma, D. P. S., Seal, S. N. & Marcus, A. (1972) *Nature* **236**, 167–168.
12. Shafritz, D. A., Laycock, D. G., Crystal, R. G. & Anderson, W. F. (1971) *Proc. Nat. Acad. Sci. USA* **68**, 2246–2251.
13. Crystal, R. G. & Anderson, W. F. (1972) *Proc. Nat. Acad. Sci. USA* **69**, 706–711.
14. Thach, S. S. & Thach, R. E. (1971) *Nature* **229**, 219–221.
15. Rudland, P. S., Whybrow, W. A. & Clark, B. F. C. (1971) *Nature* **231**, 76–78.
16. Lockwood, A. H., Chakraborty, P. R. & Maitra, U. (1971) *Proc. Nat. Acad. Sci. USA* **68**, 3122–3126.
17. Levin, D. H. & Kyner, D. (1971) *Fed. Proc.* **30**, 1289.
18. Levin, D. H., Kyner, D. & Acs, G. (1972) *Proc. Nat. Acad. Sci. USA* **69**, 1234–1238.
19. Blobel, G. & Sabatini, D. (1971) *Proc. Nat. Acad. Sci. USA* **68**, 390–394.
20. Leis, J. P. & Keller, E. B. (1970) *Biochem. Biophys. Res. Commun.* **40**, 416–421.
21. Gordon, J. (1967) *Proc. Nat. Acad. Sci. USA* **58**, 1574–1578.
22. Shorey, R. L., Ravel, J. M., Garner, C. W. & Shive, W. (1969) *J. Biol. Chem.* **244**, 4555–4564.
23. Ono, Y., Skoultchi, A., Klein, A. & Lengyel, P. (1968) *Nature* **220**, 1304–1307.
24. Moon, H. M. & Weissbach, H. (1972) *Biochem. Biophys. Res. Commun.* **46**, 254–262.
25. Wettenhall, R. E. H., Leader, D. P. & Wool, I. G. (1971) *Biochem. Biophys. Res. Commun.* **43**, 994–1000.
26. Shafritz, D. A., Prichard, P. M., Gilbert, J. M., Merrick, W. C. & Anderson, W. F. (1972) *Proc. Nat. Acad. Sci. USA* **69**, 983–987.
27. Bray, G. A. (1960) *Anal. Biochem.* **1**, 279–285.

Proc. Nat. Acad. Sci. USA
Vol. 70, No. 1, pp. 46–49, January 1973

Malignant Transformation of BHK_{21} Clone 13 Cells *In Vitro* by Nitrosamines—A Conditional State

(*in vitro* chemical carcinogenesis/transformed phenotype conditioned by high temperature)

GIAMPIERO DI MAYORCA*, MELVIN GREENBLATT†, THOMAS TRAUTHEN*, ARTHUR SOLLER*, AND ROBERTO GIORDANO*

University of Illinois at the Medical Center, Chicago, Ill. 60680; and The Eppley Institute for Research in Cancer, University of Nebraska, Medical Center, Omaha, Neb. 68105

Communicated by Hewson Swift, September 19, 1972

ABSTRACT **All the BHK_{21} Clone 13 cells transformed by dimethylnitrosamine or nitrosomethylurea, and a single "spontaneously" transformed clone obtained in our laboratory, exhibit a conditional state of the transformed phenotype. Upon growth at 38.5°, they have a transformed phenotype (clonal morphology and the ability to plate in soft agar); when grown at 32°, their phenotype is normal. The conditional state of these cells, however, does not extend to their growth characteristics; their plating efficiency at the two temperatures in liquid medium is similar. Conversion from the normal to the transformed phenotype and the reverse is possible by temperature shifts. A working hypothesis is proposed suggesting that this phenomenon may be caused by a temperature-sensitive mutation of a cellular gene whose product is responsible for maintaining the normal phenotype. The high temperature would then affect either the synthesis or the function of the protein carrying the temperature-sensitive alteration and, as a consequence, the transformed phenotype would be expressed.**

The *in vitro* malignant transformation of cells by chemical carcinogens has been reported by several investigators. However, the data available were obtained either by exposure of primary or secondary mass cultures to the chemicals for long periods of time, thereby allowing selection, through toxicity and a growing advantage of resistant variants (1–6), or, in other instances, aneuploid permanent cell lines were used (7–10). A more desirable test for *in vitro* carcinogenesis would involve the use of a standardized cell line (e.g., BHK_{21} Clone 13, 3T3, Balb/c 3T3, etc.), exposure of suspended cells to the chemicals for a brief period of time (10–60 min), and finally plating in soft agar for assay of malignant transformants. This assay, amply used for viral transformation, is the only one that allows a reasonable quantification of transformation frequency. Recently, in our laboratory, we were able to develop such a test fashioned after the well-known technique of MacPherson and Montagnier (11) for induction of malignant transformation by polyoma virus. The test involves the use of BHK_{21} Cl 13 cells. Brief exposure of a suspension of cells to various concentrations of dimethylnitrosamine (Me_2N) or nitrosomethylurea (NMeU) was followed by plating in soft agar. After 20–60 min of exposure to either of the two chemicals at a fixed concentration, the transformation frequency was 6×10^{-4}. The development of the test, the quantitative aspect of it, experiments with other chemical carcinogens, and the dose–response relationship will be reported elsewhere. In this paper, we report a common characteristic that was found for all clones of BHK_{21} Cl 13 cells obtained by transformation either by Me_2N or NMeU, and of a "spontaneously" transformed clone. So far, in our laboratory, the expression of the transformed phenotype for all these clones is dependent upon a high incubation temperature (38.5°), whereas incubation at low temperature (32°) allows the normal phenotype to be expressed.

Present address: * University of Illinois at the Medical Center, Department of Microbiology, P. O. Box 6998, Chicago, Ill. 60680. † National Cancer Research Laboratory, University of Otago, Medical School, Denedin, New Zealand.

Abbreviations: Me_2N, dimethylnitrosamine; NMeU, nitrosomethylurea.

MATERIALS AND METHODS

Tissue Culture. Standard plastic tissue culture dishes were used in all experiments. TD buffer [0.8% NaCl–0.038% KCl–0.01% Na_2HPO_4–0.3% Tris·HCl (Sigma 7-9) (all w/v)] was adjusted to pH 7.0 with 1 N HCl.

BHK_{21} Cl 13 Cells from an early passage‡ were kept frozen in liquid nitrogen. For use in experiments, cells were quickly defrosted and passed 2–3 times to obtain the necessary numbers.

Media. Eagle's standard medium with 4-times concentrated amino acids and vitamins (Dulbecco Medium), with 10% tryptose phosphate broth and 10% calf serum, was used in all experiments. Soft agar suspension medium with 10% calf serum (11) was used in the agar-plating experiments. Incubation was in 10% CO_2 in air and 99.5% humidity.

Test for Malignant Transformation. BHK_{21} Cl 13 cells were harvested from semi-confluent monolayers by trypsinization, centrifuged, and suspended by pipetting to insure single-cell dispersion. 10^6 Cells in 1 ml were exposed to several concentrations of chemical for various periods of time. After exposure, the cells were washed with medium, suspended, and plated in liquid medium at various concentrations to assess plating efficiency and survival. In general, 4×10^4 cells were plated in soft agar at the two temperatures. After incubation (14 days at 38.5° and 28 days at 32°), colonies were counted and the percent of transformation was obtained (only malignantly transformed cells give rise to

‡ Between 15th and 20th serial subculture from tissue of origin.

colonies in soft agar at the critical agar concentration of 0.3%).

Transformed colonies were individually harvested and grown both at 38.5° and 32° for two passages and frozen in liquid nitrogen.

Chemical Carcinogenesis. Dimethylnitrosamine and nitrosomethylurea were kindly provided by Dr. W. Lijinsky. Dimethylnitrosamine

Dimethylnitrosamine $\begin{matrix}CH_3\\CH_3\end{matrix}\!\!>\!N\!-\!N\!=\!O$

is a well-known very potent chemical carcinogen. It must be metabolically activated to a reactive metabolite. This metabolite, yet to be identified, probably is an alkylating agent.

Nitrosomethylurea $CH_3\!-\!N(-N=O)\!-\!C(=O)\!-\!NH_2$

is a direct alkylating agent and potent carcinogen. Dimethylnitrosamine was used in the following concentrations: 1 mg per 10^6 cells per ml for 20 min and 25 mg per 10^6 cells per ml for 1 hr in TD buffer. Nitrosomethylurea was dissolved in 5 mM citrate buffer (pH 5). Suitable amounts were added to the cells suspended in TD buffer to obtain 1, 5, or 50 μg per 10^6 cells per ml.

Nomenclature and Derivation of the Studied Clones Transformed by Treatment with Me_2N or NMeU.

Designation	*Derivation*
Me_2N1–6	1 mg of Me_2N per ml for 20 min
Me_2N7–9	25 mg of Me_2N per ml for 1 hr
NMeU2	5 μg of NMeU per ml for 1 hr
NMeU3	50 μg of NMeU per ml for 1 hr
NMeU4, 5	1 μg of NMeU per ml for 1 hr
CO_4	Untreated, spontaneously transformed
BHK21/13	From M. Stoker, low passage,§ viable frozen test line
PY_1	Transformed by polyoma virus

Spontaneously Transformed BHK_{21} Cl 13 Clone. Occasionally, 1 or 2 colonies will appear for every 4×10^4 low-passage, BHK_{21} Clone 13 cells, plated in soft agar. Upon isolation and replating in soft agar, such colonies do not grow. It is known that normal BHK cell clumps will give rise to colonies in soft agar. Spontaneously transformed BHK clones, defined as truly transformed cells by their ability to plate in agar after defrosting and a couple of passages, appear with an extremely low frequency. Clone CO_4 is one of the few spontaneously transformed BHK that we have found.

BHK_{21} Cl 13 cells transformed by polyoma virus (PY1) were used as controls.

RESULTS

Six clones transformed by Me_2N, four by NMeU, one spontaneously transformed, one transformed by polyoma virus,

§ 20th serial subculture from tissue of origin.

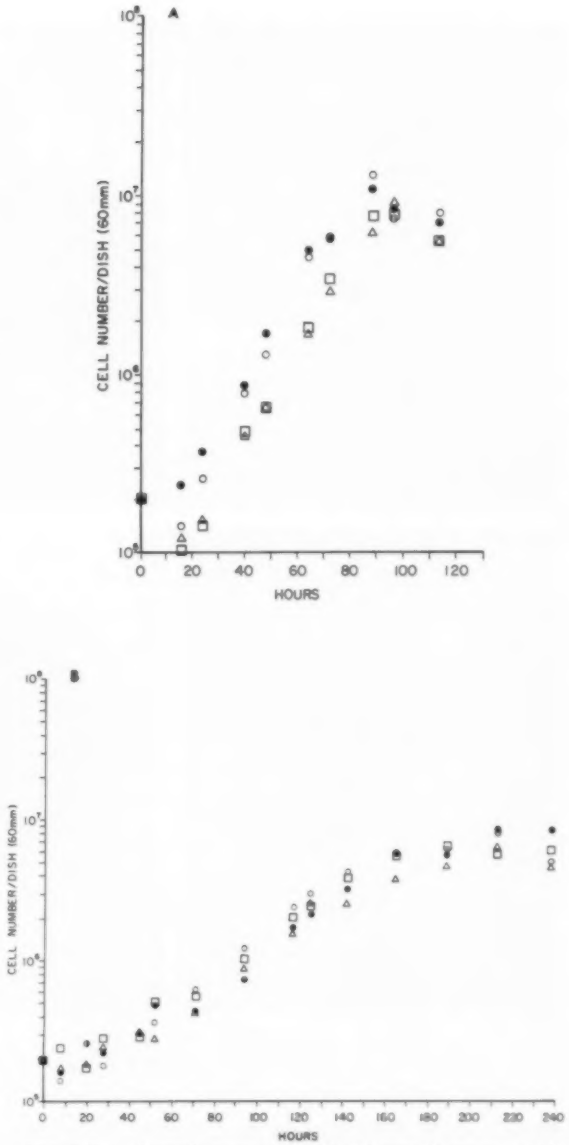

FIG. 1(*A*). Growth curve at 38.5°; (*B*) growth curve at 32°. Several dishes were seeded with 2×10^5 cells per dish. At various times, the total number of cells per dish was counted microscopically after the cells were harvested by trypsinization. Each point represents the count of 2 dishes. ○, BHK_{21} Cl 13; ●, PY1; □, Me_2N4; △, Me_2N6.

and a normal BHK_{21} Cl 13 were grown for a few passages [2–3] at 32° and 38.5°. Cells were then plated at the two temperatures. The plating efficiency of the various clones in liquid medium did not show significant differences at the two temperatures.

Figs. 1*A* and *B* represent cell growth at 38.5° and 32°, respectively. The growth rate of the chemically transformed clones is not significantly different from that of the BHK control or PY1 transformed cells at either temperature. Figs. 2–4 illustrate the morphology of the different clones at the two temperatures. BHK_{21} Cl 13

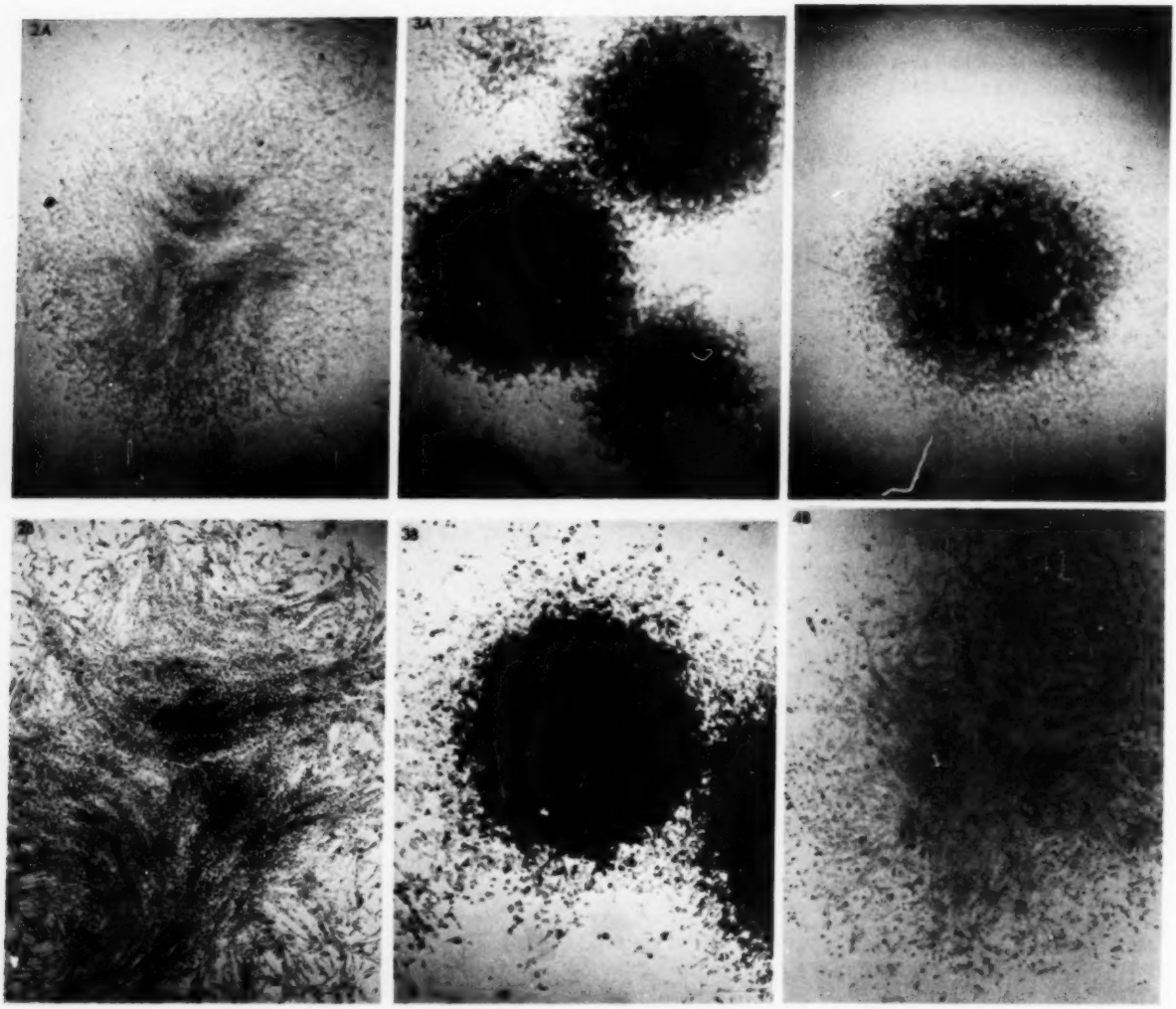

FIGS. 2–4. Microphotographs of colonies of (2*A*) BHK_{21} Cl 13 at 38.5°, (*B*) BHK_{21} Cl 13 at 32°; (3*A*) PY1 at 38.5°, (*B*) PY1 at 32°; (4*A*) typical Me_2N-transformed cells at 38.5°, (*B*) typical Me_2N-transformed cells at 32°.

exhibits normal clonal morphology at the two temperatures. PY1 clone shows transformed morphology at both temperatures. In contrast, Me_2N-, NMeU-, and spontaneously transformed clones exhibit a normal morphology at 32° and a transformed morphology at 38.5°. It should be recalled that transformed clonal morphology of BHK_{21} Cl 13 is defined by: (*A*) loss of the swirl pattern, a typical cyto-architectural feature of normal cells, (*B*) criss-cross pattern of growth, and (*C*) piling up of cells in the colony. This accounts for the dense, dark appearance of the transformed clones. Clonal morphology, however, appears to be only loosely related to the ability of a given clone to produce tumors in an animal. The ability to plate in soft agar is, however, strictly related to tumorigenicity, at least in our experience with cells transformed by polyoma virus or chemicals. Only 10% of the clones showing a "transformed" morphology plate in soft agar and produce tumors in animals. All the clones listed in this work that plated in soft agar were tumorigenic in hamsters. Within 30 days after inoculation of 10^3 cells per animal, visible tumors were observed. At this density, BHK cells did not provoke tumor formation. Only at a much greater density (10^6–10^7 cells per animal) did BHK cells provoke tumors within 30 days; however, after inoculation of similar densities of the chemically transformed clones visible tumors were found within 7 days. The spontaneously transformed clone, CO_4, was not tested. Table 1 shows the plating efficiencies of the various clones, grown and subsequently plated in soft agar at the two temperatures. Again, BHK_{21} Cl 13 does not plate at either temperature, PY1 clone plates at both temperatures, but Me_2N-, NMeU-, and the spontaneously transformed clones exhibit a temperature dependence of their plating efficiency. The transformed phenotype of these clones at 38.5° reverts to normal when the cells are shifted to 32°. Conversely, the cells express the transformed phenotype when shifted from 32° to 38.5°. The ability to plate in soft agar after the temperature shifts was used as a measure of phenotype recognition. Hence, the expression of the transformed phenotype of these clones is conditioned by tempera-

TABLE 1. *Temperature dependence of plating efficiency in soft agar of Me_2N, NMeU, polyoma, "spontaneous," and normal BHK_{21} Cl 13 clones*

	Cells grown and plated at 38°	Cells grown and plated at 32°
Me_2N1	8.6	0
2	12.9	0
3	11.4	0
4	6.1	0
5	11.8	0
6	18.5	0
NMeU2	1.2	0
3	1.0	0
4	4.7	0
5	9.2	0
BHK	0	0
PY1	30	28
CO_4	6.0	0

Each determination is based on counts of 10 plates seeded with 1000 cells per plate in Dulbecco medium with 0.3% agar, and the plating efficiency is expressed as % of cells plated.

TABLE 2. *Phenotypic lag of the expression of transformation after shift from 32° to 38.5°*

Clone	Plating efficiency of control cells in soft agar at 38.5°	Number of generations at 38.5° after shift	Plating efficiency in soft agar at 38.5°
NMeU5	9.2	—	—
		0	9.2
Me_2N6	18.5	—	—
		0	0
		1	0
		2	0.2
		3	7.0
		3.5	18.5

Several dishes were seeded with 5×10^5 cells per dish from clones carried at 32°. These dishes were shifted to 38.5°. At various times after the shift, the cells were plated in soft agar; these plates were incubated at 38.5°. The plating efficiency is compared with that of the same cells maintained at 38.5° and plated in soft agar at 38.5° (control cells). See footnote of Table 1.

ture. When the various clones grown at 32° were shifted to 38.5° and then plated in soft agar at 38.5, they were found to belong to two different classes; one that immediately expressed the transformed phenotype (as judged by the ability to plate in soft agar at the high temperature), and the other that exhibited a phenotypic lag of 3.5 generations before transformation was expressed.

Table 2 shows the behavior of clone NMeU5, a representative of the first class, and clone Me_2N6, a representative of the second class, after temperature shift. Clone NMeU5 immediately exhibits the transformed phenotype when shifted to 38.5°. In contrast, clone Me_2N6 must grow 3.5 generation times at 38.5° before full expression of the transformed phenotype occurs.

DISCUSSION

Temperature dependence of the transformed phenotype of cells transformed by two different nitrosamines and of a spontaneously transformed clone has been clearly demonstrated. These results were found to be highly reproducible in a set of several experiments. In contrast, cells transformed by polyoma virus are completely unrestricted by temperature and exhibit a transformed phenotype both at 32° and 38.5°. The conditionally transformed state of these cells may be explained by the assumption, as a working hypothesis, that nitrosoamines and the unknown causative agent of spontaneous transformation, react with the cell genome and produce a temperature-sensitive mutation in a gene whose product is essential in maintaining the normal phenotype. The temperature-sensitive mutation at the higher temperature would operationally suppress either the function or the synthesis of the gene product, and unregulated growth and malignant transformation would occur.

This research was supported by NIH Contract no. 70-2203.

1. Berwald, Y. & Sachs, L. (1965) *J. Nat. Cancer Inst.* **35**, 641–662.
2. Huberman, E. & Sachs, L. (1966) *Proc. Nat. Acad. Sci. USA* **56**, 1123–1129.
3. Medina, D. & Sachs, L. (1965) *Virology* **27**, 398–408.
4. DiPaolo, J. A., Donovan, P. J. & Nelson, R. L. (1969) *J. Nat. Cancer Inst.* **42**, 867–880.
5. DiPaolo, J. A., Nelson, R. L. & Donovan, P. J. (1969) *Science* **165**, 917–918.
6. DiPaolo, J. A., Donovan, P. J. & Nelson, R. L. (1971) *Nature New Biol.* **230**, 240–242.
7. Borenfreund, E., Krim, M., Sanders, F. K., Sternberg, S. S. & Bendich, A. (1966) *Proc. Nat. Acad. Sci. USA* **56**, 672–679.
8. Chen, T. T. & Heidelberger, C. (1969) *J. Nat. Cancer Inst.* **42**, 903–912.
9. Chen, T. T. & Heidelberger, C. (1969) *Int. J. Cancer* **4**, 166–178.
10. Mondal, S. & Heidelberger, C. (1970) *Proc. Nat. Acad. Sci. USA* **65**, 219–225.
11. MacPherson, I. & Montagnier, L. (1964) *Virology* **23**, 291–294.

Proc. Nat. Acad. Sci. USA
Vol. 70, No. 1, pp. 50–53, January 1973

Photophosphorylation by Monomolecular Films at an Air–Water Interface

(surface chemistry/chlorophyll/photosynthesis/coupling factor I/lipid membranes)

J. McPHEE AND S. S. BRODY

Department of Biology, Washington Square, New York University, New York, N.Y. 10003

Communicated by Britton Chance, October 19, 1972

ABSTRACT **An acetone extract of chloroplast particles, when layered on an aqueous surface, exhibited light-dependent phosphorylation. Studies with the firefly-tail enzyme assay, as well as with ^{32}P-labeled inorganic phosphate, show an initial release of adenosine triphosphate (a step that is apparently only light-triggered), followed by a light-dependent uptake of the labeled inorganic phosphate into adenosine diphosphate and adenosine triphosphate.**

Photophosphorylation has been demonstrated with fragments of chloroplast lamellae (1–5). It has been suggested that these fragments must be capable of maintaining a proton gradient or a pH gradient between an inner and an outer compartment in order for them to be active (6–9). Recent evidence, however, seems to indicate that some photophosphorylation can occur in the absence of a proton pump (1, 4, 10), and that the act of phosphorylation in this case is directly coupled to the electron transport chain through a "high-energy" chemical intermediate (11).

In this preliminary report, we describe an acetone extract of spinach subchloroplast particles at an air–water interface. This system is capable of photophosphorylation in the apparent absence of any intact membranes or artificially supplied electron carriers.

MATERIALS AND METHODS

The apparatus used for preparation and study of the monolayers is essentially the same as that described by Aghion *et al.* (12), the only major modification being that the trough was constructed of aluminum and coated with Teflon.

The chloroplasts were prepared from spinach leaves (*Spinacia oleracia* L.) by the method of S. Saha and N. E. Good (13). Subchloroplast particles were prepared from these by use of a modified method of Nelson *et al.* (2). A 5-min sonication in a temperature-controlled sonic oscillator (Raytheon Electronics Corp.) was used in place of digitonin treatment. The sonicated particles were first spun at 46,000 × *g* for 20 min to remove the heavier fragments. The supernatant was then spun at 95,000 × *g* in a Beckman refrigerated ultracentrifuge (model L2-65B) for 30 min, the supernatant was poured off, and the pellet was resuspended in cold acetone (−20°). The resultant solution was centrifuged again at 95,000 × *g* for 15 min; the supernatant was removed with a syringe and used on prepare the monolayer. After addition of the extract on the aqueous subphase, the film was immediately compressed to a surface tension, π, of 19.6 dynes/cm. To assay for ATP or esterified ^{32}P, 2-ml aliquots were removed from the subphase with a syringe at various time intervals.

Utilization of larger particles for preparation of the acetone extract resulted in a more unstable system, making results more difficult to reproduce. All steps were performed at 0° and in dim light. The subphase on which the monolayer was spread contained 10 μM Na_2HPO_4, 10 mM N-tris(hydroxymethyl)methyl glycine (Tricine) buffer (pH 7.8), and 50 μM ADP. The temperature was maintained at 15°. The subphase for the experiments involving $^{32}PO_4$ was prepared in the same manner (the $^{32}PO_4$ being added as part of the Na_2HPO_4 solution).

Total chlorophyll contained in the extract was estimated by the method of Vernon to be 1.6 μmol/ml (14); about 0.6 μmol was spread on the surface. For the ATP measurements, the monolayer was illuminated with two cool-white, 20-W, fluorescent lamps mounted 60 cm above the trough or a single 100-W tungsten filament bulb mounted 30 cm above the trough. In the [^{32}P]inorganic phosphate esterification measurements, only the tungsten light source was used. The average light intensity at the surface of the monolayer was measured with a thermopile (Eppley Instruments) to be 580 ergs cm^{-2} sec^{-1} for the fluorescent light source and 6.5 × 10^4 ergs cm^{-2} sec^{-1} for the tungsten source.

The extract was maintained in the dark at 4° before addition to the aqueous surface. Under these conditions, about 80% of the photophosphorylation activity was lost in the acetone extract after about 0.5 hr.

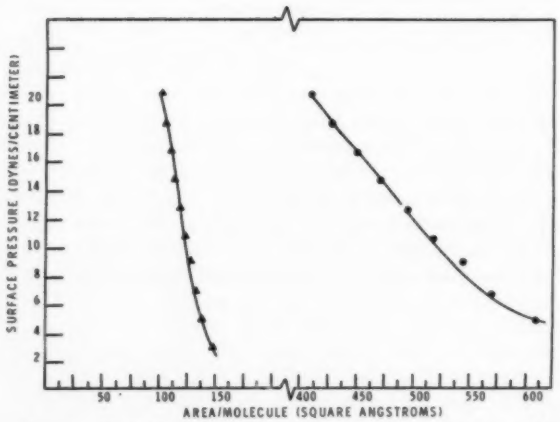

FIG. 1. (*left*) Surface isotherm of pure chlorophyll *a* in the dark and air at 15°. An acetone solution of chlorophyll *a* was spread on a buffered aqueous surface (0.01 M Tricine, pH 7.8).

FIG. 2. (*right*) Surface isotherm of the aqueous acetone extract of spinach subchloroplast particles in the dark and air at 15°. The extract was spread on a buffered aqueous surface (0.01 M Tricine, pH 7.8).

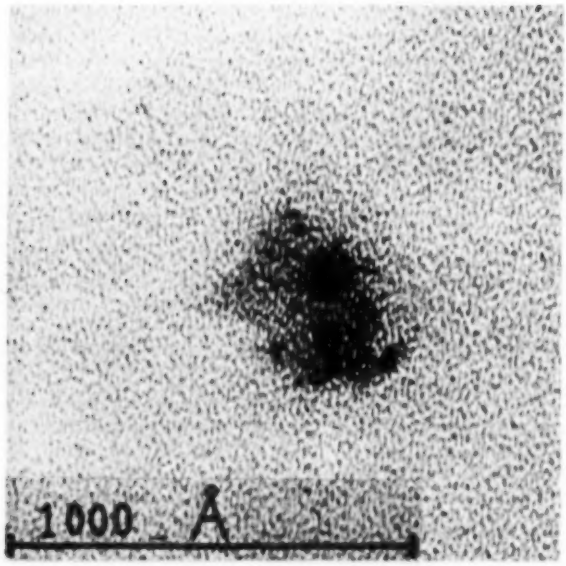

FIG. 3. An electron micrograph showing one of the particles present in the extract. These particles are about 200 Å in diameter, and are present in the extract at a concentration of 1 per 2×10^9 Å^2.

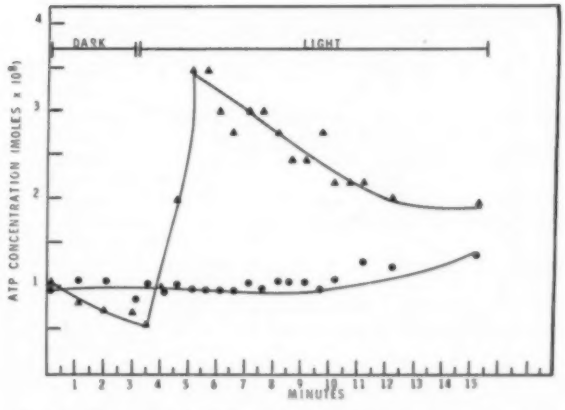

FIG. 4. Variation of ATP in the aqueous subphase, as a function of time in light and dark (*solid triangles*). As a control, ATP concentration in that portion of the subphase free of film is also shown (*solid circles*). A monolayer is formed at an air–water interface with an aqueous acetone extract of spinach subchloroplast particles. The subphase contains 0.01 M Tricine (pH 7.8), 10 μM Na_2HPO_4, and 10 μM ADP; the temperature was maintained at 15°. The monolayer is irradiated either with cool-white fluorescent lamps, (580 ergs cm^{-2} sec^{-1}) or with a tungsten filament lamp (6.5×10^4 ergs cm^{-2} sec^{-1}).

^{32}P was acquired in the phosphoric acid form from Union Carbide Corp. (Sterling Forest, N.Y.). 1.0 mCi was dissolved in 250 ml of 1 mM Na_2HPO_4 solution. 50-ml Aliquots of this solution were used as the sole source of inorganic phosphate in the ^{32}P-esterification studies. ^{32}P Esterified was assayed by the method of Pullman and Monroy (15).

All sample counts were referenced against a control sample taken from the trough before the monolayer was spread. This control sample was counted directly, without extraction for esterified ^{32}P, to give the specific activity of the 5 μmol of phosphate added. Molar concentrations in the assayed samples were then calculated by comparison of their counts to this value.

Samples for electron microscopy were prepared by dipping a Formvar disc (Ladd Research, Burlington, Vt.) three times into the compressed film. The untreated grid was then examined with a Philips 300 electron microscope (Einhoven, Netherlands).

Desiccated firefly tails and apyrase (EC 3.6.1.5) were obtained from Sigma Chemical Company (St. Louis, Mo.). ATP production was assayed quantitatively by a luciferin–luciferase bioluminescence technique, similar to that described by Nielsen and Rasmussen (16).

RESULTS

Composition of extract

In Figs. 1 and 2 are shown the isotherms of pure chlorophyll *a* and that of the extract. The ratio of the surface areas of pure chlorophyll *a* to that of a known amount (by absorption spectroscopy) of chlorophyll *a* contained in the extract yields an estimate of the percent chlorophyll content. The average surface area per chlorophyll molecule in the extract at $\pi = 10$ dynes/cm is about 530 Å^2 and that of pure chlorophyll *a* is 120 Å^2. The estimate of % chlorophyll content is then 22%. Electron microscopy indicates the presence of a small particle present in the film at a concentration of 1 particle per 2×10^9 Å^2 on the compressed surface. (Fig. 3). The particle is estimated to be 200 Å^2 in diameter, containing smaller, more electron-dense particles that average about 60 Å in diameter. The remaining material on the surface is probably a mixture of other pigments, neutral lipids, and some lipoprotein. A microkjeldahl assay of the extract indicated the presence of about 20% protein residue by weight.

ATP concentration

The variation in ATP concentration under the film is shown in Fig. 4, (*solid triangles*). In the initial dark period, a slight decline is seen. Upon illumination there is a short lag period, followed by a rapid rise, which reaches a maximum after 100 sec. This rise is followed by a slow decline, which reaches a steady state after 12 min. (Two light sources, with widely differing intensities, were used in these experiments. However, no difference was observed in either the rate of or maximum amount of ATP production). The maximum ATP concentration attained by the system is estimated to be 35 μmol. As a control, ATP concentration in a section of the subphase not covered by the film is also shown in Fig. 4 (*solid circles*). Point by point comparison of the ATP production curve and the control curve yields the net ATP production of the film. A preliminary estimate of the quantum yield for ATP synthesis (under low light intensity) gives values between 0.1 and 1.

Compression of the film to a pressure greater than 10 dynes/cm surface pressure is required in order to observe this increase in ATP concentration.

Addition of phenazine methosulfate (0.06 μmol/ml) to the subphase results in more than a doubled enhancement in ATP concentration, and a much slower decline after the initial rise (Fig. 5, *open triangles*). In Fig. 5 (*solid triangles*), a

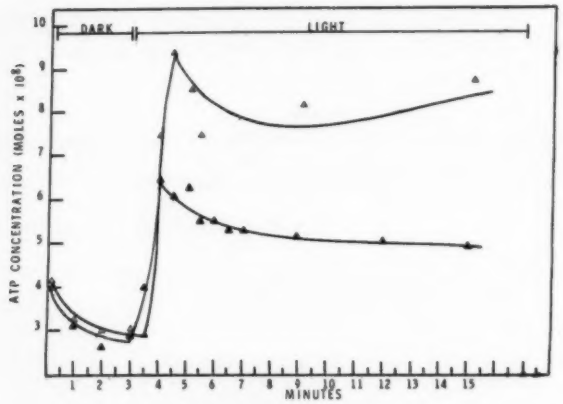

FIG. 5. Comparison of the variation of ATP concentration in light and dark in the absence (*solid triangles*) and presence (*open triangles*) of phenazine methosulfate. The subphase for both curves contained 0.01 M Tricine, (pH 7.8), 10 μM Na_2HPO_4, and 10 μM ADP. The subphase for the *open triangle curve* also contained 60 μM phenazine methosulfate. Films were prepared from acetone extracts of the same spinach subchloroplast particles.

control was provided by running another sample of the same extract on a subphase free of the reducing dye.

^{32}P Esterification

The amount of ^{32}P esterified in the subphase is shown in Fig. 6 (*solid triangles*). After the initial burst of ^{32}P esterification, there is a slow decline in the number of esterified counts. Fig. 6 (*solid circles*) indicates the esterified ^{32}P measured on a portion of the trough not covered by the film. The bulk of these counts are from a trace contaminant of inorganic pyrophosphate. Removal of pyrophosphate by filtration through activated charcoal gives values for Fig. 6 (*solid circles*) close to zero, but does not significantly alter

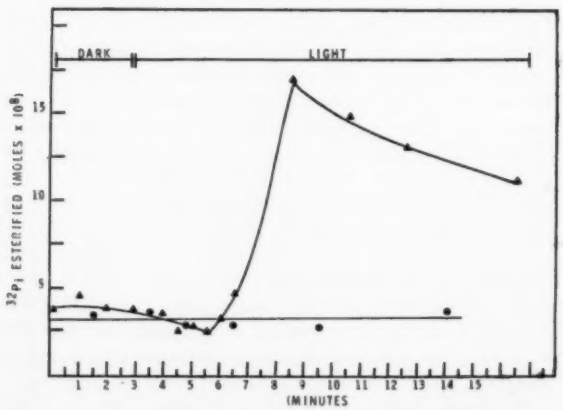

FIG. 6. Variation of ^{32}P esterified in the aqueous subphase in light and dark, as a function of time (*solid triangles*). As a control, ^{32}P esterification of the film-free portion of the subphase is shown by *solid circles*. The aqueous acetone extract of spinach subchloroplast particles was spread on an aqueous subphase containing 5 μM Na_2HPO_4 labeled with ^{32}P, 0.01 M Tricine (pH 7.8), and 10 μM ADP. The monolayer was compressed and irradiated with a tungsten filament lamp (6.5×10^4 ergs cm^{-2} sec^{-1}).

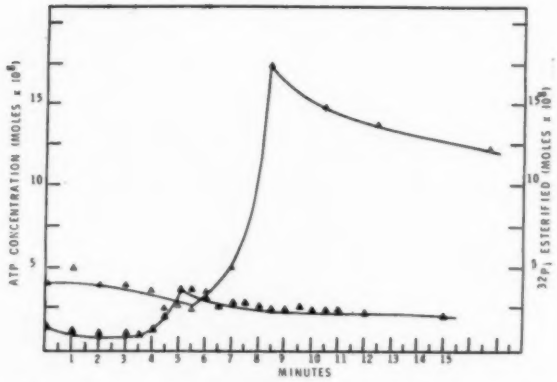

FIG. 7. Comparison of the variations of ATP concentration relative to esterification of ^{32}P: *solid triangles* and *open triangles*, respectively.

the variation in ^{32}P esterification measured in Fig. 6 (*solid triangles*). The maximum amount of $^{32}PO_4$ esterified occurs after 270 sec of illumination at 20°. The maximum of ^{32}P esterified is about 0.18 μmol. Addition of phenazine methosulfate (0.06 μmol/ml) had no apparent effect on the amount or rate of esterification.

However, light intensity was a critical factor for the esterification reaction. Utilization of the fluorescent light source with its output of only 580 ergs cm^{-2} sec^{-1} gave little or no esterification. Therefore, all reactions were run with the 100-W tungsten light source.

DISCUSSION

A comparison of the ATP produced (as determined by the firefly bioluminescence assay) and the amount of [^{32}P]-inorganic phosphate esterified is shown in Fig. 7. The maximum concentration of ^{32}P esterified occurs after 270 sec of illumination at 20°, in contrast to the ATP concentration maximum (which occurs after 100-sec of illumination). There is also an apparent 5-fold difference between the concentration of ATP and esterified $^{32}PO_4$.

The initial production of ATP in Fig. 7 (*solid triangles*) takes place with or without inorganic phosphate supplied in the subphase. It is, however, completely dependent on the presence of ADP in the subphase. It will be noted that there is very little change in the ^{32}P esterified (Fig. 7, *open triangles*) during this initial period of ATP production. It would seem that ATP is produced either by utilization of some endogenous source of inorganic phosphate, or by a transphosphorylation of the ADP supplied to it in the subphase. The stimulation of ATP production by phenazine methosulfate is an indication that this process is coupled to an electron transport system in the monolayer. The inability of the dye to stimulate ^{32}P esterification might imply that the process of esterification is not rate limited by the electron transport system. Or, perhaps more interestingly, esterification might not be dependent on electron transport, but may function instead as a separate system.

It has been proposed that photophosphorylation occurs as a two-step reaction (10). There is an initial myokinase-type reaction, in which two ADP molecules take part in a transphosphorylation to yield one molecule of AMP and one of

ATP. The second step is a phosphorylation reaction that is directly coupled to the electron transport chain, resulting in the formation of one molecule of ADP from one molecule of AMP and one of P_i.

Our results seem to fit this hypothesis in that the initial production of ATP might readily be the result of a transphosphorylation and that the ^{32}P esterification later observed might be the result of AMP phosphorylation, since most of the esterified phosphate is in the ADP form.

This work was supported in part by grants from NIH (EY-00173) and NSF (GB18354). We thank Mr. Monroe Yoder for assistance in preparation of the electron micrograph.

1. Neumann, J., Arntzen, C. J. & Dilley, R. A. (1971) *Biochemistry* **10**, 866–873.
2. Nelson, N., Dreschsler, Z. & Neumann, J. (1970) *J. Biol. Chem.* **245**, 143–151.
3. Anderson, M. M. & McCarty, R. E. (1969) *Biochim. Biophys. Acta* **189**, 193–206.
4. Arnon, D. I., Tsujimoto, H. Y., McSwain, B. D. & Chain, R. K. (1968) *Comp. Biochem. and Biophys. of Photosynthesis*, (Shibata, K., Takamiya, A., Jagendorf, A. T. & Fuller, R. C. eds. Univ. of Tokyo Press, Tokyo, Japan).
5. Wessels, J. S. C. (1964) *Biochim. Biophys. Acta* **79**, 640–642.
6. Mitchell, P. (1966) *Camb. Phil. Soc. Biol. Rev.* **41**, 445–502.
7. Witt, H. T., Doring, G., Rumberg, B., Schmidt-Mende, P., Siggel, V. & Stiehl, H. H. (1966) *Brookhaven Nat. Lab. Symp.* **19**, 161–168.
8. Izawa, S. (1970) *Biochim. Biophys. Acta* **223**, 165–173.
9. Rottenberg, H., Grunwald, T. & Avron, M. (1971) *Febs Lett.*, **13**, 41–44.
10. Roy, H. & Moudrianakis, E. N. (1971) *Proc. Nat. Acad. Sci. USA* **68**, 464–468.
11. Slater, E. C. (1967) *Eur. J. Biochem.* **1**, 317–326.
12. Aghion, J., Broyde, S. B. & Brody, S. S. (1969) *Biochemistry* **8**, 3120–3126.
13. Saha, S. & Good, N. E. (1970) *J. Biol. Chem.* **245**, 5017–5021.
14. Vernon, L. P. (1960) *Analyt. Chem.* **32**, 1144–1150.
15. Pullman, M. E. & Monroy, G. (1963) *J. Biol. Chem.* **238**, 3762–3769.
16. Nielsen, R. & Rasmussen, H. (1968) *Acta Chem. Scand.* **22**, 1746–1754.

Proc. Nat. Acad. Sci. USA
Vol. 70, No. 1, pp. 54–56, January 1973

Production of Mucopolysaccharides by Normal and Transformed Cells

(hyaluronic acid/transformed cells/hamster-embryo cultures)

C. SATOH, R. DUFF, F. RAPP, AND E. A. DAVIDSON*

Departments of Biological Chemistry and Microbiology, The Milton S. Hershey Medical Center of The Pennsylvania State University, Hershey, Pa. 17033

Communicated by Charles Tanford, October 30, 1972

ABSTRACT **The rate of hyaluronic acid and sulfated mucopolysaccharide production was measured for hamster embryo fibroblasts and for general oncogenic lines derived by virus transformation. A striking increase in both the rate of hyaluronic acid synthesis and the amount of cell-associated polymer was observed after transformation by herpes simplex type-2 or SV40 virus. Although no corresponding change was observed for the sulfated polysaccharides, the proportion of heparan sulfate increased significantly after transformation.**

Recent reports from several laboratories have described effects on cell coat properties associated with virus transformation (1–3). In general, the morphologic observations have been attributed to changes in the content of those acid polysaccharides identified with the extracellular matrix—hyaluronic acid and a group of sulfated saccharides. Although differences in the rate of synthesis of cell coat have been observed for transformed cells (4), as a rule the polysaccharides involved have not been characterized.

The present study describes the production and characterization of mucopolysaccharides by normal and virus-transformed fibroblasts from hamster embryo under cell culture conditions. An attempt was made to differentiate material adhering to cell surfaces from that released to the culture medium, although only an operational distinction was used. In most of the experiments reported, [^{3}H]glucosamine was used as a radioactive precursor for both nonsulfated (hyaluronic acid) and sulfated (chondroitin sulfates, heparan sulfate, etc.) polysaccharides.

The identification of the polysaccharides was based on elution behavior from cetylpyridinium chloride precipitates (5), high-voltage electrophoresis, enzyme susceptibilities, and characterization of the amino sugar component after acid hydrolysis. Table 1 illustrates the results obtained for several polysaccharides under consideration.

MATERIALS AND METHODS

Syrian hamster-embryo fibroblasts cells (inbred LSH strain, Lakeview Hamster Colony, New Field, N.J.) were prepared by dispersion of 13-day-old embryos with 0.25% trypsin. The dispersed cells were grown in medium 199 supplemented with 10% tryptose phosphate broth, 10% fetal-bovine serum, and 0.075% $NaHCO_3$. Primary African green monkey kidney cells were also prepared by dispersion with 0.25% trypsin, and grown in Eagle's medium (BME, Flow Laboratories Inc.) with 10% fetal-calf serum and 0.075% $NaHCO_3$.

The H-50 cell line was developed from a Syrian hamster tumor that was originally induced by SV40 (6). H-50 cells contain the SV40 T and transplantation-rejection antigens, and induce tumors when reinjected into weanling Syrian hamsters. They do not produce infectious virus. The cells were maintained in the identical manner as primary hamster embryo fibroblasts. The SV40-transformed BSC-1 cells are the results of the transformation of a stable line of African green monkey kidney cells (BSC-1) by SV40 (7). These cells synthesize the SV40-specific tumor antigen, the surface antigen, and the transplantation antigen; however, SV40 capsid antigen is not synthesized (8). BSC-1 (SV40) cells were grown in Eagle's medium (BME) supplemented as described above.

Hamster-embryo fibroblast cells were transformed (9, 10) by herpes simplex virus type-2. The 333-8-9 T no. 1 cells were maintained in medium 199 with the same supplements as used with normal fibroblast cells. Herpes virus-specific antigens are present in the 333-8-9 T no. 1 cells, which were developed from a tumor induced in a weanling Syrian hamster by the virus-transformed cells.

For polysaccharide analysis, cell cultures were maintained in medium 199 supplemented with 10% fetal-calf serum and 10% tryptose phosphate broth. The cells were passaged at 3- to 4-day intervals. Exposure to isotopically labeled glucosamine ([^{3}H]glucosamine, 10 μCi/ml final concentration, 3 Ci/mmol, New England Nuclear Corp.) was for 24 hr; 10^6 cells were used in the same medium with dialyzed serum. In a rate study, cells were labeled for 4 hr with 10 μCi/ml of [^{3}H]glucosamine, then the medium was removed and replaced with fresh medium containing an equivalent concentration of unlabeled glucosamine (1.6 pmol/ml). Cell and medium samples were collected at several intervals thereafter.

Medium was decanted from the cells and the cells were removed from the glass substrate by brief exposure to 0.1 mM EDTA or by mechanical means. The cells were collected by centrifugation and washed once with isosmotic phosphate-buffered saline (pH 7.3). The wash was combined with the decanted medium.

After the addition of 2.5 mg (each) of unlabeled hyaluronic acid and chondroitin 4-sulfate as carrier, the mucopolysaccharides were isolated by precipitation with excess cetylpyridinium chloride after 18 hr of digestion with 1 mg/ml of Pronase at pH 6.5 and 37°, 18 hr of exposure to 0.1 N NaOH, and dialysis against H_2O to remove peptides and glycopeptides. The cetylpyridinium-chloride precipitate was washed with 30 mM NaCl, and sequentially extracted with

* To whom reprints requests should be addressed.

TABLE 1. *Characterization profile of mucopolysaccharides*

	Cetylpyridinium chloride elution (M NaCl)	Enzyme susceptibility	Amino sugar
Haluronic acid	0.4	Hyalur¬nidase	Glucosamine
Chondroitin 4- and 6-sulfate*	1.2	Hyaluronidase: chondroitinase ABC	Galactosamine
Heparan sulfate†	1.2	Flavobacterium heparinase	Glucosamine
Heparin†	2.0	Flavobacterium heparinase	Glucosamine

* Differentiated by both chemical and enzymatic hydrolysis susceptibility of the sulfate ester grouping.

† Contains *N*-sulfate as well as *O*-sulfate.

0.4 M NaCl, 1.2 M NaCl, and, in some preliminary experiments, 2.0 M $MgCl_2$. The $MgCl_2$ extracts invariably contained insignificant radioactivity and were not studied further. The NaCl eluates were freed of cetylpyridinium chloride by dialysis before further analyses.

Electrophoresis was performed in pyridine–formic acid, (pH 3.0), on cellulose acetate strips for 30 min at a current of 0.22 mA/cm. Standards for hyaluronic acid and the chondroitin sulfates were prepared in this laboratory. The position of the standards was revealed by staining with Alcian Blue; the experimental strips were sectioned and assayed for radioactivity by scintillation counting. In all cases, the results obtained corresponded to those expected on the basis of the cetylpyridinium chloride elution profile. It should be noted that the sulfated polysaccharides (e.g., chondroitin 4- against 6-sulfate) are not distinguished by this procedure. We are indebted to Dr. Alfred Linker for an authentic sample of heparan sulfate.

Hyaluronidase susceptibility was observed by measurement of dialyzable radioactivity after 24 hr of digestion at pH 5.0 and 37° with 300 turbidity-reducing units of Worthington testicular hyaluronidase. Similar conditions were used for chondroitinase ABC and a flavobacterium heparinase obtained through the courtesy of Dr. Alfred Linker.

The amino sugar composition of the various fractions was measured after 24 hr of hydrolysis in an evacuated tube in 6 N HCl. Samples were resolved on a Beckman 120C aminoacid analyzer; a stream-splitting attachment was used. The radioactivity associated with the glucosamine or galactosamine peaks was determined by counting aliquots in a liquid scintillation counter in a toluene–Triton mixture as solvent and 2,5-diphenyl oxazole(PPO)–1,4-bis [2-(5-phenyl oxazole)]-benzene POPOP (40:1) as scintillators.

Estimates of molecular size are based on chromatography on porous glass beads with oligo- and polysaccharide samples of known degree of polymerization as standards. The glass beads were obtained from Corning Glass, Inc. The details of this technique will be published elsewhere.

RESULTS AND DISCUSSION

The effect of virus transformation on mucopolysaccharide production by hamster-embryo fibroblasts is notable in that there is a striking increase in label in the hyaluronic acid fraction without a corresponding effect on the sulfated polysaccharide components. Data are summarized in Table 2. Since incorporation of precursor into product under the conditions of this experiment must represent a composite of both synthesis and degradation, a time-course study was performed in an attempt to better define the nature of the observed effect. The data, shown in Table 3 and Fig. 1, clearly demonstrate an increase in the rate of glucosamine incorporation into hyaluronic acid of about tenfold that persists after 24 hr, and also suggest that greater amounts of the hyaluronic acid remain associated with the cells after viral transformation, although the nature of this association is unknown.

TABLE 2. *Mucopolysaccharide production by normal and transformed cells*

Cell line	Hyaluronic acid		Sulfated polysaccharides	
	Cell	Medium	Cell	Medium
Hamster-embryo fibroblasts	43,800	262,700	111,600	683,200
333-8-9 T no. 1	463,000	8,578,900	107,000	1,042,000
H-50	96,300	655,800	13,200	918,500

The radioactivity incorporated into the identified fraction after exposure of 10^6 cells to 5 μCi/ml of [^{3}H]glucosamine for 48 hr under standard culture conditions. The sulfated-fraction radioactivity is based on high-voltage electrophoresis after elution from cetylpyridinium chloride. Both glucosamine and galactosamine were present, suggesting the presence of heparan sulfate, as well as a chondroitin sulfate (see Table 4). 333-8-9 T no. 1: hamster-embryo fibroblasts transformed *in vitro* by herpes simplex virus type-2, cell line recovered from tumor, carried in culture, 13th passage: H-50:hamster tumor induced by SV40, cell line recovered from tumor, carried in culture, 46th passage. Both transformed lines are oncogenic. The counts identified as hyaluronic acid represent those eluted from the cetylpyridinium chloride precipitate with 0.4 M NaCl. These fractions were completely (>95%) digested by hyaluronidase, and all radioactivity was associated with glucosamine; galactosamine was not present.

Although the amount of isotope incorporated into the sulfated fraction was not significantly different from that in control cells, and the characterization of this fraction is not complete, several facets are of interest. Examination of the data presented in Fig. 1 suggests a significant effect on the rate of sulfated polysaccharide synthesis during the 4-hr period after a medium change. In addition, there is an indication of some turnover of this fraction at extended time periods, a finding

TABLE 3. *Rate of hyaluronic acid synthesis*

	Cell		Medium	
	0 Hr	4 Hr	0 Hr	4 Hr
HEF	5,300	9,000	8,100	38,900
333-8-9 T no. 1	82,400	95,600	95,600	98,300

Rate of hyaluronic acid synthesis by normal and transformed fibroblasts. 10^6 Cells were labeled for 4 hr by exposure to 10 μCi/ml of [^{3}H]glucosamine. At "zero time," fresh medium containing a comparable concentration of unlabeled glucosamine was added, and the cells were incubated for an additional 4 hr. 333-8-9 T no. 1 cells are herpes-transformed cells (see Table 2).

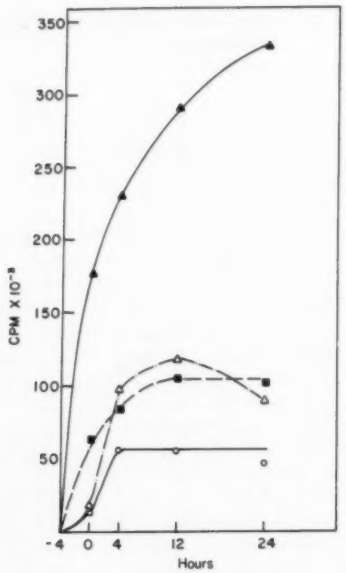

FIG. 1. Rate of hyaluronic acid and sulfated mucopolysaccharide production by hamster-embryo fibroblasts and a cell line transformed by herpes virus type-2, 333-8-9 T no. 1. O——O, [^{3}H]glucosamine incorporation into total hyaluronic acid by control cells: ▲——▲, [^{3}H]glucosamine incorporation into total hyaluronic acid by transformed line 333-8-9 T no. 1; △——△, [^{3}H]glucosamine incorporation into total sulfated polysaccharides by control lines; ■——■, [^{3}H]glucosamine incorporation into total sulfated polysaccharides by 333-8-9 T no. 1 cells.

that was not observed in several experiments with transformed cell lines. An apparent result of *in vitro* SV40 transformation on a line of monkey kidney cells was to cause a change in the average molecular size of the sulfated polysaccharide fraction and, concomitantly, to cause a marked increase in the proportion of heparan sulfate in this fraction. A similar effect was observed for herpes-transformed hamster-embryo fibroblasts. Data are summarized in Table 4.

Although accurate molecular weights cannot be determined for most of the isolated samples due to material limitations, size estimates were made based on behavior of the polysaccharide samples on columns of porous glass beads. In general, both the hyaluronic acid and the sulfated polysaccharides appeared altered in molecular size after viral transformation. The possibility of a degradative activity associated with untransformed lines cannot be excluded, either by these observations or by the rate studies. In addition, since this study was focused on the saccharide moieties, we have no information regarding effects on covalently associated protein, a normal constituent of at least the sulfated proteoglycans.

Several laboratories have observed alterations in cell-surface polysaccharides coincident with a transforming event. Changes in cell-coat thickness and rates of formation (4) have been reported, although the identification of the associated

TABLE 4. *Properties of sulfated polysaccharide fraction*

	% Low molecular weight	% Heparan sulfate
Green monkey kidney	24	2.7
BSC-1 (SV40)	45.7	16.0
Hamster embryo fibroblast	46	4.4
333-8-9 T no. 1	35	23.1

% Low molecular weight is based on the fraction of radioactively labeled material eluting after standard chondroitin 4-sulfate (molecular weight = 14,500) on a 0.9 × 50 cm column of CPG-240 porous glass beads with 0.5 M $CaCl_2$ as eluting solvent. If the profiles overlapped completely, the percentage of low molecular weight material is assumed to be 50. Heparan sulfate content is an estimate based on hyaluronidase-resistant, heparinase-sensitive material remaining after dialysis. BSC-1 (SV40), a stable line of monkey kidney cells (BSC-1) transformed by SV40 virus; 333-8-9 T no. 1 cells are described in Table 2.

macromolecule was limited to those able to bind electron-dense stain (ruthenium red) (11) or to purely physical observations (4). Similarly, the presence of heparan sulfate in several tumor cell lines has been reported, but direct comparison with control cells has not been reported (12, 13).

The physiological role of these mucopolysaccharides remains unknown, as does the nature of their association with the cell, but it is suggestive that selective differences in expression are found in the transformed lines. The possible association between the marked change in hyaluronic acid content and phenomena such as contact inhibition needs further study.

This study was supported by Contract no. 70-2024 within the Special Virus Cancer Program of the National Cancer Institute, National Institutes of Health, USPHS and by Grant AM12074 from the National Institute of Arthritis and Metabolic Diseases, USPHS.

1. Erichsen, S., Eng, J. & Morgan, H. R. (1961) *J. Exp. Med.* **114,** 435–441.
2. Martinez-Palomo, A., Braislovsky, C. & Berulvard, W. (1969) *Cancer Res.* **29,** 925–930; Tarpier, G. & Montagnier, L. (1970) *Int. J. Cancer* **6,** 529–535.
3. Moore, E. S. & Temin, H. (1971) *Nature* **231,** 117–118; Kapeller, M. & Doljanski, F. (1972) *Nature New Biol.*, **235,** 184–185; Culp, L. A. & Black, P. H. (1972) *Biochemistry*, **11,** 2161–2172.
4. Mallucci, L., Poste, G. H. & Wells, V. (1972) *Nature New Biol.* **235,** 222–223.
5. Scott, J. E. (1962) *Biochem. J.* **84,** 270–275.
6. Ashkenzai, A. & Melnick, J. L. (1963) *J. Nat. Cancer Inst.* **30,** 1227–1265.
7. Margalith, M., Volk-Fuchs, F. & Goldblum, N. (1969) *J. Gen. Virol.* **5,** 321–327.
8. Rapp, F. & Trulock, S. C. (1970) *Virology* **40,** 961–970.
9. Duff, R. & Rapp, F. (1971) *J. Virol.* **8,** 469–477.
10. Duff, R. & Rapp, F. (1971) *Nature New Biol.* **233,** 48–50.
11. Martiney-Palomo, A. (1970) *Int. Rev. Cytol.* **29,** 29–75.
12. Kraemer, P. M. (1971) *Biochemistry* **10,** 1437–1445.
13. Kraemer, P. M. (1971) *Biochemistry* **10,** 1445–1451.

Proc. Nat. Acad. Sci. USA
Vol. 70, No. 1, pp. 57–61, January 1973

Structure and Development of Neuronal Connections in Isogenic Organisms: Variations and Similarities in the Optic System of *Daphnia magna*

(neuronal specificity/serial section reconstruction/crustacea)

E. R. MACAGNO, V. LOPRESTI, AND C. LEVINTHAL

Department of Biological Sciences, Columbia University, New York, N.Y. 10027

Contributed by C. Levinthal, November 1, 1972

ABSTRACT **It is readily apparent upon examination and comparison of organisms of the same and related species that to a large extent genes control morphological features. One means to ascertain the role and degree of genetic control is to study in detail the anatomy and development of a particular structure, say an identifiable neuron, in a population with a fixed genome, and at different stages of morphogenesis. The small crustacean, Daphnia, is well suited for this type of study, since it reproduces parthenogenically, its development is easily staged, and its nervous system is reasonably simple. In this paper comparisons of detailed morphology of neurons in the visual system of adult *Daphnia magna* are considered. Results indicate that gross features of the system are reproduced within the clone, but some of the finer details are not reproduced.**

Even a casual observation of identical twins makes it clear that the morphology of an organism is largely determined by its genes. However, the observation of gross similarities raises a host of questions concerning the control of morphology at the cellular and possibly even at the subcellular level. It seems likely that an understanding of the mechanisms by which genes determine shape will require detailed knowledge of the extent to which structural similarities extend to the small features of organs and even cells. Furthermore, examining the variations that can be induced in genetically identical animals by changes in their environment should make it possible to put limits on the extent to which genetic control is, in fact, a rigid determinant of form. In order to obtain the equivalent of many identical twins, we have been examining clones of organisms that reproduce parthenogenically. In a series of papers of which this is the first, we will consider several rather specific questions concerning the anatomy and development of the visual system of *Daphnia magna*. This small crustacean is a diploid organism, which reproduces parthenogenically as long as it is well-fed, uncrowded, and growing in a constant light–dark cycle.

The compound eye of Daphnia consists of 22 ommatidial structures arranged in a raspberry fashion, each consisting of a crystalline cone and eight receptor cells. Each of the 176 receptor cells sends a fiber to the optic ganglion where the fibers make primary contact with a set of 110 neurons. Thus, we are dealing with a relatively small optic system in which each cell and each fiber can be well identified from animal to animal; in fact, the same fibers and cells can be identified at various stages during embryonic development of an organism.

With this system we have been trying to answer several specific questions:

(*a*) To what extent is there variation in the morphology of particular cells when they are examined in different but genetically identical animals raised under identical environmental conditions?

(*b*) Within the same animal, how precisely does the anatomy of a particular cell match the mirror image of its bilaterally symmetric mate?

(*c*) Mathematically precise bilateral symmetry must break down when fibers cross the midplane of an animal. Is this breaking down of symmetry a feature that occurs in the same way in different organisms?

(*d*) What is the sequence of developmental steps leading to the adult structure of the visual system, and is this sequence unique and reproducible within the clone?

(*e*) What clues concerning the means by which particular cells make specific connections can be obtained by following the progress of a particular neuron during its development?

These, as well as other questions, will be the subject of this and following papers. In this first paper we will present some results that bear upon questions (*a*) and (*b*), as well as some descriptive background of our system and technique that will serve as a basis for future papers.

Several studies of the anatomy of the visual system in various species of Daphnia have appeared in the literature. A thorough description of the general anatomy of *D. magna* has been published by Klotzsche (1), and major contributions on the genetics of different species have been made by Banta and collaborators (2). Of special interest in relation to our anatomical studies are the physiological experiments of Waterman (3) and others with the Daphnia visual system. Recently, several ultrastructural studies have been published that deal with the fine structure of the optic ganglia and the compound eye of *D. pulex* and *D. magna* (4–6). None of these studies dealt with the question central to this paper. However, their observations with respect to structures discernible in individual micrographs are in agreement with our own.

MATERIALS AND METHODS

Our starting culture of *D. magna* was obtained from the laboratory of T. H. Waterman. The present individuals are derived from the parthenogenic offspring of a single female. The culture is kept in a 24°C incubator with a 12-hr light–dark cycle (fluorescent lighting), at a maximum density of 10 adults per 100 ml of medium (0.2 g/liter of $NaHCO_3$; 25 mg/liter of K_2SO_4; 0.22 g/liter of $CaCl_2 \cdot 2H_2O$). The medium is changed every other day, at which time the animals are fed WT *Chlamydomonas reinhardi*, grown by innoculation of agar slants in SG2 medium (7). Under these growth conditions we have not observed any males or the laying of any resting eggs.

The animals chosen for the studies described in this report

were large adults, about 4 weeks old. No attempt was made to choose animals in the same instar. Careful staging is necessary, however, in our developmental studies and will be described in the next paper. The animals to be studied are removed from the medium, placed on wax plates, and cut in half to facilitate penetration during fixation and embedding.

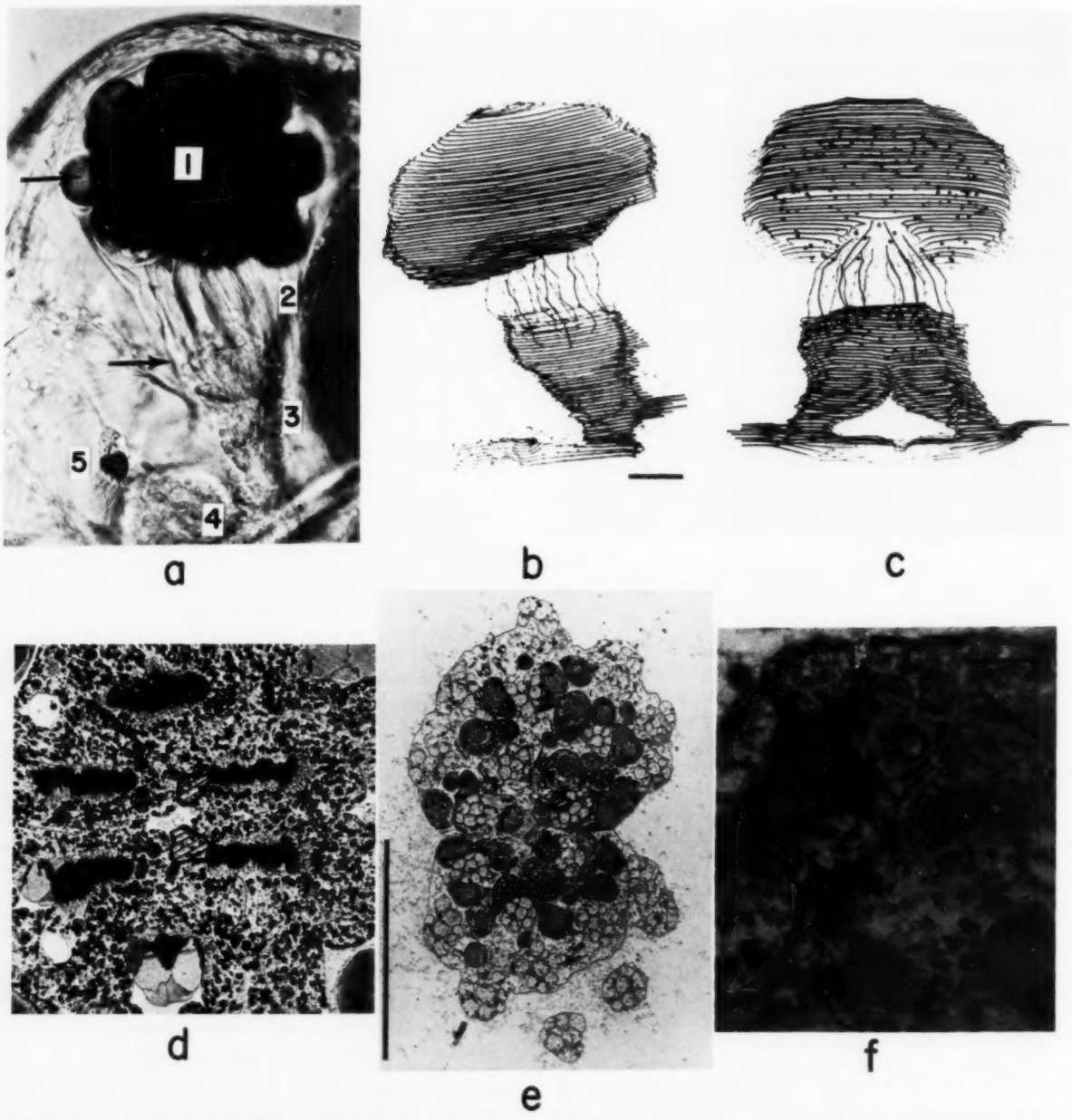

FIG. 1. (*a*) Lateral view of the visual system of a live *Daphnia magna*, showing the cyclopic eye (**1**), fibers (**2**), optic ganglion (**3**), anterior surface of the supraesophageal ganglion (**4**), and ocellus (**5**). The *arrows* show the levels of the micrographs in (*d*) and (*e*). (*b*) Computer reconstruction of the eye and optic ganglion from micrographs of serial sections; lateral view. The lines joining the eye and optic ganglion each represent a bundle of eight fibers. (*c*) Frontal view of the computer reconstruction, in this case also showing the location of the receptor-cell nuclei in the eye and the lamina-cell nuclei in the optic ganglion. Note that in this view one can see the two lobes of the optic ganglion quite clearly. (*d*) Electron micrograph of a thin section in the eye, showing some rhabdoms along the midplane. The *cross-hatched* cells are D2 on left (top) and right. The two groups of accessory cell fibers can be seen along the midline, on both sides of the rhabdoms that include cells D2. (*e*) Electron micrograph of a section in the optic ganglion, showing the 22 bundles of 8 fibers entering the lamina. Lamina cells and their nuclei are readily seen. The two *cross-hatched* fibers are the axons of cells D2 from (*d*). (*f*) High-power electron micrograph showing synaptic junctions in the neuropil of the optic ganglion. *Vesicles* fill the receptor cell terminal, which is presynaptic to a lamina cell process. *Bar* in (*b*) is 100 μm, also (*a*) and (*c*). *Bar* in (*e*) is 100 μm, also (*d*). *Bar* in (*f*) is 0.2 μm.

Immediately after cutting, the heads are placed into a 1% solution of OsO_4 in dichromate buffer (0.70% $K_2Cr_2O_7$) containing 0.85% NaCl. After an hour in the solution, the specimens are rinsed three times in buffer, then in 50% ethanol, stained in a uranyl acetate solution (0.5% in 50% ethanol) for 45 min, dehydrated with ethanol and propylene oxide, and embedded in Epon 812. The entire process is performed at room temperature (24°C). Serial sections about 1000 Å thick are cut on a Sorvall MT2B ultramicrotome and picked up on copper grids with a 1 mm × 2 mm hole previously covered with a formvar film coated with carbon. The top face of the trapezoidally trimmed epon block is coated with a glue consisting of Scotch tape adhesive dissolved from the tape with chloroform, so that the serial sections form ribbons during the cutting. Groups of from 5 to 10 sections are picked up on each grid. After post-staining with lead citrate, the sections are photographed on Kodak microfilm with a Zeiss EM-9S electron microscope modified for very low magnifications. Serial thick sections (1 μm) are cut and mounted on glass slides, stained with toluidine blue, and photographed with an optical microscope.

The original negatives are aligned and copied sequentially onto a 35-mm microfilm strip by use of an image combiner somewhat different from the one described by Levinthal and Ware (8). In this newer model, three stages are mounted at 120° on a rotating table; two can be viewed simultaneously and aligned, the third is photographed. After each negative is aligned, the table is rotated, a frame of the movie is exposed, the next negative is aligned, and so on. (A major feature of the new device was suggested to us by Dr. Sydney Brenner, who has markedly improved the version described by Levinthal and Ware.) The 35-mm movie of aligned serial sections is then projected onto a ground-glass screen at right angles to the computer oscilloscope screen, both being viewed in superposition with the aid of a half-silvered mirror at 45° to them. The recording of information from each section of tissue proceeds approximately in the manner described by Levinthal and Ware; however, the present version of the computer system by which this recording is made has been considerably modified. A detailed description of the software and hardware involved will appear elsewhere.

ORGANIZATION OF THE VISUAL SYSTEM OF *D. MAGNA*

The visual system of *D. magna* consists of a compound eye, an optic ganglion, which receives input from the compound eye and sends fibers to the central ganglion, and an ocellus, which connects directly to the central ganglion. The ocellus, which consists of some dozen pigmented cells, was not studied in any detail and will not be mentioned further. A light micrograph of the visual system is shown in Fig. 1*a*. The corresponding computer reconstruction is shown in two positions in Fig. 1*b* and *c;* Figure 1c also shows the location of the receptor- and lamina-cell nuclei. The eight receptor cells in one ommatidium that are filled with pigment granules surround the cone, and all contribute to the fused rhabdom. In any one section perpendicular to the axis of the ommatidium, only seven cells appear to contribute to this structure. Our serial section reconstructions, however, show that the eighth cell displaces one of the other cells about half-way back in the rhabdom, and that this cell also has a rhabdomere. The cross-section of the rhabdom is rectangular, with two end rhabdomeres and six lateral ones, two on one side and four on the other (Fig. 1*d*). The microvilli of the end cells and the lateral cells are perpendicular to each other and to the ommatidial axis. The receptor-cell nuclei are located near the surface of the eye, with the processes of these cells travelling centripetally to form the optic nerve. A layer of flat accessory cells lies between the crystalline cones at the surface of the eye. Two groups of small accessory cells, numbering about 10 cells each, send bundles of fibers from the surface of the eye to the center. These two groups lie on the midline of the eye, setting off the two central symmetric ommatidia, and providing an easy marker for the identification of these structures (Fig. 1*d*).

The 22 ommatidia consist of 176 receptor cells, 88 on each side of the midplane. Embryonically, this single compound eye appears to form at two loci, symmetrically located about the midplane, that later fuse into a single structure. In the adult, the receptor cells are arranged in an accurately mirror-symmetric fashion. This bilateral symmetry, however, does not hold for the accessory cells mentioned above that lie directly on and along the midline.

We have not found any synaptic or other specialized contacts between receptor cells in the eye itself. The processes from each cell, although in appearance touching other processes, make synaptic contacts only in the neuropil of the optic ganglion. We have not investigated the structure of the fused rhabdom in detail, and hence cannot altogether exclude cross-talk at this level in the eye, although random searches in single blow-ups of individual rhabdoms indicated a physical separation between rhabdomeres.

As the optic nerve exits posteriorly from the compound eye, it splits into 22 fascicles, each containing the eight processes from a single ommatidium. There are no cross-overs from different ommatidia, as is the case in some insects with unfused rhabdomeres. The 22 fascicles travel separately and diverge slightly from each other until they reach the optic ganglion, which they enter through a set of port-holes, each formed by 5 lamina neurons (see Fig. 1*e*).

The optic ganglion is a two-lobed structure with fused lobes symmetrically located about the midplane. A single layer of cells forms an anterior group, the lamina, with perikarya on the surface and processes that grow backward into the neuropil. This group is well separated from the posterior group, the medulla, by a ring of glial cells. The lamina contains 110 neurons; 5 neurons associate with each of the 22 fascicles. There are over 200 neurons in the medulla.

The lamina cells are arranged in the right and left lobes in a bilaterally symmetric fashion. A particular cell can always be identified by the position of its perikaryon in its quintet, as well as by its shape, level of branching, or connectivity pattern. Furthermore, its mirror symmetric counterpart in the other lobe has a symmetric structure except in the detailed anatomy of its branching pattern, as discussed below. For example, lamina neuron R4 (right side) is the only one of its quintet that has multiple branches leaving the perikaryon; the other four first form a narrow process, which branches further in the neuropil. Neuron L4 (left side), which occupies the mirror position, also branches from the perikaryon. The fact that any one neuron has a clear and unique geometric and connectivity signature is what permits the study of reproducibility from one specimen to the next.

The lamina neurons branch at a specific depth in the neuropil, but send a main process through and into the medulla region where they branch again. They receive their synaptic

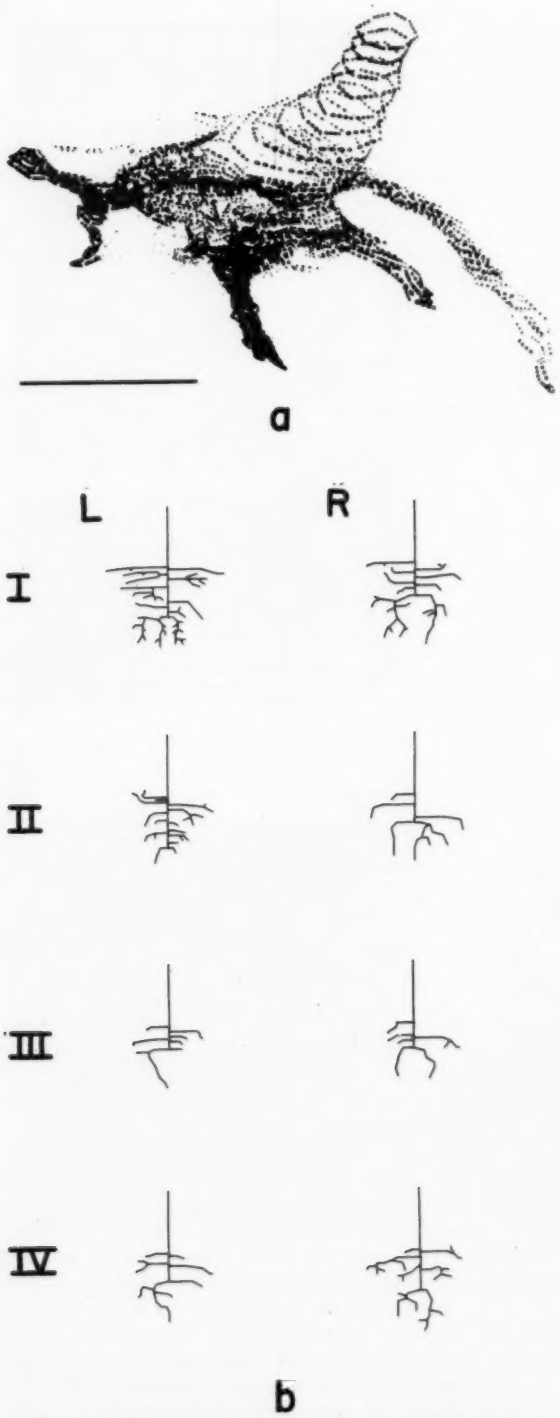

FIG. 2. (*a*) Computer reconstruction of a receptor-cell synaptic terminal. The cell body and the rest of the axon would extend above the figure. The *bar* is 10 μm. (*b*) Schematic representation of the branching sequence of the fiber shown in (*a*), but on the left (*L*) and right (*R*) of four specimens (I, II, III, and IV). The order, position and relative lengths of branches are maintained, but some angular distortion was necessary to avoid overlaps.

inputs mostly from one or two receptor cells, and make few or no synaptic contacts with other lamina cells. The receptor-cell processes show two types of behavior in the lamina uropil. Some in each bundle increase in volume and branch out profusely, making synaptic contact with specific lamina cells; others appear to go right through, making few or no connections. This behavior for any particular receptor cell is reproducible from organism to organism.

The neuropil itself is extremely complicated, because of the extensive interdigitation of the various processes. All space not occupied by neuron processes is filled by glial processes. These appear to isolate regions of synaptic contact of different pairs of cells, as well as neural processes that are passing through without making synaptic contacts. The synapses are mostly of the classic parallel type (Fig. 1*f*).

BRANCHING PATTERNS

Between the eye and optic ganglion the receptor cell axons have diameters that range between 2 and 4 μm. Within the neuropil, the axons increase in size 2- or 3-fold, and send out branches in various directions. The shape of the terminals is very irregular and very different for each of the eight axons, as is also the case for the lamina-cell processes. An example of a computer reconstruction of a retinular axon terminal is shown in Fig. 2*a*. We have performed such three-dimensional reconstructions in detail for two adjacent groups, symmetrically located about the midline, in four animals. The structures of the 16 receptor-cell terminals and the 10 associated lamina cells were recorded both as surface contours and as branching line patterns (see ref. 8), and the location and direction of identifiable synapses were noted. The volume of neuropil studied in great detail is about $20 \times 40 \times 15$ μm^3. Some axons terminate within this volume, and some continue through to the medulla region.

A great deal of variation is evident when the fine structure of a specific terminal both from left to right and from animal to animal is compared. This can be seen in Fig. 2*b*, where the branching patterns of a specific cell are shown schematically for the right and left sides of four different animals. (This is a cell that ends within the volume studied.) It is apparent from this figure that both the number and sequence of branches are variable. The differences are easily observed in the original three-dimensional recordings, which contain information such as angular distribution of branches that is difficult to represent schematically in two dimensions.

SYNAPTIC PATTERNS

The synapses found within the volume of the neuropil that we studied are classified as to whether they are pre- or post-synaptic with respect to the receptor cell in order to obtain a connectivity matrix. Such a matrix, for one group of receptor axons and associated lamina cells on one side of the optic ganglion of one animal, is presented in Table 1, which lists numbers of synapses between pairs of cells. The receptor cells (D1 to D8) make synapses with each other and with the lamina cells (R1 to R5). Some of the synapses involving a particular identified cell are to or from cells whose structure has not been traced. These are designated *Y* and *X* in Table 1. Tracing has been performed and the matrices have been constructed for the symmetric cells in the opposite side of the animal recorded in Table 1, and for both sides in three other animals. A summary of the data on the connectivity of receptor-cell

TABLE 1. *Connectivity matrix for one group of eight receptor cells (D1 to D8) and the corresponding group of lamina cells (L1 to L5)*

Pre-synaptic cell	Post-synaptic cell														
	D1	D2	D3	D4	D5	D6	D7	D8	L1	L2	L3	L4	L5	*Y*	Total
D1	0	0	1	0	3	0	2	1	0	62	0	0	0	37	106
D2	2	0	0	0	0	0	0	0	3	0	0	20	0	18	47
D3	0	2	0	0	0	0	0	6	48	1	0	0	0	40	97
D4	0	0	0	0	0	0	0	0	0	0	0	0	0	2	2
D5	3	0	0	0	0	2	3	0	0	2	0	0	82	33	125
D6	4	0	0	0	5	0	5	0	0	0	0	3	3	50	70
D7	4	0	0	0	2	1	0	0	0	0	0	0	0	1	8
D8	0	0	3	0	0	0	0	0	1	0	0	0	0	3	7
X	1	1	0	0	0	0	0	0	6	10	11	3	10	0	0

X and *Y* are unidentified processes. *The numbers* are the identified synapses between the corresponding pair of cells. *The numbers underlined* appear to be the principal connections in the volume of neuropil studied (Specimen III, *left side*).

axon D2 on the left and right of four animals is given in Table 2. It should be noted that the axon of cell D2 ends within the volume studied, and therefore the table lists all its synaptic connections onto lamina cells.

The data on the synaptic connectivity of the same group of cells on the right and left of the optic ganglion of four adult Daphnia indicates that, whereas the number of synapses between a pair of cells may vary from animal to animal, the overall pattern shows certain regularities. If we divide cell–cell interactions into three groups, (*a*) no synapses, cells topologically separate, (*b*) few synapses or zero, but cells touching and synapses possible, and (*c*) many synapses, that is, 15 or more synapses between the cells, we then find that the three groups are the same in all of the specimens studied. The variation in numbers of synapses is partly related to the variation in morphology of the synaptic terminal. This can be seen by comparison of Fig. 2*b* and Table 2, which give the branching pattern and synaptic pattern of cell D2 in the four animals. In general, an increase in branching is accompanied by an increase in synapses.

DISCUSSION AND CONCLUSION

The use of isogenic members of a single parthenogenic clone in these experiments gives us reasonable assurance that any differences we observe are not due to genetic variation. However, we have no reason to postulate that the differences observed in randomly selected members of a single species would be significantly greater. The use of isogenic animals means that we can defer consideration of genetically determined variation and concentrate for the present on the effect of environmental differences on the organisms.

As long as the position of cell bodies and the branching and synaptic pattern of nerve fibers are recorded to a resolution of a few micrometers, then great similarities are observed in different animals of the same cone and bilateral symmetry is observed between corresponding cells in the two sides of the same animal. However, when the branching and synaptic patterns are examined at levels of resolution ranging from a few tenths to a few micrometers, then significant variations are observed that seem to be approximately as great when comparing the two sides of the same animal as when comparing different members of the clone. There is, however, no reason to believe that these variations will be reflected in any physiological or behavioral observations, since they apparently correspond to differences in the strengths of interaction between specific cell pairs rather than the formation of new interactions.

Thus, our observation suggests that the location of, and the individual cells that contribute to, synaptic complexes in Daphnia are rigidly determined at least within a genetically identical clone. On the other hand, the synaptic and branching patterns that occur over distances of a few micrometers, as fibers terminate within a complex, seem to reflect the noise level of the genetic control of structure.

TABLE 2. *Connectivity matrix for cell D2, for four specimens (I to IV) on the left (L) and right (R) sides of the neuropil*

Specimen	Side	Post-synaptic cell					
		1	2	3	4	5	*Y*
I	*L*	10	0	0	54	0	42
	R	8	0	0	50	0	37
II	*L*	9	0	0	65	0	54
	R	4	0	0	36	0	38
III	*L*	3	0	0	20	0	18
	R	3	0	0	22	0	20
IV	*L*	6	0	0	41	0	54
	R	5	0	0	44	0	45

The post-synaptic cells are either those belonging to the associated lamina group (1 to 5) or unidentified (*Y*). *The numbers* are the identified synapses; *the number zero* also indicates here a topological separation, and hence no possible synapses.

We thank Mr. Kamil Ugurbil and Mr. Robert Campbell for their assistance in the work reported here, and Mr. Christos Tountas for the implementation of the computer programming system. This work was supported by NIH Grants RR00442(04) and 5RO1-A1-08902(04), and a gift from the RGK foundation.

1. Klotzsche, K. (1913) *Jena. Z. Naturwiss.* **43,** 601–646.
2. Banta, A. M. (1939) Carnegie Inst. Wash. Publ. **513,** 1–285.
3. Waterman, T. H. (1966) in *The Functional Organization of the Compound Eye,* ed. Bernhard, C. G. (Pergamon Press, New York), pp. 493–511.
4. Rohlich, P. & Toro, I. (1965) in *Eye Structure, 11 Symp.,* ed. Rohen, J. W. (Schattauer Verlag, Stuttgart), pp. 175–186.
5. Bohm, M. K. & Parker, R. A. (1968) *J. Morphol.* **126,** 373–394.
6. Wolff, J. R. & Guldner, F. H. (1970) *Z. Zellforsch. Mikrosk. Anat.* **103,** 526–543.
7. Sager, R. & Granick, S. (1953) *Ann. N.Y. Acad. Sci.* **56,** 831–838.
8. Levinthal, C. & Ware, R. (1972) *Nature* **236,** 207–210.

Proc. Nat. Acad. Sci. USA
Vol. 70, No. 1, pp. 62–65, January 1973

On the Theory of Ion Transport Across the Nerve Membrane, VII. Cooperativity Between Channels of a Large Square Lattice

(computer simulation/Ising kinetics/Adam model/correlation functions/phase transition)

YI-DER CHEN AND TERRELL L. HILL

Laboratory of Molecular Biology, National Institute of Arthritis, Metabolism, and Digestive Diseases, National Institutes of Health, Bethesda, Maryland 20014

Contributed by Terrell L. Hill, October 27, 1972

ABSTRACT **The exact kinetics of a 10 × 10 Ising system (periodic boundary conditions) with two-state channels arranged in a square lattice was studied by computer simulation. With all three values of the cooperativity parameter used, no induction in the K^+-current curve was obtained. This confirms one of our previous conclusions concerning K^+ channels in the squid axon membrane: models with interacting channels arranged in a two-dimensional lattice (Adam's model) are apparently excluded. Other topics included: equilibrium properties; short-range pair correlation functions; phase transition.**

In a previous paper (1), we investigated the exact kinetics of 2×2, 2×3, and 3×3 square Ising lattices with periodic boundary conditions to simulate Adam's model (2, 3): two-state (open and closed) K^+ channels arranged in a two-dimensional lattice with nearest-neighbor interactions between channels. It was shown that this model failed to generate induction or satisfactory superposition behavior, and therefore is presumably not applicable to K^+ transport across the nerve membrane. However, it is possible that one could be misled in the representation of a very large patch of channels by such small numbers as above. In this paper, we report the calculation of the kinetics of a much larger lattice, 10×10 with periodic boundary conditions, in order to extend the generality of the conclusion reached before with respect to induction behavior.

A system containing x channels in a lattice, each of which may be open or closed, has 2^x possible system states. In order to study the exact kinetics of this system with $x = 100$, a tremendous number of first-order differential equations would have to be solved. The formal matrix diagonalization method used before (1, 4) is not feasible in this case; both the computing time and computer memory needed would be too large. Therefore, the calculations were performed on a computer by Gordon's dynamic simulation (Monte Carlo) method (5). To check the program, the empirical results so obtained were first compared with some of the known exact properties of an infinite Ising system at equilibrium. The kinetics at three cooperativity strengths, $s = 0.7$, 0.5, and 0.4, was then investigated.

We refer the reader to similar work by Ogita *et al.* (6) in which Markov chains generated in discrete time steps were used to simulate the kinetics of an Ising system. However, their method is less efficient than the present procedure (5).

THE MODEL AND SIMULATION

Consider a 10×10 square lattice in which each site (channel) has four nearest neighbors. Each channel can be in one of two states, *i* (closed) and *ii* (open). The first row of the lattice is considered to be adjacent to the last row and the first column is considered to be adjacent to the last column (periodic boundary conditions). The notation for rate constants and nearest-neighbor interaction energies is the same as in the asymmetric (Adam) Schemes 8, 9, and 10 of ref. 1. Thus, the rate constants for the change in state of some particular channel are

$$(i \rightarrow ii)\ k_{12} = \alpha s^{2N_1} \qquad [1]$$

$$(ii \rightarrow i)\ k_{21} = \beta \qquad [2]$$

where N_1 is the instantaneous number of nearest neighbors to the particular channel that are in state *i* ($0 \leqslant N_1 \leqslant 4$) and

$$s = e^{w/2kT},\ w = w_{11} + w_{22} - 2w_{12}.$$

Here w_{11} is the $i - i$ pair interaction energy, etc. Of course N_1 fluctuates with time, but this is taken into account in the following procedure.

A state of the entire system is determined by the configuration (i.e., specification of state *i* or *ii* for each channel) of the lattice. When the system is in any given state, l, x possible events may occur, yielding a transition to a different system state m, by changing the state (*i* or *ii*) of some one channel in the lattice. Eqs. **1** and **2**, together with the complete configuration of the lattice, provide the x rate constants that are operative here. We follow Gordon (5) in using a random number generator to decide which event actually occurs and in assigning a mean time interval $\langle \Delta t_l \rangle$ to the event.

If some property of the system X (e.g., the number of open channels) has the value X_l in system state l, then at equilibrium ($t \rightarrow \infty$) the mean value of X is the time average

$$\bar{X} = \sum_l X_l \langle \Delta t_l \rangle / \sum_l \langle \Delta t_l \rangle \qquad [3]$$

where the sum is over a consecutive sequence of a very large number (e.g., tens of thousands) of system states.

If the system is not at equilibrium, we could follow by computer the event by event values of X_l and $\langle \Delta t \rangle_l$, and thus be able to plot $X(t)$. However, this is inconvenient and unnecessarily detailed. Instead, we can group together a consecutive sequence of a relatively small number of system states (say of order 10 or 100) and assign an average $\bar{X}$ from Eq. **3** to the time interval $\Sigma_l \langle \Delta t_l \rangle$, thus giving $\bar{X}(t)$. This can be done (see below for examples) with either a fixed number of consecutive system states per averaging step or a fixed time interval $\Sigma_l \langle \Delta t_l \rangle$ per averaging step. The latter procedure

is generally more convenient because what we are primarily interested in is a further average of the function $\bar{X}(t)$ over a large number of "runs" (this is equivalent to averaging over an ensemble of identical patches of channels, each with $x = 100$). Clearly, the "fixed time" procedure makes the latter averaging easier and produces points $\bar{X}(t)$ equally spaced along the time axis.

In this study, the state variables of the system of particular interest are the fraction of open channels p (the fraction of channels in state *ii*), and the short-range pair correlation functions, $\langle S_{y,z}\, S_{y,z+1}\rangle$, $\langle S_{y,z}\, S_{y,z+2}\rangle$, $\langle S_{y,z}\, S_{y+1,z+1}\rangle$, and $\langle S_{y,z}\, S_{y+1,z+2}\rangle$, where y and z denote the coordinates of a channel in the lattice and the values of S are taken to be $+1$ for channel state *i* and -1 for state *ii*. The brackets mean averaging the product over the entire lattice.

CALCULATIONS ON EQUILIBRIUM SPIN SYSTEMS AT ZERO MAGNETIC FIELD

Several exact properties of an infinite square Ising-spin system at zero magnetic field have been found by Onsager (7), Kaufman and Onsager (8), Yang (9), and others. After translating (10) some of these results into our notation, comparison with 10×10 simulated values provides a check on the correctness of the computational algorithms and on the adequacy of representing an infinite lattice by a 10×10 lattice (with periodic boundary conditions).

Zero magnetic field, $H = 0$, in the usual spin system would lead to the result (in our notation) $\bar{p} = 1/2$ (averaged over infinite time). It is easy to see, by consideration of detailed balance at equilibrium in Schemes 8 and 9 (1), that the parameter choice (equivalent to $H = 0$) required to produce $\bar{p} = 1/2$ is $\beta/\alpha = s^4$.

In the special case $\beta/\alpha = s^4$, then, we have calculated $\bar{p}$ and the four shortest-range pair-correlation functions (see above) for a few temperatures in the range $0.88 < T/T_c < 1.4$. A single long simulation run was used for each temperature. The temperature is determined by the value of s: $s = e^{w/2kT}$. The critical value of s (7) is $s_c = e^{w/2kT_c} = \sqrt{2} - 1 = 0.4142$.

A special comment is required concerning $\bar{p}$ when $T < T_c$. Over infinite time, the computer simulated system would spend equal amounts of time in two different phases with $\bar{p}$ values of, say, $\bar{p}' > 1/2$ and $1 - \bar{p}' < 1/2$, so that the overall $\bar{p} = (\bar{p}'/2) + [(1 - \bar{p}')/2] = 1/2$. However, in our calculations the system was started and then remained in the $\bar{p}'$ phase because of an extremely long nucleation time for the phase transition.

Fig. 1 shows the theoretical $\bar{p}'$ ($T < T_c$) and $\bar{p}$ ($T > T_c$) curves (infinite system), together with computer simulated points (10×10 system). The $\bar{p}'$ curve is also the "coexistence curve" (10), in lattice-gas language, or the spontaneous magnetization per spin (10) in a spin system (change the ordinate scale, in this case, from $0.5 \leftrightarrow 1.0$ to $0 \leftrightarrow 1.0$).

The length of simulation run used for each point varied from 10,000 to 40,000 consecutive events; these numbers are indicated in the figure.

Fig. 2 shows the theoretical correlation function curves and computed points from the same simulation runs as in Fig. 1. The results in both figures indicate that the 10×10 (periodic boundary conditions) system is a very good approximation to the infinite system. Of course, the scatter of points around the theoretical curves would decrease with increasing lengths of simulation runs.

The computer print-outs for both $\bar{p}(t)$ and the correlation functions exhibit two kinds of fluctuations: one with small

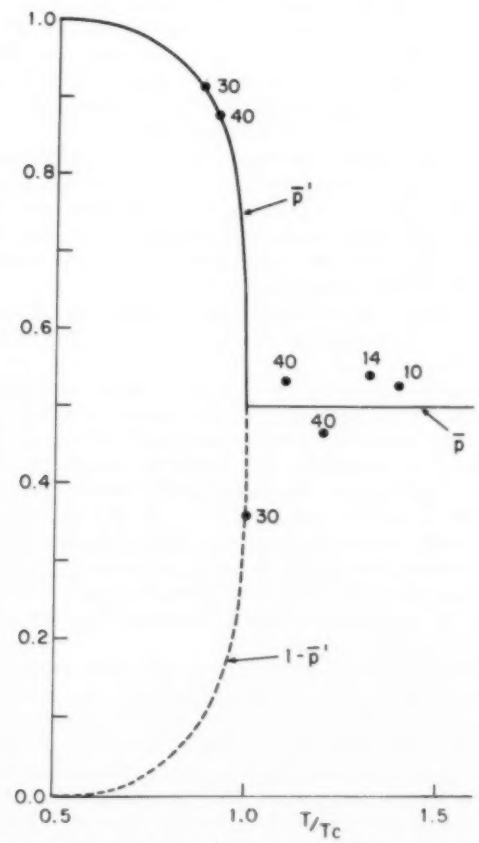

FIG. 1. Mean number of channels in state *ii* (open) at equilibrium with $\beta/\alpha = s^4$ (corresponding to zero magnetic field in a spin system). *Curves* are exact for an infinite system; *points* are computer simulated for a 10×10 system by use of a single run of the number of thousands of consecutive events indicated beside each point.

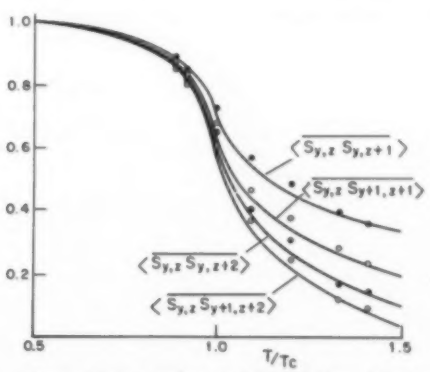

FIG. 2. Four shortest-range pair-correlation functions at equilibrium with $\beta/\alpha = s^4$ (corresponding to zero magnetic field in a spin system). *Curves* are exact for an infinite system; *points* are computer simulated for a 10×10 system by use of the same runs as in Fig. 1.

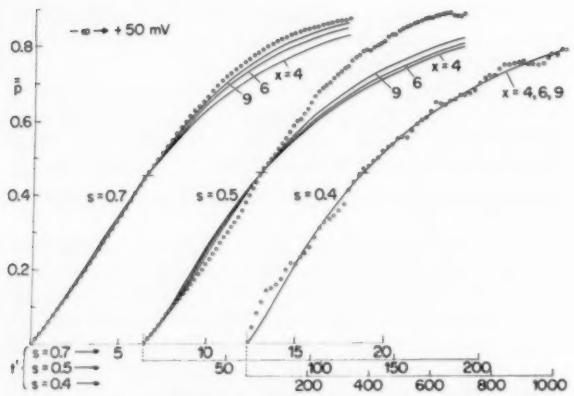

FIG. 3. $\bar{p}(t)$ points for $x = 100$ superimposed on $x = 4,6,9$ curves from Fig. 8 of ref. 1. Time scales are for the $x = 4$ cases. The time scales for $x = 6$, 9, and 100 are adjusted to give the same $t'_{1/2}$ as for $x = 4$. The definition of t' is $(\alpha + \beta)t$.

amplitude and short period; and another with large amplitude and long period (the amplitude and period of the latter increase when the temperature approaches the critical value). In general, the period of the long $\bar{p}$ fluctuation is longer than those of the pair correlation functions. In fact, as $T \to T_c+$, this long $\bar{p}$ period becomes of the same order as the length of the runs used. This accounts for the greater scatter in $\bar{p}$ points.

CALCULATION OF KINETIC PROPERTIES

In order to make a comparison with our previous results in Fig. 8 of ref. 1, we calculated $\bar{p}(t)$ starting from a system state with all channels in state i ($\bar{p} = 0$) and ending with $\bar{p} \cong 0.895$, thus simulating the depolarization of the K^+ channels of a squid axon membrane from a maximally hyperpolarized state to E_{Na} (1). Three values of the cooperativity parameter, $s = 0.7$, 0.5, and 0.4, were used. Note that $s = 0.4$ is below $s_c = 0.4142$.

For each value of s, it was first necessary to make several equilibrium runs to determine by interpolation the approximate value of β/α that leads to $\bar{p}(\infty) \cong 0.895$.

With these approximate values of β/α, 100 simulation runs were performed for $s = 0.5$ and 0.7, and 60 runs for $s = 0.4$, to obtain ensemble averaged $\bar{p}(t)$ points from the individual "fixed-time" points $\bar{p}(t)$ obtained from each run. The three sets of $\bar{p}(t)$ points ($x = 100$) are shown in Fig. 3, superimposed on the $x = 4$, 6, 9 curves taken from Fig. 8 of ref. 1. As with $x = 6$, 9 (1), the time scales of the $\bar{p}(t)$ points ($x = 100$) have been adjusted to give approximately the same $t'_{1/2}$ (1) as for $x = 4$ [t' is defined (4) as $(\alpha + \beta)t$].

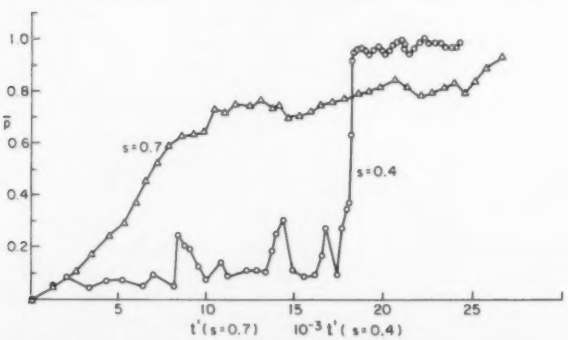

FIG. 4. The mean fraction of open channels p as a function of time in a single simulation run. Each point represents an average value of p over 10 consecutive system states for $s = 0.7$ and over 300 such states for $s = 0.4$.

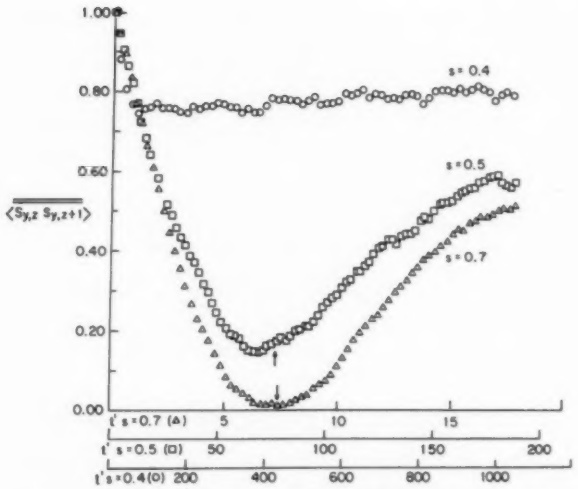

FIG. 5. Pair correlation function $\overline{\langle S_{y,x} S_{y,x+1} \rangle}$ corresponding to $x = 100$ in Fig. 3. Time scales are the same as in Fig. 3. The two small *arrows* indicate the time at $\bar{p} = 0.5$.

We used a smaller number of runs for $s = 0.4$ because of the much greater computer time required per run. Ideally, of course, since $s = 0.4$ is so near $s = s_c$, we should have used an appreciably larger number of runs for $s = 0.4$ than for $s = 0.5$ or 0.7. This would have reduced the considerable scatter apparent in the $\bar{p}(t)$ points for $s = 0.4$.

Incidentally, the average number of events per $\bar{p}(t)$ point per run in Fig. 3 is 597 for $s = 0.4$, 16.2 for $s = 0.5$, and 3.45 for $s = 0.7$.

The results shown in Fig. 3 for $x = 100$ are approximate in various ways (especially the β/α values), as indicated in the above discussion, but they seem to us to be more than adequate to demonstrate the qualitative point of primary interest in this paper: the experimentally observed induction behavior in the K^+ current near $t = 0$ (1, 4) is not recovered in a model with cooperative interactions between channels on increasing the size of the patch of interacting channels to a size, which for practical purposes, is essentially infinite. Thus, the conclusions reached in discussing Figs. 6, 7, and 8 of ref. 1 are reinforced here.

Although smooth curves through the three sets of $\bar{p}(t)$ points in Fig. 3 are very similar in shape, the behavior of the individual $\bar{p}(t)$'s from which the average $\bar{p}(t)$'s were derived is quite different. For example, at $s = 0.7$, the change of the lattice with time from the initial to the final configuration is more or less gradual, and the general appearance of $\bar{p}(t)$ does not differ much from one run to another. But at $s = 0.4$, in an individual run, the lattice tends to stay in the initial "dilute" (small $\bar{p}$) configuration for a considerable time and then changes quite suddenly to the final stable "dense" configuration when a large enough fluctuation nucleates the phase transition. The phase transition is a random process and the nucleation times are Poisson distributed.

For somewhat smaller values of s than $s = 0.4$ we would then expect a simple exponential $\bar{p}(t)$ curve. This phenomenon was already encountered (indirectly) with $x = 4$ and discussed near the end of ref. 4.

Fig. 4 contains an illustration of the above comments in which, for variety, we have used "fixed number" averaging rather than "fixed time" averaging: each point $\bar{p}(t)$ in the figure is an average over 10 consecutive system states for $s = 0.7$ and an average over 300 such states for $s = 0.4$. The two time scales used differ by a factor of 1000. In the $s = 0.4$ case, note the much shorter mean lifetime of system states after the transition (because of the factor s^{N_1}).

Finally, we supplement the $\bar{p}(t)$ results ($x = 100$) in Fig. 3 with plots in Fig. 5 of the time dependence of the shortest range correlation function obtained from the same computer runs as in Fig. 3, and using the same time scales as in Fig. 3. The $s = 0.7$ system has an almost random distribution of channels at $\bar{p} = 0.5$. The relatively flat correlation function for $s = 0.4$ arises because, roughly speaking, what is happening in this case as time passes is random and sudden phase transitions (see above) in the ensemble of 60 systems from a phase with $\bar{p} \cong 1 - 0.895$ to another with $\bar{p} \cong 0.895$. But these two phases would have approximately the same value of the correlation function, so this quantity remains roughly independent of time. The argument is not exact because the former phase is not an equilibrium phase while the latter is an equilibrium phase.

The other three correlation functions (not shown) behave in much the same way.

1. Hill, T. L. & Chen, Y. (1971) *Proc. Nat. Acad. Sci. USA* **68**, 2488–2492.
2. Adam, G. (1970) in *Physical Principles of Biological Membranes*, eds. Snell, F., Wolken, J., Iverson, G. & Lam, J. (Gordon and Breach, New York).
3. Adam, G. (1972) in *Proceedings of International Symposium on Synergetics (Cooperative Processes)*, ed. Haken, H. (Schloss Elman, W. Germany), in press.
4. Hill, T. L. & Chen, Y. (1971) *Proc. Nat. Acad. Sci. USA* **68**, 1711–1715.
5. Gordon, R. (1968) *J. Chem. Phys.* **49**, 570–580.
6. Ogita, N., Ueda, A.; Matsubara, T., Matsuda, M. & Yonezawa, F. (1969) *J. Phys. Soc. Jap.* **26** Supplement, 145–149.
7. Onsager, L. (1944) *Phys. Rev.* **65**, 117–149.
8. Kauĭman B. & Onsager, L. (1949) *Phys. Rev.* **76**, 1244–1252.
9. Yang, C. N. (1952) *Phys. Rev.* **85**, 808–816.
10. Hill, T. L. (1956) *Statistical Mechanics* (McGraw-Hill, New York), chap. 7.

Proc. Nat. Acad. Sci. USA
Vol. 70, No. 1, pp. 66–70, January 1973

Electron Spin Resonance Studies of Spin-Labeled Mammalian Cells by Detection of Surface-Membrane Signals

(lipid-soluble labels/living nucleated cells/erythrocytes/potassium ferricyanide)

JOSEPH KAPLAN*, PETER G. CANONICO, AND WILLIAM J. CASPARY†

United States Army Medical Research Institute of Infectious Diseases, Frederick, Maryland 21701

Communicated by Harden M. McConnell, October 25, 1972

ABSTRACT **Lipid-soluble spin labels were incorporated into human lymphocytes and mouse L-cells and the resulting electron spin resonance spectra were compared with spectra obtained from similarly labeled human erythrocytes. Spin labels were found in all subcellular fractions of the nucleated cells that contained membranes. Spin-labeled cells remained viable and capable of replicating *in vitro*. Electron spin resonance signals from spin-labeled nucleated cells underwent a time- and temperature-dependent decay that was reversed by bathing the cells in $K_3Fe(CN)_6$. The demonstration of a relative cell impermeability to ferricyanide, as measured by both colorimetric and radioisotopic label methods, indicated that only spin-labeled molecules in the surface membrane were reactivated when ferricyanide was added to spin-labeled cells after the electron spin resonance signal had decayed.**

Electron spin resonance (ESR) spectroscopy and spin-label techniques have been used recently to probe the structure of artificial membranes (1, 2) and membranes of erythrocytes (3), neurospora (4), viruses (5), lobster walking nerves (6), sarcoplasmic reticulum (7), and mycoplasma (8). However, information is not available regarding application of spin-label techniques to studies with intact nucleated mammalian cells. A major problem in the application of ESR techniques to studies of surface membrane phenomena in intact cells is differentiating between labels attached to cell surface and those bound to internal membrane structures.

This report describes a technique for differential detection of surface-membrane signals from spin-labeled, intact nucleated mammalian cells. The cellular distribution and spectral characteristics of various lipid-soluble spin labels incorporated in membranes of mouse L-cells and human lymphocytes are described. ESR spectra of these spin-labeled nucleated cells are compared with spectra of spin-labeled human erythrocytes. In addition, factors affecting signal stability and the effect of label incorporation on cell viability and replication are reported.

MATERIALS AND METHODS

Spin Labels. All spin labels were purchased from Syva Assoc., Palo Alto, Calif. The spin labels used were (Fig. 1): I(m,n), stearic acid analogs with the nitroxide ring located at the hydrophilic end (m,n = 12,3) or at the hydrophobic end (m,n = 5,10); II, an androstane spin label; and III, an organophosphate spin label.

Mammalian Cells. Mouse L-cells were grown in suspension in Eagle's Minimal Essential Medium (ME medium) containing 10% fetal-calf serum. Human lymphocytes, cell line RPMI 1788 derived from a normal donor (Associated Biomedia Systems, Inc., Buffalo, N.Y.), were cultured in medium RPMI 1640 (Associated Biomedia Systems, Inc., Buffalo, N.Y.) with 10% fetal-calf serum. Cells were harvested by centrifugation at 250 × g for 10 min and washed three times with 20 volumes of ME medium. Fresh human erythrocytes were prepared from heparinized venous blood obtained from healthy male donors.

Spin-Labeled Cells. 50 μl of 0.1 M label in 100% ethanol were mixed in 30-ml screw-capped glass tubes with 25 ml of 2% (v/v) L-cells or lymphocytes in ME medium, or with 2% (v/v) erythrocytes in phosphate-buffered saline. After incubation at 37° for 15 min with end-over-end rotation, cells were centrifuged at 250 × g for 10 min, and washed three times.

ESR Spectra. ESR spectra were obtained at room temperature (23°) in flat quartz cells in a Varian E-9 dual cavity ESR spectrometer. Spin-label concentrations were determined with a Fabritek 1074 Signal Averager that allowed double integration of signals from the sample and from a simultaneously run standard. All suspensions and supernates from final washes were examined for ESR signal immediately after preparation and after incubation at 23° or 37°.

Cell Fractionation. Subcellular fractions of L-cells labeled with stearic acid I(12,3) were obtained by differential centrifugation of cell homogenates. Packed cells, suspended in ME medium to yield a 20% (v/v) solution, were homogenized by 16 rapid strokes in a chilled motor-driven Duall homogenizer. Four subcellular fractions were isolated by differential centrifugation of the homogenate. A nuclear pellet, N, was separated at 2000 × g for 6 min. After suspension in ME medium to 50% of the original volume of homogenate, the nuclear pellet was given three additional strokes in the Duall homogenizer and again centrifuged. Supernates were combined and centrifuged at 25,000 × g for 10 min to obtain a mitochondrial fraction (M), and at 48,000 × g for 60 min to obtain a microsomal fraction (P). The final supernate was the soluble fraction (S). N, M, and P fractions were concentrated by suspending them to 50% or 25% of the homogenate's original volume. Relative concentrations of label in each of the subcellular fractions were determined.

* Present address: Child Research Center, Children's Hospital of Michigan, 3901 Beaubien Blvd., Detroit, Mich. 48201
† Present address: Department of Radiological Sciences, Johns Hopkins University School of Hygiene and Public Health, Baltimore, Md. 21205

$K_3Fe(CN)_6$ Studies. The ESR signal of a 50% suspension in medium RPMI 1640 of L-cells labeled with I(12,3), I(5,10), or II was allowed to decay by incubation at 37°. After signal decay, the cells were incubated with various concentrations of $K_3Fe(CN)_6$ (Sigma Chemical Co., St. Louis, Mo.) and immediately examined in the spectrometer for reactivated signal strength.

In experiments to determine the ability of $K_3Fe(CN)_6$ to penetrate cell membrane, I(5,10)-labeled L-cells were incubated as a 50% suspension in 1 mM $K_3Fe(CN)_6$ in RPMI 1640 for 10 min at 23°, and then pelleted at 1000 × *g* for 10 min and washed four times in 10 volumes of 0.01 M phosphate-buffered saline (pH 7.2), to remove unattached $K_3Fe(CN)_6$. After the final wash, cells were lysed by suspension in 10 ml of distilled water, freeze-thawed three times, and clarified by centrifugation at 30,000 × *g* for 20 min. The amount of ferrocyanide in supernates and cell lysate was determined by the colorimetric method of Avron and Shavit (9) with sulfonated 4,7-diphenyl-1,10-phenanthroline (C. F. Smith Co., Columbus, Ohio). This method allows detection of 1 μM ferrocyanide. Ferricyanide was measured as the increase in ferrocyanide after addition of excess sodium hyposulfite.

In other experiments, the distribution of ferricyanide was measured by addition of 2.5 μCi of $K_3{}^{59}Fe(CN)_6$ (Amersham-Searle Corp., Arlington Heights, Ill.) to a 25% suspension of I(12,13)-labeled L-cells after they had undergone signal inactivation at 37° and reactivation with 0.1 mM ferricyanide. 2 ml of the cell suspension was layered on top of a discontinuous gradient consisting of 2-ml portions of 2.5, 5, 8, and 10% Ficoll in RPMI 1640. The cellulose nitrate centrifuge tube was spun at 196 × *g* for 10 min. After centrifugation of the sample layer, the 5 and 8% Ficoll layers were removed by piercing the side of the tube with a 22-gauge needle. The cell pellet was suspended in 2 ml of Hank's balanced salt solution, and aliquots were assayed for radioactivity in a Nuclear Chicago gamma scintillation counter before and after repeated washing with 10 volumes of fresh RPMI 1640 medium.

Viability and Growth of Spin-Labeled L-Cells. L-Cells labeled with either androstane or stearic acid I(12,3) or I(5,10) were suspended to 0.4 × 10^6 cells per ml in ME medium with 10% fetal-calf serum and cultured in spinner flasks at 37°. At 0, 24, and 48 hr, cell counts were performed in a hemocytometer and cell viability was determined by trypan blue exclusion.

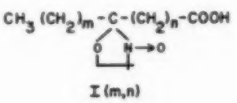

I (m,n)

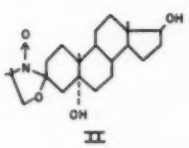

II

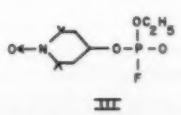

III

FIG. 1. Spin labels used in cell labeling studies.

RESULTS

ESR spectra consisting of three absorption peaks or lines are characteristic for nitroxide spin labels. The monitoring system records the first derivative of each peak. Alterations in mobility of the spin label result in changes in the line width and the splitting, or distance, between the lines of the spectra. In general, as the spin label becomes increasingly hindered by its environment, the splitting and line width increase.

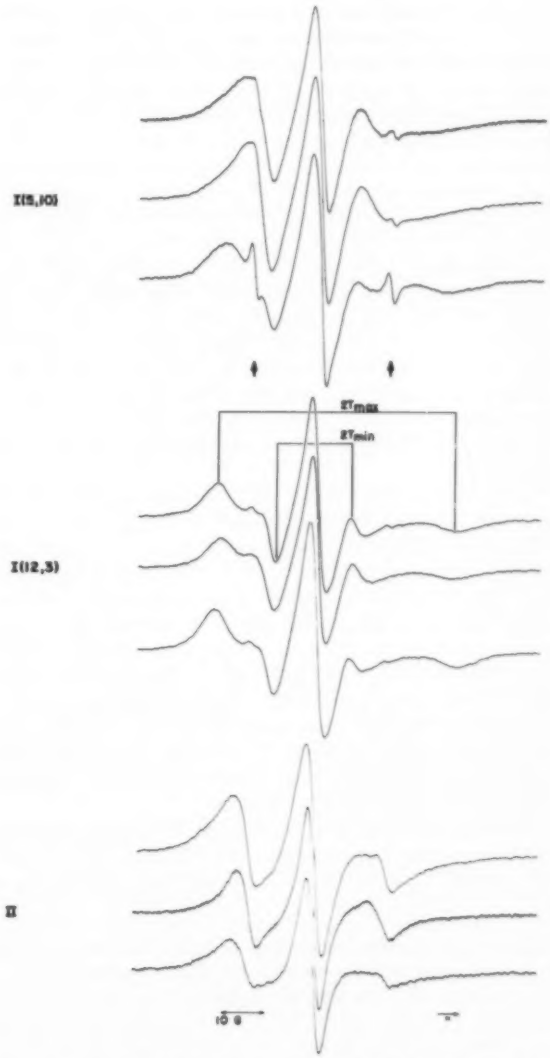

FIG. 2. Comparison of the spectra of spin labels I(5,10), I(12,3), and II incorporated into intact mouse L-cells, human lymphocytes, and human erythrocytes (*top*, *middle*, and *lower* spectra of each triad, respectively). *Vertical arrows* indicate the positions of the low-field and high-field "free-spin" peaks. T_{max} and T_{min} are the components of the hyperfine tensor as experimentally determined from the spectra as shown.

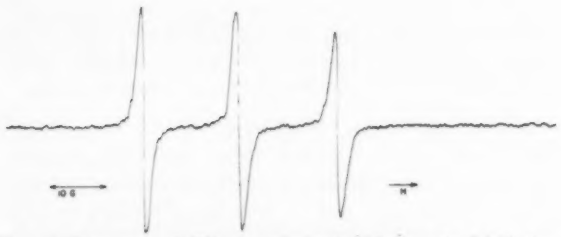

FIG. 3. Spectrum of III, an organophosphate spin label, incorporated into intact mouse L-cells.

All four lipid-soluble spin labels were readily incorporated into cells, as evidenced by a greater signal strength and different spectral shape of washed cells than of their final wash. In each case, the ESR signal from the final wash was relatively weak and consisted of three sharp, narrowly spaced lines of nearly equal height that reflected molecules undergoing rapid isotropic tumbling similar to the spectra of spin labels dissolved in medium. In contrast, spectra of stearic acid- and androstane-labeled cells (Fig. 2) were superpositions of two spectra—one due to "membrane-bound" label and the other due to "free-spin" label. "Membrane-bound" label was represented by three broad and relatively widely split peaks, while "free-spin" contributed three sharp lines (of which the outer lines are indicated by arrows) with splittings of 14.5 G. Since this "free-spin" signal was identical to that obtained from the final wash and persisted in both cell suspension and final wash regardless of the number of washes performed, it probably represented spin label released into the suspending medium and at equilibrium with "membrane-bound" label.

When spectra of the three cell types were compared, there were no differences between spectra of similarly labeled L-cells and lymphocytes. However, as shown in Fig. 2 and Table 1, splitting, reflected by T_{max}, S values (a quantitative measure of the anisotropy of the membrane), and line width were both smaller in spectra of spin-labeled L-cells and lymphocytes than in spectra of spin-labeled erythrocytes. Fig. 2 also shows that spectra of cells spin-labeled with stearic acid I(5,10), which contains the nitroxide ring attached in a hydrophobic region, were characterized by narrower line widths and smaller splittings than spectra of the same cells spin labeled with stearic acid I(12,3) in which the nitroxide ring is attached in a hydrophilic region.

The spectrum of label III, a spin-labeled phosphofluoridate inhibitor of acetylcholinesterase, in L-cells is shown in Fig. 3. It consisted of three narrowly spaced lines reflecting rapid unrestricted tumbling of the molecule. This represented cell-bound label, since the signal strength from cell suspension was at least 100 times greater than the signal obtained from the final wash. A similar spectrum was obtained from label III incorporated into erythrocyte membranes.

TABLE 1. *Hyperfine tensor components and orientation factors, S*, for labeled stearic acid, I(12,3), in erythrocytes, L-cells, and lymphocytes*

Cell	$2\,T_{max}$	$2\,T_{min}$	S
L-cell	54.7 ± 0.6	17.7 ± 0.3	0.64
Lymphocyte	53.7 ± 0.9	18.1 ± 0.2	0.61
Erythrocyte	59.8 ± 0.5	17.3 ± 0.4	0.70

* $S = (T_{||} - T_{\perp})/(T_{zz} - T_{xx})\,a^{\ddagger}/a'$ where $T_{||} = T_{max}$, $T_{\perp} = T_{min} + 0.8$ G, $T_{zz} - T_{xx} = 25$ G (10). $a = 2\,T_{xx} + T_{zz}^{\ddagger}$, $a' = 2\,T_{\perp} + T_{||}^{\ddagger}$.

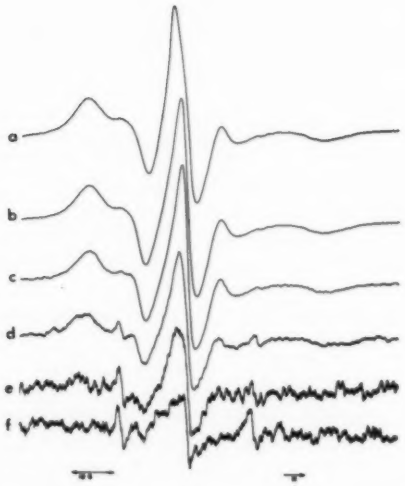

FIG. 4. Spectra of subcellular fractions from I(12,3)-labeled mouse L-cells. (*a*) Intact L cells; (b) homogenate; (*c–f*) nuclear, mitochondrial, microsomal, and soluble fractions, respectively.

Spectra of subcellular fractions from stearic acid I(12,3)-labeled L-cells are shown in Fig. 4. After exposure to 0.5 mM $K_3Fe(CN)_6$, ESR signal characteristic of "membrane-bound" label was detected in all membrane-containing fractions. Only a weak, "free-spin" signal was found in the soluble fraction. As measured by relative signal strength, most of the label was found in the "nuclear" fraction, which contains predominantly nuclei and plasma membranes (Table 2). No gross differences were found in the shapes of spectra from the different membrane-containing fractions.

Decay of cell signal observed for L-cells and lymphocytes, but not for erythrocytes, proceeded more rapidly at 37° than at 23°. Aeration of suspensions or exposure to $K_3Fe(CN)_6$ were effective means of restoring the cell signal. The lowest concentration of $K_3Fe(CN)_6$ that reactivated cell signal was 0.1 mM and resulted in a signal strength of about 0.1 mM. When ferricyanide was removed by washing, the cell signal disappeared, but reappeared immediately upon reexposure to ferricyanide. When stearic acid I(5,10)-labeled L-cells

TABLE 2. *The relative amounts of stearic acid I(12,3) incorporated into subcellular fractions of L-cells*

Fraction	% Total label*
Nuclear	87
Total mitochondria	8.4
Microsomal	1.4
Cell sap	3.2

* The amount of label in each fraction was obtained by integration of the respective spectra.

$$\%\ \text{of total label} = \frac{\text{mmol label in each fraction}}{\text{total mmol label in all fractions}}.$$

were suspended in 1 mM $K_3Fe(CN)_6$ and then washed and lysed, ferricyanide and ferrocyanide were found in initial washings; neither was detected in the cell lysate (Table 3).

After the addition of $K_4{}^{59}Fe(CN)_6$ to L-cells spin-labeled with I(12,3), only 1% of the initially added isotope was recovered with the cells after they were sedimented through a discontinuous Ficoll gradient and repeatedly washed (Table 4). Most of the isotope remained in the supernate above the Ficoll, while only trace amounts were detected in aliquots of either the 5% or 8% Ficoll layers above the cell pellet.

To determine whether spin-labeled cells maintain biological function, we studied the growth in suspension culture of L-cells labeled with stearic acid I(5,10), I(12,3), and androstane. After 48 hr, cell counts and viability of labeled and unlabeled L-cells were essentially the same. Both had approximately doubled in population.

DISCUSSION

These studies demonstrate that lipid-soluble spin labels are readily incorporated into membranes of intact viable nucleated cells. While the bulk of label incorporation probably occurs by simple solubility in hydrophobic regions, it is possible that some spin label may be enzymatically coupled with glycerol moieties to form phospholipid molecules. Keith *et al.* (4) reported that this coupling occurred after they grew neurospora in the presence of I(5,10).

It should be noted that the ease with which lipid-soluble spin labels enter membranes must be considered in the design and interpretation of studies of membrane-receptor sites when spin-labeled ligands are used. For example, our finding that the spin-labeled phosphofluoridate inhibitor of acetylcholinesterase is readily incorporated into L-cell membranes that do not contain acetylcholinesterase suggests reconsideration of the interpretation of a previous study on erythrocyte acetylcholinesterase (11), in which specific attachment of spin-labeled phosphofluoridate to erythrocyte-membrane acetylcholinesterase was reported. Our studies indicate that spin-labeled phosphofluoridate, probably by virtue of its solubility in lipids, is incorporated nonspecifically into membranes.

Each spin-labeled compound used for incorporation into cell membranes yielded nearly identical spectra for both L-cells and lymphocytes. However, comparison of these with spectra of similarly labeled erythrocytes showed a consistent difference. The immobility and anisotropy of the nitroxide was always greater in erythrocyte membranes than in L-cell or lymphocyte membranes. This greater fluidity of lipid phases of L-cell and lymphocyte membranes compared to that of erythrocyte membranes may result from differences in membrane-lipid composition since the mobility of spin-labeled fatty acids in synthetic membranes varies with changes in membrane-lipid composition (2, 12, 13).

TABLE 3. *Distribution of $Fe(CN)_6^{+3}$ and $Fe(CN)_6^{+2}$ in wash fluids and lysate of L-cells spin-labeled with I(5,10)**

	Ferricyanide (μmol)	Ferrocyanide (μmol)
Initial amount	1.0	<0.01
Wash fluid no. 1	0.11	0.65
no. 2	0.02	0.16
no. 3	<0.01	<0.01
no. 4	<0.01	<0.01
Cell lysate	<0.01	<0.01

Total recovery of ferricyanide and ferrocyanide was 93% of the amount of ferricyanide initially added.

* 1 ml of a 50% cell suspension containing 1.0 μmol of ferricyanide.

TABLE 4. *Distribution of $^{59}Fe(CN)_6^{+3}$ in L-cells spin-labeled with I(12,3)*

	cpm*	% of total radioactivity
Initial suspension placed on gradient†	69,800	100
Sample layer	64,900	93
5% Ficoll layer	279	0.43
8% Ficoll layer	209	0.33
Original cell pellet‡	1,820	2.6
after 1st wash	1,050	1.5
after 2nd wash	916	1.3
after 3rd wash	726	1.0

* cpm/50-μl aliquot (average of three experiments).

† 2 ml of a 25% L-cell suspension layered on a Ficoll gradient as described in text.

‡ Each cell pellet was resuspended in 2 ml of medium RPMI 1640.

While our data suggest that the molecular composition of erythrocyte membranes probably differs from that of L-cell and lymphocyte membranes, they also indicate that the membrane-lipid phases of all three cell types probably consist of lipid bilayers. This follows from the observation that for each of the three cells we found the same type of increase in mobility of the nitroxides located in the hydrophobic, compared to the hydrophilic, end of membrane-bound, spin-labeled stearic acid, as has been reported for comparable stearic acid spin labels incorporated into synthetic membranes with lipid bilayers (3, 10).

The fact that signals characteristic of "membrane-bound" label were detected in all subcellular fractions containing membrane could indicate that spin-labeled molecules were incorporated into intracellular as well as into surface membranes. However, it is possible that spin label was incorporated in only the outer membrane of intact cells but, during fractionation, leaked into the washing medium and was assimilated by internal membranes.

In any case, it is likely that surface-membrane signals were primarily obtained when ferricyanide was added to labeled cells after occurrence of signal decay. Cell membranes are relatively impermeable to ferricyanide, and even if small amounts of ferricyanide entered the cell, the amounts inside the cell could not account for the ESR signal strength observed. This statement is based on the following observations: (*a*) Mishra and Passow, studying erythrocytes, found cells to be impermeable to ferricyanide (14). (*b*) In our studies, decayed cell signal was immediately reactivated by addition of ferricyanide but disappeared when cells were washed free of ferricyanide. (*c*) It is unlikely that the cells were freely permeable to ferricyanide and then leaked during washing. When, after addition of $K_4{}^{59}Fe(CN)_6$, spin-labeled L-cells were sedimented through a discontinuous Ficoll gradient,

only trace amounts of isotope were detected in Ficoll layers above the cell pellet. If cells were freely permeable and then leaked, considerably more isotope should have been found in these layers. (*d*) Even if some ferricyanide entered the cells, the maximum amount of ferricyanide that could have entered to activate internal membrane signals was equivalent to a concentration no greater than 1 μM, as measured by the amount of ferricyanide found in either cell lysates by the colorimetric method, or attached to washed cells by the isotope-label method. Therefore, since the reactivated signal strength after addition of ferricyanide indicated a concentration of 0.1 mM, at most only an insignificant 1% of the observed reactivated signal could have been contributed by signals arising inside the cells from spin labels reactivated by ferricyanide molecules that had penetrated the surface membrane. However, we cannot rule out the possibility that some of the spin-labeled molecules, reactivated at the cell surface by ferricyanide, then entered the cell, were not reduced before recording the spectra, and thereby contributed to the observed signal.

As probes of local membrane viscosity, polarity, and molecular orientation, spin labels incorporated into membranes seem uniquely suitable for providing information about the interrelationship of membrane structure and function. The finding that spectra can be obtained that primarily represent surface-membrane signals from spin labels incorporated into membranes of intact and viable nucleated mammalian cells should, therefore, be useful in future applications of the spin-label method to studies of cell-surface functions.

The technical assistance of Eugene Gottfried, Daniel Graham, and Charles Ambrose is gratefully acknowledged.

1. Libertini, L. S., Waggoner, A. S., Jost, P. C. & Griffith, O. H. (1969) *Proc. Nat. Acad. Sci. USA* **64**, 13–19.
2. Hsia, J., Schneider, H. & Smith, I. C. P. (1971) *Can. J. Biochem.* **49**, 614–622.
3. Hubbell, W. L. & McConnell, H. M. (1969) *Proc. Nat. Acad. Sci. USA* **64**, 20–27.
4. Keith, A. D., Waggoner, A. S. & Griffith, O. H. (1968) *Proc. Nat. Acad. Sci. USA* **61**, 819–826.
5. Landsberger, F. R., Lenard, J., Paxton, J. & Compans, R. W. (1971) *Proc. Nat. Acad. Sci. USA* **68**, 2579–2583.
6. Hubbell, W. L. & McConnell, H. M. (1968) *Proc. Nat. Acad. Sci. USA* **61**, 12–16.
7. Kandgraf, W. C. & Inesi, G. (1969) *Arch. Biochem. Biophys.* **130**, 111–118.
8. Tourtellotte, M. E., Branton, D. & Keith, A. (1970) *Proc. Nat. Acad. Sci. USA* **66**, 909–916.
9. Avron, M. & Shavit, N. (1963) *Anal. Biochem.* **6**, 549–554.
10. Hubbell, W. L. & McConnell, H. M. (1971) *J. Amer. Chem. Soc.* **93**, 314–326.
11. Morrisett, J. D., Broomfield, C. A. & Hackley, B. E. (1969) *J. Biol. Chem.* **244**, 5758–5761.
12. Butler, K. W., Smith, I. C. P. & Schneider, H. (1970) *Biochim. Biophys. Acta* **219**, 514–517.
13. Rottem, J., Hubbell, W. L., Hayflick, L. & McConnell, H. M. (1970) *Biochim. Biophys. Acta* **219**, 104–113.
14. Mishra, R. K. & Passow, H. (1969) *J. Membrane Biol.* **1**, 214–224.

Proc. Nat. Acad. Sci. USA
Vol. 70, No. 1, pp. 71–75, January 1973

Alteration of Ribosomal Protein S4 by Mutation Linked to Kasugamycin-Resistance in *Escherichia coli*

(ribosomal proteins/ribosomal RNA/reconstitution/phosphocellulose chromatography)

ROBERT A. ZIMMERMANN*, YOSHIKO IKEYA†, AND P. FREDERICK SPARLING†§

* Département de Biologie Moléculaire, Université de Genéve, 30, Quai de l'Ecole-de-Medecine, CH-1211, Geneva 4, Switzerland; and † Departments of Medicine and Bacteriology, University of North Carolina School of Medicine, Chapel Hill, N.C. 27514

Communicated by Cyrus Levinthal, October 20, 1972

ABSTRACT **An alteration in the chromatographic mobility of 30S ribosomal protein S4 from two kasugamycin-resistant (*ksgA*) strains of *E. coli* was observed. The locus determining this alteration frequently cotransduced with *ksgA* but could be separated from it by transduction and conjugation. Since the structural gene for protein S4 is thought to lie some 30 min from *ksgA* on the *E. coli* chromosome, the product of the newly-identified gene may modify protein S4. We propose to designate this gene *ramB*.**

Reconstitution of 30S subunits from RNA and protein components of *ksgA ramB* and *ksgA*$^+$ *ramB*$^+$ strains demonstrated that ribosomal resistance to kasugamycin was due to altered 16S RNA and not to altered protein S4. The altered 16S RNA was undermethylated, and a methylating enzyme that acts on 16S RNA from *ksgA* strains was present in *ksgA*$^+$ but not in *ksgA* strains.

Resistance to the aminoglycoside antibiotic, kasugamycin results from alteration of the 30S ribosomal subunit in *Escherichia coli* (1). The gene for ribosomal kasugamycin resistance (*ksgA*) is closely linked to *leu* and maps near 0.5 min on the *E. coli* chromosome (1–3). By contrast, loci determining ribosomal resistance to the aminoglycosides, streptomycin and spectinomycin, have been placed in the cluster of 30S and 50S ribosomal protein genes near *strA* at 64 min (see ref. 4), and in both cases, antibiotic sensitivity or resistance is mediated by specific ribosomal proteins (5, 6). The unusual map position of the *ksgA* locus suggested a novel mechanism for kasugamycin resistance (1).

In a recent report, Helser, Davies, and Dahlberg demonstrated that resistance to kasugamycin is attributable to an alteration of the 16S RNA component of the 30S subunit (7). Specifically, the 16S RNA from resistant mutants lacks methylation of two adjacent adenine residues that are both dimethylated in the RNA of sensitive strains. The same authors later found that *ksgA*$^+$, but not *ksgA*, bacteria contain an enzyme that dimethylates the relevant adenine residues of "resistant" RNA and that 30S particles reconstituted from such RNA after *in vitro* methylation are sensitive to the drug (8). Moreover, the enzyme acted only on undermethylated 16S RNA from kasugamycin-resistant mutants and not on mature 16S RNA from sensitive strains, 23S RNA, or protein. It was concluded that the product of the *ksgA* gene is a methylating enzyme that modifies 16S RNA at some time during maturation of the 30S subunit.

§ To whom reprint requests should be sent.

We report experiments that confirm many of these findings. In contrast to Helser *et al.* (7, 8), however, we have found that two *ksgA* mutants possess an altered 30S subunit protein as well as undermethylated 16S RNA. Both of the mutants were obtained by nitrosoguanidine mutagenesis and are probably double mutants. The altered protein has been identified as S4 (9) or p4a (10). Several reports have described structural changes in protein S4 (11–14) resulting from mutations in the cluster of ribosomal protein genes near *strA* (12–15). The gene for alteration of protein S4 that we describe is shown to be close to, but separable from, *ksgA*, and is therefore at a considerable distance from *strA* on the *E. coli* chromosome. The implications of this finding are discussed.

MATERIALS AND METHODS

Bacterial Strains. Bacterial strains are listed in Table 1. The kasugamycin-resistant strains in which altered protein S4 was found were selected on tryptone-yeast extract plates containing 1 mg of kasugamycin/ml after nitrosoguanidine mutagenesis (16) to the extent of 10% survival of exposed cells. Spontaneous kasugamycin-resistant mutants were selected on the same plates containing 250 μg of kasugamycin per ml. Kasugamycin was a gift of Bristol Laboratories. Strains were designated *ksgA* if the locus for kasugamycin resistance cotransduced 90% with *pdxA*, and if cell-free extracts were resistant to kasugamycin (2). Strains were designated *ksgB* if they contained a locus for kasugamycin resistance that was located between 30–35 min on the *E. coli* chromosome, and if cell-free extracts were sensitive to kasugamycin (2). Transductions were performed with phage $P1_{kc}$ by standard methods (17).

Chromatography of Ribosomal Proteins. Growth of cells, preparation of ribosomal proteins, and chromatographic analysis were performed as described by Zimmerman *et al.* (11) with two exceptions: cells were labeled with either [^{3}H]- or [^{14}C]amino-acid mixtures (New England Nuclear Corp.) and high-capacity phosphocellulose (Mann, 1.1 meq/g) was used for chromatography.

Preparation of Ribosomal Components for Reconstitution. Cells were grown to mid log-phase in tryptone-yeast extract broth and harvested after pouring on ice. Ribosomes were prepared as described (18), except that no DNase was used. Ribosomes were not washed in high-salt (0.5 M NH_4Cl) buffers. 30S and 50S subunits were prepared by suspension of pelleted 70S ribosomes in standard buffer [10 mM Tris·HCl

TABLE 1. *Strains of E. coli K12 used*

Strain	Source	Genotype
JC411	W. K. Mass*	F⁻; *argG met leu his strA*
JC12	W. K. Mass*	HFr; *purC met*
FS131	Nitrosoguanidine mutagenesis	As JC12 but *ramB1 ksgA19*
FS157	Nitrosoguanidine mutagenesis	As JC12 but *ramB2 ksgA23 ksgB1*
FS215	Recombinant from FS157 x JC411	As JC411 but *his⁺ ramB2 ksgA23*
FS216	Recombinant from FS157 x JC411	As JC411 but *his⁺ ramB2 ksgB1*
FS232	Transductant of JC411 from FS131	As JC411 but *leu⁺ ramB1 ksgA19*
FS233	Transductant of JC411 from FS157	As JC411 but *leu⁺ ramB2 ksgA23*
Q13	W. Gilbert via M. Nomura†	*met tyr pnp-13*
FS240	Spontaneous mutant	As Q13 but *ksgA30*
FS241	Nitrosoguanidine mutagenesis	As Q13 but *leu*
FS242	Transductant of FS241 from FS157	As FS241 but *leu⁺ ksgA23*

* Dept. of Microbiology, New York University School of Medicine, New York, N.Y.

† Institute for Enzyme Research, Univ. of Wisconsin, Madison, Wisc.

(pH 7.6)–30 mM NH_4Cl–6 mM 2-mercaptoethanol] containing 0.3 mM $MgCl_2$, followed by dialysis against TAS buffer [20 mM Tris·HCl (pH 7.6)–100 mM NH_4Cl–1 mM $MgCl_2$–0.5 mM EDTA–4 mM 2-mercaptoethanol] for 3–4 hr at 0° (19). Subunits were separated on discontinuous 0.2–1.0 M sucrose gradients (19) by centrifugation in an SW27 rotor for 20 hr at 27,000 rpm. 30S and 50S subunits were precipitated with 0.6 volume of ethanol (19), and further purified by centrifugation on a 5–20% linear sucrose gradient in TAS buffer for 9.5 hr at 21,000 rpm in an SW27 rotor. Ribosomes and subunits were stored at −70° in standard buffer containing 10 mM $MgCl_2$.

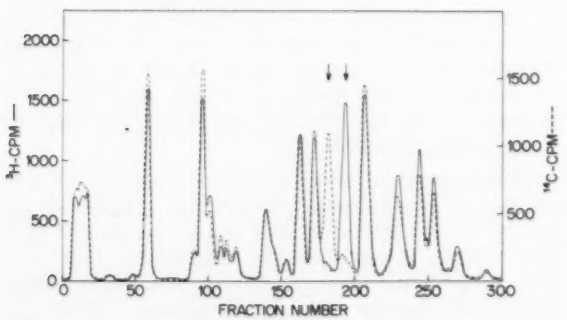

FIG. 1. Elution profile of 30S total proteins from ^{3}H-labeled JC411 and ^{14}C-labeled FS215. About 10 mg of proteins, including equal contributions from the 30S subunits of each strain, was applied to a phosphocellulose column in initial elution buffer (0.05 M NaH_2PO_4, titrated to pH 6.5 with methylamine–6 M urea–4 mM 2-mercaptoethanol) and eluted with a linear 0–0.5 M NaCl gradient in the same buffer (35). Procedures have been described (11). ^{3}H-labeled JC411 (——); ^{14}C-labeled FS215 (– – –). *Arrows* indicate displaced peaks.

TABLE 2. *Reconstitution of 30S ribosomes from total protein and 16S RNA*

Reconstituted 30S ribosomes		Incorporation cpm (% control) μg of kasugamycin per ml		
16S RNA	Total protein	0	50	100
S	S	607	367 (61)	289 (48)
S	R	503	251 (50)	179 (35)
R	S	324	281 (87)	220 (68)
R	R	357	288 (81)	290 (73)

30S ribosomal subunits were reconstituted as described in *Methods* and assayed for activity in poly(U,G)-dependent [^{14}C]valine incorporation *in vitro*. Reaction mixture (100 μl total) contained 0.7–0.8 A_{260} units each of reconstituted 30S particles and 50S subunits, 10 μl of S-100 fraction, 10 μg of poly(U,G) (1:1, Miles Laboratories), 8 mM Mg acetate, 0.01 mM [^{14}C]-valine (50 μCi/μmol, New England Nuclear Corp.), and other components as described (18). *S* indicates component derived from strain JC411 (*ksgA⁺ ramB⁺*); *R* indicates component derived from strain FS232 (*ksgA19 ramB1*).

The 16S RNA and total 30S ribosomal protein fractions were prepared by phenol extraction and urea–LiCl treatment, respectively (20). Reconstitution of 30S subunits from 16S RNA and total 30S proteins was performed according to Traub and Nomura (20). The RNA precipitate resulting from treatment of 30S subunits with urea–LiCl was also used and was as active as that prepared by phenol extraction.

Fingerprint Analysis. [^{14}C]Methyl-labeled oligonucleotides from 16S RNA were prepared and fingerprinted (21).

Methylation. 23S core particles from 30S subunits (22) were methylated by enzymes prepared from S-100 fractions and from the 1.0 M NH_4Cl supernatant of washed 70S ribosomes (8); *S*-adenosyl-[^{3}H]methionine was purchased from New England Nuclear Corp.

RESULTS

Altered Ribosomal Protein S4 in Certain Kasugamycin-Resistant Strains. In our early efforts to identify the ribosomal component altered in kasugamycin-resistant strains of *E. coli*, ^{3}H- and ^{14}C-labeled 30S subunit proteins from JC411 (*ksgA⁺*) and FS215 (a *ksgA23* recombinant derived by conjugation of JC411 with FS157) were compared by cochromatography on phosphocellulose columns. Fig. 1 demonstrates that one 30S protein from the mutant eluted at a significantly lower salt concentration than its counterpart from the wild-type strain, whereas the elution positions of all other 30S proteins from the two strains coincided. No chromatographic differences were observed in a parallel analysis of 50S subunit proteins.

To further examine the relationship between the *ksgA* locus and the altered protein, two independently isolated, kasugamycin-resistant mutations were introduced into JC411 (*ksgA⁺*) from FS131 and FS157 by cotransduction with *leu*. Chromatographic comparison of the parental 30S proteins

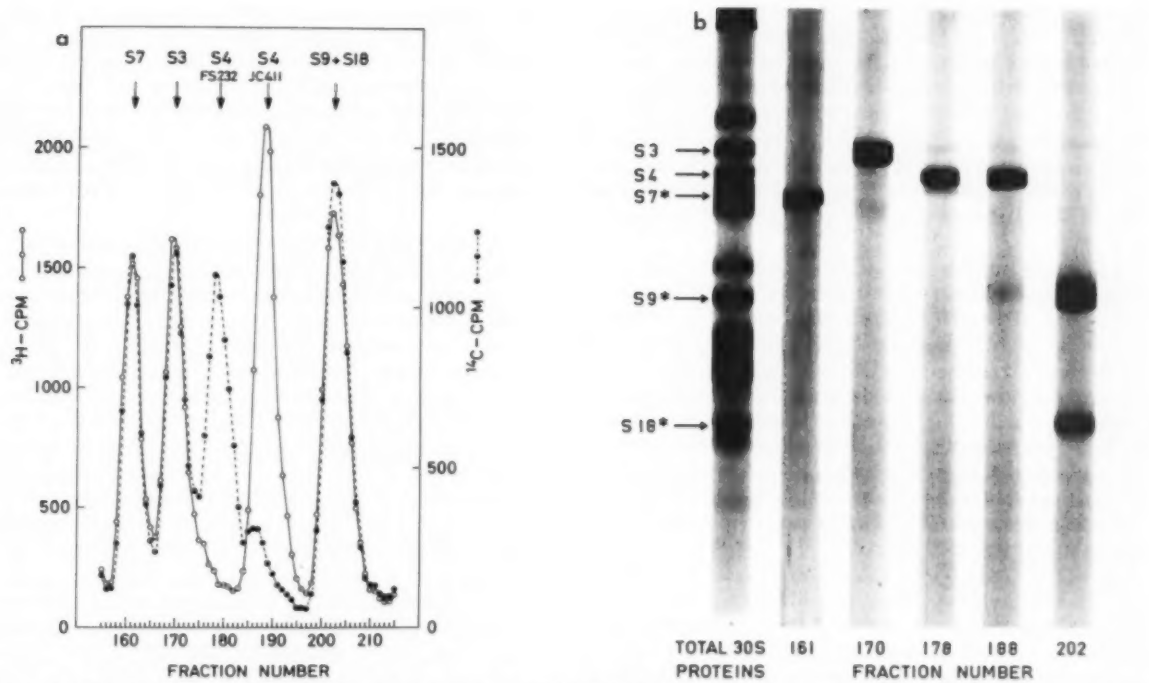

FIG. 2. (*a*) Detail of elution profile of 30S total proteins from ^{3}H-labeled JC411 and ^{14}C-labeled FS232. Preparation and chromatography of sample was performed as described in Fig. 1 and ref. 11. ^{3}H-labeled JC411 (— —); ^{14}C-labeled FS232 (– – –). (*b*) Polyacrylamide gels of peaks from chromatogram depicted in *a*. Gel of total 30S proteins is shown at *left*; gels from individual column fractions are shown at *right*. Gels contained 7.5% acrylamide and 0.8% methylene *bis*-acrylamide and were run according to Moore *et al.* (36). Protein S4 is unambiguously identified in this system since it migrates as a separate band. Similar analyses of FS215 and FS233 yielded identical results. Bands marked by asterisk (*) also contain other proteins that elute at different positions in the chromatogram. A faint band due to protein S11 is visible in tube 188 at the same level as protein S9; this band is not present in tube 178. Protein S11 most likely accounts for the small ^{14}C-peak between tubes 185 and 188.

with those from the two transductants, FS232 (*ksgA19*) and FS233 (*ksgA23*), resulted in elution patterns indistinguishable from that of Fig. 1; a detail of one of these chromatograms is presented in Fig. 2*a*. Thus, the locus that determines the altered protein must be close to or identical with *ksgA*, since it was present in two independent transductants selected for *leu*$^+$ and scored for kasugamycin resistance.

The altered 30S protein in strains FS215, FS232, and FS233 was identified by polyacrylamide gel electrophoresis of material from individual column fractions, as illustrated in Fig. 2*b* for FS232. The analysis demonstrates that samples from the displaced mutant peak (tube 178) and from the wild-type peak (tube 188) both contained a single component that migrated to a position characteristic of 30S protein S4. At the pH used for electrophoresis, there was no difference in the mobilities of the chromatographically altered and unaltered proteins.

There is considerable evidence that the structural gene for protein S4 is located in the ribosomal protein gene cluster near 64 min on the *E. coli* chromosome map (11–15). Since the original mutant of the S4 structural gene was designated *ram* (15), we propose that the new locus for altered S4 near 0.5 min be designated *ramB*, in contrast to the original locus near 64 min, which is redesignated *ramA*.

Separability of ksgA from the Locus for Altered S4. The locus for altered protein S4 (*ramB*) is apparently distinct from *ksgA*, although precise determination of its map position has been impeded by lack of a convenient method for scoring the mutant phenotype *in vivo*. Nonetheless, the separability of the two genes is strongly suggested by the following observations. (*a*) Strain FS216 (*ksgA*$^+$ *ksgB1*) has been shown to possess an altered S4 similar in its chromatographic properties to that of FS215, and is therefore *ramB*. Since FS216 was constructed by conjugation of FS157 (*ksgA23 ksgB1 ramB2*) with JC411 (*ksgA*$^+$ *ksgB*$^+$ *ramB*$^+$), the presence of the altered protein in FS216 can be most easily explained by postulation of a crossover between *ksgA* and *ramB*. (*b*) Transduction of the *ksgA23* allele into FS241, a *leu*$^-$ derivative of Q13, by the same methods used to construct FS232 and FS233 (selection for *leu*$^+$, followed by scoring for kasugamycin resistance) resulted in the *ksgA23* strain FS242 whose 30S subunits did not possess a chromatographically altered protein S4. Thus, although *ramB* and *ksgA* are sufficiently close to be cotransduced, as in the construction of FS233, they are not obligatorily cotransduced. (*c*) No chromatographic differences were observed upon comparison of 30S proteins from Q13 and FS240, a spontaneous kasugamycin-resistant derivative of Q13.

Kasugamycin Resistance Attributable to Abnormal 16S RNA. The evidence that *ramB* is genetically distinct from *ksgA* suggests that *ramB* is not directly related to the mechanism of ribosomal resistance to kasugamycin. Accordingly, 30S

ribosomal subunits were reconstituted from 30S total proteins and 16S RNA of JC411 (*ksgA*$^+$ *ramB*$^+$) and FS232 (*ksgA19 ramB1*) and tested for their susceptibility to the antibiotic in an *in vitro* polypeptide-synthesizing system. As shown in Table 2, reconstituted subunits were resistant to kasugamycin only when 16S RNA was derived from a kasugamycin-resistant strain; total proteins from the same strain, which included altered S4, did not produce kasugamycin-resistant subunits unless combined with homologous RNA.

Ribosomal subunits were also reconstituted with components from the *ksgA*$^+$ strains Q13 or FS241 and their *ksgA* derivatives, FS240 (*ksgA30*) or FS242 (*ksgA23*), all of which are *ramB*$^+$. In all cases, it was found that the presence of 16S RNA from a kasugamycin-resistant strain was required to form particles resistant to the drug *in vitro* (data not shown). Moreover, the levels of resistance observed with proteins from the *ramB*$^+$ strains were not significantly different from those obtained with protein mixtures containing altered S4. Our findings are thus consistent with the work of Helser *et al.* (7), who first demonstrated that kasugamycin resistance was due to altered 16S RNA.

In addition, fingerprint analysis of RNase T_1 digests of [^{14}C]methyl-labeled 16S RNA from JC411 and FS232 showed that the oligonucleotide AACCUG from FS232 RNA lacks the four methyl groups normally present in mature 16S molecules (21). We have also demonstrated that 23S core particles derived from the 30S subunits of *ksgA* strains are excellent substrates for a methylating enzyme present in extracts of *ksgA*$^+$ but not of *ksgA* strains; the methylase is present in the S-100 fraction, but is found in relatively higher concentration in extracts from salt-washed ribosomes (8). Core particles made from the 30S subunits of *ksgA*$^+$ strains are not substrates for the methylating enzyme. These findings are in accord with those already reported (7, 8) and are, therefore, not presented in detail here.

DISCUSSION

We have shown that mutations in a gene (*ramB*) close to *ksgA* leads to a change in the chromatographic mobility of 30S protein S4, while mutations in *ksgA* result in undermethylation of a specific nucleotide sequence in the 16S RNA (7). A possible explanation for the unexpected finding of alteration of 30S protein S4 in each of two tested nitrosoguanidine-induced mutants (FS131, FS157) selected for high-level resistance to kasugamycin is suggested by the fact that protein S4 is one of the five or six 30S ribosomal proteins that interact directly with 16S RNA during subunit assembly (23–25). If interaction of altered 16S RNA with mutant protein S4 produces a ribosome structure more resistant to kasugamycin than that resulting from altered 16S RNA alone, double mutations would be favored. Although this conjecture cannot be excluded, it is unlikely since (*a*) *ksgA ramB* strains are not significantly more resistant to kasugamycin *in vivo* or *in vitro* than other *ksgA ramB*$^+$ strains, (*b*) altered and unaltered S4 protein have approximately the same affinity for 16S RNA (P. Spierer and R. A. Zimmermann, unpublished), and (*c*) methylation of 16S RNA is thought to occur subsequent to the binding of protein S4 during subunit assembly (26). There may be other selective advantages (apart from resistance to kasugamycin) to *ksgA* mutants, which are also *ramB*. Testing this hypothesis requires construction of an isogenic set of strains carrying one or both of the same *ramB* and *ksgA* alleles, which has not yet been possible due to the cumbersome necessity of scoring for *ramB* by column chromatography. It is possible that coincidence of *ksgA* and *ramB* mutations occurred by chance in our strains because it is known that after exposure to nitrosoguanidine, multiple mutations are frequently found within a 2-min map distance of the mutation for which initial selection was made (27).

Cotransduction of a gene (*ramB*) for altered protein S4 with *ksgA*, which is located near 0.5 min on the *E. coli* linkage map, would appear to be paradoxical, since the same protein is altered by *ramA* (11) and by certain mutations reversing streptomycin dependence (12–14), all of which map near 64 min. Insofar as is known, protein S4 does not consist of more than one polypeptide chain (28). Moreover, although examples of gene duplication in bacteria are known (29), it is unlikely that both *ramA* and *ramB* are structural genes for S4. If they were, one would expect *ramA*$^+$ *ramB* strains such as FS215 and FS232 to yield two approximately equal peaks of normal and mutant S4. However, analysis of the normalized chromatograms presented in Figs. 1 and 2*a* reveals that about 85% of the ^{14}C-radioactivity in the S4 region (fractions 175–194) is associated with the mutant S4 peak; most of the remaining 15%, which is nearly coincident with, but slightly displaced from, the normal S4 peak, probably consists of protein S11 (see Fig. 2*b*). Nonetheless, since the presence of a small amount of normal S4 in the 30S subunits of *ramA*$^+$ *ramB* strains cannot be completely excluded, the existence of two structural genes for this protein remains a possibility. To explain the chromatographic results in such an event, one would have to postulate either preferential synthesis of mutant S4 or preferential incorporation of mutant S4 into the ribosomes.

A more likely explanation is that the primary structure of protein S4 is encoded only by the *ramA* (15), or *rpsD* (12), locus in the *strA* region, consistent with the mounting evidence that the ribosomal protein genes clustered near *strA* at 64 min are structural genes (30), and that the *ramB* gene product is an enzyme that modifies protein S4. It is intriguing in this regard to note that the C-terminal amino-acid sequences of several mutant forms of protein S4 have been found to vary substantially in length (31). This observation could be interpreted to mean that protein S4 is cleaved from a longer precursor molecule; if so, the *ramB* gene product would be a potential candidate for the putative cleavage enzyme. Alternatively, *ramB* might alter protein S4 by a group-transfer reaction; several enzymes that perform secondary modifications of ribosomal proteins by methylation, phosphorylation, and acylation have already been described (32–34). Finally, the presence of the *ramB* gene near *ksgA* would raise the possibility that there is a grouping of ribosome-modifying genes near 0.5 min on the bacterial chromosome.

The functional significance of protein S4 alteration resulting from mutation at the *ramB* locus remains to be clarified. It is reasonable to predict that translational fidelity should be affected in *ramB* strains, since the alteration of protein S4 in *ramA* mutants has a striking influence on accuracy of translation (11, 15). Preliminary experiments have in fact shown that the 70S ribosomes of strains FS232 and FS233 (both *ramB ksgA*) differ notably from those of strain JC411 (*ramB*$^+$ *ksgA*$^+$) in their ability to misread poly(U)

templates, as measured by the relative incorporation of isoleucine and phenylalanine *in vitro* (Ikeya, Y. & Sparling, P. F., unpublished).

We thank Miss Elly van Alphen and Mrs. Barbara Seebeck for skilled technical assistance and Mr. Alain Rifat for his enthusiastic participation in some of these experiments. R. A. Z. acknowledges with thanks the support of the Helen Hay Whitney Foundation and is indebted to Dr. A. Tissieres for making laboratory facilities available to him. P. F. S. is a recipient of a Research Career Development Award from the National Institutes of Health (1-K4-AI-33,032). This work was performed under grants from the National Institutes of Health (5R01-AI09574) and the Fonds National Suisse de la Recherche Scientifique.

1. Sparling, P. F. (1970) *Science* **167**, 56–58.
2. Sparling, P. F. (1971) *Bact. Proc.*, p. 81.
3. Helser, T. L. & Davies, J. (1971) *Bact. Proc.*, p. 82.
4. Dekio, S. (1971) *Mol. Gen. Genet.* **113**, 20–30.
5. Ozaki, M., Mizushima, S. & Nomura, M. (1969) *Nature* **222**, 333–339.
6. Bollen, A., Davies, J., Ozaki, M. & Mizushima, S. (1969) *Science* **165**, 85–86.
7. Helser, T. L., Davies, J. E. & Dahlberg, J. E. (1971) *Nature New Biol.* **233**, 12–14.
8. Helser, T. L., Davies, J. E. & Dahlberg, J. E. (1972) *Nature New Biol.* **235**, 6–9.
9. Wittmann, H. G., Stoffler, G., Hindennach, I., Kurland, C. G., Randall-Hazelbauer, L., Birge, E. A., Nomura, M., Kaltschmidt, E., Mizushima, S., Traut, R. R. & Bickle, T. A. (1971) *Mol. Gen. Genet.* **111**, 327–333.
10. Nomura, M., Mizushima, S., Ozaki, M., Traub, P. & Lowry, C. V. (1969) *Cold Spring Harbor Symp. Quant. Biol.* **34**, 49–61.
11. Zimmermann, R. A., Garvin, R. T. & Gorini, L. (1971) *Proc. Nat. Acad. Sci. USA* **68**, 2263–2267.
12. Birge, E. A. & Kurland, C. G. (1970) *Mol. Gen. Genet.* **109**, 356–369.
13. Duesser, E., Stoffler, G., Wittmann, H. G. & Apirion, D. (1970) *Mol. Gen. Genet.* **109**, 298–302.
14. Kreider, G. & Brownstein, B. L. (1971) *J. Mol. Biol.* **61**, 135–142.
15. Rosset, R. & Gorini, L. (1969) *J. Mol. Biol.* **39**, 95–112.
16. Adelberg, E. A., Mandel, M. & Chen, G. C. C. (1965) *Biochem. Biophys. Res. Commun.* **18**, 788–795.
17. Lennox, E. S. (1955) *Virology* **1**, 190–206.
18. Sparling, P. F., Modelell, J. B., Takeda, Y. & Davis, B. D. (1968) *J. Mol. Biol.* **37**, 407–421.
19. Staehelin, T. & Maglott, D. R. (1971) in *Methods in Enzymology*, eds. Moldave, K. & Grossmann, L. (Academic Press, New York), Vol. 20, pp. 449–456.
20. Traub, P. & Nomura, M. (1969) *J. Mol. Biol.* **40**, 391–413.
21. Fellner, P. (1969) *Eur. J. Biochem.* **11**, 12–27.
22. Staehelin, T. & Meselson, M. (1966) *J. Mol. Biol.* **19**, 207–210.
23. Mizushima, S. & Nomura, M. (1970) *Nature* **226**, 1214–1218.
24. Schaup, H. W., Green, M. & Kurland, C. G. (1970) *Mol. Gen. Genet.* **109**, 193–205.
25. Stoffler, G., Daya, L., Rak, K. H. & Garrett, R. A. (1971) *J. Mol. Biol.* **62**, 411–414.
26. Lowry, C. V. & Dahlberg, J. (1971) *Nature New Biol.* **232**, 52–54.
27. Cerda-Olmedo, E., Hanawalt, P. C. & Guerola, N. (1968) *J. Mol. Biol.* **33**, 705–719.
28. Dzionara, M., Kaltschmidt, E. & Wittmann, H. G. (1970) *Proc. Nat. Acad. Sci. USA* **67**, 1909–1913.
29. Folk, W. R. & Berg, P. (1971) *J. Mol. Biol.* **58**, 595–610.
30. Funatsu, G., Schiltz, E. & Wittmann, H. G. (1971) *Mol. Gen. Genet.* **114**, 106–111.
31. Funatsu, G., Puls, W., Schiltz, E., Reinbolt, J. & Wittmann, H. G. (1972) *Mol. Gen. Genet.* **115**, 131–139.
32. Pak, W. K. & Kim, S. (1971) *Science* **174**, 114–119.
33. Walton, G. M., Gill, G. N., Abrass, I. B. & Garren, L. D. (1971) *Proc. Nat. Acad. Sci. USA* **68**, 880–884.
34. Leibowitz, M. J. & Soffer, R. L. (1971) *Proc. Nat. Acad. Sci. USA* **68**, 1866–1869.
35. Hardy, S. J. S., Kurland, G. C., Voynow, P. & Mora, G. (1969) *Biochemistry* **8**, 2897–2905.
36. Moore, P. B., Traut, R. R., Noller, H., Pearson, P. & Delius, H. (1968) *J. Mol. Biol.* **31**, 441–461.

Proc. Nat. Acad. Sci. USA
Vol. 70, No. 1, pp. 76–79, January 1973

Induction of Cytolysis of Cultured Lymphoma Cells by Adenosine 3′:5′-Cyclic Monophosphate and the Isolation of Resistant Variants

(cytoplasmic receptor molecules/protein kinase)

VIOLET DANIEL*, GERALD LITWACK†, AND GORDON M. TOMKINS

Department of Biochemistry and Biophysics, University of California, San Francisco, Calif. 94122

Communicated by Bruce N. Ames, October 26, 1972

ABSTRACT **Cultured mouse lymphosarcoma cells are killed on exposure to 0.1 mM $N^6,O^{2'}$-dibutyryl-adenosine 3′:5′-cyclic monophosphate. A population of cells resistant to the killing effect of dibutyryl cyclic AMP at concentrations as high as 1 mM was selected. The growth characteristics of the resistant cells were similar to those of the sensitive parental line. However, the resistant cells contain less cytoplasmic cyclic AMP-binding proteins and decreased cyclic AMP-stimulated protein kinase activity. It is proposed that transition from sensitivity to resistance to dibutyryl cyclic AMP in lymphoma cells is connected with a modification of the cyclic AMP-binding protein, which appears to be the regulatory subunit of the cyclic AMP-activated protein kinase.**

Exposure of cultured lymphoid cells to adrenal steroid hormones leads to inhibition of cell growth and, ultimately, to cytolysis (1). Various experiments suggest that specific protein synthesis induced by steroid hormones is required for this process (2, 3). Steroid-resistant variants have been isolated that contain decreased quantities of the specific cytoplasmic receptor molecules thought to mediate steroid action (4, 5).

Adenosine 3′:5′-cyclic monophosphate (cAMP), although not a direct intermediate in glucocorticoid action (6), frequently mimics the physiological effects of the steroids. In this publication, we demonstrate that the cyclic nucleotide can also promote the death of lymphoid cells and that cAMP-resistant cells can be obtained that contain lower concentrations than normal cells of cAMP-binding proteins. Furthermore, we show that the binding proteins that are diminished in the resistant variants behave like the regulatory subunits of the cyclic AMP-dependent protein kinase. Therefore, cAMP-induced cytolysis very probably involves the combination of the cyclic nucleotide with this protein subunit.

MATERIALS AND METHODS

The mouse lymphoma line S49.1 TB4, obtained from Ruth Epstein, Salk Institute, San Diego, was propagated in Dulbecco's medium (General Biochemicals) containing 10% heat-inactivated horse serum. Cell concentrations were assayed by a Coulter Counter model F with a cell-size threshold value that excluded the majority of cells with pycnotic nuclei (1). [^{3}H]cAMP, [^{3}H]$N^6,O^{2'}$-dibutyryl cAMP (But_2cAMP), and [γ-^{32}P]ATP were obtained from New England Nuclear Corp. Unlabeled But_2cAMP was purchased from Calbiochem, and unfractionated calf-thymus histones from Sigma Co.

Cyclic AMP binding to cellular proteins was measured by the competition assay of Gilman (7). The reaction mixture contained, in a final volume of 0.1 ml: 50 mM potassium phosphate buffer (pH 7.0) or the same concentration of sodium acetate (pH 6.5), 3 mM theophylline, and 0.5 μM [^{3}H]cAMP (24 Ci/mmol). The reactions were started by addition of the protein samples.

Protein kinase activity was determined by measurement of the incorporation of ^{32}P from γ-labeled ATP into histone. The reaction mixtures contained, in a final volume of 0.2 ml: [γ-^{32}P]ATP (8×10^4 cpm/nmol), 1 mM theophylline, 10 mM dithiothreitol, and enzyme protein. Incubations were at 30° for 5 min with or without 1 μM cAMP. Protein-bound ^{32}P was determined by the method of Kabat (8).

Protein concentrations were determined by the method of Lowry *et al.* (9).

RESULTS

Killing of cultured lymphoma cells by But_2cAMP and the emergence of a resistant population

Growth of the mouse lymphoma line S49.1 TB4 that is sensitive to glucocorticoids (1) was inhibited by But_2cAMP at concentrations as low as 10 μM, and at 0.1–1 mM But_2cAMP (with 0.2 mM theophylline) there was virtually complete cytolysis 48 hr after treatment (Fig. 1). Theophylline alone, at this concentration, had no effect on cell growth. Neither cAMP itself, adenine, adenosine, nor 5′-AMP at a concentration of 0.1 mM inhibited cellular growth.

We derived a But_2cAMP-resistant population of S49.1 TB4 cells by growing the sensitive cells in the presence of 0.2 mM theophylline and increasing But_2cAMP concentrations stepwise from 1 to 100 μM over a period of about 30 days. This partially resistant population was then exposed to 1 mM But_2cAMP for a week; the survivors of this treatment were used as the cAMP-resistant cells. The growth rates of both sensitive and resistant populations are similar in the absence of But_2cAMP (Fig. 1). No cytolysis occurred in the resistant cells at 1 mM But_2cAMP with 0.2 mM theophylline (Fig. 1), and the cells remained resistant to these concentrations when cultured in medium free of But_2cAMP and theophylline for up to 6 months.

Abbreviation; $N^6,O^{2'}$-dibutyryladenosine 3′:5′-cyclic monophosphate, But_2cAMP.

* Permanent address: Weizmann Institute of Science, Rehovot, Israel.

† Permanent address: Fels Research Institute, Temple University School of Medicine, Philadelphia, Pa. 19140.

Mechanism of But$_2$cAMP resistance

Because free cAMP itself does not inhibit the growth of even But$_2$cAMP-sensitive lymphoma cells, we investigated the possibility that resistance to But$_2$cAMP might be due to inability of the substituted nucleotide to enter the resistant cells. We therefore sought to increase the intracellular cAMP concentration indirectly by adding prostaglandin to the medium of both sensitive and resistant cells. In both cases there was a marked increase in the internal cAMP concentration (manuscript in preparation); however, only the growth of the But$_2$cAMP-sensitive cells was inhibited. These results suggest that the resistant cells are truly insensitive to intracellular cAMP and are not simply unable to take up exogenous But$_2$cAMP. Consistent with this conclusion was the finding that both sensitive and reistant cells showed an identical uptake of [^{3}H]But$_2$cAMP (0.4 pmol per 4×10^6 cells in a 3-hr incubation) at an external nucleotide concentration of 1.4 μM.

We next inquired whether cAMP resistance is due to impaired binding to a specific cytoplasmic receptor. We incubated [^{3}H]cAMP with cytosols from sensitive or resistant lymphoma cells and subjected the mixtures to gel filtration on Sephadex G-25. Fig. 2 shows that there is much greater macromolecular binding by cytoplasmic extracts of sensitive than of resistant cells, as shown by the amount of radioactivity excluded by the column. In seven different experiments, the binding to sensitive cell extracts was 4–8 times higher than to cytosols from resistant cells, but in each case some residual binding by resistant cell extracts was found.

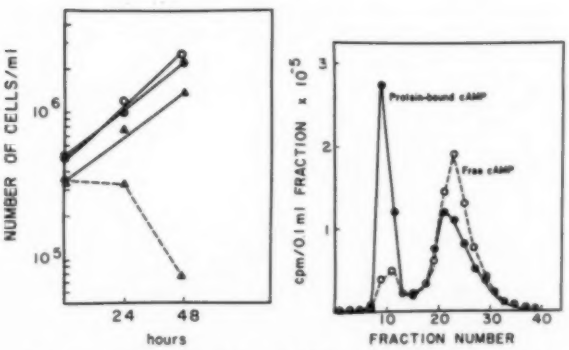

FIG. 1. (*left*). Effect of But$_2$cAMP on the growth of sensitive and resistant lymphoma cells. Cells sensitive to But$_2$cAMP were grown in the absence (▲——▲) or presence (△——△) of 1 mM But$_2$cAMP and 0.2 mM theophylline. Cells resistant to But$_2$cAMP were grown in the absence (●——●) or presence (○——○) of the same reagents.

FIG. 2. (*right*). Gel filtration of [^{3}H]cAMP-bound cytosols from But$_2$cAMP-sensitive and -resistant cells. Centrifuged packed cells (1–2 ml) were homogenized with an equal volume of 0.25 M sucrose in 0.05 M Tris·HCl buffer (pH 7.4) containing 3 mM $MgCl_2$ and 4 mM 2-mercaptoethanol. Particulate material was removed by a 90-min centrifugation in a Spinco preparative ultracentrifuge at 40,000 rpm (105,000 × *g*). The same amounts (25 mg of protein) of the resulting cytosols from both But$_2$cAMP-sensitive (●) and resistant (○) cells were incubated for 60 min at 0° with 0.5 μM [^{3}H]cAMP in the presence of 5 mM theophylline. The macromolecular-bound [^{3}H]cAMP was then separated from free [^{3}H]cAMP by filtration through a 1.2 × 20 cm Sephadex G-25 column equilibrated with 0.05 M Tris·HCl buffer (pH 7.5). 1-ml Fractions were collected, and samples of 0.1 ml were counted for radioactivity in a scintillation counter with a mixture of Triton X-100–water–Omnifluor–toluene (25:4:04:70).

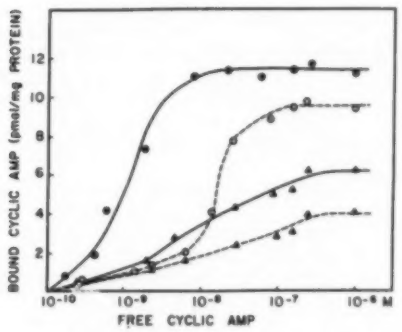

FIG. 3. Specific cAMP binding by cytoplasmic extracts from But$_2$cAMP-sensitive and resistant lymphoma cells at various cAMP concentrations. Reaction mixtures in a total volume of 0.1 ml contained 50 mM sodium acetate buffer (pH 4.5 or 6.0), 2 mM theophylline, 120 or 140 μg of cytosol protein from sensitive or resistant cells, and various concentrations of [^{3}H]cAMP (24 Ci/mmol) with or without 0.5 mM nonradioactive cAMP. The difference between the amount of [^{3}H]cAMP bound to cytoplasmic extracts in the absence and presence of excess nonradioactive cAMP is considered a measure of the "specifically-bound" cAMP. The concentration of free [^{3}H]cAMP is obtained by subtraction of the total bound [^{3}H]cAMP from total [^{3}H]cAMP present in the incubation. ●——●, sensitive cytosol (pH 4.5); ○——○, sensitive cytosol (pH 6.0); ▲——▲, resistant cytosol (pH 4.5); △——△, resistant cytosol (pH 6.0).

"Specific" binding curves were next compared at two pH values with cytosols from both types of cells. Specific binding was calculated by subtraction of a blank value (obtained at a given concentration of radioactive cAMP together with a 500- to 1000-fold excess of nonradioactive cAMP) from the value obtained with the radioactive nucleotide alone (10). Fig. 3 shows that at pH 4.5 the specific binding components in both cells become saturated at lower cAMP concentrations than at pH 6.0. At both pH values, however, there was substantially less specific cAMP binding by resistant cell cytosol at all the cAMP concentrations tested. These results, together with the experiments shown in Fig. 2, lead us to conclude that resistant cells contain fewer cAMP receptors than do sensitive cells.

Characteristics of "sensitive" and "resistant" cAMP-binding proteins

In addition to these quantitative differences, the shape of the curves in Fig. 2 suggest the possibility of qualitative differences between "sensitive" and "resistant" binding proteins. Although obviously a final decision cannot be based only on measurements made in a crude extract, this point was investigated further by examination of the influence of pH on the binding at two different concentrations of the cyclic nucleotide by "sensitive" and "resistant" cytosols. Fig. 4 shows that binding by resistant cytosol has a pH optimum of about 4.5 for both cAMP concentrations. At the lower concentrations of cAMP, sensitive cytosol shows optimal binding at the same pH. However, the pH-binding curve at the higher nucleotide concentration seems qualitatively different in the sensitive as compared to the resistant cells. The data in Fig. 4 indicate that the sensitive cytosol might contain two types of cAMP-binding sites, one with a higher affinity for the nucleo-

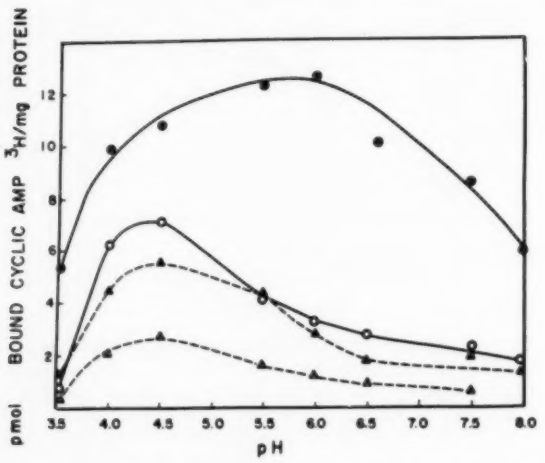

FIG. 4. Effect of pH on cAMP binding activity. In a total volume of 0.1 ml the reaction mixtures contained: 50 mM buffer (pH 3.5–6.5 sodium acetate and pH 7.5–8.0 Tris·HCl), 2 mM theophylline, 0.5 μM or 5 nM [^{3}H]cAMP (24 Ci/mmol), and 82 or 170 μg of cytosol protein from sensitive or resistant cells. The protein-bound cAMP was assayed on Millipore filters (9) with 20 mM buffers of the same pH. ●——●, sensitive cytosol (0.5 μM cAMP); ○——○, resistant cytosol (0.5 μM cAMP); ▲——▲, sensitive cytosol (5 nM cAMP); △——△, resistant cytosol (5 nM cAMP).

tide than the other. The resistant cytosol appears not to contain the lower affinity sites, and also seems to have a diminished concentration of the higher affinity sites compared to the sensitive cytosol.

We also bound ^{3}H-labeled cAMP to both sensitive and resistant extracts and subjected them to get filtration on Sephadex G-200 (data not shown). The binding activity in both extracts emerged as a single peak. The binding activity from sensitive cytosol was included in the gel and had, by comparison with known proteins, apparent molecular weights of 105,000 and 107,000 in two experiments. However, the binding activity from resistant cell cytosol (in three experiments) was excluded from the gel, suggesting that it may have a higher molecular weight. The signifiance of this apparent difference between the size of the sensitive and resistant binding activities, if any, cannot be assessed until further purification of the extracts.

Identity of the cAMP-binding protein in lymphoma cells

In many different mammalian tissues the cAMP receptor is a regulatory subunit that controls the activity of a protein phosphokinase (11, 12). Experiments were therefore performed to determine whether this is the case in our cultured lymphoma cells. Extracts of sensitive and resistant cells were chromatographed on DEAE-Sephadex, and the cAMP binding and histone kinase activities were identified (Fig. 5*A* and *B*). In both cases the cAMP-binding macromolecules migrate with the cAMP-activated kinase activity. A decreased binding activity in resistant cells was seen by this technique and was accompanied by a diminished cAMP-activated kinase. Similar conclusions were reached on the basis of sucrose density gradient centrifugation of the two cytosols (not shown). Since the cAMP-binding activity in both sensitive and resistant cell extracts cochromatographed on DEAE-Sephadex and cosedimented on sucrose gradient with their respective cAMP-activated histone kinase, it appears that in both types of cells the cAMP receptor is the regulatory subunit.

DISCUSSION

The results presented show that exogenous But_2cAMP inhibits the growth of cultured mouse lymphoma S49.1 TB4 cells and ultimately leads to their death. Experiments with prostaglandin E_1 suggest that endogenously generated cAMP has a similar effect. Variants of the parent cell line resistant to high concentrations of added But_2cAMP (and to prostaglandin) were easily derived from the sensitive parent line. Compared to the sensitive cells, these resistant variants contain lowered concentrations of cAMP-binding macromolecules, which appear to be the regulatory subunits of the cAMP-activated protein kinase. Our data suggest that cAMP resistance is accompanied by a decrease in the activity of cAMP receptors and, perhaps, by a change in their physical properties. However, none of our experiments indicates whether the transition from cAMP-sensitivity to resistance represents a genetic change or some type of heritable phontypic variation.

The mechanism by which cAMP induces the killing of sensitive lymphoma cells is unknown. The cylic nucleotide inhibits the growth of transformed, cultured mouse-embryo fibroblasts (13) and slows the uptake of added uridine, leucine, and 2-deoxyglucose by these cells (R. Kram, in preparation). Glucocorticoids that decrease the penetration of macromolecular precursors into thymic lymphocytes (2, 3) also

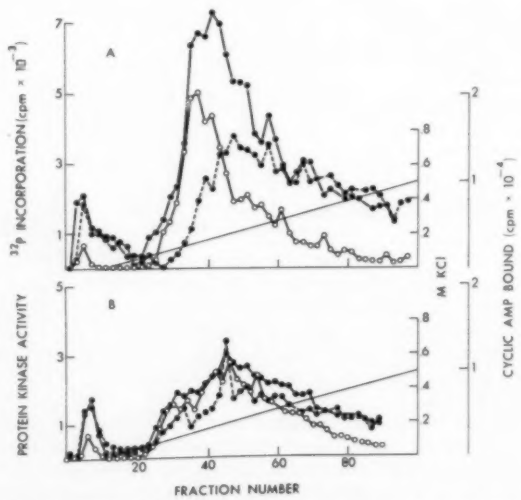

FIG. 5. DEAE-Sephadex A-50 chromotography of cytosols from But_2cAMP-sensitive or resistant cells. 60 mg of cytosol protein (prepared as described in legend to Fig. 2) was applied to a DEAE–Sephadex A-50 column (2.5 × 4 cm) equilibrated with 0.05 M Tris·HCl buffer (pH 7.4) containing 4 mM 2-mercaptoethanol and then eluted with a 100-ml linear (0.05–0.5 M) KCl gradient in the same buffer. 1.0-ml Fractions were collected and 50 1-ml samples were assayed for [^{3}H]cAMP binding (○——○), protein kinase (●——●), and cAMP-activated protein kinase (●——●) activities (see *Methods*). (*A*) Chromatography of But_2cAMP-sensitive cell cytosol; (*B*) chromatography of But_2cAMP-resistant cell cytosol.

induce lympholysis (1). We imagine, therefore, that the cytolytic effect of cAMP on lymphoma cells may also be related to decreased membrane transport.

This study was supported by Contract no. 72-3236 within the Special Virus–Cancer Program of the National Cancer Institute, and Grant GM 17239 from the National Institute of General Medical Sciences of the National Institutes of Health. The work reported in this paper was undertaken during the tenure of an American Cancer Society–Eleanor Roosevelt-International Cancer Fellowship awarded by the International Union Against Cancer.

1. Horibata, K. & Harris, A. W. (1970) *Exp. Cell Res.* **60**, 61–77.
2. Makman, M. H., Dvorkin, B. & White A. (1971) *Proc. Nat. Acad. Sci. USA* **68**, 1269–1273.
3. Munck, A. & Wira, Ch. (1970) *in Advances in the Biosciences* (Schering Workshop on Steroid Hormone 'Receptors', Berlin), Vol. 7, pp. 300–327.
4. Baxter, J. D., Harris, A. W., Tomkins, G. M. & Cohn, M. (1971) *Science* **171**, 189–191.
5. Rosenau, W., Baxter, J. D., Rousseau, G. G. & Tomkins, G. M. (1972) *Nature* **237**, 20–23.
6. Granner, D. K., Chase, L. R., Aurbach, G. D. & Tomkins, G. M. (1968) *Science* **162**, 1018.
7. Gilman, A. G. (1970) *Proc. Nat. Acad. Sci. USA* **67**, 305–312.
8. Kabat, D. (1971) *Biochemistry* **10**, 197–203.
9. Lowry, O. H., Rosebrough, N. J., Farr, A. L. & Randall, R. J. (1951) *J. Biol. Chem.* **193**, 265–275.
10. Rousseau, G. G., Baxter, J. D. & Tomkins, G. M. (1972) *J. Mol. Biol.* **67**, 99–115.
11. Walsh, D. A., Perkins, J. P. & Krebs, E. G. (1968) *J. Biol. Chem.* **243**, 3763–3765.
12. Kuo, J. F. & Greengard, P. (1969) *Proc. Nat. Acad. Sci. USA* **64**, 1349–1355.
13. Johnson, G. S., Friedman, R. M. & Pastan, I. (1971) *Proc. Nat. Acad. Sci. USA* **68**, 425–429.

Proc. Nat. Acad. Sci. USA
Vol. 70, No. 1, pp. 80–83, January 1973

Release of Amplified Ribosomal DNA from the Chromomeres of *Acheta*

(RNA cistrons/hybridization/oocytes/pachytene/meiosis)

A. LIMA-DE-FARIA, HALINA JAWORSKA, AND T. GUSTAFSSON

Institute of Molecular Cytogenetics, University of Lund, Lund, Sweden

Communicated by Åke Gustafsson, October 20, 1972

ABSTRACT The major chromomeres of pachytene chromosomes 6 and 11 in the oocytes of *Acheta* (Orthoptera) are regions of amplification for ribosomal RNA cistrons (28 S and 18 S). During late prophase the amplified DNA copies are released from the chromomeres, which decrease in size as the amount of DNA decreases. The number of nucleotide pairs released from the major chromomere of chromosome 11 is about 1.38×10^9.

The concept of chromomere–band–gene was determined by cytological and genetic studies (1, 2) of polytene and pachytene chromosomes. Recently, on the basis of new data from structural, genetic, and molecular analyses of chromomeres, this concept is being expanded and revised.

Structural analysis of pachytene and diplotene chromosomes established that the chromomeres consist of spiralized segments of the chromosome (3, 4). Later, studies on the DNA of higher organisms disclosed that (*a*) there is no correlation between large amounts of DNA and obvious developmental complexity, (*b*) repeated DNA sequences occur in most eukaryotes (5), and (*c*) in certain bands of giant chromosomes of insects the amount of DNA increases differentially (6–8). As a result of this evidence the chromomere was looked upon, not as a single genetic unit, but as a structure with multiple genetic functions consisting of repeated copies of given cistrons or given DNA sequences (9–11). Recently, a more radical model has been proposed in which the chromomeres or bands would be the control elements, whereas the interbands or fibrils between the chromomeres would be the coding sequences of the chromosomal DNA (12).

Before presentation of the data on the release of DNA copies from the chromomeres the principal data on gene amplification in *Acheta* should be mentioned. (*a*) At early pachytene there are five major chromomeres or DNA bodies in *Acheta* oocytes that are not present in the spermatocytes. The major chromomeres are formed by extra DNA synthesis occurring at the interphase and early prophase of meiosis (13, 14). (*b*) Besides the main band, there is a DNA satellite, which has a calculated GC content of 56% (buoyant density 1.716 g/ml). (*c*) The DNA satellite of ovaries at the interphase of meiosis, where the major chromomeres are largest, contains 14% of the ovarian DNA, whereas the DNA satellite of testes, where no major chromomeres are present, contains 0.8% of the total testes DNA (15). This result suggested that the large DNA satellite seen in ovaries represents the DNA of the major chromomeres. (*d*) To test this assumption *Acheta* DNA from ovaries (fractionated on CsCl gradients) and 28S and 18S ribosomal RNA of *Acheta* labeled with ^{32}P or ^{3}H were hybridized. The hybridization peak occurred at the position of the DNA satellite. This shows that the ribosomal cistrons are present in the satellite DNA (15, 16). (*e*) To check the amplification process further, [^{3}H]RNA–DNA hybridization at saturation was performed. The percentage of ribosomal RNA bound to DNA was nearly the same in testes and somatic tissues but it was 4- to 5-times higher in ovaries (16). (*f*) Further confirmation that the major chromomeres represent amplified regions of ribosomal DNA was obtained by isolation of the DNA satellite on CsCl gradients and by preparation, with RNA polymerase, of complementary [^{3}H]RNA from satellite DNA. This complementary RNA was then hybridized *in situ* with the pachytene chromosomes of *Acheta* oocytes, and it hybridized mainly with the major chromomeres (17). (*g*) The amounts of DNA in each pachytene chromosome of the oocytes, in the pachytene chromosomes of the spermatocytes, and in the major chromomeres were measured (18).

This evidence indicates that the major chromomeres present in *Acheta* oocytes at early pachytene contain amplified ribosomal RNA cistrons.

MATERIALS AND METHODS

The amount of DNA in Feulgen-stained pachytene chromosomes was measured by a Zeiss Scanning Microscope Photometer 05 connected to a Facit Tape Punch. The tapes were then analyzed by a computer, the values being displayed as contour maps of iso-brightness or as a volumetric display on an incremental plotter. For the measurements, the chromomeres of every chromosome and all the chromosomes of a cell must lie on a single plane. Human lymphocytes and rat-kidney nuclei were used as standards. Details of the procedures used were described (18).

RESULTS AND DISCUSSION

In *Acheta*, every chromosome of the complement can be identified at pachytene, by its size and chromomere markers. This allows us to establish the number of amplification sites and to locate them in specific chromomeres (19).

The number of major chromomeres, their size from early to late pachytene, and their DNA content have been recorded. The amount of DNA in the five major oocyte chromomeres at early pachytene is 4.18 pg, and 9.11 pg in the rest of the chromosomes. Three of the major chromomeres release their DNA copies early in development, and they are hardly visible by middle pachytene. The two largest chromomeres are of about the same size at early pachytene (Fig. 1), and at this stage contain, on the average, 2.00 pg and 1.48 pg of DNA. The average amount of DNA per chromomere pair for the other chromomeres of the pachytene chromosomes of *Acheta* is 0.04 pg. It can then be seen by middle–late pachytene that one of

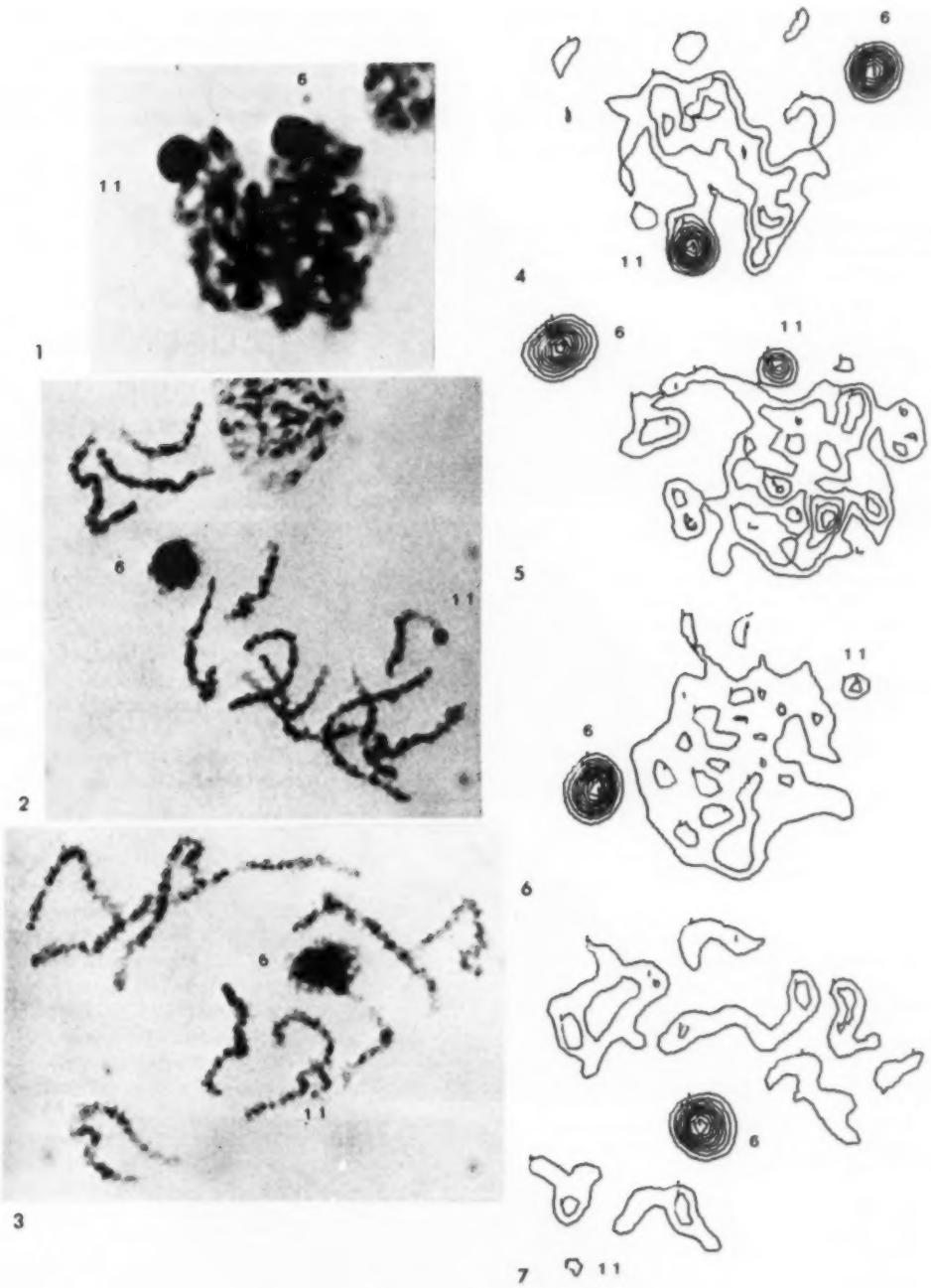

FIGS. 1–3. Feulgen-stained nuclei of *Acheta* at pachytene. At early pachytene (Fig. 1) the two major chromomeres, belonging to chromosomes 6 and 11, are about the same size. At late pachytene, stage 1 (Fig. 2), the major chromomere of chromosome 6 (which was separated from its chromosome by the squash) becomes a "puff" with the DNA copies separating from each other. The major chromomere of chromosome 11 has in the meantime released some of its DNA copies, becoming now only what could be called a large chromomere. Later, at late pachytene, stage 2 (Fig. 3), the major chromomere of chromosome 11 has released most of its copies and it is indistinguishable from the smallest chromomeres of the chromosome complement, ×1,700.

FIGS. 4–7. DNA measured in Feulgen-stained nuclei of *Acheta* at pachytene by the Zeiss Scanning Microscope Photometer 05. The extinction values were recorded on tape and processed by a computer. They are displayed as a contour map of iso-brightness curves. The amount of DNA in the major chromomere of chromosome 6 remains practically constant, whereas that of the major chromomere of chromosome 11 decreases from early (Fig. 4) to middle (Fig. 5) to late, stage 1 (Fig. 6), and late, stage 2 (Fig. 7), pachytene. The amount of DNA released is 1.43 pg.

the amplified chromomeres is located at one end of chromosome 6 and the other is located at one end of chromosome 11 (Figs. 2 and 3). At this stage, the DNA copies in the amplified chromomere of chromosome 6 open out in the form of a "puff." The DNA copies are active in RNA synthesis, as checked by [^{3}H]uridine incorporation (13, 14). No appreciable number of copies is released from the amplified chromomere of chromosome 6 throughout pachytene (Figs. 4–8). Only at late diplotene do most copies leave this chromomere. On the other hand, the amplified chromomere of chromosome 11 starts releasing

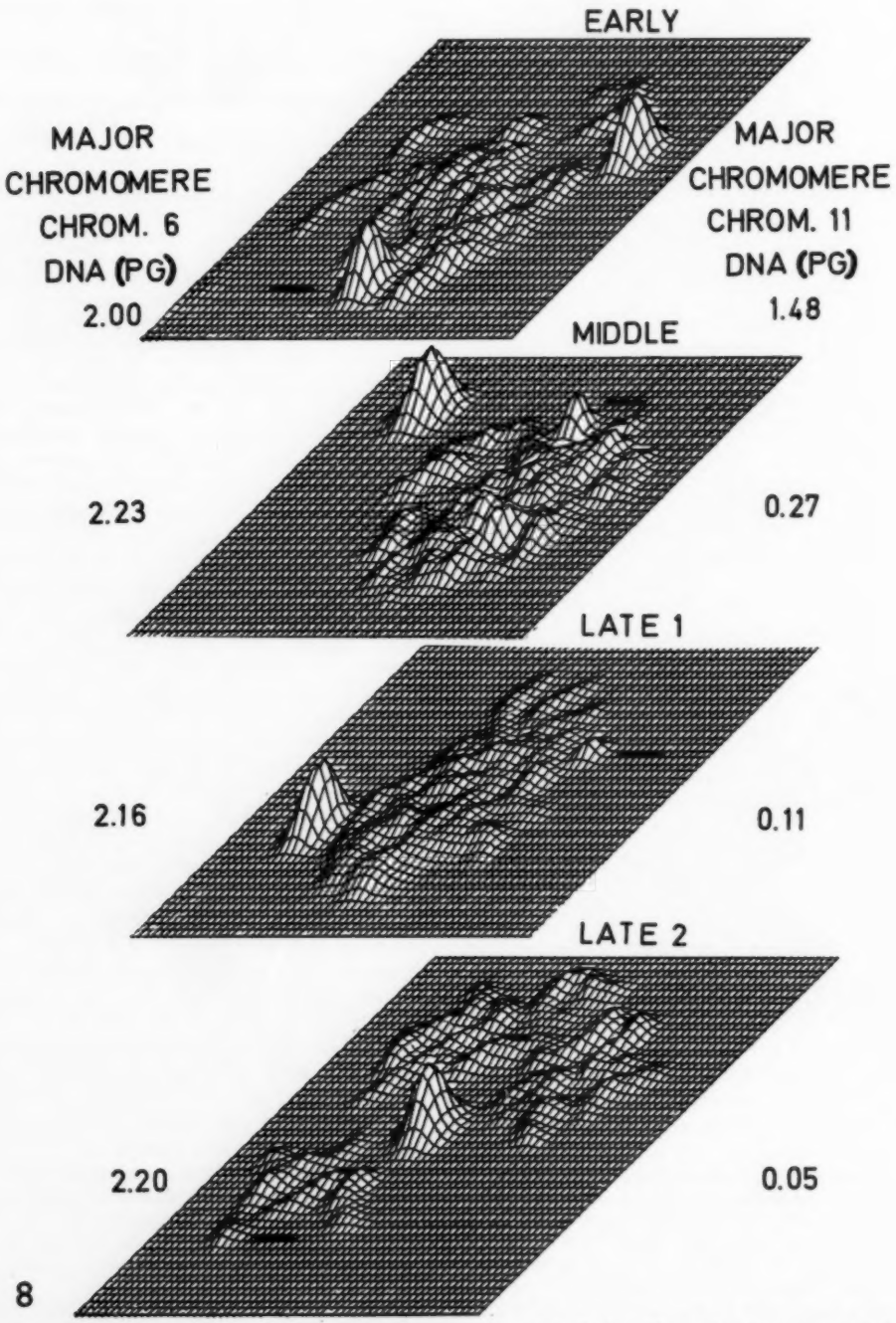

FIG. 8. The same cells measured in Figs. 4–7 are shown in computer volumetric display. The major chromomere of chromosome 11 is indicated by an *arrow*. The average amount of DNA in pg is given on the left side for the major chromomere of chromosome 6 and on the right side for the major chromomere of chromosome 11. At late pachytene, stage 2 (bottom of figure) every chromosome could be identified separately.

its copies during early pachytene. Its diameter decreases, from early to late pachytene (stage 2), from 1.8 μm to 0.4 μm. What was a DNA body or major chromomere at early prophase becomes a large chromomere, then a chromomere of average size, and finally a minute chromomere (see Figs. 4–7). During this process the DNA copies separate and the major chromomere builds a smaller "puff" than that formed on chromosome 6. As the copies are released, the amount of DNA decreases from an average of 1.48 pg (early pachytene) to 0.27 pg (middle pachytene) to 0.11 pg (late pachytene, stage 1) and, finally, to 0.05 pg (late pachytene, stage 2, Fig. 8). This means that as much as 1.4 pg of DNA is released from a single major chromomere during pachytene, transforming it into a minor chromomere. This amount of DNA corresponds to 1.38×10^9 nucleotide pairs.

From the saturation experiments and the haploid DNA value of *Acheta* (2.00 pg) it has been calculated that in somatic tissues there are about 171 cistrons (single strand) for ribosomal RNA (28 S and 18 S). Since most of these sites are located in the two major chromomeres of chromosomes 6 and 11, as shown by hybridization *in situ* with complementary RNA and with 28 S and 18 S *Xenopus* RNA (17, 20), the major chromomeres of these chromosomes contain redundant, tandemly duplicated ribosomal DNA sequences, as well as extra DNA copies that result from localized amplification of cistrons coding for ribosomal RNA.

What distinguishes the present data from previous information on localized DNA increase and decrease is the following. (*a*) Chromomeres are shown to contain (not necessarily to consist of) gene redundancy and gene amplification. (*b*) Chromomeres are not only spiralized regions of the chromosome, as has been shown in several other species, but, at least for the cases described here, extra DNA copies are also an integral part of their structure. (*c*) This redundancy and amplification is for well-defined cistrons (the DNA sites that code for 28S and 18S RNA), whereas in most previous cases it was not known which genes were involved in DNA increase. (*d*) The chromomeres studied here are not part of a somatic tissue, such as the salivary glands, but are part of the germ line. (*e*) Not only the increase in DNA but also the decrease due to the release of the copies could be measured in the very small pachytene chromomere pairs, which are on the average about $^1/_5$ and $^1/_{10}$ of the diameter of the salivary gland chromosomes of *Drosophila* and *Chironomus*, respectively.

Several questions arise. Do other chromomeres contain amplified copies of other genes? Once these copies are released are they destroyed at once? If not, do they still have a function? Chromomeres are present at every prophase but are particularly large and distinct at the first prophase of meiosis. Is this connected with the more elaborate type of genetic information needed at this stage, in which more significant genetic events take place than in mitosis, and which precedes fertilization?

NOTE ADDED IN PROOF

Ribosomal DNA is the DNA that contains the segments (cistrons) coding for 28 S and 18 S ribosomal RNA together with sequences not homologous to this RNA ("spacer").

Supported by research grants from the Swedish Natural Science Research Council, the Knut and Alice Wallenberg Foundation, the Bank of Sweden Tercentenary Fund, and the Torsten and Ragnar Söderberg Foundation.

1. McClintock, B. (1931) *Proc. Nat. Acad. Sci. USA* **17**, 485–491.
2. Muller, H. J. (1935) *Amer. Nat.* **69**, 405–411.
3. Ris, H. (1957) in *A Symposium on the Chemical Basis of Heredity*, eds. McElroy, W. D. & Glass, B. (The Johns Hopkins Press), pp. 23–62.
4. Callan, H. G. (1955) in *Symposium on the Fine Structure of Cells (Leiden, 1954)* (P. Noordhoff, Groningen, The Netherlands) *Int. Union Biol. Sci. Ser. B* **21**, 89.
5. Britten, R. J. & Kohne, D. E. (1969) in *Handbook of Molecular Cytology*, ed. Lima-de-Faria, A. (North-Holland Publ. Co., Amsterdam, London), pp. 21–36.
6. Ficq, A. & Pavan, C. (1957) *Nature* **180**, 983–984.
7. Rudkin, G. T. & Corlette, S. L. (1957) *Proc. Nat. Acad. Sci. USA* **43**, 964–968.
8. Keyl, H.-G. (1965) *Experientia* **21** (191), 1–7.
9. Callan, H. G. (1967) *J. Cell Sci.* **2**, 1–7.
10. Beermann, W. (1967) in *Heritage from Mendel*, ed. Brink, R. A. (Univ. of Wisconsin Press), pp. 179–201.
11. Edström, J. E. (1968) *Nature* **220**, 1196–1198.
12. Crick, F. (1971) *Nature* **234**, 25–27.
13. Heinonen, L. & Halkka, O. (1967) *Ann. Med. Exp. Fenn.* **45**, 101–109.
14. Lima-de-Faria, A., Nilsson, B., Cave, D., Puga, A. & Jaworska, H. (1968) *Chromosoma* **25**, 1–20.
15. Lima-de-Faria, A., Birnstiel, M. & Jaworska, H. (1969) *Genetics Supplement* **61** (1), 145–159.
16. Pero, R., Lima-de-Faria, A., Ståhle, U., Granström, H. & Ghatnekar, R. (1973) *Hereditas* **73**, in press.
17. Ullman, J., Lima-de-Faria, A., Jaworska, H. & Bryngelsson, T. (1973) *Hereditas* **73**, in press.
18. Lima-de-Faria, A., Gustafsson, T. & Jaworska, H. (1973) *Hereditas* **73**, in press.
19. Lima-de-Faria, A., Daskaloff, S. & Enell, A. (1973) *Hereditas* **73**, in press.
20. Cave, M.D. (1971) *Amer. Soc. Cell Biol. 11th Ann. Meeting* **1971**, 48 abstr.

Proc. Nat. Acad. Sci. USA
Vol. 70, No. 1, pp. 84–87, January 1973

Genetic Transformation in *Escherichia coli* K12

(DNA/$CaCl_2$/recombination/genetic linkage)

SHARON D. COSLOY AND MICHIO OISHI

The Public Health Research Institute of the City of New York, Inc., 455 First Avenue, New York, N.Y. 10016

Communicated by Maclyn McCarty, October 24, 1972

ABSTRACT **An auxotrophic strain of *E. coli* K12 treated with $CaCl_2$ was transformed for several markers at a frequency of up to 10^{-4} per recipient cell by a DNA preparation isolated from a prototrophic strain. The transforming activity of the DNA preparation was eliminated by treatment with DNase, heat, or sonication, whereas RNase or Pronase treatment had little effect. Two closely linked genetic markers (*leu* and *ara*) showed a high degree of cotransformation linkage when high molecular weight DNA was used, but the linkage was almost completely eliminated when sheared, smaller molecular weight DNA was used. There is genetic evidence that the transformation is a result of the replacement of the preexisting genetic marker on the chromosome by that of the donor DNA.**

Since its discovery in Pneumococcus (1, 2), genetic transformation has been reported among several other bacterial species such as *Haemophilus influenzae* (3) and *Bacillus subtilis* (4). In *Escherichia coli*, especially in its K12 strain, however, attempts to demonstrate genetic transformation have been unsuccessful.

Several unique systems are known in *E. coli* in which the biological activity of isolated DNA can be assayed directly, such as transformations by bacteriophage λ DNA with helper phages (5). More recently, an efficient transfection system was developed by Mandel and Higa using $CaCl_2$-treated cells (6). In most examples of transfection and transformation, the DNA is either phage or plasmid (7) DNA, which is circular (or converts to circular forms in the cells).

During studies on the mechanism of ATP-dependent DNase (8–11) from *E. coli* in this laboratory, we have observed that the enzyme does not attack double-stranded circular DNA with or without nicks, whereas it causes extensive degradation of linear DNA molecules. Since fragments of bacterial chromosome are the source of genetic material in other general transformation systems, one of the reasons for the failure of genetic transformation in *E. coli* cells might be extensive degradation by the enzyme of linear DNA molecules lacking any protection mechanism. These characteristics of the enzyme plus reports of a mutant that lacks ATP-dependent DNase yet retains the capacity for genetic recombination (12) prompted us to examine the possibility of genetic transformation in *E. coli* K12. In this paper, we report the genetic transformation of *E. coli* K12 and some of its basic characteristics.

MATERIALS AND METHODS

Bacterial Strains used in this study are listed in Table 1. Genetic symbols are those used by Taylor (13).

Abbreviation: SDS, sodium dodecyl sulfate.

Reagents. RNase (pancreas, crystalline RNase A), DNase (pancreas, crystalline), and calf-thymus DNA were purchased from Worthington Biochemical Co. Pronase (grade B) was purchased from Calbiochem.

Isolation of Transforming DNA. Cells were grown in Pen assay broth (Difco), chilled, and harvested at the late exponential or early stationary phase by centrifugation. They were then suspended in one-fortieth of the original volume of cold 0.1 M NaCl–0.1 M EDTA (pH 8.5). 1 M Tris·HCl (pH 9.0)–10% SDS (sodium dodecyl sulfate) was added to give a final concentration of 0.1 M Tris·HCl and 1% SDS, followed by incubation at 42° for 2–5 min until the cell suspension became viscous. Immediately afterwards an equal volume of redistilled phenol (saturated with water) was added, and the samples were gently shaken for 20 min at room temperature. After centrifugation, the aqueous phase was carefully withdrawn and mixed with two volumes of 95% ethyl alcohol. Crude DNA was picked up with a glass rod while the samples were being mixed with alcohol. The DNA was then dissolved in the same volume of 0.1 strength of standard saline–citrate (15 mM NaCl–1.5 mM Na_3-citrate) that contained 5 mM EDTA. After the DNA was dissolved completely, one-tenth volume of 10-times the strength of standard saline–citrate (1.5 M NaCl–0.15 M Na_3-citrate) and 25 μg/ml of pancreatic RNase [treated in 0.1 M NaCl–10 mM acetate buffer (pH 5.2) by the method of Marmur (14)] were added, and the sample was incubated at 37° for 30 min. After incubation, 1 M Tris·HCl (pH 9.0) was added to give a final concentration of 0.1 M. After the phenol treatment was repeated, the aqueous phase was treated with ethyl ether (equal volume, 3 times) to extract the remaining phenol. The DNA was then precipitated with alcohol as described above and dissolved in an appropriate volume of 0.1 strength standard saline citrate (final DNA concentration, 100–400 μg/ml). For certain strains (MO611 and its derivatives), it was necessary that 200 μg/ml of Pronase (previously treated at 70° for 10 min) was present during the Tris–SDS treatment. Incubation at 42° was done for 60 min. The DNA thus prepared can be kept in a refrigerator with a drop of chloroform without measurable loss of biological activity for at least 8 months. As will be discussed later, biologically active DNA can be obtained reproducibly only when an endonuclease I-negative mutant strain (15) is used as the source of transforming DNA.

Transformation. The procedure was a modification of that originally discovered by Mandel and Higa for transfection of *E. coli* cells by bacteriophage λ DNA (6). All treatments

TABLE 1. *Bacterial strains used in this study*

E. coli K12 strain	Derived from	Relevant genetic characteristic used in this study*	Source
HfrC6		*end* (endonuclease I negative)	H. Hoffmann–Berling
AB1157(F^-)		*leu-6 ara-14 his-4*	B. Low
MO609(F^-)	AB1157	*end leu-6 ara-14 his*$^+$	This laboratory†
W3110			F. Imamoto
JC5519(F^-)	AB1157	*recB21 recC22 leu-6 ara-14 his-4*	A. J. Clark
JC7623(F^-)	AB1157	*recB21 recC22 sbcB15 leu-6 ara-14 his-4*	A. J. Clark
MO611(F^-)	JC7623	*end recB21 recC22 sbcB15 leu-6 ara-14 his-4*	This laboratory‡
MO617(F^-)	MO611	*end recB21 recC22 sbcB15 leu*$^+$ *ara-14 his-4*	This laboratory§
MO618(F^-)	MO611	*end recB21 recC22 sbcB15 lell*$^+$ *ara*$^+$ *his-4*	This laboratory§
MO626(F^-)	JC5519	*recB*$^+$ *recC*$^+$ *leu-6 ara-14 his-4*	This laboratory¶
MO627(F^-)	JC7623	*recB*$^+$ *recC*$^+$ *sbcB15 leu-6 ara-14 his-4*	This laboratory¶
MO619(F^-)	JC7623	*recB21 recC22 sbcB15 leu-6 ara*$^+$ *his*$^+$	This laboratory§

* Besides genetic characteristics listed here, the following markers are known: HfrC6 (*met*); W3110 (*trp*); AB1157, JC5519, JC7623, and their derivatives (*thr-1 thi-1 lacY-1 mtl-1 xyl-5 galK2 proA2 argE3 str-31 tex-33 sup-37 amber*). MO611, MO617, and MO618 require tryptophan (*trpBC-27*).

† Constructed by conjugation with HfrC6.

‡ *end* was introduced by a mutation with *N*-methyl-*N'*-nitro-*N*-nitrosoguanidine.

§ Constructed by transformation with HfrC6 DNA.

¶ Constructed by conjugation with HfrKL16(*leu*).

and manipulations were done at 0°–2°, unless specified. Three ml of overnight culture of the recipient cells grown in P medium (16) (supplemented with 100 μg/ml of required amino acids and 10 μg/ml of vitamin B1) were transferred to fresh medium (usually 80 ml) and incubated at 37° with rotatory shaking until the cell density reached 3×10^8/ml. The culture was chilled, centrifuged (6000 × *g*, 10 min), washed once with 40 ml of 10 mM $CaCl_2$, and suspended in the same volume of 25 mM $CaCl_2$. After having been kept at 0° for 20 min, the cells were centrifuged and suspended in 4–8 ml of 25 mM $CaCl_2$. 0.3 ml of the cell suspension was transferred to tubes that contained DNA (0.1 ml) and $CaCl_2$ (50 mM, 0.1 ml). The reaction mixture (0.5 ml) was incubated for 45 min at 0° followed by 10 min at 37°. The reaction was terminated by chilling the tubes at 0°, followed by addition of 1 μg of pancreatic DNase [50 μl of 20 μg/ml in 10 mM Tris·HCl–1 mM $CaCl_2$ (pH 7.6)]. 0.1 ml of samples (usually duplicate) was plated on selective plates (17) that contained minimal medium supplemented with required (nonselective) amino acids and vitamins. Transformants were counted after 36–48 hr of incubation at 37°. The same plates supplemented with all the requirements were used for counting of the total viable cells in the transformation mixture.

RESULTS

When the multi-auxotrophic *E. coli* K12 strain (JC7623), which lacks ATP-dependent DNase (*recB*$^-$ *recC*$^-$) and exonuclease I (*sbcB*$^-$) but retains recombination capacity, was treated with $CaCl_2$ and then exposed to DNA isolated from a prototrophic *E. coli* strain (HfrC6), a significant number of colonies arose on agar medium that would not support the growth of the original strain. For example (Table 2), after exposure to DNA, a small percentage of original strain that had required both leucine and histidine was now capable of growing without leucine in some cases and without histidine in others. $CaCl_2$ treatment of the recipient cells was essential for production of the colonies. These apparent transformants were stable for their newly acquired genetic characters and maintained them for many generations. The number of such apparent genetic transformants produced per test tube was roughly proportional to the amount of DNA added to it, up to 10 μg/0.5 ml. The maximum frequency of transformation under these conditions was about 10^{-6} for each genetic marker, which is considerably lower than that observed in the other bacterial transformation systems. Besides leucine (*leu-6*) and histidine (*his-4*) markers, the other available genetic markers, arginine (*argE3*), threonine (*thr-1*), and proline (*proA2*) requirements and ability to use arabinose (*ara-14*) as a sole carbon source, were also transformable. The transformation frequency for all these markers was similar to that observed for leucine and histidine. These results indicate that transformation events are not limited to a few particular genetic markers but occur generally for the available markers located at several places on the *E. coli* chromosome, thus suggesting that this system is similar to the other known bacterial transformation systems.

TABLE 2. *Transformation with various concentrations of DNA*

DNA (μg/0.5 ml)	No. of transformants	
	Leu$^+$	His$^+$
0	1	2
1	53	28
2	109	38
4	128	62
6	184	68
10	354	126
10 (no cells)	0	0
10 (no $CaCl_2$ treatment)	3	10

Transformation was performed with HfrC6 DNA as donor DNA and JC7623 cells as recipients. Number of transformants is the sum of transformants produced on four plates with a total of 2.8×10^8 recipient cells. For cells without $CaCl_2$ treatment, the same cells were resuspended in P-medium instead of in $CaCl_2$ solution, and transformation was performed. Total recipient cells were 8×10^8.

TABLE 3. *Effect of various treatments of DNA on the transforming activity*

Treatment of DNA	No. of Leu$^+$ transformants
(*A*) No treatment	335
DNase (1 μg/ml)	1
RNase (20 μg/ml)	349
Sonication	1
Denaturation (100°, 5 min)	4
Denaturation-renaturation	21
No DNA	2
(*B*) No treatment	280
Pronase (500 μg/ml)	411

(*A*) DNA (5 μg/0.5 ml) from HfrC6 and JC7623 cells were used as donor DNA and recipient cells, respectively. The number of Leu$^+$ transformants is the sum of the transformants produced on four plates with a total of 2.8×10^8 recipient cells. All the treatments of DNA were done in 0.1 standard saline–citrate unless specified. Treatment with DNase was done at 37° for 20 min at DNA concentration of 50 μg/ml in 0.1 standard saline–citrate with 5 mM $CaCl_2$. Treatment with RNase was done at 37° for 20 min at DNA concentration of 50 μg/ml in 0.1 standard saline–citrate. For sonication, DNA solution (100 μg/ml) was treated by sonic oscillation (Raytheon, model DF 101) at maximum capacity for 5 min. For denaturation, DNA (100 μg/ml in 0.1 standard saline–citrate) was heated at 100° for 5 min, followed by quick chilling in ice-water. For renaturation, the heated denaturated DNA (100 μg/ml) was incubated at 69° for 4 hr in 2 × standard saline–citrate, followed by slow cooling to room temperature over a 10-hr period. After pulse heating (78°, 5 min), the DNA solution was dialyzed against 0.1 standard saline–citrate. (*B*) Same as (*A*), but total recipient cells were 2.1×10^8. Treatment with Pronase was done at 37° for 15 min at DNA concentrations of 268 μg/ml in standard saline–citrate, followed by one phenol treatment (see *Methods*).

We further investigated the nature of the active component in the DNA preparation. As shown in Table 3, prior treatment of the DNA preparation with pancreatic DNase completely eliminated the transforming activity, whereas treatment with RNase or Pronase had little effect. The activity was also lost after sonication or denaturation by heat treatment (100°, 5 min). In another experiment (not shown), when the DNA preparation was centrifuged in CsCl, the active transforming fraction coincided with the DNA fraction having the buoyant density of *E. coli* DNA (1.710 g/ml). These results indicate that the biologically active component in the DNA preparation is DNA, and that only double-stranded DNA is active for the transformation. We tested DNA preparations isolated from various sources. DNA from various *E. coli* K12 strains (Hfr as well as F$^-$) could transform the auxotrophic recipients (Table 4). This was also the case when DNA from transformed cells was used as donor DNA for a second transformation. It should be noted, however, that we sometimes encountered difficulties in attempting to isolate active DNA from endonuclease I-positive cells, probably due to damage by the enzyme to the DNA during its isolation. DNA from *E. coli* B had essentially no transforming activity. This lack of activity may be due to restriction of *E. coli* B DNA in K12 cells.

TABLE 4. *Transformation with DNA from various sources*

Source of DNA (genotype)	No. of transformants Leu$^+$	His$^+$
No DNA	0	1
E. coli K12 HfrC6 (*leu*$^+$ *his*$^+$)	235	100
E. coli K12 F$^-$MO609* (*leu*$^-$ *his*$^+$)	0	75
E. coli W3110 (*leu*$^+$ *his*$^+$)	65	25
E. coli B	2	2
B. subtilis†	0	0
Calf thymus	0	1

Transformation was performed with 5 μg/0.5 ml of DNA and JC7623 as recipient cells. Number of transformants is the sum of the transformants produced on four plates with a total of 8×10^7 recipient cells.

* Derivative of AB1157 (see Table 1).

† Transforming DNA (168W DNA, gift from Dr. I. Smith).

TABLE 5. *Evidence for linkage by transformation*

Selected marker	Cotransformation with	No. cotransformants/no. examined (%) Untreated DNA	Sheared DNA
Leu$^+$	Ara$^+$	20/50 (40)	1/50 (2)
	His$^+$	0/50 (0)	0/50 (0)
Ara$^+$	Leu$^+$	20/50 (40)	3/50 (6)
	His$^+$	0/50 (0)	0/50 (0)
His$^+$	Leu$^+$	0/50 (0)	0/50 (0)
	Ara$^+$	0/50 (0)	0/50 (0)

Transformation was performed with 2 μg/0.5 ml of HfrC6 DNA as donor DNA and JC7623 as recipient cells. Fifty randomly selected transformants were purified and examined for cotransformation.

We next compared the degree of the linkage of two very close genetic markers, using both high and low molecular weight DNA. The linkage between the leucine (*leu-6*) and arabinose (*ara-14*) markers was chosen for this purpose. The cotransduction frequency with bacteriophage P1 is close to 50% or more for various mutational markers in these two loci (13, 18). As shown in Table 5, when transformation was performed with high molecular weight DNA (untreated, estimated molecular weight 30 to 300×10^6), selecting separately for Leu$^+$, Ara$^+$, and His$^+$ transformants, about 40% (20/50) of the leucine transformants were also Ara$^+$, whereas none (0/50) of the Leu$^+$ transformants was His$^+$. This result was to be expected since the *his* marker is very distant from

TABLE 6. *Cotransformation of closely linked negative genetic markers*

DNA (genotype)	Selected marker	No. cotransformants/no. Leu$^+$ transformants (%) Ara$^-$	His$^-$
MO617 (*leu*$^+$ *ara*$^-$ *his*$^-$)	Leu$^+$	17/50 (34)	0/50 (0)
MO618 (*leu*$^+$ *ara*$^+$ *his*$^-$)	Leu$^+$	0/50 (0)	0/50 (0)

Transformation was performed with 6 μg/0.5 ml of DNA as donor DNA and MO619 (*leu*$^-$ *ara*$^+$ *his*$^+$) as recipient cells. Fifty randomly selected Leu$^+$ transformants were purified and examined for cotransformation.

the *leu* and *ara* genes on the *E. coli* chromosome. Reciprocal tests confirmed the same degree of linkage between leucine and arabinose markers. The fact that the reciprocal linkages are identical is not significant, since the numbers tested are relatively small. The observed cotransformation frequency (40%) between leucine and arabinose with high molecular weight DNA seems to be a reasonable one relative to the linkage value found with P1 transduction, in which the transducing fragment has a molecular weight of 6×10^7 (19). In similar experiments with sheared, smaller molecular weight DNA (estimated average molecular weight, 8×10^6), only one of 50 leucine transformants was Ara$^+$ and three of 50 arabinose transformants were Leu$^+$. These results indicate that physical breakage of the DNA molecules causes loss of the genetic linkage originally observed, and further support the interpretation that the biologically active fraction in the DNA preparation must be DNA itself.

Another question to be answered in this transformation system was whether the donor DNA was integrated into the recipient chromosome. Although the observation that transformants are stable for their acquired characteristics suggested that integration occurred, we performed the following experiment: A recipient strain (*leu*$^-$ *ara*$^+$ *his*$^+$) was transformed with DNA derived from a strain possessing *leu*$^+$, *ara*$^-$, and *his*$^-$ markers. Leu$^+$ transformants were selected and tested to determine if they had incorporated the donor's *ara*$^-$ marker. As seen in Table 6, 34% of the Leu$^+$ transformants were Ara$^-$. In the control experiment (MO617 DNA) (Table 6), the absence of Leu$^+$ His$^-$ types demonstrated that the Leu$^+$ Ara$^-$ transformants were not due to double transformation events. The same control experiment with MO618 (*leu*$^+$ *ara*$^+$ *his*$^-$) DNA showed that the Leu$^+$ Ara$^-$ transformants are not the result of production of *ara*$^-$ mutations in or near recombination sites such as those reported by Yoshikawa (20). The transformation to a negative phenotype (Ara$^-$) makes it reasonable to conclude that the donor marker integrates into the homologous site of the recipient chromosome, replacing the preexisting marker.

The genetic basis for the transformability of the JC7623 (*recB21 recC22 sbcB15*) strain is not yet clear. Preliminary experiments with its parental strain, AB1157 (*recB*$^+$ *recC*$^+$ *sbcB*$^+$), as well as with two recombinants for these genes (MO626 and MO627) obtained by conjugation, has produced evidence for significantly less transformability. The strain that lacks a functional *rec* system (JC5519) is the only one that gave absolutely no evidence of transformability. These studies are continuing.

DISCUSSION

From our results it seems that transformation in *E. coli* K12 strains is similar to that of other bacterial transformation systems. There are, of course, other possibilities that could explain these results. For example, DNA of some thus far undetected phages or plasmids may be present widely in *E. coli* K12 strains and become associated with various chromosomal genetic segments. This DNA could be the source of the transforming activity in bulk DNA preparations. Alternatively, it is also conceivable that DNA of a particular structure, which represents only a small portion of the total DNA preparation, is responsible for the transformation. Such DNA could be derived from the *in vivo* intermediate of a cellular process such as DNA replication, recombination, or repair.

The reason for the low frequency of transformation and the requirement for high concentrations of DNA in this system is not clear. Perhaps *E. coli* cells inherently do not have an active uptake system for incorporating DNA so that a high concentration of DNA outside the cells is necessary. On the other hand, the failure to detect a double transformation of two unlinked markers (i.e., Leu$^+$ His$^+$) among transformants at even very high DNA concentrations seems to diminish the possibility that only certain highly transformable recipient cells are responsible for the transformation.

The possibilities of this transformation system in *E. coli* with its wealth and diversity of genetic and biochemical background material is for the most part self evident. Among the more intriguing possibilities is the potential for using this extremely well-characterized organism as a model to study the introduction and integration of genetic information from various sources.

NOTE ADDED IN PROOF

After submission of this manuscript we completed experiments that allowed us to conclude that the absence of both ATP-dependent DNase (*recB*$^-$ *recC*$^-$) and exonuclease I (sbcB$^-$) activity are major factors contributing to the transformability of the *E. coli* K12 strain (Oishi, M. & Cosloy, S. D., *Biochem. Biophys. Res. Commun.* in press).

We thank Drs. P. Margolin and S. Basu for helpful discussions and Ms. J. Tamayo for preparing the manuscript. This work was supported by NSF (GB 14313) Grant awarded to M. O. S. D. C. was supported by Public Health Science Research Fellowship (GM 50531). M. O. is a U.S. Public Health Service Research Career Development Awardee (GM 70538).

1. Griffith, F. (1928) *J. Hyg.* **27**, 113–159.
2. Avery, O. T., MacLeod, C. M. & McCarty, M. (1944) *J. Exp. Med.* **79**, 137–157.
3. Alexander, H. E. & Leidy, G. (1951) *J. Exp. Med.* **93**, 345–359.
4. Spizizen, J. (1958) *Proc. Nat. Acad. Sci. USA* **44**, 1072–1078.
5. Kaiser, A. D. & Hogness, D. S. (1960) *J. Mol. Biol.* **2**, 392–415.
6. Mandel, M. & Higa, A. (1970) *J. Mol. Biol.* **53**, 159–162.
7. Cohen, S. N., Chang, A. C. Y. & Hsu, L. (1972) *Proc. Nat. Acad. Sci. USA* **69**, 2110–2114.
8. Wright, M. & Buttin, G. (1969) *Bull. Soc. Chim. Biol.* **51**, 1373–1383.
9. Oishi, M. (1969) *Proc. Nat. Acad. Sci. USA* **64**, 1292–1299.
10. Barbour, S. D. & Clark, A. J. (1970) *Proc. Nat. Acad. Sci. USA* **65**, 955–961.
11. Goldmark, P. J. & Linn, S. (1970) *Proc. Nat. Acad. Sci. USA* **67**, 434–441.
12. Kushner, S. R., Nagaishi, H., Templin, A. & Clark, A. J. (1971) *Proc. Nat. Acad. Sci. USA* **68**, 824–827.
13. Taylor, A. L. (1970) *Bacteriol. Rev.* **34**, 155–175.
14. Marmur, J. (1961) *J. Mol. Biol.* **3**, 208–218.
15. Dürwald, H. & Hoffmann-Berling, H. (1968) *J. Mol. Biol.* **34**, 331–346.
16. Kaiser, A. D. (1962) *J. Mol. Biol.* **4**, 275–287.
17. Margolin, P. (1963) *Genetics* **48**, 441–457.
18. Gross, J. & Englesberg, E. (1959) *Virology* **9**, 314–331.
19. Ikeda, H. & Tomizawa, J. (1965) *J. Mol. Biol.* **14**, 85–109.
20. Yoshikawa, H. (1966) *Genetics* **54**, 1201–1214.

Proc. Nat. Acad. Sci. USA
Vol. 70, No. 1, pp. 88–92, January 1973

RNA-Linked DNA Fragments *In Vitro**

(*E. coli*/toluene-treated cells/DNA synthesis/discontinuous replication/RNA synthesis/nucleotide sequence)

AKIO SUGINO AND REIJI OKAZAKI

Institute of Molecular Biology, Faculty of Science, Nagoya University, Nagoya, Japan 464

Communicated by Arthur Kornberg, October 24, 1972

ABSTRACT **RNA-linked DNA fragments are intermediates in DNA replication in *Escherichia coli* cells made permeable to nucleoside triphosphates by treatment with toluene. Covalent linkage of a short RNA stretch to the 5′ end of the DNA is proved by transfer of ^{32}P from [α-^{32}P]-dNTP to ribonucleotides upon digestion with alkali or pancreatic RNase, and by a small decrease in the molecular size upon alkaline hydrolysis. The ^{32}P transfer experiments reveal a unique structure...p(rPy)p(rA)p(rU or rC)p-(dC)p... at the RNA–DNA junction.**

We have shown (1, 2) that a short stretch of RNA is linked to the nascent DNA fragments isolated from exponentially growing cells of *Escherichia coli*. The RNA seems to be removed before the fragments are joined by ligase and become a part of the long DNA strand. These findings suggest that RNA synthesis (transcription) is involved in the initiation of synthesis of these fragments, which would occur at specific sites on the template strands in the discontinuous mode of DNA replication.

To obtain further information on the structure and metabolism of the RNA-linked nascent DNA fragments, we have investigated the synthesis of these molecules in *E. coli* cells made permeable to nucleoside triphosphates by treatment with toluene (3). The results presented here indicate that toluene-treated cells synthesize RNA-linked DNA fragments—as do intact cells—and that the RNA is covalently linked at the 5′ end of the DNA by a phosphodiester bond. Furthermore, unique primary structures at the RNA–DNA junction are demonstrated.

MATERIALS AND METHODS

Unlabeled dNTPs were purchased from Schwarz BioResearch, dT, rATP, DPN from Sigma Chemical Co., and [^3H]dTTP (17.4 Ci/mmol) from the Radiochemical Centre (Amersham). [α-^{32}P]dCTP, [α-^{32}P]dGTP, and [α-^{32}P]dATP (14–21 Ci/mmol) were obtained from International Chemical and Nuclear Corp. and treated with periodate (4) to degrade any contaminating ribonucleotides. [α-^{32}P]dTTP (9 Ci/mmol) was prepared as follows: dT was first phosphorylated by *E. coli* dT kinase (5) with [γ-^{32}P]rATP (11.5 Ci/mmol), prepared by a described method (6), and the reaction mixture was treated with periodate to destroy the remaining [γ-^{32}P]rATP. [^{32}P]dTMP was recovered by charcoal treatment and converted to [α-^{32}P]dTTP with unlabeled rATP and dNMP kinase from bacteriophage T4-infected *E. coli*. The labeled dTTP was isolated by paper electrophoresis at pH 3.5, followed by charcoal treatment.

E. coli P3478 *thy*$^+$ (*polA1′*) (7) was grown in Bacto Tryptose Broth to a titer of 6×10^8 cells per ml, suspended in 50 mM potassium phosphate buffer (pH 7.6) at a density of 3×10^9 cells per ml, and treated with 1% toluene for 15 min at 37°. The standard incubation mixture for DNA synthesis contained 70 mM potassium phosphate buffer (pH 7.6), 13 mM $MgCl_2$, 1.3 mM rATP, 0.3 mM DPN, 33 μM (each) of four dNTPs, and 1.5×10^9 toluene-treated cells per ml. The reaction was performed at 30° and terminated by addition of two volumes of an ethanol–phenol mixture (18), and cells were collected by centrifugation. Cells were lysed either by incubation in 0.2 N NaOH–20 mM EDTA–0.5% sodium *N*-lauroyl sarcosinate at 37° for 20 min (method A) or by heating in 0.5% sodium dodecyl sulfate (SDS)–10 mM NaCl–10 mM EDTA–10 mM Tris·HCl (pH 7.6) at 100° for 5 min (method B). Cs_2SO_4 equilibrium centrifugation and alkaline sucrose gradient sedimentation were performed as before (1, 9).

Paper electrophoresis was performed on Toyo no. 50 paper at 60 V/cm in 50 mM sodium citrate buffer at pH 5.0 or 3.5. Two-dimensional paper chromatography was performed on Toyo no. 50 paper in 95% ethanol–1 M ammonium acetate (pH 6.8) 75:30 and saturated $(NH_4)_2SO_4$–1 M sodium acetate 80:18. Thin-layer chromatography was done on an Avicel SF cellulose plate (Funakoshi Pharmaceutical Co.) in isopropanol–HCl–H_2O 65:17:18 or in saturated $(NH_4)_2SO_4$–1 M ammonium acetate–isopropanol 40:9:1. To fractionate oligonucleotides, the sample in 7 M urea–20 mM Tris·HCl (pH 7.6) was applied to a DEAE-cellulose (Whatman DE52) column (0.2×30 cm) and eluted with a 60-ml linear gradient of 0–0.25 M NaCl in 7 M urea–20 mM Tris·HCl (pH 7.6). For Dowex-1 chromatography, the sample was applied to a Dowex AG1 X2 (Bio-Rad) column (0.3×12 cm) and eluted first by a linear gradient with 20 ml of 4 mM HCl in the mixing vessel and 20 ml of 0.15 M NaCl–10 mM HCl in the reservoir, then with 20 ml of 0.3 M NaCl–12 mM HCl. Gel filtration through Sepharose 2B (Pharmacia) was performed with upward flow of 0.05 M NaCl–10 mM EDTA–5 mM Tris·HCl (pH 8.0).

RESULTS

The patterns of alkaline sucrose gradient sedimentation of DNA pulse-labeled with [^3H]dTTP for various times (Fig. 1) show that DNA replication in this system occurs by a discontinuous mechanism, as does DNA replication in intact

Abbreviations: SDS, sodium dodecyl sulfate: SSC, standard saline–citrate (0.15 M NaCl–0.015 M sodium citrate).

* This paper is no. X in a series; "Mechanism of DNA Chain Growth." The preceding paper is ref. 1.

cells. Isopycnic analysis (Fig. 2) showed that very nascent DNA in toluene-treated cells has a higher density than does standard *E. coli* DNA, as does nascent DNA of intact cells. Thus RNA-linked DNA fragments seem to be formed as intermediates in DNA replication also in this *in vitro* system.

To test if RNA is linked covalently to the 5′ end of DNA by a 3′:5′-phosphodiester bond, toluene-treated cells were incubated for 5 min in four reaction mixtures, each containing a different dNTP labeled with ^{32}P at the α position. The product of each reaction was hydrolyzed with alkali, and the distribution of ^{32}P in the four 2′(3′)-rNMPs was examined. If covalently linked RNA–DNA molecules are formed with incorporation of the labeled dNTP into the RNA–DNA linkage (the 5′ end of the DNA segment), the ^{32}P originally linked to the 5′ position of that deoxynucleotide should be transferred to the adjacent ribonucleotide (the 3′-terminal nucleotide of the RNA segment) upon alkaline hydrolysis.

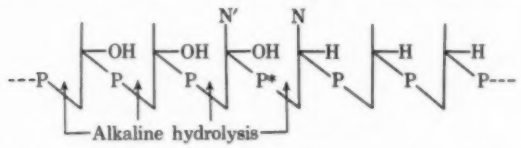

As shown in Table 1, transfer of ^{32}P from the α position of 5′-dNTPs to 2′(3′)-rNMPs did occur, indicating the presence of the phosphodiester linkage between ribo- and deoxyribonucleotides in the product. While a relatively large amount of ^{32}P was transferred from [α-^{32}P]dCTP or [α-^{32}P]dGTP to rUMP, and some ^{32}P transfer from dCTP to rCMP, rAMP, and rGMP was found, little other transfer was detected. Thus, unique base sequences exist at the RNA–DNA linkage: (rU)p(dC) is the most common sequence, which occurs at about half of the linkages, and the sequence (rU)p(dG) occurs at about a quarter of the linkages, whereas most of the rest of the RNA–DNA linkages have the structure (rC)p(dC), (rG)p(dC), or (rA)p(dC).

Pancreatic RNase splits the bond between the 3′-pyrimidine ribonucleotide and the 5′ position of the adjacent deoxy-,

TABLE 1. *Distribution of radioactivity in 2′(3′)-rNMPs after alkaline hydrolysis of products formed with* [α-^{32}P]*dNTP*

[α-^{32}P]dNTP substrate	% of acid-insoluble ^{32}P transferred to:			
	CMP	AMP	GMP	UMP
dCTP	0.08	0.03	0.05	0.34
dATP	<0.01	<0.01	<0.01	0.01
dGTP	<0.01	<0.01	0.01	0.20
dTTP	<0.01	<0.01	<0.01	<0.01

The reaction was performed in four 0.43-ml reaction mixtures for 5 min under the standard conditions, except that one of the four dNTPs was labeled with ^{32}P at the α position as indicated and used at a concentration of 16 μM. The specific activity of dCTP, dATP, dGTP, and dTTP was 9.8, 9.5, 7.0, and 8.9 Ci/mmol, respectively. Cells were lysed by method B and the lysate was subjected to Cs_2SO_4 equilibrium centrifugation. Material banded at densities of 1.40–1.59 g/cm^3 (2.1 to 2.9 $\times$ 10^9 cpm) was dialyzed against 0.1 $\times$ SSC–0.01% SDS, precipitated by ethanol with *E. coli* tRNA (400 μg), and dissolved in 50 μl of 0.3 M KOH. After incubation for 16 hr at 37°, 5 μl of 1% bovine-serum albumin and 3 μl of 60% $HClO_4$ were added and the mixture was centrifuged. The supernatant was neutralized with KOH and the precipitate of $KClO_4$ was removed. The radioactivity of both the supernatant and pellet was measured upon aliquots. The supernatant was subjected to paper electrophoresis at pH 5.0. The rNMP region was cut out, eluted with water, and subjected to a second electrophoresis at pH 3.5. After location of four 2′(3′)-rNMPs under a UV lamp, the paper was cut into 1-cm strips and the radioactivity in each strip was counted. The radioactive nucleotides were eluted from the paper and subjected to thin-layer chromatography, along with authentic 2′(3′)-rNMPs and 5′-dNMPs to confirm identification.

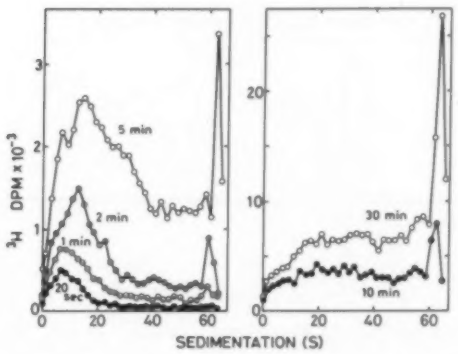

FIG. 1. Alkaline sucrose gradient sedimentation of DNA from toluene-treated cells pulse-labeled with [^{3}H]dTTP. Toluene-treated cells were incubated for 2 min at 30° in the standard reaction mixture (1 ml) with four unlabeled dNTPs. [^{3}H]dTTP (17.4 Ci/mmol) was then added to 2.9 μM, and the reaction was terminated after the times indicated. Cells were lysed by method A and the lysate was subjected to sedimentation through a 5–20% alkaline sucrose gradient made on a 82% sucrose cushion, along with [^{14}C]ϕA DNA (a 19S internal reference).

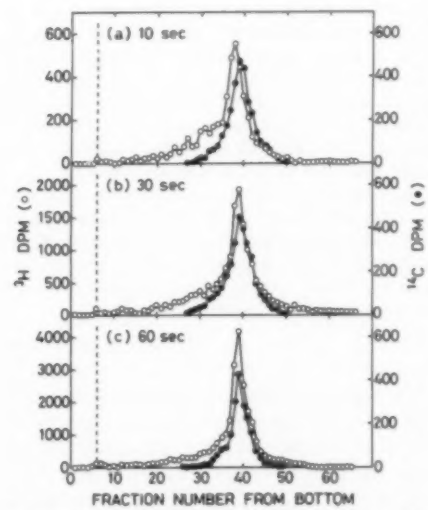

FIG. 2. Cs_2SO_4 equilibrium centrifugation of DNA from toluene-treated cells pulse-labeled with [^{3}H]dTTP. Toluene-treated cells were incubated in the 1-ml standard reaction mixture with [^{3}H]dTTP (3 Ci/mmol) at 30° for the times indicated. Cells were lysed by method B, and the lysate was subjected to equilibrium density centrifugation in a Beckman SW50L rotor, together with denatured *E. coli* [^{14}C]DNA. The vertical *dotted lines* indicate the position of the peak of RNA.

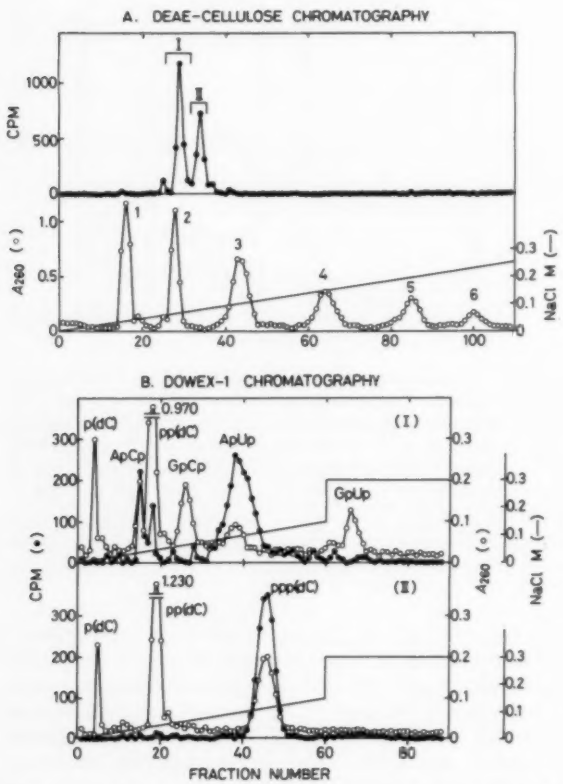

FIG. 3. Identification of radioactive products formed by pancreatic RNase digestion of RNA–DNA molecules synthesized with [α-^{32}P]dCTP. DNA synthesis with [α-^{32}P]dCTP (9.8 Ci/mmol) was performed as in Table 1. Cells were lysed by method B, and the material banding near the density of DNA in Cs_2SO_4 (ρ = 1.40–1.47 g/cm^3; total radioactivity = 3.2 × 10^5 cpm) was dialyzed against 0.1 × SSC–0.01% SDS, and precipitated by ethanol with 300 μg of tRNA as carrier. The sample was dissolved in 50 μl of 20 mM Tris·HCl (pH 7.5)–20 mM NaCl–2 mM EDTA containing 6 μg of pancreatic RNase and incubated at 37° for 2 hr. The mixture was diluted with 2 ml of 7 M urea–20 mM Tris·HCl (pH 7.6) and subjected to chromatography on a DEAE-cellulose–urea column. *Bracketed fractions* (I and II) were diluted 5-fold with water and applied to a Dowex AG1 column along with dCMP and dCDP (*I*) or with dCMP, dCDP, and dCTP (*II*), respectively. The column was eluted as described in *Methods*, and nucleotides were identified by their elution positions and their absorption spectra.

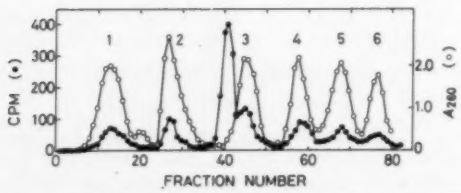

FIG. 4. DEAE-cellulose chromatography of radioactive products formed by pancreatic RNase digestion of RNA–DNA molecules synthesized with [α-^{32}P]dGTP. The experiment was performed as in Fig. 3, except that [α-^{32}P]dGTP (5.5 Ci/mmol) was used as labeled substrate for DNA synthesis.

as well as ribonucleotide (10). Therefore, if the RNA–DNA molecules synthesized with [α-^{32}P]dCTP or [α-^{32}]dGTP are digested with pancreatic RNase, radioactive ribonucleotides (oligo- or mononucleotides) will be produced as the result of cleavage of the linkage as (rU)p(dC), (rC)p(dC), and (rU)-p(dG), and at the nearest pyrimidine nucleotides in the RNA.

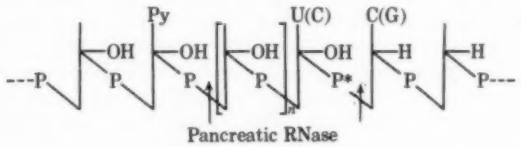

When the product synthesized in the presence of [α-^{32}P]-dCTP was hydrolyzed with pancreatic RNase and subjected to DEAE-cellulose chromatography, 0.7% of the radioactivity was eluted in the position of dinucleotide (Fig. 3*A*, Peak *I*). Of the radioactivity in this peak, 79% cochromatographed with ApUp on Dowex-1, while 15% was eluted in the region of ApCp; no radioactivity was found in the other possible dinucleotides, GpCp and GpUp (Fig. 3*B I*). 0.46% of the total radioactivity was eluted from DEAE-cellulose between di- and trinucleotides (Fig. 3*A*, Peak *II*); this material was contaminating dCTP (Fig. 3*B II*). No radioactivity was found in mono-, tri-, tetra-, penta-, and hexanucleotides. Thus, ApUp and ApCp are the only major radioactive ribonucleotides produced by the RNase digestion of the product formed in the presence of [α-^{32}P]dCTP. The yields of these radioactive dinucleotides are in rough agreement with the amounts of the (rU)p(dC) and (rC)p(dC) linkages indicated by the alkaline hydrolysis experiments. Thus, on the 5′ side of these linkages is the definite structure (rPy)p(rA)p, and the predominant structure at the RNA–DNA junction is:

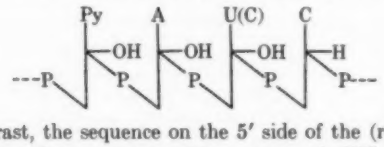

In contrast, the sequence on the 5′ side of the (rU)p(dG) linkage seems heterogeneous. After pancreatic RNase digestion of the product synthesized with [α-^{32}P]dGTP as labeled substrate, various sizes of radioactive products from mono- to hexanucleotides were found (Fig. 4). The radioactive material eluted immediately before trinucleotides was contaminating [α-^{32}P]dGTP.

In the ^{32}P transfer experiments described above, the reaction was allowed to proceed for 5 min. The essential fea-

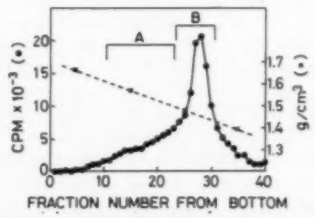

FIG. 5. Cs_2SO_4 equilibrium centrifugation of product synthesized in a 1-min incubation with [α-^{32}P]dCTP. The experiment was performed as in Table 1, except that the reaction was for 1 min with [α-^{32}P]dCTP (14.6 Ci/mmol). *Bracketed fractions* (*A* and *B*) were used for the analysis shown in Table 2.

tures of the results were confirmed with the reaction for 1 min. As shown in Fig. 5, the product of the 1-min reaction with [α-^{32}P]dCTP banded heterogeneously in the Cs_2SO_4 gradient between the densities of RNA and DNA. It was divided into two fractions (*A* and *B*) with relatively high and low densities, and each was hydrolyzed with alkali. As seen from Table 2, 2.82 and 1.10% of the total radioactivity in *A* and *B*, respectively, were transferred to rNMPs. In both fractions, the largest portion of the transferred ^{32}P (78% in *A* and 72% in *B*) was in 2′(3′)-UMP. When the whole product of the 1-min reaction with [α-^{32}P]dCTP was digested by pancreatic RNase and subjected to DEAE-cellulose chromatography, 1.9% of the radioactivity was recovered in dinucleotide; virtually no radioactivity was found in mono-, tetra-, penta-, and hexanucleotides. Of the radioactive dinucleotides, 22% and 77% were ApCp and ApUp, respectively.

From the data of the ^{32}P transfer experiments, the number of total deoxynucleotides per RNA–DNA linkage in the product of the 5-min reaction is calculated to be about 500. If it is assumed that dCMP is contained in three quarters of the RNA–DNA linkages synthesized in the 1-min reaction (as shown for the product of the 5-min reaction), the total number of deoxynucleotides per RNA–DNA linkage is estimated to be about 200 for whole product formed in 1 min, and about 100 and 270 for the product of the 1-min reaction with the high and low densities (*A* and *B* in Fig. 5), respectively. These results are in line with the idea that RNA is linked only to very nascent short DNA, degraded by nuclease action as the DNA segment elongates, and removed completely before ligation of the DNA segments.

In further support of this idea, pancreatic RNase digestion of the product yielded virtually no radioactive dinucleotide (20 cpm in an experiment comparable to that of Fig. 3) when the synthesis with [α-^{32}P]dCTP was followed by incubation in the presence of a 100-fold excess of unlabeled dCTP for 20 min.

Although the ^{32}P transfer experiments prove the RNA–DNA linkage in the product, they do not exclude the possibility that the RNA is located in the middle of the chain or that ribonucleotide sequences are scattered in the molecule. To clarify this point, the molecules of various sizes, synthesized by a 1-min reaction with [^{3}H]dTTP as labeled substrate, were isolated by gel filtration on Sepharose 2B, and the change of their size upon alkaline hydrolysis, as well as their density, was analyzed (Fig. 6). Only small decreases in molecular size were observed, excluding the above possibilities. Thus, the RNA is attached to the 5′ end of the DNA. The size of the RNA segments of the molecules of various sizes is suggested by both size change and density analyses to be about 50–100 nucleotides, in agreement with the results obtained with the *in vivo* RNA–DNA molecules (2).

TABLE 2. *Distribution of radioactivity in 2′(3′)-rNMPs after alkaline hydrolysis of products formed in a 1-min reaction with* [α-^{32}*P*]*dCTP*

Fraction	% of acid-insoluble ^{32}P transferred to:			
	CMP	AMP	GMP	UMP
A	0.23	0.10	0.31	2.18
B	0.18	0.03	0.11	0.78

Fraction A (4.2×10^4 cpm) and Fraction B (1.1×10^6 cpm) in Fig. 5 were dialyzed against 0.1 × SSC–0.01% SDS and precipitated by ethanol with 600 μg of *E. coli* tRNA. After hydrolysis in 50 μl of 0.3 M KOH at 37° for 15 hr, cold $HClO_4$-soluble supernatant was neutralized, concentrated, and subjected to two-dimensional paper chromatography. The 2′(3′)-rNMP spots were cut out and their radioactivity was counted. In addition, all rNMP spots were eluted and subjected to thin-layer chromatography to confirm their identification.

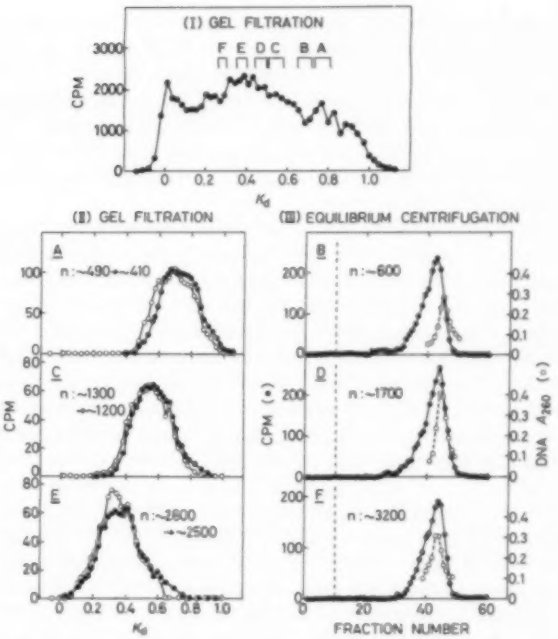

FIG. 6. Fractionation and analysis of RNA–DNA molecules of various sizes. (*I*) Toluene-treated cells were incubated in a 6-ml standard reaction mixture with [^{3}H]dTTP (3 Ci/mmol) for 1 min at 30°. Cells were lysed by method B. The lysate was treated with Pronase E (1 mg/ml, 4 hr at 37°) and then with phenol, and dialyzed against 50 mM NaCl–10 mM EDTA–5 mM Tris·HCl (pH 8.0). After it was heated at 100° for 5 min and quickly chilled, the sample was subjected to gel filtration on a Sepharose 2B column (1.6 × 95 cm). The indicated fractions (*A–F*) were precipitated by ethanol with *E. coli* tRNA as carrier and dissolved in a small volume of 50 mM NaCl–10 mM EDTA–5 mM Tris·HCl (pH 8.0). (*II*) Fractions A, C, and E were divided into two portions: one portion was treated with 0.3 M NaOH at 37° for 4 hr and neutralized. After they were heated at 100° for 5 min and quickly chilled, the untreated (○) and alkali-treated (●) samples were subjected to gel filtration on a Sepharose 2B column (1.6 × 40 cm). (*III*) Fractions *B*, *D*, and *F* were heated at 100° for 5 min, chilled quickly, and subjected to Cs_2SO_4 equilibrium centrifugation in a Beckman SW56Ti rotor with denatured *E. coli* DNA. The *dotted lines* indicate the position of RNA. The chain length (*n*) was estimated from the *K*d values by use of a calibration curve prepared with single-stranded *E. coli* DNA of known chain lengths (Hirose, Okazaki, and Tamanoy, in preparation).

DISCUSSION

Based on studies with intact cells, we have postulated (1, 2) a replication mechanism involving: (*i*) unwinding of the

parental strands; (*ii*) synthesis of short RNA chains along the parental strands beginning at specific initiation signals and stopping at termination signals; (*iii*) extension of the chains by a DNA polymerase in the 5′ → 3′ direction with the RNA as primer; (*iv*) removal of the RNA segments by RNase activity; (*v*) filling the gaps between the DNA fragments by a DNA polymerase; and (*vi*) joining of the DNA fragments by ligase.

The present study performed with toluene-treated cells of a *polA*⁻ strain, an *in vitro* replication system that closely resembles viable cells, lends strong support for this hypothetical mechanism. It demonstrates that RNA-linked DNA fragments are also synthesized *in vitro* (Figs. 2 and 6) and provides definitive evidence for the covalent attachment of RNA to the 5′ end of the DNA (Tables 1 and 2, Fig. 3). That the attachment of RNA is characteristic of nascent short DNA chains is confirmed (Tables 1 and 2, Fig. 6, and the chase effect of unlabeled dCTP on the ^{32}P transfer from [α-^{32}P]-dCTP).

Furthermore, the ^{32}P transfer experiments (Tables 1 and 2, Fig. 3) reveal that ...p(rPy)p(rA)p(rU)p(dC)p..., with occasional replacement of (rU) with (rC), is a predominant sequence at the RNA–DNA junction. Although the linkage (rU)p(dG) occurs fairly frequently, the sequence at its 5′ side is random. A recent study (ref. 2, Hirose, Okazaki, and Tamanoy, in preparation) has shown that the RNA-linked DNA fragments isolated from growing *E. coli* cells accept ^{32}P from [γ-^{32}P]rATP in the polynucleotide kinase reaction after alkaline hydrolysis. The ^{32}P linked to the 5′ end of the DNA is recovered quantitatively in dCMP upon digestion with pancreatic DNase and venom phosphodiesterase. Moreover, almost the same number of 5′-OH ends of DNA are created by pancreatic RNase digestion as by alkaline hydrolysis. Therefore, most of the *in vivo* RNA–DNA fragments contain the linkage (rPy)p(dC). This remarkable agreement of the *in vitro* and *in vivo* results points to the possibility that ...p(rPy)p(rA)p(rU or rC)p(dC)p... is a universal sequence of the RNA–DNA junction of the *E. coli* fragments, which may reflect the nucleotide sequence on the template strands designating the termination of synthesis of the RNA segment (and/or the initiation of the DNA segment). The (rU)p(dG) linkage might have a similar significance as the (rPy)p(dC) linkage. However, we think it more likely that this linkage is an *in vitro* artifact, because the sequence in its 5′ side is random and because no dGMP is detected at the RNA–DNA linkage of the *in vivo* fragments.

Wickner *et al.* (11) and Scheckman *et al.* (12) have demonstrated the synthesis of covalently linked RNA–DNA molecules in *E. coli* extracts using M13 and ϕX DNA as template. The rNMP in the RNA–DNA linkage is largely AMP in the case of M13, whereas all four rNMPs are found in the linkage in the case of ϕX. Keller (13) has obtained similar results with ϕX using *E. coli* RNA polymerase and DNA polymerase II from KB cells. Covalently linked RNA–DNA molecules are also synthesized by RNA-dependent DNA polymerase. Flügel and Wells (14) found only (rU)p(dC) and (rA)p(dA) linkages in such molecules formed by avian myelobalastosis virus DNA polymerase. The relationship between these and the present findings is an interesting question to be clarified by future studies.

Synthesis of the RNA-linked DNA fragments in toluene-treated cells occurs in the absence of rNTP other than rATP. While this fact suggests enough endogenous supply of RNA precursors, a labeled rNTP is incorporated into the RNA–DNA molecules when it is added to the reaction mixture. Our results, to be detailed elsewhere, show that [γ-^{32}P]-rGTP is incorporated into the 5′ ends of the RNA-linked DNA fragments and recovered as radioactive ppp(rG)p after alkaline hydrolysis. This finding provides further support for the 5′-terminal location of the RNA segment and indicates that the RNA is formed not by a reaction primed by a preexisting chain, but by *de novo* synthesis. The specific labeling of the 5′ end of the RNA segment by [γ-^{32}P]dGTP would facilitate analysis of its structure and elucidation of the mechanism of its synthesis and degradation.

Our work with *E. coli*, work of Kornberg and coworkers (11, 12, 15) with M13 and ϕX, and work of Helinski's group with *Col*E$_1$ (16) provide strong evidence for primer functions of RNA in DNA replication. Other possible roles of RNA or RNA synthesis in DNA replication have been suggested by Lark (17) and by Dove *et al.* (18).

This work was supported by grants from the Ministry of Education of Japan, the Jane Coffin Childs Memorial Fund for Medical Research, and the Toray Science Foundation.

1. Sugino, A., Hirose, S. & Okazaki, R. (1972) *Proc. Nat. Acad. Sci. USA* **69**, 1863–1867.
2. Okazaki, R., Sugino, A., Hirose, S., Okazaki, T., Imae, Y., Kainuma-Kuroda, R., Ogawa, T., Arisawa, M. & Kurosawa, Y. (1973) in *DNA Synthesis In Vitro*, eds. Wells, R. D. & Inman, R. B. (University Park Press, Baltimore), in press.
3. Moses, R. E. & Richardson, C. C. (1970) *Proc. Nat. Acad. Sci. USA* **67**, 674–681.
4. Lehman, I. R., Bessman, M. J., Simms, E. S. & Kornberg, A. (1958) *J. Biol. Chem.* **233**, 163–170.
5. Okazaki, R. & Kornberg, A. (1964) *J. Biol. Chem.* **239**, 269–274.
6. Glynn, I. M. & Chappell, J. B. (1964) *Biochem. J.* **90**, 147–149.
7. Okazaki, R., Sugimoto, K., Okazaki, T., Imae, Y. & Sugino, A. (1970) *Nature* **228**, 223–226.
8. Sugino, A. & Okazaki, R. (1972) *J. Mol. Biol.* **64**, 61–85.
9. Okazaki, R., Arisawa, M. & Sugino, A. (1971) *Proc. Nat. Acad. Sci. USA* **68**, 2954–2957.
10. Van de Sande, J. H., Loewen, P. & Khorana, H. G. (1972) *Fed. Proc.* **31**, 426 Abstr.
11. Wickner, W., Brutlag, D., Schekman, R. & Kornberg, A. (1972) *Proc. Nat. Acad. Sci. USA* **69**, 965–969.
12. Schekman, R., Wickner, W., Westergaard, O., Brutlag, D., Geider, K., Bertsch, L. L. & Kornberg, A. (1972) *Proc. Nat. Acad. Sci. USA* **69**, 2691–2695.
13. Keller, W. (1972) *Proc. Nat. Acad. Sci. USA* **69**, 1560–1564.
14. Flügel, R. M. & Wells, R. D. (1972) *Virology* **48**, 394–401.
15. Brutlag, D., Schekman, R. & Kornberg, A. (1971) *Proc. Nat. Acad. Sci. USA* **68**, 2826–2829.
16. Blair, D. G., Sherratt, D. J., Clewell, D. B. & Helinski, D. R. (1972) *Proc. Nat. Acad. Sci. USA* **69**, 2518–2522.
17. Lark, K. G. (1972) *J. Mol. Biol.* **64**, 47–60.
18. Dove, W. F., Hargrove, E., Ohashi, M., Haugli, F. & Guha, A. (1969) *Japan. J. Genet.* **44**, suppl. 1:11–22.

Proc. Nat. Acad. Sci. USA
Vol. 70, No. 1, pp. 93–97, January 1973

Surface Circulation of Lakes and Nearly Land-Locked Seas

(marginal seas/wind drive/water movements)

K. O. EMERY AND G. T. CSANADY

Woods Hole Oceanographic Institution, Woods Hole, Massachusetts 02543

Contributed by K. O. Emery, October 30, 1972

ABSTRACT **The pattern of surface circulation has been mapped for more than 40 lakes, marginal seas, estuaries, and lagoons. All are within the northern hemisphere, and all except one are known to have a counterclockwise pattern. This consistent pattern is attributed to the drag of wind blowing across the bodies of water. Warmer surface water is displaced to the right-hand shore zone (facing downwind), where it produces greater surface turbulence and, thus, greater wind drag. This effect leads to counterclockwise water circulation regardless of the direction and, within limits, the duration of the wind.**

During studies of northern hemisphere lakes and water bodies marginal to the ocean, we have noted a consistent counterclockwise circulation of surface waters. "Circulation" is here defined to mean a long-term pattern of motion, or residual motion remaining after the irregular water movements involved in wind drift, seiches, and other short-term phenomena are averaged. The averaging period is taken to be long compared with the typical passage time of weather cycles. Experimentally, such long-term patterns of flow may be directly determined, e.g., by releasing batches of drift bottles and tracing their paths of long period drift.

Charts of this circulation pattern were assembled, and the cause of the pattern was examined in the expectation that it may be useful to other workers, particularly in connection with predictions of pollution down-current from points of sewage and industrial discharge into large bodies of water. Information about circulation patterns of lakes is very scarce in limnological journals, as these mainly are limited to strictly biological problems. Moreover, most studies of water movements in lakes are restricted to seiches, internal waves, and other movements in a vertical plane. Investigations of circulation in marginal seas and estuaries are more common than in lakes, possibly because of the natural landward extension of oceanographic methods. Many marginal seas are separated from the ocean by barriers caused by crustal deformation that allow little exchange of water. These are included in the discussion below. Estuaries and lagoons separated from the ocean by barriers produced by sand deposition, and marginal seas widely open to the ocean (Kara Sea, Chukchi Sea, Norwegian Sea, Bering Sea, and the North Sea) often have circulation patterns similar to those of lakes and the nearly land-locked seas, but they are omitted here because of possible control by currents from the open ocean.

Patterns

The charts of horizontal circulation in lakes and nearly land-locked bodies of ocean water are so thinly and widely scattered in physical and geological literature that we probably have missed some of the published examples. Most of the ones we found are illustrated in simplified form in Figs. 1 and 2. Examples of patterns from lakes of North America listed from north to south are: Lake Superior (1), Lake Huron (1–3), Lake Michigan (1, 4), Lake Ontario (1, 5), Lake Erie (1, 6), Great Salt Lake (7), and the Salton Sea (8, 9). Patterns also are available for the following lakes of Eurasia: Lake Constance–*Bodensee* (10, 11), Lake Neuchâtel (12), Lake Geneva–*Léman* (13), Aral Sea (14), Caspian Sea (A. F. Mikhalevskii in ref 15), Dead Sea (16); and Bitter Lake (17).

Circulation patterns for water bodies of North America that are nearly separated from the ocean or from large adjacent lakes by structural barriers have been published for: Baffin Bay (18, 19), Hudson Bay (20, 21), Gulf of St. Lawrence (22, 23), Passamaquoddy Bay (24), Grand Traverse Bay (25), Bay of Fundy (26, 27), Gulf of Maine (22), and Long Island Sound (28). In South America the circulation in Lake Maracaibo (29) has been mapped. Similar water bodies of Eurasia for which surface circulation are known are: the White Sea (V. Timonov in ref. 30), Baltic Sea (31), Black Sea (32), Adriatic Sea (33, 34), Japan Sea (ref. 35, Sizova in refs. 30 and 36), the Mediterranean Sea (37), and the Persian Gulf (38, 39).

These enclosed or nearly enclosed bodies of water span a range from 72° to 9° North latitude; unfortunately, no data of surface circulation were found for similar water bodies in the southern hemisphere. Where the methods by which the circulation was measured were reported, they consisted variously of drift bottles or drift cards, drogues, buoyed fishing nets, measurements with drift lines and current meters from anchored ships, tracing of increased salinity caused by excess evaporation, and computations from dynamic topography above prominent thermoclines. The short-term methods are significant only during average conditions. Some examples are based upon several methods.

The circulation patterns for all but one of the lakes and seas of Figs. 1 and 2 are generally counterclockwise. The pattern for the Aral Sea, however, is reported to have a clockwise circulation; whether this uniqueness is due to peculiarities of bottom topography or to perhaps erroneous interpretation of measurements is unknown, and it must remain an exception for the time being.

Cause of counterclockwise circulation: physical description

The general consistency in circulation patterns demands a general explanation. For estuaries and some small marginal seas the chief mechanism may be the inflow of light fresh water at the landward side and the outflow of mixed water at the mouth, where it is largely counterbalanced by inflow of denser ocean water. Similarly, the flow of light fresh water into lakes having no outlet (Salton Sea and Dead Sea) may be important. Such inflows of light water would produce a surface slope down which movement of water would be de-

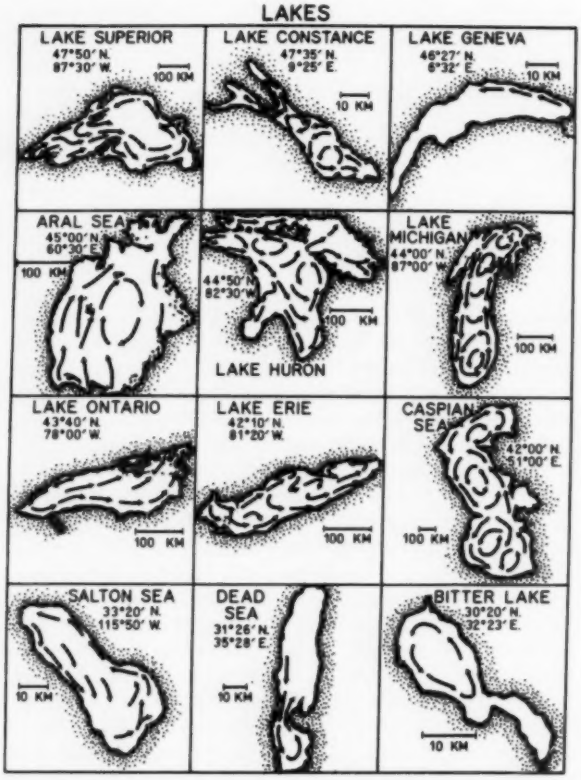

FIG. 1. Circulation patterns for lakes simplified from original illustrations cited in the text: Lake Superior, Lake Constance, Lake Geneva, Aral Sea, Lake Huron, Lake Michigan, Lake Ontario, Lake Erie, Caspian Sea, Salton Sea, Dead Sea, and Bitter Lake.

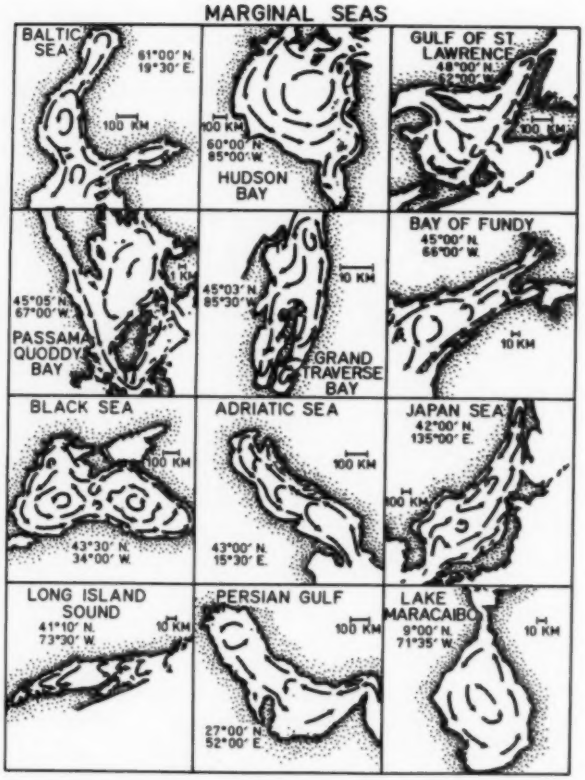

FIG. 2. Circulation patterns for nearly land-locked bodies of water separated from the open sea by structural barriers. Patterns are simplified from original illustrations cited in the text: Baltic Sea, Hudson Bay, Gulf of St. Lawrence, Passamaquoddy Bay, Grand Traverse Bay, Bay of Fundy, Black Sea, Adriatic Sea, Japan Sea, Long Island Sound, Persian Gulf, and Lake Maracaibo.

flected to the right (in the northern hemisphere) by the Coriolis force of earth rotation. In most examples, however, the water bodies are too large to be much affected by the relatively small inflow of light water. Likewise, a decrease in density of water above the shoal nearshore zone through solar heating could produce a slope that may give rise to a counterclockwise current, but this effect must be small; if it were important, the current would be counterclockwise only during the spring and early summer—before the development of a homogeneous surface layer—a restriction that seems not to be present. In some specific instances one would be inclined to attribute the observed circulation pattern to the topography of the basin, but in most examples such an argument also is unconvincing. The generality of the counterclockwise circulation in the northern hemisphere suggests that the cause is independent of basin shape and depth distribution, and within limits also of size. Therefore, it will be convenient to examine how a counterclockwise circulation pattern may be set up in a circular basin of constant depth, which represents a theoretical model sufficiently idealized to exclude irrelevancies.

It is well known that water movements in lakes and shallow seas are produced mainly by wind, that they are strongly influenced by the vertical stratification of the water column, and that in the larger bodies of water they are also affected by the rotation of the earth. In a circular basin, constant-depth model of a stratified lake, the motions produced by the irregularly occurring wind impulses may be elucidated in considerable detail analytically (40), by use of linearized equations of motion. These equations describe large bodies of water quite faithfully, and the qualitative features of the analytical solutions are in good agreement with observation. With a uniform wind blowing over the basin, "coastal jets" more or less along the direction of the wind are produced at both right-hand and left-hand shores, with Ekman drift occupying the central part of the basin.

One key property of wind-induced motions in a symmetrical basin is that the circulation pattern is also symmetrical, unless the wind stress distribution itself possesses significant asymmetry or "curl." If the basin is small compared to the dimensions of weather systems (this is true even for very large lakes), any such asymmetry, if present, must be produced by the basin itself, through some interaction with the air flow above. To explain an anticlockwise average circulation, we have to show why there should be a positive (cyclonic) curl in the wind stress, regardless of the direction in which the wind blows. In simple terms, we have to show why the wind should drag the water along more effectively on the right-

hand shore than on the left-hand one (in the northern hemisphere, and "right" and "left" if we look downwind).

As shown by Roll (41), the stress exerted by the wind on a water surface depends critically on the air–water temperature difference. The stability of the air layer in contact with a water surface colder by several degrees than the air some distance above may completely suppress turbulence and reduce wind stress to zero. In the Great Lakes it is common to observe a completely smooth band of cold water, while the warmer water a few hundred meters away is covered by capillary waves, a clearly visible sign of wind stress. Even when the contrast is not quite so extreme, the wind stress magnitude is significantly affected by surface temperature changes of the order of 1°, or even 0.5°. This effect is further discussed quantitatively below.

It is also clear that in the presence of net surface heating a horizontal temperature gradient tends to become established, positive in the direction of surface drift. In sufficiently large basins (in practice, larger than a few km in size) and in the northern hemisphere the surface drift has a large component to the right of the wind ("Ekman drift"). Therefore, in the presence of net surface heating the water becomes warmer on the right-hand shore and is, in fact, dragged along more effectively by the wind. Aerial temperature surveys of the Great Lakes, for example, show clear evidence of this warming trend across wind, the temperature contrast being of the order of 1–2°. Fig. 3 illustrates this point. A much more pronounced temperature difference occurs between left- and right-hand shores when the wind stress is strong enough and acts long enough to produce upwelling of cold water. The upwelling occurs on the left-hand shore in the northern hemisphere, and it is under such circumstances that absence of wind stress may be observed over the upwelled water, while the warmer water not too far away is clearly acted upon by the wind. The exact dynamical effects on a stratified lake of such an asymmetrical distribution of wind stress are complicated, but they undoubtedly include a tendency to produce counterclockwise circulation of the wind-driven surface waters.

At least in temperate latitudes the winds are variable: as weather systems pass over a lake or marginal sea, wind-stress impulses are exerted on the water surface that change irregularly both in magnitude and direction. As a result, currents observable at any fixed point in such a lake or sea are highly variable. Near shore, for example, they alternate irregularly between the two shore-parallel directions. According to the above argument, however, the currents are somewhat stronger when they leave the shore to the right than in the opposite case. When the flow is averaged over a longer period, most of the irregular motion is cancelled out, but not the portion directly due to wind-stress curl; this portion is of the same sense regardless of wind direction or velocity and it should add up to a significant component of the mean flow pattern.

In concluding this section, it may be useful to point out two nonexplanations of counterclockwise circulation. One is the well-known property of certain long waves to progress in a counterclockwise direction along the periphery of a sufficiently large basin. Thus, the phase of the seiches or "wind tides" of Lake Erie progresses counterclockwise (42), as do tides in the Gulf of St. Lawrence (43) or long internal Kelvin waves in Lake Michigan (44). However, particle orbits associated with such wavelike motions are closed in a first approximation, i.e., there is no net drift in the direction of phase propagation. A second-order drift akin to Stokes drift in surface waves is possible (45), but such an effect has not yet been shown to be quantitatively significant in the above types of waves.

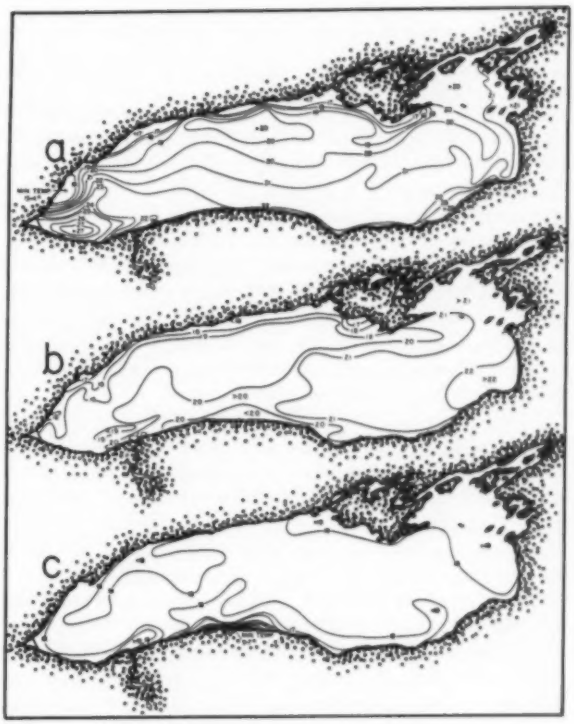

FIG. 3. Observed surface temperature patterns of Lake Ontario from aerial infrared radiation surveys. Before surveys (*a*) and (*b*), the winds were generally westerly; before survey (*c*), they were easterly. Larger temperature contrast in (*a*) is typical of summer conditions, while that of (*b*) is typical of early autumn. Redrawn from illustrations by Irbe (48).

A second plausible explanation that does not work is that nonlinear momentum transport by the mean motion fortifies the right-hand shore "coastal jet." This momentum transport is in fact to the right on both shores, i.e., shoreward on the right and offshore on the left. However, its net effect is to displace the left-hand jet somewhat offshore and to stabilize the right-hand jet against the shore, without interfering very significantly with the overall flow pattern.

Possibly other nonlinear or more complicated effects also contribute to the maintenance of anticlockwise mean circulation in enclosed bodies of water, but we have not been able to identify any that were quantitatively significant. By contrast, the surface heating–Ekman drift coupling of air and water should be able to maintain a significant circulation amplitude, as shown by the calculations below.

Quantitative considerations

To calculate the "typical" magnitude of the cross-wind temperature gradient, we assume that the wind has blown long enough from a constant direction to establish equilibrium between surface heating and advective heat transport in the

water, i.e.

$$\frac{\partial \theta}{\partial y} = \frac{H}{c_p \rho V} \qquad [1]$$

where θ is temperature (°C), H is net heat absorption by the water in cal cm^{-2} sec^{-1}, c_p and ρ are the specific heat and density of water, y is the direction perpendicular to the wind, and V is Ekman transport to the right of the wind (cm^2 sec^{-1}). A typical magnitude of the net heat flux is $2 \cdot 10^{-3}$ cal cm^{-2} sec^{-1} (about 180 cal cm^{-2} day^{-1}), while the Ekman drift in a 6 m/sec wind ("10 meter level wind") at mid-latitudes is close to 10^4 cm^2 sec^{-1}. These data yield a temperature gradient $\partial\theta/\partial y$ of $2 \cdot 10^{-7}$ °C cm^{-1}, or 2° per 100 km. Actual observed temperature gradients in the central part of Lake Ontario, during the heating season for example, (see Fig. 3*a*), are of a similar magnitude to several times greater.

In the absence of surface heating, temperature contrasts in a cross-wind direction are also observed, although they tend to be somewhat smaller; in Lake Ontario, these effects are of the order of 1° across the 70-km wide lake. An examination of successive surveys suggests that these temperature differences are caused by intermittent upwelling of cold water on the left-hand shore, followed by some horizontal mixing.

The wind-stress differences corresponding to temperature contrasts of the above order of magnitude may be estimated on a theoretical basis by the use of geostrophic drag coefficients presented in (46). These drag coefficients are functions of two nondimensional parameters, the surface Rossby number and the Lettau number

$$Ro = \frac{U_g}{f z_0}$$
$$Le = \frac{\Delta T\, g}{T f^2 z_0} \qquad [2]$$

where U_g is geostrophic wind speed, f is the Coriolis parameter, z_0 the roughness length of the surface, ΔT the temperature difference between air at geostrophic level and surface below, T the absolute air temperature, and g is the acceleration of gravity. As a typical roughness length, we take $z_0 = 0.1$ cm. Assuming also $U_g = 10$ m sec^{-1}, $f = 10^{-4}$ sec^{-1}, we calculate $Ro = 10^8$. Suppose that the air–water temperature difference on the right-hand shore is exactly zero, while on the left-hand shore the water surface is 1° cooler than the air—then $Le = 0$ on the right, $Le = 10^9$ on the left. The corresponding drag coefficients and surfaces stresses are

Right $c_d = 0.55 \cdot 10^{-3}$

$\tau_0 = c_d \rho_a U_g^2 = 0.7$ dyne cm^{-2}

Left $c_d = 0.15 \cdot 10^{-3}$

$\tau_0 = 0.2$ dyne cm^{-2}

The theoretically predicted wind stress is thus 3.5 times greater on the right than on the left, a very significant variation indeed, considering the smallness of the temperature contrast. Direct experimental evidence to support these rather surprising results does not seem to be available, but even if these figures are overestimates, they suggest that substantial wind-stress curl due to surface temperature contrasts is, in fact, a likely possibility.

Linear theory (47) shows that the circulation set up by a nonuniform wind stress is proportional to the time-integral of the wind-stress curl, i.e., to

$$W = \int \frac{\partial}{\partial y} \left| \frac{\tau_0}{\rho} \right| dt \qquad [3]$$

Suppose that the above wind-stress curl was acting for a period of $t = 8$ hr, over a circular basin of 50 km in diameter, i.e.,

$$\frac{\partial}{\partial y}\left(\frac{\tau_0}{\rho}\right) = \frac{\Delta(\tau_0/\rho)}{50\,\text{km}} = 10^{-7}\text{cm sec}^{-2}$$
$$W = 8 \cdot 3600 \cdot 10^{-7} = 2 \cdot 88 \cdot 10^{-3}\ \text{cm sec}$$

where we have assumed a linear change in stress across the basin. The circulation produced by this wind stress curl is characterized by a tangential velocity at the shores of

$$v_t = \frac{Wr}{2h} \qquad [4]$$

where r is the basin radius and h is the mixed-layer depth. For $r = 25$ km and taking $h = 10$ m, we find

$$v_t = 3.6 \text{ cm/sec}$$
$$\equiv 3.1 \text{ km/day}$$

Note that v_t is proportional to Wr, so that it does not directly depend on radius, given a certain temperature contrast, and with it $\Delta(\tau_0/\rho)$ across the basin, W containing the gradient $\Delta(\tau_0/\rho)/2r$. Similar tangential velocities v_t can, therefore, develop in smaller or larger basins, as long as the temperature contrast remains significant.

Concluding remarks

To sum up briefly, we have presented a possible physical mechanism to explain the observed universal tendency toward counterclockwise circulation in northern hemisphere lakes and marginal seas. The salient parts of our argument are: (*i*) there is usually a temperature contrast between the right- and left-hand shore, (looking downwind), the former being warmer; (*ii*) the observed temperature differences are sufficient to produce cyclonic wind-stress curl of appreciable magnitude, which sets up the counterclockwise circulation. Climatic conditions allowing these physical factors to operate prevail from early spring to late fall. In midwinter, the circulation pattern should be different. In some lakes and other water bodies, this appears to be true, but the evidence is scant as most observations of circulation are made during the warmer seasons. The rotation of the earth is involved in the establishment of the temperature contrast across wind, either through Ekman drift to the right, or the production of an upwelling on the left. In the southern hemisphere the opposite circulation should be observable. Unfortunately, as we remarked before, evidence on this point is insufficient to confirm our reasoning.

We thank the Office of Naval Research, which supported this work under Contract N00014-66-C0241. This is Contribution 2965 of the Woods Hole Oceanographic Institution.

1. Harrington, M. W. (1895) *Surface Currents of the Great Lakes as Deduced from the Movements of Bottle Papers During the Seasons of 1892, 1893, and 1894* (U.S. Dept. of Agriculture, Washington, D.C., Weather Bureau, Bull. B), 16p.
2. Ayers, J. C. (1956) "A dynamic height method for the determination of currents in deep lakes," *Limnol. Oceanogr.* 1, 150–161.

3. Ayers, J. C., Anderson, D. V., Chandler, D. C. & Lauff, G. H. (1956) "Currents and water masses of Lake Huron (1954 synoptic surveys)," *Great Lakes Res. Div. Univ. Mich.* Publ. **1**, 101p.
4. Ayers, J. C., Chandler, D. C., Lauff, G. H. Lauff & Powers, C. F. (1958) "Currents and water masses of Lake Michigan," *Great Lakes Res. Div. Univ. Mich. Publ.* **3**, 168p.
5. Bruce, J. P. (1960) "Great Lakes Research," *Great Lakes Res. Div. Univ. Mich. Publ.* **4**, 3–8.
6. Ayers, J. C. (1960) "Status and programs," *Great Lakes Res. Div. Univ. Mich. Publ.* **4**, 61–74.
7. Greer, D. C. (1971) *A map of Great Salt Lake, Utah, scale 1:125,000* (Assoc. Amer. Geographers, Washington D.C.).
8. Arnal, R. E. (1961) "Limnology, sedimentation, and microorganisms of the Salton Sea, California," *Geol. Soc. Amer. Bull.* **72**, 427–478.
9. Office of Technology Utilization (1967) "*Earth Photographs from Gemini III, IV, and V*, (National Aeronautics and Space Administration, SP-129, Washington, D.C., Supt. of Docs., U.S. Govt. Printing Office), 266p.
10. Wasmund, E. (1928) "Die Strömungen im Bodensee, verglichen mit bisher in Binnenseen bekannten Strömen," *Int. Rev. Gesamten Hydrobiol.* **19**, 21–155.
11. Auerbach, M. & Ritzi, M. (1937) "Oberflächen und Tiefenströme des Bodensees, IV," *Arch. Hydrobiol.* **32**, 409–433.
12. Quartier, A. A. (1959) "Étude preliminaire des courants du lac de Neuchatel," *Schweiz. Z. Hydrol.* **21**, 7–18.
13. Mercanton, P.-L. (1932) "Étude de la circulation du lac Léman," *Mem. Soc. Vaudoise Sci. Natur.* **4**, 225–271.
14. Brodskaya, N. G. (1954) "Osadkoobrazovanie v ozerax zaschshlivoi zoni SSR. Aralskoe ozero-more (Sediment formation in lakes of the arid zones of the USSR Urals. The Aral Lake-Sea)," in *Obrazovanie osadkov v sovremennich bodoemax* (*Formation of Sediments in Present Day Waters*), ed. Bezrukov, P. L. (Izdat. Akad. Nauk SSSR, Moscow), pp. 237–282.
15. Batyrin, V. P. & Kopilova, I. K. (1956) "Geologichsekii ocherk yuzhnoi i srednei chastei kaspiiskogo morya (Geological sketch of the southern and central parts of the Caspian Sea)," in *Sovremennie osadki Kaspiiskogo morya* (*Recent Sediments of the Caspian Sea*), ed. Teodorovich, G. I. (Izdat. Akad. Nauk SSSR, Moscow), pp. 272–302.
16. Neev, David, & Emery (1967) "The Dead Sea: Depositional processes and environments of evaporites," *Geol. Survey of Israel, Bull.* **41**, 147p.
17. Miller, A. R. & Munns, R. G. (1973) "The Bitter Lake salt barrier," *IAPSO Symposium on the "Physical Oceanography of the Red Sea,"* Sponsored by SCOR and UNESCO, Paris, 9–10 October 1972.
18. Collin, A. E. & Dunbar, M. J. (1964) "Physical oceanography in Arctic Canada," ed. Barnes, H. in *Oceanography and Marine Biology Annu. Rev.*, **2**, 45–95.
19. Marlowe, J. I. (1968) "Unconsolidated marine sediments in Baffin Bay," *J. Sediment Petrology* **38**, 1065–1078.
20. Hachey, H. B. (1935) "The circulation of Hudson Bay waters as indicated by drift bottles," *Science* **82**, 275–276.
21. Leslie, R. J. (1963) "Sedimentology of Hudson Bay, District of Keewatin," *Bedford Inst. of Oceanogr. Rept.* **63-4**, 20p.
22. Bumpus, D. F. & Lauzier, L. M. (1965) "Surface circulation on the continental shelf off eastern North America between Newfoundland and Florida," *Serial Atlas of the Marine Environment, Amer. Geogr. Soc.*, Folio 7, 8 plates.
23. Blackford, B. L. (1965) "Some oceanographic observations in the southeastern Gulf of St. Lawrence—summer 1964," *Canada Fisheries Res. Board Rept. Ser.* (*Oceanog. & Limnolog.*) **190**, 22p.
24. Chevrier, J. R. (1959) "Drift bottle experiments in the Quoddy region," in *International Passamaquoddy Fisheries Board, Report to International Joint Commission* (Ottawa, Ontario and Washington, D.C.), chapt. 2, 13p.
25. Lauff, G. H. (1957) "Some aspects of the physical limnology of Grand Traverse Bay," *Great Lakes Res. Div. Univ. Mich. Publ.* **2**, 56p.
26. Godin, G. (1968) "The 1965 current survey of the Bay of Fundy—A new analysis, etc.," *Can. Dep. Energy, Mines Resour. Marine Sci. Br. ms. Rept.* **8**, 97p.
27. Swift, D. J. P., Pelletier, B. R., Lyall, A. K. & Miller, J. A. (1969) "Sediments of the Bay of Fundy—A preliminary report," *Maritime Sed.*, **5**, 95–100.
28. Riley, G. A. (1952) "Hydrography of the Long Island and Block Island sounds," *Bull. Bingham Coll. Yale Univ.* **13**, 5–39.
29. Redfield, A. C. (1958) "Preludes to the entrapment of organic matter in the sediments of Lake Maracaibo," in *Habitat of Oil*, ed. Weeks, L. G. (Amer. Ass. Petroleum Geologists, Tulsa, Oklahoma) pp. 968–981.
30. Zenkevitch, L. (1963) in *Biology of the Seas of the U.S.S.R.* (Interscience, New York), 955p., (translation).
31. Palmén, E. (1930) "Untersuchungen uber die Strömungen in den Finnland umgebenden Meeren," *Soc. Sci. Fenn. Commentat. Phys. Math.* **12**, 45–94.
32. Neumann, G. (1942) "Die absolute topographie des physikalischen Meeresnivaeaus und die Oberflächenströmungen des Schwarzen Meeres," *Ann. Hydr. Marit. Meteorol.* **70**, no. 9, 265–282.
33. Chierici, A., Busi, T. & Cita, B. (1962) "Contribution à une étude écologique des foraminiferes dans la mer Adriatique," *Rev. Micropaléont.* **5**, 123–142.
34. van Straaten, L. M. J. U. (1965) "Sedimentation in the north-western part of the Adriatic Sea," in Submarine Geology and Geophysics, eds. Whittard, W. F. & Bradshaw, R. (17th Symposium Colston Res. Soc., Univ. Bristol, England; Butterworths, London), pp. 143–173.
35. Hata, Katsumi (1965) "Seasonal variation of the volume transport in the northern part of the Japan Sea," *J. Oceanogr. Soc. Jap.* **20th Anniv. Vol.**, 168–179.
36. Yasui, M., Yasuoka, T., Tanioka, K. & Shiota, O. (1967) "Oceanographic studies of the Japan Sea, (1) Water characteristics," *Oceanogr. Mag.* **19**, 177–192.
37. Nielsen, J. J. (1912) "Hydrography of the Mediterranean and adjacent waters," *Danish Oceanogr. Exped. 1908–1910, Rept.* **1**, 77–191.
38. Emery, K. O. (1956) "Sediments and water of the Persian Gulf," *Bull. Amer. Ass. Petrol. Geol.* **40**, 2354–2383.
39. Peery, K. (1965) *Results of the Persian Gulf—Arabian Sea oceanographic surveys 1960–61* (U.S. Naval Oceanogr. Office, Washington, D.C., Tech. Rept. 176), 239p.
40. Csanady, G. T. (1972a) "Response of Large Stratified Lakes to Winds," *J. Phys. Oceanogr.* **2**, 3–13.
41. Roll, H. U. (1965) *Physics of the Marine Atmosphere* (Academic Press, New York), 426p.
42. Platzman, G. W. (1963) "The Dynamic Prediction of Wind Tides on Lake Erie," *Met. Monogr. 4, No. 26*, 44 pp.
43. El-Sabh, M. I., Forrester, W. D. & Johannessen, O. M. (1969) "Bibliography and some aspects of physical oceanography in the Gulf of St. Lawrence," *Marine Sciences Centre Manuscript Report No. 14*, McGill University.
44. Mortimer, C. H. (1965) "Spectra of Long Surface Waves and Tides in Lake Michigan and at Green Bay, Wisconsin," *Proc. 8th Conf. Great Lakes Res., pub. No. 13* (Great Lakes Res. Div., Univ. of Michigan), pp. 304–325.
45. Longuet-Higgins, M. S. (1969) "On the transport of mass by time-varying ocean currents," *Deep Sea Res.* **16**, 431–447.
46. Csanady, G. T. (1972b) "Geostrophic Drag, Heat, and Mass Transfer Coefficients for the Diabatic Ekman Layer," *J. Atmos. Sci.* **29**, 488–496.
47. Csanady, G. T. (1968) "Wind-driven Summer Circulation in the Great Lakes," *J. Geophys. Res.* **73**, 2579–2589.
48. Irbe, J. G. (1972) "Aerial Surveys of Great Lakes Water Temperatures, April 1968 to March 1970," *Climatological Studies No. 19* (Dept. Environment, Canada), 57p.

Proc. Nat. Acad. Sci. USA
Vol. 70, No. 1, pp. 98–102, January 1973

Stimulation of Mitochondrial Adenosine Diphosphate Uptake by Thyroid Hormones

(mitochondrial O_2 uptake/mitochondrial respiratory control/atractyloside/2,4-dinitrophenol)

BERNARD M. BABIOR*†, SUSAN CREAGAN‡, SIDNEY H. INGBAR§, AND RUBY S. KIPNES†

Thorndike Memorial Laboratory, Harvard Medical Unit, Boston City Hospital, and the Department of Medicine, Harvard Medical School, Boston, Massachusetts 02118

Communicated by Konrad Bloch, November 3, 1972

ABSTRACT **Thyroid hormone administered *in vivo* increased carrier-mediated (atractyloside-sensitive) ADP uptake by rat liver mitochondria. 3 Days after a single large dose of triiodothyronine (20 μg/100 g of body weight), mitochondrial uptake of ADP measured at 6° was 2.35 ± 0.17 nmol/min per mg of protein, compared with an uptake of 1.81 ± 0.19 nmol/min per mg of protein in mitochondria from untreated rats ($P < 0.025$). Cyanide (1.33 mM) had no effect on ADP uptake by mitochondria from either untreated or triiodothyronine-treated animals. Uptake of ADP by mitochondria from thyroidectomized rats treated with thyroxine for 7 days was 2.89 ± 0.40 nmol/min per mg in mitochondria from thyrotoxic rats (20 μg of thyroxine per 100 g per day) and 1.98 ± 0.22 nmol/min per mg in mitochondria from euthyroid rats (2 μg of thyroxine per 100 g per day) ($P < 0.025$). Mitochondria from both untreated and thyroid hormone-treated rats displayed a highly significant linear correlation between ADP uptake and ADP-dependent (i.e., state 3 minus state 4) oxygen consumption. There was, however, no difference in respiratory control ratios between mitochondria from euthyroid and thyrotoxic animals. Administration of dinitrophenol (2 mg/100 g) also stimulated carrier-mediated ADP uptake, but respiratory control of mitochondria from dinitrophenol-treated animals was virtually abolished. Triiodothyronine *in vitro*, at concentrations of 100 and 0.1 nM, appeared to inhibit rather than stimulate the uptake of mitochondrial ADP. The relationship between these observations and the clinical manifestations of thyrotoxicosis is discussed from the point of view of the possible effects of increased mitochondrial ADP transport on oxidative phosphorylation and adenosyl nucleotide metabolism.**

It has long been known that an increase in metabolic rate follows administration of a sufficient dose of thyroid hormone. Animals treated with large doses of thyroxine manifest an increased rate of oxygen consumption, a rise in body temperature, and a loss in weight, all consequent to an increase in the rate of oxidation of substrate (1, 2). Since most substrate oxidation takes place in mitochondria, many studies on the mechanism of action of thyroid hormone have involved these organelles. These studies have shown, for example, that thyroid hormone increases the rate of mitochondrial oxidation of succinate, glutamate, β-hydroxybutyrate, and isocitrate (3); the activity of the electron transport chain is increased without an increase in the concentrations of the chain components (4); and there is an increase in the activity of membrane-bound α-glycerophosphate dehydrogenase (5). In addition, thyroid hormone affects mitochondrial swelling (6, 7) and respiratory control (8), but these effects are only observed with rather large doses of hormone.

The mitochondrion is composed of an outer membrane, an inner membrane, and two spaces: the intermembrane space, which lies between the membranes, and the matrix, which is enclosed within the inner membrane. The matrix contains the substrates necessary for oxidative phosphorylation, a process that takes place on the inner surface of the inner membrane (9). It has recently been shown that the transport of ADP, one of the substrates of oxidative phosphorylation into the matrix, is a carrier-mediated process in which an ADP molecule is conveyed into the matrix in exchange for an ATP molecule, which is then transported out of the mitochondrion (10, 11). Since there is evidence that under physiological conditions, the rates of both substrate oxidation and oxidative phosphorylation are limited by the availability of ADP (12–14), we thought it of interest to investigate whether thyroid hormone might increase the availability of ADP through an effect on the carrier-mediated transport.

MATERIALS AND METHODS

Male and female CD rats weighing 250–400 g were obtained from the Charles River Breeding Laboratories. In some cases rats underwent surgical thyroidectomy before delivery. Where normal rats were used, the control and treated groups each contained about the same proportion of animals of a given sex. Thyroidectomized rats were all males.

Thyroxine and triiodothyronine were obtained from Sigma Chemical Co. Each was dissolved in a minimum volume of 0.1 M NaOH and added through a Millipore Sterilizing Apparatus® to sterile 0.9% saline (triiodothyronine) or to a sterile solution of 1 part 10% bovine-serum albumin to 4 parts 0.9% saline (thyroxine). For the experiments with triiodothyronine, a comparable volume of 0.1 M NaOH was added to saline for injection into control animals. Potassium atractyloside, succinic acid, ethylene glycol-*bis* (β-aminoethyl ether) *N,N'*-tetraacetic acid (EGTA), and ADP were also obtained from Sigma. [^{14}C]ADP was purchased from New England Nuclear Corp. Other reagents were the best quality available com-

* To whom to address correspondence.

† Present address: New England Medical Center Hospital, 171 Harrison Ave., Boston, Mass. 02111.

‡ Present address: Duke Medical Center, Box 2731, Durham, N.C. 27710.

§ Present address: Veterans Administration Hospital, 4150 Clement St., San Francisco, Calif. 94121.

mercially, and were used without further purification. Water was distilled, deionized, redistilled from glass, and stored in polyethylene containers.

Mitochondria. Rats were killed by a single blow on the head. The livers were quickly removed and washed in 0.25 M sucrose containing 1.0 mM Tris·HCl (pH 7.9 at 23°) and 0.25 mM EGTA. The livers were squeezed through an aluminum-plated garlic press, and the resulting pulp was homogenized together with 5 volumes of sucrose–Tris–EGTA solution, at slow speed in a Potter–Elvehjem glass homogenizer with a loose-fitting Teflon pestle. The homogenate was centrifuged twice for 10 min at 1000 × *g* to remove the debris. The supernatant was then centrifuged at 6000 × *g* for 10 min. The resulting pellet was washed once in the sucrose–Tris–EGTA solution and then once in sucrose–Tris without EGTA. The pellet was centrifuged at 6000 × *g* for 10 min after each wash. The final pellet was suspended in about 2 ml of sucrose–Tris. Care was taken to keep the mitochondria, solutions, and instruments ice-cold at all times.

Mitochondrial Oxygen Uptake and Respiratory Control were determined by the method of Estabrook (15), with succinate as substrate. Measurements of oxygen uptake were made with either a model 53 oxygen electrode or a model 55 oxygen electrode (both manufactured by Yellow Spring Instruments). Except in experiments with dinitrophenol, mitochondria with respiratory control ratios of < 2 were discarded.

Mitochondrial ADP Uptake. Carrier-mediated mitochondrial ADP uptake was determined by a modification of the filtration method described by Winkler *et al.* (16). Mitochondria were diluted to a concentration of 30 mg of protein per ml of sucrose–Tris (assayed by the biuret method, with bovine-serum albumin as standard). The assay was begun by addition of 20 μl of mitochondria to 180 μl of a solution containing 0.2 μmol (0.1 μCi) of [^{14}C]ADP, 13 μmol of K_2HPO_4, 3 μmol of KH_2PO_4, 58 μmol of KCl, and 30 μmol of NaCl per ml. After 10 sec, ADP uptake was arrested by the rapid addition of 100 μl of 0.2 mM potassium atractyloside, a powerful specific competitive inhibitor of mitochondrial ADP–ATP exchange [K_i = 20 nM (11)]. Immediately, 100 μl of the reaction mixture was drawn into a microliter syringe and injected into the center of a Millipore paper filter (0.65-μm pore size, 2.5-cm diameter), which was held in a filtration apparatus under reduced pressure. The mitochondria were quickly washed with 10 ml of 0.15 M NaCl solution. The entire operation was conducted in a cold room at 6°. From beginning to end, the procedure took less than 25 sec.

The filter was removed from the apparatus, placed in a liquid scintillation vial containing 15 ml of Bray's solution, and allowed to stand overnight to permit the filter to dissolve. After vigorous shaking to disrupt the mitochondrial precipitate, the sample was counted in a Mark I liquid scintillation counter (Nuclear Chicago). Counting efficiency was determined by internal standardization with [^{14}C]toluene of known specific activity.

Nonspecific ADP uptake was determined similarly, except that mitochondria were added after the addition of atractyloside. For a given set of mitochondria, total ADP uptake was determined in duplicate, and nonspecific uptake was determined once. Carrier-mediated ADP transport was calculated by subtraction of the value of nonspecific ADP uptake from the average of the values for total ADP uptake. Nonspecific uptake generally represented less than 20% of the total uptake.

TABLE 1. *Uptake of ADP by mitochondria from triiodothyronine-treated animals*

Interval between injection and death	ADP uptake (nmol/min per mg of protein)		Significance of difference (P value)
	Thyrotoxic	Control	
20 hr	1.94 ± 0.23 (13)	1.55 ± 0.19 (15)	<0.1
3 days	2.35 ± 0.17 (12)	1.81 ± 0.19 (11)	<0.025

Experiments were performed as described in the text. Numbers in parentheses represents the number of animals used in each experiment.

Statistical Analyses. Statistical significances were determined by Student's *t*-test. Regression lines were calculated by the method of least squares. Data are expressed as means ± 1 standard error.

RESULTS

Initial experiments were performed with two groups of normal rats. Animals from each group were treated either with a large dose of triiodothyronine (20 μg/100 g) or with an equivalent volume of NaOH–saline, administered as a single intraperitoneal injection. Animals from one group were killed 20 hr after injection, while animals from the other group were killed 3 days after treatment with triiodothyronine. Liver mitochondria were prepared as previously described and tested for oxygen consumption with succinate as the oxidizable substrate, as well as for carrier-mediated ADP uptake.

Results of the determinations of mitochondrial ADP uptake are shown in Table 1. Significant differences in ADP uptake between the two groups of animals were observed. In mitochondria from rats killed 20 hr after injection, atractyloside-sensitive ADP uptake was 25% greater in mitochondria from triiodothyronine-treated animals than in those from control animals ($P < 0.1$). At 3 days, the time at which effects on basal metabolic rate are greatest (17), the difference between the two groups was 30% and was now statistically significant ($P < 0.025$). It thus appears that treatment with triiodothyronine increased carrier-mediated ADP uptake by rat-liver mitochondria.

Oxygen uptake by mitochondria from triiodothyronine-treated animals was also increased when compared with values in controls. Moreover, there was a close correlation between ADP-dependent (state 3 minus state 4) oxygen uptake and carrier-mediated ADP transport into the mitochondrial matrix (Fig. 1), a finding consistent with the previously reported dependence of mitochondrial substrate oxidation on availability of ADP (12–14). Nevertheless, the respiratory control ratios of the two groups were the same (2.95 ± 0.17 and 2.83 ± 0.14). Thus, at the dose given, triiodothyronine increased both carrier-mediated ADP uptake and ADP-dependent respiration in rat-liver mitochondria, but did not appear to affect respiratory control.

Similar results were obtained with rats treated with thyroxine. For these experiments, thyroidectomized rats were used.

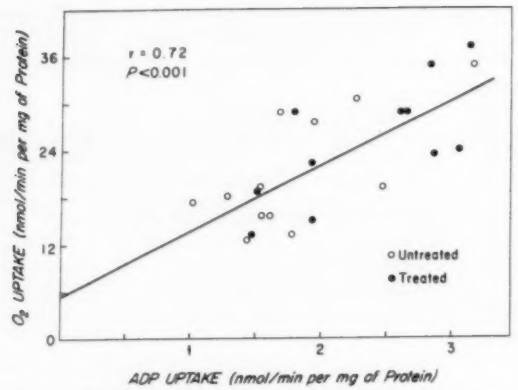

FIG. 1. Correlation between ADP-dependent oxygen consumption and ADP uptake by mitochondria from normal and triiodothyronine-treated animals. The values shown represent those of the thyrotoxic and control rats that were killed 3 days after injection (see Table 1). Oxygen consumption was measured at 34°. ADP-dependent oxygen consumption was calculated by subtraction of the state 4 from the state 3 respiratory rate. The line was fitted by least-squares regression analysis. The parameters for the regression line are: slope, 8.6 ± 1.8; intercept, 5.2 ± 3.8.

2 Weeks after thyroidectomy, the animals were divided into two groups. One group received seven daily intraperitoneal injections of 2 μg of thyroxine/100 g of body weight (10 μg/ml in 2% bovine-serum albumin), a quantity sufficient to restore the animals to euthyroid status; the other group received a similar number of injections of thyroxine (100 μg/ml in 2% bovine-serum albumin), but at the 10-fold greater dose of 20 μg/100 g. 24 hr after the final injection, the animals were killed, liver mitochondria were prepared, and determinations of oxygen consumption and ADP uptake were performed as described above. Uptake of ADP in mitochondria from rats made thyrotoxic with thyroxine was 34% greater ($P < 0.025$) than in mitochondria of euthyroid animals (Table 2). A significant correlation between ADP-dependent oxygen uptake and carrier-mediated ADP transport was also observed (Fig. 2). Finally, despite the differences between the two groups of thyroxine-treated animals with respect to mitochondrial ADP uptake and oxygen consumption, respiratory control of euthyroid mitochondria (2.84 ± 0.23) was almost identical with that of thyrotoxic mitochondria (2.79 ± 0.20). Thus, the findings obtained with the thyroxine-treated animals accord in all respects with those obtained with the triiodothyronine-treated animals. Moreover, regression equations for the relation between ADP uptake and ADP-dependent oxygen uptake in the two groups of experiments were very similar (Figs. 1 and 2). The slightly greater slope seen in experiments with triiodothyronine may reflect the slightly higher temperature (34°) at which oxygen uptake was measured with triiodothyronine, compared to thyroxine (30°).

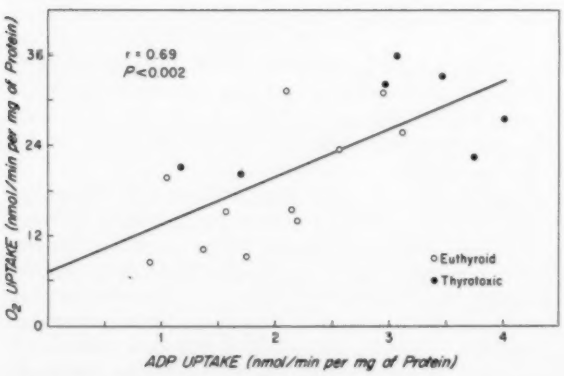

FIG. 2. Correlation between ADP-dependent oxygen consumption and ADP uptake by mitochondria from euthyroid and thyrotoxic thyroxine-treated animals. Oxygen consumption was measured at 30°. ADP-dependent oxygen consumption was calculated by subtraction of the state 4 from the state 3 respiratory rate. The line was fitted by least-squares regression analysis. The parameters for the regression line are: slope, 6.2 ± 1.7; intercept, 7.5 ± 4.1.

TABLE 2. *Uptake of ADP by mitochondria from thyroidectomized, thyroxine-treated animals*

Dose of thyroxine (μg/100 g)	ADP uptake (nmol/min per mg of protein)
2	1.98 ± 0.22 (11)
20	2.89 ± 0.40 (7)

Numbers in parentheses represent the number of animals used in each experiment. The difference between the two groups is significant at the level of $P < 0.025$.

Although uptake experiments were performed in the absence of oxidizable substrate, it could be argued that the differences in the rates of uptake of ADP by mitochondria from euthyroid and hyperthyroid animals were a consequence of differences in the rates of oxidation of endogenous substrates by the two groups of mitochondria. Evidence against this possibility was provided by the observation that cyanide had no effect on ADP uptake by mitochondria from either untreated or triiodothyronine-treated animals. The ratios of mitochondrial ADP uptake rates in the absence and presence of cyanide (1.33 mM KCN) were 1.00 ± 0.08 and 0.99 ± 0.06 for mitochondria from untreated rats (5 animals) and triiodothyronine-treated rats (4 animals), respectively.

Experiments were also performed to determine whether triiodothyronine *in vitro* has a direct effect on mitochondrial ADP uptake. ADP uptake was determined in mitochondria from the livers of normal rats in the absence and presence of triiodothyronine. ADP uptake was measured both before and after incubation of the mitochondria with triiodothyronine. For these experiments a total of five animals was used. Mitochondria prepared by the usual technique were diluted to a concentration of 30 mg of protein per ml of sucrose–Tris to which sufficient triiodothyronine had been added to bring the final concentration to that indicated in Table 3. A portion of these mitochondria was assayed immediately, while another portion was assayed after incubation for 60 min at 23°. In all instances, triiodothyronine was present in the ADP-uptake assay mixture at the concentration shown in Table 3. To avoid adsorption of triiodothyronine to the walls of the vessel, all operations subsequent to the preparation of the mitochondria were performed in polyethylene tubes. No increase in mitochondrial ADP uptake was produced by exposure of mitochondria to triiodothyronine either before or during the

period of ADP accumulation (Table 3). Rather, mitochondrial uptake of ADP was decreased significantly in the presence of triiodothyronine.

The increase in basal metabolic rate and body temperature seen in animals with thyrotoxicosis can also be produced by the administration of 2,4-dinitrophenol, an agent that uncouples oxidative phosphorylation (18). These similarities between the effect of dinitrophenol and thyrotoxicosis led us to study the effect of exposure to dinitrophenol *in vivo* on mitochondrial ADP transport. For these experiments, four pairs of normal rats were used. One animal from each pair was injected intraperitoneally with sterile sodium dinitrophenolate (pH 7.4) in 0.9% NaCl (2 mg/kg of the freshly prepared solution), while the other was given 0.9% NaCl alone. After 90 min (18), the animals were killed, liver mitochondria were prepared, and ADP uptake and oxygen consumption were assayed. With dinitrophenol, as with both thyroxine and triiodothyronine, there was an increase in mitochondrial uptake of ADP (3.77 ± 0.22 against 2.36 ± 0.22 nmol/min per mg of protein; $P < 0.05$). However, the changes induced by dinitrophenol were substantially larger than those produced by either of the thyroid hormones. In further contrast to the effects seen with thyroid hormone, and in confirmation of earlier reports, respiratory control of mitochondria obtained from dinitrophenol-treated animals was virtually abolished (1.26 ± 0.15 against a normal value of 2.72 ± 0.23; $P < 0.05$).

DISCUSSION

These experiments have shown that the *in vivo* administration of triiodothyronine or thyroxine in doses sufficient to produce thyrotoxicosis in rats led to an increase in the rate of uptake of ADP by liver mitochondria. Presumably, this uptake was accompanied by the discharge of an equivalent amount of ATP from the mitochondrial matrix. An increase in mitochondrial oxygen consumption proportional to the increase in ADP uptake was also observed. There was, however, no evidence that either hormone caused an uncoupling of oxidative phosphorylation, since respiratory control ratios in the thyrotoxic and euthyroid groups were the same. The last result is in accord with previous observations in tissues from both animals made thyrotoxic (1) and thyrotoxic patients (19).

Even though the ADP–ATP exchange rate correlated well with the rate of ADP-dependent oxygen uptake, the difference in the temperatures at which the two reactions were measured precluded a direct comparison of their absolute velocities. From the measurements made at 6°, however, an estimate can be made of the ADP–ATP exchange rate at the temperature at which oxygen uptake was measured. This estimate is based on the observation that the Arrhenius plot for the ADP–ATP exchange reaction is linear between 1° and 25° (14). If we assume that the plot is also linear at temperatures slightly greater than 25°, the activation energy of 28 kcal obtained from this plot can be used to calculate that an increase in the ADP–ATP exchange rate of 1 nmol/min per mg at 6°, the temperature at which the exchange reaction was measured, corresponds to an increase of 37 nmol/min per mg at 30°, the temperature at which ADP-dependent oxygen uptake was measured. Application of this factor to the data of Fig. 2 shows that at 30°, an increase in ADP transport of 3.0 nmol/min per mg of protein is accompanied by an increase in oxygen uptake of 1 nanoatom/min per mg of protein.

TABLE 3. *Effect of in vitro exposure to thyroid hormone on mitochondrial ADP uptake*

Duration of incubation with triiodothyronine (min)	ADP uptake (nmol/min per mg of protein)		
	[Triiodothyronine] = 0	[Triiodothyronine] = 0.1 nM	[Triiodothyronine] = 100 nM
0	2.52 ± 0.50	1.73 ± 0.37	1.64 ± 0.31
60	0.70 ± 0.15	0.63 ± 0.15	0.53 ± 0.16

The difference in uptake of ADP between mitochondria incubated in the presence or absence of triiodothyronine is significant at the level of $P < 0.05$ for all cases.

The ratio of these two values agrees surprisingly well with the figure of 2.0 expected on the basis of the P:O ratio of mitochondria performing oxidative phosphorylation with succinate.

An increase in ADP uptake also followed administration of dinitrophenol. This result is in agreement with the observations of previous workers (10), who found that dinitrophenol stimulated mitochondrial uptake of both ADP and ATP. This effect was accompanied by a loss of specificity of nucleotide uptake that normally favors ADP. In the presence of dinitrophenol, ADP and ATP were transported indiscriminately into the mitochondrial matrix.

In contrast to the effect observed when triiodothyronine was administered *in vivo*, the addition of this hormone *in vitro* was found to inhibit ADP uptake. Additional investigation will be necessary before the significance of the difference between the *in vivo* and *in vitro* actions of thyroid hormone becomes clear.

The fact that there was no oxidizable substrate present in the reaction mixture in which ADP uptake was measured and the observation that cyanide was without effect on ADP uptake indicate that the increase in nucleotide transport cannot be ascribed to an increase in the rate of oxidation of substrate. Conversely, however, it is possible that the increase in oxygen consumption observed in thyrotoxic mitochondria may reflect increased availability of ADP as a substrate for oxidative phosphorylation. An additional observation supporting this conclusion is the similarity of the correlation between ADP uptake and ADP-dependent oxygen consumption for triiodothyronine- and thyroxine-treated animals. Such a finding would be expected if the thyroid hormone-induced increase in mitochondrial oxygen consumption was a consequence of an increase in ADP uptake. Many of the changes in mitochondrial function reported to be induced by thyroid hormone may be due to an increase in the rate of oxidative phosphorylation that would accompany an increased rate of transport of ADP into the mitochondrion, if in fact ADP availability is the limiting parameter in mitochondrial function.

If thyroid hormone affects mitochondrial ADP–ATP exchange *in vivo* as it does *in vitro*, then thyrotoxicosis might be associated with an increase in the energy charge† of the cell

† Energy charge, defined as ([ATP] + 0.5[ADP])/([ATP] + [ADP] + [AMP]), is proportional to the number of moles of high energy phosphate per mole of adenosyl nucleotide.

resulting from an increased output of ATP by the mitochondrion. Such an increase in energy charge would be expected to be accompanied by an increase in the activity of ATP-consuming enzymes due to a direct effect of energy charge on existing enzymes (20, 21) and perhaps also due to a stimulation of synthesis of new enzymes. Ismail-Beigi and Edelman recently reported a rise in membrane-bound Na,K-dependent ATPase induced by high doses of thyroid hormone (22, 23). This increase might be the result of an alteration in the energy charge of the cell, although alternatively it might represent an independent action of the hormone. In any case, the additional ADP produced as a consequence of the increase in activity of Na,K-dependent ATPase and other ATP-consuming reactions, added to mitochondria whose capacity to take up the nucleotide is already augmented, would lead to still further increases in the rate of oxidative phosphorylation. The end result would be an increase in the rate of turnover of both ADP and oxidizable substrate. These considerations suggest the possibility that certain of the clinical and biochemical manifestations of thyrotoxicosis can be attributed at least in part to an effect of thyroid hormone on mitochondrial nucleotide transport.

This research was supported in part by Public Health Service Grants AM-09115, AM-5413, AM-09753, by a Research Career Development Award (AM-11950) awarded to B. M. B., and by Grant RR-0076 from the Division of Health Resources and Facilities, National Institutes of Health, Bethesda, Md.

1. Tata, J. R. (1964) "Biological action of thyroid hormones at the cellular and molecular levels," in *Actions of Hormones on Molecular Processes*, eds. Litwack, G. & Kritchevsky, D. (John Wiley & Sons, Inc., New York), pp. 58–131.
2. Hoch, F. L. (1962) "Thyrotoxicosis as a disease of mitochondria," *N. Engl. J. Med.* **266**, 446–454.
3. Hoch, F. L. & Lipmann, F. (1953) "Inhibition of mitochondria phosphorylation by thyroxine," *Fed. Proc.* **12**, 218–219.
4. Bronk, J. R. (1966) "Thyroid hormone: effects on electron transport," *Science* **153**, 638–639.
5. Lee, Y. P. & Lardy, H. A. (1965) "Influence of thyroid hormones on L-alphaglycerophosphate dehydrogenases and other dehydrogenases in various organs of the rat," *J. Biol. Chem.* **240**, 1427–1436.
6. Lehninger, A. L. (1965) *The Mitochondrion* (W. A. Benjamin, Inc., New York), p. 185.
7. Shaw, W. V., Lannon, T. J. & Tapley, D. F. (1959) "The effect of analogues of thyroxine and 2,4-dinitrophenol on the swelling of mitochondria," *Biochim. Biophys. Acta* **36**, 499–504.
8. Hoch, F. L. (1962) "Biochemical actions of thyroid hormones," *Physiol. Rev.* **42**, 605–673.
9. Racker, E. (1970) "The two faces of the inner mitochondrial membrane," *Essays Biochem.* **6**, 1–22.
10. Pfaff, E. & Klingenberg, M. (1968) "Adenine nucleotide translocation of mitochondria. 1. Specificity and control," *Eur. J. Biochem.* **6**, 66–79.
11. Klingenberg, M. (1970) "Metabolite transport in mitochondria: an example for intracellular membrane function," *Essays Biochem.* **6**, 119–159.
12. Lehninger, A. L. (1965) *The Mitochondrion* (W. A. Benjamin, Inc., New York), p. 132.
13. Chance, B. & Williams, G. R. (1956) "The respiratory chain and oxidative phosphorylation," *Advan. Enzymol.* **17**, 65–134.
14. Klingenberg, M. & Pfaff, E. (1968) "Metabolic control in mitochondria by adenine nucleotide translocation," in *The Metabolic Roles of Citrate*, ed. Goodwin, T. W. (Academic Press, New York), pp. 105–122.
15. Estabrook, R. W. (1967) "Mitochondrial respiratory control and the polarographic measurement of ADP: O ratios," *Methods Enzymol.* **10**, 41–47.
16. Winkler, H. H., Bygrave, F. L. & Lehninger, A. L. (1968) "Characterization of the atractyloside-sensitive adenine nucleotide transport system in rat-liver mitochondria," *J. Biol. Chem.* **243**, 20–28.
17. Tata, J. R., Ernster, L., Lindberg, O., Arrhenius, E., Pederson, S. & Hedman, R. (1963) "The action of thyroid hormones at the cell level," *Biochem. J.* **86**, 408–428.
18. Bianchetti, A., Pugliatti, C. & Jori, A. (1967) "On the hyperthermia induced by 2,4-dinitrophenol," *Med. Pharmacol. Exp.* **17**, 401–408.
19. Stocker, W. W., Samaha, F. J. & DeGroot, L. J. (1968) "Coupled oxidative phosphorylation in muscle of thyrotoxic patients," *Amer. J. Med.* **44**, 900–909.
20. Atkinson, D. E. (1968) "The energy charge of the adenylate pool as a regulatory parameter. Interaction with feedback modifiers," *Biochemistry* **7**, 4030–4034.
21. Atkinson, D. E. & Walton, G. M. (1967) "Adenosine triphosphate conservation in biosynthetic regulation. *Escherichia coli* phosphoribosylpyrophosphate synthase," *J. Biol. Chem.* **242**, 3239–3241.
22. Ismail-Beigi, F. & Edelman, I. S. (1970) "Mechanism of thyroid calorigenesis: role of active sodium transport," *Proc. Nat. Acad. Sci. USA* **67**, 1071–1078.
23. Ismail-Beigi, F. & Edelman, I. S. (1971) "The mechanism of the calorigenic action of thyroid hormone. Stimulation of $Na^+ + K^+$-activated adenosine-triphosphatase activity," *J. Gen. Physiol.* **57**, 710–722.

Proc. Nat. Acad. Sci. USA
Vol. 70, No. 1, pp. 103–107, January 1973

Inhibition of a DNA Polymerase from *Bacillus subtilis* by Hydroxyphenylazopyrimidines

(base-pairing/antimicrobials/DNA replication)

KENNETH B. GASS, ROBERT L. LOW, AND NICHOLAS R. COZZARELLI

Departments of Biochemistry and Biophysics, University of Chicago, Chicago, Illinois 60637

Communicated by Josef Fried, October 24, 1972

ABSTRACT **The antimicrobial agent, 6-(*p*-hydroxyphenylazo)-uracil, specifically inhibits DNA polymerase III of *Bacillus subtilis* with a K_i of less than 1 μM. The inhibition requires prior reduction of the drug, is reversible, and is competitive with dGTP. High amounts of dATP prevent inhibition by the closely related drug, 6-(*p*-hydroxyphenylazo)-isocytosine. A model is presented in which the inhibitors base-pair with the template while part of a ternary complex with the enzyme. These results imply that DNA polymerase III of *B. subtilis* is necessary for chromosomal replication.**

The antimicrobial agent, 6-(*p*-hydroxyphenylazo)-uracil (HPUra), specifically inhibits DNA synthesis in several Gram-positive bacteria (1). In *Bacillus subtilis*, the inhibition is limited to replicative synthesis, while repair synthesis and DNA synthesis directed by several bacteriophages is unimpaired (2, 3). Semiconservative DNA synthesis in toluene-treated *B. subtilis* cells is inhibited by HPUra in the presence of reducing agents (4).

Recently, we described a mutant of *B. subtilis* lacking the DNA polymerase isolated by Okazaki and Kornberg (polymerase I) (5, 6). In these *polA*$^-$ cells, the residual DNA-polymerizing activity has markedly different properties from polymerase I (5). During the analysis of this residual activity we have isolated two additional DNA polymerases that we call polymerases II and III, in order of discovery. The three *B. subtilis* polymerases are similar to the correspondingly numbered *Escherichia coli* enzymes (7–10), but there are clear differences (11). In this report, we show that HPUra specifically inhibits DNA polymerase III of *B. subtilis* by an unexpected mechanism.

MATERIALS AND METHODS

Bacteria. Strain BC26 (*phe*$^-$, *argA*$^-$) was obtained from Dr. J. Copeland. The *polA59* locus in HA101(59)F (5) was introduced into BC26 by transduction with bacteriophage PBS1 to form BC26(F). Among the *phe*$^+$, *argA*$^+$ transductants, the frequency of *polA*$^-$ bacteria is 95%.

Nucleotides and Nucleic Acids. Unlabeled nucleotides, poly(dA), poly(dT), and $(dT)_{10}$ were purchased from P. L. Biochemicals, poly[d(A-T)] from Miles Laboratories, and salmon-testes DNA from Worthington Biochemical Corp. The deoxynucleotides were purified before use (5). Labeled nucleotides were purchased from Schwarz BioResearch. Activation of salmon-testes DNA for use as a template-primer for DNA polymerase used limited digestion by pancreatic DNase (4% acid-soluble A_{260}) (11). The concentration of nucleic acids is expressed as nucleotide equivalents.

Drugs. HPUra and 6-(*p*-hydroxyphenylazo)-2-amino-4-hydroxypyrimidine (HPIso) were generously provided by Dr. Bernard Langley of Imperial Chemical Industries, Ltd., Macclesfield, England. The removal of minor contaminants from HPUra by paper or column chromatography (1) did not alter the inhibitory activity of the drug. To convert the drug to an active inhibitor, 2.0 mM HPUra was treated with 25 mM dithiothreitol in 50 mM Tris·HCl (pH 7.5) at 37° for 21 min; longer incubation times result in a gradual loss of inhibitory activity. During the activation reaction the red color of the drug is lost at a rate that is directly proportional to the concentration of both HPUra and dithiothreitol; the second-order rate constants are 4.4 and 6.5 M^{-1} min^{-1} at 30° and 37°, respectively. Although the activated form (absorption maximum at 260–265 nm) can be readily purified from dithiothreitol and inactive drug by DEAE-cellulose chromatography, it rapidly reoxidizes in air to the colored form. Thus, for the experiments in this report, the activated drug was used without purification, and its concentration was assumed to be equal to the input inactive form.

Enzymes. Deoxyribonuclease I was purchased from Worthington Biochemical Corp. *E. coli* DNA polymerase I, Fraction 7 (12), and T4 DNA polymerase, Fraction VII (13), were gifts of Dr. P. T. Englund. *B. subtilis* polymerase I was purified through the phosphocellulose chromatography step by the published method (6). Purification and properties of polymerases II and III of *B. subtilis* are detailed elsewhere (11). The specific activity of the polymerases II and III preparations used here were increased 2700-fold and 210-fold, respectively, over that of the crude extract of BC26(F) used in the purification. The preparations of each of three *B. subtilis* DNA polymerases are free of cross contamination by the other two, and polymerases I and II contain negligible nuclease activity. Polymerase III, unlike the other two *B. subtilis* enzymes, is inhibited (>90%) by 2.0 mM *N*-ethyl maleimide and 100 μM HPUra, and by raising the assay temperature to 56°. It is also the most salt-sensitive (95% inhibition at 0.20 M KCl). Both polymerases II and III, unlike polymerase I, are inhibited by *p*-chloromercuriphenyl sulfonic acid, single-

Abbreviations: HPUra, 6-(*p*-hydroxyphenylazo)-uracil; HPIso, 6-(*p*-hydroxyphenylazo)-2-amino-4-hydroxypyrimidine; ara-CTP, 1-β-D-arabinofuranosylcytosine triphosphate.

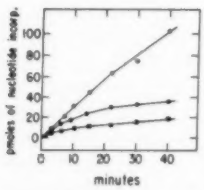

Fig. 1. Time-course of HPUra inhibition of polymerase III. The standard assay with 6 mM dithiothreitol in place of 2-mercaptoethanol was done at 37°, with 0.075 unit of enzyme in a total volume of 0.5 ml. At the times indicated, 60 μl was removed for determination of acid-precipitable material. ○——○, no HPUra; ●——●, 0.32 mM HPUra; ■——■, 2.0 mM HPUra.

stranded DNA, and 1-β-D-arabinofuranosylcytosine triphosphate (ara-CTP).

Enzyme Assay. In the assay for *B. subtilis* DNA polymerase III, the reaction mixture contained in a total volume of 0.1 ml, 65 mM Tris·HCl (pH 7.5), 6.5 mM $MgCl_2$, 3 mM 2-mercaptoethanol, 40 μM each of dATP, dCTP, and dGTP, 10 μM [^{3}H]dTTP, 300 μM activated DNA, 10% glycerol, and 0.003–0.02 units of enzyme in 10 μl of diluent. A unit of enzyme activity catalyzes the incorporation of 10 nmol of total nucleotide into an acid-precipitable product in 30 min at 37°; the enzyme diluent contains 50 mM Tris·HCl (pH 7.5), 10 mM 2-mercaptoethanol, 0.15 M KCl, 1.0 mg/ml of bovine-serum albumin, and 20% glycerol. The assay procedure is the same as described previously (5).

RESULTS

Activation of HPUra. The effect of HPUra on the time-course of a reaction of *B. subtilis* DNA polymerase III is shown in Fig. 1. The degree of inhibition by the drug increases with time. Preincubation experiments with various components of the reaction mixture showed that the lag in inhibition is eliminated only when the preincubation mix contained HPUra and dithiothreitol. With preincubated drug, the onset of inhibition is immediate and the incorporation rate is linear with time (see Fig. 5), even when the drug is added after the polymerization reaction has begun. Therefore, dithiothreitol chemically converts the drug to an active form. The activation is essential; no inhibition is obtained with unactivated drug even at 500-times the concentration, that gives 50% inhibition with the activated form. During activation the drug becomes colorless and a new absorption peak in the UV appears. The decoloration is a second-order reaction, but at the high dithiothreitol to HPUra ratios used in the activation reactions, pseudo first-order kinetics are observed. As shown in Fig. 2, the conversion of HPUra to an active inhibitor is also a first-order reaction. Like the rate of color loss, the rate of formation of active inhibitor is augmented by an increase in the dithiothreitol concentration. For unknown reasons, the the calculated rate of activation is about twice that of color loss. Several other reducing agents such as reduced glutathione, cysteine, TPNH, and ascorbic acid both activate and reduce the drug, although all do so more slowly than dithiothreitol. Oxidized glutathione neither activates nor decolorizes HPUra. Fig. 3 shows a dose–response curve for inhibition by activated HPUra; the linear relationship between reciprocal velocity and HPUra concentration implies that the reaction of drug with the enzyme is uncomplicated (14).

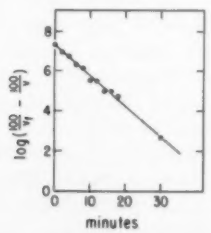

Fig. 2. Activation of HPUra at 30°. The preincubation mixture contained 25 mM potassium phosphate (pH 7.4), 5 mM dithiothreitol, and 0.8 mM HPUra. At the times indicated aliquots were diluted 5-fold into an assay mixture with 0.025 unit of polymerase III and 40 μM triphosphates; the incorporation in a 5-min assay was monitored. The units of v are nucleotides incorporated, and v_f is the velocity at maximal (83%) inhibition. The form of the plot is derived from the basic kinetic equations for inhibition and the definition of a first-order reaction (14).

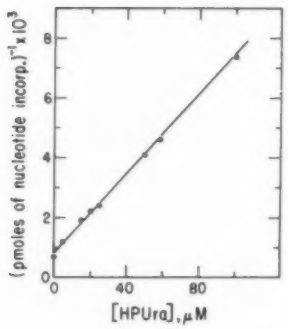

Fig. 3. Dose–response curve for activated HPUra. The reaction mix contained 10 μM triphosphates, 0.025 unit of polymerase III, and the indicated activated HPUra concentrations. The assay was done at 30° for 20 min.

Enzyme Specificity of HPUra. With the activated drug in hand, we tested the effect of HPUra on four other DNA polymerases. An activated DNA template was used in all cases. Even at 100- to 1000-times the HPUra concentration that gives 50% inhibition of *B. subtilis* polymerase III, there was no inhibition of *B. subtilis* polymerase I, *E. coli* polymerase I, and T4 polymerase (the unactivated drug was also impotent). *B. subtilis* polymerase II was slightly inhibited; however, it was at least 500-fold less sensitive than *B. subtilis* polymerase III. Therefore, HPUra is a highly specific inhibitor of *B. subtilis* polymerase III.

Site of Action of HPUra. Since HPUra does not inhibit several DNA polymerases, it is unlikely that it affects the template and not the enzyme, as some other DNA polymerase inhibitors (15). Indeed, preincubation of the drug and template did not alter the degree of inhibition, nor did the addition of more template to an inhibited reaction. Increasing the template concentration from 0.3 mM, already a saturating level, to 1.0 mM also did not diminish inhibition. Therefore, it seems likely that HPUra interacts directly with DNA polymerase III.

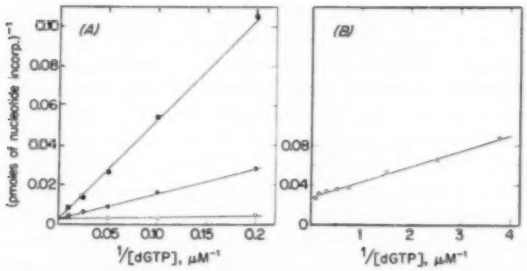

FIG. 4. Lineweaver-Burk plots of the relationship between dGTP, HPUra, and polymerase III. (*A*) Reaction mixtures contained 40 μM each of dATP, dCTP, and dTTP, the indicated amounts of dGTP, and 0.025 unit of enzyme. The assay was at 30° for 20 min. ○——○, no HPUra; ●——●, 25 μM HPUra; ■——■, 100 μM HPUra. (*B*) To minimize dGTP depletion during the assay in the absence of HPUra, the reaction mixture was altered by increasing the total volume to 0.3 ml and decreasing the enzyme to 0.004 unit and the reaction time to 7 min.

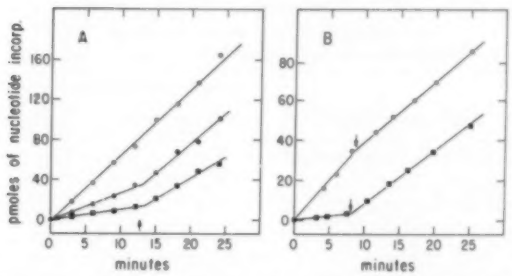

FIG. 5. Reversal of HPUra inhibition. (*A*) Reaction mixtures contained in a total volume of 0.3 ml, 0.18 unit of polymerase III and activated HPUra at either 0 μM, ○——○; 13 μM, ●——●; or 67 μM, ■——■; temperature is 30°. At the indicated time (*arrow*), 0.15 ml of each reaction mixture was diluted with 0.85 ml of assay mixture without drug and enzyme. For measurement of incorporation, 30- and 200-μl aliquots were withdrawn before and after dilution, respectively. (*B*) Reaction mixtures at 30°, contained in a total volume of 0.4 ml, 10 μM triphosphates, 0.1 unit of polymerase III, and activated HPUra at 0 μM, ○——○ or 100 μM, ■——■. At the indicated times (*arrows*), dGTP to 0.4 mM was added to each. For measurement of incorporation, 40-μl aliquots were withdrawn.

Competitive Attenuation of Inhibition by dGTP. An unexpected finding of the study of toluene-treated cells was that HPUra inhibition is abolished by high amounts of dGTP (16). The effect is the same on polymerase III. In Fig. 4, double-reciprocal plots of reaction velocity as a function of dGTP concentration at two concentrations of activated HPUra are shown. HPUra inhibition is competitive with dGTP concentration since the maximum velocity is not altered by the presence of inhibitor. From these and other data the K_m for dGTP is calculated to be 6×10^{-7} M and the K_i for HPUra to be 3 to 6×10^{-7} M. The following nucleotides at 0.2 mM did not alter the degree of inhibition by 20 μM HPUra: rGTP, dGDP, dGMP, dATP, dTTP, and dCTP; in the same experiment 0.2 mM dGTP abolished inhibition. The only nucleotide, other than dGTP, that we have found to attenuate inhibition is dITP, which, like dGTP, base-pairs with C residues. Maximal activity requires a higher concentration of dITP than dGTP, and thus a higher concentration of dITP is needed to diminish inhibition. With no dGTP in the assay mixture, the inhibition by 3 μM drug was 86, 63, 25, and 6% at 0, 4.0, 90, and 480 μM dITP, respectively.

Inhibition by HPUra Is Reversible. Addition of dGTP or dilution of the reaction mix reduced the inhibition by activated HPUra to the level expected of a reversible inhibitor (Fig. 5). Thus, polymerase III is not irreversibly inactivated by HPUra.

Inhibition by HPIso Is Reversed by dATP. HPIso is an analogue of HPUra in which the pyrimidine 2-keto group in HPUra is replaced by an amino moiety. Like HPUra, HPIso must be reduced to be an inhibitor of *B. subtilis* polymerase III. Unlike HPUra, the inhibition is attenuated by dATP and not dGTP, as also found in toluene-treated *B. subtilis* cells (17). Thus, an increase in the concentration of dATP from 5 μM to 200 μM in an assay reduced the inhibition by 20 μM HPIso from 87% to 17%, while addition of dAMP, dGTP, dTTP, or dCTP to 200 μM was without effect.

Template Specificity of Inhibition by Hydroxyphenylazopyrimidines. The data presented thus far can be explained by postulating that HPUra and HPIso are simple competitive inhibitors of the reaction of dGTP and dATP, respectively, with *B. subtilis* polymerase III. Polymerase III catalyzes an extensive end-addition reaction in the absence of a full triphosphate complement (11). Under these conditions, it is clear that HPUra inhibits the incorporation of each of the four triphosphates. HPUra (100 μM) inhibited the incorporation of 10 μM dATP, dTTP, dCTP, and dGTP alone by 92, 96, 85, and 77%, respectively. A dose–response curve for the inhibition of synthesis with dGTP missing from the full triphosphate complement is plotted in Fig. 6. The K_i is 6×10^{-7} M or about the same as that obtained in the presence of dGTP. Thus, HPUra prevents the incorporation of all four triphosphates while only dGTP attenuates inhibition.

A simple model consistent with the data postulates that HPUra binds to an enzyme–template replicative complex only when C is the base to be copied (T for HPIso); the HPUra hydrogen-bonds to the C residue. This ternary complex, enzyme–template–inhibitor, decreases the amount of enzyme available for polymerization. Since only dGTP is accepted by a polymerase copying a C residue, only dGTP competes with HPUra.

One test of the model is provided by the experiments reported in Table 1. Synthetic polymers were used to limit the template residues to A alone for $(dT)_{10} \cdot$poly(dA) and to A

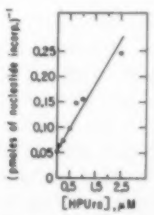

FIG. 6. Inhibition by HPUra in the absence of dGTP. The conditions are the same as in Fig. 3 except that the assay mixture contained no dGTP.

TABLE 1. *Inhibition of oligo(dT)·poly(dA)- and poly[d(A-T)]-promoted synthesis*

Template-primer	Incorporation (pmol) No drug	HPUra	HPIso
1. $(dT)_{10}$·poly(dA), 0.25 mM	4.6	5.5	4.2
2. Activated DNA, 0.004 mM	<0.1	<0.1	<0.1
3. $(dT)_{10}$·poly(dA), 0.25 mM and activated DNA, 0.004 mM	4.4	0.6	0.9
4. Poly[d(A-T)], 0.28 mM	0.12	0.11	<0.01

The homopolymer experiments used 83 μM $(dT)_{10}$, 165 μM poly(dA), 50 μM [^{3}H]dTTP, and 0.025 unit of enzyme in a total volume of 0.1 ml. The reaction was done at 25° for 15 min. Exp. 4 contained 0.28 mM poly[d(A-T)], 7 μM [^{3}H]dTTP, and 0.025 unit of enzyme. The reaction was at 37° for 15 min. (Note that poly[d(A-T)] is a poor template for polymerase III.) The drug concentration was 200 μM in Exp. 4 and 100 μM in the others.

and T residues for poly[d(A-T)]. The incorporation of dTTP into 0.25 mM oligo(dT)·poly(dA) and 0.28 mM poly[d(A-T)] was not inhibited by HPUra. However, the addition of only 0.004 mM activated DNA, an amount that by itself promoted negligible synthesis, caused the incorporation into the homopolymers to be inhibited 87% by 100 μM HPUra. Even at one-tenth this amount of DNA the activity is halved by HPUra. HPIso, however, markedly inhibited poly[d(A-T)] but not oligo(dT)·poly(dA)-primed synthesis. We interpret these results as indicating that the activated DNA provides a C residue for the HPUra ternary complex and the poly[d-(A-T)] provides the T residue for the HPIso complex; evidently these complexes scavenge free enzyme efficiently.

DISCUSSION

In order for HPUra to inhibit DNA polymerase activity four conditions must be fulfilled. First, the drug must be chemically modified; reaction with several reducing agents including dithiothreitol, reduced glutathione, cysteine, TPNH, and ascorbic acid is sufficient. While the structure of the active form is unknown, a hydrazine derivative of HPUra is compatible with the data. The reduction of the azo linkage would interrupt the conjugated double-bond system and thereby cause a loss of the visible spectrum, and, typically, hydrazine derivatives oxidize rapidly in air (18), as does activated HPUra. Second, the enzyme must be *B. subtilis* polymerase III (or presumably similar polymerases from other Gram-positive bacteria); the other four DNA polymerases tested from *B. subtilis*, *E. coli*, and T4-infected cells are resistant to the drug. Third, the template probably must contain a C residue for HPUra inhibition (a T residue for HPIso inhibition). Fourth, the dGTP to HPUra ratio must not be too high (dATP for HPIso inhibition).

The inhibition model postulates that HPUra and HPIso occupy the triphosphate binding site of polymerase III, hydrogen bonding to C and T on the template, respectively. These are, of course, not the expected base pairs, but if an enol tautomer of the drug is present, then these specific pairs can be drawn. The 4-hydroxy tautomer of HPIso can make three good hydrogen bonds to T but cannot readily form two hydrogen bonds to the other bases within wobble limits (19). Since HPUra has two carbonyl groups, two monoenolic isomers are possible. With the 4-hydroxy form, two hydrogen bonds can be formed to C but two hydrogen bonds cannot be made readily to G or A within wobble limits; bonding to T brings the keto groups rather close together. It is interesting to note that another uracil analogue, 3-deazauridine, has an enolic 4-hydroxyl group (20). The 2-hydroxy derivative of HPUra can make three hydrogen bonds to C and cannot pair effectively to T and G; base pairing with A may be excluded on geometric grounds since HPUra and HPIso apparently bond like purines. These postulated base pairs do not require any significant tilting of the pyrimidine ring of the drug from the position of this ring in the purines of the Watson–Crick base pairs.

Whatever the precise structure of the base pairs*, the evidence that the drugs hydrogen-bond to the template is quite good. The binding of each of the drugs (which differ only in the pyrimidine moiety) to the template–enzyme complex is strong, but reversible, and base-specific both in its formation and its competition by triphosphates. Hydrogen bond-mediated base pairing is the most reasonable explanation of these properties. It is striking, and somewhat surprising, that the apparent affinity of the enzyme for HPUra and dGTP is the same, while dGDP and rGTP do not compete effectively with dGTP for polymerase III.

The contrast of HPUra with ara-CTP is instructive. While the effect of both drugs is enzyme-specific and reversed by a specific triphosphate for both *E. coli* (21) and *B. subtilis* DNA polymerases (11), ara-CTP has no effect on synthesis in the absence of dCTP (11). Ara-CTP acts as a simple competitive inhibitor of dCTP incorporation while HPUra prevents the incorporation of all four triphosphates.

Evidence was presented that HPUra does not alter the template nonspecifically; nor does it inhibit by binding to a triphosphate to form a toxic analogue, since raising the concentration of either dATP, dCTP, or dTTP does nor reverse inhibition, even though the incorporation of each of these triphosphates is prevented by the drug.

There are several persuasive arguments for the inhibition of polymerase III being the site of action of HPUra *in vivo*. First, the reaction of HPUra with *B. subtilis* polymerase III is highly selective. Second, the *in vitro* reaction, like the inhibition of toluene-treated cells, is rapid in onset, is reversible by dilution or by dGTP (dATP for HPIso), and requires a reduced drug at only very low concentrations (the K_i, *in vitro*, is less than 1 μM). Third, the pattern of inhibition *in vivo* in affecting only the host, replicative DNA synthesis is clearly compatible with an action on a specific DNA polymerase. Therefore, it seems likely that *B. subtilis* polymerase III, like the correspondingly numbered *E. coli* enzyme (22), is necessary for DNA replication (see note added in proof).

NOTE ADDED IN PROOF

We have selected a spontaneous mutant of *B. subtilis* resistant to HPUra and HPIso. The polymerase III of this mutant is resistant to the drugs, thereby confirming polymerase III is necessary for replication.

* Dr. R. Wells has suggested an alternative bonding scheme that does not postulate enolic tautomers but rather base-pairing through the N-1 hydrogen, a hydrogen from the proximal nitrogen of the presumed hydrazine link, and the 2-carbonyl of HPUra or the amino of HPIso (personal communication).

We thank R. Depew, F. Kézdy, and R. Wells for many helpful discussions and S. Rashbaum for purification of active inhibitor. This work was supported by grants from the National Science Foundation (GB-32243) and the National Institutes of Health (GM-19425). K. B. G. and R. L. L. were supported by Public Health Service Grant HD-00001.

1. Brown, N. C. & Handschumacher, R. E. (1966) *J. Biol. Chem.* **241**, 3083–3089.
2. Brown, N. C. (1971) *J. Mol. Biol.* **59**, 1–16.
3. Brown, N. C. (1970) *Proc. Nat. Acad. Sci. USA* **67**, 1454–1461.
4. Brown, N. C., Wisseman, C. L. & Matsushita, T. (1972) *Nature New Biol.* **237**, 72–74.
5. Gass, K. B., Hill, T. C., Goulian, M., Strauss, B. S. & Cozzarelli, N. R. (1971) *J. Bacteriol.* **108**, 364–374.
6. Okazaki, T. & Kornberg, A. (1964) *J. Biol. Chem.* **239**, 259–268.
7. Moses, R. E. & Richardson, C. C. (1970) *Biochem. Biophys. Res. Commun.* **41**, 1557–1564.
8. Kornberg, T. & Gefter, M. L. (1971) *Proc. Nat. Acad. Sci. USA* **68**, 761–764.
9. Wickner, R. B., Ginsberg, B., Berkower, I. & Hurwitz, J. (1972) *J. Biol. Chem.* **247**, 489–497.
10. Kornberg, T. & Gefter, M. L. (1972) *J. Biol. Chem.* **247**, 5369–5375.
11. Gass, K. B. & Cozzarelli, N. R. (1973) in *Methods in Enzymology*, eds. Grossman, L. & Moldave, K. (Academic Press, New York), in press.
12. Jovin, T. M., Englund, P. T. & Bertsch, L. L. (1969) *J. Biol. Chem.* **244**, 2996–3008.
13. Goulian, M., Lucas, Z. L., & Kornberg, A. (1968) *J. Biol. Chem.* **243**, 627–638.
14. Dixon, W. & Webb, E. C. (1964) *Enzymes* (Academic Press, New York).
15. Falaschi, A. & Kornberg, A. (1964) *Fed. Proc.* **23**, 940–945.
16. Brown, N. C. (1972) *Fed. Proc.* **31**, 442 Abstr.
17. Brown, N. C. (1972) *Biochim. Biophys. Acta*, **281**, 202–215.
18. Overberger, C. G., Anselme, J-P. & Lombardino, J. G. (1966) *Organic Compounds with Nitrogen-Nitrogen Bonds* (The Ronald Press Co., New York).
19. Crick, F. H. C. (1966) *J. Mol. Biol.* **19**, 548–555.
20. Schwalbe, C. H., Gassen, H. G. & Saenger, W. (1972) *Nature New Biol.* **238**, 171–173.
21. Rama Reddy, G. V., Goulian, M. & Hendler, S. S. (1971) *Nature New Biol.* **234**, 286–288.
22. Gefter, M. L., Hirota, Y., Kornberg, T., Wechsler, J. A. & Barnoux, C. (1971) *Proc. Nat. Acad. Sci. USA* **68**, 3150–3153.

Proc. Nat. Acad. Sci. USA
Vol. 70, No. 1, pp. 108–110, January 1973

Extranuclear Temperature-Sensitive Lethality in *Nicotiana tabacum* L.

(cytoplasmic inheritance/genetics/tobacco)

D. F. MATZINGER AND E. A. WERNSMAN

Departments of Genetics and Crop Science, North Carolina State University, Raleigh, N.C. 27607

Communicated by S. G. Stephens, November 2, 1972

ABSTRACT **Tobacco seedlings from progeny of a single aberrant plant, either self-fertilized or used as the female in crosses, failed to become autotrophic at 13° day and 8° night temperatures, but grew normally at 26° day and 20° night temperatures. After initial normal growth at 26° day and 20° night temperatures, autotrophic plants from the aberrant line also died after subsequent exposure to 13° day and 8° night temperatures. The temperature-sensitive lethality was transmitted only through the female parent. When seedlings were grown at normal 26° day and 20° night temperatures, mutant selfs, normal selfs, and reciprocal F_1 hybrids were indistinguishable.**

In a recent study sponsored by the National Research Council (1), evidence was presented for the dangers associated with the restricted germ plasm base in many plant species. In addition, attention was directed to the greater uniformity of cytoplasmic, as compared with nuclear, genes. Such uniformity of cytoplasm in male sterile *Zea mays* L. exposed this species to extreme vulnerability to a plant pathogen that led to widespread yield reductions in 1970. It was suggested that additional attention should be given to the cytoplasm of plants to increase cytoplasmic genetic diversity as a safeguard against major crop losses.

Recent information from investigations of extrachromosomal genetic factors has been summarized and elucidated (2, 3). Many studies are currently being directed toward identification of specific cytoplasmic organelles and the mechanisms of biochemical control. Both plastids and mitochondria have been shown to possess their own DNA, RNA, and protein synthetizing systems.

Temperature-sensitive nuclear alleles have served as useful source material for the study of biochemical functions in many species. Examples of the type of studies enhanced by these techniques can be seen for bacteria (4), bacteriophage (5), and *Drosophila* (6). Many of the alleles in these species cause lethality at critical temperatures.

The detection of temperature-sensitive extrachromosomal factors has not been as widespread, and we know of no documented examples in higher plants. Cytoplasmic male sterility in *Zea mays* L. reverts to partial fertility under certain environmental conditions, but this reversion is apparently related more to the presence of nuclear factors that control partial restoration than to the cytoplasm *per se* (7). Temperature-sensitive cytoplasmic genes in *Chlamydomonas* have been mapped into linkage groups (8). Identification of cytoplasmic temperature-sensitive mutants in higher plants would be useful in characterizing the related functions of the nucleus and cytoplasm. The present report describes an extrachromosomal temperature-sensitive factor lethal to growth of *Nicotiana tabacum L.*

An F_2 tobacco population was created by self-fertilizing a single F_1 plant from a Hicks Broadleaf (♀) x Coker 139 (♂) cross, each parent representing a long-time inbred line. Random reciprocal crosses were made among the F_2 plants for a study of the inheritance of quantitative characters within the population. Seeds were sown in outdoor plant beds in North Carolina during February to obtain plants for transplanting to fields in May. The seeds from one F_2 plant used as the female parent in crosses with four other random F_2 plants produced only a few very small plants, whereas reciprocal crosses were normal. Several of the aberrant seedlings were transplanted to fields. They were delayed in flowering by about 10 days, but the flowers were normal in morphology and fertility. Since no self seeds were obtained from the F_2 plants, only the four reciprocal cross pairs were available for further study. The aberrant F_2 parent plant was designated **5,** and the four normal plants were designated **1–4**.

The self generation, S_1, from each of the four reciprocal-cross pairs was seeded in plant beds in fields the next year. The four self families that involved plant **5** as the female in the previous generation produced only a few plants and they were retarded in growth. Self progenies from the reciprocal crosses developed normally. There was no evidence of segregation in any of the crosses.

Studies were restricted to reciprocal crosses of parents **1** (normal) and **5** (aberrant) in subsequent years. In the S_2 and S_3 generations of **1** x **5** and **5** x **1,** each was crossed reciprocally to the initial Hicks and Coker 139 parents. Aberrant seedlings were always associated with the cytoplasm of parent **5;** this parent will hereafter be referred to as a mutant type. Although field studies established that aberrant growth was associated with the cytoplasm of parent **5,** it was not possible to establish whether crosses with parent **5** cytoplasm failed to germinate or died after germination. Air temperatures in the vicinity of the field beds during February and March were often below 0°, followed by warmer temperatures in April and May. We suspected that the cold temperatures influenced or controlled expression of the mutant phenotype.

Seeds were evaluated in environmental growth chambers to determine the effect of temperature on germination and seedling survival. Crosses evaluated were the mutant **5** x **1** S_s, normal **1** x **5** S_s, and the two reciprocal F_1 hybrids. 25 Seeds of each cross were sown on a soil mixture in 15-cm clay pots, with five replications of each cross. The growth chamber operated on a 12-hr day, with a 17,222 lux (lumens/meter^2) light regime.

In the first experiment, the chamber was set for 9° day and 7° night temperatures. No germination was observed for any seeds after 15 days, at which time the temperatures were

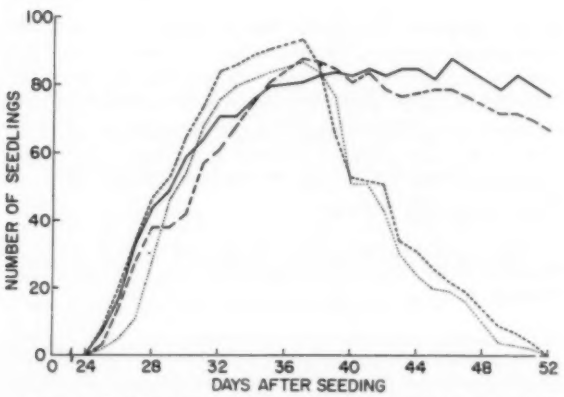

FIG. 1. Seedling emergence and survival at 13° day and 8° night temperatures. (——) Normal self; (— — —), normal x mutant; (– – –), mutant self; (· · · ·) mutant x normal.

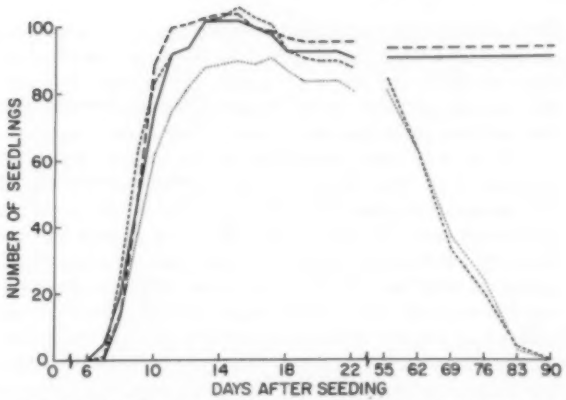

FIG. 2. Seedling emergence and survival at initial 26° day and 20° night temperatures, followed by 13° day and 8° night temperatures after the 29th day. (——), Normal self; (— — —) normal x mutant; (– – –), mutant self; (· · · · · ·), mutant x normal.

elevated to 13° during the day and 8° at night. Germination began 10 days later; the number of plants showing green cotyledons was scored each day. The cumulative number of germinated seedlings is shown in Fig. 1.

The normal and mutant lines and the reciprocal crosses germinated at the same rate and to the same total number of plants. The normal parent and the hybrid where the normal parent was used as a female continued to grow and develop new leaves. The mutant line and the hybrid with mutant cytoplasm failed to become autotrophic. These seedlings failed to produce any leaves beyond the cotyledons, and death occurred about 2 weeks after germination of each seed.

A second experiment was conducted to evaluate the ability of the mutant plants to survive cold temperatures after they had become autotrophic at normal temperatures. The same four crosses were seeded as in the first experiment. The initial temperatures of the chamber were 26° during the day and 20° at night. The numbers of germinated seedlings are presented

FIG. 3. Normal self-fertilized plant (*left*) and mutant self-fertilized plant (*right*) 70 days after seeding. Initial 26° day and 20° night temperatures, followed by 13° day and 8° night temperatures after the 29th day.

in Fig. 2. Again all entries began germinating at the same time and produced about the same number of plants. Germination occurred earlier and the total number of seedlings was somewhat greater at these higher temperatures than at the lower temperatures of the first experiment. After 29 days there was no difference in vigor among the crosses, and all plants had produced four true leaves in addition to the cotyledons. The temperatures were then reduced to the conditions of the first experiment, 13° day and 8° night. The mutant line and the hybrid with mutant cytoplasm began to slow in growth, as compared with the normal plants; on the 48th day after seeding the mutants and hybrids began to wilt. Thereafter, the plants began to die; 90 days after seeding, all plants of the two crosses with plant **5** cytoplasm were dead. A comparison of the normal and mutant parents 70 days after seeding is shown in Fig. 3. The increased food reserves in plants that developed four true leaves before they were subjected to low temperatures lengthened the interval before the plants died, as compared with the plants in the first experiment that supported only cotyledons.

The two growth-chamber studies verified that the mutant characteristic was associated with the female parent. The differences between normal and mutant types were not related to a germination phenomenon, but to the ability of the plants to grow beyond the cotyledons under low-temperature stress. Although a plant with mutant cytoplasm can become autotrophic when germinated and grown at normal temperatures, it has not overcome its inherent inability to survive if it is subjected to cold temperatures.

We do not know whether a new mutation has occurred in a cytoplasmic organelle or whether heterogeneity for cytoplasmic organelles exists within the population from which this mutant was derived. The original cross was produced on Hicks cytoplasm. The parent line of Hicks strain had been maintained for over 10 generations of single plant self-pollination; therefore, one would expect that the cytoplasm was homogeneous. However, quantitative genetic studies of segregating families within this Hicks Broadleaf x Coker 139 population give evidence of some departure from normal Mendelian inheritance, and the present mutant verifies at least one qualitative change.

This is paper number *3890* of the Journal Series of the North Carolina State University Agricultural Experiment Station, Raleigh N.C.

1. Committee on Genetic Vulnerability of Major Crops, National Research Council (1972) *Genetic Vulnerability of Major Crops* (National Academy of Sciences, Washington, D.C.).
2. Sager, R. (1972) *Cytoplasmic Genes and Organelles* (Academic Press, New York).
3. Harvey, P. H., Levings, C. S., III & Wernsman, E. A. (1972) "The role of extrachromosomal inheritance in plant breeding," *Advan. Agron.* **24,** in press.
4. Gross, J. D., Karamata, D. & Hempstead, P. G. (1968) "Temperature-sensitive mutants of *B. subtilis* defective in DNA synthesis," *Cold Spring Harbor Symp. Quant. Biol.* **33,** 307–312.
5. Epstein, R. H., Bolle, A., Steinberg, C. M., Kellenberger, E., de la Tour, E. B., Chevalley, R., Edgar, R. S., Susman, M., Denhardt, G. H. & Lielausis, A. (1963) "Physiological studies of conditional lethal mutants of bacteriophage T4D," *Cold Spring Harbor Symp. Quant. Biol.* **28,** 375–392.
6. Suzuki, D. T. (1970) "Temperature-sensitive mutations in *Drosophila melanogaster*," *Science* **170,** 695–706.
7. Duvick, D. N. (1965) "Cytoplasmic pollen sterility in corn," *Advan. Genet.* **13,** 1–56.
8. Sager, R. & Ramanis, Z. (1970) "A genetic map of non-mendelian genes in *Chlamydomonas*," *Proc. Nat. Acad. Sci. USA* **65,** 593–600.

Proc. Nat. Acad. Sci. USA
Vol. 70, No. 1, pp. 111–114, January 1973

Autonomy of Mitochondria in *Saccharomyces cerevisiae* in Their Production of Messenger RNA

(RNA synthesis/polysomes/inhibition/ethidium bromide/mitochondrial genome)

HENRY R. MAHLER AND KARL DAWIDOWICZ

Chemical Laboratories, Indiana University, Bloomington, Indiana 47401

Communicated by Marcus Rhoades, October 26, 1972

ABSTRACT **In *ts*$^{-}$136, a temperature-sensitive mutant of *Saccharomyces cerevisiae*, nuclear and mitochondrial RNA production can be inhibited selectively by exposure to 36° and ethidium bromide, respectively. Using the programming of mitochondrial polysomes, as measured by their ability to form nascent polypeptide chains, as an assay for functional messenger RNA, we have determined its response to temperature shifts and ethidium bromide. Only ethidium bromide produced a measurable effect; in contrast the cell-sap system responded exclusively to temperature shifts. We conclude that transcription of mitochondrial DNA is sufficient and that import of messenger RNA transcribed from nuclear chromosomes makes no measurable contribution to intramitochondrial protein synthesis.**

Mitochondria, ubiquitous organelles of eukaryotic cells, contain their own semi-autonomous system of gene expression. The current view is that only the primary structure of the constituent stable RNA species [ribosomal RNAs (rRNAs), some or all transfer RNAs (tRNAs)] but not of its multitudinous polypeptides (ribosomal proteins and initiation, elongation, and termination factors, etc.) is encoded in mitochondrial (mt)DNA (1). A major uncertainty remains: to what extent is mtDNA competent to code for mitochondrial mRNA, or, in other words, which, if any, of the polypeptides synthesized by the mitochondrial machinery are actual products of mitochondrial genes? Some investigators believe that most, or perhaps all, of mitochondrial mRNA is an import of nuclear origin (2, 3), while others have provided evidence for mitochondrial transcripts with at least some of the properties expected of a mRNA (4), and even for the export of such species into the cell sap (5).

A critical inquiry into this problem requires the following: (*i*) a means for effectively shutting down nuclear and mtRNA selectively, and (*ii*) some way for assessing the presence and activity of mRNA as well as its response to (*i*). These conditions can be met, particularly in *Saccharomyces cerevisiae*, since it has been shown that: (*i*) ethidium bromide inhibits transcription and appears to be restricted to mitochondrial events in its specificity (1, 6–8); a temperature-sensitive mutant (*ts*$^{-}$136) is available that shuts down production of all nuclear RNA including mRNA (9, 10), and (*ii*) the ability to program polyribosomes, as measured by their capacity to support initiation and propagation of nascent polypeptide chains, provides a sensitive operational assay for mRNA in both the cell-sap and the mitochondrial systems (9–11).

In this communication, we show that cells and spheroplasts of *ts*$^{-}$136 can be used to demonstrate that all functional mitochondrial mRNA is produced inside the organelle and that effective mitochondrial protein synthesis does not depend on the import of mRNA.

METHODS

Strains and Culture Conditions. Strains (obtained from L. H. Hartwell, University of Washington, Seattle) used in these studies were: (*1*) *S. cerevisiae* A364A, haploid, P ρ^{+} (*a ade*$_1$ *ade*$_2$ *ura*$_1$ *tyr*$_1$ *his*$_1$ *lys*$_2$ *gal*$_1$); (*2*) *S. cerevisiae ts*$^{-}$136, derived from A364A by treatment with *N*-methyl-*N'*-nitro-*N*-nitrosoguanidine. They were grown to midexponential phase at 23° in medium YM-1L that contained (g/liter): yeast extract, 5; peptone, 10; yeast nitrogen base (filter-sterilized), 6.7; adenine sulfate, 0.01; uracil, 0.01; succinic acid, 10; NaOH, 6; Na-D,L-lactate, 30, final pH 6.8. The labeling medium was YM-5L, which is the same as YM-1L except that the peptone and yeast extract are reduced 5-fold.

Labeling of Spheroplasts. Cells were converted into spheroplasts as described (11), suspended in the original volume of YM-5L plus 1 M sorbitol, and incubated with the appropriate precursors ([^{3}H]uracil, 40 Ci/mmol; [^{3}H]leucine, 36 Ci/mmol, and [^{14}C]formate, 59 Ci/mol, all from New England Nuclear). Reaction was stopped by addition of crushed ice, 4 mg/ml of chloramphenicol, and 100 μg/ml of cycloheximide, and centrifugation at 3° (10 min at 4000 rpm in a Sorval RC-1). The pellet was suspended in one-twentieth of the original volume of 0.5 M sorbitol-NMT [10 mM $MgCl_2$–100 mM NH_4Cl–10 mM Tris·HCl (pH 7.4)] and blended for 15 sec.

Isolation of Mitochondria and Cell Sap. Lysed spheroplasts were centrifuged 3 times at 600 × *g* for 10 min. The pellets were discarded and the supernatant was centrifuged at 20,000 × *g* for 20 min. The pellet, resuspended in 0.01 of the original volume of 0.5 M sorbitol-NMT, constitutes the mitochondrial fraction; the supernatant is the cell-sap fraction.

Isolation of Ribosomes, Samples for Counting, etc. are described in ref. 11 and in the figure legends.

RESULTS

Experimental design

The experiments to be described have been designed to answer the following question: Is transcription by either of the two systems *sufficient* for mitochondrial mRNA function or are both *necessary?* This question is asked in two ways. After the specificity of the two blocks of RNA synthesis (exposure to 36° for nuclear RNA synthesis, and to ethidium bromide for mtRNA synthesis) is first established by measuring their effect on the kinetics of incorporation of uracil into mitochondrial and cell-sap RNA of the ts mutant, is a shift to this nonpermissive temperature (nuclear block) sufficient, necessary, or ineffective in the absence of a subsequent or simultaneous exposure to ethidium bromide (mitochondrial

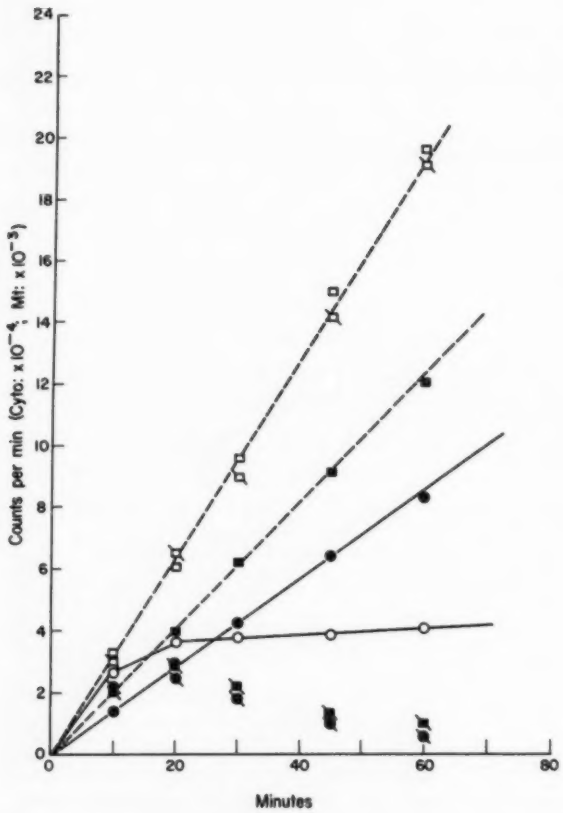

FIG. 1. Incorporation of [³H]uracil at 36°. A364A (wild type) and *ts*⁻136 were grown (50 ml each) in YM-1L at 23° until A_{600} = 0.5. The cells were harvested and spheroplasts were made. The spheroplasts were suspended in YM-5L–1 M sorbitol and transferred to a 36° incubator; after 20 min [³H]uracil (5 μCi/ml) was added. 12-ml samples were taken from each flask at the times indicated, iced, and harvested. The spheroplasts were lysed and mitochondrial (*Mt*)(1 ml) and cell-sap (*Cyto*) (5 ml) fractions were isolated. 0.2-ml aliquots were put on filter paper discs. The discs were put in 10% cold trichloroacetic acid for 2 hr, washed twice with 10% cold trichloracetic acid, suspended in EtOEt–EtOH (2:1), washed twice with this mixture and once with EtOEt, and dried. Their radioactivity was then measured (11). The values shown are total cpm determined on replicate samples. (□, ■) cell-sap and mitochondrial fractions, respectively, from A364A; (○, ●) cell-sap and mitochondrial fractions, respectively, from *ts*⁻136. *Crossed symbols* (⊠, ⊠, ⊘, ⊘) represent data obtained when 10 μg/ml of ethidium bromide was added to the spheroplast suspension at the time of the shift to 36°.

block) to eliminate mRNA function? After all functional mRNA is first eliminated as a result of the double block, is a shift down (selective release of nuclear block) sufficient to re-establish a functional system?*

* The converse, i.e., release of the mitochondrial block by removal of ethidium bromide is not feasible because, in addition to the transcriptional block, exposure to this agent also produces irreversible effects on mtDNA; experiments with acriflavine, which circumvent this difficulty, are in progress.

Blocks exerted by shift-up and ethidium bromide are specific

The data shown in Fig. 1 demonstrate that in *ts*⁻136 a shift-up to 36°, a restrictive temperature for nuclear RNA synthesis in this strain (9), blocks incorporation of uracil into RNA outside, but is without effect on this process inside, the mitochondria. Conversely, exposure to ethidium bromide for 10 min completely blocks incorporation of this precursor into mtRNA at the restrictive temperature, or at 23°, the permissive temperature—as well as into mtRNA of the wild type at either temperature—without affecting cell-sap RNA.

Functional mitochondrial mRNA is unaffected by a shift-up but blocked by ethidium bromide

A shift-up of *ts*⁻136 to 36°, followed by incubation at this temperature for 60 min, is sufficient to eliminate all mRNA function in the cell sap, as measured by the disappearance of polysomal structures (9, 10), and the inability of these structures to catalyze polypeptide chain initiation or elongation (Table 1). As judged by any of these criteria cell-sap functions are, however, inert to exposure to ethidium bromide at either 36° or 23° (compare Fig. 3*A* and *C*) (as they are in the wild type). Conversely, functional mRNA-containing ribonucleoprotein particles, isolated from highly purified mitochondria, are unaffected by the elevated temperature, as measured by

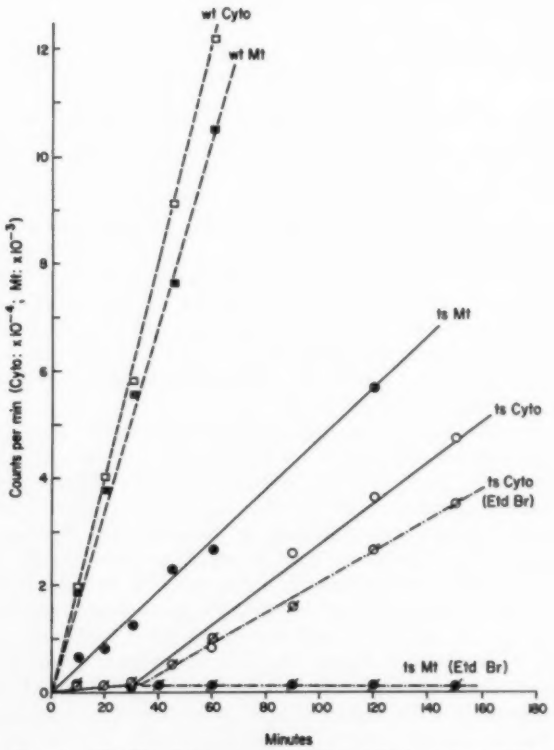

FIG. 2. [³H]Uracil incorporation after shift-down from 36° to 23°. Procedure as in Fig. 1, except that the spheroplasts were kept for 60 min at 36 and shifted down to 23°. Then 10 μg/ml of ethidium bromide was added to one sample and no drug to another. 20 min later [³H]uracil (5 μCi/ml) was added to the samples, and 10-ml aliquots were taken at the appropriate time. Symbols are as in Fig. 1.

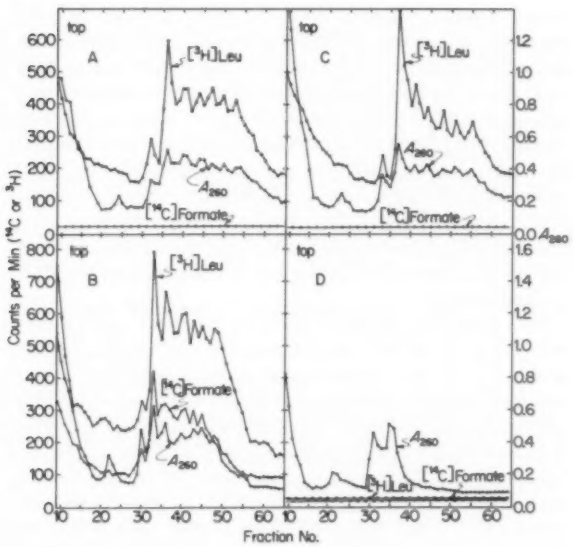

FIG. 3. Polypeptide synthesis on ribosomes. *ts*−136 cells were grown in YM-1L medium (200 ml each) to A_{600} = 0.4 and then shifted to 36°; after 60 min at this temperature one-half of the cells received 10 μg/ml of ethidium bromide. Then both samples were incubated 60 min longer at 36° before they were shifted down to 23° and incubated for 30 min. The cells were harvested and spheroplasts were made at 23°. They were suspended in YM-5L (supplemented with 10 μg/ml of ethidium bromide for the cells treated with this agent at 36°). After 30 min, [³H]leucine (5 μCi/ml) and [¹⁴C]formate (2.5 μCi/ml) were added. The reaction was stopped after 10 min by addition of crushed ice plus 100 μg/ml of cycloheximide and 4 mg/ml of chloramphencol. The spheroplasts were sedimented and lysed by blending in 0.5 M sorbitol–NMT buffer. Mitochondrial and cell-sap fractions were isolated. Mitochondria were washed by sedimentation from 5 mM EDTA–100 mM NH_4Cl–10 mM Tris·HCl in 0.5 M sorbitol and lysed in 2 ml of 2% Triton X-100–NMT buffer. The lysates were layered on top of a 0.3–1.4 M sucrose in NMT buffer linear gradient and centrifuged for 4 hr in an SW27 rotor in an L2 Beckman centrifuge, at 26,000 rpm. The gradients were fractionated from the top, and A_{260} and radioactivity were measured (11). *A* and *C*, cell sap; *B* and *D*, mitochondria; *A* and *B* in the absence of, *C* and *D* in the presence of ethidium bromide. Results similar to *D* were obtained when the cells incubated with ethidium bromide were analyzed just before the shift-down; analogous results for leucine were also found when 4 mg/ml of chloramphenicol was substituted for ethidium bromide. However, with this inhibitor the A_{260} profile resembled that shown in *B*! Thus, the technique can distinguish between programmed functional, but inhibited, particles and nonfunctional ones.

A_{260}, incorporation of leucine into nascent polypeptide chains or by chain initiation with formate (all in Fig. 3*B*). They also retain their ability to catalyze initiation of polypeptide chains, as measured by formation of fMet puromycin (11) or incorporation of leucine or formate into nascent chains (all shown in Table 1): all these activities, at either temperature, are eliminated by prior exposure to ethidium bromide. Similar results (not shown) are obtained with chloramphenicol, a specific inhibitor of mitochondrial translation, except that in this instance polysomal structures are retained.

TABLE 1. *Incorporation of leucine and formate into mitochondrial and cell-sap nascent chains (cpm)*

	Leucine		Formate		
Addition	Mt*	Cell sap	Mt	Cell sap	fMet puromycin Mt
	wild type (A364A)				
36°					
None	1970	9000	440	46	5790
Chloramphenicol	320	—	67	—	720
Cycloheximide	1830	240	460	42	5730
Ethidium bromide	510	—	130	—	1470
36 → 23°					
None	1080	5050	240	22	5140†
	ts−136				
36°					
None	1810	315	460	45	4320
Chloramphenicol	325	—	65	—	540
Cycloheximide	1690	270	440	45	4330
Ethidium bromide	520	—	100	—	990
36 → 23°					
None	1080	850	290	29	5240†
Cycloheximide	1130	35	280	24	
Chloramphenicol	150	—	54	—	

* Mt, mitochondria.

† 23° without prior incubation at 36°.

All data are the means of duplicate or triplicate determinations of total cpm by spheroplasts. A *dash* indicates not measured. Spheroplasts (prepared at 23°!) were equilibrated for 10 min at 23° and then shifted to 36°; after 20 min aeration at this temperature they were divided into 50-ml aliquots. Appropriate drugs (4 mg/ml of chloramphenicol; 100 μg/ml of cycloheximide; 10 μg/ml of ethidium bromide) were added, and the samples were aerated for an additional 10 min (ethidium bromide, for 20 min). Precursors (5 μCi/ml of [³H]leucine; 2.5 μCi/ml of [¹⁴C]formate) were added, and incorporation was for 10 min. Spheroplasts were harvested, lysed, and ribosomes were isolated from the mitochondrial and cell-sap fractions (11; see also Fig. 3) by sedimentation for 120 min at 105,000 × *g*. Aliquots on filters were processed for counting. In the 36 → 23° experiment, prior incubation at 36° was for 60 min, followed by equilibration at 23° for 35 min, before addition of inhibitors. fMet puromycin was determined in a separate experiment, for measurement of chain initiation (11).

Shift-down restores function only to cell-sap ribosomes

When cells, previously incubated at 36° for 60–120 min, are restored to the permissive temperature of 23°, incorporation of uracil into cell-sap RNA resumes after a characteristic lag of 30 min. No such lag is observed for incorporation into mtRNA (Fig. 2). When these cells, previously completely blocked in *all* RNA synthesis by exposure to ethidium bromide at 36°, are restored to 23°, the rate of uracil-incorporation returns (after a similar lag) to that characteristic for this regime (Fig. 2). Coincident with this return the residual ribosomes in the cell sap (9) become reprogrammed into functional polysomal structures, whether or not ethidium bromide is present (Compare Fig. 3*A* and *C*, and Table 1). On the other hand, there is no evidence for import of any labeled RNA into mitochondria (Fig. 2). In another experiment, spheroplasts were exposed to a 30-min labeling period (with ethidium bromide added) 20

min after the shift-down and then to a chase of unlabeled uracil for an additional 60 min. 8600 cpm were incorporated into the cell sap, of which 1300 were retained after the chase (i.e., most was probably mRNA); no incorporation above background was observed in the mitochondrial fraction either before or after the chase. More conclusively, perhaps, in the presence of ethidium bromide polysomes decay and, in contrast to the cell-sap structures, the residual intramitochondrial ribosomes and subunits do not become reprogrammed for the support of polypeptide chain elongation or even initiation (compare Fig. 3*B* with Fig. 3*D*).

DISCUSSION

Our results show that the temperature-sensitive mutant, *ts*$^{-}$136, in conjunction with the inhibitor ethidium bromide, can be used to study the relative contribution and importance of nuclear and mitochondrial RNA synthesis. They also indicate that formation and decay of *functional* polysomes measured by incorporation of a radioactive precursor into nascent polypeptide chains on these particles provides a sensitive, qualitative assay for the presence of functional mRNA not only in the cell sap (9, 10), but in mitochondria (11) as well.

By means of our particular experimental design we have attempted to answer whether import of mRNA into mitochondria is either necessary or sufficient to program their ribosomes for active polypeptide synthesis; we find that such import is completely dispensable, while the converse holds for mRNA synthesized inside the particle in a process sensitive to ethidium bromide—presumably on mtDNA. One possible source of ambiguity in the interpretation of these results resides in the observation that ethidium bromide may inhibit mitochondrial translation directly, and not just as a consequence of its interference with transcription (1, 12). The results of the temperature-shift experiments could then be interpreted in terms of such a translational inhibition of mitochondrial polysomes programmed with a population of very long-lived mRNAs of nuclear origin. We consider this alternative unlikely for the following three reasons: (*i*) Since we have shown that ethidium bromide is a specific and potent inhibitor of mitochondrial transcription under precisely the conditions of this particular experiment, the most parsimonious interpretation would rely on this demonstrated fact. (*ii*) Since we have repeated the shift-down experiments after prior exposure to 36° for as long as 2 hr, the half-life of the hypothetical mRNA would have to be >2 hr, i.e., half a generation time under conditions where the same species in the cell-sap breaks down within 23 min (9). (*iii*) This "stable" mRNA would then have to decay rapidly under conditions of the postulated translation block by ethidium bromide (at either 36° or 23°); this decay is contrary to the effect of most translational inhibitors on polysomal stability (13), including that of cycloheximide on cell-sap polysomes (10), or of chloramphenicol on mitochondrial ones in these strains. Another possible source of ambiguity is that many of the experiments made use of spheroplasts rather than intact cells, and it might be argued that these structures are no longer capable of supporting certain events required for complete cellular function, specifically the mitochondrial import of nuclear mRNA. This *ad hoc* hypothesis is highly unlikely; yeast spheroplasts have been shown to be fully competent to biosynthesize nucleic acids and proteins in Hartwell's laboratory (9, 10) as well as in our own (11), including the elaboration of active mitochondria after release from catabolite repression. Finally, one might argue that ethidium bromide blocks not the synthesis of mitochondrial mRNA but precisely the transport into mitochondria of the nuclear variety: any substantial contribution of this mechanism is ruled out by the results of the shift-up experiments.

We, therefore, conclude that, at least in ascomycetes, transcripts of mtDNA are sufficient to account for the programming of the protein-synthesizing machinery of the organelle, and the latter need not depend on the import of mRNA transcribed from nuclear genes. Similar inferences have been drawn by Reijnders *et al.* from hybridization data of total stable mtRNA with nuclear DNA (14). Therefore, for these organisms at least, the only polypeptide products translated by the organelle are the ones encoded in the genome of the organelle.

We thank Prof. Leland H. Hartwell for supplying us with the strains required for this investigation and for his counsel concerning their use, and Dr. Fred Feldman for many stimulating discussions. This research was supported by Research Grant PHS R01 GM 12228 from the Institute of General Medical Sciences. HRM is a recipient of a Research Career Award K06 GM 05060 from this Institute. KD was supported by Consejo de Desarrollo Cientifico y Humanistico, Universidad Central de Venezuela. This is publication no. 2137 from the Chemical Laboratories, Indiana University.

1. For recent references see Borst, P. (1972) *Annu. Rev. Biochem.* **41,** 333–376; Küntzel, H. (1971) *Curr. Top. Microbiol. Immunol.* **54,** 94–118.
2. Dawid, I. B. (1970) "The Control of Organelle Development," in Symp. 24 of *Soc. for Exp. Biol.* ed. Miller, P. L. (Cambridge University Press), p. 227; (1972) *Oogenesis.* ed. Biggers, J. D. & Schuetz, A. W. (Government Printing Office, Washington, D.C.).
3. Swanson, R. F. (1971) *Nature* **231,** 31–33.
4. Aloni, Y. & Attardi, G. (1971) *J. Mol. Biol.* **55,** 251–270; *Proc. Nat. Acad. Sci. USA* **68,** 1737–1761.
5. Attardi, B. & Attardi, G. (1967) *Proc. Nat. Acad. Sci. USA* **58,** 1051–1058.
6. South, D. J. & Mahler, H. R. (1968) *Nature* **216,** 1226–1232; Mahler, H. R. & Perlman, P. (1971) *Biochemistry* **10,** 2979–2990.
7. Fukuhara, H. & Kujawa, C. (1970) *Biochem. Biophys. Res. Commun.* **41,** 1002–1008; Zylber, E., Vesco, C. & Penman, S. (1969) *J. Mol. Biol.* **44,** 195–204.
8. Weislogel, P. O. & Butow, R. A. (1971) *J. Biol. Chem.* **246,** 5113–5119.
9. Hutchison, H. T., Hartwell, L. H. & McLaughlin, C. S. (1969) *J. Bacteriol.* **99,** 807–814.
10. Hartwell, L. H., Hutchison, H. T., Holland, T. M. & McLaughlin, C. S. (1970) *Mol. Gen. Genet.* **106,** 347–361.
11. Mahler, H. R., Dawidowicz, K. & Feldman, F. (1972) *J. Biol. Chem.*, **247,** 7439–7442.
12. Kellerman, G. M., Biggs, D. R. & Linnane, A. W. (1969) *J. Cell Biol.* **42,** 378–391.
13. Pestka, S. (1971) *Annu. Rev. Biochem.* **40,** 697–710.
14. Reijnders, L., Kleisen, C. M., Grivell, L. A. & Borst, P. (1972) *Biochim. Biophys. Acta* **272,** 396–407.

Proc. Nat. Acad. Sci. USA
Vol. 70, No. 1, pp. 115–119, January 1973

Stability of Cytoplasmic Messenger RNA in HeLa Cells

(actinomycin D/benzoylated-DEAE-cellulose/poly(T)-cellulose/nucleoside triphosphate pools/cold chase)

WILLIAM MURPHY AND GIUSEPPE ATTARDI

Division of Biology, California Institute of Technology, Pasadena, Calif. 91109

Communicated by Norman Davidson, October 24, 1972

ABSTRACT **The metabolic stability of pulse-labeled or long-term labeled messenger RNA (mRNA) from cytoplasmic free polysomes was measured in HeLa cells, with chase conditions that do not involve inhibitors of RNA synthesis, and chromatography on benzoylated-DEAE-cellulose or poly(T)-cellulose for isolation of mRNA. For these studies, a new chase technique was developed that allows analysis of the stability of mRNA labeled during a short [^{3}H]uridine pulse. Pulse-labeled and long-term labeled mRNA were found to decay with an estimated average half-life of about 2 and 3 days, respectively, much longer than hitherto assumed.**

Because of the lack of an effective cold-chase technique and of methods for purification of messenger RNA (mRNA), the main approach used for the study of metabolic stability of cytoplasmic mRNA in animal cells has been the analysis of the quantitative behavior and synthetic capacity of cytoplasmic polysomes after further mRNA synthesis has been arrested by actinomycin D. The results of these experiments have suggested that, while in differentiated cell types such as erythrocytes (1, 2) or liver cells (3) the bulk of the mRNA is considerably stable, the half-life of cytoplasmic mRNA in rapidly growing cells is relatively short, 3–4 hr (4, 5). The basic premise upon which these experiments rely is that polysome breakdown is a direct measurement of normal degradation of pre-existing mRNA. Recent studies on the secondary toxic effects of actinomycin D raise serious doubts as to the validity of this assumption (6–8).

Because most of these toxic effects of the drug would lead to an underestimate of the stability of mRNA in rapidly growing cells, we felt it to be essential that this question be again examined under physiological conditions. In the present work, we report experiments by which we have measured the half-life of mRNA of cytoplasmic free polysomes in HeLa cells, using chase conditions that do not involve inhibitors of RNA synthesis, and chromatography on benzoylated-DEAE–cellulose or poly(T)–cellulose for isolation of mRNA. We found that the stability of the bulk of the free polysome mRNA population is much greater than previously reported, with an estimated average half-life of about 3 days.

MATERIALS AND METHODS

Cells and Method of Growth. HeLa cells were grown in suspension in modified Eagle's medium (9) with 5% calf serum.

Abbreviations: SDS, sodium dodecyl sulfate; BDC, benzoylated-DEAE–cellulose.

Labeling Conditions. For short-term labeling of RNA or DNA, HeLa cells (1 to 2 × 10^5/ml) were exposed to [5-^{3}H]-uridine (20–30 Ci/mmol; 0.1 μCi/ml in the kinetic experiments, 2.5–5.0 μCi/ml in the experiments for RNA analysis), or to [8-^{3}H]adenosine (28 Ci/mmol, 1.0 μCi/ml), or to [*methyl*-^{3}H]thymidine (29 Ci/mmol, 1 μCi/ml), for the times indicated.

Long-term labeling of mRNA for stability measurements was performed by growth of the cells (0.5 to 1.0 × 10^5/ml) in the presence of 2.5 μCi/ml of [5-^{3}H]uridine (20–30 Ci/mmol) for 24 hr. In order to ensure, as much as possible, a uniform incorporation of the precursor into the mRNA over the entire 24-hr period, additional label was administered at 8, 16, and 22 hr of incubation to bring the amount of radioactivity in the medium to its original level (10). As an internal control to monitor the recovery of mRNA from various samples in the analysis of mRNA stability, a constant amount of cells grown for 1 or 2 generations in the presence of 0.03 μCi/ml of [2-^{14}C]uridine (62 Ci/mol), with an additional 0.03 μCi/ml of label being administered 2–3 hr before harvesting, was added to the sample for each time point.

For measurement of the rate of protein synthesis, HeLa cells, suspended at 1 × 10^5/ml in modified Eagle's medium with 0.2 mM leucine and 5% dialyzed serum, were incubated with 0.2 μCi/ml of [^{3}H]leucine (40 Ci/mmol). Total acid-precipitable, alkali-resistant radioactivity incorporated was determined (11).

For analysis of labeling of nucleotide pools, HeLa cells, suspended at 1 × 10^6/ml in modified Eagle's medium with 1 mM phosphate and 5% dialyzed serum, were grown in the presence of carrier-free [^{32}P]orthophosphate (1 μCi/ml) for 12–24 hr. By this time, the nucleoside triphosphate pools are uniformly labeled with ^{32}P (12). After ^{32}P labeling, [5-^{3}H]uridine (2.5–5.0 μCi/ml), or [*methyl*-^{3}H]thymidine (1 μCi/ml), or [8-^{3}H]adenosine (1.0 μCi/ml) was added to the cultures for the times indicated.

Chase Conditions. "Cold" Chase: After cells were labeled for 30 min or 24 hr with [5-^{3}H]uridine, unlabeled 10 mM uridine and 5 mM cytidine were added. The culture was then cooled in an ice bath to 4° (in a 12-min period), allowed to remain at this temperature for 3 hr under gentle stirring, warmed in a water bath to 37° (in 12 min), and kept thereafter at this temperature. Warm Chase: 10 mM unlabeled uridine (in some experiments, also 5 mM unlabeled cytidine) were added to the growth medium, or the cells were centrifuged and suspended in fresh medium, as specified below.

Free Polysome Isolation. A HeLa-cell extract was prepared (13), with 1.5 mM $MgCl_2$ in the homogenization medium. Free polysomes were isolated from the postmitochondrial supernatant by centrifugation through a discontinuous sucrose gradient (14). The polysome pellet was suspended in 1.0 ml TKM [50 mM Tris buffer, pH 6.7 (25°)–25 mM KCl–2.5 mM $MgCl_2$], layered on a 15–30% sucrose gradient in TKM, and centrifuged for 90 min at 25,000 rpm at 2° in an SW25.1 Spinco rotor. For analysis of EDTA sensitivity of the polysomes, the polysome pellet was dissolved in TKV (TKM, with 10 mM EDTA instead of $MgCl_2$) and centrifuged, as described above, through a 15–30% sucrose gradient in TKV.

RNA Extraction and Analysis. RNA was extracted from polysomes by the sodium dodecylsulfate (SDS)–Pronase–phenol method (15). For sedimentation analysis, the RNA was centrifuged for 15 hr at 26,000 rpm at 20° in an SW25.3 Spinco rotor through a 15–30% sucrose gradient (prepared over a 1-ml cushion of 64% sucrose) in SDS buffer.

Benzoylated-DEAE-Cellulose (BDC) Chromatography. Polysomal RNA was analyzed on BDC columns (16). The resin was either prepared in this laboratory or purchased from Schwarz/Mann or Boehringer–Mannheim Corp.

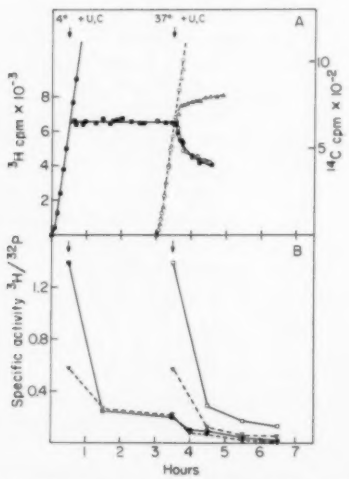

FIG. 1. (*A*) Kinetics of net incorporation of [^{3}H]uridine by HeLa cells and decay of labeled RNA by three different pulse-chase techniques. Three HeLa cell cultures were labeled for 30 min with [^{3}H]uridine; one was cooled for 3 hr in the presence of 10 mM uridine and 5 mM cytidine, and then warmed to 37° (■——■), the other two were chased at 37° by addition of 10 mM uridine (△——△), or 5 μg/ml of actinomycin D (○——○). The data plotted are the acid-precipitable cpm in aliquots of the cultures after the cells were washed with a salt solution. The labeling data for the latter two cultures are displaced on the axis of abscissae, so as to compare the effectiveness of the chase at 37° with that of the cold-treated culture. The actinomycin experimental data are redrawn from Houssais and Attardi (20). (*B*) Specific activities of the UTP and CTP acid-soluble pools in cells labeled for 30 min with [^{3}H]uridine and either subjected to a "cold" chase and then warmed, or directly chased at 37° with 10 mM uridine and 5 mM cytidine. The cells had been previously labeled for 24 hr with [^{32}P]orthophosphate, and the specific activity data are expressed as ^{3}H to ^{32}P ratios (11). "Cold" chase: ■——■, UTP; ▼——▼,C TP. Warm chase: □——□, UTP; ▽——▽, CTP.

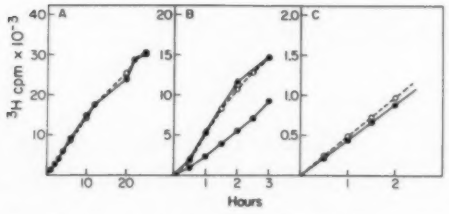

FIG. 2. Kinetics of net protein (*A*), RNA (*B*), or DNA synthesis (*C*) in cells subjected to "cold" chase. The time-courses of synthesis measured in "cold" chased cultures immediately after the cooling period, ●——● or, for RNA, also after 3 hr rewarming ▲——▲, are compared to those of untreated cultures at the same cell concentration ○——○. The incorporation of [*8*-^{3}H]adenosine into RNA was measured as acid-precipitable cpm solubilized by treatment with 0.5 N NaOH at 30° for 22 hr. The [*8*-^{3}H]-adenosine- and [^{3}H]thymidine-labeling data are corrected for differences in specific activity of the ATP and TTP pools, respectively.

Poly(T)-Cellulose Chromatography was performed according to Kates *et al.* (17), except that RNA was applied to the column in 0.12 M NaCl–10 mM Tris, pH 7.4–1 mM EDTA, and the column was washed with the same buffer.

Nucleotide Pool Analysis. The nucleoside triphosphates were isolated from cells long-term labeled with [^{32}P]orthophosphate, and labeled for different times with tritiated precursors, by two-dimensional thin-layer chromatography on PEI-cellulose, as described (11).

RESULTS

Effectiveness and physiological effects of the "cold" chase technique

The conventional pulse-chase technique, involving the use of a large excess of unlabeled precursor to dilute the intracellular pools, is ineffective in the study of RNA metabolism in animal cells because of the continued RNA labeling from the large triphosphate pools, which are fed by the turnover of unstable RNA species. In view of the need for an effective chase technique in the present work, an effort was made to develop chase conditions that would overcome this difficulty.

Since at least some of the enzymes involved in nucleotide phosphorylation may remain active at reduced temperatures (18, 19), a chase procedure was devised in which addition of an excess of unlabeled precursors was coupled with a relatively brief cold treatment, in an attempt to wash out the triphosphate pools while RNA synthesis and degradation are arrested*. A comparison of this "cold" chase with a warm chase using an equal concentration of exogenous unlabeled uridine is shown in Fig. 1*A*. After a 30-min [^{3}H]uridine pulse, the warm chase fails to stop further incorporation of label into RNA, which continues for at least 2 hr. By contrast, after the "cold" chase, there is an immediate decay of the incorporated label, with a reduction of about 35% during a 40-min period after the culture is rewarmed. The initial kinetics of decline in acid-precipitable counts per min (cpm) is similar to that found after further RNA synthesis is blocked with 5 μg/ml of actinomycin D; this decay represents in most part the turnover of heterogeneous nuclear RNA (20), which

* A detailed description of this procedure will be published elsewhere.

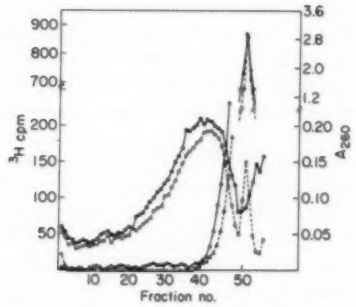

FIG. 3. Sedimentation patterns in sucrose gradients of free polysomes from cells labeled with [^{3}H]uridine for 20 min before and after disruption with EDTA. The free polysome pellet from 1.6×10^8 cells was divided into two equal parts: one half was analyzed in sucrose gradient in TKM, the other half was analyzed in sucrose gradient in TKV. O- - -O, A_{260} TKM; Δ- - -Δ, A_{260} TKV; ●——●, ^{3}H cpm TKM; ▲——▲, ^{3}H cpm TKV.

in the warm chase is masked by a continued high rate of incorporation. The basis for the effectiveness of the "cold" chase procedure is shown in Fig. 1*B*. During the 3-hr "cold" treatment, there is no change in the amount of incorporated radioactivity, while the specific activities of the UTP and CTP pools are reduced to 13 and 38%, respectively, of their original values. This reduction in specific activity is the result of two cooperative effects: the increase by a factor of about 2.5 in the UTP pool size, due to the high uridine concentration in the medium†, and a loss of 70% of the total acid-soluble radioactivity from the cells.

In Fig. 2, the kinetics of net synthesis of RNA, DNA, and protein after the "cold" chase are compared to control kinetics. The net incorporation of [^{3}H]leucine into protein starts immediately after rewarming (within 2 min from transfer of the culture to the 37° water bath), and proceeds at a rate identical to that of the control culture, when analyzed both within the first few minutes after rewarming (not shown) and over an extended period (Fig. 2). These observations suggest that not only does the "cold" chase not impair polysome protein synthesis, but also it allows the arrival of mRNA at the polysomes to occur at a normal rate. Similarly, the measured rate of DNA synthesis is about 90% that of control, the difference being presumably not significant. This result, coupled with an observed steady exponential increase in cell number and a normal generation time (about 24 hr), indicates that no significant degree of synchronization was induced by the cold shock. There does exist, however, a transitory inhibition of about 35% of the rate of net RNA synthesis in the cell. This inhibition, which is caused by the high concentration of exogenous uridine, gradually disappears until, by 3 hr, the rate of net RNA synthesis returns to normal.

Isolation of free polysome mRNA

Since benzoylated-DEAE-cellulose (BDC) chromatography has been successfully used in purification of bacterial mRNA (16), isolation of HeLa cell mRNA was attempted by such a procedure. Free polysomes from cells pulse-labeled for 20 min with [^{3}H]uridine and uniformly labeled with [^{14}C]uridine were isolated. These polysomes are more than 95% pure, as judged by the sensitivity to EDTA of both the UV absorbing and the radioactive material (21) (Fig. 3). Fig. 4*A* shows the sedimentation profile of polysomal RNA. Clear [^{14}C]-uridine peaks corresponding to ribosomal RNA (rRNA) and transfer RNA (tRNA) are seen, while the pulse-labeled mRNA shows a heterogeneous sedimentation profile extending from about 8 S to more than 40 S, with a broad peak centered around 20 S. The small peak of ^{3}H label found at the bottom of the tube is RNA that has been prevented from pelleting by the cushion of 64% sucrose.

The portion of the gradient indicated by arrows in Fig. 4*A* was pooled and chromatographed on BDC at pH 3.5. Fig. 4*B* shows the RNA eluted, as a single peak, with 1 M NH_4Cl in urea buffer (8 M urea–0.1 M acetic acid, pH 3.5); this RNA includes about 90% of the ^{3}H-labeled mRNA (in different experiments, the yield of mRNA varied between 70 and 95%) and only about 5% of the ^{14}C-labeled RNA. The sedimentation profile of the eluted pulse-labeled material is identical to that shown in the original gradient (Fig. 4*C*), showing that there was no degradation or preferential isolation of any size class of mRNA. The ^{14}C curve shows a small peak at 18 S and a smaller one at 28 S; these peaks presumably represent a small amount of eluted rRNA, corresponding to about 2% of that originally present in the preparation.

The basis of the separation on BDC at pH 3.5 of mRNA and rRNA is not clear (16). Thus, although this procedure appeared to be effective for isolation of HeLa cell mRNA, we felt it to be desirable to check the results with an independent technique. For this purpose, the procedure for isolation of mRNA from mammalian and other eukaryotic polysomes on poly(U)- or poly(T)-cellulose columns (22, 23) [exploiting the existence of poly(A) stretches covalently linked to the mRNA molecules (22–24)] was used. The sedi-

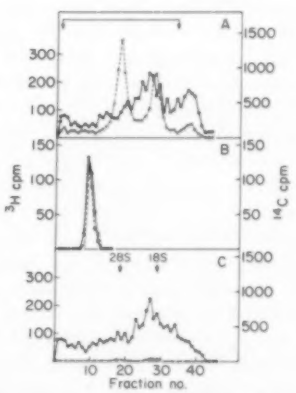

FIG. 4. Sedimentation patterns in sucrose gradients of HeLa cell polysomal RNA before and after BDC chromatography. (*A*) Sedimentation profile of RNA extracted from a mixture of cells labeled for 20 min with [^{3}H]uridine and cells labeled for 48 hr with [^{14}C]uridine and chased for 24 hr with 1 mM uridine. (*B*) The portion of the gradient indicated by *arrows* in (*A*) was collected by ethanol precipitation and centrifugation, and chromatographed on BDC, pH 3.5. The RNA eluted with 1 M NH_4Cl in urea buffer is shown. (*C*) A portion of the RNA eluted from the BDC column was run in sucrose gradient as in (*A*). ●——●, ^{3}H cpm; O- - -O, ^{14}C cpm.

† No such effect was observed for the CTP pool (its size was about one-tenth of that of UTP after the chase), while the ATP pool was reduced to one half.

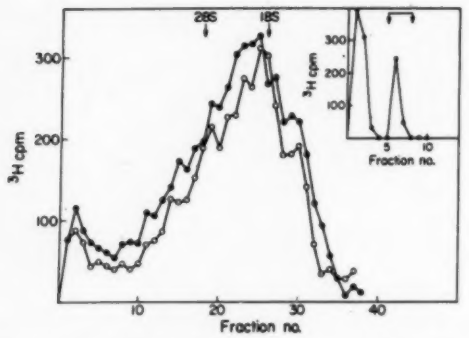

FIG. 5. Comparison of sedimentation patterns of pulse-labeled polysomal RNA isolated by BDC or poly(T)–cellulose chromatography. A portion of polysomal RNA from cells labeled with [^{3}H]uridine for 30 min was run on a poly(T)–cellulose column (*insert*), and an equal portion on a BDC column. The material eluted with 10 mM Tris, pH 7.4–1 mM EDTA from the poly(T)–cellulose column (*arrows* in *insert*) and that eluted from the BDC column were collected by ethanol precipitation and centrifugation, and run on sucrose gradients, as in Fig. 4. ●——●, poly(T)–cellulose-isolated RNA; ○——○, BDC-isolated RNA.

mentation patterns of mRNA pulse-labeled for 30 min isolated on a BDC and a poly(T)–cellulose column (insert) are compared in Fig. 5. The ^{3}H profiles of the mRNA are substantially identical, with the recovery of the ^{3}H label being about 15% higher with the poly(T)–cellulose column. A similar sedimentation pattern of HeLa mRNA separated on a poly(T)–cellulose column has been recently published (25). In the present work, both BDC and poly(T)–cellulose chromatography were used to isolate mRNA for analysis of its metabolic stability.

Metabolic stability of free polysome mRNA

By the techniques described above, the metabolic stability of free polysome mRNA was investigated. In order to be able to follow the fate of both the faster turning over and the more stable components of mRNA, the cells were labeled either for a short time (30 min) or for 24 hr.

Fig. 6 summarizes the results of several experiments measuring the rate of decay, after "cold" chase, of free polysome mRNA labeled for 30 min or for 24 hr with [^{3}H]uridine, and isolated by either BDC or poly(T)–cellulose chromatography. The zero-time point in these experiments was measured immediately after the temperature of the rewarmed culture reached 37°. In the experiments involving a 30-min pulse, this zero-time value was corrected (see legend of the figure) both for the arrival at the polysomes of mRNA labeled during the pulse (insert) and for continued incorporation of the label remaining in the nucleotide pools. No such correction was applied to the 24-hr labeled mRNA, because of its small value. mRNA labeled with [^{3}H]uridine for 30 min and isolated by BDC or poly(T)–cellulose chromatography decays with an approximately first-order kinetics, with a half-life of about 2 days (Fig. 6*A*). mRNA labeled with [^{3}H]uridine for 24 hr and isolated by BDC chromatography also appears to decay exponentially with a half-life that, by extrapolation of the curve, was estimated to be about 3 days (Fig. 6*B*).

As a control for any possible side effects of the "cold" chase that might lengthen the life-time of the mRNA, HeLa cells were labeled for 24 hr with [^{3}H]uridine and suspended in fresh medium without added uridine or cytidine. Fig. 6*B* shows that the metabolic stability of the mRNA chased in this manner, isolated by either BDC or poly(T)–cellulose chromatography, is close to that obtained after "cold" chase.

DISCUSSION

The main observation reported here is that in HeLa cells cytoplasmic mRNA is endowed with a much greater stability than has been assumed up to now. The average half-life of the bulk of free polysome mRNA in these cells is estimated to be about 3 days.

The similarity of half-life between mRNA labeled for 30 min and for 24 hr suggests that there is no large subpopulation of unstable mRNA in HeLa cells. We do not know, however, whether the measured decay results from a random degradation of the various molecular species of mRNA, or whether there are different classes of mRNA with different half-lives. The existence of mRNA species less stable than

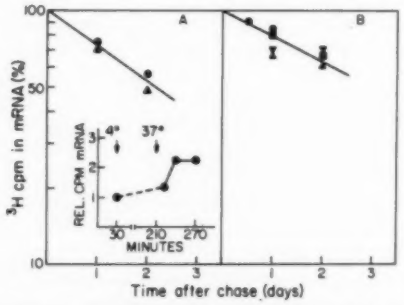

FIG. 6. Kinetics of decay of free polysome mRNA. (*A*) Equal samples of HeLa cells, labeled for 30 min with [^{3}H]uridine and subjected to the "cold" chase, were mixed, at different times, with the same amount of long-term [^{14}C]uridine-labeled cells; free polysome mRNA was extracted and purified by BDC (●) or poly(T)–cellulose(▲) chromatography. The amounts of [^{3}H]-uridine-labeled mRNA at different times have been normalized for recovery on the basis of the ^{14}C label. The zero-time value (determined after warming the culture to 37°) has been corrected: (*i*) for the continued arrival at the polysomes of mRNA labeled during the 30-min pulse, on the basis of the increment in labeled mRNA isolated on poly(T)–cellulose 1 hr after rewarming (*insert*), after subtraction of the small contribution of new synthesis from the labeled pools, estimated as described below [the increment measured relative to the amount at the end of the pulse would correspond to a mRNA pool equivalent to 12 min of synthesis, in good agreement with previous observations (21)]; (*ii*) for the continued synthesis from the labeled uridine and cytidine nucleotides; the fractional increase due to these nucleotides was estimated from the ratio of the integral of the UTP and CTP pool labeling in the 3-hr interval after warming (Fig. 1*B*) to that in the interval 0–30 min (estimated from Fig. 1, ref. 26). No account was taken of the 35% depression in rate of RNA synthesis; its effect would be small and in any case would increase the estimate of mRNA stability. (*B*) Equal samples of HeLa cells were labeled for 24 hr with [^{3}H]uridine and subjected either to the "cold" chase, with the mRNA being isolated by BDC (●,■), or to resuspension in fresh medium at 37°, with the mRNA being isolated by BDC(▼) or poly(T)–cellulose (▲) chromatography. The data have been normalized for recovery of the mRNA on the basis of long-term [^{14}C]labeled mRNA from cells added as internal control.

bulk RNA is hinted at by the somewhat shorter lifetime measured for the mRNA labeled for 30 min, as compared to that labeled for 24 hr. One component of this shorter-lived mRNA fraction is possibly the histone messenger (5, 27). Likewise, the analysis of the decay of mRNA has not been extended for a long enough time to exclude the existence of a fraction of the mRNA population with a half-life considerably longer than the average. Although there is a slight suggestion of a leveling off of the decay curve of mRNA labeled for 24 hr, further work is needed to verify this point.

The considerable stability shown here for the bulk of free polysome mRNA in a rapidly growing mammalian cell line provides a striking contrast to the situation in bacteria, where the majority of mRNA is short-lived (28). This difference presumably underlies a fundamental difference in regulation of genetic expression in the two types of organisms. While in bacteria this regulation operates mainly at the level of transcription (29), in animal cells translational mechanisms of control are likely to play a prominent role.

The average half-life of cytoplasmic mRNA previously estimated in HeLa and L cells with actinomycin D (4, 5) (3–4 hr) was much shorter than that measured here. This result implies that the assumption that the polysome breakdown caused by actinomycin D is the consequence of normal degradation of pre-existing mRNA was not correct. The actual mechanism of drug-induced polysome decay is not known. This polysome breakdown may represent only one aspect of the general cellular deterioration that actinomycin induces in HeLa cells (6–8). An alternative explanation is that the cells may possess a labile RNA or protein factor needed for polysome stability, whose continued synthesis or function is inhibited by the drug.

The new chase procedure described here has allowed the analysis of the stability of mRNA labeled during a short [^{3}H]uridine pulse. The mechanism by which the intracellular pools become depleted of radioactivity during the "cold" chase has not been studied in detail, although the experimental evidence indicates that expansion of the pools and release of the labeled precursors into the medium, presumably after dephosphorylation, play a role. With the exception of a transient depression by 35% of the rate of net RNA synthesis, no side effects of the "cold" chase were observed. A possible cause for this depression are the changes induced by the excess of uridine in the intracellular concentration of several nucleotides, which persist for at least 5 hr after rewarming the culture. The 3-hr recovery period may represent the time needed for the cells to adapt to these pool changes. The chase procedure described here provides a valuable alternative to the use of inhibitors of RNA synthesis for the study of the stability or processing of RNA species in animal cells under more physiological conditions.

In the present work, chromatography on BDC columns, first used for purification of bacterial mRNA (16), has been applied with success to isolation of mammalian mRNA. The observation that messenger of animal and bacterial cells behaves alike on this resin may point to a common property of mRNA of all organisms. The recovery of mRNA labeled with [^{3}H]uridine or [^{14}C]uridine for 30 min or 24 hr was slightly better (about 15%) after poly(T)–cellulose than after BDC chromatography. In the light of this observation, the finding that the BDC consistently gave a better yield of mRNA (6–9%) than the poly(T)–cellulose from the 1-day chased samples, and even better (16–18%) from the 2-day chased samples, may be significant as a possible indication of changes occurring in the mRNA with ageing, which affect its retention on poly(T)–cellulose columns.

These investigations were supported by a research grant from the U.S. Public Health Service (GM-11726) and by a National Science Foundation Predoctoral Fellowship to W. M. The help of Mrs. L. Wenzel and Miss G. Engel and the excellent technical assistance of Mrs. B. Keeley are gratefully acknowledged. The poly(T)-cellulose used here was a generous gift of Dr. J. Kates.

1. Djaldetti, M., Chui, D., Marks, P. A. & Rifkind, R. A. (1970) *J. Mol. Biol.*, **50**, 345–358.
2. Kabat, D. & Attardi, G. (1967) *Biochim. Biophys. Acta* **138**, 382–399.
3. Revel, M. & Hiatt, H. H. (1964) *Proc. Nat. Acad. Sci. USA* **51**, 810–818.
4. Penman, S., Scherrer, K., Becker, Y. & Darnell, J. (1963) *Proc. Nat. Acad. Sci. USA* **49**, 654–662.
5. Craig, N., Kelley, D. E. & Perry, R. P. (1971) *Biochim. Biophys. Acta* **246**, 493–498.
6. Sawicki, S. & Godman, G. (1971) *J. Cell Biol.* **50**, 746–761.
7. Soeiro, R. & Amos, H. (1966) *Biochem. Biophys. Acta* **129**, 406–409.
8. Revel, M., Hiatt, H. H. & Revel, J. P. (1964) *Science* **146**, 1311–1313.
9. Levintow, L. & Darnell, J. E. (1960) *J. Biol. Chem.* **235**, 70–73.
10. Aloni, Y. & Attardi, G. (1971) *J. Mol. Biol.* **55**, 251–270.
11. Pica-Mattoccia, L. & Attardi, G. (1972) *J. Mol. Biol.* **64**, 465–484.
12. Jeanteur, P. Amaldi, F. & Attardi, G. (1968) *J. Mol. Biol.* **33**, 757–775.
13. Attardi, B., Cravioto, B. & Attardi, G. (1969) *J. Mol. Biol.* **44**, 47–70.
14. Attardi, G., Parnas, H. & Attardi, B. (1970) *Exp. Cell Res.* **62**, 11–31.
15. Aloni, Y. & Attardi, G. (1971) *Proc. Nat. Acad. Sci., USA* **68**, 1757–1761.
16. Sedat, J., Lyon, A. & Sinsheimer, R. L. (1969) *J. Mol. Biol.* **44**, 415–434.
17. Sheldon, R., Jurale, C. & Kates, J. (1972) *Proc. Nat. Acad. Sci. USA* **69**, 417–421.
18. Scholtissek, C. (1967) *Biochim. Biophys. Acta* **145**, 228–237.
19. Scholtissek, C. (1971) *Eur. J. Biochem.* **24**, 358–365.
20. Houssais, J. F. & Attardi, G. (1966) *Proc. Nat. Acad. Sci. USA* **56**, 616–623.
21. Penman, S., Vesco, C. & Penman, M. (1968) *J. Mol. Biol.* **34**, 49–69.
22. Kates, J. (1970) *Cold Spring Harbor Symp. Quant. Biol.* **35**, 743–752.
23. Edmonds, M., Vaughan, M. H., Jr. & Nakazato, H. (1971) *Proc. Nat. Acad. Sci. USA* **68**, 1336–1340.
24. Darnell, J., Wall, R. & Tushinski, R. J. (1971) *Proc. Nat. Acad. Sci. USA* **68**, 1321–1325.
25. Nakazato, H. & Edmonds, M. (1972) *J. Biol. Chem.* **247**, 3365–3367.
26. Attardi, G. & Attardi, B. (1968) *Proc. Nat. Acad. Sci. USA* **61**, 261–268.
27. Borun, T. W., Scharff, M. D. & Robbins, E. (1967) *Proc. Nat. Acad. Sci. USA* **58**, 1977–1983.
28. Geiduschek, E. P. & Haselkorn, R. (1969) *Annu. Rev. Biochem.* **38**, 647–676.
29. Attardi, G., Naono, S., Rouviere, J., Jacob, F. & Gros, F. (1963) *Cold Spring Harbor Symp. Quant. Biol.* **28**, 363–372.

Proc. Nat. Acad. Sci. USA
Vol. 70, No. 1, pp. 120–123, January 1973

Structure and Chemical Synthesis of a Biologically Active Form of *Renilla* (Sea Pansy) Luciferin*

(bioluminescence/pyrazine derivative/coelenterates)

KAZUO HORI AND MILTON J. CORMIER

Department of Biochemistry, University of Georgia, Athens, Ga. 30601

Communicated by William D. McElroy, October 30, 1972

ABSTRACT **The structure of a biologically active form of *Renilla* (sea pansy) luciferin has been elucidated; this structure, confirmed by total chemical synthesis, is 3,7-dihydro-2-methyl-6-(*p*-hydroxyphenyl)-8-benzylimidazo [1,2-*a*] pyrazin-3-one. In the natural compound the methyl group at the 2 position is replaced by an unknown, more complex group. For this reason the synthetic compound is 10% as active as the natural compound in producing light with *Renilla* luciferase. However, the spectral properties of the two compounds are identical. In addition the rates of the luminescent reaction with both compounds are similar, and the color of the light produced is identical in each case.**

A compound isolated from the calcium-triggered photoprotein aequorin has been identified by Shimomura and Johnson [(1972) *Biochemistry* 11, 1602] to be 2-amino-3-benzyl-5-(*p*-hydroxyphenyl)pyrazine. This compound forms an integral part of the structure of *Renilla* luciferin. This, and other evidence, suggests that the structure elucidated for *Renilla* luciferin is a more general one associated with the luciferins of most, if not all, bioluminescent coelenterates.

From about 40,000 sea pansies (*Renilla reniformis*), obtained by dredging the ocean bottom at depths of 10–20 meters, one can obtain about 0.5 mg of pure *Renilla* luciferin. It is for this reason that elucidation of the structure of *Renilla* luciferin has been a difficult problem. We have accumulated a considerable amount of absorption data (U.V., visible, I.R.), as well as chemical and high-resolution mass spectroscopy data, over the last 10 years (1–3). These data, and the observation that several of the physical and chemical properties of *Renilla* luciferin were similar to those of *Cypridina* luciferin (1), led us to propose a partial tentative structure for *Renilla* luciferin that was similar to the structure of *Cypridina* luciferin (1). Due to the small amount of *Renilla* luciferin available and the ease with which luciferin is autooxidized good NMR data have never been available to us. Thus, several alternative structures were possible based on the mass spectroscopy data.

A choice between the various possible structures might have been a more difficult problem if it were not for several observations made by us and by other investigators in the field of bioluminescence who were working on problems that seemed at first unrelated. The key observations and ideas that led to the proper choice of structure are outlined below.

When the luminous tissues of bioluminescent coelenterates are extracted with EDTA-containing buffers, a protein can be isolated that exhibits a bluish luminescence upon the addition of calcium ions (4–7). Such proteins were termed "photoproteins." Recently, the existence of calcium-triggered photoproteins have been demonstrated in extracts of a wide variety of coelenterates such as *Obelia*, *Aequorea*, *Pelagia*, *Renilla*, *Mnemiopsis*, *Campanularia*, *Clytia*, *Phialidium*, *Lovenella*, *Ptilosarcus*, and *Diphyes* (7). Furthermore, the characteristics of these photoproteins were for the most part similar to those described for *Aequorea*.

These and other observations led us to look for possible biochemical similarities in the bioluminescence of coelenterates. Such similarities were indeed found. For example, components required for luminescence in *Renilla* were also found in several bioluminescent coelenterates examined such as *Aequorea*, *Obelia*, *Cavernularia*, *Ptilosarcus*, *Stylatula*, *Acanthoptilum*, *Parazoanthus*, and *Mnemiopsis* (8). Depending on the organism, these included one or more of the following: luciferyl sulfate, luciferase, photoprotein, and luciferin sulfokinase. The luciferyl sulfates isolated, including the one from *Aequorea*, produced light when added to the *Renilla* system, suggesting that the luciferins and luciferases from these coelenterates were either identical or very similar.

When *Aequorea* photoprotein is treated with urea and mercaptoethanol, a compound is released that has been designated AF-350 (9). We have noted that the absorption and fluorescence characteristics reported for AF-350 are very similar to those observed by us for *Renilla*-autooxidized luciferin (1).

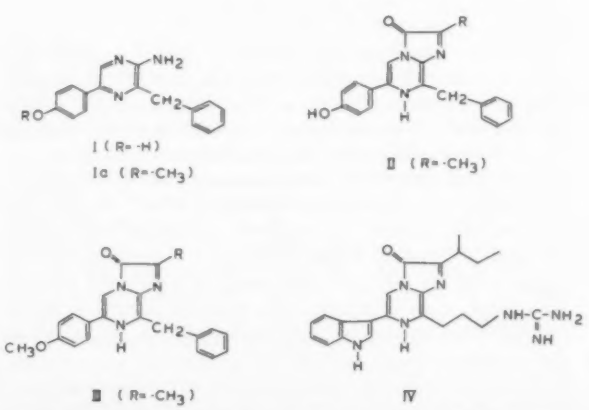

FIG. 1. Luciferin structures and some of their derivatives.

* This is paper no. XII of a series entitled, "Studies on the Bioluminescence of *Renilla reniformis*."

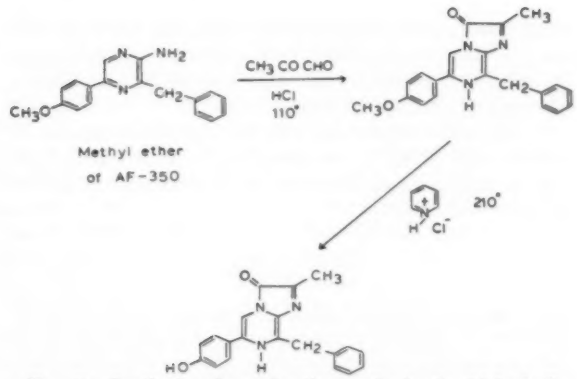

FIG. 2. Synthetic scheme for the synthesis of a biologically active form of *Renilla* luciferin.

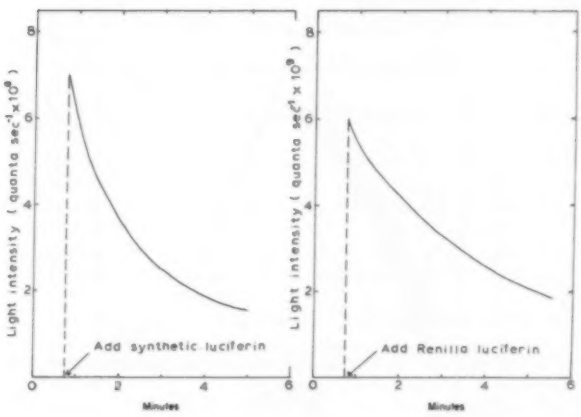

FIG. 3. A comparison of the rates of the luminescent reaction upon initiation with synthetic luciferin and *Renilla* luciferin. In each case, 1 nmol of luciferin was injected into a solution of *Renilla* luciferase.

The reported molecular weight of AF-350 is 277, which is also the strongest peak observed when *Renilla* luciferin is analyzed in a mass spectrometer. Further, the mass spectroscopy patterns of AF-350 and *Renilla* luciferin are essentially the same up to a mass of 277.

The structure of AF-350 (I in Fig. 1) was reported recently (10), and this structure has been confirmed by synthesis (11).

We noted that with minor modifications of our proposed structure of *Renilla* luciferin (1, 2) AF-350 becomes an integral part of the structure of *Renilla* luciferin.

Based on the above observations, as well as a consideration of the energetics of the luminescent reaction, we felt that a likely ring structure for *Renilla* luciferin would involve fusing an imidazole ring to structure I, thus converting it to structure II. With this in mind, structure II was synthesized and was found to be biologically active. This paper describes the synthesis and some of the biological properties of this newly synthesized luciferin.

MATERIALS AND METHODS

Luciferase was purified as described (12), with elimination of the acetone powder step. Native *Renilla* luciferyl sulfate was isolated as described (2), and was then converted to luciferin (15).

Absorption spectra were determined on a Cary model 14 Spectrophotometer. Absolute bioluminescence and fluorescence emission spectra were determined by use of an on-line spectrofluorimeter system (14) derived from a component fluorimeter (13).

Low-resolution mass spectral data were obtained on a Dupont Instrument model 21-490 single-focusing mass spectrometer equipped with a solid sample inlet probe, variable ionizing voltage control, and electrical ion detection. High-resolution mass spectral data were obtained with a CEC 21-110B mass spectrometer with photoplate recording of the spectra.

The methyl ether of AF-350 (Structure Ia) was synthesized as described (11). A biologically active *Renilla* luciferin derivative (Structure II) was synthesized from Ia by modification of the final steps involved in the synthesis of *Cypridina* luciferin (16). The method used was as follows: Compound Ia was reacted with methyl glyoxal in ethanol–12 N HCl 1:1 under an argon atmosphere in a sealed tube at 110° for 1.5 hr. The hydrochloride of Compound III was obtained in good yield (85%). It was converted to Compound II by treatment with anhydrous pyridine hydrochloride at 210° for 2 hr under an argon atmosphere in a sealed tube. The hydrochloride of Compound II was isolated from the reaction mixture in good yield (90%) by chromatography of the reaction mixture through LH-20 (2). The elution solvent was 80% methanol made 0.1 N with HCl. The hydrochloride of II was converted to free luciferin (II) by neutralizing it with phosphate buffer. Yellow crystals of II were obtained by heating an aqueous suspension of II at pH 2 under a hydrogen atmosphere, and allowing the solution to slowly cool. It should be noted that by use of derivatives of glyoxal other than methyl any desired substitution can be made at the 2-position of luciferin (II).

RESULTS

Structure II was synthesized from AF-350 (Structure I) according to procedures outlined under *Methods*. The synthetic scheme is shown in Fig. 2.

Absorption and fluorescence properties of II are identical to those observed for *Renilla* luciferin (1). In methanol solutions at pH 7.0, they both absorb at 262 and 433 nm and they both exhibit the same bathochromic shifts in acidic and basic environments.

The molar extinction coefficients of these two transitions were essentially the same as those reported for *Renilla* luciferin (1). In methanol solution at pH 7.0, both *Renilla* luciferin and II exhibit identical yellow–green fluorescence emissions (λ_{max} = 538 nm).

The molecular weight of II is 331. The mass spectral pattern of this compound was identical to that of *Renilla* luciferin up to a mass of 331. High-resolution mass analysis of *Renilla* luciferin, however, shows it to have a molecular weight of 513. Thus, the R group of II is rather complex in natural luciferin. However, it does not influence the spectral characteristics of luciferin, as judged by the absorption, fluorescence, and bioluminescence emission of luciferin as compared with II.

The synthetic compound (II) was biologically active, while I was totally inactive. When II was added to *Renilla* luciferase, light production occurred. As shown in Fig. 3, the rates of the light reaction were similar whether we used II or *Renilla* luciferin. Furthermore, the color of bioluminescence was identical

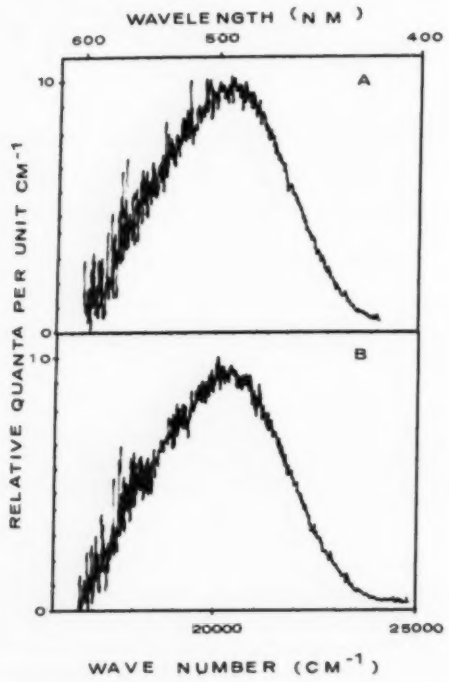

FIG. 4. A comparison of the color of bioluminescence upon initiation of the reaction with synthetic luciferin (*A*) and *Renilla* luciferin (*B*). In each case, the reaction was initiated by injection of about 0.1 μmol of luciferin into a solution of luciferase. These spectra were corrected for instrument spectral response with quinine bisulfate as spectral standard.

in both cases, as shown in Fig. 4. In each case the typical emission spectrum of the *Renilla in vitro* reaction was observed.

Because of the differences in the R group of II and that of *Renilla* luciferin as outlined above, II is only 10% as active as *Renilla* luciferin in producing light with *Renilla* luciferase. We compared the two compounds by comparing the peak intensities of the bioluminescent flash when equimolar amounts were injected into solutions of luciferase.

It was interesting to note that the methylated form of II (structure III in Fig. 1) was totally inactive in producing light with luciferase. Upon demethylation, biological activity was restored.

DISCUSSION

From the data reported here it appears that, with the exception of the R group in II, the structure of II and *Renilla* luciferin are identical. It is interesting to compare the structure of II with that of *Cypridina* luciferin (IV), whose structure and synthesis has also been accomplished (16–18). They both contain a pyrazine ring with a fused imidazole nucleus. The side chains, however, are considerably different. Side chains derived from tryptophan and arginine in *Cypridina* luciferin are replaced by those derived from tyrosine and phenylalanine in II. Since the heterocyclic ring structures of both compounds are the same, it is not surprising that we noted striking similarities in the absorption and fluorescence properties when *Renilla* and *Cypridina* luciferins were compared (1). A published tentative structure of *Renilla* luciferin (1, 2), which included an indole nucleus, was based on mass spectral data and a color test when *Renilla* luciferin is reacted with *p*-dimethylaminobenzaldehyde (3). However, the mass spectral data on *Renilla* luciferin can now be easily explained based on structure II.

As mentioned above, AF-350 (I) can be isolated when the calcium-triggered photoprotein of *Aequorea* is treated with urea and mercaptoethanol (9). It is most interesting to find that this structure is an integral part of the structure of *Renilla* luciferin. This observation reinforces our recent proposal that the luciferins and luciferases of bioluminescent coelenterates are similar or identical (8). In this connection, it should be mentioned that both *Renilla* luciferin and II will produce light

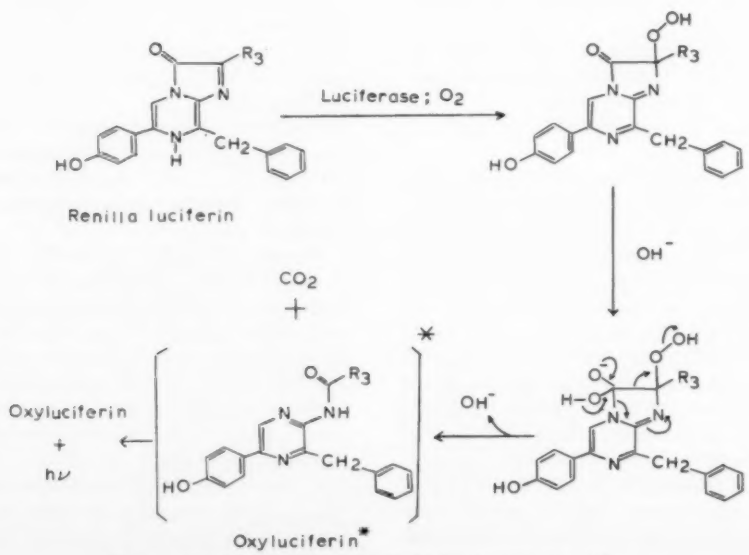

FIG. 5. Mechanism of the *Renilla* bioluminescence reaction.

when mixed with luciferases isolated from several coelenterates such as *Renilla*, *Ptilosarcus*, and *Stylatula*.

When the problem of the nature of photoproteins is considered, it is also interesting that we have isolated from *Aequorea*, and several other bioluminescent coelenterates, a *Renilla*-like luciferyl sulfate (8). Since *Renilla* extracts also contain luciferyl sulfate, as well as calcium-triggered soluble photoprotein, it seems reasonable to assume that luciferin, derived from luciferyl sulfate, somehow becomes an integral part of the photoprotein complex in coelenterates. This is an important consideration when one considers the overall energetics of the *Renilla* luminescent reaction, since about 70 kcal/mol quanta are required for the creation of the electronically excited state of the emitter. Based on structure II and on previous work on the mechanism of the luminescent reaction in *Renilla* with ^{18}O (19), a mechanism that satisfies the energy requirements and predicts the structure of the emitter (oxyluciferin) is shown in Fig. 5. Hydrolysis of the peptide bond in oxyluciferin would lead to the formation of AF-350 (I).

We thank Dr. R. E. Lovins of this department for providing the low- and high-resolution mass spectral data and Dr. J. E. Wampler for providing the absolute fluorescence and bioluminescence emission data. This work was supported by grants from the National Science Foundation and the U.S. Atomic Energy Commission. M. J. C. is a Career Development Awardee no. 1-K3-6M-333-07 of the U.S. Public Health Service. This is contribution no. 235 from the University of Georgia Marine Institute, Sapelo Island, Ga.

1. Hori, K. & Cormier, M. J. (1973) in *Chemiluminescence and Bioluminescence*, eds. Cormier, M. J., Hercules, P. M. & Lee, J. (Plenum Press, New York), in press.
2. Hori, K., Nakano, Y. & Cormier, M. J. (1972) *Biochim. Biophys. Acta* **256**, 638–644.
3. Hori, K. & Cormier, M. J. (1966) *Biochim. Biophys. Acta* **130**, 420–425.
4. Shimomura, O., Johnson. F. H. & Saiga, Y. (1962) *J. Cell. Comp. Physiol.* **59**, 223–240.
5. Shimomura, O., Johnson, F. H. & Saiga, Y. (1963) *J. Cell. Comp. Physiol.* **62**, 1–8.
6. Shimomura, O., Johnson, F. H. & Saiga, Y. (1963) *J. Cell. Comp. Physiol.* **62**, 9–16.
7. Morin, J. G. & Hastings, J. W. (1971) *J. Cell Physiol.* **77**, 305–311.
8. Cormier, M. J., Hori, K., Karkhanis, Y. D., Anderson J. M., Wampler, J. E., Morin, J. G. & Hastings, J. W. (1973) *J. Cell. Physiol.*, in press.
9. Shimomura, O. & Johnson, F. H. (1969) *Biochemistry* **8**, 3991–3997.
10. Shimomura, O. & Johnson, F. H. (1972) *Biochemistry* **11**, 1602–1608.
11. Kishi, Y., Tanino, H. & Goto, T. (1972) *Tetrahedron Lett.* **27**, 2747–2749.
12. Karkhanis, Y. D. & Cormier, M. J. (1971) *Biochemistry* **10**, 317–326.
13. Cormier, M. J. & Prichard, P. M. (1968) *J. Biol. Chem.*, **243**, 4706–4714.
14. Wampler, J. E. & DeSa, R. J. (1971) *Appl. Spectros.* **25**, 623–627.
15. Cormier, M. J., Hori, K. & Karkhanis, Y. D. (1970) *Biochemistry* **9**, 1184–1189.
16. Inoue, S., Sugiura, S., Kakoi, H. & Goto, T. (1969) *Tetrahedron Lett.* **20**, 1609–1610.
17. Kishi, Y., Goto, T., Hirata, Y., Shimomura, O. & Johnson, F. H. (1966) *Tetrahedron Lett.* **29**, 3427–3436.
18. Kishi, Y., Goto, T., Inoue, S., Sugiura, S. & Kishimoto, H. (1966) *Tetrahedron Lett.* **29**, 3445–3450.
19. DeLuca, M., Dempsey, M. E., Hori, K., Wampler, J. E. & Cormier, M. J. (1971) *Proc. Nat. Acad. Sci. USA* **68**, 1658–1660.

Proc. Nat. Acad. Sci. USA
Vol. 70, No. 1, pp. 124–128, January 1973

Thermal Motion and Forced Migration of Colloidal Particles Generate Hydrostatic Pressure in Solvent

(osmotic pressure/ferrofluid)

H. T. HAMMEL AND P. F. SCHOLANDER

Physiological Research Laboratory, Scripps Institution of Oceanography, University of California, San Diego, La Jolla, Calif. 92037

Contributed by P. F. Scholander, October 30, 1972

ABSTRACT **A colloidal solution of ferrite particles in an osmometer has been used to demonstrate that the property that propels water across the semipermeable membrane is the decrease in hydrostatic pressure in the water of the solution. A magnetic field gradient directed so as to force the ferrite particles away from the semipermeable membrane of the osmometer and toward the free surface of the solution enhanced the colloidal osmotic pressure. The enhancement of this pressure was always exactly equal to the augmentation of the pressure as measured by the outward force of the particles, against the area of the free surface. Contrariwise, directing the magnetic field gradient so as to force the ferrite particles away from the free surface and toward the semipermeable membrane diminished the colloidal osmotic pressure of the solution. For a sufficiently forceful field gradient, the initial colloidal osmotic pressure could be negative, followed by an equilibrium pressure approaching zero regardless of the force of the particles against the membrane. Thus, the osmotic pressure of a solution is to be attributed to the pressure in the solvent generated in opposition to the pressure of the solute particles caused by their interaction with the free surface (Brownian motion and/or an external field force), or by their viscous shear when they migrate through the solvent, or both.**

Recently, Scholander (1) has emphasized the view that the lowering of the chemical potential of water caused by adding microsolutes or colloidal particles to the water or by placing the water in a matrix is a direct and exclusive result of lowering the internal hydrostatic pressure in the water. Colloidal particles in Brownian motion in water disperse throughout the volume and exert an outward pressure on all boundaries. The colloidal pressure develops an internal hydrostatic tension in the water if there is an unrestrained surface. The magnitude of the colloidal particle pressure and the opposing internal negative hydrostatic pressure in the water may be ascertained by separation of the suspension from pure water by a membrane permeable only by the water. The magnitude of that negative hydrostatic pressure in the pure water sufficient to prevent water from passing through the membrane to the suspension, designated as the colloidal osmotic pressure (COP), is exactly equal to the internal negative hydrostatic pressure in the water of the suspension. Thus, the COP is a consequence of, and is equal to, the internal negative hydrostatic pressure generated in the water of the suspension by the thermal pressure of the colloidal particles against the free boundary of the suspension.

By using a colloidal suspension of magnetic particles in water, Scholander and Perez (2) have experimentally verified that the pressure exerted by the colloidal particles at the free surface generates the colloidal osmotic pressure of the suspension. By applying a magnetic field so as to attract the magnetic particles toward the free surface and away from the semipermeable membrane, they showed that the COP increased directly as the attractive force between the particles and the magnet increased. Contrariwise, by applying the magnetic field so as to attract the magnetic particles away from the free surface and toward the semipermeable membrane, they found that the COP decreased. However, they supposed they were measuring the equilibrium COP, and did not recognize the transient effects induced by the migrating magnetic particles. The purpose of this report is to describe an experiment that demonstrates a transient COP caused by migration or dispersal of particles toward or away from the free surface. Since osmotic equilibrium often does not exist in biological systems, osmotic effects induced by migrating solutes are a principal concern.

Abbreviations; COP, colloidal osmotic pressure.

PROCEDURES

Fig. 1*A* illustrates how the colloidal suspension of colloidal magnetic particles* was retained in an osmometer, and how a heterogenous magnetic field was applied to the colloidal suspension. The strength of the vertical component of the attractive force between the suspension and the magnet was measured by a calibrated Statham gauge supported above the osmometer coupled to it. COP of the suspension was measured before, during, and after application of a magnetic field to the suspension. Experiments were done with the vertical attractive force ranging from 0 to 35 g by variation of the separation between the magnet and the colloidal suspension. Since the cross-sectional area of the suspension in the osmometer was 4.89 cm^2, the vertical attraction pressure ranged from 0 to 7.0 $\times 10^3$ dyne $\cdot$ cm^{-2}.

The osmometer (3) was assembled by stretching a wet dialyzing membrane over a convex plastic disc that was 28 mm in diameter. A 28-cm length of 0.3-mm inner diameter polyethylene tubing was passed through a hole at the center of the disc (Fig. 1*B*). Between the disc and the membrane was placed a 25-mm disc of 0.1-mm thick lens paper, which served as a spacer. The lens-tissue disc was soaked in distilled water overnight to cleanse it of osmotically active substances. The

* The colloidal magnetic particles of the ferrofluid used in this experiment were ferrite, and were about 100 Å in diameter. In the manufacture of the ferrofluid, molecules of oleic acid were bound to the finely ground magnetic particles so as to prevent any close approach on collision that would flocculate the particles. The magnetization of the ferrofluid was 100 G and its concentration was on the order of 10^{17} per cm^3. The ferrofluid was obtained from Ferrofluidics Corp., Burlington, Mass., and is more fully described by Rosensweig (4).

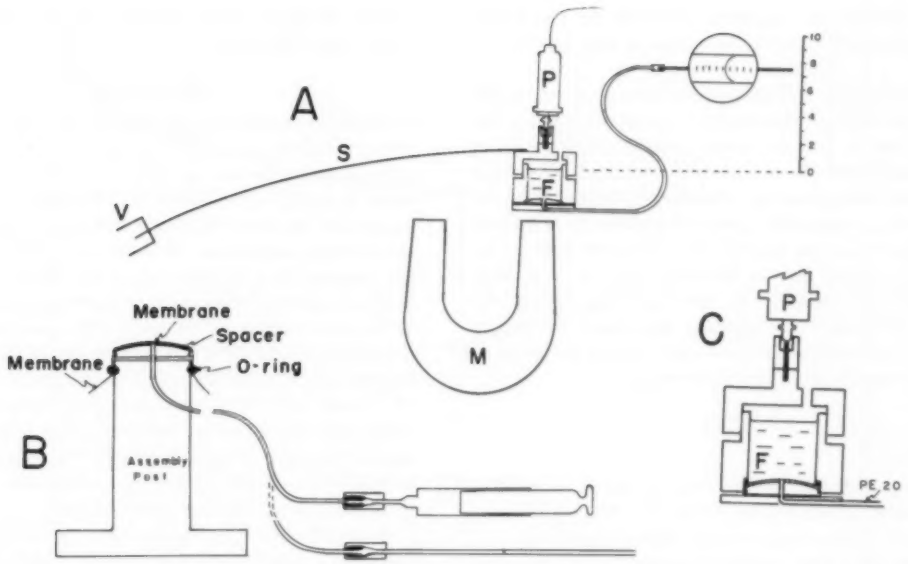

FIG. 1. (*A*) Apparatus for measurement of colloidal osmotic pressure of ferrofluid, F, and for measurement of change in force by magnetic particles when they are forced to migrate toward the semipermeable membrane by the field gradient of magnet *M*. Transducer *P* measures the change in force. Spring *S* and adjustable vise *V* support the weight of the osmometer and exert an additional force on *P*. (*B*) Procedure for mounting membrane and attaching capillary. (*C*) Details of osmometer.

dialyzing membrane was stretched by placement of the disc on a post and retention of the membrane with a stretched rubber O-ring. By pulling on the free edges of the membrane, taking care to eliminate all creases over the edge of the disc, one caused the membrane to stretch and compress the tissue spacer. A thread of dental floss was tied around the stretched membrane. A razor blade was used to cut the excess of membrane between the disc and the assembly post. The apparatus must be assembled with gas-extracted distilled water in the syringe, rubber coupling, tubing, spacer, and dialyzing membrane—as shown in Fig. 1*B*—and care must be taken to avoid trapping bubbles below the membrane. The disc and membrane were pressed tightly against an *O*-ring in the osmometer by a larger plastic disc, as shown in Fig. 1*C*, and held by three flat-head brass screws (not shown in Fig. 1*C*). Approximately 10 ml of ferrofluid was placed in the osmometer through a hole in the cover. In the middle of the upper surface of the cover was mounted a brass pin for exerting a force against the Statham transducer (model UC3). A flat spring was attached to the cover and was clamped in a vise, which could be rotated such that the weight of the osmometer was supported by the spring, and an additional force of about 40 g was pressed against the transducer. As one pole of a magnetron magnet was raised toward the ferrofluid in the osmometer, the ferrite was drawn downward exerting a force against the membrane. This magnetic force diminished the force against the transducer. The magnetic field had no direct effect on the transducer. The output of the transducer was recorded on a strip chart millivolt recorder; the system was calibrated by adding known weights of ferrofluid to the osmometer and recording the output.

The COP was ascertained by adjustment of the height of the capillary, Fig. 1*A*, in relation to the level surface of the suspension until there was no drift in the meniscus as viewed against an ocular scale with a 20-power microscope. The position of the meniscus could be determined within ±0.1 division (± 2.6 μm). The COP was equal to the capillary pressure† minus the hydrostatic pressure. When 10 min was allowed to detect zero drift in the meniscus, the height of the capillary and the COP could be obtained with an accuracy within ±0.03 cm of H_2O. Only when the COP changed slowly was there sufficient time to obtain full accuracy by this method. When COP changed rapidly, another method was used. Upon elevation of the magnet, the capillary was immediately raised to just below the height for the lowest anticipated COP. At this capillary level the meniscus drifted to the right in Fig. 1*A* (away from the membrane). As the transient COP increased, the capillary pressure minus the preset hydrostatic height became equal to the COP, and the drift to the right became zero. Subsequently, the meniscus began to drift to the left at an accelerating rate. After a few minutes, the capillary was adjusted to a lower level, and again the COP was determined when the drift of the meniscus was zero. By this procedure, the COP was determined several times after applying and removing the magnetic field.

When the magnetic field was applied so that a pressure was exerted against the membrane, there was an immediate small shift in the meniscus, possibly due to compression of the spacer. This shift showed no hysteresis and was complete in less than 5 sec.

The volume of the water on the water side of the membrane was kept very small by the thin spacer, the small bore of the polyethylene tubing, and the small volume of the capillary, so as to minimize thermal drifts. In a room without forced con-

† The capillaries used in this experiment were 20-μl micropipettes from Yankee. The capillary pressure of each was 46.5 ± 0.1 mm of H_2O.

vection these drifts were negligible. The meniscus was displaced by 1 division by a change in volume of only 8.4×10^{-3} mm^3.

In other experiments, the pressure transducer was mounted below the osmometer and the magnet was supported above the ferrofluid in order to pull the ferrite particles away from the membrane and toward the surface of the ferrofluid. For these experiments the osmometer cup was filled to the rim. The rim was coated with Vaseline and a film of Saran was loosely layed on the ferrofluid so as to exclude air. The cover pressed an O-ring onto the Saran film to maintain the film in a slack condition, while it retained the ferrofluid. The spring was adjusted so as to allow the pressure transducer to support about 40 g of the weight of the osmometer. As the magnet was lowered to the ferrofluid the weight decreased.

RESULTS

Magnet below

When the magnet was raised beneath the ferrofluid so as to draw the ferrite particles away from the free surface and toward the membrane, there was an immediate transient reduction in the COP from -1.55 cm of H_2O to $+2.90$ cm of H_2O (Fig. 2*A*). Subsequently, the COP increased rapidly, then gradually, until it read nearly zero after 33 hr. Conversely, when the magnet was removed, the COP increased immediately to more than the equilibrium COP before it gradually returned toward the equilibrium value, as indicated in Fig. 2*A*; the ferrofluid was stirred to hasten return to the final equilibrium value of -1.70 cm of H_2O, indicating a drift of only 0.15 cm of H_2O in 47 hr. Fig. 2*A* also shows the force (grams) and corresponding pressure (cm of H_2O) induced by the magnetic field acting on the ferrofluid as a function of time. There was an immediate increase in the magnetic pressure, followed by a period of rapid increase lasting about 30 min, followed by a slow increase over many hours.

The initial reduction in COP, as well as the subsequent values, were dependent upon the proximity of the pole of the magnet to the suspension. The smaller the gap, the greater the magnetic pressure and the greater the reduction in the initial COP. The initial reduction in COP was plotted for several experiments as a function of the magnetically induced pressure of the ferrite particles migrating toward the membrane (Fig. 3, upper-right quadrant). The equivalent line for COP and magnetic pressure (both expressed as cm of H_2O) is drawn for comparison. The data for the initial reduction in COP fall very nearly on the equivalent line. Also plotted in Fig. 3 (upper-right quadrant) is the net reduction in COP at 0.5 hr against the magnetic pressure.

Magnet above

In Fig. 2*B* is plotted the COP before, during, and after the magnet was placed above the ferrofluid. There was an immediate increase in the COP from a value of -1.1 cm of H_2O before placement of the magnet to -4.25 cm of H_2O, and a further increase to -5.45 cm of H_2O after 2 hr, there was no further increase for another 2 hr. When the magnet was removed the COP snapped back to nearly the initial value (without the magnet). All points from Fig. 2*B* are replotted in Fig. 3 (lower-left quadrant). With the magnet above the suspension and drawing the magnetic particles away from the membrane and toward the free surface, all points fell on the equivalent line. The plot of the enhancement of colloidal osmotic pressure versus induced magnetic pressure was no longer time-dependent.

DISCUSSION

The experiments on the colloidal osmotic pressure of a suspension of magnetic particles demonstrate that (*i*) the role of the colloidal particles was to exert a pressure of the solvating water to change the pressure of the water and (*ii*) it was the pressure of the water that determined the osmotic behavior of the colloidal suspension. It makes no difference (*a*) whether the pressure was transmitted to the water by the random Brownian motion of the colloidal particles exerting a pressure at the free surface of the suspension, as when equilibrium osmotic pressures were observed, or (*b*) whether the pressure exerted by the colloidal particles was transmitted to the water by viscous shear. Viscous shear transmitted pressure to the water when the particles were forced by a magnetic field to migrate toward or away from the membrane or when the particles were dispersing toward or away from the membrane by diffusion after removal of the magnet.

An explanation of osmosis found in current textbooks in physiology (5, 6) is invalidated by these experiments. It suggests that the presence of the solute or colloidal particles lowers the concentration of the water at the membrane that results in the diffusion of water from the region of higher water concentration beyond the membrane to the region of lower water concentration on the solution side of the membrane. The fact that when the colloidal particles are forced to migrate toward the membrane generates a strongly negative COP, followed by an equilibrium osmotic pressure that approaches zero (or, if more than zero, then less positive than without the magnetic force) cannot be explained by supposed effects on the concentration of water at the membrane.

We conclude that the equilibrium effect of colloidal particles is a positive pressure exerted on all boundaries retaining the particles, first proposed by Van't Hoff for solutions as the bombardment pressure (7). The secondary effect is the response of the water to this colloidal particle pressure, that is, a negative hydrostatic pressure (with respect to the suspension's ambient pressure) in the water of the suspension, an effect that was first fully developed by Hulett (8) as a basis for explaining the lowering of vapor pressure and osmosis. A similar view was accepted by Herzfeld (9), Mysels (10), and Duclaux (11), and by Scholander *et al.* (12) as a basis for osmosis. This secondary effect was first demonstrated experimentally by Scholander and Perez (2). The effects of lowering the chemical potential of water on the colligative properties (osmotic pressure, vapor pressure, and melting point) in a solution at ambient pressure are entirely due to the lowering of the internal hydrostatic pressure in the water below ambient pressure. For example, the molecules of 1 mol of an ideal microsolute, which does not dissociate when dissolved in 1 liter of water at 0°, would disperse throughout the volume and would exert a pressure of $+22.4$ atm on all boundaries, including the free surface of the solution in an open container, and on the boundaries with all inclusions within the solution such as ice crystals or bubbles. As there are strong forces between the molecules of water, the pressure of the solute molecules against all surfaces develops a tension in the water, i.e., an internal hydrostatic pressure of -22.4 atm in the water on the solution. The net pressure on any inclusion would be 0, or the same as the ambient pressure. The vapor pressure of the 1 molal solution would be lowered

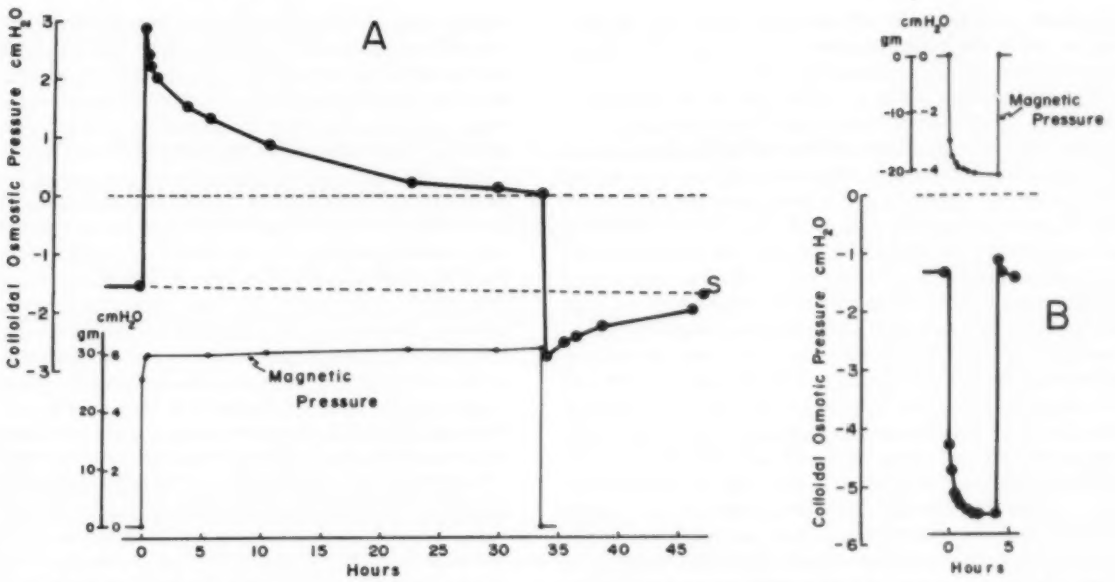

FIG. 2. (*A*) Colloidal osmotic pressure (COP) and magnetic force induced by the magnetc field (*gm*) as a function of time after raising and lowering magnet from below osmometer. The magnetic force is also expressed as the corresponding magnetic pressure in cm of H_2O. *S* indicates COP after ferrofluid is stirred in osmometer. (*B*) COP and magnetic pressure as a function of time before and after lowering magnet from above the osmometer and then raising it again.

by exactly the same amount as the lowering caused by a tension of 22.4 atm in pure water at 0°, and for exactly the same reason, i.e., the water in the solution is under a tension of 22.4 atm, a view first proposed by Hulett (8). Lowering of the melting point of a solution is also a consequence of the tension in the water of the solution. Hydrostatic tension in the water lowers its vapor pressure, whereas the vapor pressure of ice is not lowered since the net pressure at its boundary

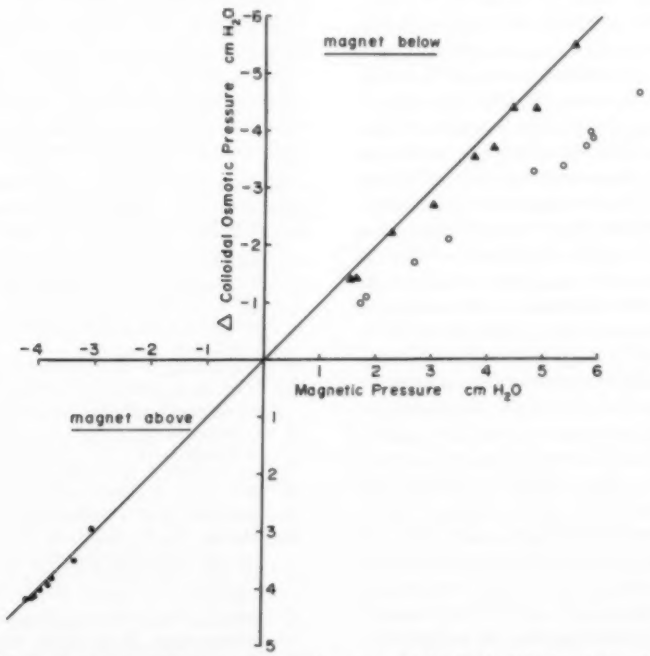

FIG. 3. *Upper-right quadrant.* Reduction in COP against magnetic pressure initially (*solid triangles*) and after 0.5 hr (*open circles*). Data were obtained by raising magnet from below up to several levels beneath the osmometer. The *solid line* is the equivalent pressure line. *Lower-left quadrant.* Enhancement of COP versus magnetic pressure at several times after the magnet was lowered to osmometer from above (*solid circles*, data from Fig. 2*B*).

is ambient pressure, as for all inclusions. Thus, the temperature at which the vapor pressures of the water and ice are equal is lowered by the tension in the water.

The results shown in Fig. 2*A*, after removal of the magnet, and in Fig. 2*B* demonstrate that one sufficient condition for a COP is the dispersal of particles away from the membrane. By their viscous shear these dispersing particles transmitted to the solvating water a negative hydrostatic pressure, which was the transient portion of the COP. Fig. 2*A* also shows that pulling the particles away from the free surface reduced the pressure exerted by the particles against the free surface and, thereby, reduced the COP toward zero. The magnetic force on the particles also caused them to migrate toward the membrane, transmitting by viscous shear hydrostatic pressure to the solvating water that could yield, if sufficient, a COP that was negative. For strong magnetic forces, the COP remained negative so long as the particles migrated toward the membrane. In time, the particles distributed themselves in the magnetic field in accordance with the Boltzman distribution, i.e., highest concentration at the membrane and lowest concentration at the free surface and no net migration. As the magnetic field gradient increased, the initial migration of the particles toward the membrane increased and the initial negative COP decreased without limit, but the equilibrium COP only decreased toward zero as the equilibrium distribution of particles left fewer and fewer particles at the free surface. The overshooting and undershooting of the COP about its equilibrium value in Fig. 2*A* also illustrates that the pull on the magnetic particles by the magnet could cause the particles to migrate toward the membrane at a higher rate than was the rate of migration away from the membrane by thermal dispersal when the magnet was removed.

Only the qualitative features of the curves in Fig. 2*A* and *B* were subject to analysis. The unknown distribution of the magnetic particle size and dipole moment in the ferrofluid and assymetries in the heterogenous magnet field used in these experiments prevented a quantitative analysis of the curves. However, an important quantitative feature revealed by Fig. 3 is that when all of the magnetic particles were exerting a pressure on the solvating water, there was an exact equivalence between the COP and the induced magnetic pressure measured by the transducer. This effect always occurred when the magnet was above. When the magnet was below the colloidal suspension, the only time when all the magnetic particles were exerting a pressure on the water was before any of the migrating particles had arrived at the membrane. When the magnet was above the colloidal suspension and pulling the colloidal particles toward the free surface and away from the membrane, then the magnetic particles were always exerting a pressure on the solvating water, either by viscous shear as they were migrating toward the free surface or by pressure applied to the free surface as they were reflected from the free surface. Since the particles were either migrating toward the surface or exerting their pressure at the surface, the equivalence of the enhanced COP and the magnetic pressure demonstrates that the pressure in the water caused by the viscous shear of the migrating particles was indistinguishable from the pressure in the water caused by the equilibrium pressure of the particles against the free surface.

When the magnet was below the suspension and pulling the particles toward the membrane, there was an approximate proportionality between the colloidal osmotic pressure and the induced magnetic pressure when they were measured at a fixed interval after application of the magnetic field, e.g., at 30 min in Fig. 3. The proportionality constant diminished with time from the initial value, rapidly at first and then more slowly as more and more particles arrived at the membrane and could exert no further influence on the water.

Even the monomers and polymers of pure water must be exerting a pressure against all boundaries, causing the binding forces between these moieties to be under tension. If all the water were monomeric, the maximum internal tension would be $55.5 \times 22.4 = 1243$ atm at 0°, well under the tensile strength of water, which has been estimated at some 2000 atm (13). At temperatures between 0 and 25°, the majority of the water molecules are considered to be combined in clusters of various sizes (14). However, the molecules of water in a cluster may be so loosely joined that they exhibit their own Brownian motion. At the free surface of the water they would then exert a pressure against the surface as if they were monomers. If this model is correct, then the internal hydrostatic tension of pure water would be approximately RT/V°_{w}, where the partial molar volume V°_{w} is not a function of temperature.

CONCLUSIONS

The primary effect of the colloidal particles in a water suspension is the outward pressure they exert against all boundaries. The colligative properties are the consequences of the negative hydrostatic pressure generated in the solvating water. As Perrin (15) recognized in his studies on the molecular basis of Brownian motion, the effects on the solvent in a solution of microsolutes must be the same as for a colloidal suspension. Thus, we can generalize from our experiments on the colloidal suspensions that (*i*) microsolutes also exert a pressure on all boundaries of the solution, (*ii*) the solvating water opposes this pressure by a negative hydrostatic pressure within the water, a tension made possible by the strong binding forces between molecules of water, and (*iii*) the colligative properties of the solution are a direct consequence of the hydrostatic tension in the water of the solution.

We thank J. Raymond and Dr. A. A. Yayanos for reading the manuscript and suggesting improvements. This work was supported by NSF Grant GB 8343 and NIH Grant HE 13893-01.

1. Scholander, P. F. (1971) *Microvascular Res.* **3**, 215–232.
2. Scholander, P. F. & Perez, M. (1971) *Proc. Nat. Acad. Sci. USA* **68**, 1093–1094.
3. Hargens, A. R. & Scholander, P. F. (1969) *Microvascular Res.* **1**, 417–419.
4. Rosensweig, R. E. (1966) *Int. Sci. Technol.* **55**.
5. Guyton, A. (1971) in *Textbook of Medical Physiology* (W. B. Saunders Co., Phila.), pp 44–47.
6. Gordon, M. S. (1972) in *Animal Function: Principles and Adaptations* (MacMillan Co., London), pp. 243–245.
7. Van't Hoff, J. H. (1887) *Z. Phys. Chem.* **1**, 481–508.
8. Hulett, G. A. (1902) *Z. Phys. Chem.* **42**, 353–368.
9. Herzfeld, K. F. (1937) *Phys. Z.* **38**, 58–64.
10. Mysels, K. J. (1959) in *Introduction to Colloid Chemistry* (Intersciences Publishers Inc., New York), pp. 134–136.
11. Duclaux, J. (1965) *J. Chim. Phys. Physicochem. Biol.* **62**, 435–438.
12. Scholander, P. F., Hammel, H. T., Bradstreet, E. D. & Hemmingsen, E. A. (1965) *Science* **148**, 339–346.
13. Yayanos, A. A. (1970) *J. Appl. Phys.* **41**, 2259–2260.
14. Nemethy, G. & Scheraga. H. A.(1962) *J. Chem. Phys.* **36**, 3382–3400.
15. Perrin, M. J. (1910) in *Brownian Movement and Molecular Reality* (Taylor and Francis, London).

Proc. Nat. Acad. Sci. USA
Vol. 70, No. 1, pp. 129–133, January 1973

Ultraviolet-Stimulated DNA Synthesis in Toluenized *Escherichia coli* Deficient in DNA Polymerase I

(temperature-sensitive mutants/nonconservative/*dnaE*/repair synthesis)

WARREN E. MASKER AND PHILIP C. HANAWALT

Department of Biological Sciences, Stanford University, Stanford, California 94305

Communicated by Allan Campbell, October 26, 1972

ABSTRACT **Ultraviolet (UV)-stimulated nonconservative DNA synthesis has been observed in *E. coli* rendered permeable to nucleoside triphosphates by exposure to toluene. This synthesis is detected in toluenized cells in which the background of UV-independent DNA synthesis is reduced by use of *dnaB* mutants temperature-sensitive for DNA replication and additionally deficient in DNA polymerase I. UV-stimulated nonconservative synthesis is also seen in *polA dnaE* mutants that are deficient in two of the three known DNA polymerases. The observed UV-stimulated repair-like synthesis requires the presence of the four deoxyribonucleoside triphosphates and ATP. This mode of synthesis appears to differ from the ATP-independent nonconservative DNA synthesis previously reported to occur in toluenized bacteria.**

Recent attempts to elucidate the mechanism of DNA replication in bacteria have demonstrated both repair-like and replicative-like DNA synthesis in cells made permeable to nucleoside triphosphates and other small molecules by exposure to toluene (1). The semiconservative, ATP-dependent, replicative DNA synthesis observed in toluenized bacteria resembles *in vivo* DNA replication in many respects (1–4). The modes of DNA synthesis that occur in toluenized bacteria in the absence of ATP have received less attention. This repair-like synthesis is most readily observed in strains with normal levels of DNA polymerase I, and it can be enhanced by treatment with DNase during toluenization (1). Although it was suggested that this nonconservative synthesis might be similar to the repair resynthesis observed as a consequence of ultraviolet (UV) damage to DNA (1), no study of DNA synthesis in toluenized bacteria after UV irradiation has yet been reported.

In spite of the apparent involvement of DNA polymerase I in the ATP-independent DNA synthesis in permeabilized cells, doubts remain as to whether this polymerase is responsible for observably large amounts of repair resynthesis *in vivo*. *In vivo* studies (5, 6) have suggested that DNA polymerase I performs only a limited amount of resynthesis in the excision-repair of UV-induced dimers, and that it produces repair patches consisting of only a few ($\lesssim 30$) nucleotides (5). The *recA recB* gene products appear to be involved in a pathway of excision-repair in which longer patches are produced (6). In view of the uncertainties surrounding the exact mechanisms of excision-repair resynthesis, the question of whether toluenized bacteria can perform repair resynthesis of UV damage appears to be significant. Moreover, such a quasi-*in vitro* system offers a potentially powerful tool for investigating the enzymatic basis of excision-repair.

We report here a study of DNA synthesis in toluenized mutants of *Escherichia coli* that have suffered UV damage. Our experiments have revealed that UV-stimulated DNA synthesis can be observed in toluenized *E. coli* if special conditions are imposed to eliminate the high background of nonconservative DNA synthesis that occurs even in unirradiated cells. The observed UV-stimulated DNA synthesis, which is most easily detected in strains that are *polA* and temperature sensitive for DNA replication, shows a strong dependence upon the presence of ATP. We have also observed UV-stimulated repair-like synthesis in a strain that is deficient in both DNA polymerases I and III. Our results suggest that enzymes other than DNA polymerase I are active in UV-stimulated repair-like synthesis in toluenized bacteria and that such enzymes may be part of the alternate excision-repair resynthesis system thought to operate *in vivo* (6).

MATERIALS AND METHODS

The following strains of *E. coli* were used: D110: *polA1 end thy* (1); TG149: *dnaB thy his leu thr thi*, a derivative of CR34/43 (7); CRT 266: F⁻ *thr leu met thy tonA dnaB* (8); BT 1026: *polA1 end thy dnaE* (9); and TG169 a Thy⁻, Thi⁺ derivative of CRT 2667 (F⁻ *his thi malA polA1 dnaB* Str^r) (2). Cultures were routinely diluted from overnight cultures and incubated with shaking at 37° (33° for temperature-sensitive strains) in M-9 medium (10) with glucose as carbon source. Required amino acids were supplied at 20 μg/ml. Thiamine (when required) and thymine were added at 2 μg/ml. Casamino acids were provided at 0.2%. Cultures of BT 1026 were supplemented with arginine at 20 μg/ml and thymine at 4 μg/ml in addition to 0.2% casamino acids. In experiments where a prior labeling step was required, [^{14}C]thymine was added at 6 nCi/ml for 2–3 generations.

Before irradiation, exponentially growing cultures at a density of 2 to 3 × 10^8 cells per ml were harvested by centrifugation and resuspended in one-third of the original volume of M-9 medium without glucose or other additives. 30-ml portions were irradiated in 14-cm diameter petri dishes by exposure to a Phillips low-pressure germicidal lamp (incident dose rate 9.3 ergs per mm^2 per sec). All steps after irradiation were performed either in the dark or in yellow light.

Toluenization was performed essentially as described by Moses and Richardson (1). Bacteria were concentrated 50-fold from the original density in 0.05 M potassium phosphate buffer (pH 7.4), into which 1% toluene (Baker, spectrophotometric grade) had been "dissolved" by sonication. The cells

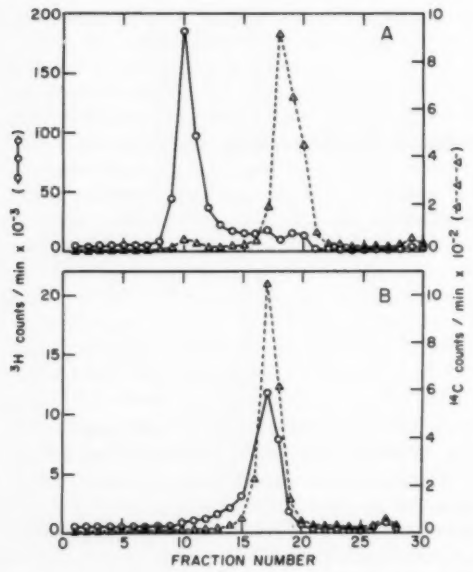

FIG. 1. Isopycnic analysis of DNA from a culture of toluenized strain D110. A culture uniformly labeled with [^{14}C]thymine was divided and half was exposed to 500 ergs/mm^2. The irradiated cells (*lower*) along with an unirradiated control (*upper*) were toluenized and incubated in assay mix containing BrdUTP and [^{3}H]dATP. *Triangles*, [^{14}C]thymine; *circles*, [^{3}H]dATP.

were shaken in toluenized buffer at 37° (33° for temperature-sensitive strains) for 1–10 min, depending on the strain. The duration of exposure to toluene was chosen to maximize the ATP-dependent synthesis for each strain. After toluenization the cells were diluted 1:4.6 in warmed assay mix consisting of a final concentration of 0.07 M potassium phosphate buffer (pH 7.4), 12 mM $MgCl_2$, 0.13 mM NAD, and 35 μM (each) dATP, dCTP, dGTP, and dTTP. When present, ATP was 1.2 mM. Deoxyribonucleoside triphosphates, ATP, and NAD were purchased from Calbiochem or Schwartz/Mann. Radioactive labeling was done with [^{3}H]dTTP or [^{3}H]dATP (Schwartz/Mann) at 20 μM and 20–30 μCi/ml. For density labeling, bromodeoxyuridine triphosphate (BrdUTP) was prepared from dUTP as described by Chamberlin *et al.* (11).

Reactions in the toluenized cells were terminated by the addition of ice-cold 5% Cl_3CCOOH–0.1 M PP_i or, when density analysis was required, by the addition of ice-cold NET buffer [0.1 M NaCl–0.01 M EDTA–0.01 M Tris·HCl (pH 8.0)]. Lysis and isopycnic gradient analysis were performed essentially as described by Hanawalt and Cooper (12), except that the Pronase–Sarkosyl treatment was continued for 2 hr.

Alkaline sucrose-gradient analysis was by a modification of the method described by Kato and Kondo (13). To linear gradients of 5–20% sucrose in 0.2 M NaOH–0.8 M NaCl–5 mM EDTA a 0.1-ml top layer of 0.5 M NaOH–0.01 M EDTA–1% Sarkosyl was added. 10 μl of a suspension of 2 to 3 × 10^9 cells per ml of bacteria was gently stirred into the top layer and allowed to incubate at 22° for 45 min. Gradients were spun at 30,000 rpm in a Spinco SW50.1 rotor at 20° for 80 min.

Radioactively labeled DNA was routinely precipitated with 5% Cl_3CCOOH–0.1 M PP_i and filtered onto glass-fiber filters (Reeve–Angel) or Millipore filters (HAWP) that had been soaked in 0.2 M sodium pyrophosphate. Filters were then washed twice with 5% Cl_3CCOOH–0.1 M PPi, twice with distilled water, dried, and counted in toluene-based scintillation fluid containing PPO and POPOP (12).

RESULTS

Before we studied DNA synthesis in toluenized, UV-irradiated bacteria, we examined the characteristics of DNA synthesis in permeabilized unirradiated cells for each strain. DNA synthesis, as measured by incorporation of [^{3}H]dTTP or [^{3}H]dATP into acid-precipitable material, was linear with time for 45–60 min. After this time, synthesis gradually leveled off. The length of exposure to toluene was chosen for each strain so as to maximize the amount of ATP-dependent synthesis relative to the amount of ATP-independent synthesis. In agreement with earlier reports (1), CsCl gradient analysis revealed that semiconservative synthesis in toluenized *E. coli* is virtually totally dependent upon the presence of ATP, and that semiconservative synthesis is diminished in preparations overexposed to toluene. Based on the amount of label carried into the hybrid density position during subsequent isopycnic analysis, less than 5% of the parental DNA in a toluenized culture is replicated during 60 min under our optimal conditions.

When BrdUTP is provided in place of TTP as a substrate for DNA synthesis in toluenized cells, repair replication should be evidenced by the synthesis of relatively short stretches of DNA that appear at normal (parental) density in an isopycnic gradient; this result should be distinguishable from replicative synthesis, which yields DNA of hybrid density. The result of an examination of the effect of UV on DNA replication in toluenized cells of D110 (*polA1 end*$^-$) is shown

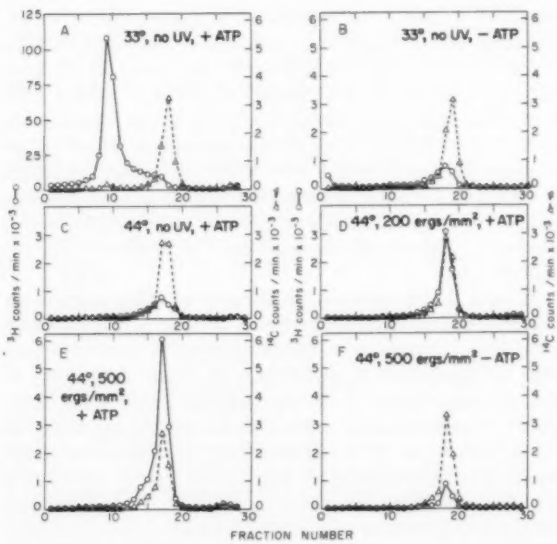
A 33°, no UV, + ATP
B 33°, no UV, − ATP
C 44°, no UV, + ATP
D 44°, 200 ergs/mm², + ATP
E 44°, 500 ergs/mm², + ATP
F 44°, 500 ergs/mm² − ATP
^{3}H counts / min x 10^{-3} (—o—)
^{14}C counts / min x 10^{-3} (-Δ-Δ-)
FRACTION NUMBER

FIG. 2. Isopycnic analysis of DNA from strain TG169. A culture uniformly labeled with [^{14}C]thymine was divided, irradiated, and toluenized along with unirradiated controls. The cells were incubated in assay mix containing [^{3}H]dATP and BrdUTP at permissive and restrictive temperatures in the presence or absence of ATP. *Triangles*, [^{14}C]thymine; *circles*, [^{3}H]dATP.

in Fig. 1. A culture growing exponentially in the presence of [^{14}C]thymine was harvested and resuspended in M-9 medium minus glucose and other additives. Half of the culture was exposed to 500 ergs/mm^2 of UV radiation. The cells were pelleted, toluenized for 2.5 min at 37°, and incubated for 50 min at 37° in assay mix containing [^{3}H]dATP and BrdUTP in place of dTTP. The reaction was stopped and the cells were harvested and lysed; their DNA was examined by CsCl isopycnic gradient analysis. The ^{14}C label marks the position of DNA of normal density, and serves as an indication of the relative amount of DNA in each gradient. Although a dramatic decrease in the amount of semiconservative DNA synthesis in the UV-treated cells relative to the unirradiated control is apparent, no increase in newly replicated normal density DNA, characteristic of repair re-

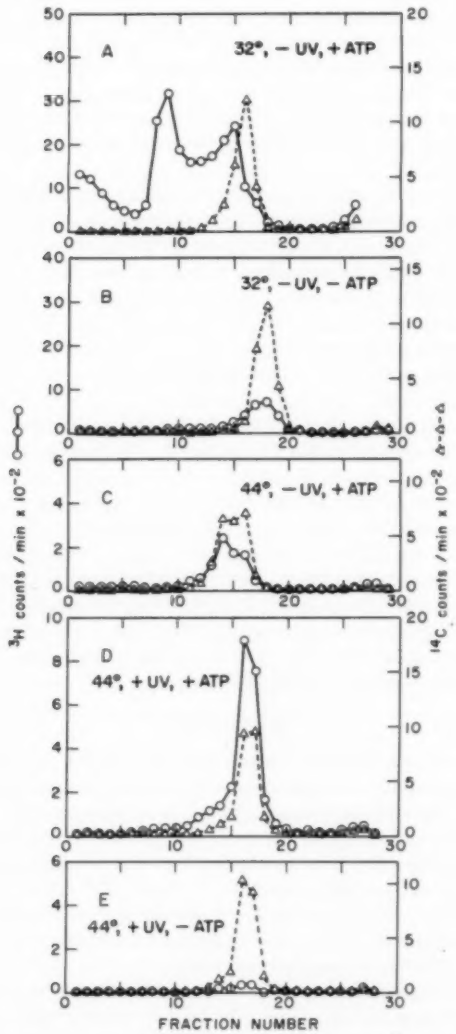

FIG. 3. Isopycnic analysis of DNA from strain BT 1026. A culture labeled uniformly with [^{14}C]thymine was divided and a portion was irradiated with 500 ergs/mm^2. The cells were toluenized and incubated in assay mixture with BrdUTP and [^{3}H]dATP under the conditions indicated. *Triangles*, [^{14}C]thymine; *circles*, [^{3}H]dATP.

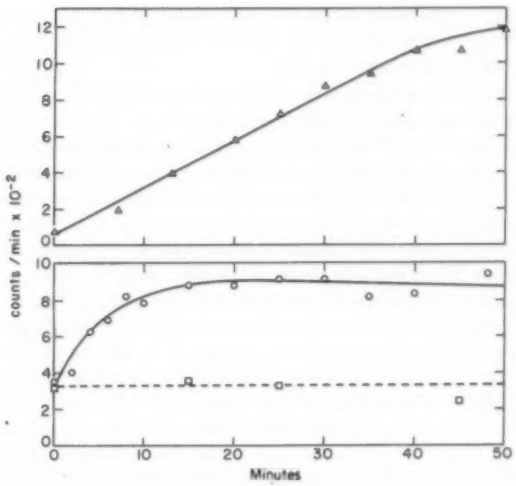

FIG. 4. DNA synthesis in toluenized strain TG169. An exponentially growing culture was harvested and divided; a portion was irradiated with 500 ergs/mm^2. The cells were toluenized and added to assay mix plus ATP; 0.1-ml portions were withdrawn and precipitated with Cl_3CCOOH–PP_i at the times indicated. *Upper frame:* Unirradiated cells incubated at 33° (permissive temperature) in the presence of 20 μM [^{3}H]dATP (7.5 μCi/ml). *Lower frame:* Unirradiated cells (*squares*) and irradiated cells (*circles*), both incubated at 44° in assay mix containing 20 μM [^{3}H]dATP (39 μCi/ml).

synthesis, can be seen. It appears from this result that any study of UV-stimulated repair-like synthesis in toluenized bacteria will be hampered by the significant amount of newly synthesized DNA of normal density found in unirradiated cells undergoing semiconservative replication. In order to eliminate contributions from semiconservative synthesis to the "background" of DNA banding at normal density, several approaches were tried that might inhibit replicative synthesis while allowing repair resynthesis to continue. The most obvious scheme, that of removing ATP from the assay mix, eliminated semiconservative synthesis almost completely, but it also prevented UV-stimulated repair-like resynthesis, as discussed below. The method finally chosen was that of

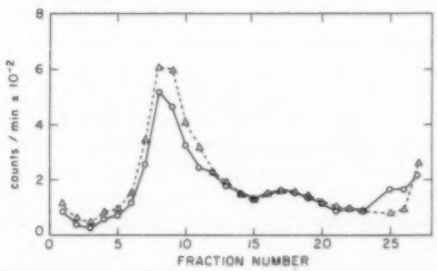

FIG. 5. Comparison of toluenized and untreated cells of strain D110 in an alkaline sucrose gradient. A culture of D110 was divided and uniformly labeled with [^{3}H]thymine (*circles*) or [^{14}C]-thymine (*triangles*). The ^{14}C-labeled cells were resuspended in phosphate buffer and the ^{3}H-labeled cells were toluenized for 10 min and incubated in assay mix minus 4dNTPs for 10 min. Equal amounts of each preparation were mixed on top of an alkaline sucrose gradient, gently lysed, and centrifuged.

using temperature-sensitive DNA mutants that are able to perform repair resynthesis but not DNA replication at the restrictive temperature (14).

In Fig. 2 we show the results of an experiment performed upon strain TG169 (*polA1 dnaB*), which is temperature sensitive for DNA replication. An exponentially growing culture was harvested by centrifugation and resuspended in M-9 medium without additives. Portions were exposed to 500 ergs/mm², 200 ergs/mm², or no UV. The cells were pelleted, and each portion was toluenized separately for 2 min at 37°. The toluenized cells were diluted in warmed assay mixtures containing [³H]dATP and BrdUTP, and were incubated for 60 min at the indicated temperature in the presence or absence of ATP. As seen in Fig. 2*A*, most of the synthesis in the unirradiated control at the permissive temperature is semiconservative. In the absence of ATP (Fig. 2*B*) essentially all semiconservative synthesis is eliminated, although a small amount of repair-like synthesis persists. At 44°, a restrictive temperature for this strain, no semiconservative synthesis occurs in the unirradiated control (Fig. 2*C*), although the nonconservative synthesis is about equal to that seen in absence of ATP at the permissive temperature. A UV dose of 200 ergs/mm² enhances the amount of nonconservative synthesis seen at the restrictive temperature (Fig. 2*D*), and this UV-stimulated synthesis is increased by a factor of about 2.5 in cells that have been exposed to 500 ergs/mm² (Fig. 2*E*). Removal of ATP from the incubation mixture prevented any UV-stimulated synthesis above the background seen in the unirradiated control (Fig. 2*F*). These results show that UV-stimulated repair-like synthesis is detectable in toluenized bacteria lacking DNA polymerase I, and that this synthesis is totally dependent upon the presence of ATP.

Fig. 3 shows results from an experiment similar to that seen in Fig. 2, except that strain BT 1026 (*polA1 end dnaE*) was used. At the restrictive temperature this strain lacks normal levels of both polymerase I and polymerase III (9). Again, cells toluenized for one min at 32° and incubated in assay mix at the restrictive temperature for 45 min show a distinct enhancement of nonconservative DNA synthesis after UV irradiation. The UV-stimulated synthesis appears to be totally dependent upon ATP. A control (not shown) in which irradiated toluenized cells were incubated in assay mix complete (including ATP) except for dCTP and dGTP showed no DNA synthesis at all. Strain BT 1026 appears to be more sensitive to toluenization than others used in this experiment. Even with short (1 min or less) exposure to toluene, the amount of semiconservative DNA synthesis seen at the permissive temperature is much less than that seen with strain TG169 under similar conditions. When using strain BT 1026, we have also had difficulty reproducing the approximately linear relationship between UV dose and amount of nonconservative DNA synthesis seen with strain TG169.

In Fig. 4 is shown the incorporation of [³H]dATP into acid-precipitable material as a function of time for toluenized preparations of strain TG169 irradiated with 500 ergs/mm² and incubated at the restrictive temperature along with an unirradiated control (lower frame). A portion of the unirradiated control was also incubated at the permissive temperature in assay mix containing [³H]dATP at 20% of the specific activity used in the 44° experiment (upper frame). Although synthesis in the permissive temperature control remains linear for about 45 min, all UV-stimulated synthesis has ceased within 15 min after toluenization. The short duration of UV-stimulated synthesis, which presumably limits the total incorporation of labeled precursors seen in isopycnic gradient experiments, may reflect gradual diffusion of unknown cofactors that may be required for repair resynthesis, a phenomenon that might be more serious at the higher (restrictive) temperatures used here. This result might also obtain if toluenized bacteria are unable to perform the incision or excision steps that must precede resynthesis in the repair process.

Experiments similar to those shown in Figs. 2 and 3 were performed upon strains TG149 and CRT266, both of which are Pol I⁺ and *dnaB*. Although the levels of nonconservative DNA synthesis seen in the unirradiated controls were generally 2- to 5-fold higher in these strains than in *polA1* strains, no significant stimulation of nonconservative synthesis was detected after irradiation. Assuming that the lower levels of polymerase I limit the amount of repair, our result suggests that residual DNA polymerase I activity is not responsible for the UV-stimulated synthesis observed in *polA1* strains.

In order to test the hypothesis that the ATP-independent nonconservative DNA synthesis reported by other workers (1–4) using Pol I⁺ strains represents repair of damage to DNA introduced by toluenization, perhaps as a result of release of periplasmic enzymes into the cytoplasm, we compared the molecular weights of DNA from toluenized bacteria and an untreated control. A culture of D110 was split and equal portions were grown exponentially in the presence of [³H]-thymine or [¹⁴C]thymine, respectively, for several generations. The cells were harvested, and the ¹⁴C-labeled culture was resuspended in phosphate buffer. The ³H-labeled culture was resuspended in phosphate buffer containing 1% toluene, shaken at 37° for 10 min, and then incubated for 10 min at 37° in assay mix that was complete (including ATP) except for the 4 dNTPs. Equal amounts of each preparation were layered upon an alkaline sucrose gradient, gently lysed, and centrifuged as described in *Methods*. The resultant distribution of acid-precipitable material, shown in Fig. 5, indicates no significant difference in molecular weight between the DNA of toluenized and untreated cultures.

DISCUSSION

We have shown that nonconservative DNA synthesis in toluenized *E. coli* can be stimulated by irradiation of the bacteria with ultraviolet light. This synthesis differs from the repair-like synthesis reported by Moses and Richardson (1) in that it is readily observed in *polA* strains and shows an almost complete dependence upon ATP. The UV-stimulated synthesis persists for a shorter period of time after toluenization than either replicative synthesis or ATP-independent nonconservative synthesis.

The short duration of UV-stimulated synthesis in toluenized bacteria is not surprising. The *in vivo* excision repair process is known to be complex, involving recognition of an imperfection, incision, excision of the defect, resynthesis of the excised region with the complementary DNA strand as a template, and, finally, rejoining to the contiguous parental strand by ligase action (15). If any step before resynthesis is blocked in toluenized bacteria, the repair-like synthesis

observed will be limited by the amount of excision completed before toluenization. Another possibility is that the repair-resynthesis complex may require cofactors not provided in an assay mixture that maximizes semiconservative replication.

We have thus far detected only insignificant amounts of UV-stimulated synthesis in toluenized strains with normal polymerase I levels. Frequently a higher background of UV-independent nonconservative synthesis occurs in Pol I^+ strains than in their Pol I^- derivatives. This background is presumably the same ATP-independent repair-like synthesis reported by Moses and Richardson (1). The origin of this synthesis remains obscure. Since the number of single-strand breaks put into DNA during toluenization is so small as to be insignificantly different from that in untreated cells, it does not seem that the damage caused by toluenization should saturate the resources of the repair system. Therefore, it might be expected that the usual amount of UV-stimulated DNA synthesis would be superimposed upon the higher background in Pol I^+ strains. However, when viewed within the framework of earlier *in vivo* studies of repair resynthesis (5, 6), our difficulty in detecting UV-stimulation of repair-like synthesis in Pol I^+ strains is less surprising. Excision of UV-induced dimers produces gaps in the DNA that could act as primers for polymerase I or could invite degradation by nucleases. Polymerizing enzymes could then use the exposed single-strand regions as templates for resynthesis of relatively long repair patches. The short duration of the observed synthesis presumably limits the repaired regions to lengths that are not sufficient to significantly increase the buoyant density of the DNA. With competition of pol I for excision sites reduced in *polA* mutants, such extensive repair-like synthesis might well be more abundant in *polA* strains. The observation of greater amounts of repair resynthesis *in vivo* in *polA* mutants (5) favors such an explanation. Since this type of extensive repair resynthesis does not occur *in vivo* in *recA recB* strains (6), the *recB* nuclease, known to be ATP-dependent (16), may be involved in the ATP-dependent UV-stimulated synthesis we observe in toluenized *E. coli*.

The observation of UV-stimulated synthesis in a strain that is deficient in DNA polymerases I and III at the restrictive temperatures used in these experiments reemphasizes the question of which DNA polymerizing enzyme is responsible for this type of synthesis. Residual pol III activity undoubtedly persists in strain BT 1026 at the restrictive temperature (9), and this residual activity might suffice to perform the small amount of UV-stimulated synthesis we detect with this strain. Since no physiological function has been reported for pol II (17), we must, at present, remain open minded about its possible involvement in repair resynthesis. Also, we can not dismiss the possibility that a fourth DNA polymerase may exist.

The class of DNA synthesis we report here resembles *in vivo* repair resynthesis in that it is nonconservative, UV-stimulated, and persists at the restrictive temperature in mutants temperature-sensitive for DNA replication. The resemblance to *in vivo* studies that show greater amounts of repair resynthesis in *polA* strains has already been discussed. Actual completion of the repair process in toluenized *polA* mutants of *E. coli* is likely to be difficult to demonstrate because of the short duration of repair-like synthesis and because even unirradiated toluenized cells are nonviable (1). A recent report (18) has presented indirect evidence for repair of γ-ray damage in toluenized *Bacillus subtilis*. The experiments we report here constitute the first direct measurement of UV-stimulated DNA synthesis in permeabilized *E. coli*, and show that this synthesis is ATP-dependent.

We thank Drs. K. Geider and C. C. Richardson for bacterial strains and Dr. A. R. Grivell for producing strains TG149 and TG169. Ms. J. Spranza provided technical assistance. This work was supported by a postdoctoral fellowship from the Helen Hay Whitney Foundation to W.E.M. and a Research Grant GM09901 from the National Institutes of Health.

1. Moses, R. E. & Richardson, C. C. (1970) *Proc. Nat. Acad. Sci. USA* **67**, 674–681.
2. Mordoh, J., Hirota, Y. & Jacob, F. (1970) *Proc. Nat. Acad. Sci. USA* **67**, 773–778.
3. Burger, R. M. (1971) *Proc. Nat. Acad. Sci. USA* **68**, 2124–2126.
4. Matsushita, T., White, K. P. & Sueoka, N. (1971) *Nature New Biol.* **232**, 111–114.
5. Cooper, P. K. & Hanawalt, P. C. (1972) *J. Mol. Biol.* **67**, 1–10.
6. Cooper, P. K. & Hanawalt, P. C. (1972) *Proc. Nat. Acad. Sci. USA* **69**, 1156–1160.
7. Bonhoeffer, F. (1966) *Z. Vererbungslehre* **98**, 141–149.
8. Kohiyama, M., Cousin, D., Ryter, A. & Jacob, F. (1966) *Ann. Inst. Pasteur* **110**, 465–486.
9. Gefter, M., Hirota, Y., Kornberg, T., Barnoux, C. & Wechslen, J. (1971) *Proc. Nat. Acad. Sci. USA* **68**, 3150–3153.
10. Lark, K. G. Repko, T. & Hoffman, E. J. (1963) *Biochim. Biophys. Acta* **76**, 9–24.
11. Chamberlin, M., Baldwin, R. L. & Berg, P. (1963) *J. Mol. Biol.* **7**, 334–349.
12. Hanawalt, P. C. & Cooper, P. C. (1971) in *Methods in Enzymology*, eds. Grossman, L. & Moldare, K. (Academic Press, New York), Vol. XXI, pp. 221–230.
13. Kato, T. & Kondo, S. (1970) *J. Bacteriol.* **104**, 871–881.
14. Couch, J. & Hanawalt, P. (1967) *Biochem. Biophys. Res. Commun.* **29**, 779–784.
15. Howard-Flanders, P. (1968). *Annu. Rev. Biochem.* **67**, 175–200.
16. Oishi, M. (1969) *Proc. Nat. Acad. Sci. USA* **64**, 1292–1299.
17. Campbell, J. L., Soll, L. & Richardson, C. C. (1972). *Proc. Nat. Acad. Sci. USA* **69**, 2090–2094.
18. Noguti, T. & Kada, T. (1972) *J. Mol. Biol.* **67**, 507–512.

Proc. Nat. Acad. Sci. USA
Vol. 70, No. 1, pp. 134–137, January 1973

Biosynthesis of the Photosystem I Chlorophyll–Protein Complex in Greening Leaves of Higher Plants

(photosystem I/chloroplast development/lamellar proteins/P700)

RANDALL S. ALBERTE, J. PHILIP THORNBER*, AND AUBREY W. NAYLOR

Department of Botany, Duke University, Durham, North Carolina 27706; and * Department of Biology and Molecular Biology Institute, University of California, Los Angeles, Calif. 90024

Communicated by Paul J. Kramer, November 13, 1972

ABSTRACT **Biosynthesis of photosystem I chlorophyll–protein complex, derived from chloroplast lamellae solubilized with Triton X-100, was examined in rapidly greening primary leaves of the jack bean. It was found that the chlorophyll/P700 ratio of the complex was low (35/1) in the early stages of greening, and increased steadily to a stable level (75/1) during continued chloroplast development. It is suggested from these results that in the initial stages of greening, and probably throughout synthesis, the P700–chlorophyll–protein molecules are first inserted into the developing lamellae, and those photosystem I chlorophyll–protein molecules functioning solely in a light-harvesting capacity are added subsequently.**

Information about the time course of biosynthesis of the photochemical apparatus of plants has been derived from examination of the activities of photosystems I and II during greening of dark-grown tissues (see refs. 1–3). Several investigators (4–11) have reported that photosystem I activity appears before that of photosystem II, while we (12) have observed the reverse order of biosynthesis in leaves greened under high relative humidity conditions and showing no lag in chlorophyll accumulation. The differences in results are most probably a reflection of environmental conditions during greening, rather than of species differences. It has been shown (13, 14) that low relative humidity conditions result in sufficient water stress to greening leaves to cause a lag in chlorophyll accumulation during the early stages of chloroplast development (see ref. 12). Under greening conditions with high relative humidity, however, the lag in chlorophyll accumulation is eliminated and there is rapid and uniform chloroplast development (12, 14, 15). In etiolated tissues greening under high relative humidity conditions, photosystem II becomes functional before photosystem I. Thus, it appears that assembly processes for photosystem II are more responsive to water stress than are those for photosystem I (16).

Further, our work (12) supports the generally accepted view (13, 17–20) that a step-wise, rather than a simultaneous, synthesis of the components of the thylakoid membranes occurs. We (12) detected the first signs of photosystem II activity after 2 hr of greening of etiolated jack bean leaves, while photosystem I activity was first observed 4 hr later.

With respect to the photosystem I activity, a correlation was observed between the appearance of a photo-oxidizable P700 molecule (the photochemical reaction center of photosystem I) and that of the photosystem I chlorophyll–protein complex (21) after 6 hr of greening. In fully green tissues the heart of the photosystem I unit is composed of 6–8 of these chlorophyll–protein molecules, each having a molecular weight of 100,000 and each containing about 12 molecules of chlorophyll *a* (21–25). One of the 6–8 chlorophyll–protein molecules contains the P700 assembly, but in all other respects it is identical to the other chlorophyll–protein molecules (22, 23). The function of these latter molecules is to feed absorbed light energy to the P700-containing entity, the site of the primary photochemical event.

As an extension of our previous investigations, we have studied the assembly of the P700-containing molecules and the light-harvesting molecules into functional photosystem I units. This has been done by examination of the composition of the photosystem I chlorophyll–protein complex isolated from leaves at different stages of greening, i.e., after 6 hr or more of illumination of etiolated leaves. In this manner it has been possible to determine whether the P700-containing chlorophyll–protein molecule is synthesized initially followed by addition of chlorophyll–protein molecules devoid of P700, or whether the 6–8 chlorophyll–protein molecules without P700 are assembled first and only later is the P700 inserted. The working hypothesis was that a preponderance of P700-containing chlorophyll–protein molecules should be present in preparations of the complex from leaves at early stages of photosystem I development, if the first alternative was correct. This would be reflected in a low chlorophyll/P700 ratio that would increase after further greening. If the second alternative was correct, however, the composition of the chlorophyll–protein preparation should be constant at all stages of greening after initiation of P700 synthesis. The results obtained support the view that the first alternative is correct.

MATERIALS AND METHODS

Plant Material. Jack beans [*Canavalia ensiformis* (L.) DC.] were germinated and grown for 7 days in total darkness at 28° with 80–85% relative humidity as described (12). On the seventh day, the etiolated seedlings were illuminated with incandescent light (General Electric 150-W cool beam flood lamps) at 750–1000 ft-cd.

Preparation of Triton Lamellar Extracts. Primary leaves were harvested at specific times during greening and chloroplast lamellar extracts were prepared. The leaves were homogenized in a Waring Blendor in 0.50 M sucrose–50 mM Tris·HCl (pH 8.0), and the brei was filtered through cheesecloth.

The cellular debris was removed by centrifugation at 10,000 × *g* for 1 min and a chloroplast lamellar pellet was collected from the supernatant by centrifugation at 20,000 × *g* for 10 min. The lamellar pellet was washed twice with 50 mM Tris·HCl (pH 8.0) to remove most of the soluble proteins; a Kontes glass homogenizer was used to suspend the lamellae in buffer, and the centrifugation was at 40,000 × *g* for 10 min. The final pellet was homogenized with a sufficient volume of 1% Triton X-100 in 50 mM Tris·HCl (pH 8.0) to yield a detergent/chlorophyll ratio of 75/1 (w/w). The Triton-solubilized lamellae were used for purification of the photosystem I chlorophyll–protein complex and for measurement of light-induced absorbance changes of P700.

Chlorophyll Determinations. A portion of the leaf samples harvested for lamellar preparations was used to determine the rate of chlorophyll accumulation during greening. Chlorophyll was measured by the procedure of Arnon (26).

Isolation of the Photosystem I Chlorophyll–protein Complex. The photosystem I chlorophyll–protein complex was isolated by the methods of J. P. Thornber, R. S. Alberte, M. Frick, and J. Shiozawa (in preparation). The Triton extract was run into a column of hydroxyapatite (27) equilibrated with 10 mM sodium phosphate (pH 7.0). A large portion of the pigmented material was eluted from the column with the 10 mM sodium phosphate buffer. The photosystem I complex was eluted subsequently with 0.2 M sodium phosphate (pH 7.0) after a brief wash of the column with 0.2 M sodium phosphate–0.1% sodium dodecyl sulfate–10 mM $MgCl_2$.

Determination of the Chlorophyll/P700 Ratio. The reversible light-induced absorbance changes due to P700 in Triton-solubilized lamellar extracts and in isolated chlorophyll–proteins were measured on an Aminco DW-2 spectrophotometer by described procedures (22). The concentration of P700 was estimated from the light-oxidized against reduced difference spectrum by use of a differential extinction coefficient for P700 at 697 nm of 100 mM^{-1} cm^{-1}. Also used was a reference wavelength of 715 nm, an isobestic point in the P700 difference spectrum. Sodium ascorbate was added to samples to fully reduce P700 in the dark, while methyl viologen was added to aid in obtaining the P700 in a fully oxidized state in the light. The chlorophyll concentration of the test sample was determined from the absorbance maximum at 676–678 nm, with an extinction coefficient of 60 mM^{-1} cm^{-1} (J. P. Thornber, R. S. Alberte, M. Frick, and J. Shiozawa, in preparation).

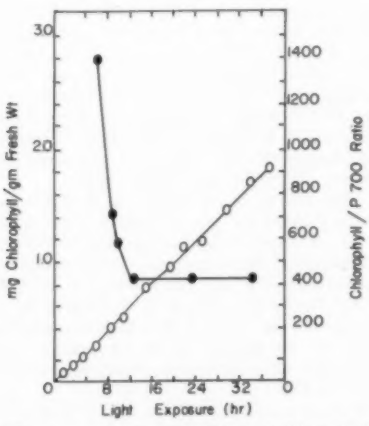

FIG. 1. Time course of accumulation of chlorophyll (○——○) and of appearance of photo-oxidizable P700 (●——●) in primary leaves of jack bean greening under high relative humidity conditions. P700 content is expressed as the chlorophyll/P700 ratio in the Triton X-100-lamellar extracts prepared from leaves after various periods of illumination.

TABLE 1. *P700 content of fractions of jack bean leaves at various stages of greening*

Light exposure (hr)	Chlorophyll/P700 ratio		Percentage of leaf chlorophyll in CPI*
	Triton extract	CPI*	
6	1400	35	2
8	720	45	6
10	600	48	8
12	395	63	16
24	400	69	17
36	380	77	22
∞	430	75	17

* CPI is the photosystem I chlorophyll–protein complex described in the text.

RESULTS

Jack bean leaves greening under the described conditions show a rapid and uniform accumulation of chlorophyll with no lag in accumulation rate (Fig. 1). These results are in agreement with those reported (12).

No P700 could be detected during the very early stages of greening in jack bean (12). Light-induced bleaching of P700 was first detected in very low concentration (chlorophyll/P700 = 1400) in leaves receiving light for 6 hr. The chlorophyll/P700 ratios in the leaf decreased during subsequent greening in a manner in agreement with that reported (12), and stabilized after about 12 hr of illumination (Fig. 1).

Analysis of the photosystem I chlorophyll–protein complex isolated from leaves greened for 6 hr gave low chlorophyll/P700 ratios (35/1). The ratio steadily increased in preparations of the complex from leaves illuminated for longer periods (Table 1), and reached a steady-state level of about 75/1 after 36 hr of greening. The same concentration of P700 was observed in preparations from leaves fully developed in the light. Table 1 includes determinations of the percentage of the total chlorophyll associated with the photosystem I chlorophyll–protein fractions at several stages of greening. It is clear that after 6 hr in the light, only a very small portion (2%) of the total chlorophyll present in the developing chloroplasts was associated with the photosystem I complex, and that during subsequent greening the amount of chlorophyll associated with this complex increases about ten times, to 22%. These results are in agreement with the observations of Kung and Thornber (24) and unpublished data of R. S. Alberte and J. P. Thornber indicating that only about 20% of the lamellar chlorophyll is associated with the photosystem I complex in higher plants.

DISCUSSION

An attempt has been made by us to answer a frequently posed question (see refs. 17, 28, 29) about one aspect of the

biogenesis of the photosynthetic membrane. Is the reaction center of a photosystem inserted into the membrane before or after the assembly of its associated light-harvesting chlorophyll? The most likely interpretation of the increase in the chlorophyll/P700 ratio of the isolated photosystem I chlorophyll–protein complex during greening (Table 1) in the present work is that the P700-containing chlorophyll–protein molecule is synthesized first and is later embellished with light-harvesting chlorophyll–protein molecules. Thus, in the case of photosystem I of the jack bean it appears that the reaction center is inserted into the membrane before the addition of much of the light-harvesting chlorophyll during chloroplast development. The only way in which our results could be interpreted to show that insertion of the reaction center is the final step in the assembly of a photosystem is to presume the photosystem I chlorophyll–protein complex, made in the early stages of greening and having a chlorophyll/P700 ratio of 35/1, receives no further additions of light-harvesting chlorophyll–protein molecules during biogenesis of other photosynthetic units. This latter interpretation seems unlikely since the chlorophyll–protein molecules probably self-assemble *in vivo* into a unit of uniform size of about 6–8 molecules—the concentration of P700 in the photosystem I chlorophyll–protein isolated from such widely different sources as seed plants and blue-green algae is the same (J. P. Thornber, R. S. Alberte, M. Frick, and J. Shiozawa, in preparation; ref. 22). Thus, it would be unlikely that synthesis of the complex during greening would be arrested at a smaller than normal size. Further support for our view on the biogenesis of photosystem I chlorophyll–protein is given by the work of Herron and Mauzerall (30), who have suggested from analysis of light-saturation curves in a greening mutant of *Chlorella* that there is a progressive addition of light-harvesting chlorophyll to rapidly formed reaction centers during greening.

The increase in the percentage of the total chlorophyll of the leaf associated with the photosystem I chlorophyll–protein during greening (Table 1) quantitates and confirms our earlier observation (12) that synthesis of the reaction center of photosystem I begins after about 6 hr of greening, and that during the next 30 hr the photosystem I chlorophyll–protein complex accounts for an increasing portion of the chlorophyll of the leaf; after 36 hr of greening the proportion of chlorophyll–protein is the same as that found in normal light-grown plants. These observations are precisely what would be expected if biosynthesis of photosystem I followed that of photosystem II.

If the generally accepted Z-scheme of photosynthesis is to function at maximum efficiency with an equal division of labor between the two photosystems, it has been maintained (see refs. 28, 29) that there should be approximately equal distribution of chlorophyll between the two photosystems. Inasmuch as the percentage of chlorophyll associated with the photosystem I chlorophyll–protein complex is only about 20% of the total, other chlorophyll molecules must be able to transfer light energy to P700 *in vivo*. It is most probable that these other chlorophyll molecules are localized in the major light-harvesting chlorophyll–protein of the chloroplast, which is a complex of chlorophylls *a* and *b* and protein previously termed the photosystem II chlorophyll–protein (23, 24, 31). Perhaps the chlorophyll *a*/*b*–protein complex performs a less-specific function than heretofore envisaged. It is a matter for future investigation to determine when and how molecules of the chlorophyll *a*/*b*–protein are added to the photosystem I unit, and whether the first photosystem I chlorophyll–protein molecule inserted into the developing thylakoids obtains its P700 in a functional form before or immediately after insertion into the membrane.

Much research during the last decade has been devoted to the isolation of P700 in a highly enriched form (32). Enrichment of seed plant and algal P700 has proved to be more difficult than for the bacterial reaction center. Thus far, the most enriched material has been isolated from spinach stroma lamellae and exhibits a chlorophyll/P700 ratio of sixteen (33), when a millimolar extinction coefficient for P700 of 60 cm^{-1} (100 cm^{-1} in this paper) is used. Owing to the small quantities present it is likely to be difficult to isolate the photosystem I chlorophyll–protein complex from tissues allowed to green for less than 6 hr. The attempt should be made, however, because that is almost certainly the best material for study of the nature of P700.

The senior author wishes to acknowledge the use of facilities made available by the Department of Biology, University of California, Los Angeles, where this research was conducted. This work was supported by National Science Foundation Grant NSF GB-31207 awarded to J. P. Thornber, and by a grant from the University Research Committee, U.C.L.A.

1. Kirk, J. T. O. & Tilney-Bassett, R. A. E. (1967) *The Plastids* (Freeman, London and San Francisco).
2. Kirk, J. T. O. (1970) "Biochemical aspects of chloroplast development," *Annu. Rev. Plant Physiol.* **21**, 11–42.
3. Boardman, N. K., Anderson, J. M., Kahn, A., Thorne, S. W. & Treffy, T. E. (1971) "Formation of photosynthetic membranes during chloroplast development," in *Autonomy and Biogenesis of Mitochondria and Chloroplasts*, eds. Boardman, N. K., Linnane, A. W. & Smillie, R. M. (North Holland, Amsterdam and London), pp. 70–84.
4. Butler, W. L. (1965) "Development of photosynthetic systems 1 and 2 in a greening leaf," *Biochim. Biophys. Acta* **102**, 1–8.
5. Thorne, S. W. & Boardman, N. K. (1971) "Formation of chlorophyll *b*, and the fluorescence properties and photochemical activities of isolated plastids from greening pea seedlings," *Plant Physiol.* **47**, 252–261.
6. Gyldenholm, A. O. & Whatley, F. R. (1968) "The onset of photophosphorylation in chloroplasts isolated from developing bean leaves," *New Phytol.* **67**, 461–468.
7. Bradbeer, J. W., Gyldenholm, A. O., Wallis, M. E. & Whatley, F. R. (1969) "Studies on the biochemistry of chloroplast development," in *Progress in Photosynthesis Research*, ed. Metzner, H. (Tübingen, Germany), Vol. 1, pp. 272–279.
8. Oelze-Karow, H. & Butler, W. L. (1971) "The development of photophosphorylation and photosynthesis in greening bean leaves," *Plant Physiol.* **48**, 621–625.
9. Phung Nhu Hung, S., Horarau, A. & Moyse, A. (1970) "Etude de l'Evolution en chloroplastes des plastes etioles d'Orge II. Photophosphorylation et photoreduction du NADP, formation de ferredoxine en eclairement continu et par l'action d'eclairs," *Zt. Pflanzenphysiol.* **62**, 245–258.
10. Remy, R., Phung Nhu Hung, S. & Moyse, A. (1972) "La differenciation fonctionnelle et structurale au cours du verdissement des etioplastes. Quelques apercus sur la mise en place des deux systemes photochimiques," *Physiol. Veg.* **10**, 269–290.
11. Hiller, R. G. & Boardman, N. K. (1971) "Light driven redox changes of cytochrome *f* and the development of photosystems I and II during greening of bean leaves," *Biochim. Biophys. Acta* **253**, 449–458.
12. Alberte, R. S., Thornber, J. P. & Naylor, A. W. (1972) "Appearance of photosystems I and II in greening jack bean leaves," *J. Exp. Bot.* **23**, in press.
13. Bourque, D. P. & Naylor, A. W. (1971) "Large effects of small water deficits on chlorophyll accumulation and ribo-

nucleic acid synthesis in etiolated leaves of jack bean (*Canavalia ensiformis* (L.) DC.)," *Plant Physiol.* **47,** 591–594.

14. Alberte, R. S. & Naylor, A. W. (1970) "Studies on the relation of humidity and food supply to greening jack bean (*Canavalia ensiformis* (L.) DC.) seedlings," *ASB Bull.* **17,** 28.
15. Bourque, D. P., McMillan, P. N., Clingenspeel, W. J. & Naylor, A. W. (1971) "Effect on chloroplast development in jack bean (*Canavalia ensiformis* (*L.*) DC.) of water stress and inhibitors of protein and nucleic acid synthesis," *Proc. A.S.A.W. Proc. Assoc. Southern Agr. Workers* **68,** 202–203.
16. Bourque, D. P. (1967) "Hill reaction activity in chloroplasts and cellular ribonucleic acid distribution in greening leaves of *Canavalia ensiformis* (L.) DC.," M.A. thesis. Duke University, Durham.
17. Kirk, J. T. O. (1971) "Chloroplast structure and biogenesis," *Annu. Rev. Biochem.* **40,** 161–198.
18. Hoober, J. K., Siekevitz, P. & Palade, G. E. (1969) "Formation of chloroplast membranes in *Chlamydomonas reinhardi* y-1. Effects of inhibitors of protein synthesis," *J. Biol. Chem.* **244,** 2621–2631.
19. Eytan, G. & Ohad, I. (1972) "Biogenesis of chloroplast membranes VIII. Modulation of chloroplast lamellae composition and function induced by discontinuous illumination and inhibition of ribonucleic acid and protein synthesis during greening of *Chlamydomonas reinhardi* y-1 mutant cells," *J. Biol. Chem.* **247,** 122–129.
20. Bar-Nun, S., Wallach, D. & Ohad, I. (1972) "Biogenesis of chloroplast membranes X. Changes in the photosynthetic specific activity and the relationship between the light harvesting system and photosynthetic electron transfer chain during greening of *Chlamydomonas reinhardi* y-1 cells," *Biochim. Biophys. Acta* **267,** 125–137.
21. Thornber, J. P. (1969) "Comparison of a chlorophyll *a*–protein isolated from a blue-green alga with chlorophyll–protein complexes isolated from green bacteria and higher plants," *Biochim. Biophys. Acta* **172,** 230–241.
22. Dietrich, W. E., Jr. & Thornber, J. P. (1971) "The P700-chlorophyll *a*-protein of a blue-green alga," *Biochim. Biophys. Acta* **245,** 482–493.
23. Thornber, J. P. & Olson, J. M. (1971) "Chlorophyll–proteins and reaction center preparations from photosynthetic bacteria, algae and higher plants," *Photochem. Photobiol.* **14,** 329–341.
24. Kung, S. D. & Thornber, J. P. (1971) Photosystem I and II chlorophyll–protein complexes of higher plant chloroplasts," *Biochim. Biophys. Acta* **253,** 285–289.
25. Thornber, J. P. & Benson, D. (1971) *Comparative Biochemical Studies on Reaction Center Containing Chlorophyll-Protein Complexes,* Abstract from Conference on Primary Photochemistry of Photosynthesis, Argonne National Laboratory, p. 8.
26. Arnon, D. I. (1949) "Copper enzymes in isolated chloroplasts; Polyphenoloxidase in isolated chloroplasts," *Plant Physiol.* **24,** 1–15.
27. Siegelman, H. W., Wieczorek, G. A. & Turner, B. C. (1965) "Preparation of calcium phosphate for protein chromatography," *Anal. Biochem.* **13,** 402–404.
28. Boardman, N. K. (1968) "The photochemical systems of photosynthesis," in *Advances in Enzymology,* ed. Nord, F. F. (Interscience Publishers, John Wiley & Sons, New York), Vol. 30, pp. 1–79.
29. Clayton, R. K. (1971) "The biological part," in *Light and Living Matter, Vol. 2: The Biological Part* (McGraw-Hill Book Company, New York).
30. Herron, H. A. & Mauzerall, D. (1972) "The development of photosynthesis in a greening mutant of *Chlorella* and an analysis of the light saturation curve," *Plant Physiol.* **50,** 141–148.
31. Thornber, J. P., Gregory, R. P. F., Smith, C. A. & Bailey, J. L. (1967) "Studies on the nature of the chloroplast lamellae. I. Preparation and some properties of two chlorophyll-protein complexes," *Biochemistry* **6,** 391–396.
32. Boardman, N. K. (1970) "Physical separation of the photosynthetic photochemical systems," *Annu. Rev. Plant Physiol.* **21,** 115–140.
33. Sane, P. V. & Park, R. B. (1970) "Purification of photosystem I reaction centers from spinach stroma lamellae," *Biochem. Biophys. Res. Commun.* **41,** 206–210.

Proc. Nat. Acad. Sci. USA
Vol. 70, No. 1, pp. 138–142, January 1973

Bromodeoxyuridine Dependence—A New Mutation in Mammalian Cells

(hamster cells/drug dependence/DNA)

RICHARD L. DAVIDSON* AND MICHAEL D. BICK†

* Clinical Genetics Division and Department of Medicine, Children's Hospital Medical Center and Department of Microbiology and Molecular Genetics; and † Department of Biological Chemistry, Harvard Medical School, Boston, Massachusetts 02115

Communicated by Edward A. Adelberg, October 30, 1972

ABSTRACT **When cells of a Syrian hamster melanoma were grown in increasing concentrations of bromodeoxyuridine (BrdU), lines of mutant cells able to grow well at high concentrations of BrdU were isolated. The mutant cells were characterized by BrdU dependence. In the absence of BrdU, the cells grew very poorly. The requirement for BrdU was specific for both the bromine and the deoxy sugar. The mutant cells incorporated BrdU into the DNA, replacing about 50% of the thymine residues with bromouracil. The reason for the BrdU dependence is not known.**

The drug 5-bromodeoxyuridine (BrdU), which can be incorporated into DNA in place of thymidine, has many types of effects on cells. It has been shown to act as a mutagen (1), to suppress differentiated functions (2), to induce latent viruses (3), and to affect the strength of binding of a bacterial repressor to its operator (4). Mammalian cells resistant to the drug have been isolated (5). A search for additional cell lines able to grow in BrdU has led to the discovery of a new type of mutation in mammalian cells, BrdU dependence. The isolation and properties of the mutant cells are described in this paper.

MATERIALS AND METHODS

Isolation of Cells in BrdU. The cells were derived from the pigmented Syrian hamster melanoma line RPMI 3460 (6). This line has been maintained in culture for several years, and its derivatives have been used extensively in cell hybridization studies (7). A pigmented clone called 3460 W1 (referred to below as W1) was used as the parental line for the isolation of the mutant cells. The cells were grown in Dulbecco's modified Eagle's medium supplemented with 10% fetal-calf serum (E medium).

For the isolation of cells able to grow in BrdU, 60-mm (Falcon) plastic tissue culture dishes were inoculated each with 2×10^6 W1 cells in E medium containing 3 μg/ml BrdU (Sigma Chemical Co.). After 3 weeks in this medium, about 20 large colonies of cells were present in each dish. The colonies from two dishes were pooled, and the cells were passed two more times in medium with 3 μg of BrdU per ml, and then passed two times in medium containing 30 μg of BrdU per ml. (E medium containing 30 μg of BrdU per ml will be referred to as E–B medium.) During these passages, the cells were transferred at 2- to 3-week intervals. 2 Weeks after the second passage in E–B medium, large colonies of cells were observed. Several colonies were picked and subcultured individually in E–B medium. The lines obtained were called 3460 B1, B2, B3, etc., and as a group will be referred to as 3460 B. Because of the repeated transfers in BrdU before the isolation of colonies, it is not certain that all of the colonies are of independent origin.

Pyrimidine Requirements. The 3460 B cells were tested for the ability to grow in E medium alone or supplemented with one of the following: BrdU, thymidine, uridine, deoxyuridine, bromouracil, bromouridine, and iododeoxyuridine. Since cells resistant to BrdU often lack the enzyme thymidine kinase (EC 2.7.1.21), and are therefore unable to grow in HAT medium [E medium supplemented with 0.1 mM hypoxanthine, 0.4 μM aminopterin, and 16 μM thymidine (8)], the 3460 B cells were also tested for their ability to grow in HAT medium. For the growth tests, 60-mm dishes were inoculated with 10^4 cells (maintained in E–B medium until harvested for the tests) in E medium containing different additives. After 1 week the dishes were renewed with fresh medium; after 2 weeks, the cells (from two dishes with each medium) were counted.

Labeling of Cells and DNA Isolation. Cells were grown in E or E–B medium to which was added the appropriate radiolabel at an activity of 10 μCi/ml for 2–3 population doublings before harvesting the cells. Cells were labeled with either [^{3}H]thymidine (6.7 Ci/mmol), [^{3}H]BrdU (26.4 Ci/mmol), or $H_3{}^{32}PO_4$. (All three compounds were purchased from New England Nuclear Corp.)

The cells were collected by trypsinization, centrifuged, resuspended in 1 ml of 0.01 M Tris·HCl–0.01 M KCl–1.5 mM $MgCl_2$ (pH 8.5), containing 5% NP-40 detergent, and lysed by vigorous agitation with a Vortex mixer. The nuclei were collected and resuspended in 0.1 M NaCl, 0.03 M Tris·HCl (pH 7.5) 0.01 M EDTA, and 2% Sarkosyl. Previously digested Pronase (Calbiochem) was added to a concentration of 1 mg/ml, and the mixture was gently rocked at 37° for 1 hr, extracted twice with phenol, then extracted once with chloroform, and finally dialyzed overnight against 0.01 M Tris·HCl–1 mM EDTA (pH 7.5). When ^{32}P was used as the label, the DNA was subjected to a 30-min treatment with RNase A (previously boiled for 10 min) before dialysis.

CsCl Gradient Centrifugation. Neutral gradients were prepared by the addition of CsCl to an initial density of either 1.700 g/ml (for 3460 and W1) or 1.750 g/ml (for 3460 B) in a total volume of 5 ml. Gradients were run for 72 hr in a Beckman L2-65B ultracentrifuge at 35,000 rpm. For alkaline CsCl gradients, the DNA sample was denatured and the gradient was prepared as described (9), at an initial density of either 1.760 g/ml (for 3460 and W1) or 1.790 g/ml (for 3460 B). The tubes were punctured and 10-drop fractions were collected. Samples were taken for scintillation counting and determination of refractive indices.

Radiation Sensitivity. 0.2-ml DNA samples were irradiated in small, open petri dishes with a UV Germicidal Lamp (Syl-

vania G15T8) at a distance of 10 cm for 10 min at room temperature (24°). After irradiation, samples were denatured in 0.3 N NaOH and analyzed for single-chain scissions on alkaline sucrose gradients. The gradients were run on 5–25% sucrose in 0.3 N NaOH–0.7 M NaCl for 90 min at 49,000 rpm in an SW50.1 rotor. Denatured bacteriophage T7 DNA was used as a marker.

Cells were irradiated with light from a fluorescent source (ITT F40, Cool White) at a distance of 10 cm at room temperature. The cells were growing in (Falcon) plastic tissue culture dishes, and the medium was left in the dishes with the top on during irradiation.

RESULTS

The 3460 B sublines were maintained in E–B medium after their isolation. All of the lines were maintained for at least 6 weeks, during which time they were subcultured at least four times. One of the sublines, 3460 B4 (referred to below as B4), was maintained in continuous multiplication in BrdU for more than 6 months, undergoing more than 75 cell divisions with no decrease in growth rate. Cells of the B4 subline had as much thymidine kinase activity as the 3460 cells. (Thymidine kinase assays were kindly performed by Dr. S. J. Adelstein.) Cells of all of the 3460 B sublines were unpigmented, consistent with previous observations of the effect of BrdU on pigment cells (10).

Soon after their isolation, it became apparent that the 3460 B cells were not simply BrdU resistant but were actually BrdU dependent. When transferred to E medium, the cells stopped growing. The cell morphology was also altered in the absence of BrdU, with the cells becoming flattened and enlarged. [This is the reverse of the effect of BrdU on the morphology of mouse melanoma cells, in which case the cells exposed to BrdU became more flattened (11).] Seven of the 3460 B sublines were tested for their ability to grow in medium without BrdU, and it can be seen from Table 1 that all of the sublines grew very poorly in the absence of the drug. On the average, the increase in cell number over the 2-week period of the test was 20-fold greater in E–B medium than in E medium.

Cloning experiments were performed in an effort to determine the significance of the small increase in the number of 3460 B cells in the absence of BrdU. The B4 line was subcloned

TABLE 1. *BrdU dependence of 3460 B sublines*

Cell line*	Cell number† (×10⁻⁴) +BrdU	−BrdU	Cell line*	Cell number† (×10⁻⁴) +BrdU	−BrdU
3460 B4	150	4	3460 B4(A)	330	12
B8	110	3	B4(B)	380	15
B9	130	6	B4(C)	430	8
B10	72	8	B4(D)	580	10
B11	24	2			
B12	36	5			
B13	28	2			

* 3460 B4, B8, B9, etc. are independent clones of cells isolated in E–B medium. 3460 B4(A), B4(B), etc. are subclones of 3460 B4.

† The cell number is the total number of cells per 60-mm dish (average of two dishes), counted 14 days after inoculation with 10^4 cells in medium containing either 30 μg of BrdU per ml or no BrdU.

TABLE 2. *BrdU concentration and thymidine competition*

Medium additive*	Cell number† (×10⁻⁴)	Medium additive*	Cell number† (×10⁻⁴)
None	12	BrdU (30)	415
BrdU (0.03)	12	BrdU (30) + Thymidine (3)	402
BrdU (0.3)	75		
BrdU (3)	180	BrdU (30) + Thymidine (30)	365
BrdU (30)	445		
BrdU (90)	2	BrdU (3)	192
Thymidine (3)	10	BrdU (3) + Thymidine (3)	152
Thymidine (30)	12		
		BrdU (3) + Thymidine (30)	26

* 60-mm Dishes were inoculated with 10^4 B4 cells in E medium, supplemented as indicated in the Table. The concentrations of the additive, in μg/ml, are indicated in parentheses.

† See note to Table 1.

in BrdU, and four subclones were tested for their ability to grow in the absence of the drug (see Table 1). It can be seen that all of the subclones were BrdU dependent and, like the parental population, underwent a small increase in cell number in the absence of BrdU.

Cells of the B4 line and of one of the subclones, B4(D), were cloned in E and E–B medium, to determine whether all of the cells in the BrdU-dependent populations could grow slowly in the absence of BrdU or whether a small fraction of the cells could survive and grow rapidly without the drug. The cloning dishes were stained and counted after 2 weeks, and it was seen that the cloning efficiency of the dependent cells was about the same in medium with or without BrdU (8% in E medium and 11% in E–B medium). However, the average colony size in E medium was less than 10 cells, whereas the average colony size in E–B medium was more than 200 cells. These results suggested that all of the cells in the dependent populations could grow very slowly, at least for a few generations, in the absence of BrdU.

Since BrdU-dependent cells had not been observed previously, it was necessary to show that these cells actually required BrdU and not some trace contaminant in the commercially supplied material. Two different lots of the drug were tested and both gave the same results. One sample of BrdU was further purified by paper chromatography [with Whatman 3Mm paper and a solvent of butanol–formic acid–water 770:108:122]. The BrdU spot was detected with UV light, cut out, and eluted. The chromatographed BrdU was tested for its ability to support the growth of B4 cells at two different concentrations (15 μg/ml and 3 μg/ml); the dependent cells grew as well with the chromatographed BrdU as with nonchromatographed material. These results suggested that the cells actually required BrdU itself.

The B4 line was used to study in detail the requirement for BrdU. The rate of growth of the cells was dependent upon the concentration of BrdU (Table 2). Over a thousandfold range of concentrations, from 0.03 μg/ml to 30 μg/ml (about 0.1 μM–100 μM) BrdU, the cells grew faster as the concentration of the drug was increased. At a concentration of 90 μg of BrdU per ml, the cells did not grow at all. It was mentioned earlier that the dependent cells in the absence of drug became very flattened and enlarged. In this experiment, it was observed that the

TABLE 3. *Thymidine requirement of BrdU-dependent cells*

Medium additive*	Cell number† ($\times 10^{-4}$)
None	18
BrdU	425
HAT	20
HA + BrdU	2
HAT + BrdU	127

* BrdU was used at a concentration of 30 μg/ml. H, A, and T represent hypoxanthine, aminopterin, and thymidine at the concentrations indicated in *Methods*.

† See note to Table 1.

extent of enlargement decreased progressively as the concentration of BrdU was increased.

Experiments were performed to determine if thymidine could be substituted for BrdU (Table 2). The results demonstrated that thymidine could not satisfy the requirement for BrdU. The fact that the cells could not survive when thymidine was substituted for BrdU in the medium demonstrated that the BrdU was not being used by the cells to compensate for an inability to synthesize thymidine.

The B4 cells were grown in mixtures of BrdU and thymidine to test whether there was any competition between them (see Table 2). With equal amounts of BrdU and thymidine in the medium, the presence of thymidine had no effect on cell growth. However, with a 10-fold excess of thymidine over BrdU, cell growth was significantly inhibited. Thus, even though thymidine could not be utilized in place of BrdU, it did compete with BrdU.

Experiments were also performed to determine whether the cells could survive without any thymidine at all. The *de novo* synthesis of thymidine was blocked by aminopterin, forcing the cells to obtain any necessary thymidine from the medium. As shown in Table 3, when aminopterin was added to the medium, the cells could not grow in the presence of BrdU without added thymidine (E medium contains no thymidine), nor could they grow with thymidine in the absence of BrdU. However, if both thymidine and BrdU were present when aminopterin was in the medium, the cells could grow. These results showed that the cells required both thymidine and BrdU for growth and that neither one alone was sufficient. The necessary thymidine could be provided by the cell's own synthetic mechanisms (indicated by the fact that exogenous thymidine was not required for growth in the absence of aminopterin) or, in the presence of aminopterin, thymidine had to be obtained from the medium.

TABLE 4. *Specificity of BrdU requirement*

Medium additive*	Cell number† ($\times 10^{-4}$)	Medium additive*	Cell number† ($\times 10^{-4}$)
None	6	None	18
BrdU	298	BrdU	425
Bromouracil	10	Bromouridine	18
Uridine	8	Iododeoxyuridine	2
Deoxyuridine	10		

* All of the additives were tested at a concentration of 30 μg/ml.

† See note to Table 1.

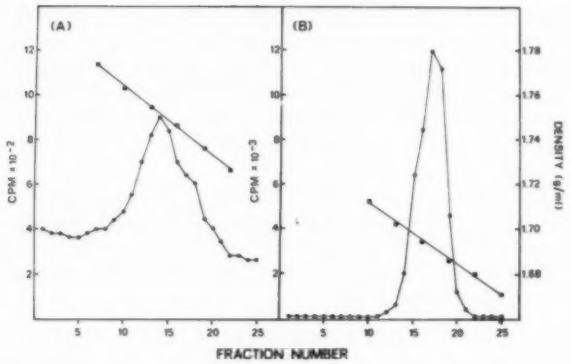

FIG. 1. Incorporation of BrdU into DNA of dependent cells. Neutral CsCl gradients were prepared as described in *Methods*. (*A*) B4 DNA, labeled with ^{32}P; (*B*) 3460 DNA, labeled with [^{3}H]-thymidine. ●——● radioactivity; ■——■, density.

The specificity of the requirement for BrdU was tested by culturing the B4 cells in medium in which BrdU was replaced by uridine, deoxyuridine, bromouracil, bromouridine, or iododeoxyuridine. The results of the tests are shown in Table 4, and it is clear that none of the compounds tested could be substituted for BrdU, indicating that the requirement for BrdU was specific for both the bromine and the deoxy sugar.

The specificity of the requirement for BrdU suggested that the BrdU was being incorporated into the DNA of the dependent cells. Since cells with BrdU-substituted DNA have been shown to be sensitive to visible light (12), the effect of fluorescent light on the B4 cells was determined. It was found that the cells were extremely light-sensitive, with a 10-min exposure reducing the fraction of surviving cells to 0.01%. The same exposure had no effect on cells not growing in the presence of BrdU.

In order to test more directly whether the dependent cells were incorporating BrdU into DNA, the buoyant density of the DNA was examined. The 3460 and W1 cells were grown in E medium containing [^{3}H]thymidine or $H_3{}^{32}PO_4$, and the B4 cells were grown in E–B medium plus [^{3}H]thymidine, [^{3}H]-BrdU, or $H_3{}^{32}PO_4$. The DNA from the labeled cells was extracted, and the buoyant density of the DNA was determined in neutral CsCl. As shown in Fig. 1, the DNA from the 3460 cells gave a single peak with a density of 1.693 g/ml. The DNA from W1 cells (not shown) gave an identical result. The DNA from the B4 cells also gave a single peak, but the peak was much more disperse, and the mean density had increased to 1.753 g/ml. No labeled DNA with the density of 3460 DNA was detected in the dependent cells. The large increase in the density of the B4 DNA indicated a significant incorporation of BrdU into the DNA of the dependent cells. Table 5 shows the density ranges from five different CsCl gradients with four different DNA preparations and all three labeled precursors. While the peak of radioactivity for the B4 cells was heterogeneous, the mean density, as well as the upper and lower extremes, were always the same, regardless of the labeled precursor used. The fact that the distribution of label showed the same density ranges with both [^{3}H]thymidine and [^{3}H]BrdU suggested that BrUra was evenly distributed throughout the DNA.

The extent to which T residues had been replaced by BrUra

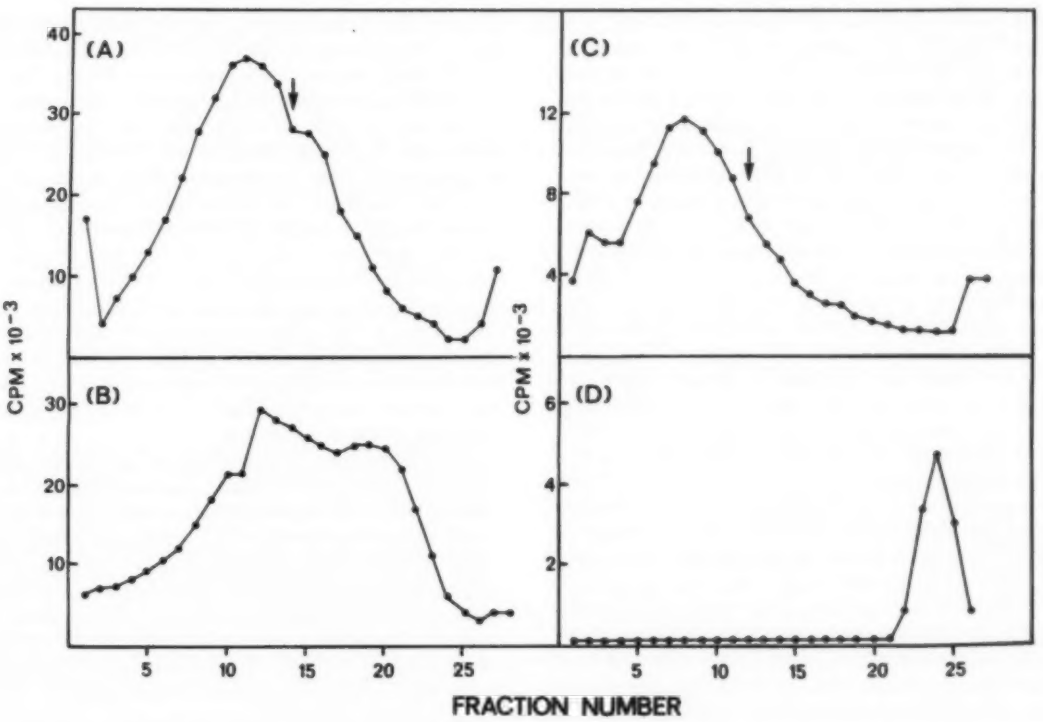

FIG. 2. Effect of UV irradiation on DNA of BrdU-dependent cells. Alkaline sucrose gradients of irradiated and unirradiated DNA, treated and centrifuged as described in *Methods*. (*A*) 3460 DNA, unirradiated; (*B*) 3460 DNA, irradiated; (*C*) B4 DNA, unirradiated; (*D*) B4 DNA, irradiated. DNA of both cell lines was labeled with [^{3}H]thymidine. *Arrow* indicates position of T7 DNA marker.

in the DNA of the dependent cells was calculated on the basis of the shift in density. The density of the 3460 DNA corresponded to a G-C content of 40% or a T content of 30%. In CsCl, the density of poly(dA-dT) is 0.20 g/ml less than that of poly(dA-dBrUra) (13). Thus, the shift in density from 1.693 (for 3460 DNA) to 1.753 (for B4 DNA) indicated a replacement of 50% of the T residues by BrUra in B4. The extremes of density of the B4 DNA corresponded to a range of 33–66% substitution, if we assume that all of the DNA fragments would contain 30% T. The density shifts described above were obtained with DNA at a molecular weight of 10^8. Identical results were obtained with DNA sheared to 6–8 $\times$ 10^6 daltons.

Labeled DNA from B4 cells was run on alkaline CsCl gradients to determine if the BrdU was being incorporated uniformly into both strands of DNA. The DNA of the dependent cells was found to band with a single peak. The fact that the two strands did not separate in alkaline CsCl indicated that approximately equal amounts of BrUra were incorporated into both strands of the DNA.

BrdU-substituted DNA has been shown to be much more light-sensitive than unsubstituted DNA (14). Labeled DNA from 3460 and B4 cells was exposed to UV light and then run on alkaline sucrose gradients to detect single-strand scissions (see Fig. 2). The unirradiated, single-stranded DNA of the 3460 cells had a single broad peak, with a mean molecular weight of about 2 $\times$ 10^7. After irradiation, some DNA of 2 $\times$ 10^7 molecular weight still remained, but the size distribution became more heterogeneous, with an obvious production of some smaller fragments. The unirradiated single-stranded DNA of the dependent cells had a molecular weight of 2 $\times$ 10^7, similar to that of the 3460 cells. However, after irradiation, no label at all was detectable in high molecular weight DNA. All of the label appeared in a single peak, with a molecular weight of less than 2 $\times$ 10^6. The fact that no single-stranded DNA of high molecular weight remained after irradiation suggested again that the BrUra was located in both strands of the DNA, and further suggested that there were very few, if any, long stretches of DNA into which BrdU was not incorporated.

In an effort to further characterize the BrdU-dependence mutation, a population of "revertant" cells able to grow rapidly without BrdU was isolated and studied. The revertant population, called B4-E, was derived from B4 after the cells

TABLE 5. *Density range of B4 DNA*

Label*		Density range†	Peak
[^{3}H]Thymidine		1.736–1.772	1.757
[^{3}H]BrdU		1.733–1.778	1.752
$H_2{}^{32}PO_4$		1.732–1.774	1.752
$H_2{}^{32}PO_4$		1.733–1.766	1.751
$H_2{}^{32}PO_4$		1.731–1.774	1.753
	Average	1.733–1.773	1.753

* B4 cells were labeled with [^{3}H]thymidine, [^{3}H]BrdU, or $H_2{}^{32}PO_4$ as described in *Methods*.

† Extremes of density of B4 DNA, run on neutral CsCl gradients prepared as described in *Methods*.

had undergone 25 generations in the presence of BrdU, and was obtained after several passages of B4 in the absence of BrdU. B4-E cells were cloned in E and E–B medium; the cloning efficiency of the cells was about 60% in E medium and 5% in E–B medium, with the colonies in both media being about the same size suggesting that about 10% of the cells in the B4-E population were again able to grow rapidly in the presence of BrdU. A new population of cells growing in BrdU, called B4-E-B, was isolated from B4-E; after 15 generations in BrdU, the B4-E-B cells were again tested for BrdU incorporation and dependence. The density of B4-E-B DNA was determined, and it was found that B4-E-B cells incorporated as much BrdU into DNA as B4 cells. However, in contrast to B4, B4-E-B cells were able to grow as well in E medium as in E–B medium. The B4-E-B cells were thus unlike the B4 cells from which they had been derived, even though both populations grew rapidly at high concentrations of BrdU and incorporated BrdU into the DNA. The reason for this difference is not understood.

The mutagenic effect of BrdU is thought to be due to pairing errors during DNA replication, resulting in the replacement of A-T pairs by G-C pairs (15). A progressive increase in G-C content in cells grown in BrdU might, therefore, be expected. The buoyant density of the DNA of the revertant B4-E cells, which had undergone 25 generations in the presence of BrdU before being reselected in E medium, was determined after the cells had grown 30 generations in the absence of the drug. The DNA of these cells was found to have a buoyant density of 1.693, identical to that of 3460 cells. The absence of a detectable shift in buoyant density indicated that the presence of BrUra in the DNA during 25 generations did not result in a large-scale increase in G-C content.

DISCUSSION

This paper has described the characteristics of a new mutation in mammalian cells, BrdU dependence. (The term "mutation" is used to indicate that the variant phenotype is heritable, and it is not meant to imply that a change at the genetic level has been demonstrated.) The requirement for BrdU was specific for both the bromine and the deoxy sugar. Thymidine could not satisfy the BrdU requirement, but the cells needed thymidine in addition to BrdU for survival. The mutation was leaky, in the sense that some growth occurred when the dependent cells were removed from BrdU.

Tests of the physical properties of the DNA of the dependent cells demonstrated that the BrdU was being incorporated into the DNA of the cells. About 50% of the T residues were replaced by BrUra in the dependent cells, and the BrUra seemed to be evenly distributed throughout the DNA. Some of the dependent cells have undergone more than 75 cell divisions in the presence of BrdU, indicating that cells can survive for long periods of time with highly substituted DNA.

The isolation of these BrdU-dependent cells recalls the effect of BrdU on the growth of infectious bovine rhinotracheitis virus. When the virus was grown for one cycle in the presence of BrdU, it was found that BrdU was required for the growth of the virus in the subsequent cycle (16). The reason that BrdU was necessary for viral growth was not determined.

Cells able to grow in media with high concentrations of BrdU have been isolated previously from many different mammalian cell lines. Two classes of BrdU-resistant mutants have been described, one class in which the cells lacked the enzyme thymidine kinase (5) and the other class in which the cells had thymidine kinase activity, but were deficient in the thymidine uptake system (17). In both cases resistance to the drug was associated with the absence of incorporation of BrdU into the DNA. The mutant cells described in this paper differ from those previously isolated in that the 3460 B cells have both thymidine kinase activity and an active thymidine uptake system, incorporate BrdU into the DNA, and, most strikingly, are BrdU dependent.

The existence and properties of the BrdU-dependent cells raise many questions, especially the question of why do the cells require BrdU. Some of the possibilities that are being considered are based on the many effects that BrdU has been shown to have in other systems, e.g., as a mutagen, as a suppressor of differentiated functions, and as an inducer of latent viruses. Another possibility is that the BrdU dependence is not based on the action of the drug itself or on the effect of its incorporation into the DNA, but is due instead to an alteration in the DNA-synthesizing system of these cells.

We acknowledge the excellent technical assistance of Miss Gayle Forbes and Mr. Dennis Sabourin. This work was supported in part by NICHD Grants HD 04807 and HD 06276. M. D. B. is a Damon Runyon fellow in the laboratory of Dr. C. A. Thomas, Jr., where the work was supported by NIH Grant AI 08186-03 and NSF Grant 31118X.

1. Litman, R. & Pardee, A. (1956) *Nature* **178,** 529–531.
2. Stockdale, F., Okazaki, K., Nameroff, M. & Holtzer, H. (1964) *Science* **146,** 533–535.
3. Lowy, D., Rowe, W., Teich, N. & Hartley, J. (1971) *Science* **174,** 156.
4. Lin, S. & Riggs, A. (1972) *Proc. Nat. Acad. Sci. USA* **69,** 2574–2576.
5. Kit, S., Dubbs, D., Piekarski, L. & Hsu, T. (1963) *Exp. Cell Res.* **31,** 297–312.
6. Moore, G. (1964) *Exp. Cell Res.* **36,** 422–423.
7. Davidson, R. L. (1971) *In Vitro* **6,** 411–426.
8. Littlefield, J. (1964) *Science* **145,** 709.
9. Flamm, W., McCallum, M. & Walker, P. (1967) *Proc. Nat. Acad. Sci. USA* **57,** 1729–1734.
10. Coleman, A., Kunkel, D., Werener, I. & Coleman, J. (1968) *J. Cell Biol.* **39,** 27 abstr.
11. Silagi, S. & Bruce, S. (1970) *Proc. Nat. Acad. Sci. USA* **66,** 72–78.
12. Puck, T. & Kao, F. (1967) *Proc. Nat. Acad. Sci. USA* **58,** 1227–1234.
13. Wake, R. & Baldwin, R. (1962) *J. Mol. Biol.* **5,** 201–216.
14. Lion, M. (1970) *Biochim.Biophys. Acta* **209,** 24–33.
15. Freese, E. (1959) *J. Mol. Biol.* **1,** 87–105.
16. Stevens, J. (1965) *Virology* **25,** 379–386.
17. Breslow. R. & Goldsby, R. (1969) *Exp. Cell Res.* **55,** 339–346.

Proc. Nat. Acad. Sci. USA
Vol. 70, No. 1, pp. 143–146, January 1973

Photooxidation of Chlorophyll *b* by Quinones Studied by Chemically-Induced Dynamic Nuclear Polarization

(NMR/excited states/radical pairs)

MICHA TOMKIEWICZ* AND MELVIN P. KLEIN

Laboratory of Chemical Biodynamics, Lawrence Berkeley Laboratory, University of California, Berkeley, Calif. 94720

Communicated by Melvin Calvin, November 6, 1972

ABSTRACT **The photooxidation of chlorophyll *b* by 1,4-benzoquinone and 2,6-dimethyl-1,4-benzoquinone was investigated by the technique of chemically-induced dynamic nuclear polarization. Polarization of the proton magnetic resonance lines of the quinone was detected. A mechanism for the photooxidation was postulated that invokes the reaction of the quinone with the excited singlet state of the chlorophyll to form a radical pair. This mechanism, together with a theoretical model and parameters taken from the literature, yields a theoretical proton magnetic resonance spectrum for the polarized quinone that agrees well with that observed experimentally.**

The photosensitized oxidation of chlorophyll by different oxidizing agents is being investigated in several laboratories (1–17), in order to provide guidelines for understanding the primary steps in photosynthesis. Among the various oxidants, the reaction of chlorophyll with various quinones is of special interest. It is well established that this reaction proceeds through free-radical intermediates, but the mechanistic details are still controversial (16). There are conflicting data on the nature of the excited states of chlorophyll with which the quinones react. The main sources of information about the nature of the precursors involved were obtained from flash photolysis, electron spin resonance (ESR), and fluorescence studies with β-carotene as a competing quencher of the excited states. It was assumed that β-carotene reacts only with the triplet state of the excited chlorophyll. Addition of quinone reduced the concentration of the excited triplet of the chlorophyll, but not its lifetime (13, 14), suggesting that the quinone reacts with a precursor of the chlorophyll triplet. However, ESR studies showed that β-carotene quenches the semiquinone radical formation, a finding that was explained in terms of competition between the quinones and the β-carotene for the chlorophyll triplet (9, 11).

As a way out of this dilemna, Tollin (13, 14, 17) suggested that a reaction occurs involving a ternary complex of the form:

$$(\text{solvent}\cdots\text{Chl}\cdots\text{Q}) \xrightarrow{h\nu} (\text{solvent}_{ox} + \text{Chl} + \text{Q}^-).$$

The suggestion was that the chlorophyll photosensitizes the oxidation of solvent molecules and the solvent radical that is formed reacts with the quinone. Recently, Harbour and Tollin (17) reported observations of the solvent radical in low-temperature ESR experiments; for ethanol as the solvent, the ethoxy radical was identified.

Chemical reactions involving radical pairs can give rise to nuclear spin polarization, which is manifest by enhanced nuclear magnetic resonance (NMR) absorption and/or emission. This phenomenon is commonly denoted as chemically-induced dynamic nuclear polarization (CIDNP) (18, 19). This technique appeared to be eminently suitable for attacking this problem, and we report here direct evidence of the nature of the precursors in the photooxidation of chlorophyll by quinones.

A necessary condition for producing polarized NMR spectra of this sort is a competition between spin-dependent annihilation of the radical pair to form a singlet and spin-independent scattering to form the two separate radicals (20–26). This condition seems to be satisfied in this case, since the reaction is reversible and the radicals of both Chl^+ and semiquinone have been observed by electron paramagnetic resonance (EPR) (16). Furthermore, some data obtained by fluorescence, flash photolysis, and ESR were interpreted in terms of the existence of radical pairs (1, 3, 16). Since the CIDNP technique is sensitive to the multiplicity of the precursor of the radical pair, as well as to the chemical nature of the participants, it seemed to be a promising approach for clarification of some of the mechanistic aspects of this reaction.

MATERIALS AND TECHNIQUE

The light-induced PMR spectra were recorded with a Varian A-60 spectrometer equipped with a light guide, as described elsewhere (27). 1,4-Benzoquinone was purified by vacuum sublimation. Chlorophyll *b* supplied by Sandoz Pharmaceuticals (crystallizable product) and by Sigma (highly purified) was used without further purification. All other chemicals were the most highly purified among those commercially available, and were used without further purification. Corning glass filters were used to select the desired spectral range. Calibrated mesh filters were used to change the light intensity. A Hanovia 1000-W high-pressure mercury xenon lamp in a Schoeffel housing was used as the light source.

We found no effect upon deoxygenating the sample, except for the observation that the deoxygenated samples remained stable for longer periods of irradiation. Fresh solutions were used for each experiment.

Abbreviation: CIDNP, chemically-induced dynamic nuclear polarization.

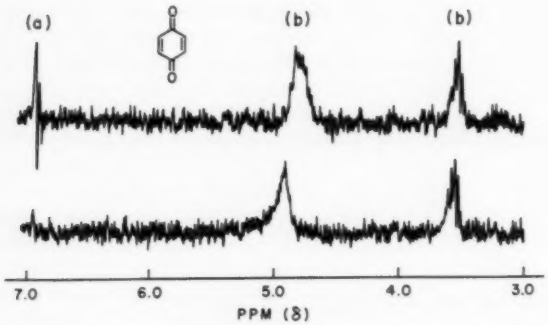

FIG. 1. 60-MHz PMR spectra of a solution of 10 mM 1,4-benzoquinone and 50 μM chlorophyll *b* in CD_3OD. *Lower trace:* before irradiation. *Upper trace:* during irradiation with visible light. (*a*) 1,4-benzoquinone; (*b*) CD_3OD.

RESULTS

Fig. 1 shows spectra for a solution of 50 μM chlorophyll *b* with 10 mM 1,4-benzoquinone in perdeuterated methanol. The lower trace shows the spectrum before irradiation and the upper trace shows the spectrum during irradiation with visible light passed through an O-51 Corning filter, which removes all light with wavelengths shorter than 400 nm. The magnetic field increases from left to right. The line that appears in the low-field part of the spectrum is due to the ring protons of 1,4-benzoquinone. The remaining features are due to the solvent. It can be seen that upon irradiation the ring protons of the 1,4-benzoquinone are enhanced in intensity, while the shape and intensity of the methyl protons of the solvent remained unchanged. The absorption peak of the OH protons changes shape and shifts to higher field due to local heating, but integration of the signal revealed that there is no change in intensity.

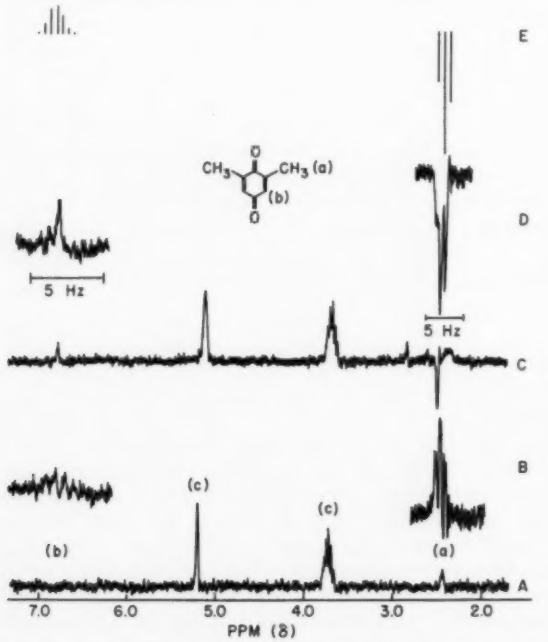

FIG. 2. 60-MHz PMR spectra of a solution of 10 mM 2,6-dimethyl-1,4-benzoquinone and 50 μM chlorophyll *b* in CD_3OD. (*A*) and (*B*): before irradiation. (*C*) and (*D*): during irradiation with visible light. (*E*) Theoretically constructed stick spectrum. (*a*) Methyl protons of the quinone; (*b*) aromatic protons of the quinone; (*c*) solvent lines.

Fig. 2 shows spectra of 2,6-dimethyl-1,4-benzoquinone taken under the same conditions as in Fig. 1. *A* and *B* are scans recorded before irradiation under low- and high-resolution conditions, respectively, while *C* and *D* were recorded during irradiation.

The PMR spectrum of 2,6-dimethyl-1,4-benzoquinone is of the type $AX_3A'X'_3$ (28). While we were unable to resolve the ring proton lines, the methyl lines were fully resolved, with a coupling constant of $J_{ax} = 0.7 \pm 0.2$ Hz. Upon irradiation, the ring protons of 2,6-dimethyl-1,4-benzoquinone are enhanced in intensity, while the signals due to the methyl protons appear as emission lines with a different distribution of intensities within the triplet as compared to the unirradiated sample. In addition, an unidentified peak appears on the low-field side of the methyl protons of the quinone in trace *C*. This peak arises from some unidentified polarized irradiation product. Another feature of the spectra (not shown) is that after prolonged irradiation the enhanced absorption lines of the ring protons become emission lines. We will not deal with this problem here, as we are not sure of the mechanisms involved. Our working hypothesis is that these inverted lines occur from new product(s), whose chemical shift does not differ from that of the aromatic protons of the original quinones.

The polarization of an NMR line that results from transitions between nuclear states *n* and *m* is defined by:

$$P_{mn} = \frac{V_{mn} - V^{\circ}_{mn}}{V^{\circ}_{mn}}, \qquad [1]$$

where V_{mn} is the observed intensity of the NMR signal and V°_{mn} is the intensity of the signal at Boltzman equilibrium.

No polarization of the quinone peaks occurred in the absence of chlorophyll. No polarization was observed when the chlorophyll was replaced with chlorophyllin. Also, no polarization was observed when the deuterated methanol solvent was replaced by CCl_4.

When the system chlorophyll + quinone was excited with red light by use of a Corning filter 2–61, which removed all wavelengths shorter than 600 nm, the same pattern of polarization was observed, but the magnitude was reduced by more than 50%; this result indicates that both visible-absorption bands of the chlorophyll participate in the reaction. No further enhancement of the polarization was observed by removal of all filters and extension of the spectral range of the excitation into the ultraviolet. The polarization was proportional to the light intensity.

Theory

Details of the theory used to calculate the polarized spectra can be found elsewhere (23). Here, we will give only the final formulas involved in those calculations, and we mention the physical meaning of the parameters involved.

Based on the density matrix treatment of the radical pair, the theoretical expression for P_{mn} in Eq. **1** is:

$$P_{mn} = \frac{LkT}{g_N\beta_N H_O \sum_n [D \cdot P]_n} \gamma T_1^{nm} (\rho^n_{ss} - \rho^m_{ss}) \qquad [2]$$

In this equation, $D \cdot P$ describes the diamagnetic product formed by annihilation of the radical pair, $L = \prod_i (2I_i + 1)$, the total number of nuclear levels of $D \cdot P$, g_N is the nuclear g factor, β_N is the nuclear magneton, T is the absolute temperature, H_0 is the intensity of the magnetic field, k is the Boltzman factor, $\gamma = k_1/k_{-2}$ where k_1 is the rate constant for the radical-pair annihilation and k_{-2} is the rate constant for scattering of the radical pair to give two separate radicals (see scheme I), T_1^{nn} is the spin-lattice relaxation time from state m to state n, and ρ_{ss} is the diagonal density matrix element for the singlet state of the radical pair, which is given by:

$$\rho_{ss} = \frac{\alpha_{ss} + \mu(2 + \gamma)\alpha_{TT}}{1 + \gamma + \mu(2 + \gamma)} \quad [3]$$

In Eq. **3**, α is a matrix that describes the rate of formation of the radical pair; its exact form will depend on the nature of the precursor of the radical pair. If the total rate of formation of the radical pair is given by k^*, then for a singlet precursor

$$\alpha_{TT} = 0 \text{ and } \alpha_{ss} = k^*,$$

for a triplet precursor

$$\alpha_{ss} = 0 \text{ and } \alpha_{TT} = k^*/3$$

and if the radical pair is formed from two separate radicals, then

$$\alpha_{ss} = \alpha_{TT} = k^*/4.$$

μ is given by

$$\mu = \frac{H^2_{ST}/k^2_{-2}}{(1 + \gamma/2)^2 + 4J^2_e/k^2_{-2} + (2 + \gamma)H^2_{ST}/k^2_{-2}} \quad [4]$$

In Eq. **4**, J_e is the electron exchange integral in energy units, which is related to the energy separation of the singlet and the T_0 triplet state of the radical pair, and H_{ST} is the off-diagonal matrix element of the spin-Hamiltonian that mixes the singlet with the T_0 state of the triplet manifold, and is given by:

$$H_{ST} = 1/2[\beta H_0 \Delta g + \sum_j^a A_j N_j - \sum_j^b A_k N_k] \quad [5]$$

In Eq. **5**, a and b are the two radicals that form the radical pair, Δg is the difference in their electronic g factors, A_j and A_k are their scalar nuclear hyperfine interactions, N_j and N_k are their nuclear spin quantum numbers that describe the state of the jth and kth spin (for protons 1/2 and $-1/2$), and β is the electron Bohr magneton.

DISCUSSION

The stick spectrum given in Fig. 2(*E*) was constructed by use of Eq. **2** with the appropriate parameters, based on the following mechanism:

$$\text{Chl} + \text{Q} \underset{k_1}{\overset{h\nu}{\rightleftarrows}} \text{Chl}^{*S} + \text{Q} \rightarrow \text{Chl}^{*T} + \text{Q}$$

$$\text{Chl}^{*S} \xrightarrow{k^*} \overline{\text{Chl}^+ \text{Q}^-} \xrightarrow{k_{-2}} \text{Chl}^+ + \text{Q}^-$$

Scheme I

The chlorophyll is excited to its singlet excited state, from which it can go by intersystem crossing to the excited triplet state. The quinone quenches the excited *singlet*. As a result, the radical pair $\overline{\text{Chl}^+ \text{Q}^-}$ is formed. The radical pair can dissociate to give the semiquinone radical and Chl^+ or it can annihilate to give back the starting materials. This mechanism can account for the reversibility of the reaction, as well as for the fact that both the semiquinone radical and Chl^+ have been detected by EPR (16).

According to this scheme, the constituents of the radical pair are Chl^+ and Q^-. The g value of Chl^+ is 2.0025 (29) and that of 2,6-dimethyl-1,4-semiquinone radical is 2.00445 (30). The magnitudes of the hyperfine interaction of the CH_3 protons is $A_{CH_3} = +1.87\ g$, and that of the aromatic protons $A_H = -2.22\ g$ (30). The signs were deduced from the well-known difference in coupling mechanism between these two kinds of protons and the unpaired electron spin density in semiquinone radicals. While the coupling of the CH_3 protons is via hyperconjugation and, hence, A_{CH_3} will be positive, the coupling of the aromatic protons is via polarization of the C–H σ electrons by the unpaired π electron and, hence, A_{CH_3} will be negative (31).

The asymmetry of the methyl triplet is determined by the sign of the indirect coupling constant, J_N. For the calculated stick spectrum in Fig. 2*E*, which agrees reasonably well with the experimentally observed spectrum, Fig. 2*D*, a negative sign was required, in agreement with other allylic coupling constants, e.g., toluene (32). The electron–electron exchange interaction was taken as $J_e = 10^8$ Hz; the justifications for use of this value are given elsewhere (23). The parameters given thus far are sufficient for calculating H_{ST} from Eq. **5**.

Much less is known about the kinetic parameters that appear in Scheme I. The existence of biradicals of the nature postulated here was suggested previously to explain various optical and EPR observations (1, 3, 16). Hales and Bolton (16) postulate that they observe the EPR spectrum of the $\text{Chl}^+ \text{Q}^-$ biradical at room temperature and that the biradical decays with a first-order rate constant of 1.2×10^3 sec^{-1}. We have some reservations as to the correctness of the assignment of their rapidly decaying ESR signal as the $\text{Chl}^+ \text{Q}^-$ biradical, and thus do not choose to use their value for the rate of disappearance in our calculations. In view of lack of other sources of information, we took the literature value for the rate constant for the reaction $\text{Chl}^+ + \text{Q}^-$, which is $(3.0 \pm 1.0) \times 10^9$ liter mol^{-1} sec^{-1} (10, 7, 12). We normalized this value to an apparent quinone concentration in which the distance between the quinone and the chlorophyll would be 6 Å, and multiplied the result by a steric factor that accounts for only one semiquinone radical per Chl^+. Assuming that the radical pair dissociates with equal probabilities through its singlet and the three triplet channels, we arrived at the following values for the rate constants:

$$k_1 = 5 \times 10^9 \text{ sec}^{-1} \text{ and } k_{-2} = 1.5 \times 10^9 \text{ sec}^{-1}$$

In view of the fact that we did not measure quantum yields for the polarization, the only information that we have about k^* is its linear dependence upon the light intensity, which derives from the predicted linear dependence of the polarization. It should be mentioned that the accuracy of our estimation of the rate constants will have only a marginal effect on the relative shape of the simulated spectrum, but will have a pronounced effect on the absolute magnitude of the

observed polarization. The shape of the polarized spectrum is very sensitive to the relative values of Δg and the hyperfine constants of the various protons.

Finally, as the precursor is a singlet

$$\alpha_{ss} = k^* \text{ and } \alpha_{TT} = 0$$

Attempts to fit the spectra for a triplet precursor or two separate radicals gave spectra inverted relative to the experimental. It was impossible to fit the spectra to the radical pair proposed by Tollin *et al.* (13, 14, 17), namely, $\overline{CH_3O\ Q^-}$. Using the g value assigned by Harbour and Tollin (17) for the ethoxy radical, $g = 2.0049$, and assuming that the methoxy radical will have a similar g value, we find that the Δg between the methoxy and the semiquinone radicals is too small as compared to the hyperfine interactions to account for the observed polarization. Simulated spectra that are based on those values look totally different from those observed experimentally.

Although the experimental results presented here are in reasonable agreement with the postulate of a singlet precursor of the radical pair, we cannot exclude some participation of the chlorophyll triplet. From Eqs. **2–5**, one can see that if the same products are formed from singlet and triplet precursors, the condition for the absence of any polarization is that $\alpha_{ss} = \alpha_{TT}(1 + \gamma)$. The fact that we observe polarization characteristic of a singlet precursor is indicative that at least 30% of the radical pairs form through the singlet channel. We cannot assign a more accurate fraction, as the absolute quantum yield of the polarization was not measured.

This work was performed under the auspices of the U.S. Atomic Energy Commission. M. T. was a postdoctoral fellow of the National Institutes of Health (NIGMS).

1. Livingston, R. & Ke, C-L. (1950) *J. Amer. Chem. Soc.* **72**, 909–915.
2. Linschitz, H. & Rennert, J. (1952) *Nature* **169**, 193–194.
3. Tollin, G. & Green, G. (1962) *Biochim. Biophys. Acta* **60**, 524–538.
4. Tollin, G., Chatterjee, K. K. & Green, G. (1965) *Photochem. Photobiol.* **4**, 593–600.
5. Chibisov, A. K., Karyakin, A. V., Drozdova, N. N. & Krasnovskii, A. A. (1967) *Dokl. Akad. Nauk SSSR* **175**, 737–740.
6. Evstigneev, V. B. (1968) *J. Chim. Phys. Physicochim. Biol.* **65**, 1447–1456.
7. Seifert, K. & Witt, H. (1968) "Progress in Photosynthesis Research," *Proc. Int. Congr. Biochem.* **2**, 750–756.
8. Chibisov, A. K. (1972) *Dokl. Akad. Nauk SSSR* **205**, 142–145.
9. White, R. A. & Tollin, G. (1967) *J. Amer. Chem. Soc.* **89**, 1253–1257.
10. Chibisov, A. K. (1969) *Photochem. Photobiol.* **10**, 331–347.
11. Mukherjee, D. C., Cho, D. H. & Tollin, G. (1969) *Photochem. Photobiol.* **9**, 273–289.
12. Kelly, J. M. & Porter, G. (1970) *Proc. Roy. Soc. Ser. A* **319**, 319–329.
13. Raman, R. & Tollin, G. (1971) *Photochem. Photobiol.* **13**, 135–145.
14. White, R. A. & Tollin, G. (1971) *Photochem. Photobiol.* **14**, 15–63.
15. Quinlan, K. P. (1971) *Photochem. Photobiol.* **13**, 113–121.
16. Hales, B. J. & Bolton, J. R. (1972) *J. Amer. Chem. Soc.* **94**, 3314–3320.
17. Harbour, J. R. & Tollin, G. (1972) *Proc. Nat. Acad. Sci. USA* **69**, 2066–2068.
18. Bargon, J., Fisher, H. & Johnson, U. (1967) *Z. Naturforsch. A.* **22**, 1551–1555.
19. Ward, H. R. & Lawler, R. G. (1967) *J. Amer. Chem. Soc.* **89**, 5518–5519.
20. Kaptein, R. & Oosterhoff, L. (1969) *Chem. Phys. Lett.* **4**, 195–197, 214–216.
21. Closs, G. & Trifunac, A. (1970) *J. Amer. Chem. Soc.* **92**, 2183–2187.
22. Fisher, C. H. (1970) *Z. Naturforsch.* **25a**, 1957–1962.
23. Tomkiewicz, M., Groen, A. & Cocivera, M. (1972) *J. Chem. Phys.* **56**, 5850–5857.
24. Ward, H. R. (1972) *Accounts Chem. Res.* **5**, 18–24.
25. Lawler, R. G. (1972) *Accounts Chem. Res.* **5**, 25–33.
26. Kaptein, R. (1972) *J. Amer. Chem. Soc.* **94**, 6521–6279.
27. Tomkiewicz, M. & Klein, M. P. (1972) *Rev. Sci. Instrum.* **43**, 1206–1207.
28. Norris, R. K. & Sternhell, S. (1966) *Aust. J. Chem.* **19**, 617–627.
29. Borg, D. C., Fajer, J., Felton, R. H. & Dolphin, D. (1970) *Proc. Nat. Acad. Sci. USA* **67**, 813–820.
30. Adams, J. M., Blois, Jr., M. S. & Sands, R. H. (1958) *J. Chem. Phys.* **28**, 774–776.
31. Carrington, A. & McLachlan, D. (1967) in *Introduction to Magnetic Resonance* (Harper & Row, New York), chap. 6.
32. Williamson, M. P., Kostelnik, R. J. & Castellano, S. M. (1968) *J. Chem. Phys.* **49**, 2218–2224.

Proc. Nat. Acad. Sci. USA
Vol. 70, No. 1, pp. 142–150, January 1973

Identity of the Ribosomal Proteins Involved in the Interaction with Elongation Factor G*

(*E. coli*/ribosomal protein antibodies/translocation/GTP/fusidic acid)

JOSEPH H. HIGHLAND†‡, JAMES W. BODLEY§, JULIAN GORDON¶, RENATE HASENBANK†, AND GEORG STÖFFLER†

† Max-Planck Institut für Molekulare Genetik, Abteilung Wittmann, Berlin-Dahlem; § Department of Biochemistry, University of Minnesota, Minneapolis, Minn. 55455; and Friedrich Miescher Institut, Basel, Switzerland¶

Communicated by Bernard D. Davis, October 24, 1972

ABSTRACT **Rabbit antibodies produced against 50 of the 55 individually purified ribosomal proteins of *Escherichia coli* were tested for their ability to interfere with the formation of the ribosome·EF-G·GDP complex. Only antibodies produced against proteins L7 and L12 inhibited complex formation, and they did so completely. These two proteins were previously shown to be immunologically indistinguishable and necessary for the interaction between ribosomes and EF-G. The present data are consistent with the view that the interaction between ribosomes and EF-G that results in GTP hydrolysis occurs on, and is limited to, proteins L7 and L12 on the surface of the 50S ribosomal subunit.**

Establishment of the structure–function relationships of ribosomes and the mechanisms of GTP involvement in ribosome function are two of the major goals in defining the process of translation of the genetic code (for recent reviews, see refs. 3 and 4).

Elucidation of ribosomal structure–function relationships has been thwarted by the complexity and cooperativity of ribosomal structure (the ribosome is composed of more than 50 distinct macromolecules), as well as the complexities of its functions. The availability of antibodies produced against individually purified ribosomal proteins now provides a potentially powerful tool with which to investigate the functional topology of ribosomes. Already, experiments involving the use of antibodies have successfully defined the specific ribosomal proteins involved in streptomycin and spectinomycin binding (5)**,††, yielded information on the identity of the ribosomal proteins that bind ribosomal RNA (6, 7), and implicated proteins L7 and L12 in the interaction between ribosomes and EF-G (8).

Similarly, elucidation of the roles of GTP in ribosome function has been hampered by the complexities of the reactions and their participants. An experimental approach to this problem is provided by the "single step" hydrolysis of GTP by EF-G and the 50S ribosomal subunit in the presence of fusidic acid (9, 10). This system is one of the simplest manifestations of GTP participation in protein synthesis, and recent results suggest that it may involve a ribosomal site in common with the other GTP-requiring elongation step of protein synthesis, aminoacyl-tRNA binding (2, 11–14).

In the experiments to be reported here, we have simply asked, which antibodies to ribosomal protein (when reacted with the ribosome) will prevent the formation of the ribosome·EF-G·GDP complex? The results are surprisingly simple; only antibodies prepared against proteins L7 and L12 inhibit this reaction, suggesting that they are the only proteins physically involved in this interaction. To our knowledge these results provide the first direct definition of a ribosomal site of interaction with a factor, and support earlier work that suggested this relationship (8, 15, 16).

MATERIALS AND METHODS

Preparation of Materials. The preparation of antisera against individual ribosomal proteins, and the purification and characterization of IgGs and their corresponding Fab-fragments from these sera were as described (17, 18)‡‡. The methods of preparation of *E. coli* EF-G and ribosomes were also described (19). [^{3}H]GTP was obtained from New England Nuclear Corp. and had a specific activity of 5.7 Ci/mmol. Miss Barbara Stearns of E.R. Squibb kindly provided the fusidic acid.

Reaction of Antibodies with the Ribosome. Ribosomes (30 μg) were reacted for 3 min at 0° with the appropriate IgG or Fab preparation in the amounts indicated. The reaction (final volume, 20 μl) contained, in addition to ribosomes and antiserum: 10 mM Tris·HCl (pH 7.4), 10 mM magnesium acetate, 60 mM NH_4Cl, and 1 mM dithiothreitol.

Formation of the Ribosome·EF-G·[^{3}H]GDP Complex. 15 μl of the ribosome–antibody reaction mixture described above was added to 35 μl of a solution that contained 10 mM Tris·HCl (pH 7.4), 10 mM magnesium acetate, 28 mM

* This is paper no. XLII in the series "Ribosomal Proteins" and paper no. XIII in the series "Studies on Translocation." The preceding papers in these series are refs. 1 and 2, respectively.

‡ To whom reprint requests should be sent. Current address: Friedrich Miescher Institut, Postfach 273, CH-4002, Basel, Switzerland.

** Bollen, A., Maschler, R. & Stöffler, G., *J. Mol. Biol.*, submitted for publication.

†† Lelong, J. C., Gros, F., Bollen, A., Maschler, R. & Stöffler, G. *Proc. Nat. Acad. Sci. USA*, to be submitted for publication.

‡‡ Maschler, R., Hasenbank, R. & Stöffler, G., *Biochemistry*, submitted for publication.

NH_4Cl, 1 mM dithiothreitol, 11 units of EF-G (19), 3 mM fusidic acid, and 10 pmol of [^{3}H]GTP. Under these conditions the antigen–antibody complex remained in solution. The mixture was incubated for 5 min at 0°. The ribosome·EF-G·[^{3}H]GDP complex was measured by a Millipore filtration method (20). Under these conditions, the binding of [^{3}H]GDP to Millipore filters was limited by ribosomes; in the absence of IgG, about 2 pmol was bound.

RESULTS

As summarized in Table 1, only two types of results characterized the effect of antibodies prepared against individual 50S ribosomal proteins on the ability of 70S ribosomes to participate in the subsequent formation of the ribosome·EF-G·[^{3}H]GDP complex. All but two IgG preparations either were without effect or stimulated the interaction somewhat. By contrast, the IgGs prepared in response to proteins L7 and L12 suppressed this interaction by more than 90%. In similar experiments with IgGs prepared in response to proteins of the 30S subunit (Table 2), only the neutral or stimulatory effect was observed. These results should be compared to earlier findings†,‡ (also ref. 5 and G. S., unpublished data) that the majority of IgG preparations inhibited the ability of ribosomes to participate in overall protein synthesis, i.e., polyphenylalanine formation.

TABLE 1. *The effect of IgG binding (specific for 50S proteins) on the formation of the ribosome·EF-G·[^{3}H]GDP complex*

Ribosomal protein specificity of IgG preparation	% [^{3}H]GDP binding
L1	140
L2	126
L3	122
L4	120
L5	164
L6	126
L7	*4*
L8	116
L9	138
L10	130
L11	122
L12	*6*
L13	113
L14	96
L15	138
L16	138
L17	118
L18	115
L19	100
L20	140
L21	114
L22	144
L23	130
L24	116
L25	142
L26	N.D.
L27	140
L28	120
L29	135
L30	120
L31	N.D.
L32	N.D.
L33	108
L34	N.D.

The reaction conditions were as described in the text. 0.32 A_{280} units of IgG was present in the initial reaction with ribosomes, yielding an IgG/ribosome ratio of 135. The amount of [^{3}H]GDP binding observed in the absence of IgG is defined as 100%.

The concentration dependence of the inhibition of complex formation by anti-L7 and -L12 IgGs is compared in Fig. 1 with the response to a typical noninhibitory IgG. Since proteins L7 and L12 are immunologically identical (18), the difference in the ability of these two IgG preparations to inhibit complex formation presumably reflects only a difference in antibody titer. The significance of the stimulation of complex formation observed with low amounts of the IgG preparations is not clear. However, since it is known that only a portion of the ribosomes is capable of binding EF-G and GDP (20), it is likely that IgG binding (either specific or nonspecific) alters ribosome conformation so as to increase this fraction.

In order to eliminate the possibility that the observed inhibitions by antibodies to proteins L7 and L12 resulted from nonspecific precipitation of ribosomes, monovalent Fab-fragments were prepared from both antibodies. These Fab-fragments yielded inhibition curves essentially identical to those shown in Fig. 1 (data not shown).

The ribosome·EF-G·GDP complex was shown (10) to result from the direct interaction of ribosomes, EF-G, and GDP. Inhibition curves similar to those shown in Fig. 1 for IgG L7 were also obtained when this complex was formed starting with GDP rather than GTP (data not shown). These results are consistent with the view that all of the interactions between EF-G and ribosomes that are necessary for GTP hydrolysis occur on, and are limited to, proteins L7 and L12 on the surface of 50S ribosomal subunits.

DISCUSSION

Proteins L7 and L12 are acidic 50S ribosomal proteins that can be removed from ribosomes either with CsCl or with ethanol and NH_4Cl. Neither the resulting protein-deficient particles nor the separated proteins themselves are able, by various criteria, to interact with EF-G and GTP. However, this interaction can be readily restored by the readdition of proteins L7 and L12 to the protein-deficient particles (8, 15, 16). These results suggest, but by no means prove, that EF-G interacts with these proteins on the ribosome, for it is known that the conformation of ribosomes is important to this interaction (21), and these proteins may simply promote the required conformation.

The ribosome·EF-G·GDP complex forms on the 50S subunit (9); the present experiments demonstrate that of antibodies prepared against 30 individual purified 50S ribosomal proteins (thus far, preparation of the remaining four antibodies has not succeeded for technical reasons), only antibodies produced in response to proteins L7 and L12 prevent formation of this complex. In addition, we have tested antibodies prepared against 20 of the 21 30S proteins, and found all of them to be without inhibitory activity. These results, taken together with the fact, as mentioned above, that the presence of proteins L7 and L12 on ribosomes is required for this interaction, lead us to conclude that these proteins, and probably only these proteins, comprise the physical region of contact between elongation factor G and ribosomes. However, we have no information with respect to the possible involvement of the four 50S proteins for which we are presently unable to obtain antisera.

TABLE 2. *The effect of IgG binding (specific for 30S proteins) on the formation of the ribosome·EF-G·[^{3}H]GDP complex*

Ribosomal protein specificity of IgG preparation	% [^{3}H]GDP binding
S1	116
S2	123
S3	122
S4	115
S5	104
S6	150
S7	97
S8	96
S9	119
S10	125
S11	128
S12	116
S13	149
S14	124
S15	108
S16	119
S17	N.D.
S18	132
S19	101
S20	99
S21	118

The reaction conditions were as described in Table 1.

Proteins L7 and L12 are, in several respects, unique among ribosomal proteins. (*i*) They are acidic, while the majority of ribosomal proteins are basic (22–24). (*ii*) Their amino-acid compositions are distinctive: each contains ϵ-*N*-monomethyllysine and about 25 mol % alanine (22–24). (*iii*) Compared to other ribosomal proteins, they have a high α-helix content (about 50–60%) (24, 25). (*iv*) Proteins L7 and L12 are immunologically identical (18) and, except for an *N*-acetyl-blocked terminal serine in L7, they appear to be identical in sequence (26, 27)¶¶. Such extensive structural homologies between other ribosomal proteins have not been found. (*v*) Together, proteins L7 and L12 appear to be present in at least two, but probably three, copies per 50S subunit (18, 26, 28, 29)§§, while the majority of ribosomal proteins appear to be present in one or fewer copies per particle (3, 28)§§.

GTP is hydrolyzed in at least three distinct steps of protein synthesis. During initiation, it is required for the binding of fMet-tRNA to 30S subunits, and its hydrolysis is mediated by initiation factor IF-2 and requires the addition of 50S subunits. In elongation, GTP hydrolysis occurs during EF-Tu-mediated aminoacyl-tRNA binding, and during EF-G-mediated translocation. In the first case hydrolysis requires the 50S subunit, and in the second it can occur entirely upon this subunit. Three independent lines of evidence suggest that at least these latter two hydrolytic events involve a common region of 50S subunits. (*i*) Thiostrepton, an antibiotic that binds to 50S subunits, prevents both the EF-G- and EF-Tu-associated hydrolyses (30). (*ii*) Protein L7 and/or L12 are required for both reactions (15, 16). (*iii*) The two

§§ Thammana, P., Weber, H. J., Deusser, E., Maschler, R., Kurland, C. G., Stöffler, G. & Wittmann, H. G., *Nature*, in press.
¶¶ Terhorst, C., Möller, W., Laürsen, R. & Wittmann-Liebold, B., *Eur. J. Biochem.*, submitted for publication.

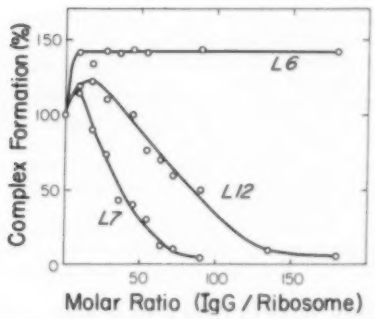

FIG. 1. Concentration dependence of the effect of IgG on the formation of the ribosome·EF-G·[^{3}H]GDP complex. Conditions are described in the text.

hydrolytic reactions cannot occur simultaneously on a single ribosome (2, 11–13). Additionally, it has recently been suggested that GTP hydrolysis during initiation might also involve this ribosomal site (31).

In the light of these relationships and the observations reported here, an attractive hypothesis is that proteins L7 and L12, perhaps present as a triad, constitute a "universal" GTPase region on the ribosome. In combination with either EF-G or EF-Tu, proteins L7 and L12 would participate in GTP hydrolysis and, in some way, transduce the energy derived from these hydrolyses to the ribosome so as to promote the conformational changes required for translocation and for aminoacyl-tRNA binding, respectively.

Whatever the case, it is clear that ribosomal protein-specific antibodies will be of considerable importance in defining the functional and structural topology of the ribosome.

We thank H. G. Wittmann for stimulating discussions. This research was supported in part by grants to J. W. B. from the American Cancer Society (NP-460), the National Science Foundation (GB-19164), and the National Institutes of Health (GM-17101) and an EMBO travel fellowship to J. H. H.

1. Schulte, C. & Garrett, R. A. (1972) "Ribosomal proteins XLI optimal conditions for the interaction of ribosomal protein S8 and 16S RNA and studies on the reaction mechanism," *Mol. Gen. Genet.*, in press.
2. Richman, N. & Bodley, J. W. (1972) "Ribosomes cannot interact simultaneously with elongation factors EF-Tu and EF-G," *Proc. Nat. Acad. Sci. USA* **69**, 686–689.
3. Kurland, C. (1972) "Structure and function of the bacterial ribosome," *Annu. Rev. Biochem.* **41**, 377–408.
4. Lucas-Lenard, J. & Lipmann, F. (1971) "Protein biosynthesis," *Annu. Rev. Biochem.* **40**, 409–448.
5. Wittmann, H. G. & Stöffler, G. (1972) *The Mechanism of Protein Synthesis and Its Regulation*, ed. Bosch, L. (North-Holland, Amsterdam).
6. Stöffler, G., Daya, L., Rak, K. H. & Garrett, R. A. (1971), "Ribosomal proteins XXVI. The number of specific protein binding sites on 16S and 23S RNA of *E. coli*," *J. Mol. Biol.* **62**, 411–414.
7. Gray, P. N., Garrett, R. A., Stöffler, G. & Monier, R. (1972) "An attempt at the identification of the proteins involved in the incorporation of 5sRNA during 50S ribosomal subunit assembly," *Eur. J. Biochem.* **28**, 412–421.
8. Kischa, K., Möller, W. & Stöffler, G. (1971) "Reconstitution of a GTPase activity by a 50S ribosomal protein," *Nature* **233**, 62–63.
9. Bodley, J. W. & Lin, L. (1970) "Interaction of *E. coli* G factor with the 50S ribosomal subunit," *Nature* **227**, 60–62.

10. Bodley, J. W., Zieve, F. J. & Lin, L. (1970) "Studies on translocation IV. The hydrolysis of a single round of guanosine triphosphate in the presence of fusidic acid," *J. Biol. Chem.* **245**, 5662–5667.
11. Cabrer, B., Vazquez, D. & Modelell, J. (1972) "Inhibition by elongation factor EF-G of amino acyl-tRNA binding to ribosomes," *Proc. Nat. Acad. Sci. USA* **69**, 733–736.
12. Miller, D. L. (1972) "Elongation factors EF-Tu and EF-G interact at related sites on the ribosome," *Proc. Nat. Acad. Sci. USA* **69**, 752–755.
13. Richter, D. (1972) "Inability of *E. coli* ribosomes to interact simultaneously with the bacterial elongation factors EF-Tu and EF-G," *Biochem. Biophys. Res. Commun.* **46**, 1850–1856.
14. Cundliffe, E. (1972) "The mode of action of fusidic acid," *Biochem. Biophys. Res. Commun.* **46**, 1794–1801.
15. Hamel, E. & Nakamoto, T. (1972) "Requirement of an *E. coli* 50S ribosomal protein component for effective interaction of the ribosome with T and G factors and with guanosine triphosphate," *J. Biol. Chem.* **247**, 805–814.
16. Brot, N., Yamasaki, E., Redfield, B. & Weissbach, H. (1972) "The properties of an *E. coli* ribosomal protein required for the function of factor G," *Arch. Biochem. Biophys.* **148**, 148–155.
17. Stoffler, G. & Wittmann, H. G. (1971) "Sequence differences of *E. coli* 30S ribosomal proteins by immunochemical methods," *Proc. Nat. Acad. Sci. USA* **68**, 2283–2287.
18. Stöffler, G. & Wittman, H. G. (1971) "Ribosomal proteins XXV. Immunological studies on *E. coli* ribosomal proteins," *J. Mol. Biol.* **62**, 407–409.
19. Highland, J. H., Lin, L. & Bodley, J. W. (1971) "Protection of ribosomes from thiostrepton inactivation by the binding of G-factor and guanosine diphosphate," *Biochemistry* **10**, 4404–4409.
20. Bodley, J. W., Zieve, F. J., Lin, L. & Zieve, S. T. (1970) "Studies on translocation III. Conditions necessary for the formation and detection of a stable ribosome·G factor-guanosine diphosphate complex in the presence of fusidic acid," *Biol. Chem.* **245**, 5655–5661.
21. Bodley, J. W. & Lin, L. (1972) "Studies on the nature of the G factor binding site on the 50S ribosomal subunit," *Biochemistry* **11**, 782–786.
22. Kaltschmidt, E., Dzionara, M. & Wittmann, H. G. (1970) "Ribosomal proteins XV. Amino acid compositions of isolated ribosomal proteins from 30S and 50S subunits of *E. coli*," *Mol. Gen. Genet.* **109**, 292–297.
23. Mora, G., Donner, D., Thammana, P., Lutter, L., Kurland, C. G. & Craven, G. R. (1971) "Purification and characterization of 50S ribosomal proteins of *E. coli*," *Mol. Gen. Genet.* **112**, 229–242.
24. Dzionara, M. (1970) "Ribosomal proteins. Secondary structure of individual ribosomal proteins of *E. coli* studied by circular dichroism," *FEBS Lett.* **8**, 197–200.
25. Möller, W., Castlemen, H. & Terhorst, C. (1970) "Characterization of an acidic protein in 50S ribosomes of *E. coli*," *FEBS Lett.* **8**, 192–196.
26. Möller, W., Groene, A., Terhorst, C. & Amons, R. (1972) "50S Ribosomal proteins. Purification and partial characterization of two acidic proteins A_1 and A_2 isolated from 50S ribosomes of *E. coli*," *Eur. J. Biochem.* **25**, 5–12.
27. Terhorst, C., Wittmann-Liebold, B. & Möller (1972) "50S Ribosomal proteins. Peptide studies on two acidic proteins, A_1 and A_2, isolated from 50S ribosomes of *E. coli*," *Eur. J. Biochem.* **25**, 13–19.
28. Weber, H. J. (1972) "Stoichiometric measurements of 30S and 50S ribosomal proteins from *E. coli*," *Mol. Gen. Genet.*, in press.
29. Deusser, E. & Wittmann (1972) "Ribosomal proteins: Variations of the protein composition in *Escherichia coli* ribosomes as function of growth rate," *Nature* **238**, 269–270.
30. Modolell, J., Cabrer, B., Parmeggiani, A. & Vazquez, D. (1971) "Inhibition by siomycin and thiostrepton of both aminoacyl-tRNA and factor G binding to ribosomes," *Proc. Nat. Acad. Sci. USA* **68**, 1796–1800.
31. Grunberg-Manago, M., Dondon, J. & Graffe, M. (1972) "Inhibition by thiostrepton of the IF-2 dependent ribosomal GTPase," *FEBS Lett.* **22**, 217–221.

Proc. Nat. Acad. Sci. USA
Vol. 70, No. 1, pp. 151–155, January 1973

Requirement of Proteins S5 and S9 from 30S Subunits for the Ribosome-Dependent GTPase Activity of Elongation Factor G

(CsCl 30S core/ribosomal split proteins/30S reconstitution/30S–50S association)

ROBERT C. MARSH AND ANDREA PARMEGGIANI

Gesellschaft für Molekularbiologische Forschung, 3301 Stöckheim, Germany

Communicated by Fritz Lipmann, October 30, 1972

ABSTRACT **During CsCl isopycnic centrifugation at 20 mM Mg^{++}, *Escherichia coli* 30S ribosomal subunits specifically lose proteins S1, S2, S3, S5, S9, S10, and S14. The resultant 30S core is unable to stimulate the GTPase activity of EF-G in the presence of 50S subunits. Activity could be restored to a small extent by adding back S2, S5, or S9. However, when S5 and S9 were added together, they cooperatively produced 30S particles 1.5 times more active than the original native 30S subunits. The small amount of activity restored by S2 was simply additive to that restored by S5 or S9. None of the other split proteins showed any restoring capability. Ability of the various protein-deficient 30S particles to couple with 50S subunits corresponded closely to their activity in the EF-G GTPase reaction. It is concluded that S5 and S9 together enable the 30S subunit to participate in the formation of a GTPase-active 30S–50S–EF-G complex.**

Elongation factor G(EF-G) is essential for ribosomal polypeptide synthesis. Its presence is required for expression of a GTPase activity involved in translocation of the peptidyl-tRNA from the acceptor to the donor site of a ribosome. The ribosome–EF-G GTPase activity can be manifested also in the absence of elongation or of amino-acyl-tRNA and mRNA (1). In 1966, Nishizuka and Lipmann (2) found that both ribosomal subunits participate in this GTPase reaction. Since then, most work has pointed out the central role of the 50S ribosomal subunit in the interaction of ribosomes with EF-G (3–5). As will be shown in this communication and in more detail elsewhere, the level of GTPase activity is, however, dependent upon the additional presence of the 30S subunit. Recently, proteins L7 and L12 from the 50S subunit were found to be required for the EF-G GTPase reaction (6, 7). We now report our studies on the 30S subunit designed to determine its active components in this GTPase reaction.

Hosokawa *et al.* (8) and Staehelin and Meselson (9) have shown that CsCl isopycnic centrifugation of 30S subunits produces protein-deficient cores and a fraction of seven specific split proteins—S1, S2, S3, S5, S9, S10, and S14 (10–13)—neither of which can substitute for the 30S subunit in protein synthesis. Recombined, however, they form fully functional 30S subunits. The 30S cores specifically lack the ability to bind mRNA and, in turn, cannot bind tRNA (10, 14). We have now observed that this 30S core is also inactive in promoting the ribosome-dependent GTPase activity of EF-G, apparently due to a failure to couple with 50S subunits. A test of the purified split proteins for their ability to restore this activity has shown S5 and S9 to be the necessary components for restoration.

MATERIALS AND METHODS

EF-G and Ribosomal Particles. Pure EF-G and 70S ribosomes were isolated from *Escherichia coli* B/2 as described (15). The NH_4Cl-washed ribosomes were separated into 30S and 50S subunits by sucrose density gradient centrifugation at 0.5 mM Mg^{++} with a Spinco 15 Ti rotor, and further purified by another zonal centrifugation in a Spinco 14 Ti rotor. The 30S subunits were 99% pure and the 50S subunits were 96–97% pure, as measured by sedimentation in linear 7–30% sucrose density gradients. The 30S cores were prepared by CsCl density gradient centrifugation of 30S subunits in the presence of 20 mM Tris·HCl (pH 7.8)–20 mM $MgCl_2$–7 mM 2-mercaptoethanol (16). The CsCl was optical grade from the Harshaw Chemical Co. All ribosomal particles were stored at −35° in 10 mM Tris·HCl (pH 7.8)–10 mM $MgCl_2$–15 mM KCl–15 mM NH_4Cl–50% glycerol. One A_{260} unit was taken to represent 25 pmol of 70S, 39 pmol of 50S, or 67 pmol of 30S particles (7).

Split Proteins. Individual split proteins were purified from total 30S protein extracted with LiCl–urea (17) by a scheme inspired by methods that have been used by Nomura, Traut, and Wittmann (11, 18, 19). A correlation of the different 30S protein nomenclatures used by these groups is given in ref. 13. All chromatography was performed at 4° in a 10 mM Na-phosphate buffer containing 3 mM 2-mercaptoethanol and 6 M urea (reagent grade, Merck), which had been freshly deionized. The pH was adjusted with NaOH to the desired value. Proteins S1 and S2 were separated from the other 30S proteins by chromatography on DEAE-cellulose (Whatman DE 52) at pH 8.0 with a linear 0–200 mM LiCl gradient. S1 and S2 were then individually purified from minor contaminants by elution from CM-cellulose (Whatman CM 52) at pH 5.6 with a linear 0–200 mM LiCl gradient. The 30S proteins that did not absorb to the DEAE-cellulose at pH 8.0 were applied to a column of carboxymethyl (CM)-cellulose at pH 5.6 and eluted with a linear 80–425 mM LiCl gradient. So chromatographed, S3 and S14 were essentially pure, S9 was still somewhat contaminated, and S5 and S10 were mixed with one another. S9 was purified by CM-cellulose chromatography at pH 6.6 with a linear gradient of 150–250 mM LiCl; S5 was separated from S10 by CM-cellulose chromatography at pH 3.8 with a linear 75–200 mM LiCl gradient. After being concentrated to about 1 mg/ml with Aquacide II (Calbiochem), the proteins were stored at 4° in 50 mM Tris·HCl (pH 7.8)–2 M NH_4Cl–3 mM 2-mercaptoethanol. Purity of the proteins was monitored at all steps by polyacrylamide gel electrophoresis at pH 4.5 in 8 M urea (20). So judged, the isolated split proteins were more than 95% pure and contained no cross-contamination. Protein concentrations were measured by the method of Lowry *et al.* (21) with crystalline bovine-serum albumin as standard. Molecular weights of S1, S2, S3, S5, S9, S10, and S14 were

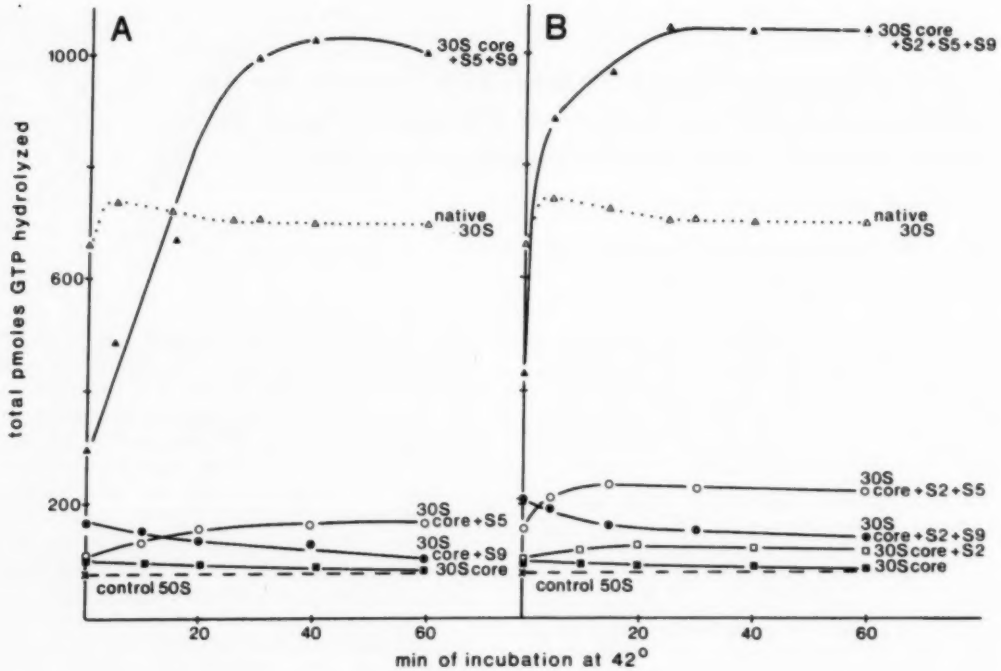

FIG. 1. Ability of S2, S5, and S9—individually and in all possible combinations—to restore activity in the ribosome–EF-G GTPase reaction to CsCl-prepared 30S cores as a function of the time of reconstitution at 42°. Each reconstitution mixture contained 8 pmol of 30S cores and a 1.2-molar excess of each of the split proteins, added as indicated in the figure. To assay GTPase activity after reconstitution 10 pmol of native 50S subunits was added to each reaction mixture. As controls, the 50S subunits were assayed alone (×) and in the presence of either (■) 30S core or (△) native 30S particles.

assumed to be 65,000, 30,000, 32,000, 24,000, 21,000, 16,000, and 15,600, respectively (22).

Reconstitution and GTPase Assay. For reconstitution of 30S particles, the 20-μl reaction mixture contained 0.12 A_{260} units of CsCl 30S cores (8 pmol) and various concentrations and combinations of the individual split proteins in 10 mM Tris·HCl (pH 7.8)–25 mM $MgCl_2$–300 mM NH_4Cl–5 mM KCl–1 mM mercaptoethanol–12% glycerol. After incubation at 42°, 0.25 A_{260} units of 50S subunits (10 pmol), 5.0 μg of EF-G (60 pmol), and 5.0 nmol of [γ-^{32}P]GTP (43–63 Ci/mol, prepared as in ref. 7) were added to the reaction mixture, which was then brought to a final volume of 75 μl containing the following concentrations: 100 mM Tris·HCl (pH 7.8)–20 mM $MgCl_2$–80 mM NH_4Cl–2 mM KCl–15 mM mercaptoethanol–3% glycerol. GTPase activity was measured as the amount of $^{32}P_i$ liberated during a 15-min incubation at 30° (7).

30S–50S Reassociation. Ability of the various 30S particles to couple with 50S subunits was measured by sedimentation in linear 7–30% sucrose gradients in 20 mM Tris·HCl (pH 7.8)–20 mM $MgCl_2$–30 mM NH_4Cl–30 mM KCl. For this procedure, the 20-μl reconstitution mixture described above was doubled in volume and constituents and incubated 20 min at 42°. After addition of 0.50 A_{260} units of 50S subunits along with 250 μl of 25 mM Tris·HCl (pH 7.8)–20 mM $MgCl_2$–50 mM NH_4Cl and incubation for 10 min at 30°, the mixtures were layered on the sucrose gradients. The gradients were spun for 3 hr at 38,000 rpm at 4° in a Spinco SW40 rotor, and the resultant absorption patterns at 254 nm were measured with an ISCO fractionator connected to an external Servogor recorder.

RESULTS

Role of 30S subunits in the EF-G-dependent GTPase reaction

As shown in Table 1 and Figs. 1 and 2, preparations of 50S ribosomal subunits that were contaminated 3–4% with measurable 30S subunits possessed a small residual capability to promote the EF-G-dependent hydrolysis of GTP. Upon addition of native 30S subunits at a 0.8 molar ratio to the 50S subunits, the GTPase activity increased 10-fold or more. Results to be published elsewhere show that the GTPase activity can be further increased when more 30S subunits are added, a plateau in activity being reached only after 30S subunits are present at a several-fold excess over the 50S.

Activity of protein-deficient 30S particles in the GTPase reaction

Under our EF-G GTPase assay conditions, designed to measure the full stimulatory activity of the average 30S subunit by including a slight—but sufficient—excess of 50S subunits, little or no activity was observed for CsCl-prepared protein-deficient 30S cores (Table 1). This variation in activity depended upon the individual 30S core preparation; the best preparations were made at 10–20 mM Mg^{++}, as opposed to 40 mM Mg^{++}. Residual activity, when present, could be

lowered or eliminated by a second centrifugation in CsCl. Addition of all purified split proteins, each at a 1.2-molar excess over core, produced 30S particles more active in the GTPase reaction than the original 30S subunits. Without the 30S core, the split proteins showed no ability to stimulate the GTPase reaction.

To determine which of the split proteins were essential for restoring activity, a series of reconstitutions and assays was performed; a different split protein was omitted from each reconstitution mixture. As Table 1 shows, S5 and S9 proved to be the necessary components, the absence of S5 having a somewhat more dramatic effect than that of S9. Only minor variations from the activity of the fully reconstituted 30S particles were observed upon omission of any one of the other five split proteins. The requirement for S5 and S9 was independent of Mg^{++} concentration over the range (10–20 mM) tested.

Restoring ability of individual split proteins

The lack of restored 30S activity in the EF-G GTPase reaction in the absence of proteins S5 and S9 naturally leads to the question: can they alone impart activity to the cores? Fig. 1*A* shows that only about 13% of the native 30S activity could be restored by either S5 or S9 alone at the 1.2-molar excess of protein over core used. Combined, however, the action of S5 and S9 proved to be extremely cooperative; particles 1.5-times more active than the native 30S control were produced. The reason for this greater activity is unclear since one copy of both S5 and S9 appears to be present in the native 30S subunit (23).

Although formation of fully active 30S particles from cores and proteins did not stringently require a 42° incubation, such an incubation was necessary to restore maximal activity in a reasonable period of time. The reactivation time could also be decreased by use of concentrations of S5 and S9 proteins higher than the 1.2-molar excess over 30S core used for the experiment illustrated in Fig. 1*A*. However, no further increase in activity of the final GTPase was observed.

A further examination of the individual split proteins revealed that the 30S restoring ability of S5 or S9 depended upon their concentration in the reaction mixture. As Fig. 2 shows, S5 could maximally restore 38% of the native 30S activity when present at more than a 5-fold excess over 30S core. With S9, a maximum restoration of 19% of native activity was reached at a 2-fold excess. Surprisingly, S2 also showed activity, restoring 20% of the native 30S activity when present at a 13.5-molar excess over core, the highest ratio tested. The presence of S2 failed, however, to have any striking effect on the restoring ability of either S5 or S9, the restoration of 30S activity in both cases being simply additive (Fig. 1*B*). Moreover, S2, S5, and S9 together showed no significant increase in final 30S activity restored over the combination of S5 and S9 alone. However, with S2 present, the rate at which S5 and S9 were able to restore 30S activity in the GTPase reaction was markedly increased (Fig. 1*A* and *B*).

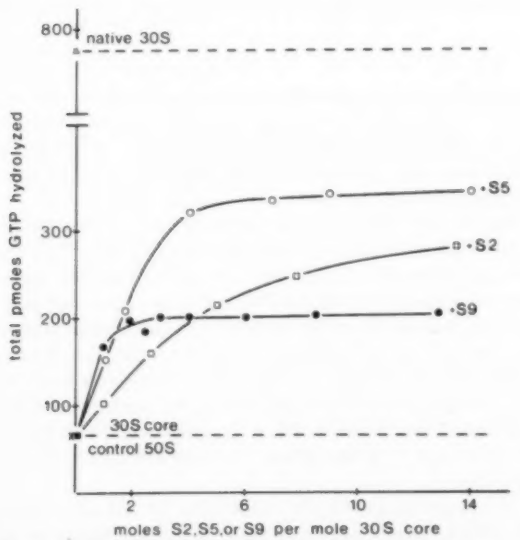

FIG. 2. The individual ability of proteins (□) S2, (○) S5, and (●) S9 to restore activity in the ribosome–EF-G GTPase reaction to 30S cores, as a function of their relative concentrations in the reconstitution mixture. All GTPase assays were performed in the presence of 10 pmol of 50S subunits. Each *point* represents the total activity observed with 8 pmol of 30S particles. These particles had been reconstituted in the presence of increasing concentrations of the given split proteins under the following observed optimal conditions: a 60-min incubation at 42° with S2 and S5, or without a 42° incubation with S9. As controls, 50S particles were assayed alone (×) and in the presence of either (■) 30S core or (△) native 30S subunits.

50S coupling ability of protein-deficient 30S particles

As a step toward elucidation of the mechanism by which S5 and S9 restore activity to 30S cores in the ribosome–EF-G GTPase reaction, the various protein-deficient 30S particles were tested for their ability to associate with 50S subunits, as judged by the production of particles sedimenting faster than

TABLE 1. *Activity of various split protein-deficient 30S particles in the ribosome–EF-G GTPase reaction*

30S particles	mol of GTP hydrolyzed per mol of 30S particles
Native 30S	82.2
30S core	4.2
30S core + (S1,S2,S3,S5,S9,S10,S14)	92.4
30S core + (—,S2,S3,S5,S9,S10,S14)	79.7
30S core + (S1,—,S3,S5,S9,S10,S14)	83.1
30S core + (S1,S2,—,S5,S9,S10,S14)	85.0
30S core + (S1,S2,S3,—,S9,S10,S14)	15.2
30S core + (S1,S2,S3,S5,—,S10,S14)	29.8
30S core + (S1,S2,S3,S5,S9, —, S14)	81.5
30S core + (S1,S2,S3,S5,S9,S10, —)	75.0

Protein-deficient 30S cores prepared by CsCl isopycnic centrifugation of native 30S subunits were incubated with a 1.2-molar excess of each of the given split proteins and tested in the presence of a 1.25-molar excess of native 50S subunits for activity in the EF-G-dependent GTPase reaction. When the 50S subunits were assayed alone, 5.4 mol of GTP were hydrolyzed per mol of 50S subunits; this background activity has been subtracted from the values given in the table. When all split proteins were tested only in the presence of 50S subunits and the background was subtracted, 0.3 mol of GTP was hydrolyzed per mol of 50S particles.

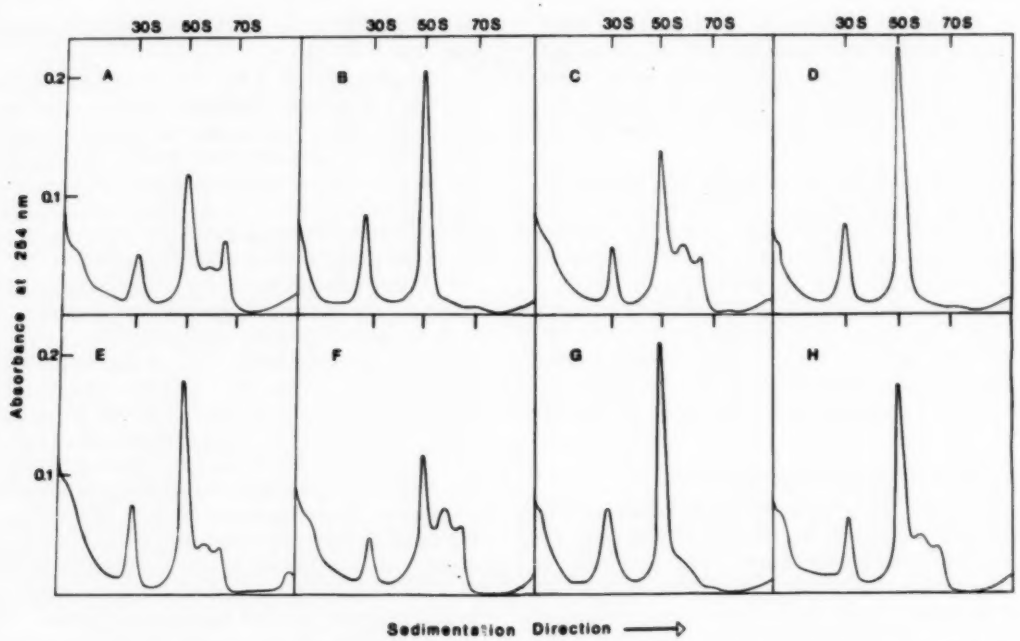

FIG. 3. 50S coupling ability of protein-deficient 30S particles as measured in linear 7–30% sucrose gradients containing 20 mM Mg^{++}. The gradients were layered with mixtures containing native 50S subunits incubated together with either (*A*) native 30S subunits, (*B*) CsCl 30S cores; or with 30S particles reconstituted from 30S cores and (*C*) all seven split proteins, (*D*) all split proteins except S5, (*E*) all split proteins except S9, (*F*) all split proteins except S10, (*G*) S5 alone, (*H*) S5 and S9 together. Each split protein was present at a 1.2-molar excess over 30S core during reconstitution except for S5 in (*G*), which was present at a 3-fold excess. Centrifugation conditions: Spinco SW40 rotor, 38,000 rpm, 3 hr at 4°. Absorption at the top of the gradients was due to the presence of mercaptoethanol in the 30S reconstitution mixture.

50S in sucrose density gradients. In direct correlation with the GTPase results, 30S cores failed to associate with 50S subunits (Fig. 3*B*) but could be restored to full activity upon addition of all seven split proteins (Fig. 3*A* and *C*). Again, this restoration depended primarily upon the presence of protein S5 (Fig. 3*D*) and, to a lesser extent, upon that of S9 (Fig. 3*E*). No difference in restored 50S coupling ability was observed when either S1, S2, S3, or S14 was omitted from the mixture of split proteins; sedimentation patterns identical with Fig. 3*C* were obtained in each case. Upon omission of S10, however, a small but reproducible stimulation in coupling occurred (Fig. 3*F*). Although this apparent inhibition of 30S–50S association by S10 may be physiologically significant, it is more likely due to nonspecific binding of S10, which is known to aggregate readily (18), to the ribosomal subunits.

Alone, S5 at high molar ratios to core could impart a small amount of 50S coupling activity (Fig. 3*G*); but, as with GTPase activity, S9 together with S5 was required to restore essentially full 50S coupling ability to the 30S cores (Fig. 3*H*).

Our failure to observe a sedimentation constant of 70 S for reassociated 30S–50S subunits is probably due to a combination of great hydrostatic pressure during the high-speed sedimentation analysis (24) and to weakened interaction between subunits in the absence of mRNA and tRNA.

DISCUSSION

Our experimental results point out the importance of 30S subunits in the ribosome–EF-G GTPase reaction and show that their activity depends upon the presence of proteins S5 and S9. Proteins S1, S3, S10, and S14 are dispensible—at least in the 10–20 mM Mg^{++} range tested. In general, S2 is also dispensible; however, it does appear capable of inducing a minor amount of 30S activity that becomes apparent in the absence of S5 and S9.

Because the 50S coupling ability of the various protein-deficient particles tested corresponded almost directly to their activity in the EF-G GTPase reaction and because the 50S subunit is known to bind EF-G under several experimental conditions (3, 4), S5 and S9 undoubtedly function by enabling the 30S subunit to participate in the formation of a GTPase-active 30S–50S–EF-G complex. Such a central role for S5 and S9 in protein synthesis is in agreement with the low capability of 30S particles reconstituted in the absence of either S5 or S9 to participate in protein synthesis, as determined by Nomura *et al.* (11).

The tempting possibility exists that S5 and S9 sit at the 30S–50S interface and in so doing directly regulate or help mediate the GTPase reaction. In support of this possibility, Huang and Cantor (25) have recently found S5 and S9 to be among six 30S proteins strongly shielded by the 50S subunit from reaction with fluorescein isothiocyanate. Alternatively, binding of S5 and S9 may simply induce conformational changes that activate other portions of the core responsible for coupling with 50S and stimulation of the GTPase reaction.

The extreme cooperativity of S5 and S9 in activating the 30S core is most exciting in light of the recent finding by Bickle *et al.* (26) that S5 and S9 can be crosslinked by reaction of 30S subunits with bis-(methyl)suberimidate and are, there-

fore, close neighbors. This result suggests that S5 and S9 interact directly, perhaps inducing conformational changes in one another that enable the 30S to couple with the 50S subunit. That the cooperativity shown by S5 and S9 is not due to any interdependency in binding to the 30S subunit during reconstitution has been observed by Mizushima and Nomura (12).

The fact that S5 plays a vital role in the ribosome–EF-G GTPase reaction is consistent with earlier work on the antibiotic spectinomycin. Spectinomycin appears to inhibit protein synthesis by blocking some aspect of ribosomal translocation (27), and S5 has been identified as the component responsible for the sensitivity of ribosomes to this antibiotic (28).

Our results indicate that S2 plays some role in the GTPase reaction and also facilitates the reconstitution of 30S particles by S5 and S9. These activities cannot be explained by contamination. It is interesting to note that S2 has also been indicated to contribute to the aminoacyl-tRNA binding site (29).

The results reported here do not affect the fact that the GTP cleavage center seems to be localized on a 50S–EF-G complex (3–5) but point out the great importance of S5 and S9 from the 30S subunit in the EF-G–ribosome GTPase reaction. Elucidation of the mechanism of the EF-G–ribosome GTPase reaction during elongation can be expected only when the role of the different components has been clarified with respect to the complete system, which alone allows polypeptide synthesis.

We thank Drs. G. Chinali and G. Sander for critically reviewing the manuscript, and are especially appreciative of the technical assistance provided by Mrs. B. Foellmer. This investigation was supported by Sonderforschungsbereich 75 of the Deutsche Forschungsgemeinschaft.

1. Lucas-Lenard, J. & Lipmann, F. (1971) *Annu. Rev. Biochem.* **40,** 409–448.
2. Nishizuka, Y. & Lipmann, F. (1966) *Arch. Biochem. Biophys.* **116,** 344–351.
3. Bodley, J. W. & Lin, L. (1971) *Nature* **227,** 60–61.
4. Brot, N., Spears, C. & Weissbach, H. (1971) *Arch. Biochem. Biophys.* **143,** 286–296.
5. Modolell, J., Vazquez, D. and Monro, R. E. (1971) *Nature New Biol.* **230,** 109–112.
6. Kischa, K., Möller, W. & Stöffler, G. (1971) *Nature New Biol.* **233,** 62–63.
7. Sander, G., Marsh, R. C. & Parmeggiani, A. (1972) *Biochem. Biophys. Res. Commun.* **47,** 866–873.
8. Hosokawa, K., Fujimura, R. K. & Nomura, M. (1966) *Proc. Nat. Acad. Sci. USA* **55,** 198–204.
9. Staehelin, T. & Meselson, M. (1966) *J. Mol. Biol.* **16,** 245–249.
10. Traub, P. & Nomura, M. (1968) *J. Mol. Biol.* **34,** 575–593.
11. Nomura, M., Mizushima, S., Ozaki, M., Traub, P. & Lowry, C. V. (1969) *Cold Spring Harbor Symp. Quant. Biol.* **34,** 49–61.
12. Mizushima, S. & Nomura, M. (1970) *Nature* **226,** 1214–1218.
13. Wittmann, H. G., Stöffler, G., Hindennach, I., Kurland, C. G., Randall-Hazelbauer, L., Birge, E. A., Nomura, M., Kaltschmidt, E., Mizushima, S., Traut, R. R. & Bickle, T. A. (1971) *Mol. Gen. Genet.* **111,** 327–333.
14. Raskas, H. & Staehelin, T. (1967) *J. Mol. Biol.* **23,** 89–97.
15. Parmeggiani, A., Singer, C. & Gottschalk, E. M. (1971) in *Methods in Enzymology,* eds. Grossmann, L. & Moldave, K. (Academic Press, New York), Vol. 20, part C, pp. 291–302.
16. Meselson, M., Nomura, M., Brenner, S., Davern, C. & Schlessinger, D. (1964) *J. Mol. Biol.* **9,** 696–711.
17. Spitnik-Elson, P. (1965) *Biochem. Biophys. Res. Commun.* **18,** 557–562.
18. Moore, P. B., Traut, R. R., Noller, H., Pearson, P. & Delius, H. (1968) *J. Mol. Biol.* **31,** 441–461.
19. Hindennach, I., Stöffler, G. & Wittmann, H. G. (1971) *Eur. J. Biochem.* **23,** 7–11.
20. Leboy, P. S., Cox, E. C. & Flaks, J. G. (1964) *Proc. Nat. Acad. Sci. USA* **52,** 1367–1374.
21. Lowry, O. H., Rosebrough, N. J., Farr, A. L. & Randall, R. J. (1951) *J. Biol. Chem.* **193,** 265–275.
22. Craven, G. R., Voynow, P., Hardy, S. J. S. & Kurland, C. G. (1969) *Biochemistry* **8,** 2906–2915.
23. Traut, R. R., Delius, H., Ahmad-Zadeh, C., Bickle, T. A., Pearson, P. & Tissières, A. (1969) *Cold Spring Harbor Symp. Quant. Biol.* **34,** 25–38.
24. Infante, A. A. & Baierlein, R. (1971) *Proc. Nat. Acad. Sci. USA* **68,** 1780–1785.
25. Huang, K. & Cantor, C. R. (1972) *J. Mol. Biol.* **67,** 265–275.
26. Bickle, T. A., Hershey, J. W. B. & Traut, R. R. (1972) *Proc. Nat. Acad. Sci. USA* **69,** 1327–1331.
27. Anderson, P., Davies, J. & Davis, B. D. (1967) *J. Mol. Biol.* **29,** 203–215.
28. Bollen, A., Davies, J., Ozaki, M. & Mizushima, S. (1969) *Science* **165,** 85–86.
29. Randall-Hazelbauer, L. L. & Kurland, C. G. (1972) *Mol. Gen. Genet.* **115,** 234–242.

Proc. Nat. Acad. Sci. USA
Vol. 70, No. 1, pp. 156–160, January 1973

Colicin E3: A Unique Endoribonuclease

(ribosomes/16S rRNA/gel electrophoresis/RNase-less mutants)

BERND MEYHACK, IRENE MEYHACK, AND DAVID APIRION

Department of Microbiology, Washington University School of Medicine, St. Louis, Missouri 63110

Communicated by Allan Campbell, August 30, 1972

ABSTRACT **The question of whether or not a cellular ribonuclease is involved in the cleavage of 16S ribosomal RNA by colicin E3 was investigated. For this purpose ribosomes from strains devoid of some ribonucleases or ribosomes in which ribonucleases had been inactivated by heat or removed by extensive washings were used for the colicin reaction. Since the 16S RNA of all these different ribosomes, and even of the most extensively washed ribosomes, was cleaved by colicin E3, it is suggested that cellular ribonucleases are not involved in colicin E3 action. Thus, colicin E3 seems to be a unique endoribonuclease.**

Colicin E3 (1) cleaves 16S ribosomal RNA from *Escherichia coli* into two unequal fragments (2–4). The smaller fragment is about 50 nucleotides long and contains the 3′ end of the molecule (2, 3). The cleavage reaction can take place *in vivo* after infection of sensitive *E. coli* cells with colicin (2, 3), or *in vitro* by incubation of ribosomes with colicin (4, 5). The reaction requires the presence of both ribosomal subunits (6, 7). Purified 16S ribosomal RNA is not cleaved by colicin E3 (2, 4). Moreover, colicin E3 has not been reported to possess any other ribonuclease activity.

Under the reported conditions for *in vitro* colicin action on ribosomes (4, 6–8) there are a number of known, and perhaps several unknown, ribonucleases that are still attached to the ribosomes. Therefore, it is possible that an adventitious ribonuclease is involved in colicin action. We shall consider here the following possibilities: (*a*) Colicin itself is the ribonuclease and has a unique substrate specificity; (*b*) Colicin activates a pre-existing ribonuclease to function as a very specific endoribonuclease; (*c*) Colicin, in conjunction with a ribosomal protein(s) becomes a ribonuclease, which is an elaboration of the first possibility. The experiments reported here suggest that either possibility *a* or *c* is the most likely explanation of colicin action.

MATERIALS AND METHODS

Ribosomes from *Escherichia coli* strains D10 (8), MRE 600 (9), and N7060 (10) were used for *in vitro* colicin assays. These strains are all devoid of ribonuclease I (8–10). Strain N7060 is further characterized by a thermolabile ribonuclease II and a modified polynucleotide phosphorylase (10). Highly purified colicin E3 was kindly provided by Dr. D. R. Helinski (this preparation did not have any measurable ribonuclease activity). Colicin E3 activity was assayed according to Herschman and Helinski (11), by use of the colicin-sensitive strain D10. Kodak x-ray film (NS2T, 12.5 × 17.5 cm) was used for autoradiography. Carrier-free $H_3{}^{32}PO_4$ (50 mCi/ml) was purchased from New England Nuclear Corp.

Isolation of Ribosomes from Colicin-Sensitive Cells. Cells of strain D10 were grown at 37° in 500 ml of mimimal medium (per liter: 14.5 g Tris, 100 mg $MgSO_4$, 500 mg NaCl, 150 mg KCl, 500 mg NH_4Cl, adjusted to pH 7.4 with HCl) containing 0.2% glucose, 25 mg of L-methionine, and 16 mg of KH_2PO_4. In this medium phosphate limited the growth of cells. They were labeled by the addition of carrier-free $H_3{}^{32}PO_4$ (5 mCi) at an A_{560} of 0.15 and harvested at an A_{560} of 0.7, together with unlabeled cells of strain D10, grown in 2.5 liters of minimal medium containing 40 mg of KH_2PO_4 per liter. The cells were washed twice in TM2 buffer [0.01 M Tris·HCl (pH 7.5)–0.01 M magnesium acetate]. Cells of strain N7060 and MRE600 were grown at 37° (each) in 100 ml of phosphate-deprived rich medium (8 g of Difco Nutrient Broth and 8 g of Difco Casamino Acids per liter; inorganic phosphate was precipitated with 66 ml of 1 M $MgCl_2$ at pH 10.5; the pH of the filtrate was readjusted to pH 7.0 with HCl). (This medium was developed by Dr. D. Stroman from this laboratory.) Cells were labeled by the addition of carrier-free $H_3{}^{32}PO_4$ (2 mCi) at an A_{560} of 0.15. The cultures were harvested at an A_{560} of 1.0 and mixed with unlabeled cells of the same strains, grown in 400 ml (each) of rich medium at 37°. Cells were washed twice in TM2 buffer.

All subsequent steps in the preparation of ribosomes were done at 4°. Cells were ground with alumina (12) and extracted with TM2 buffer with the addition of 1 mM dithioerythritol. The clarified extract (20,000 × *g*) was centrifuged in a fixed-angle rotor for 2 hr at 200,000 × *g*. The pellet was resuspended in TMA buffer (TM2 buffer containing 0.03 M NH_4Cl). This suspension was centrifuged as before.

Ribosome Washings. Ribosomes of strain D10, as obtained above, were resuspended in TMA buffer containing 0.3 M NH_4Cl (650 A_{260} units/ml; 2 × 10^5 cpm/A_{260} unit). This suspension was clarified by low-speed centrifugation (20,000 × *g*), then centrifuged for 2 hr at 200,000 × *g*. The pellet was resuspended in TMA buffer and NH_4Cl was added to a final concentration of 1 M. The clarified suspension was centrifuged for 2 hr at 200,000 × *g*. Four washes in 1 M NH_4Cl were performed successively in the same way. The last pellet was resuspended in TMA buffer, layered on top of a linear sucrose gradient (5–20% in TMA buffer) and centrifuged 10 hr at 200,000 × *g*. The pellet was resuspended in TMA buffer. This step was repeated. Finally the ribosomes were dialyzed against TMA buffer and stored at −70°. At each step a sample was withdrawn, dialyzed against TMA buffer, and stored at −70° for further analysis. (1 unit of ribosomes corresponds to an A_{260} of 1.0).

Isolation of Ribosomal Proteins. Ribosomal proteins were isolated with 2 M LiCl–4 M urea (13) or with acetic acid (14) from ribosomes that had been washed four times in 1 M NH_4Cl, and from those centrifuged two additional times through sucrose.

Assays for Ribonuclease II, ribonuclease III, and Polynucleotide Phosphorylase. RNase II was assayed according to Singer and Tolbert (15) in 0.01 M Tris·HCl (pH 7.6)–0.1 M KCl–2 mM magnesium acetate. The mixture contained 1 μg of [^{3}H]poly(adenylic acid) (about 3500 cpm) per assay (25 μl). After 30 min of incubation at 37°, the reaction was stopped by addition of 50 μl of unlabeled carrier RNA [yeast RNA (5 mg/ml), 0.1 M Tris·HCl (pH 7.6)–0.6 M NaCl] and 1 ml of cold 80% ethanol. The mixtures were allowed to stand in ice for 30 min and then centrifuged. 0.5 ml of the supernatant solution was taken for radioactivity counting (in a Packard scintillation counter) in 10 ml of Bray's (16) scintillation fluid.

RNase III was assayed for 2 hr at 37°, according to the method of Robertson, Webster, and Zinder (17), with 6 μg of poly(C)·(I) per assay (50 μl). The reaction was stopped by addition of 50 μg of unlabeled carrier RNA and 1 ml of cold 70% ethanol. The assay mixtures were processed as for RNase II.

Polynucleotide phosphorylase (EC 2.7.7.8) was assayed for 60 min at 37°, according to Chou and Singer (18), with 2 μg of poly(adenylic acid) as substrate and 20 mM phosphate (including [^{32}P]phosphate [about 5×10^4 cpm per assay]).

Assay for Colicin E3 Action. Under standard conditions 0.4 unit of ^{32}P-labeled 70S ribosomes in TMA buffer was mixed with 1.2 μg of purified colicin E3 (1200 units; ref. 11) in TMAl buffer (TMA buffer containing 6 mM 2-mercaptoethanol). TMAl buffer was added to give a total volume of 15 μl. After incubation for 30 min at 37°, sodium dodecyl sulfate (final concentration 0.1%), EDTA (final concentration 2 mM), sucrose (final concentration 20%), and bromphenol blue (dye marker) were added. After 20 min of incubation at room temperature, the samples were applied to 12% polyacrylamide slab gels (see below) and run in Tris–glycine buffer (pH 8.6) for 3 hr at 100 V. After it was dried the gel was exposed for 12 hr to an x-ray film.

Polyacrylamide Gel Electrophoresis. RNA was analyzed in slab gel systems ($100 \times 145 \times 1.5$ mm) (2, 5, 19) in 3.2 and 12% polyacrylamide gels. To separate large RNA molecules, 3.2% polyacrylamide gels were prepared in 0.04 M Tris–acetate buffer (pH 7.6). Acrylamide (recrystallized in chloroform) and bisacrylamide (recrystallized in acetone) were used at a ratio of 15 to 1; TEMED (*N,N,N'N'*-tetramethylethylenediamine) and ammonium persulfate were added to a final concentration of 0.08%. Electrophoresis was run in 0.04 M Tris–acetate buffer (pH 7.6) containing 0.2% sodium dodecyl sulfate for 3 hr at 100 V. 12% Polyacrylamide gels were prepared in 0.375 M Tris·HCl buffer (pH 8.9). The gel contained acrylamide and bisacrylamide at a ratio of 30 to 0.8, TEMED 0.03%, and ammonium persulfate 0.09%. After polymerization, a stacking gel was applied on top of the separation gel (about 15% of the total volume). This gel contained 5% acrylamide in 0.06 M Tris·HCl buffer (pH 6.7) bisacrylamide at the same ratio to acrylamide as in the separation gel, TEMED, and ammonium persulfate at a final concentration of 0.06%. Samples were run in Tris–glycine buffer (pH 8.6) (5.9 g Tris, 29 g glycine per liter) for 3 hr at 100 V and 4°.

RESULTS

Analysis of colicin E3 action

There are two ways to show colicin E3 action, to demonstrate the appearance of the small RNA fragment (2, 5), or to show that the 16S rRNA is decreased in size (4). In the studies reported here we used the first method. Low molecular weight RNAs were separated from large RNA molecules and from one another in 12% polyacrylamide slab gels with 5% acrylamide stacking gels on top of them. This system apparently concentrates each RNA species in the stacking gel before it moves into the separation gel [as is the case for proteins (20, 21)] and, thus, results in better separation of small RNA species as compared to electrophoresis where only a separation gel is used.

To test for colicin E3 action on ribosomes, ^{32}P-labeled ribosomes were prepared and incubated with colicin. After addition of sodium dodecyl sulfate and EDTA, the RNA species were analyzed on 12% polyacrylamide slab gels. Ribosomes without colicin (control) show 23S rRNA, 16S rRNA (better resolved in 3.2% gels), 4S RNA, and smaller material that migrates with the dye marker, (see Figs. 1–3). The appearance of an additional, distinct RNA piece (E3-fragment) is absolutely colicin-dependent. The fragment is smaller than 4S RNA; we never found it in any control devoid of colicin. Colicin itself did not show any nuclease activity when it was incubated with ^{32}P-labeled total *E. coli* RNA.

The formation of E3-fragment was assayed in the linear range of colicin activity (Fig. 1). Under standard conditions for colicin action, enough ^{32}P-labeled E3-fragment was released to cause a clearly visible spot on an autoradiogram after a given time of exposure to the film. Reduction of the concentration of colicin decreased the intensity of this spot. This is shown in Fig. 1, in which ribosomes washed in TMA buffer were used. Similar results were obtained with well-washed ribosomes (twice in 1 M NH_4Cl).

Are ribonucleases involved in colicin action?

It is possible that colicin acts by activating one of the cellular ribonucleases. We tested this hypothesis for known RNases.

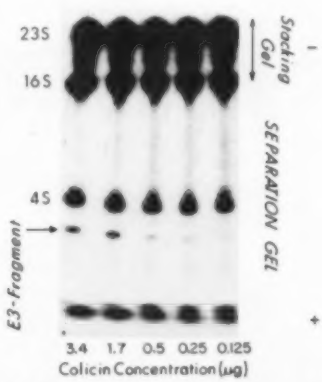

FIG. 1. Formation of colicin E3-fragment as a function of colicin concentration. ^{32}P-Labeled ribosomes from strain D10 washed in TMA buffer were incubated with different concentrations of colicin (as indicated) under standard assay conditions.

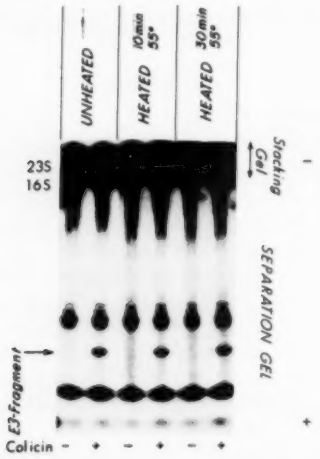

FIG. 2. Action of colicin E3 after heat inactivation of RNase II activity. ^{32}P-Labeled ribosomes from strain N7060 washed in TMA buffer (0.55 unit) were incubated for 2 hr at 37° with 5 μg of colicin. (Similar results were obtained with standard levels of ribosomes and colicin.) In this experiment the stacking gel was shorter than usual; therefore, 23S RNA is not clearly separated from 16S RNA.

To find out whether ribonuclease I (EC 2.7.7.8) is involved in the process, ^{32}P-labeled ribosomes from strains D10 and MRE600, both devoid of RNase I, were prepared and assayed in the colicin reaction. The 16S rRNA from both strains was cleaved by colicin E3. (The experiments in Figs. 1 and 3 were done with strain D10; similar results were obtained with ribosomes from strain MRE600.) This same result was shown by Bowman *et al.* (2, 5) for *E. coli* Q13, which has a low level of RNase I (8, 22). Therefore, we conclude that RNase I does not participate in colicin action.

To test for RNase II we used ribosomes of strain N7060, which possesses a heat-labile RNase II enzyme (10). As shown in Fig. 2, colicin action can be observed even after ribosomes have been heated at 55° for 0.5 hr, conditions that completely inactivate RNase II (Table 1) but leave the ribosomes functionally active (23). Moreover, since strain N7060 contains a modified polynucleotide phosphorylase that is also inactivated under these conditions (refs. 10, 22, and Krishna, unpublished observations), we conclude that these two enzymes, RNase II and polynucleotide phosphorylase, are not involved in colicin E3 action. This conclusion is further supported by the experiments discussed below.

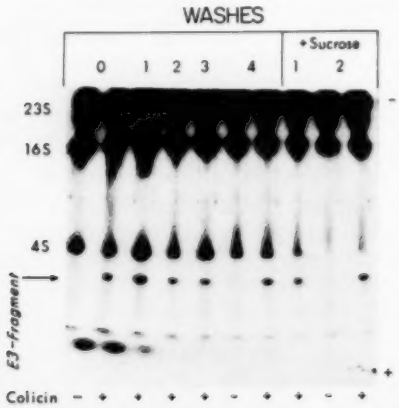

FIG. 3. Colicin E3 action on differently washed ribosomes. Number of washes with 1 M NH_4Cl in TMA buffer as indicated; + sucrose indicates the number of additional washes in a 5–20% sucrose gradient in TMA buffer, as indicated.

In order to find out whether any other known, or even an unknown, RNase is involved in the reaction, ^{32}P-labeled ribosomes from strain D10 were washed extensively to remove attached RNases. Ribosomes were washed twice in TMA buffer, once in TMA buffer containing 0.3 M NH_4Cl, then four times in TMA buffer containing 1.0 M NH_4Cl, followed by two centrifugations through 5–20% sucrose gradients (see *Methods*). Colicin action on the differently washed ribosomes was tested (Fig. 3), and their ribonuclease (II, III, and polynucleotide phosphorylase) activities were measured. We found (Table 2) high RNase II activity on the ribosomes washed in TMA buffer and about 12% RNase II activity even on those ribosomes washed once with 1 M NH_4Cl. No measurable RNase II activity could be detected on the extensively washed ribosomes. Essentially the same result was obtained for RNase III and polynucleotide phosphorylase activities on ribosomes from the last three steps of the washing procedure. Since of these enzymes RNase II sticks most tenaciously to the ribosomes (15, 17, 24), we show in Table 2 the data for ribonuclease activity under RNase II assay conditions. Ribosome concentrations and incubation times were comparable to those used in the standard colicin assay. For samples with low activities, the assays were performed more rigorously (higher concentrations of ribosomes and 2 hr of incubation), and the results were normalized for colicin assay conditions. Although there is no detectable RNase activity left on the well-washed ribosomes, they are still cleaved by colicin E3 under standard conditions to an extent similar to that of unwashed ribosomes (Fig. 3).

To find out whether or not there might be a hidden ribonuclease activity in the ribosomes, we extracted the ribosomal proteins from extensively washed ribosomes by acetic acid (14) and by LiCl–urea (13), techniques widely used for the

TABLE 1. *Heat inactivation of RNase II on ribosomes from strain N7060*

Min of heating at 55°	RNase activity	
	cpm	%
0	10,200	100.0
10	62	0.6
30	16	0.2

^{32}P-Labeled ribosomes from strain N7060 were prepared as described in *Methods*. Ribosomes (108 units/ml) were heated in TMA buffer and kept on ice: samples were assayed for RNase II activity. Assays with heated ribosomes contained 0.55 unit of ribosomes (according to the concentration used in the colicin assay, see Fig. 2). For the unheated ribosomes, however, only 0.18 units were used to determine the 100% value in the linear range of the assay. The data were normalized for 0.55 units. All data are averages of four determinations after 120 min of incubation at 37°. Blanks (without ribosomes 77 cpm; with ribosomes, but without substrate, 35–100 cpm, from which the counter background, 15 cpm, was subtracted) were subtracted from each value.

isolation of ribosomal proteins; the LiCl–urea method is regularly used in experiments for reconstitution of ribosomes (25). These ribosomal proteins were assayed for RNase II and III activities. Even under assay conditions that were more rigorous than those in the standard colicin assay, we could not find any of these enzymatic activities in the ribosomal protein preparations (Table 3).

DISCUSSION

The experiments presented here suggest that colicin E3 is a unique endoribonuclease that can specifically cleave 16S rRNA when it is part of the structure of the ribosome.

The gel electrophoresis system we used for the analysis of colicin action is very suitable for demonstration of the fragment that is released from 16S rRNA as a result of colicin action (2–4). The fact that in none of the experiments did we ever find a similar RNA fragment when colicin was not added strengthens our contention that the action of colicin is unique and that none of the cellular ribonucleases that sediment with the ribosomes can mimic it.

Colicin E3 could degrade 16S RNA from ribosomes of strains that lack RNase I (ref. 5 and Figs. 1–3) or from ribosomes of strains under conditions in which RNase II and PNPase are inactivated (Fig. 2 and Table 1). Moreover, the ribosomes from strain D10 can be a substrate for colicin action even after very extensive washes of ribosomes (Fig. 3), when no measurable amounts of any known ribonuclease activity could be detected on the ribosomes (Table 2). Since after these washings only ribosomal proteins should be retained in the centrifuged particles (14, 26, 27), and since we could not detect ribonuclease activity in the ribosomal proteins prepared from washed ribosomes (Table 3), we conclude that all the unknown ribonuclease activities were also washed away from the ribosomes by these treatments. These results indicate very strongly that colicin, by itself or in collaboration with one or more ribosomal proteins, is the endoribonuclease.

The suggestion that a cellular ribonuclease is not involved in the colicin E3 reaction described here should be qualified somewhat. Our experiments suggest that colicin can cleave 16S rRNA, even though no ribonuclease activity can be detected on ribosomes. However, we can only state that these ribosomes had, at most, 0.1% of the original RNase II activity. (This is the ribonuclease that seems to stick to the ribosome most tenaciously.) If this level of activity is still on the washed ribosomes, then there should be about 1 molecule of enzyme per 3000 ribosomes. If the enzyme can act catalytically in the colicin reaction, it can be argued that even our best-washed ribosomes (Fig. 3) or the heated ribosomes (Fig. 2) contained enough RNase II, or some other ribonuclease, to facilitate this reaction, so that no decrease in the level of the E3-fragment could be detected. However, this conclusion seems to be unlikely since a decrease of the enzyme concentration by a factor of a thousand (0.1%, Table 2) should reduce the concentration of the product of an enzymatic activity. This negative conclusion is further supported by the fact that more E3-fragment could be obtained per unit time than under standard conditions when the concentration of colicin in the reaction mixture was increased while the amount of ribosomes remained constant (see Fig. 1).

Thus, the experiments reported here suggest that none of the ribonucleases attached to unwashed ribosomes is involved in the colicin reaction. Whether or not a ribosomal protein is involved in the reaction (possibility *c*, see *Introduction*) cannot be answered by these experiments.

TABLE 2. *RNase II activity of washed ribosomes*

Number of washes in 1 M NH_4Cl	RNase activity	
	cpm	%
0	9170	100.0
1	1060	11.6
4	116	1.3
4 plus 2 sucrose washes	7	0.1

^{32}P-Labeled ribosomes from strain D10 were prepared and washed. The assays for the well-washed ribosomes (4 times with 1 M NH_4Cl and 4 times plus 2 sucrose washes) contained 0.4 unit of ribosomes, and were incubated for 2 hr at 37°. The unwashed and once-washed ribosomes were further diluted to measure RNase II activity in the linear range of the assay. All values are averages for four determinations and were normalized to 0.4 unit of ribosomes and 30 min of incubation at 37° (according to colicin standard assay conditions). For blank corrections, see Table 1. (Blanks with ribosomes, but without substrate, varied for the differently washed ribosomes; 0, 135 cpm; 1, 89 cpm; 4, 70 cpm; 4 + 2 sucrose washes, 48 cpm).

TABLE 3. *RNase II activity of ribosomal proteins*

Wash of ribosomes	Extraction of proteins	RNase activity	
		cpm	%*
Four times in 1 M NH_4Cl	LiCl–urea	25	0.27
	Acetic acid	0	0.00
As above, plus two times in sucrose	LiCl–urea	10	0.11
	Acetic acid	4	0.04

In these assays ribosomal proteins, equivalent to 1.2 units of ribosomes, were incubated at 37° for up to 120 min. The results were normalized for standard colicin assay conditions (proteins equivalent to 0.4 unit of ribosomes, 30 min at 37°) in order to compare the RNase activities in Tables 2 and 3. For corrections, see Table 1; values represent averages of four determinations.

* The 100% value is the same as in Table 2.

We thank Dr. Donald R. Helinski (University of California, San Diego) for a gift of colicin E3, Dr. H. Raskas (St. Louis University) for advice concerning gel electrophoresis, Dr. M. Schlesinger (Washington University) for advise with autoradiography, and Dr. D. Stroman of this laboratory for the receipe for phosphate-deprived rich medium. B. M. is a recipient of a fellowship from the Deutsche Forschungsgemeinschaft. This study was supported by National Science Foundation Grant GB-34158.

1. Nomura, M. (1967) *Annu. Rev. Microbiol.* **21**, 257–284.
2. Bowman, C. M., Dahlberg, J. E., Ikemura, T., Konisky, J. & Nomura, M. (1971) *Proc. Nat. Acad. Sci. USA* **68**, 964–968.
3. Senior, B. W. & Holland, J. B. (1971) *Proc. Nat. Acad. Sci. USA* **68**, 959–963.
4. Boon, T. (1971) *Proc. Nat. Acad. Sci. USA* **68**, 2421–2425.
5. Bowman, C. M., Sidikaro, J. & Nomura, M. (1971) *Nature New Biol.* **234**, 133–137.
6. Boon, T. (1972) *Proc. Nat. Acad. Sci. USA* **69**, 549–552.
7. Bowman, C. M. (1972) *FEBS Lett.* **22**, 73–75.
8. Gesteland, R. F. (1966) *J. Mol. Biol.* **16**, 67–84.
9. Cammack, K. A. & Wade, H. E. (1965) *Biochem. J.* **96**, 671–680.
10. Weatherford, S. C., Rosen, L., Gorelic, L. & Apirion, D. (1972) *J. Biol. Chem.* **247**, 5404–5408.

11. Herschman, H. R. & Helinski, D. R. (1967) *J. Biol. Chem.* **242,** 5360–5368.
12. Tissières, A., Watson, J. D., Schlessinger, D. & Hollingworth, B. R. (1959) *J. Mol. Biol.* **1,** 221–233.
13. Spitnik-Elson, P. (1964) *Biochim. Biophys. Acta* **80,** 594–600.
14. Hardy, S. J. S., Kurland, C. G., Voynow, P. & Mora, G. (1969) *Biochemistry* **8,** 2897–2905.
15. Singer, M. F. & Tolbert, G. (1965) *Biochemistry* **4,** 1319–1330.
16. Bray, G. A. (1960) *Anal. Biochem.* **1,** 279–285.
17. Robertson, H. D., Webster, R. E. & Zinder, N. D. (1968) *J. Biol. Chem.* **243,** 82–91.
18. Chou, J. Y. & Singer, M. F. (1970) *J. Biol. Chem.* **245,** 995–1004.
19. Reid, M. S. & Bieleski, R. L. (1968) *Anal. Biochem.* **22,** 374–381.
20. Williams, D. E. & Reisfeld, R. A. (1964) *Ann. N.Y. Acad. Sci.* **121,** 373–381.
21. Ornstein, L. (1964) *Ann. N.Y. Acad. Sci.* **121,** 321–349.
22. Reiner, A. M. (1969) *J. Bacteriol.* **97,** 1431–1436.
23. Apirion, D. (1966) *J. Mol. Biol.* **16,** 285–301.
24. Bothwell, A. L. M. & Apirion, D. (1971) *Biochem. Biophys. Res. Commun.* **44,** 844–851.
25. Traub, P., Misushima, S., Lowry, C. V. & Nomura, M. (1971) in *Methods in Enzymology,* eds. Colowick, S. P. & Kaplan, N. O. (Academic Press, Inc., New York), Vol. XX, part C, pp. 391–407.
26. Nomura, M. (1970) *Bacteriol. Rev.* **34,** 228–277.
27. Hindennach, I., Stöffler, G. & Wittmann, H. G. (1971) *Eur. J. Biochem.* **23,** 7–11.

Proc. Nat. Acad. Sci. USA
Vol. 70, No. 1, pp. 161–163, January 1973

The Nature of the Ground States of Cobalt(II) and Nickel(II) Carboxypeptidase A

(metallocarboxypeptidase A/magnetic susceptibility/coordination geometry/spectra)

ROBERT C. ROSENBERG*, CHARLES A. ROOT*‡, RUN-HAN WANG†, MASSIMO CERDONIO†§, AND HARRY B. GRAY*¶

* Arthur Amos Noyes Laboratory of Chemical Physics; and † Alfred P. Sloan Laboratory of Mathematics and Physics; California Institute of Technology, Pasadena, Calif. 91109

Contributed by Harry B. Gray, November 10, 1972

ABSTRACT **The magnetic susceptibilities of cobalt(II) and nickel(II) derivatives of carboxypeptidase A (CPA) follow the Curie law over a wide temperature range. The observed magnetic moments of Co(II)CPA and Ni(II)CPA are 4.77 ± 0.15 and 2.53 ± 0.10 Bohr Magnetons, respectively. The magnetic and spectral properties of Ni(II)CPA are consistent only with an octahedral ground-state geometry, whereas Co(II)CPA has a probable five-coordinate structure. The results establish ordinary metal-ion ground states for two metallocarboxypeptidase A derivatives which exhibit full peptidase activity.**

We have been concerned lately with the role of the metal ion in the catalytic activity of carboxypeptidase A. The Zn(II) ligands contributed by the polypeptide chain at the active site have been identified through a combination of x-ray diffraction (1–3) and sequence (4, 5) studies as His 69, Glu 72, and His 196. The x-ray results have shown further that the probable coordination geometry of the Zn(II) site is distorted tetrahedral, with the fourth ligand presumably being a H_2O molecule in the resting enzyme. A distorted tetrahedral coordination site assignment also appears to be compatible with the electronic absorption spectrum of Co(II)-CPA (6), which is a fully active derivative (7, 8).

Our efforts have been channeled into experiments designed to elucidate the electronic ground and excited states of several metallocarboxypeptidase A derivatives, in the hope of establishing some connection between metal-ion structure and activity. We have been particularly interested in the question of whether the metal ion in its role in the multifunctional catalytic apparatus has been endowed with enhanced substrate-attacking properties by virtue of a special (9, 10) ground-state structure. The present paper deals with the ground states of cobalt(II)CPA and nickel(II)CPA, as characterized by measurements of variable-temperature magnetic susceptibility by our ultrasensitive, superconducting, quantum mechanical magnetometer.

MATERIALS AND METHODS

Preparation of Sample. Bovine carboxypeptidase A, prepared by the method of Cox (11), was obtained from Sigma Chemical Co. Cobalt(II) and nickel(II) carboxypeptidase A derivatives were prepared by the method of Coleman and Vallee (12). Extreme care was taken to eliminate metal contamination. Plastic laboratory ware was used throughout and all buffers were extracted with dithizone in CCl_4 (13). Metal solutions were prepared from minimum 99.9% pure metal powders obtained from Alfa Inorganic, Inc. Crystalline metallocarboxypeptidase A, spread on a clean slide and allowed to air dry in a scrupulously dust-free enclosure, was placed in a quartz tube for magnetic measurements. A sample of Co(II)CPA treated in this manner retains its red–purple color through the entire procedure. The principal visible absorption spectral band of a pellet of air-dried Co(II)CPA has a maximum at 558 nm, in excellent agreement with the reported (6) solution spectrum. Total metal analysis on each sample was performed by digestion of the protein in 1:1 HNO_3–H_2SO_4, dilution to a known volume, and determination of the metal concentration by means of a Varian Techtron Atomic Absorption Spectrometer.

Measurements of Magnetic Susceptibility. All measurements were made on a superconducting, quantum mechanical magnetometer of ultrahigh sensitivity. Full details of the operation of the system will be described elsewhere (Wang, R. H., Hoenig, H. E., Rossman, G. R., and Mercereau, J. E., to be published). In our experimental setup, a superconducting sensor inductively coupled to an rf tank circuit induces a current due to a change of magnetic flux in the sample, arising either from movement of the sample or change of sample temperature. This induced current is used to drive a feedback loop so that the compensation current, which depends linearly on the sample-related flux, can be accurately converted into magnetic flux.

Two types of magnetic susceptibility measurements were made. In the first type, the total magnetic susceptibility in an axial field was determined by moving the sample from one pickup coil into another wound in the opposite direction so as to compensate the effect of the sample holder, which extends through both primary coils of the dc superconducting flux transformer. In a second mode of operation, the relative change of susceptibility was measured as a function of temperature up to 120°K. This change is independent of the large diamagnetic background arising from the host protein. The relative susceptibility measurement on Ni(II)CPA was made on a 14-mg sample containing 16.8 μg of Ni^{2+} in a field of 150 G from 8 to 75°K. A total susceptibility measurement

Abbreviations: CPA, Carboxypeptidase A; B. M., Bohr Magnetons.

‡ On leave from Department of Chemistry, Bucknell University, Lewisburg, Pa. 17837.

§ On leave from Institute of Physics, University of Rome, Rome, Italy.

¶ To whom correspondence should be addressed.

TABLE 1. *Visible spectral band maxima and magnetic moments of cobalt(II) complexes*

Compound	Donor set	μ_{eff} (B.M.)	$\bar{\nu}_{max}$, cm^{-1} (ϵ_{molar})
Four coordinate			
Co(EDM)Cl_2[a]	N_2Cl_2	4.48	14,600 (320), 15,070 (311) 17,250 (232), 18,200 (70 sh)
Co(Me_4en)Cl_2[b]	N_2Cl_2	4.65	15,200 (447), 17,300 (214)
Co(MOBenNEt_2)-Cl_2[c]	N_2Cl_2	4.50	15,400 (410), 15,750 (425), 17,150 (425)
Co(PA)$_2$[d]	N_4	4.67	16,000 (58), 17,100 (129) 19,610 (600), 20,830 (629)
Co(MBrPM)$_2$[e]	N_4	4.53	13,010 (498), 14,090 (383)
Co(Barb)$_2$(Im)$_2$[f]	N_4	4.54	17,270 (about 350), 18,867 (150 sh)
Five coordinate			
Co(Et_4dien)Cl_2[g]	N_3Cl_2	4.71	18,300 (60), 19,200 (58)
[Co(Me_6tren)Br]-Br[h]	N_4Br_2	4.47	15,600–16,100 (128) 19,200–19,800 (112)
Co(Me_5dien)Cl_2[i]	N_3Cl_2	4.60	16,100 (106), 18,800 (112)
β-Co(Paphy)Cl_2[j]	N_3Cl_2	4.84	15,700, 20,000
Co(Terpy)Cl_2[j]	N_3Cl_2	5.03	15,850, 20,000
Co(Me_4daeo)Cl_2[k]	N_2OCl_2	4.70	16,200 (225), 18,500 (151)
Co(Py(Cy)$_2$)Cl_2[l]	N_3Cl_2	4.85	16,500 (52), 17,900 (52)
Cobalt enzymes			
Co(II)CPA		4.77[m]	17,480–18,020 (150)[n]
Co(II)CA[o]		4.23	15,670 (250), 16,180 (250) 18,180 (400), 19,600 (240)

[a] Lott, A. L. III & Rasmussen, P. G. (1970) *J. Inorg. Nucl. Chem.*, **132**, 101–107. EDM, ethylenedimorpholine.

[b] Sacconi, L., Bertini, I. & Mani, F. (1967) *Inorg. Chem.* **6**, 262 267. Me_4en, *N,N,N'N'*-tetramethylethylenediamine.

[c] Sacconi, L. & Bertini, I. (1968) *Inorg. Chem.* **7**, 1178–1183. MOBenNEt_2, *N,N*,-diethyl-*N'*(*o*-methoxybenzylidene)ethylenediamine.

[d] Holm, R. H., Chakravorty, A. & Theriot, L. (1966) *Inorg. Chem.* **5**, 625–635. PA, *N*-*t*-butyl-pyrolle-2-aldimine.

[e] Fergusson, J. E. & Ramsay, C. A. (1965) *J. Chem. Soc. London*, 5222–5225. MBrPM, 5'-bromo-3,4',5-trimethyldipyrromethene-3'-4-dicarboxylate.

[f] Wang, B. C. & Craven, B. M. (1971) *Chem. Commun.* 290–291; R. C. Rosenberg, unpublished results. Barb, 5,5-diethylbarbituric acid; Im, imidazole.

[g] Dori, Z. & Gray, H. B. (1968) *Inorg. Chem.* **7**, 889–892. (Et_4dien), 1,1,7,7-tetraethyldiethylenetriamine.

[h] Ciampolini, M. & Nardi, N. (1966) *Inorg. Chem.* **5**, 41–44. Me_6tren, tris-(2-dimethylaminoethyl)amine.

[i] Ciampolini, M. & Speroni, G. P. (1966) *Inorg. Chem.* **5**, 45–49. Me_5dien, bis(2-dimethylaminoethyl)methylamine.

[j] Lions, S. F., Dance, I. B. & Lewis, J. (1967) *J. Chem. Soc. A* 565–572. Paphy, pyridine-2-aldehyde-2-pyridylhydrazone; Terpy, terpyridine.

[k] Ciampolini, M. & Nardi, N. (1967) *Inorg. Chem.* **6**, 445–449. Me_4daeo, bis(2-dimethylaminoethyl)oxide.

[l] Sacconi, L., Morassi, R. & Midolfini, S. (1968) *J. Chem. Soc. A* 1510–1515. Py(Cy)$_2$, *N,N'*-dicyclohexyl-2,-6-diacetylpyridinebisimine.

[m] This work.

[n] Latt, S. A. & Vallee, B. L. (1971) *Biochemistry* **10**, 4263–4270.

[o] Lindskog, S. & Ehrenberg, A. (1967) *J. Mol. Biol.* **24**, 133–137. CA, Carbonic anhydrase.

was performed for 24.4 mg of Co(II)CPA containing 29.7 μg of Co^{2+} over the temperature range 30–130°K in fields between 31 and 47 G. In each case the data were corrected for the temperature-independent susceptibility contribution and the magnetic moment was calculated from the slope of the χ versus 1/T plot.

RESULTS

A plot of χ against 1/T for Co(II)CPA is shown in Fig. 1. The magnetic behavior of the metalloprotein is strictly in accordance with the Curie law over the temperature range investigated. The magnetic moment (μ_{eff}) obtained of 4.77 ± 0.15 Bohr Magnetons (B.M.) confirms that the ground state of Co(II)CPA arises from a high-spin (spin-quartet) electronic configuration.

The visible absorption spectral maxima and magnetic moments of Co(II)CPA, Co(II) carbonic anhydrase, and selected Co(II) model complexes are given in Table 1. Only four- and five-coordinate Co(II) complexes are included in the comparison, as both the positions and the intensities of the visible absorption bands of Co(II)CPA rule out an octahedral active-site geometry (6).

The temperature dependence of the magnetic susceptibility of Ni(II)CPA is shown in Fig. 2. The μ_{eff} of 2.53 ± 0.10 B.M. conclusively establishes an orbitally nondegenerate, spin-triplet ground state. The observed nonlinearity in the χ against 1/T curve below 10°K is attributable to a zero-field splitting of the spin-triplet ground state (14).

DISCUSSION

The observed magnetic moment of Ni(II)CPA suggests very strongly that the metal center be assigned an octahedral geometry. The electronic ground state is not compatible with either a four- or five-coordinate high-spin Ni(II) configuration, as all such complexes have μ_{eff} values that exceed 3.2 B.M., due to substantial orbital contributions (15). Furthermore, the visible absorption spectrum of Ni(II)CPA, which exhibits band maxima at 14,600 (ϵ 9) and 24,270 cm^{-1} (ϵ 27), is consistent only with an octahedral ground state (Rosenberg, R. C., Root, C. A., and Gray, H. B., unpublished results). Apparently, in the Ni(II) enzyme, there are three H_2O molecules included in a distorted octahedral coordination core of the type $Ni(II)N_2O_4$.

The magnetic properties of Co(II)CPA can be accommodated more or less satisfactorily in terms of a five-coordinate or a distorted tetrahedral metal center. The μ_{eff} values

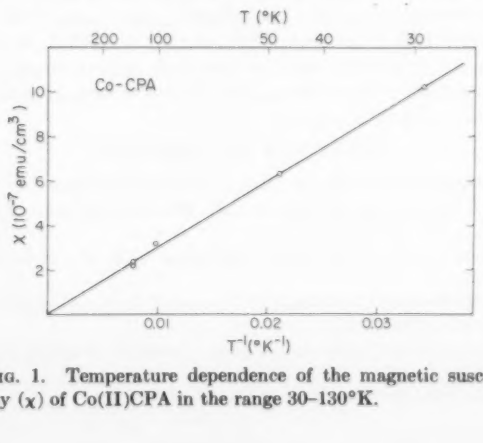

FIG. 1. Temperature dependence of the magnetic susceptibility (χ) of Co(II)CPA in the range 30–130°K.

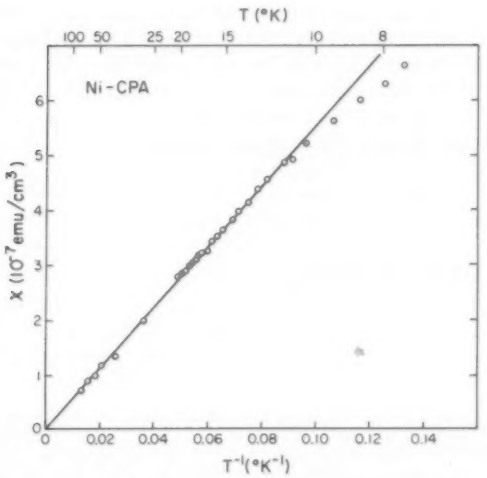

FIG. 2. Temperature dependence of the magnetic susceptibility (χ) of Ni(II)CPA in the range 8–75°K.

of the model complexes we have selected as being representative of Co(II) in distorted tetrahedral coordination are all less than 4.7 B.M., whereas all but one of the five-coordinate Co(II) complexes exhibit magnetic moments between 4.6 and 5.0 B.M. The μ_{eff} of 4.77 B.M. for Co(II)CPA thus suggests that five-coordinate Co(II) is the likely ground state, although distorted tetrahedral coordination cannot be completely eliminated as a possibility.

The intensities of the visible absorption bands attributable to electronic transitions from the ground state to the ligand field levels derived from the free-ion ^4P (Co^{2+}) excited state are often used as indicators of coordination structure for Co(II) complexes. The most intense visible bands in distorted tetrahedral Co(II) complexes generally have molar extinction coefficients that exceed 250, whereas the effective ϵ_{max} range for five-coordinate Co(II) is 80–225. The observed molar extinction coefficient of 150 for the principal visible band maximum of Co(II)CPA, thus, is in much better agreement with a five-coordinate ground state. In contrast, much higher visible absorption band intensities are observed for the enzyme Co(II) carbonic anhydrase, where a distorted tetrahedral active-site geometry, as suggested earlier (16), is probable. It is to be noted further that the large difference in the magnetic moments of Co(II)CPA and Co(II) carbonic anhydrase also suggests that the metal centers in the two enzymes are not analogously structured.

The magnetic and spectroscopic properties of Co(II)CPA and Ni(II)CPA show that the ligand environment of the enzyme is sufficiently flexible to allow changes in coordination number and geometry. The change from five or distorted tetrahedral to octahedral coordination does not drastically affect enzymatic reactivity, as the peptidase and esterase activities of Co(II)CPA and Ni(II)CPA toward several model substrates are of the same order of magnitude (7, 8), with a peptidase activity order Co(II)CPA > Ni(II)CPA = Zn(II)-CPA observed (8) in most cases. The fact that full peptidase activity can originate in M(II)CPA enzymes for which we have established very ordinary metal-ion ground states is not easily reconciled with the entatic state concept (9, 10) of catalytic activity.

Our finding of octahedral coordination for Ni(II)CPA and a probable five-coordinate structure for Co(II)CPA opens the possibility that at least one H_2O molecule remains bound to the metal center in the enzyme–substrate complex. Direct participation of coordinated H_2O in the active intermediate could be accommodated nicely in the recent mechanistic proposals of metallocarboxypeptidase A action (1, 3, 5, 17, 18), but has not been considered in any detail previously because of the generally accepted view of a four-coordinate metal center. Whether coordinated H_2O is of any importance at all in the catalytic activity of the enzyme is a question deserving of further study.

We thank Barry Dohner for technical assistance. Special thanks are due to Dr. R. J. P. Williams for a stimulating discussion. Our research was supported by the National Science Foundation and Office of Naval Research contract no. N00014-67-A-0094-0013. C.A.R. acknowledges a sabbatical leave from Bucknell University and partial support from a National Science Foundation Science Faculty Fellowship. This is Contribution no. 4588 from the Arthur Amos Noyes Laboratory.

1. Lipscomb, W. N., Hartsuck, J. A., Reeke, G. N., Jr., Quiocho, F. A., Bethge, D. H., Ludwig, M. L., Steitz, T. A., Muirhead, H. & Coppola, J. C. (1968) "Structure, function and Evolution in proteins," *Brookhaven Symp Biol.* **21**, 24–88.
2. Lipscomb, W. N., Reeke, G. N., Jr., Hartsuck, J. A., Quiocho, F. A. & Bethge, P. H. (1970) *Phil. Trans. Roy Soc., London Ser. B*, **257**, 177–214.
3. Lipscomb, W. N. (1970) *Accounts Chem. Res.* **3**, 81.
4. Bradshaw, R. A., Ericsson, L. H., Walsh, K. A. & Neurath, H. (1969) *Proc. Nat. Acad. Sci USA* **63**, 1389–1394.
5. Neurath, H. & Bradshaw, R. A. (1970) *Accounts Chem. Res.* **3**, 249–257.
6. Latt, S. A. & Vallee, B. L. (1971) *Biochemistry* **10**, 4263–4270.
7. Coleman, J. E. & Vallee, B. L. (1961) *J. Biol. Chem.* **236**, 2244–2249.
8. Auld, D. S. & Vallee, B. L. (1970) *Biochemistry* **9**, 602–609.
9. Vallee, B. L. & Williams, R. J. P. (1968) *Proc. Nat. Acad. Sci. USA* **59**, 498–505.
10. Williams, R. J. P. (1971) *Inorg. Chim. Acta Rev.* **5**, 137–155.
11. Cox, D. J., Bovard, F. C., Bargetzi, J. P., Walsh, K. A. & Neurath, H. (1969) *Biochemistry* **3**, 44–47.
12. Coleman, J. E. & Vallee, B. L. (1960) *J. Biol. Chem.* **235**, 390–395.
13. Thiers, R. E. (1957) in *Methods of Biochemical Analysis*, ed. Glick, D. (Interscience Publishers, Inc., New York), Vol. V, pp. 273–335.
14. Haseda, T. & Date, M. (1958) *J. Phys. Soc. Jap.* **13**, 175–178.
15. Sacconi, L. (1967) *Transition Metal Chem.* **4**, 199–298.
16. Lindskog, S. & Ehrenberg, A. (1967) *J. Mol. Biol.* **24**, 133–137.
17. Vallee, B. L. & Riordan, J. E. (1968) "Structure, function and Evolution in proteins," *Brookhaven Symp. Biol.* **21**, 91–117.
18. Kaiser, E. T. & Kaiser, B. L. (1972) *Accounts Chem. Res.* **5**, 219–224.

Proc. Nat. Acad. Sci. USA
Vol. 70, No. 1, pp. 164–168, January 1973

Inhibition of RNA-Dependent DNA Polymerase of Rous Sarcoma Virus by Thiosemicarbazones and Several Cations

(RNA tumor viruses/DNA synthesis/viral inactivation/chelation)

WARREN LEVINSON, ANTHONY FARAS, BRUCE WOODSON, JEAN JACKSON, AND J. MICHAEL BISHOP

Department of Microbiology, University of California, San Francisco, Calif. 94122

Communicated by K. F. Meyer, November 3, 1972

ABSTRACT **The RNA-dependent DNA polymerase of Rous sarcoma virus is inhibited by *N*-methyl isatin β-thiosemicarbazone and by thiosemicarbazide, but not by semicarbazide. These inhibitors also inactivate, upon contact with the virion, the transforming ability of Rous sarcoma virus. Sulfhydryl donors, such as 2-mercaptoethanol, can prevent these effects. The RNA-directed activity of the purified polymerase is inhibited to a greater degree than is the DNA-directed activity.**

Two cations, Cu^{++} and Hg^{++}, can inhibit RNA-dependent DNA polymerase and inactivate the transforming ability of the virus. Synergism between *N*-methyl isatin β-thiosemicarbazone and Cu^{++} occurs, since treatment of the virus with a low dose of either *N*-methyl isatin β-thiosemicarbazone or Cu^{++} has little effect; however, when the two compounds are mixed together, significant inactivation occurs. This observation supports the hypothesis that the antiviral action of thiosemicarbazones is a function of their ability to act as a ligand for metallic ions.

Several cations (Ag^{+}, Co^{++}, Zn^{++}, Cd^{++}, and Ni^{++}) significantly inactivate the RNA-dependent DNA polymerase, but have little effect on the transforming ability. In view of this result, the conclusion that the enzyme activity is required for transformation remains open to question.

N-methyl isatin β-thiosemicarbazone (Me-IBT) inhibits the growth of pox viruses (1, 2), and is effective in the prophylaxis of smallpox (3) and in the treatment of eczema vaccinatum, a complication of smallpox vaccination (4). Additional *in vitro* studies have extended the spectrum of action of this drug to include other groups of viruses, such as adenovirus, herpesvirus, picornavirus, reovirus, arbovirus, and myxo- and paramyxovirus viruses (5, 6). In these cases, inhibition of the virus was obtained by treatment of the cells after infection.

In contrast, we have recently reported that Rous sarcoma virus (RSV) can be inactivated by exposure to the drug before infection (7). Other RNA tumor viruses, such as mouse sarcoma virus, and leukemia virus, and feline sarcoma virus, are similarly inactivated (unpublished observations). However, RNA-containing cytopathic viruses, including Newcastle disease virus, poliovirus, and vesicular stomatitis virus, are not affected (ref. 7, and unpublished results).

In our previous paper (7), we described several negative attempts to determine the mechanism of inactivation (including inhibition of the RNA-dependent DNA polymerase). Subsequent experiments, reported here, have demonstrated that the RNA-dependent DNA polymerase of RSV is, indeed, inhibited by Me-IBT and that the presence of 2-mercaptoethanol prevented the action of IBT in our original experiments. The observation that a drug that inhibits the RNA-dependent DNA polymerase also inactivates the transforming ability of the virus provides evidence for the importance of this enzyme to malignant transformation by RSV.

Since thiosemicarbazones are strong chelators of copper (8, 9), a role for the cupric ion in the antiviral and antitumor activity of these drugs has been postulated and supported experimentally (10, 11). Therefore, we tested the effect of copper and several other cations on the transforming ability and on the RNA-dependent DNA polymerase activity of RSV. It was found that, at a concentration of 40 μM, Cu^{++} and Hg^{++} inhibited both the transforming ability and the enzyme activity. In addition, low doses of Cu^{++} and Me-IBT, which had little effect on the virus, caused significant inhibition of enzyme activity and inactivation of transforming ability when mixed together. These findings lend support to the previously stated hypothesis that the action of thiosemicarbazones is related to their ability to chelate metallic ions (16).

Other cations (Ag^{+}, Co^{++}, Zn^{++}, Cd^{++}, and Ni^{++}) can significantly inactivate the RNA-dependent DNA polymerase but have a minor effect on transforming ability. This could be interpreted as evidence that the enzyme is not required for transformation but can be explained in other ways (see below). In addition, a third group of cations that has a smaller or no effect on enzyme activity and on transformation was demonstrated.

MATERIALS AND METHODS

Virus. The Schmidt–Ruppin strain (Group A) of RSV was propagated and purified as described (12).

Chemicals. The drugs were obtained from the following sources: Me-IBT and methyl isatin from K & K Rare Chemicals, thiosemicarbazide and semicarbazide from Eastman Kodak, thiourea from Calbiochem, and the $(CH_3)_2SO$ used as the solvent from Matheson, Coleman and Bell. Stock solutions at 40 mM in $(CH_3)_2SO$ were prepared. Reagent grade inorganic compounds from either Baker or from Matheson, Coleman and Bell were used. Stock solutions at 40 mM were prepared in double-distilled H_2O.

RNA-Dependent DNA Polymerase Was Assayed in one of two solutions. Solution A, used when the thiosemicarbazones were being tested, was composed of 100 mM Tris·HCl (pH 8.1), 10 mM $MgCl_2$, and 0.1 mM dATP, dGTP, and dCTP.

Abbreviations: RSV, Rous sarcoma virus: Me-IBT, *N*-methyl isatin β-thiosemicarbazone.

Since it was found that both Tris buffer and deoxynucleoside triphosphates decreased the antiviral activity of the cations, Solution B, composed of 150 mM NaCl, 8 mM Na_2HPO_4, 1.5 mM KH_2PO_4, 10 mM $MgCl_2$, and 25 μM dATP, dGTP, and dCTP, was used when the cations were being tested. After suitable incubation in the presence of the drug, [^{3}H]TTP (17 Ci/mmol) and 0.05% v/v (final concentration) NP-40 (Nonidet P40, Shell Chemical Co.) were added. The reaction mixtures were incubated at 37° for 30 min and acid-precipitable counts were measured (13).

Transformation Assay. The focus-forming ability of the virus was assayed on chick-embryo cells in culture as described (14). A 1:200 dilution of the virus–drug mixture was made before infection, ensuring that the remaining drug had no effect on focus formations (unpublished results).

Partial Purification of RNA-Dependent DNA Polymerase. This procedure and the assay of the enzyme with RNA and DNA template have been described (15).

RESULTS

In the initial experiment, either Me-IBT or one of several analogues was added to a suspension of RSV at a final concentration of either 400 μM or 40 μM, and the mixture was incubated at 37° for 60 min. After samples were taken for transformation assay, [^{3}H]TTP and NP-40 were added, the reaction mixture was incubated at 37° for an additional 30 min, and the activity of RNA-dependent DNA polymerase was determined. In this experiment, the 2-mercaptoethanol (1% v/v) was added after Me-IBT had interacted with RSV. In contrast, the experiments previously reported (7) were performed with 2-mercaptoethanol (2.5% v/v) present when the Me-IBT was added. The data in Table 1 demonstrate the inhibition of RNA-dependent DNA polymerase activity by Me-IBT and by the thiosemicarbazide side chain. Me-IBT is clearly the more effective compound. Methyl isatin, semicarbazide, and thiourea analogues have no activity. The infectivity data demonstrate that those compounds that inhibit the enzyme activity also inactivate the transforming ability of RSV.

TABLE 1. *Inhibition of RNA-dependent DNA polymerase of RSV by Me-IBT*

Compounds	Enzyme*	Transforming*
None	100	100
$(CH_3)_2SO$ (1%)	100	100
Me-IBT (40 μM)	2	1
Me-IBT (4 μM)	31	30
Thiosemicarbazide (400 μM)	14	10
Thiosemicarbazide (40 μM)	88	63
Semicarbazide (400 μM)	100	100
Thiourea (400 μM)	90	100
Methyl isatin (400 μM)	88	100

10 μl of purified RSV, suspended in 200 μl of solution A, was exposed to different concentrations of the various compounds by addition of a 2-ul aliquot of the substance to be tested. After 60 min at 37°, a 5-μl sample was taken for transformation assay and 2 μl of 2-mercaptoethanol, 2 μCi of [^{3}H]TTP, and 10 μl of 1% NP-40 were added. The reaction mixture was incubated at 37° for 30 min, and acid-precipitable counts were obtained. 34,811 cpm and 116 foci were assayed in the untreated control sample.

* % Activity.

TABLE 2. *Effect of 2-mercaptoethanol on the interaction between Me-IBT and RSV*

Compounds	Enzyme*	Transforming*
$(CH_3)_2SO$	100	100
Me-IBT	4	1
Me-IBT + 0.1% 2-mercaptoethanol	92	100
Me-IBT + 0.01% 2-mercaptoethanol	46	33

Purified RSV, suspended in 200 μl of solution A, was exposed to 40 μM Me-IBT in the presence or absence of 2-mercaptoethanol. The mixture was incubated at 37° for 30 min, a 5-μl sample was taken for transformation assay, and 2 μCi of [^{3}H]TTP and 10 μl of 1% NP-40 were then added. After incubation at 37° for an additional 30 min, acid-precipitable counts were measured. 15,770 cpm and 214 foci were assayed in the untreated control sample.

* % Activity.

In the experiment just described, 2-mercaptoethanol was added after a 60-min exposure to the drugs. If 2-mercaptoethanol is omitted from the reaction entirely, the incorporation of [^{3}H]TTP is 2- to 4-fold lower, but the inhibition and inactivation by the various compounds remain relatively the same (data not shown). In the following experiment, we demonstrate directly that 2-mercaptoethanol prevents the inhibition by Me-IBT. As seen in Table 2, there is no inhibition of either enzyme activity or transforming ability of the virus that received 0.1% (14 mM) 2-mercaptoethanol at the same time as the Me-IBT, but inhibition did occur when Me-IBT alone was added. When 0.01% (1.4 mM) 2-mercaptoethanol is used, the protective effect is incomplete. Two other sulfhydryl compounds, dithiothreitol and glutathione, have a similar protective effect.

The effect of Me-IBT on the purified DNA polymerase from RSV was also determined, with both RNA and DNA templates. The data in Table 3 demonstrate that with 400 μM

TABLE 3. *Inhibition of the purified RNA-dependent DNA polymerase of RSV by Me-IBT*

	RSV DNA Polymerase Template		*E. coli* Polymerase I Template
Compounds	RNA	DNA	DNA
$(CH_3)_2SO$	100*	100	100
Me-IBT (400 μM)	12	50	3
Me-IBT (40 μM)	44	82	54

Enzyme reactions were performed with a 500-fold purified preparation of the RSV DNA polymerase, with purified 70S RSV-RNA and calf-thymus DNA templates at a concentration of 2 μg/ml. The enzyme–template combination, in 200 μl of solution A, was exposed to either 400 μM or 40 μM Me-IBT and incubated for 15 min at 37°. 2 μl of 2-mercaptoethanol and 5 μCi of [^{3}H]TTP were then added. The reaction was incubated for 1 hr at 37° and acid-precipitable counts were obtained. The cpm incorporated in the $(CH_3)_2SO$-treated control samples of the RNA-directed and DNA-directed RSV polymerase and of the *E. coli* polymerase were 923, 1,194, and 11,417, respectively.

* % Enzyme activity.

TABLE 4. *Effect of EDTA on the interaction between Me-IBT and RSV*

Compounds	Enzyme*	Transforming*
None	100	100
Me-IBT	15	19
EDTA	280	100
Me-IBT + EDTA	120	110

Purified RSV, suspended in 100 μl of a solution composed of solution A without $MgCl_2$, was exposed to 40 μM Me-IBT in the presence or absence of mM EDTA. After 30 min at 37°, a 2-μl sample was taken for transformation assay. The solution was then made 10 mM with respect to $MgCl_2$, and 1 μCi of [^{3}H]TTP and 0.05% NP-40 were added. The reaction mixture was incubated at 37° for 30 min and acid-precipitable counts were obtained. 5687 cpm and 183 foci were assayed in the untreated control sample.

* % Activity.

Me-IBT the RNA-directed activity of the purified DNA polymerase of RSV is inhibited by 88%, while the DNA-directed activity is inhibited by 50%. One explanation for the difference in the degree of inhibition is that the DNA-directed activity may be more efficiently protected by 2-mercaptoethanol, another is that the polymerase may contain a different active site for each of the two activities. Since 1% 2-mercaptoethanol was necessary in order to obtain efficient activity of the purified RNA-dependent DNA polymerase, it is probable that the 400 μM concentration of Me-IBT needed to demonstrate significant inhibition was due to the protective effect of 2-mercaptoethanol. In order to determine whether the action of Me-IBT was specific for the DNA polymerases of RSV, we exposed *Escherichia coli* DNA polymerase I (Kornberg polymerase) to the drug and found its activity to be markedly inhibited.

Since thiosemicarbazide inhibits the enzyme activity and inactivates the infectivity of RSV, but semicarbazide and thiourea do not, it appears that the activity requires the presence of both the thio and the hydrazine moieties. These groups are also necessary for the strong binding of transitional metal ions exhibited by thiosemicarbazide, and there is data implicating copper in the biological action of this compound (8–10). The hypothesis that metal ions are involved in the action of these drugs is supported by the observation (Table 4) that the presence of 1 mM EDTA can prevent the inhibition of enzyme activity and the inactivation of infectivity by Me-IBT. It was observed also that EDTA alone enhances the activity of the RNA-dependent DNA polymerase but does not affect the transforming ability of the virus. It is possible that low concentrations of cations inhibitory to the enzyme may be present in the reaction mixture, and these cations are removed by EDTA.

In view of this result, we investigated the effect of copper and several other cations on the activity of RNA-dependent DNA polymerase and the transforming ability of RSV. The data in Table 5 demonstrate that two cations, Cu^{++} and Hg^{++} (40 μM each), have the ability to inactivate the transforming ability and inhibit the enzyme activity of the virus (Group A). Cu^{+} ion has no effect on either function (Group C).

Several other cations (Ag^{+}, Co^{++}, Zn^{++}, Cd^{++}, and Ni^{++}) have the ability to inhibit RNA-dependent DNA polymerase but have little effect on the transforming ability of RSV (Group B). This finding can be interpreted in several ways. One conclusion is that the activity of RNA-dependent DNA polymerase is not necessary for transformation. However, since the sample for transformation assay must be taken before the addition of the detergent NP-40, it is possible that these cations cannot affect the enzyme in the intact virion but are capable of inhibiting the enzyme activity of the disrupted particle. We have tested several polyene detergents (Tween 20, 40, 60, 80, 85, Brij 35, 56, and 58) but were unable to retain infectivity in a concentration of detergent that allowed enzyme activity.

We therefore performed an experiment in which the intact virion was exposed to the Co^{++} ion for 30 min at 37°, diluted 4-fold, then treated with NP-40, and assayed for enzyme activity in the usual manner. The *extent* of inactivation of the diluted suspension was the same as the inactivation of the undiluted suspension; the extent of inactivation of the suspension treated with one-fourth as much Co^{++} was significantly less. This indicates that the Co^{++} ion does affect the enzyme within the virion. The effect of this group of cations cannot, therefore, be explained on the basis of an inability to penetrate the inact virion.

One additional possibility that makes the interpretation of the effect of this group of cations difficult is that the cations could be removed from the site of enzyme inhibition during the infection of the chick embryo cell. In contrast, Cu^{++} and Hg^{++} ions would remain bound during infection and transformation would be inhibited. In view of this possibility we cannot conclude that the activity of RNA-dependent DNA polymerase is not required for transformation.

TABLE 5. *Inhibition of the RNA-dependent DNA polymerase of RSV by cations*

Compounds	Enzyme*	Transforming*
None	100	100
Group A		
$CuSO_4$	5	4
$HgCl_2$	1	1
Group B		
$AgNO_3$	5	41
$Co(NO_3)_2$	7	100
$ZnCl_2$	6	50
$CdSO_4$	5	82
$NiCl_2$	5	100
Group C		
CuCl	91	93
$PbCl_2$	23	100
$FeSO_4$	21	63
$FeCl_2$	98	69
$InCl_3$	50	97
$RhCl_3$	23	34
$PtCl_4$	24	83

Purified RSV, suspended in 200 μl of solution B, was exposed to 40 μM of the various compounds. The mixture was incubated at 37° for 30 min, a 5-μl sample was taken for transformation assay, and 4 μCi of [^{3}H]TTP and 10 μl of 1% NP-40 were then added. After incubation at 37° for an additional 30 min, acid-precipitable counts were obtained. 1127 cpm and 293 foci were assayed in the untreated control sample. The enzyme activity is lower in this experiment than in previous ones because phosphate buffer (solution B) is less efficient than Tris buffer (solution A).

* % Activity.

Other cations (Group 4) that have a smaller or no effect on enzyme activity and on transformation were also found. These include indium, rhodium, and platinum, which were found to inhibit vaccinia growth in mice (10), and ferrous, ferric, lead, and, as mentioned above, cuprous ions.

At a lower concentration (4 μM), only Hg^{++} has a significant effect on the enzyme activity and transforming ability; all the other ions have little effect on either function. The activity of Hg^{++} can no longer be demonstrated at a concentration of 0.4 μM.

In an experiment performed in the same manner as that described in Table 3, it was found that copper sulfate inhibited the purified polymerase activity in a similar manner as did Me-IBT, namely, the RNA-directed reaction was significantly more inhibited at 400 μM than the DNA-directed reaction and little inhibitory activity remained at 40 μM. The *E. coli* polymerase I had 1% activity after treatment with 400 μM copper sulfate and 20% activity when exposed to 40 μM $CuSO_4$ (data not shown).

The nature of this antiviral activity was investigated further by determining whether a synergistic effect occurs between Me-IBT and Cu^{++}. In this experiment, the virus was exposed to low doses of the compounds (1 μM), separately as well as mixed together. It can be seen in Table 6 that there is a minor effect on the virus when the compounds are used by themselves, but a significant inactivation of the transforming ability and inhibition of the enzyme activity occurs when they are present together.

TABLE 6. *Synergistic effect of Me-IBT and Cu^{++} on the RNA-dependent DNA polymerase of RSV*

Compounds	Enzyme*	Transforming*
$(CH_3)_2SO$	100	100
Me-IBT	42	50
$CuSO_4$	86	90
Me-IBT + $CuSO_4$	1	1

Purified RSV, suspended in 200 μl of solution B, was exposed to either 1 μM Me-IBT, 1 μM $CuSO_4$, or both. The mixture was incubated at 37° for 30 min, a 5-μl sample was taken for transformation assay, and 4 μCi of [^{3}H]TTP and 10 μl of 1% of NP-40 were then added. After incubation at 37° for an additional 30 min, acid-precipitable counts were obtained. 3370 cpm and 300 foci were assayed in the untreated control sample.

* % Activity.

DISCUSSION

We have demonstrated that two classes of compounds, the thiosemicarbazones and the inorganic cations, can inhibit the RNA-dependent DNA polymerase activity and the transforming ability of RSV. The correlation between the effect of these agents on the enzyme activity and transformation supports the contention that the product of the RNA-dependent DNA polymerase is necessary for transformation. This correlation is not complete since several cations inhibit the enzyme but do not inactivate transformation. However, for the reason previously mentioned, it is difficult to conclude on the basis of this finding that the enzyme activity is not required for transformation.

One interpretation of the synergistic effect seen when Me-IBT and Cu^{++} are mixed is that a chelate compound is the active material. This possibility is supported by the known affinity of thiosemicarbazones for Cu^{++} (8, 9) and other cations of the first transition series (9). Biologically, Cu^{++} has been shown to be necessary for the antitumor activity of a thiosemicarbazone derivative (11) and is suspected to be involved in the antitumor activity of several other derivatives (16, 17). More speculatively, the inhibition of the recently purified DNA polymerase of chick embryo cells by *o*-phenanthroline (18) could be due to a chelate since this compound strongly binds cupric ions.

Another explanation of the synergistic effect of Me-IBT and Cu^{++} is that the action of one predisposes to the action of the other. It is also possible that the Me-IBT could act by the removal of the metal component of one of the virion enzymes and the Cu^{++} could further inhibit either that enzyme or a different one.

If the chelate is the active compound then an explanation is required for the activity of the Me-IBT when used alone, as seen in Table 1. It is possible that sufficient copper ion is provided as a trace contamination in the solutions or in the glass test tube to make the active complex. This possibility is supported by the observation that EDTA can increase the activity of the enzyme and can inhibit the action of the Me-IBT.

It is not at all clear that the site of action of these compounds is the enzyme itself since there is evidence that Cu^{++} and other cations bind to and degrade synthetic polyribonucleotides (19) and inactivate the infectivity of tobacco mosaic virus RNA (20). There is also evidence that Cu^{++} binds to DNA (21, 22). This interaction reduces the stability of the DNA, as demonstrated by a marked decrease in the melting temperature, and is thought to occur specifically at the guanine and cytosine residues (23). There are no data regarding the relationship between thiosemicarbazones and RNA or DNA. There is evidence that derivatives of thiosemicarbazide such as *1*-formyl isoquinoline thiosemicarbazone and *2*-formyl pyridine thiosemicarbazone can inhibit DNA synthesis in tumor cells and *in vitro* by the inhibition of ribonucleoside reductase (24, 25). Clearly, however, this cannot be the mechanism of action in the case of RNA-dependent DNA polymerase since the deoxynucleoside triphosphates are provided as substrates.

Sulfhydryl compounds, such as 2-mercaptoethanol, protect the virus from the effect of Me-IBT (and Cu^{++}, unpublished results). This type of protective effect has been reported previously; namely, dithiothreitol can protect ribonucleotide reductase from inhibition by *1*-formyl-isoquinoline thiosemicarbazone (24). In either case, the mechanism of this protection is unknown; it could be due to the preservation of the reduced (functional) state of the enzyme or to the binding, by the thiol, of a cation required for the action of the thiosemicarbazone.

The inhibition of RNA-dependent DNA polymerase activity and the inactivation of transforming ability of mouse sarcoma virus has been reported recently with derivatives of the drug rifamycin (26). The experiments with mouse sarcoma virus were performed in a similar fashion to those described in this paper with RSV. Similar results were obtained in so far as a direct correlation between the inhibition of the enzyme activity and the inactivation of transformation is concerned. However, no protection with sulfhydryl compounds was observed and no effect of cations was tested. It

will be of interest to determine whether the relationship of these factors is the same for rifamycin as it is for the thiosemicarbazones.

NOTE ADDED IN PROOF

In experiments performed in the same manner as those in Table 5, we found that *o*-phenanthroline (40 μM), a heavy-metal chelating agent, inactivates RNA-dependent DNA polymerase activity, but not the transforming ability of RSV. This finding supports the contention that the enzyme activity is not required for transformation, but is subject to the same criticism as mentioned with results.

This work was supported by USPHS Grants AI 08864, CA 12705, AI 06862, AI 08293, AI 00299, Contract no 71-2147 of the Special Virus Cancer Program of the National Cancer Institute, and American Cancer Society Grant VC-70. We thank Mrs. Ruby Pruitt and Mrs. Lillie Labat for their excellent technical assistance. We thank Dr. R. Shihman Chang, University of California, Davis and Dr. Alice S. Huang, Boston City Hospital for performing the studies on feline sarcoma virus and vesicular stomatitis virus, respectively.

1. Bauer, D. & Sadler, P. (1960) *Brit. J. Pharmacol.* **15,** 101–110.
2. Bauer, D., Dumbell, K., Fox-Hulme, P. & Sadler, P. (1962) *Bull. WHO* **26,** 727–732.
3. Bauer, D., St. Vincent, L., Kempe, C. & Downie, A. (1963) *Lancet* 494–496, Sept. 7.
4. Turner, W., Bauer, D. & Nimmo-Smith, R. (1962) *Brit. Med. J.* 1317–1319, May 12.
5. Bauer, D. & Apostolov, K. (1966) *Science* **154,** 796–797.
6. Bauer, D., Apostolov, K. & Selway, J. (1970) *Ann. N.Y. Acad. Sci.* **173,** 314–319.
7. Levinson, W., Woodson, B. & Jackson, J. (1971) *Nature* **232,** 116–118.
8. Taylor, M., Gabe, E., Glusher, J., Minkin, J. & Patterson, A. (1966) *J. Amer. Chem. Soc.* **88,** 1845–1846.
9. Burns, G. (1968) *J. Inorg. Chem.* **7,** 277–283.
10. Bauer, D. (1958) *Brit. J. Exp. Pathol.* **39,** 480–489.
11. Petering, H. & Van Giessen, G. (1966) in *The Biochemistry of Copper* (Academic Press, New York), pp. 197–209.
12. Bishop, J. M., Levinson, W., Quintrell, N., Sullivan, D., Fanshier, L. & Jackson, J. (1970) *Virology* **42,** 182–195.
13. Garapin, A., McDonnell, J., Levinson, W., Quintrell, N., Fanshier, L. & Bishop, J. M. (1970) *J. Virol.* **6,** 589–598.
14. Levinson, W. (1967) *Virology* **32,** 74–83.
15. Faras, A., Taylor, J., McDonnell, J., Levinson, W. & Bishop, J. M. (1972) *Biochemistry* **11,** 2334–2342.
16. French, F. & Blantz, E. (1966) *J. Med. Chem.* **9,** 585–589.
17. French, F., Blantz, E., DeAmoral, J. & French, D. (1970) *J. Med. Chem.* **13,** 1117–1124.
18. Stavrianopoulos, J., Karkas, J. & Chargaff, E. (1972) *Proc. Nat. Acad. Sci. USA* **69,** 1781–1785.
19. Butzow, J. & Eichhorn, G. (1965) *Biophysics* **3,** 95–107.
20. Fraenkel-Conrat, H. (1959) *Harvey Lect.* **53,** 56–68.
21. Eichhorn, G. & Clark, P. (1965) *Proc. Nat. Acad. Sci. USA* **53,** 586–593.
22. Hiai, S. (1965) *J. Mol. Biol.* **11,** 672–691.
23. Sundaralingam, M. & Carrabine, J. (1971) *J. Mol. Biol.* **61,** 287–309.
24. Moore, E., Zedeck, M., Agrawal, K. & Sartorelli, A. (1970) *Biochemistry* **9,** 4492–4498.
25. Moore E., Booth, B. & Sartorelli, A. (1971) *Cancer Res.* **31,** 235–238.
26. Ting, R., Yang, S. & Gallo, R. (1972) *Nature New Biol.* **236,** 163–166.

Proc. Nat. Acad. Sci. USA
Vol. 70, No. 1, pp. 169–172, January 1973

Changes in Alkaline Ribonuclease Activity During Compensatory Renal Growth

PEDRO ROSSO*, JAMES DIGGS†, AND MYRON WINICK*

* Division of Growth and Development, Department of Pediatrics, Cornell University Medical College, New York, New York 10021

Communicated by C. G. King, October 30, 1972

ABSTRACT **Unilateral nephrectomy in rats produces an increase in ribonuclease activity in both nuclear and cytoplasmic fractions of the contralateral kidney. The timing of this increase and the changes in the proportion of free activity to protein-bound activity are different in each fraction. A peak in inhibitor-bound ribonuclease, suggesting a higher amount of inhibitor, was found in the cytoplasmic fraction before the increase in RNA/DNA ratio. Ninety-six hours after the operation, ribonuclease was still significantly increased in both the nuclear and cytoplasmic fractions. The inhibitor-bound activity was increased in proportion to cellular RNA, maintaining a ribonuclease activity per μg of RNA similar to the controls.**

Alkaline ribonuclease (RNase) activity (pH 7.8) is present in the nucleus and the cytoplasm of most mammalian cells in both the free form and bound to an inhibitor protein. The inhibitor-bound activity may be released *in vitro* by addition of *p*-chloromercuribenzoate (PCMB) or other substances that react with –SH groups (1).

It has been hypothesized that RNase may regulate the quantity of cytoplasmic RNA by influencing the rate of RNA degradation (2). This idea is based upon the fact that RNase activity is elevated under several circumstances in which the RNA/DNA ratio is reduced (3–5) and conversely, activity of this enzyme decreases under certain conditions in which the RNA/DNA ratio increases (6, 7). RNA turnover studies indicate that in these situations the changes in cellular RNA content are due to changes in the rate of RNA catabolism rather than in the rate of RNA synthesis (8, 9). However, other data do not seem to support such a role for RNase. For example, RNase activity increases in the remaining kidney within 1 hr after uninephrectomy (10), a stimulus that increases the rate of RNA synthesis and elevates the RNA/DNA ratio in the contralateral kidney (11). However, this study measured the activity of only free RNase in whole organ homogenate. Consequently, it is impossible to know whether these changes in RNase activity are occurring in the cytoplasmic or nuclear fraction, where presumably different influences on RNA metabolism are exerted, or if the changes in activity correspond to a *de novo* synthesis of enzyme or to a decrease in the amount of RNase inhibitor.

The present study was undertaken to examine both free and total RNase activity in the nuclear and cytoplasmic fractions of the contralateral kidney after uninephrectomy and to correlate alterations in these activities with changes in DNA and RNA content of the organ.

In addition, since changes in the RNA/DNA ratio in sham-operated mice have been reported (11), the effects of sham operation have also been studied.

MATERIALS AND METHODS

Male Sprague–Dawley rats weighing 300–350 g were fed a standard diet (Purina lab chow) *ad libitum* and kept on a 12-hr light–dark cycle. Without previous starvation of the rats, a left uninephrectomy or a sham operation was performed under light ether anesthesia. The entire procedure was done within 5 min, and, in the long-term experiments, all animals included in the study had resumed normal activity within 24 hr. Four sham-operated and four uninephrectomized animals were killed at intervals from 90 min to 96 hr after the operation, and, except for the 6- and 12-hr groups, all animals were killed between 9 and 10 a.m. A group of animals was also killed without any previous operation, and their right kidneys were used as 0-time or nonoperated controls.

Immediately after the rats were killed, the right kidney was removed and chilled in ice-cold 0.25 M sucrose in TKM buffer (pH 7.4) (50 mM Tris·HCl–25 mM KCl–5 mM $MgCl_2 \cdot 6H_2O$). All subsequent procedures were done at 0–4°. Kidneys were weighed, minced with scissors, and made up to 20% homogenate (w/v) in 0.25 M sucrose in TKM buffer. Final homogenization was performed with 2 up-and-down strokes of a motor-driven Teflon pestle (2000 rpm) in a Potter-Elvehjem homogenizer. The homogenate was then filtered through six layers of cheesecloth; 2 ml of the filtered homogenate was underlaid by 20 ml of 0.34 M sucrose in TKM buffer (pH 7.4) and centrifuged at 1000 × *g* for 15 min. The resulting supernatant was taken as the "cytoplasmic fraction."

The crude nuclear pellet was then suspended in 2.3 M sucrose in TKM buffer (pH 7.4) and centrifuged at 40,000 × *g* for 60 min in a SW25.1 rotor of a Beckman ultracentrifuge. The supernatant was discarded, and the thin nuclear pellet, suspended in 0.34 M sucrose, was used as the "nuclear fraction."

Free RNase activity was measured by the method of Roth (1), but the final volume of the reaction mixture was reduced to 0.6 ml. Total RNase activity was measured after addition of 0.1 ml of a 10 mM PCMB solution to the incubation mixture, without previous freezing and thawing of the samples as recommended by Shortman (12). Inhibitor-bound activity was then calculated as the difference between free and PCMB-released activities. RNase units were calculated arbitrarily, assuming that an absorbance at 260 nm of 1.00 was equal to 100 units. Highly polymerized yeast RNA (Calbiochem, Calif.) was used as substrate without previous dialysis.

Abbreviation: PCMB, *p*-chloromercuribenzoate.

* Present address: Dr. Pedro Rosso, Institute of Human Nutrition, Columbia University, 511 West 166th St, New York, N.Y. 10032.

† Summer research student, Dept. of Pediatrics, Cornell University Medical College.

TABLE 1. *Changes in nucleic acids and protein content in kidney 96 hr after unilateral nephrectomy**

Group	DNA (mg)	RNA (mg)	Protein (mg)
Unoperated control	3.92 ± 0.20	4.97 ± 0.21	312.8 ± 17.0
Sham-operated	3.86 ± 0.16	4.93 ± 0.22	302.9 ± 13.2
Experimental	3.98 ± 0.07†	5.91 ± 0.15‡	400.3 ± 18.4‡

* Results are ± SD.
† Not significant.
‡ $P > 0.001$.

DNA, RNA, and protein were extracted by the method of Munro and Fleck (13), and DNA and RNA were subsequently assessed by UV absorption in a Beckman DU spectrophotometer. Proteins were measured by the biuret reaction.

RESULTS

Nucleic Acids and Proteins. DNA content was similar at 96 hr in unoperated control, sham-operated, and experimental animals, indicating that uninephrectomy did not induce DNA synthesis during this period.

RNA content was slightly increased by 12 hr and significantly increased by 24 hr after surgery in the experimental group, as indicated by a higher RNA/DNA ratio. No change occurred in the RNA content after sham operation. The sham-operated group shows lower values at 12 and 24 hr, but the differences are not significant.

Protein was also increased in the experimental group, and the changes in the protein/DNA ratio parallel the changes in the RNA/DNA ratio. No changes in protein content were found throughout this period in the sham-operated group (Tables 1 and 2).

RNase Activity in the Nuclear Fraction. Total RNase expressed per μg of DNA was elevated in the nuclear fraction of the remaining kidney of the experimental animals at 3 hr, and subsequently decreased (Fig. 1). Except at 24 hr, these values were always higher than those in the sham-operated or unoperated control groups up to 96 hr. This elevation is due to a proportional increase in free activity and in inhibitor-bound activity up to 24 hr. Subsequently, the amount of bound RNase remains elevated while free activity drops to normal levels.

TABLE 2. *Changes in RNA/DNA ratio and protein/DNA ratio in kidney after unilateral nephrectomy in sham-operated and experimental animals*

Hr after operation	Experimental		Sham-operated	
	RNA/DNA	Protein/DNA	RNA/DNA	Protein/DNA
1.5	1.26	78.5	1.25	77.7
3	1.25	76.7	1.25	76.0
6	1.25	78.0	1.24	76.5
12	1.29	81.5	1.20	78.2
24	1.34*	85.2*	1.21	77.0
48	1.40*	93.7*	1.24	77.2
96	1.50*	101.5*	1.25	76.7

* $P < 0.001$.

In the sham-operated group, total RNase activity compared to the 0-time unoperated group was significantly increased only at 6 hr, and both free and bound RNase were proportionally elevated.

RNase Activity in the Cytoplasmic Fraction. Total RNase per μg of DNA increased in the experimental rats by 1.5 hr, reached a peak at 6 hr, and subsequently remained elevated at about twice the normal level. The sham-operated group showed a similar pattern of change in the first 12 hr, but values were back to normal by 24 hr and remained there for the rest of the experiment (Fig. 2). Qualitatively similar changes were found when total enzymatic activity was expressed per μg of RNA or per mg of protein.

These changes in total activity in the experimental group are due mainly to an increase in free activity that is reflected by a decrease in the ratio of total to free activity. In the sham-operated animals similar changes occurred only within the first 6 hr, and the total/free ratio was again similar to unoperated control values at 12 hr (Fig. 3).

In the experimental group, the amount of protein-bound RNase was reduced at 90 min and subsequently elevated at 6 and 12 hr compared to the unoperated animals, and at 96 hr the elevation was still significant. In the sham-operated group, the protein-bound activity was slightly reduced at 90 min and at 3 hr, but after a peak similar to the experimental group the values were back to nonoperated control levels at 12 hr (Fig. 4). The increment in bound activity in the experimental group is proportional to the increment in protein and RNA per cell at 96 hr. Thus, the bound activity per μg of RNA or per mg of protein remains unchanged (Table 3).

DISCUSSION

These data, in agreement with previous studies, indicate that uninephrectomy in adult rats induces purely hypertrophic growth in the contralateral kidney, as reflected by an increased RNA/DNA and protein/DNA ratio without changes in DNA content (14). Also in agreement with other studies, these changes in RNA/DNA ratio are occurring within 12 hr after the operation, indicating a rapid and active response in the contralateral kidney (11). With the method of separation of nuclear and cytoplasmic fractions used in this study it

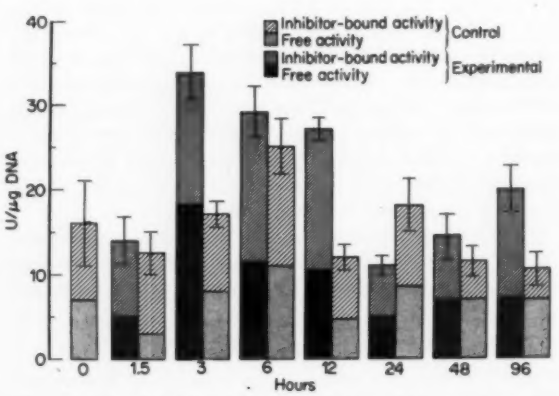

FIG. 1. Total, inhibitor-bound, and free RNase activity per μg of DNA in nuclear fraction in unoperated, 0-time control, sham-operated, and experimental animals at various times. Values represent mean and SD of four different determinations.

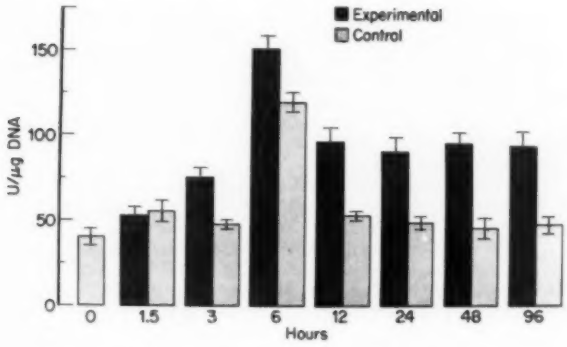

FIG. 2. Total RNase activity per μg of DNA in the cytoplasmic fraction of unoperated control, sham-operated, and experimental animals at various times. Mean and SD of four different determinations are indicated.

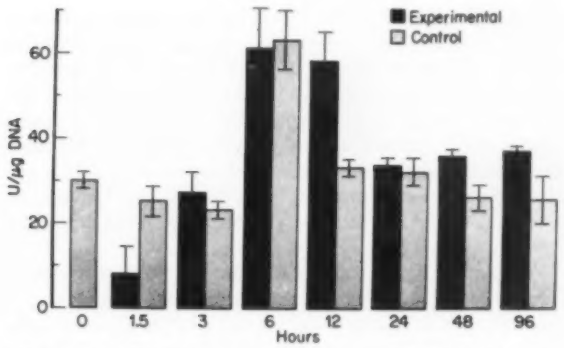

FIG. 4. Inhibitor-bound activity per μg of DNA in the cytoplasmic fraction of unoperated control, sham-operated, and experimental animals at different times after operation. Mean and SD of four different determinations are indicated.

is impossible to avoid translocation of some components between these two fractions, and it is conceivable that some degree of contamination with RNase belonging to the other fraction may have occurred in the nuclear and cytoplasmic samples. Although at present it is impossible to know how much absolute error is introduced by this method of separation, it is fair to assume that such error would be present in a similar proportion throughout the experiment. Consequently, although it influences the absolute values, this method of separation will not invalidate the qualitative data reflecting the changes in both fractions. The small degree of variability of our results and the similar values found in the control group at the beginning and at the end of the experiment further support this assumption. The elevation of nuclear RNase activity in the experimental group under these circumstances suggests some role for nuclear RNase in RNA synthesis or in RNA hydrolysis within the nucleus. The participation of RNA synthesis is probably localized in the nucleolus, where active synthesis of ribosomal RNA is accompanied by elevation of nucleolar RNase (15). However, RNase activity is also present in the nucleoplasm. Too few data are available at present to allow further speculation about the role of RNase in the nucleoplasm, but it is significant that most of the nuclear RNA is hydrolized intranuclearly (16) and that different kinds of RNA molecules have different degrees of resistance to RNase hydrolysis (17). This observation suggests selective degradation before RNA is transported into the cytoplasm. Enhanced catabolism of nuclear RNA after uninephrectomy in rats results in virtual disappearance of RNA <28 S within 60 min after the operation (18).

A decrease in RNA/DNA ratio in the kidney in mice during the first 24 hr after a sham operation has been reported (11), and our study shows a similar trend in rats. This decreased ratio, which is probably accounted for by a reduction in ribosomal RNA, may trigger synthesis of RNA by way of a feedback mechanism similar to that described in liver (19). This enhanced synthesis would replace the cytoplasmic loss and explain the changes in the nuclear RNase fraction found in the sham-operated group.

The changes in RNase activity in the cytoplasmic fraction of the experimental group differ markedly from those found in the nucleus. Shortly after the operation the most striking changes are a reduction in the amount of inhibitor-bound RNase per cell and a marked (3-fold) increase in free RNase. The increased free RNase activity reached a maximum at 6 hr and then returned to a new base line higher than the unoperated control and sham-operated values throughout the rest of the experiment. After the initial drop, inhibitor-bound activity increases, reaching a peak at 6 and 12 hr and remaining elevated throughout the experiment. The rapid drop in the amount of inhibitor may be related to the effects of operative stress, perhaps acting through hor-

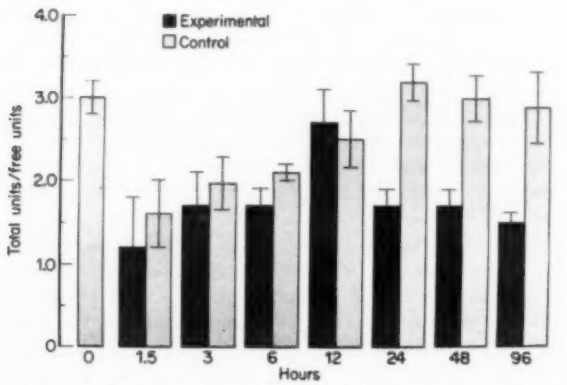

FIG. 3. Total units/free units ratio in unoperated, sham-operated, and experimental animals at various times. Marked reduction of this ratio in the experimental group is due to an increase in the amount of free activity. Mean and SD of four different determinations are indicated.

TABLE 3. *Inhibitor-bound RNase per μg of RNA or per mg of protein (mean ± SD) in the cytoplasmic fraction of unoperated control, sham-operated, and experimental groups 96 hr after operation*

Group	Bound RNase μgRNA	Bound RNase mg protein
Unoperated controls	22.6 ± 1.16	350 ± 24.2
Sham-operated	22.9 ± 0.70	343 ± 32.3
Experimental	24.6 ± 0.70	367 ± 21.3

monal influences, although there are no available data to support this assumption. How these marked changes in RNase activity can be related to RNA synthesis is unclear. The amount of inhibitor increases before RNA synthesis (2). Our data reinforce this concept, since inhibitor in the experimental group reaches its peak before the RNA/DNA ratio starts to increase. Similar changes in inhibitor in sham-operated animals, as pointed out above, may also indicate renewed RNA synthesis after the initial reduction in RNA content.

Although it is not known whether free RNase or bound RNase is the active form *in vivo*, several studies indicate that when free RNase is increased cellular RNA tends to decrease (3–5). In fact, Shortman has postulated that this is the mechanism by which RNase regulates the amount of RNA (2). Our data showing a constantly elevated free RNase activity in the experimental group are not easily fitted into this concept. Moreover, the lasting 3-fold elevation of free RNase in this group poses a new problem in understanding the role of RNase, since it is hard to imagine why uninephrectomy can influence free activity so markedly in the face of a 20% increase in the amount of cellular RNA. Data collected from other tissues in our laboratory indicate that this high amount of free RNase is unique to the kidney, since in brain, liver, or placenta the amount of free activity in a whole homogenate is only a small fraction of the inhibitor-bound RNase. One explanation of this characteristic of the kidney might be that two kinds of free RNase are being measured when an assay is done in the kidney cytoplasmic fraction. One type of RNase would be "intracellular" in the sense that it is actively participating in RNA metabolism of the cell, and the other an "extra-renal" RNase that has been "included" by the cell after it has been filtered and is being kept only momentarily before its excretion into urine, transport back into the plasma, or intracellular degradation. The possibility of RNase being taken up by the kidney has been previously considered to explain differences in the concentration of RNase between the renal artery and the renal vein (10). Consequently, the increased amount of free RNase in this experiment might indicate an increased physiological "load" of RNase on the remaining kidney and would, therefore, not be expected to correlate with concomitant changes in cellular growth. By contrast, inhibitor-bound RNase activity increases proportionally to the increase in protein and RNA per cell, suggesting that a new steady state in the relationship of bound RNase to cellular RNA has been achieved.

This study was supported by Nutrition Foundation Grant 398 and National Foundation Grant CRCS-45.

1. Roth, J. S. (1968) "Some observations on the assay and properties of ribonuclease in normal and tumor tissues," in *Methods in Cancer Research*, ed. Busch, H. (Academic Press, New York), Vol. 2, pp. 152–242.
2. Kraft, N. & Shortman, K. (1970) "A suggested control function for the animal tissue ribonuclease–ribonuclease inhibitor system, based on studies of isolated cells and phytohemagglutinin-transformed lymphocytes," *Biochim. Biophys. Acta* **217**, 164–175.
3. Quirin–Stricker, C., Gross, M. & Mandel, P. (1968) "Effects of protein deprivation on the activity of rat liver ribonuclease and their inhibitor," *Biochim. Biophys. Acta* **159**, 75–80.
4. Girija, N. S., Pradham, D. S. & Sreenivasan, A. (1965) "Effects of protein depletion on ribonucleic acid metabolism in rat liver," *Indian J. Biochem.* **2**, 85–90.
5. Brewer, E. N., Foster, L. B. & Sells, B. H. (1969) "A possible role for ribonuclease in the regulation of protein synthesis in normal and hypophysectomized rats," *J. Biol. Chem.* **244**, 1389–1392.
6. Sarkar, N. K. (1969) "The effect of synthetic corticosteroids on liver RNA, hepatic ribonuclease and ribonuclease inhibitor activities in rats," *FEBS Lett.* **4**, 37–41.
7. Louis–Ferdinand, R. T. & Fuller, G. C. (1967) "Suppression of hepatic ribonuclease during phenobarbital stimulation of drug metabolism," *Biochem. Biophys. Res. Commun.* **38**, 811–816.
8. Cohen, A. M. & Ruddon, R. W. (1970) "The metabolism of RNA in rat liver after phenobarbital administration," *Mol. Pharmacol.* **6**, 540–547.
9. Quirin–Stricker, C. & Mandel, P. (1968) "Etude du renouvellement du RNA des polysomes, du RNA de transfert et du RNA 'Messager' dans le foie de rat soumis a un jeune proteique," *Bull. Soc. Chim. Biol.* **50**, 31–45.
10. Royce, P. C. (1967) "Role of renal uptake of plasma protein in compensatory renal hypertrophy," *Amer. J. Physiol.* **212**, 924–930.
11. Malt, R. A. (1969) in *Compensatory Renal Hypertrophy*, ed. Gross, R. J. (Academic Press, New York), pp. 131–156.
12. Shortman, K. (1961) "Studies on cellular inhibitors of ribonuclear I. The assay of the ribonuclease inhibitor-system and the participation of the inhibitor from rat liver," *Biochim. Biophys. Acta* **51**, 37–49.
13. Munro, H. N. & Fleck, A. (1966) in *Methods in Biochemical Analysis*, ed. Glick, D. (Interscience Publishers, New York), Vol. 14, pp. 113–176.
14. Karp, R., Brasel, J. A. & Winick, M. (1971) "Compensatory kidney growth after uninephrectomy in adult and infant rats," *Amer. J. Dis. Child.* **121**, 186–188.
15. Villalobos, J. G., Jr., Steele, W. J. & Bush, H. (1965) "Ribonuclease activity of isolated nucleoli of livers of thioacetamide-treated rats," *Biochim. Biophys. Acta* **103**, 195–200.
16. Darnell, J. E., Jr. (1968) "Ribonucleic acids from animal cells," *Bacteriol. Rev.* **32**, 262–290.
17. Faiferman, I., Hamilton, M. G. & Pogo, A. O. (1970) "Nucleoplasmic ribonucleoprotein particles of rat liver. I.—Selective degradation by nuclear nucleases," *Biochim. Biophys. Acta* **204**, 550–563.
18. Willems, M., Musilova, H. A. & Malt, R. A. (1969) "Giant nucleoplasmic RNA in the switch-on of compensatory renal growth," *Proc. Nat. Acad. Sci. USA* **62**, 1189–1194.
19. Rizzo, A. J. & Webb, T. E. (1969) "Ribosomal formation in rat liver: evidence for post-transcriptional control," *Biochim. Biophys. Acta* **195**, 109–122.

Proc. Nat. Acad. Sci. USA
Vol. 70, No. 1, pp. 173–178, January 1973

Estimation of Light-Chain Gene Reiteration of Mouse Immunoglobulin by DNA–RNA Hybridization

(12S RNA/myeloma/protein synthesis/variable region)

T. L. DELOVITCH AND C. BAGLIONI

Department of Biology, Massachusetts Institute of Technology, Cambridge, Mass. 02139

Communicated by Baruj Benacerraf, November 6, 1972

ABSTRACT **A 12S species of RNA has been isolated from membrane-bound polyribosomes of MPC-11 mouse myeloma cells. This 12S RNA is translated by an extract of Krebs-II mouse ascites cells into immunoglobulin light chain. Labeled 12S RNA has been prepared by incubation of myeloma cells with [^{3}H]uridine in the presence of low concentrations of actinomycin D and ethidium bromide. This RNA has been hybridized under conditions of DNA excess to mouse myeloma DNA and to liver DNA. A $C_0t_{1/2}$ of about 150 has been obtained, corresponding to a reiteration frequency of about 40. Unlabeled 12S RNA competes with the labeled species in hybridization experiments, whereas globin mRNA or mouse ascites 12S RNA does not. It is suggested that 12S RNA hybridizes only to V_κ-genes of the same subclass, and that there may be several hundred genes coding for V_κ-regions of all subclasses in a mouse genome. Moreover, gene amplification in myeloma cells is not detected.**

Two main theories have been proposed to explain the origin of variability in the aminoacid sequence of immunoglobulin polypeptide chains (1). The germ line theory postulates that each aminoacid sequence is specified by a corresponding structural gene. Alternatively, somatic variation theories favor only a restricted number of basic sequences encoded by structural genes; during development, such basic sequences are subject to somatic mutations. Both theories have previously received extensive consideration (1–3).

One way of experimentally testing these theories is to measure the number of polynucleotide sequences in a genome that are complementary to immunoglobulin mRNA. However, this direct approach to the choice of germ line against somatic theories is complicated by several technical and theoretical problems. The following prerequisites must be satisfied: (*i*) isolation of an mRNA for either light or heavy chains; (*ii*) demonstration of the identity of the mRNA by its translation in a cell-free system; (*iii*) recovery of this mRNA, or its complementary DNA (cDNA), labeled with high specific activity; (*iv*) determination of the rate of hybridization of the labeled mRNA (or cDNA) to DNA, from which rate an estimate of the number of complementary polynucleotide sequences may be obtained (the interpretation of the latter reaction is rather complex). Progress toward these goals has been recently reported: mRNAs for some myeloma light chains have been isolated and translated (4–7), DNA complementary to various mRNAs has been synthesized with viral RNA-directed DNA polymerase (8–10), and preliminary data on the hybridization of light-chain mRNA have been obtained (11).

Abbreviation: SDS, sodium dodecyl sulfate.

We describe here the isolation from MPC-11 mouse myeloma cells, which secrete K chains, maintained in tissue culture (12, 13) of a 12S RNA that is translated into light chain in a cell-free extract of Krebs II mouse ascites cells (14). Hybridization experiments between the labeled 12S RNA and either mouse myeloma DNA or liver DNA suggest that immunoglobulin structural genes are not extensively reduplicated. In addition, specific gene amplification was not detected.

MATERIALS AND METHODS

Cell Culture. Mouse myeloma cells of the 66-2 clone (K-chain secretor) of the MPC-11 line (kindly provided by Dr. Matthew D. Scharff) were grown as described (15).

Preparation of RNA. Unlabeled 12S RNA was prepared from 2 liters of cells (5×10^5 cells per ml), which were washed with Earle's saline and homogenized (15). Nuclei were spun down for 5 min at $400 \times g$, and membrane-bound polyribosomes were pelleted by centrifugation for 5 min at $27{,}000 \times g$ (15). This pellet was resuspended in 1.5 ml of TNMD buffer [10 mM Tris·HCl (pH 7.4)–10 mM NaCl–1.5 mM $MgCl_2$–50 μg/ml of dextran sulphate], then mixed with an equal volume of 1 M KCl–10 mM $MgCl_2$–20 mM Tris·HCl (pH 7.4). The suspension was layered over 15–30% linear sucrose gradients in TNMD buffer, underlaid with a 0.2-ml cushion of 2 M sucrose. Membrane-bound polyribosomes were sedimented for 30 min at 25,000 rpm ($84{,}000 \times g$), and recovered at the interphase between 30% and 2 M sucrose; the top portion of the gradient was discarded and 5 ml of TNMD buffer was added to the bottom 0.3–0.5 ml. This solution was centrifuged 5 min at $27{,}000 \times g$; the pellet was rinsed with 1 ml of RSB buffer [10 mM NaCl–1.5 mM $MgCl_2$–10 mM Tris·HCl (pH 7.4)] dissolved in 3 ml of 1% sodium dodecyl sulfate in 5 mM Tris·HCl (pH 7.4) and layered over 5–20% sucrose gradients in dodecyl sulfate buffer [0.1 M NaCl–1 mM EDTA–10 mM Tris·HCl (pH 7.4)–0.5% SDS]. The RNA was fractionated by three successive 24-hr centrifugations at 26,000 rpm in an SW27 rotor. Each time, the RNA sedimenting at about 12 S was collected, precipitated with ethanol, redissolved in 1% SDS, and recentrifuged. The final centrifugation yielded a homogeneous peak at about 12 S, as estimated from the sedimentation of appropriate RNA markers in parallel gradients.

Labeled 12S RNA was prepared from 1 liter of cells, concentrated by centrifugation (15) and resuspended at 2×10^6 cells per ml in the same medium, to which 40 ng/ml of actino-

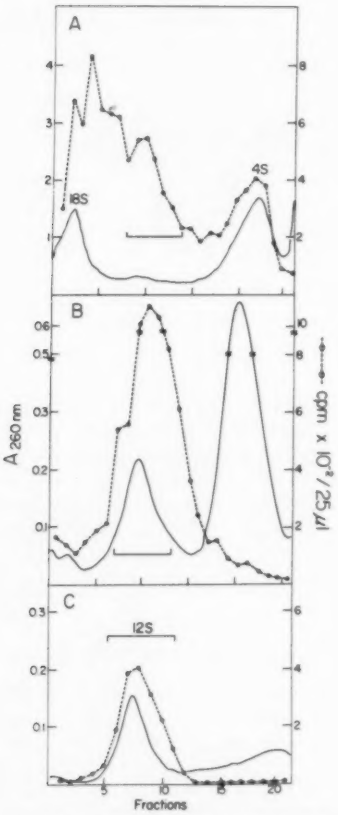

FIG. 1. Preparation of labeled 12S RNA from myeloma cells. The RNA of membrane-bound ribosomes isolated from two liters of MPC-11 cells was applied to six sucrose gradients and fractionated. The absorbance at 260 nm was monitored in a Gilford recording spectrophotometer (*A*); the RNA sedimenting at about 12 S was precipitated with ethanol after addition of carrier 4S yeast tRNA, applied to three gradients, and similarly fractionated (*B*). A further fractionation of this RNA was performed (*C*); the peak sedimenting at 12 S was isolated. The *brackets* indicate the fractions combined at each step.

mycin D and 1 µg/ml of ethidium bromide were added. After 30 min at 37°, 75 µCi/ml of [^{3}H]uridine (25 Ci/mmol) was added and the incubation was continued for 4 hr. The procedures described above were followed to prepare membrane-bound polyribosomes and 12S RNA. The RNA was fractionated on three successive sucrose gradients, as indicated in Fig. 1, and finally analyzed by electrophoresis on a 4% acrylamide gel according to Weinberg *et al.* (16). The specific activity of the 12S RNA was about 3×10^4 cpm/µg.

18S rRNA was isolated from polyribosomes of cells incubated 18 hr with 5 µCi/ml of [^{3}H]uridine, as described above for 12S RNA. This RNA was further purified by electrophoresis on preparative 2.6% acrylamide gels (17), precipitated with ethanol, and dissolved in water. The specific activity of the 18S RNA was about 2×10^4 cpm/µg.

Translation of mRNA and Analysis of the Cell-Free Product. The Krebs II ascites cell-free system (18) was used with minor modifications (14). Appropriate amounts of RNA were added to 0.6 volumes of ascites extract and 0.1 volume of master mix containing the components of the cell-free system (14). The final volume was adjusted by the addition of labeled amino acids (New England Nuclear), a complement of unlabeled amino acids (to 0.1 mM), and water. Incubations were performed at 30° for 60 min, and aliquots were counted (19).

After the incubation, aliquots were analyzed by indirect immunoprecipitation with a rabbit antiserum prepared against Fab-fragment from MPC-11 IgG (kindly provided by Dr. M. D. Scharff) and goat antiserum prepared against rabbit IgG (20). Samples were prepared for gel electrophoresis by precipitation with 5% Cl_3CCOOH in acetone, collected by centrifugation, dissolved in 0.5 ml of 0.1 N NaOH, reprecipitated with 5% Cl_3CCOOH, and then washed twice with 5% Cl_3CCOOH and twice with acetone. The precipitates were dissolved in 6 M urea–1% SDS–0.1 M mercaptoethanol–50 mM phosphate buffer (pH 7), heated at 70° for 2 min, and electrophoresed on 18-cm 10% acrylamide gels for 14 hr at 8 mA/gel; the gels were then crushed and counted (21). Samples to be digested with trypsin were first aminoethylated, dialyzed against water, and lyophilized; they were then digested (22). The tryptic peptides were separated by paper electrophoresis at pH 3.6 for 6 hr at 4500 V (21). The papers were cut into 1-cm strips and counted (21).

Preparation of DNA, and DNA–RNA Hybridization. DNA was prepared from MPC-11 myeloma and liver tissue essentially as described (23). DNA extracted from isolated nuclei was sonicated to a molecular weight of about 200,000, as estimated by the method of Studier (24), precipitated with ethanol (23), and further purified by filtration through Sephadex SP-50. The DNA collected in the excluded volume was dialyzed extensively against deionized water and lyophilized. The yields obtained were about 1 mg/g of liver and 1.5 mg/g of tumor.

TABLE 1. *Translation of myeloma 12S RNA in cell-free systems from ascites and HeLa cells*

Exp. I	RNA	µg	Reticulocyte factors	cpm
(Ascites)	12S myeloma	1.30	−	3,500
	12S myeloma	2.60	−	8,470
	12S myeloma	1.30	+	7,320
	Globin	0.45	−	9,740
	Globin	0.45	+	13,650
	—	—	−	445
	—	—	+	921
Exp. II				
(HeLa)	12S myeloma	1.30	−	1,330
	12S myeloma	1.30	+	4,560
	Globin	0.45	−	2,060
	—	—	−	394

Each reaction mixture contained the components of the cell-free system described in *Methods*, 1 or 2 µl of RNA solution, 2 µCi of [^{3}H]tyrosine (44 Ci/mmol), 1 µl of reticulocyte factors (where indicated), and water to a final volume of 10 µl. After 60 min at 30°, 4-µl aliquots were sampled in duplicate and counted as described (21). The reticulocyte initiation factors were prepared free of globin mRNA according to Shafritz *et al.* (44). Globin mRNA was prepared as described (45).

DNA–RNA hybridization was performed under conditions of DNA excess (23). Reaction mixtures in 0.12 M phosphate buffer (pH 6.8) contained 1% SDS, 10–12 mg/ml of sonicated DNA, and RNA in an overall DNA to RNA ratio of 1 to 5×10^4. In a typical experiment, aliquots were drawn into alkali-washed, silicone-treated, capillary tubes and the ends were sealed. The tubes were heated for 5 min at 100° to denature DNA, and the reactions were then performed at 70°. "Zero time" controls were determined as described (23). After incubation, the samples were diluted 1:100 into ice-cold 0.3 M NaCl–0.030 M Na citrate. Equal aliquots were treated 30 min at 37° with or without 20 μg/ml of pancreatic ribonuclease. The samples were precipitated with 5% Cl_3-CCOOH in the presence of 100 μg/ml of carrier RNA and were collected on Millipore filters for counting.

RESULTS

Translation of 12S RNA and Characterization of Its Cell-Free Product. More than 50% of the proteins synthesized by membrane-bound polyribosomes of mouse myeloma 66-2 cells consist of immunoglobulin chains (20). Whereas this clone secretes only light chains, it also synthesizes heavy chains at a rate similar to that of the parent cell line (13); these heavy chains are not assembled into IgG and are, presumably, degraded (20). We have chosen to isolate light-chain mRNA from membrane-bound polyribosomes, since it is presumably present in this fraction in higher concentration relative to other mRNAs. The preparation of membrane-bound polyribosomes was treated with 0.5 M KCl to remove contaminating free polyribosomes (25), and the RNA was fractionated by sucrose density-gradient centrifugation. Previous reports have shown that light-chain mRNA sediments around 12 S (4–7, 26). We precipitated the RNA from the region of the gradient corresponding to 12 S, and fractionated it twice further, as described in *Methods* (see also Fig. 1).

The 12S RNA isolated in this way is translated efficiently by an ascites (18) or HeLa (27) cell-free system (Table 1). Translation is stimulated by the addition of rabbit reticulocyte initiation factors, as reported (28) for globin mRNA (Table 1). The cell-free product of 12S RNA has been characterized by immunoprecipitation, acrylamide gel electrophoresis, and analysis of its tryptic peptides. Rabbit anti-MPC 11 (Fab), followed by the addition of goat antiserum prepared against rabbit IgG to equivalence (20), precipitated 38% of the labeled cell-free product of 12S RNA, whereas only 4% was precipitated when normal rabbit serum was substituted for the specific antiserum. 4% precipitation was also attained when rabbit anti-MPC 11 Fab was added to the cell-free product of globin mRNA.

Acrylamide gel electrophoresis (Fig. 2) showed that the bulk of the cell-free product synthesized by 12S RNA migrated in the position of the marker light chain; however, a large portion of the radioactive protein migrated faster than the light chain, close to the position of an immunoglobulin fragment present in the marker used (secreted IgG of P-3 myeloma cells). We have observed the formation of fragments of MPC-11 IgG in cell-free incubations containing MPC-11 polyribosomes and an ascites S-100 fraction (20). Brownlee *et al.* (5) and Swan *et al.* (6) have also observed the presence of proteins smaller than light chain when 12S myeloma RNA was translated by an ascites cell-free extract.

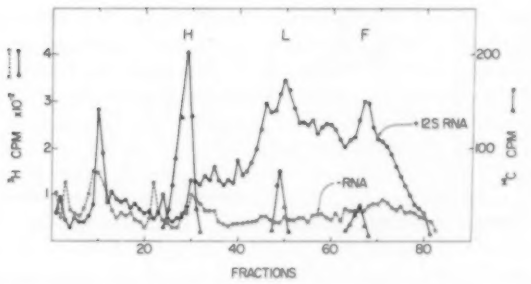

FIG. 2. Acrylamide gel electrophoresis of the product of myeloma 12S RNA synthesized in an ascites cell-free extract. Two reaction mixtures similar to those described in Table 1 were scaled up to a final volume of 60 μl, and incubated with 60 μCi of [^{3}H]aminoacids, 7.8 μg of 12S RNA, or no added RNA. The samples were analyzed on 10% acrylamide gels. Mouse IgG, of the P-3 tissue culture line, uniformly labeled with [^{14}C]proline was added as marker (20): this IgG was resolved into three peaks (*triangles*) corresponding to heavy chains (*H*), light chains (*L*), and a fragment (*F*). The pattern of the cell-free product of 12S RNA (*closed circles*) has been superimposed on that of the control without added RNA (*open circles*).

It is unclear whether these fragments are products of translation of degraded RNA molecules or whether they are formed by the action on light chains of proteases present in the cell-free extract. Fragments of human light chains are found in the urine of myeloma patients (29), and can also be produced by proteolytic cleavage of Bence–Jones proteins (30, 31).

Finally, the tryptic peptides of [^{35}S]methionine-labeled cell-free product were analyzed (Fig. 3). MPC-11 light chain uniformly labeled with [^{3}H]methionine was combined with the incubation mixture before digestion with trypsin and analysis by paper electrophoresis. The ^{3}H-labeled marker contained three peptides, which coincided in electrophoretic mobility with those obtained from the cell-free product of 12S RNA. This result indicates that our preparation of 12S RNA does not contain any major contaminating species of mRNA, unless this contaminant does not contain methionine.

Isolation of Labeled 12S RNA and Its Use in DNA–RNA Hybridization. Clone 66-2 cells were incubated with [^{3}H]-uridine, in the presence of 40 ng/ml of actinomycin D and 1 μg/ml of ethidium bromide to inhibit the synthesis of ribosomal RNA (32) and mitochondrial RNA (33). The RNA of membrane-bound polyribosomes was fractionated (Fig. 1). A peak at 4 S and two additional ones at about 12 S and 14–16 S were observed (Fig. 1*A*). Repeated gradient centrifugation of the 12S RNA yielded a symmetrical peak (Fig. 1*C*). Acrylamide gel electrophoresis (16) of this RNA showed a major peak at 12 S and a minor one at about 28 S, possibly an aggregate (Fig. 4). From the estimated molecular weight of the 12S RNA, we calculated that it contains about 800–900 nucleotides, in agreement with previous determinations (6).

Hybridization experiments with labeled 12S RNA have been performed under conditions of DNA excess (23) in 0.12 M phosphate buffer at 70°. The C_0t curve (34) of the transition of 12S RNA from the single-stranded to the duplex form is shown in Fig. 5. The results have been corrected for background ribonuclease resistance (7–10%). A $C_0t_{1/2}$ of about

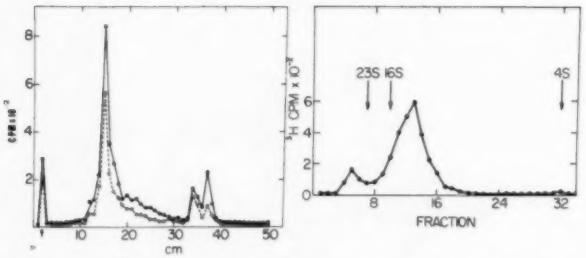

FIG. 3 (*left*). Paper electrophoresis of a tryptic digest of the cell-free product of myeloma 12S RNA. Two reaction mixtures (similar to the ones described in Fig. 2) were incubated with 50 μCi of [^{35}S]methionine (150 Ci/mmol) and either 15 μg of 12S RNA or no RNA. A total of 1,560,000 cpm was incorporated with added 12S RNA and 160,000 cpm was incorporated without added RNA. The samples were diluted with 1 ml of 10 mM NaCl–10 mM Tris·HCl (pH 7.4)–1.5 mM $MgCl_2$ and centrifuged 2 hr at 160,000 $\times$ *g* to remove ribosomes. About 75% of the total radioactivity in the samples was recovered in the supernatants. Aliquots of these solutions were combined with an appropriate amount of MPC-11 light chain uniformly labeled with [^{3}H]methionine before aminoethylation and digestion with trypsin (22). The samples were then dialyzed, lyophilized, and analyzed by paper electrophoresis at pH 3.6. The *arrow* indicates the point of sample application. No methionine-containing peptides were observed for the control sample to which no RNA was added (results not shown). (●——●), ^{3}H radioactivity: (○- - -○), ^{35}S radioactivity.

FIG. 4 (*right*). Acrylamide gel electrophoresis of myeloma 12S RNA. The 12S RNA obtained by density-gradient centrifugation (Fig. 1*C*) was electrophoresed on a 6-cm long 4% acrylamide gel for 3 hr at 5 mA/gel. The positions of ^{14}C-labeled *E. coli* 23S and 16S rRNA and 4S tRNA markers are indicated by *arrows*.

150 was observed, corresponding to a reiteration frequency (*F*) of about 40, as calculated by comparison with the $C_0t_{1/2}$ and the analytical complexity of *Escherichia coli* cRNA and DNA (35). Due to thermal degradation of mRNA and failure to operate in sufficient DNA excess $C_0t_{1/2}$ values may be underestimated by a factor of about two (35); these conditions could reduce by a similar factor our estimate of *F*. However, $C_0t_{1/2}$ determined in phosphate buffers is usually underestimated by a factor of 2–3 (36). Hence, these effects tend to cancel each other, and the experimental $C_0t_{1/2}$ provides a reasonable estimate of *F*.

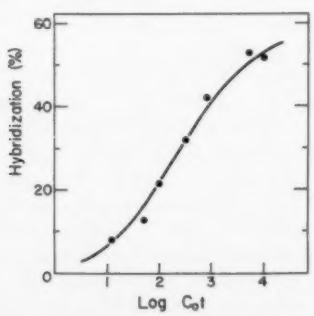

FIG. 5. Hybridization of myeloma DNA and 12S RNA. Sonicated, denatured DNA and labeled 12S RNA, prepared as indicated in *Methods*, were annealed in 0.12 M phosphate buffer at 70°. The overall DNA to RNA ratio used was about 3 $\times$ 10^4.

A maximum slightly above 50% hybridization was observed for the 12S RNA at a C_0t of 10,000. A biphasic transition curve was not obtained, as would have been expected if the 12S RNA hybridized to light chain variable (*V*) and common (*C*) region genes at different rates. Perhaps we have observed hybridization to *V*-genes exclusively, and have not detected annealing to a unique *C*-gene; we have calculated the $C_0t_{1/2}$ for the latter reaction to be about 6000 (35). Our reaction mixtures were incubated only to a C_0t of 10,000, since preliminary experiments indicated that longer incubations lead to extensive RNA degradation. Consequently, a second transition may not have been observed.

The 12S RNA hybridized to mouse liver DNA with a $C_0t_{1/2}$ similar to that observed for myeloma DNA (results not shown). This finding suggests that immunoglobulin gene amplification does not occur in myeloma cells. As a control, 18S rRNA was hybridized to myeloma DNA; a $C_0t_{1/2}$ of 20 (results not shown) was obtained, indicating an *F* corresponding to 300 copies of rDNA, in close agreement with the value previously reported (23).

The translation experiments demonstrated that unlabeled 12S RNA contains light-chain mRNA. Although the labeled 12S RNA was fractionated in an identical manner, it was necessary to prove that this RNA contains labeled light-chain mRNA. Thus, competition–hybridization experiments were performed between labeled and unlabeled 12S RNA and myeloma DNA in an attempt to establish an identity between these RNA species.

Competition experiments are more efficiently performed at a complementary sequence ratio of DNA to RNA of 1:1, rather than under conditions of DNA excess. Hybridization was thus measured as a function of the overall DNA to RNA ratio (Fig. 6*A*); about 55% hybridization was reached at an overall DNA to RNA ratio of 10^4. This ratio was chosen as the starting point for the competition analysis of labeled with unlabeled 12S RNA (Fig. 6*B*). Unlabeled 12S RNA com-

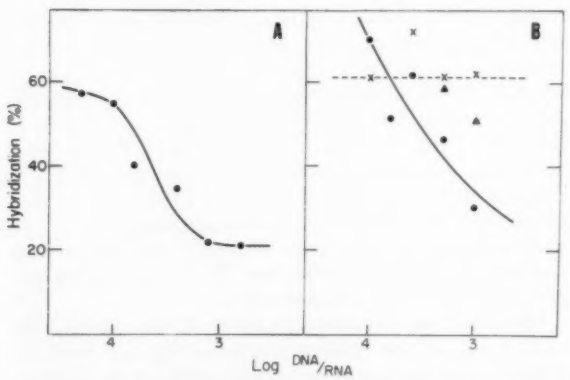

FIG. 6. (*A*) Hybridization of myeloma DNA and 12S RNA at different overall DNA to RNA ratios. Various amounts of DNA and a constant amount of RNA were hybridized in different reaction volumes as described in *Methods*. All samples were incubated to a C_0t of 10,000. (*B*) Competition–hybridization of myeloma DNA and labeled 12S RNA. Constant amounts of DNA and labeled 12S RNA were annealed with various amounts of either unlabeled myeloma 12S RNA (●——●), rabbit globin 10S mRNA (×- - -×), or Krebs-II ascites 12S RNA (▲) to a C_0t of 10,000.

peted effectively with labeled 12S RNA at DNA to RNA ratios between 10^4 and 10^3. A greater degree of competition would be expected upon further reduction of the DNA to RNA ratio. By contrast, 10S globin mRNA and 12S RNA isolated from membrane-bound polyribosomes from Krebs-II ascites cells did not compete with labeled myeloma 12S RNA, and the 12S RNA preparation is not highly contaminated with different mRNAs of similar size present in other mouse cells.

DISCUSSION

We have isolated a 12S RNA from membrane-bound polyribosomes of MPC-11 mouse myeloma cells. This RNA contains the mRNA for the MPC-11 light chain, since it can be translated into this protein. Nevertheless, we lack absolute proof that the 12S RNA is coding exclusively for light chains. Immunoprecipitation of light chains synthesized *in vitro* is not quantitative, since these light chains lack the proper disulfide bridges and tertiary configuration (20). Gel electrophoresis shows the presence of proteins with molecular weight lower than that of a light chain. However, fragments of light chains can be formed by proteolysis (29–31), and are indeed formed during the cell-free synthesis of light chains (20). The most conclusive test, the analysis of the tryptic peptides, may not reveal contamination of light-chain mRNA with other mRNAs, each present in relatively small amounts.

In addition, it is possible that the 12S RNA contains other RNAs that are not translated, i.e., RNA of the small ribosomal subunit of mitochondrial ribosomes (37) and breakdown products of rRNA. Hence, during the labeling of RNA, we have included ethidium bromide and low concentrations of actinomycin D to inhibit the synthesis of mitochondrial RNA (33) and rRNA (32), respectively. Previous reports have shown that mRNA metabolism is essentially unaltered for several hours in the presence of these drugs (33, 38).

The presence of unlabeled RNA species other than mRNA does not alter the C_0t curve obtained with labeled mRNA (35). The transition to duplex formation for at least half of the sequence of the labeled 12S RNA shows a single transition curve (Fig. 5). This result indicates that about 50% of the labeled 12S RNA behaves as a homogeneous species during hybridization. The remaining labeled RNAs may not form duplexes, since either we have failed to operate in sufficient DNA excess (23) or these RNAs are transcribed from DNA sequences present as a single copy in the genome (34).

Light-chain mRNA codes for the *V* and *C* regions of the protein. Genetic studies of alleles for *C*-region genes suggest that they are present as either single or double copies in the genome (1–3). Hence, we have probably failed to hybridize that part of light-chain mRNA coding for the *C*-region. If we assume that the C_0t curve observed represents the annealing of that part of 12S RNA coding for the V_κ-region of the MPC-11 light chain, the results suggest that under the conditions used we detect about 40 DNA sequences per genome complementary to the 12S mRNA. The interpretation of these data is complicated by the existence in mice of several subclasses of V_κ-chains, characterized by a different basic aminoacid sequence (39), and by the minimal information on the variability of aminoacid sequences within each subclass.

Human V_κ-chains of one subclass are identical for 73–87% of their sequences (42). Most of the aminoacid interchanges are localized in two or three hypervariable regions (40), and can be attributed to single nucleotide changes (42). V_κ-chains of different subclasses differ in about 40% of their sequences (42). The minimal stable length for duplex formation is 10–20 nucleotides (41); thus, there is a high probability of duplex formation between the mRNA of one particular V_κ-chain and the polynucleotide sequences coding for other V_κ-chains of the same subclass, but hybridization with V_κ-genes of other subclasses seems less likely. The hybrids between mRNA and V_κ-genes of the same subclass may be mismatched at single base pairs, except for hypervariable regions (40). Ribonuclease digestion may remove groups of mismatched nucleotides, but probably does not remove single mismatched nucleotides; therefore, it seems possible to obtain a reasonable estimate of F for V_κ-genes of one particular subclass by the method used.

If we have measured the number of structural genes coding for V regions of one V_κ-subclass, then the value of F obtained represents an underestimate of F for the total number of V_κ-genes. This value can only be obtained by summing F for each subclass. If the V_κ-sequence of the MPC-11 light chain belongs to a subclass of average size, and there are at least nine V_κ-subclasses in mice (39), we can postulate that there are probably no more than 500 structural genes for V_κ-regions in a mouse genome. Since the aminoacid sequence of the V_κ-region of the MPC-11 light chain and the relative frequency of proteins in its subclass are both unknown, it remains inconclusive whether our results provide an accurate measure of the number of structural genes coding for V_κ-regions. We estimate this number to be no less than 40 and, probably, not more than 500–1000. This estimate differs from a previous one obtained by hybridization under conditions of RNA excess (42). It has been pointed out recently that the latter method does not measure gene reiteration accurately, since part of the mRNA transcribed from a single gene hybridizes to short polynucleotide sequences common to many unrelated genes (43).

This work has been supported by the National Institute of Health (AI 08116). We are grateful to Dr. Marcelo Jacobs-Lorena for performing the translation experiments and to Gloria Mao and Rebecca Hinderlie for excellent technical assistance.

1. Lennox, E. A. & Cohn, M. (1967) *Annu. Rev. Biochem.* **36**, 365–406.
2. Hood, L. & Talmage, D. W. (1970) *Science* **168**, 325–334.
3. Gally, J. A. & Edelman, G. M. (1970) *Nature* **227**, 341–348.
4. Stavnezer, J. & Huang, R. C. C. (1971) *Nature New Biol.* **230**, 172–176.
5. Brownlee, G. G., Harrison, T. M., Mathews, M. B. & Milstein, C. (1972) *FEBS Lett.* **23**, 244–248.
6. Swan, D., Aviv, H. & Leder, P. (1972) *Proc. Nat. Acad. Sci. USA* **69**, 1967–1971.
7. Stevens, R. H. & Williamson, A. R. (1972) *Nature* **239**, 143–146.
8. Ross, J., Aviv, H., Scolnick, E. & Leder, P. (1972) *Proc. Nat. Acad. Sci. USA* **69**, 264–268.
9. Kacian, D. L., Spiegelman, S., Bank, A., Terada, M., Metafora, S., Dow, L. & Parks, P. A. (1972) *Nature New Biol.* **235**, 167–169.
10. Verma, I. M., Temple, G. F., Fan, H. & Baltimore, D. (1972) *Nature New Biol.* **235**, 163–167.
11. Delovitch, T. & Baglioni, C. (1972) *Scand. J. Immunol.* **1**, 284–285.
12. Laskov, R. & Scharff, M. D. (1970) *J. Exp. Med.* **131**, 515–539.
13. Coffino, P. & Scharff, M. D. (1971) *Proc. Nat. Acad. Sci. USA* **68**, 219–223.

14. Jacobs-Lorena, M. & Baglioni, C. (1972) *Biochemistry*, in press.
15. Baglioni, C., Bleiberg, I. & Zauderer, M. (1971) *Nature New Biol.* **232**, 8–12.
16. Weinberg, R., Loening, U., Willems, M. & Penman, S. (1967) *Proc. Nat. Acad. Sci. USA* **58**, 1088–1095.
17. McCarthy, D., Hawkes, S. P. & Lander, D. E. (1972) *Biochim. Biophys. Acta* **277**, 301–305.
18. Mathews, M. B. & Korner, A. (1970) *Eur. J. Biochem.* **17**, 328–343.
19. Nishimura, S. & Novelli, G. D. (1964) *Biochim. Biophys. Acta* **80**, 574–586.
20. Delovitch, T. L. & Baglioni, C. (1972) *J. Immunol.*, in press.
21. Jacobs-Lorena, M., Baglioni, C. & Borun, T. W. (1972) *Proc. Nat. Acad. Sci. USA* **69**, 2095–2099.
22. Baglioni, C., LaVia, M. & Ventruto, V. (1965) *Biochim. Biophys. Acta* **111**, 479–484.
23. Melli, M., Whitfield, C., Rao, K. V., Richardson, M. & Bishop, J. O. (1971) *Nature New Biol.* **231**, 8–12.
24. Studier, F. W. (1965) *J. Mol. Biol.* **11**, 373–390.
25. Zauderer, M. (1972) Doctoral Thesis, Massachusetts Institute of Technology.
26. Delovitch, T. L., Davis, B. K., Holme, G. & Sehon, A. H. (1972) *J. Mol. Biol.* **69**, 373–386.
27. McDowell, M. J., Joklik, W. K., Villa-Komaroff, L. & Lodish, H. F. (1972) *Proc. Nat. Acad. Sci. USA* **69**, 2649–2653.
28. Metafora, S., Terada, M., Dow, L. W., Marks, P. A. & Bank, A. (1972) *Proc. Nat. Acad. Sci. USA* **69**, 1299–1303.
29. Baglioni, C., Cioli, D., Gorini, G., Ruffilli, A. & Alescio-Zonta, L. (1967) *Cold Spring Harbor Symp. Quant. Biol.* **32**, 147–159.
30. Solomon, A. & McLaughlin, C. (1969) *J. Biol. Chem.* **244**, 3393–3404.
31. Karlsson, F. A., Peterson, P. A. & Berggard, I. (1969) *Proc. Nat. Acad. Sci. USA* **64**, 1257–1263.
32. Perry, R. P. (1962) *Proc. Nat. Acad. Sci. USA* **48**, 2179–2186.
33. Zylber, E., Vesco, C. & Penman, S. (1969) *J. Mol. Biol.* **44**, 195–204.
34. Britten, R. D. & Koyne, D. E. (1968) *Science* **161**, 529–540.
35. Bishop, J. O., Pemberton, R. & Baglioni, C. (1972) *Nature New Biol.* **235**, 231–234.
36. Kedes, L. H. & Birnstiel, M. L. (1971) *Nature New Biol.* **230**, 165–169.
37. Brega, A. & Vesco, C. (1971) *Nature New Biol.* **229**, 136–139.
38. Roberts, W. K. & Newman, T. F. E. (1966) *J. Mol. Biol.* **20**, 63–73.
39. Hood, L., Potter, M. & McKean, D. J. (1970) *Science* **170**, 1207–1210.
40. Wu, T. T. & Kabat, E. A. (1970) *J. Exp. Med.* **132**, 211–246.
41. McCarthy, B. J. & Church, R. B. (1970) *Annu. Rev. Biochem.* **39**, 131–150.
42. Storb, U. (1972) *J. Immunol.* **108**, 755–764.
43. Harrison, P. R., Hell, A., Birnie, G. D. & Paul, J. (1972) *Nature* **239**, 219–221.
44. Shafritz, D. A., Pritchard, P. M. & Anderson, F. W. (1972) in *Methods in Molecular Biology*, eds. Last, J. A. & Laskin, A. I. (M. Dekker, Inc., New York), Vol 2, pp. 265–321.
45. Jacobs-Lorena, M. & Baglioni, C. (1972) *Proc. Nat. Acad. Sci. USA* **69**, 1425–1428.

Proc. Nat. Acad. Sci. USA
Vol. 70, No. 1, pp. 179–182, January 1973

Transfer RNA Synthesis *In Vitro*

(T4 DNA/RNA transcription/RNA processing/sequence analysis)

DONALD P. NIERLICH*, HILDEGARD LAMFROM, ANAND SARABHAI, AND JOHN ABELSON

Department of Chemistry, University of California, San Diego, La Jolla, Calif. 92037

Communicated by Robert W. Holley, November 13, 1972

ABSTRACT **During infection of *Escherichia coli*, bacteriophage T4 directs the synthesis of at least eight transfer RNAs and of two stable RNA species of low molecular weight, of unknown function. When T4 DNA is incubated with purified RNA polymerase and the appropriate substrates, a high molecular weight RNA is produced. This RNA, on further incubation with a supernatant fraction prepared from *E. coli*, is cleaved to several species of RNA. These cleaved RNAs were analyzed by gel electrophoresis and fingerprint techniques, and were found to be similar or identical to those made *in vivo*. The fingerprint analysis of one of these, a $tRNA^{Gly}$, is presented. The molecule made *in vitro*, except for the absence of modified bases, appears to be identical to the RNA made by T4-infected cells. Therefore, in this system the tRNA genes are transcribed with fidelity, the transcript is cleaved correctly, and the tRNAs are made in good yield.**

Since transfer RNAs play a central role in cellular metabolism, it is important to understand the details of their synthesis. In the case of the tyrosine suppressor tRNA encoded by bacteriophage ϕ80pSu$^+$III, the Su$^+$III $tRNA^{Tyr}$ is transcribed with additional residues at the 3′ and 5′ ends of the molecule. This unmodified precursor RNA must be further cleaved and modified to yield the functional tRNA (1, 2). Several enzymes have been described that catalyze these modifications (3). However, it is not completely understood how the tRNA genes are arranged on the chromosome, how such genes are transcribed, or what special features allow for their regulation.

Clearly much more could be learned about the synthesis of tRNA and its control by study of tRNA synthesis *in vitro*. Several groups have reported the *in vitro* synthesis of tRNA with the Su$^+$III system (4–6). We have developed an *in vitro* system that synthesizes several of the tRNAs coded by bacteriophage T4, and we have shown the fidelity of their transcription by fingerprint analysis.

After infection of its host, *Escherichia coli*, bacteriophage T4 directs the synthesis of some ten stable RNA species, eight of which are tRNAs (7–10, 23). The genes for these stable RNA species are all clustered together in a region of about 3000 base pairs on the T4 genome (11). Our working hypothesis is that these tRNA genes are part of a single transcription unit, and may constitute a tRNA operon. Thus, the T4 system provides us with the opportunity to study in detail the processing and modification of several tRNAs from a large precursor.

When T4 DNA is transcribed *in vitro*, RNA molecules of tRNA size are not made (12–14). However, it has been observed (*i*) that mature tRNAs are stable to nucleases present in a crude extract of *E. coli* (2), whereas other RNAs are degraded, and (*ii*) that the incubation of a large ϕ80pSu$^+$III transcript with an *E. coli* supernatant yields molecules of about tRNA size (6). Our experiments have thus been directed toward testing the possibility that tRNA sequences might be revealed after the incubation of such T4 transcripts with an *E. coli* extract.

In this communication, we show that the T4 tRNAs can be accurately transcribed *in vitro* from T4 DNA and processed correctly. We have analyzed one of the *in vitro* products, a T4 $tRNA^{Gly}$, and have concluded that the *in vitro* product has the same nucleotide sequence as that made *in vivo*.

MATERIALS AND METHODS

Phage T4D and phage T4 $pSu_b^-\Delta 33$ (11) were purified by equilibrium density centrifugation in cesium chloride. The DNA was extracted with phenol (15) and dialyzed against a solution containing 0.01 M Tris·HCl (pH 7.4)–0.05 M NaCl.

The supernatant fraction was prepared from *E. coli* Q13 (16). Cells were grown in broth to late-log phase and harvested by centrifugation. The cells were washed and resuspended in a buffer containing 0.01 M Tris·HCl (pH 8.0)–0.01 M $Mg(OAc)_2$–0.06 M KCl–6 mM 2-mercaptoethanol. After disruption of the cells in a French press at 15,000 lb/in^2, the extract was centrifuged for 30 min at 31,000 × *g* and the upper $^1/_2$ volume was collected. This fraction was extensively dialyzed against a solution containing 0.01 M Tris·HCl (pH 8.0)–0.01 M $Mg(OAc)_2$–0.06 M NH_4Cl–6 mM 2-mercaptoethanol, quick frozen, and stored at −20°.

RNA polymerase was isolated according to the method of Berg, Barrett, and Chamberlin (17). Fraction V enzyme had a protein concentration of 2.5 mg/ml.

The reaction mixture for RNA synthesis (18) contained in a volume of 0.5 ml: 0.04 M Tris·HCl (pH 7.9), 0.01 M $MgCl_2$, 0.16 M KCl, 0.1 mM EDTA, 0.1 mM dithiothreitol, 0.4 mM potassium phosphate (pH 7.5), 0.16 mM each of ATP, CTP, and UTP, 0.12 mM [α-^{32}P]GTP (6 Ci/mmol; New England Nuclear Corp., Boston, Mass.), 100 μg/ml of DNA, and 50 μg/ml of RNA polymerase. The reaction was incubated for 20 min at 37° and terminated by the addition of 10 μg of actinomycin D and 50 μg of DNase I (RNase-free, Worthington, Freehold, N.J.), immediately followed by the addition of 20 μl of supernatant fraction from *E. coli* Q13 and 90 μg of carrier *E. coli* tRNA. The incubation was continued for 30 min at 37°, and terminated by the addition of 0.75 ml of 0.25 M NaOAc (pH 5.0) and 0.5 ml of 0.01 N HCl.

The incorporation of [^{32}P]GTP was followed by the precipi-

* Permanent address: Department of Bacteriology, and Molecular Biology Institute, University of California, Los Angeles, Calif. 90024.

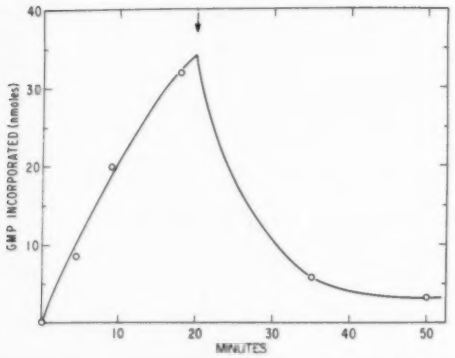

FIG. 1. Rate of [α-^{32}P]GTP incorporation by RNA polymerase with T4 DNA as template. At 20 min (*arrow*), *E. coli* Q13 supernatant fraction was added to hydrolyze the unstable RNA species and to cleave the tRNA precursor.

tation of 2-ul aliquots from the reaction mixture with 5% Cl_3CCOOH. Radioactivity was measured in a liquid scintillation counter.

The RNA was extracted by shaking the reaction mixture with an equal volume of H_2O-saturated phenol for 30 min at room temperature. The aqueous phase was fractionated on a column of Sephadex G-25 (1.8 × 25 cm) that had been equilibrated with 0.01 M NaOAc (pH 5.0). The column was eluted with the same buffer. Fractions comprising the excluded peak of radioactivity were pooled and precipitated with ethanol.

RNA was fractionated on acrylamide gels by the method described by DeWachter and Fiers (19). The 40-cm 10% gels (39:1, acrylamide–bisacrylamide) were prepared and run in 0.1 M Tris acetate (pH 8.3) at about 30 mA for 16–18 hr. Marker tRNAs were labeled *in vivo* with ^{32}P as described by Wilson and Abelson (20). Radioactive species on the gel were located by autoradiography.

The RNA species that were to be fingerprinted were recovered from the gel by homogenization of cut-out gel bands in 0.3 M NaCl. Acrylamide was removed by centrifugation and filtration through a Millipore filter.

The fingerprint analysis was performed according to the procedure of Sanger *et al.* (21), and involved T1 RNase digestion followed by two-dimensional electrophoresis on cellulose acetate and DEAE-paper.

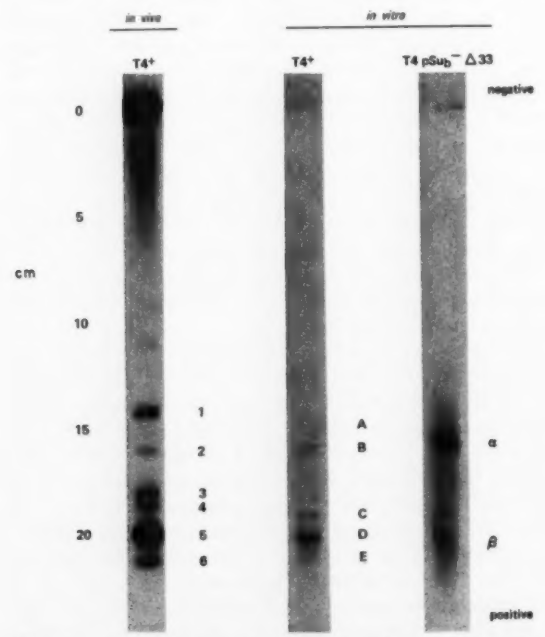

FIG. 2. Autoradiogram of acrylamide gel separations. Comparison of stable RNA species made *in vivo* and made *in vitro* with T4 or T4 pSub⁻Δ33 DNA as template, as described in the legend to Fig. 1.

RESULTS AND DISCUSSION

Fig. 1 shows the incorporation of [α-^{32}P]GTP into RNA in an experiment in which T4D DNA served as template. After 20 min of incubation at 37°, RNA synthesis was terminated by the addition of actinomycin D and DNase I. A crude S-30 supernatant fraction from *E. coli* was added and incubation was continued for 30 min. At the end of the incubation, only 10% of the labeled RNA that was acid-precipitable at 20 min remained. This RNA was purified by passage through Sephadex G-25 (exclusion molecular weight about 10,000) and precipitated with ethanol. The RNA was subjected to electrophoresis in a 10% polyacrylamide gel. As a control, RNA prepared similarly with T4 pSub⁻Δ33 DNA was used. All ten stable RNAs are deleted in this mutant. T4 [^{32}P]tRNA made *in vivo* served as a reference marker. Fig. 2 shows an autoradiogram of the gel separation.

The ten stable RNA species produced during T4 infection give rise to six bands in the gel separation. Bands *1* and *2*

TABLE 1. *Nearest-neighbor analysis of RNase T1 oligonucleotides from band E*

RNase T1 product	Sequence	Nearest neighbor predicted	Nearest neighbor found
1	G(A) G(D)	None	G
2	CG(G)	C,G	C,G
3	AG(T), AG(A)	A	A
4	UG(A) UG(A)	U	U
5	pG(C)	pGp	pGp
6	AUG(A) AUG(U)	U	U
7	TψCG(A)	C	C
8	AUAUCG(U)	C	C
9	UAUAAUG(G)	U,G	U,G
10	UAUAAUGmeG(D)	—	Not present
11	AUUCUCAUUAUCCG(C)	C	C
12	AUUUACCUCAG(A)	A	A*
13	ACUmCCAAψCUG(A)	U	U*
15	CUCCA$_{OH}$	None	Not present

The oligonucleotides were eluted from DEAE-paper and hydrolyzed by treatment with 0.2 N NaOH. The 3′ nucleotides were separated by electrophoresis at pH 3.5 on Whatman no. 52 paper.

* Oligonucleotides 12 and 13 were not resolved in Fig. 3*B*.

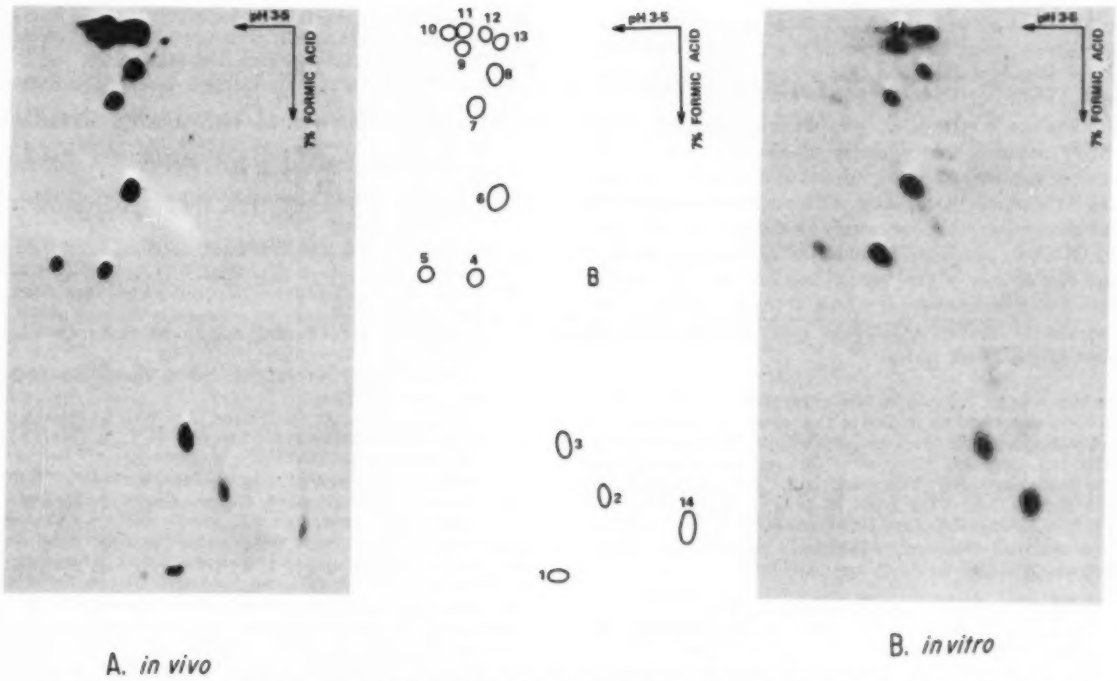

FIG. 3. Autoradiograms of fingerprints of $tRNA^{Gly}$ made *in vivo* (Band *6*, Fig. 1) and made *in vitro* (Band *E*, Fig. 1).

contain stable RNAs of unknown function. Band *1* RNA is 140 nucleotides long; it does not contain modified nucleosides, and its sequence is known (Paddock and Abelson, manuscript in preparation). Band *2* is about 100 nucleotides long. Band *3* is a $tRNA^{Ser}$ whose sequence has been determined by McClain and Barrell (personal communication). Band *4* contains a $tRNA^{Leu}$ whose sequence is known (22). Band *5* contains at least five tRNA species (23). Band *6* is a $tRNA^{Gly}$ whose sequence has been determined (Stahl, Paddock, and Abelson, manuscript in preparation). Studies of these T4 tRNAs by sequence analysis and by DNA–RNA hybridization indicate that all of them have distinctly different sequences from those of the host tRNAs (refs. 7, 9, 11, 22, 23, and unpublished results).

The electrophoretic gel pattern of stable T4 RNA made *in vitro* strongly resembles the RNA made *in vivo*, and is quite distinct from that produced when T4 $pSu_b^-\Delta 33$ DNA is used as a template. Fingerprint analysis of these RNAs by the methods of Sanger, Brownlee, and Barrell (21) confirm the identity of the *in vitro* and *in vivo* bands. By these criteria, band *A* is similar or identical to band *1*, band *C* to band *4*, and band *E* to band *6*. Band *D* is similar to band *5*, but may be contaminated by the material in band *β*. Apparently, neither band *3*, the $tRNA^{Ser}$, nor band *2* are made *in vitro*. (Band *B* does not have the same fingerprint as band *2*, and appears to correspond to band *α*.)

RNase T1 fingerprints of band *E* (*in vitro*) and band *6* (*in vivo*) are shown in Fig. 3. The *in vitro* labeling was performed with [α-^{32}P]GTP. Since RNase T1 cleaves adjacent to GMP residues, each fragment contains a labeled 3′-terminal GMP (except the 3′-terminal fragment of the molecule, which contains no GMP). Thus, differences in the fingerprint patterns will arise primarily from differences in sequences or from the presence of modified bases in the tRNA made *in vivo*, but possibly not formed *in vitro*. Table 1 lists the sequences of the *in vivo* RNase T1 fragments (Stahl, Paddock, and Abelson, in preparation). In the *in vivo* tRNA fingerprint there are two oligonucleotides (*9* and *10*) derived from the same original sequence. Fragment *9* is shorter than *10* by one residue, due to incomplete methylation *in vivo* (methylation forms the RNase T1-resistant sequence 2′-*O*-methylguanosyl GMP). Only the shorter fragment appears in the *in vitro* fingerprint, indicating the absence of this modification. The nucleotide representing the 5′-end of the tRNA molecule, pGp (guanosine 3; 5′-diphosphate), is found in the fingerprint of the *in vitro* product. In other experiments, we have synthesized T4 tRNA labeled with [α-^{32}P]CTP. RNase T1 fingerprints of band *E* from this preparation show a spot with a mobility identical to spot *14*, the 3′-terminal oligonucleotide. Thus, the cleavages at both ends of the molecule are identical to those occurring *in vivo*.

To further examine the fidelity of this transcriptional system, we have determined the nearest neighbor distribution of labeled GMP in the fragments isolated in the fingerprint shown in Fig. 2*B*. Alkaline hydrolysis of the RNase T1 fragments should lead to the transfer of ^{32}P to the nucleotide adjacent to the terminal G, while in a fragment where a terminal G is followed by another G in the tRNA sequence, the terminal G will also be labeled. Table 1 shows the results of this analysis. The distribution of ^{32}P in each fragment derived from the RNA made *in vitro* is as predicted by the sequence of $tRNA^{Gly}$. One exception is the presence of some free GMP in the analysis; this GMP probably arises from a slight contamination of the *in vitro* product.

These results allow and encourage further studies of tRNA transcription, processing, and modification. Since we suspect

that the tRNA genes are part of a large transcription unit, we are investigating the nature of the primary transcript. We have already determined that it is quite large (our unpublished results).

The absence in the *in vitro* product of bands *2* and *3* ($tRNA^{Ser}$) suggests that some factor, specified by the phage genome, is required for the synthesis or maturation of these RNAs. At least one bacteriophage T4 function, the product of the *mb* gene, appears to be necessary for the complete synthesis of T4 tRNA *in vivo*, since *mb* mutants fail to make bands *2*, *3*, and one or two of the band *5* species (20). In order to achieve a complete *in vitro* synthesis of the T4 tRNAs, it will presumably be necessary to supplement the system with the product of the T4 *mb* gene.

We thank Peter Johnson for the fingerprint analysis, Stephen Stahl and Gary Paddock for use of their data on the sequence of T4 $tRNA^{Gly}$, and M. Hayashi for a gift of RNA polymerase. D.P.N., H.L., and A.S. thank all of the members of the Abelson lab for their hospitality. This research was supported by Public Health Service Grants CA 10984 (to J.A.) and GM CA 15381 (to D.P.N.). H.L. thanks Dr. Harvey Itano for support. J. A. is a Faculty Research Associate of the American Cancer Society.

1. Altman, S. (1971) *Nature New Biol.* **229,** 19–21.
2. Altman, S. & Smith, J. D. (1971) *Nature New Biol.* **233,** 35–39.
3. Hall, R. H. (1971) *The Modified Nucleosides in Nucleic Acids* (Columbia University Press, New York).
4. Daniel, V., Sarid, S., Beckman, J. S. & Littauer, U. Z. (1970) *Proc. Nat. Acad. Sci. USA* **66,** 1260–1266.
5. Zubay, G., Cheong, L. & Gefter, M. (1971) *Proc. Nat. Acad. Sci. USA* **68,** 2195–2197.
6. Ikeda, H. (1971) *Nature New Biol.* **234,** 198–201.
7. Hsu, W. T., Foft, J. W. & Weiss, S. B. (1967) *Proc. Nat. Acad. Sci. USA* **58,** 2028–2035.
8. Daniel, V., Sarid, S. & Littauer, U. Z. (1970) *Science* **167,** 1682–1688.
9. Scherberg, N. & Weiss, S. B. (1970) *Proc. Nat. Acad. Sci. USA* **67,** 1164–1171.
10. Waters, L. C. & Novelli, G. D. (1969) *Proc. Nat. Acad. Sci. USA* **57,** 979–985.
11. Wilson, J., Kim, J. S. & Abelson, J. (1972) *J. Mol. Biol.*, in press.
12. Millet, R. L. & Trotter, C. D. (1970) *Proc. Nat. Acad. Sci. USA* **66,** 701–708.
13. Bremer, H. (1970) *Cold Spring Harbor Symp. Quant. Biol.* **35,** 109–119.
14. Richardson, J. P. (1970) *Cold Spring Harbor Symp. Quant. Biol.* **35,** 127–133.
15. Thomas, C. A., Jr. & Abelson, J. (1966) in *Procedures in Nucleic Acid Research*, eds. Cantoni, G. L., & Davies, D. R. (Academic Press, New York), pp. 553–561.
16. Reiner, A. M. (1969) *J. Bacteriol.* **97,** 1431–1436.
17. Berg, D., Barrett, K. & Chamberlin, M. (1971) *Methods Enzymol.* **21,** 506–519.
18. Burgess, R. R. (1969) *J. Biol Chem.* **244,** 6160–6167.
19. DeWachter, R. & Fiers, W. (1971) *Methods Enzymol.* **21,** 167–178.
20. Wilson, J. & Abelson, J. (1972) *J. Mol. Biol.* **69,** 57–73.
21. Sanger, F., Brownlee, G. & Barrell, B. (1965) *J. Mol. Biol.* **13,** 373–398.
22. Pinkerton, T. C., Paddock, G. & Abelson, J. (1972) *Nature New Biol.* **240,** 88.
23. McClain, W. H., Guthrie, C. & Barrell, B. G. (1972) *Proc. Nat. Acad. Sci. USA* **69,** 3703–3707.

Proc. Nat. Acad. Sci. USA
Vol. 70, No. 1, pp. 183–186, January 1973

Prevention of Simian Virus 40 Tumors by Hamster Fetal Tissue: Influence of Parity Status of Donor Females on Immunogenicity of Fetal Tissue and on Immune Cell Cytotoxicity

(primiparous and multiparous hamsters/lymph node cells/peritoneal exudate cells)

ANTHONY J. GIRARDI, PHYLLIS REPPUCCI, PEGGY DIERLAM, WILLIAM RUTALA, AND JOSEPH H. COGGIN, JR.

The Wistar Institute of Anatomy and Biology, Philadelphia, Pennsylvania 19104; the Molecular Anatomy (MAN) Program, Oak Ridge National Laboratory, Oak Ridge, Tennessee 37830; and the University of Tennessee, Knoxville, Tenn. 37916

Communicated by Alexander Hollaender, November 13, 1972

ABSTRACT **Fetal tissue from primiparous hamsters prevented simian virus 40 (SV40) tumorigenesis in male hamsters, whereas fetal tissue from multiparous hamsters did not. The parity status of normal (uninoculated) hamsters also influenced the cytotoxicity of their lymphoid cells against tumor cells. Lymph node cells from nonpregnant primiparous and multiparous animals were cytotoxic in microcytotoxicity tests against SV40, polyoma, and adenovirus 7 tumor cells, but were not active against control BHK cells. Lymph node cells from virgin female donors were inactive. Peritoneal exudate cells from these donors reacted in similar fashion against SV40 tumor cells *in vitro* and in adoptive transfer tests *in vivo*. However, the cytotoxicity of peritoneal exudate cells from multiparous hamsters was greatly reduced during pregnancy, a time when noncytotoxic humoral antibody reactive with surface antigen of SV40 tumor cells is present. This humoral antibody is not detected during first pregnancy, and peritoneal exudate cells obtained from pregnant primiparous hamsters demonstrated a high degree of cytotoxicity.**

Many reports have described antigens that are shared by normal fetal cells and tumor cells (reviewed in ref. 1), and some described protection against tumor formation in hosts inoculated with fetal tissues (2–9). In addition, normal pregnant multiparous hamsters develop antibody against surface antigens of simian virus 40 (SV40) hamster tumor cells (5, 8, 10), and serum obtained from guinea pigs immunized with unfertilized mouse eggs is cytotoxic for SV40-transformed mouse cells (11).

Inoculation of adult male hamsters with irradiated hamster, mouse, or human fetal tissue produces immunity to challenge by SV40 tumor cells and can induce cytostatic antibody formation (4–6, 8). Adenovirus 31 and SV40 tumorigenesis could be interrupted in males by inoculation of hamster fetal tissue administered to hamsters infected at birth before the appearance of tumors (5, 8). In addition, SV40 tumorigenesis could be interrupted in about 50% of hamsters by immunization with irradiated human embryo kidney (6).

Prehn (2) noted that prior immunization with fragments of isogeneic mouse embryos inhibited growth of syngeneic tumor transplants. Hanna *et al.* (7) reported that immunization with mouse fetal tissues suppressed growth of cells infected with Rauscher leukemia virus and plasma cell tumors. Brawn (12) reported that multiparous mice possessed cytotoxic lymph node cells that destroyed several methylcholanthrene tumors *in vitro* and that soluble fetal extracts desensitized cytotoxic effector cells.

In this report, we extend the initial observations (5) that hamster fetal tissue could delay the appearance of, and reduce the final incidence of, SV40-induced tumors. Further, we show the differential effect obtained with embryonic tissue derived from primiparous and multiparous females. Also, we studied cell-mediated immunity to SV40, adenovirus, and polyoma tumors, using lymphoid elements from normal multiparous and virgin female hamsters.

MATERIALS AND METHODS

Hamsters. LVG/LAK, Syrian golden hamsters, less than 24-hr old, were inoculated subcutaneously into the interscapular space with $10^{7.5}$ plaque-forming units of SV40, and at weaning were segregated by sex and randomized. Immunization was by intraperitoneal inoculation of test vaccines before the appearance of tumors. *Normal embryos* were harvested when 9–10 or 14 days of age. A finely minced preparation was made, washed with minimum essential medium (MEM), and finally aspirated through a 17-gauge needle. The final suspension was adjusted to contain 1 embryo equivalent per 1 or 2 ml, held in an ice bath, and irradiated in a cesium source at 5000 R delivered in 28 min. One embryo equivalent was inoculated per hamster at each of three weekly intervals beginning 5–6 weeks after administration of SV40 at birth.

Microcytotoxicity Procedure. The SV40 hamster tumor cell line, F5-1 (13), the adenovirus 7 tumor line, Pinckney (14), and the polyoma-transformed hamster line, TT109 (Flow Lab.), used as target cells were cultured in medium 199 containing 10% calf serum (heat inactivated). Microcytotoxicity tests were performed according to Brawn (12, 15), with several additional modifications (16). Target cells were grown overnight in suspension culture in Waymouth's medium (GIBCO) with 10% fetal-calf serum, enriched by addition of 1 ml of 100 mM sodium pyruvate (Microbiological Ass.), 1 ml of nonessential aminoacid solution, and 14.6 mg of L-glutamine per 100 ml of medium, and buffered to pH 7.2–7.4 with $NaHCO_3$. The target cells were washed twice before they were suspended in Waymouth's medium without serum for experiments with lymphoid cells.

Animals that served as effector cell donors were stimulated intraperitoneally with 1 ml of 1% oyster glycogen initially and again 24 hr later, 1 hr before harvesting. At harvest of

Abbreviation: SV40, simian virus 40.

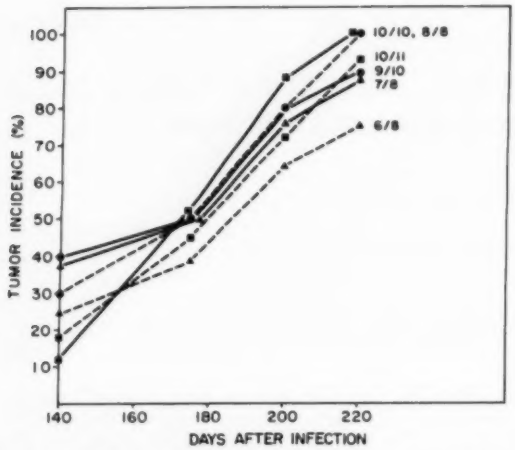

FIG. 1. The lack of immunization against SV40 tumorigenesis with hamster-fetal tissues derived from multiparous females. ●, controls; ■, 9-day fetus; ▲, 14-day fetus; – – –, male; ——, female.

peritoneal exudate cells, animals were injected with 15 ml of warm medium plus heparin (0.5 units/ml), and the fluid was aseptically collected by paracentesis with a 16-gauge needle. After the peritoneal exudate cells were washed twice with medium, they were incubated for 2–3 hr at 37° in a plastic petri plate for removal of adherent macrophages. The cells in the supernatant fluid were collected and suspended in serum-free medium to a concentration of 10^7 cells per ml.

For lymph node cell suspensions, cervical, inguinal, and mesenteric lymph nodes were removed aseptically and pressed gently through stainless steel wire mesh, washed three times with 10 ml of enriched Waymouth's medium, and suspended to a concentration of 10^7 cells per ml in serum-free medium.

Tumor cells in 0.5 ml of medium (3750 or 7500 cells; >95% viable by dye-exclusion test) were placed in a screw-cap plastic tube with 0.5 ml of peritoneal exudate or lymph node cells (5×10^6 cells), incubated for 4–5 hr in a 37° shaker-incubator, and suspended by repeated pipetting. 0.1 ml was placed in each of eight wells of a microtest tissue-culture plate (Falcon Plastics). Peritoneal exudate and lymph node cells were also "plated" in the absence of tumor cells. The plates were incubated for 2 hr, after which 1 ml of Waymouth's medium with 20% heat-inactivated fetal-calf serum was added to each well. The plates were then incubated for 2 days at 37°, fixed with methanol, stained with crystal violet, and washed. The number of attached cells was determined by visual count under 100× magnification.

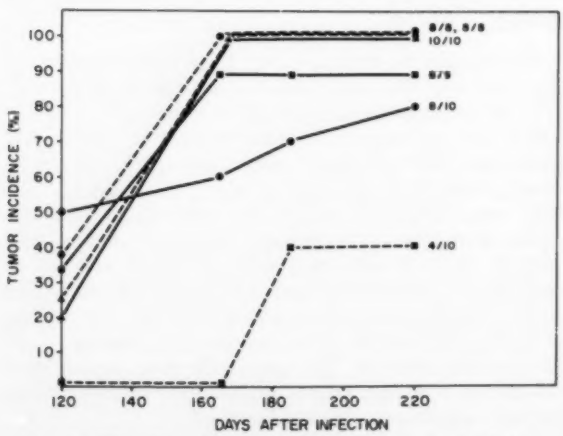

FIG. 2. The effect of immunization with hamster-fetal tissues derived from primiparous females on SV40 tumorigenesis. Symbols: same as in Fig. 1.

RESULTS

In Vivo Immunization Studies. Figs. 1 and 2 compare the results of two studies in which either multiparous or primiparous females were the source of fetal tissue. There was no significant delay (Fig. 1) in SV40 tumorigenesis in either male or female recipients of 9- or 14-day fetal tissue deriving from multiparous females, and the final tumor incidence was essentially unaffected. However, when primiparous females served as the source of fetal tissue (Fig. 2), males inoculated with 10-day fetal tissue responded with both a delay in the appearance of the first tumor and a significantly reduced incidence of tumors; females showed no such response. The differences noted were reproducible.

In both studies, normal hamsters subcutaneously inoculated with fetal tissues did not develop embryomas, indicating that adequate irradiation procedures for the fetal vaccines were used.

In Vitro Cytotoxicity Tests. Brawn (12, 15) reported that multiparous mice possessed cytotoxic lymph node cells that destroyed several methylcholanthrene tumors *in vitro*. Soluble components from fetal-mouse tissues in midgestation desensitized *specifically* immune lymph node cells, preventing cytotoxicity against tumor cells.

In our studies, normal multiparous (4 times pregnant) hamsters and age-matched virgin females were examined for cytotoxic cells. The results (Table 1) indicate reproducible and significant cytotoxicity against SV40 hamster tumor target

TABLE 1. *Cytotoxicity of peritoneal exudate cells from multiparous and age-matched virgin hamsters against SV40 hamster tumor target cells*

Target cells	Parity state	No. cells per well ± *SE**	% Cytotoxicity	*P*
SV40 tumor cells	Virgin	26 ± 3.6	—	—
	Multiparous	10 ± 2.2	62	<0.01
	Virgin	18 ± 1.8	—	—
	Multiparous	7 ± 1.8	62	<0.001
	Virgin	190 ± 24.3	—	—
	Multiparous	106 ± 16.8	44	<0.02
	Virgin	209 ± 20.0	—	—
	Multiparous	101 ± 14.2	52	<0.001
	SV40 Immune	104 ± 26.4	50	<0.01
	SV40 Immune	123 ± 25.6	41	<0.050
BHK-21 cells "normal cells"	Virgin	86 ± 7.6	—	—
	Multiparous	113 ± 6.9	0	

—, Control value.

* Standard error: results are average counts of 20 wells.

cells but not against "normal" cells with peritoneal exudate cells from normal primiparous or multiparous females. Peritoneal exudate cells from virgin female hamsters were active only after immunization with SV40 on three weekly occasions as adults. Peritoneal exudate cells from normal virgin females were not cytotoxic; the results of cell counts with them served as the 100% viability control for all the calculations.

The results shown in Table 2 with lymph node cells from primiparous and multiparous hamsters compare favorably with those with peritoneal exudate cells. The activity was directed against SV40, adenovirus 7, and polyoma tumor cells. Lymph node cells from normal virgin females were not cytotoxic. It has been noted that lymph node cells were sometimes less reactive than peritoneal exudate cells. Lymph node cells from virgin females immunized with SV40 were specifically cytotoxic (37–50%) against SV40 tumor cells, but were inactive against polyoma tumor cells.

In Vivo Cytotoxicity (Adoptive Transfer) Tests. Peritoneal exudate cells were collected from several female donors in different states of parity, washed without removal of adherent macrophages, standardized, mixed with SV40 tumor cells, and incubated in Waymouth's medium for 30 min at 37°. The cells were gently resuspended; a sample was counted and injected subcutaneously in the subscapular space of 4- to 6-week-old normal male hamsters. Each hamster received a mixture of 10^4 target tumor cells and 10^6 peritoneal exudate cells. Animals were palpated weekly for tumors. The results (Fig. 3) indicate that 10-day *pregnant* primiparous as well as nonpregnant multiparous donors possessed peritoneal exudate cells cytotoxic for SV40 tumor cells, whereas virgin donors did not. However, the cytotoxicity of peritoneal exudate cells of the multiparous females was absent during pregnancy. One is reminded that multiparous hamsters, *while pregnant*, develop cell-surface antibody (5, 8, 10), and this antibody might be responsible for the observed blocking of the cytotoxicity of peritoneal exudate cells. *Primiparous*, 10-day pregnant hamsters do *not* have detectable titers of this antibody, and, as noted in Fig. 3, their peritoneal exudate cells were as cytotoxic as those obtained from animals immune to SV40 tumors.

TABLE 2. *Cytotoxicity of lymph node cells from primiparous, multiparous, and virgin hamsters against SV40, polyoma, and adenovirus hamster tumor cells*

Target cells	Parity state	No. cells per well ± *SE**	% Cytotoxicity	*P*†
	Primiparous lymph node cells			
SV40	Virgin	166 ± 10.4	—	—
	Primiparous	108 ± 11.4	35	<0.001
Adenovirus 7	Virgin	24.4 ± 2.6	—	—
	Primiparous	10.0 ± 1.9	58	<0.001
Polyoma	Virgin	47 ± 3.2	—	—
	Primiparous	20 ± 2.8	42	<0.001
BHK-21	Virgin	204 ± 19.9	—	—
	Primiparous	251 ± 21.9	0	
	Multiparous lymph node cells‡			
SV40	Virgin	160 ± 12.0	—	—
	Multiparous	87 ± 6.3	45	<0.001
Adenovirus 7	Virgin	24.5 ± 3.7	—	—
	Multiparous	9.6 ± 1.7	61	<0.01
Polyoma	Virgin	38 ± 8.0	—	—
	Multiparous	14 ± 2.7	63	<0.02
BHK-21	Virgin	140 ± 27.0	—	—
	Multiparous	161 ± 7.0	0	

—, Control value.
* Standard error: 20 wells counted and averaged per value.
† Probability determined by Student's *t*-test.
‡ 3–4 times pregnant.

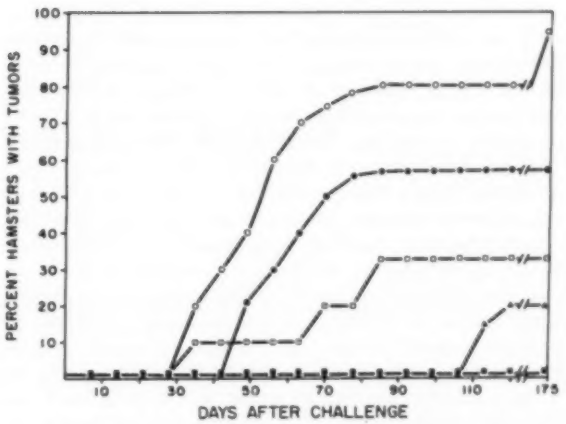

FIG. 3. SV40 tumor development in male hamsters challenged subcutaneously with 10^4 SV40 tumor cells mixed with 10^6 peritoneal exudate cells from hamsters in various states of parity. ○, Virgins; ●, 10-day pregnant multiparous; □, nonpregnant multiparous; ▲, 10-day pregnant primiparous; ■, SV40.

DISCUSSION

Our results on the prevention of SV40 tumorigenesis extend previous studies establishing that males are more responsive than females to inoculation with irradiated 9- to 10-day fetal tissue and that irradiated 14-day fetal tissue is ineffective in both sexes. Furthermore, they indicate the advantage of embryonic cells from primiparous females.

Multiparous animals possessed lymph node and peritoneal exudate cells cytotoxic for hamster tumor cells *in vitro*, while virgin animals did not. This finding confirms the principle of autosensitization during pregnancy reported by Brawn (12, 15), extending it to three tumors transformed by oncogenic DNA viruses. Also, primiparous as well as multiparous hamsters possessed cytotoxic peritoneal exudate cells capable of protecting normal male hamsters against SV40 tumor cell challenge in adoptive transfer tests, supporting *in vitro* results. Direct challenge of the *donors* of peritoneal exudate cells resulted, however, in equivalent tumor development in all donors, and one might postulate that blocking factors are present coordinately with cytotoxic cells, impairing the toxicity of sensitized cells in the donors. The data in Fig. 3 would support such a hypothesis, since the cytotoxic peritoneal exudate cells from multiparous hamsters had greatly reduced activity *during* pregnancy when it is known that noncytotoxic antibody, reactive with the cell surface of SV40 tumors, is present (5, 8, 10). Enhancement of SV40 tumor takes coordinate with increased numbers of pregnancies has been noted recently in other experiments.

In addition, normal females sensitized to fetal tissue developed such cytostatic antibody (as did males), but showed no capacity to reject tumors, either autochthonous or transplanted (5, 8). These immunologic findings possibly have evolutionary significance in females, representing a two-way protective mechanism in the maternal–fetal relationship. The cytostatic antibody developed normally during pregnancy may have a dual function: (*a*) to protect the fetus from cell-mediated rejection, and (*b*) to prevent "metastases" at ectopic sites from accidentally released fetal cells. Perhaps females have evolved this humoral mechanism more efficiently in order to suppress its ability to respond *functionally* with cellular immunity to fetal homograft, even though active peritoneal exudate and lymph node cells can be demonstrated to be present normally (Table 2 and Fig. 3). Thus, males but not females would be free to respond protectively when inoculated with appropriate fetal tissue.

Why then do females respond to inoculation of irradiated SV40 tumor cells with tumor resistance if the protective (surface) tumor transplantation antigen of SV40 tumor cells is the same antigen present in 10-day fetal tissue? Perhaps the embryonic cells contain many antigenic sites involved in stimulating the humoral antibody response, which blocks cell-mediated immunity, while the tumor cells may contain masked or fewer of these sites and stimulate the cell-mediated response more selectively. Also, fetal cells may respond to hormonal stimuli in adult female tissue and undergo membrane maturation and masking of the antigen inducing tumor resistance. In recent studies we have demonstrated that females develop weaker transplantation resistance than males when immunized with SV40 tumor cells (9).

The humoral response of the *donor* female may play an important role in determining whether the tissue of her fetus can effectively immunize recipient hamsters. During early embryogenesis in *primiparous* females, the autosensitive antibody response may be quite low, presumably due to inexperience of the females with the antigen; thus, 10-day fetal tissue would be immunogenic. During late term, the 14-day fetal tissue would be ineffective if the primary antibody response resulted in blocking. Although the antibody has not been detected *in circulation* in 14-day *primiparous* females, a sufficient amount might be absorbed on fetal tissue *in utero*. In *multiparous* females where humoral antibody is detected, an anamnestic response could ensure production of sufficient antibody to cover embryonic sites even at day 9, thereby explaining the lack of protective immunization with such tissue. Some support for this concept was obtained in preliminary experiments. Females splenectomized to reduce the humoral response react protectively to fetal vaccine (9). In addition, quantitative cytofluorograph measurements of the amount of antibody on fetal cells indicate a 4-fold increase in antibody on fetal cells in multiple pregnancy as compared to that on primiparous fetuses (9).

Alternatively, the important immunizing antigen might not be expressed during late embryogenesis, or if expressed, could be masked by other than immunologic means. Mild trypsinization of ineffective fetal tissue may remove either cellular components or antigen–antibody complexes that block the sites important for development of cell-mediated immunity. Then even females might be expected to react with tumor resistance after inoculation of fetal tissue. This seems to be the case in our initial study previously reported (17).

The observed phenomenon of specific resistance stimulated by tumors and the broad, crossreacting response of active fetal tissues may have an explanation in that different repressed genetic sites may become activated by different oncogenic agents. This could result in tumors that vary from each other in antigenic reexpression, but that crossreact with fetal tissue since, in the latter, the various sites would be expressed normally, Neither the data reported here nor in previous publications contest the idea that oncogenic stimuli may, in themselves, induce new antigens of a "nonfetal" type (18), but they do stress that antigenic sites important for tumor (and fetus?) survival or rejection are expressed during normal embryogenesis and during tumorigenesis.

This study was conducted at the Wistar Institute under Contract nos. 43-62-157 and 71-2092, and at ORNL and The University of Tennessee under Contract No. FS-7, within the Special Virus Cancer Program of the National Cancer Institute, NIH, PHS. A.J.G. is a Leukemia Scholar of the Leukemia Society of America. MAN program is Supported by the National Cancer Institute, The National Institutes of General Medical Sciences, The National Institute of Allergy and Infectious Diseases, and the U.S. Atomic Energy Commission, and in part by U.S.A.E.C. Contract AT(40-1) 3646. Oak Ridge National Laboratory is Operated for the U.S.A.E.C. by Union Carbide Corp. Nuclear Division.

1. *Embryonic and Fetal Antigens in Cancer*, eds. Anderson, N. G. & Coggin, J. H., Jr. (U.S. Department of Commerce, Springfield, Va. 1971), Vol. I, pp. 7–37.
2. Prehn, R. T. (1967) in *Cross Reacting Antigens and Neoantigens*, ed. Trentin, J. T. (Williams and Wilkins, Baltimore), pp. 105–117.
3. Pearson, G. & Freeman, G. (1968) *Cancer Res.* **28,** 1665–1673.
4. Coggin, J. H., Jr., Ambrose, K. R. & Anderson, N. G. (1970) *J. Immunol.* **105,** 524–526.
5. Coggin, J. H., Jr., Ambrose, K. R., Bellomy, B. B. & Anderson, N. G. (1971) *J. Immunol.* **107,** 526–533.
6. Ambrose, K. R., Anderson, N. G. & Coggin, J. H., Jr. (1971) *Nature* **233,** 194–195.
7. Hanna, M. G., Jr., Tennant, R. W. & Coggin, J. H., Jr. (1971) *Proc. Nat. Acad. Sci. USA* **68,** 1748–1752.
8. Coggin, J. H., Jr., Ambrose, K. R. & Anderson, N. G. (1971) in *Embryonic and Fetal Antigens in Cancer*, eds. Anderson, N. G. & Coggin, J. H., Jr. (U.S. Department of Commerce, Springfield, Va.), Vol. I, pp. 185–198.
9. Coggin, J. H., Jr. & Anderson, N. G. (1972) in *Embryonic and Fetal Antigens in Cancer*, eds. Anderson, N. G. & Coggin, J. H., Jr. (U.S. Department of Commerce, Springfield, Va.), Vol. II, in press.
10. Duff, R. J. & Rapp. F. (1970) *J. Immunol.* **105,** 521–523.
11. Baranska, W., Koldovský, P. & Koprowski, H. (1970) *Proc. Nat. Acad. Sci. USA* **67,** 193–199.
12. Brawn, R. J. (1971) In *Embryonic and Fetal Antigens in Cancer*, eds. Anderson, N. G. & Coggin, J. H., Jr. (U.S. Department of Commerce, Springfield, Va.), Vol. I, pp. 143–149.
13. Girardi, A. J., Sweet, B. H. & Hilleman, M. R. (1963) *Proc. Soc. Exp. Biol. Med.* **112,** 662–667.
14. Girardi, A. J., Hilleman, M. R. & Zwickey, R. E. (1964) *Proc. Soc. Exp. Biol. Med.* **115,** 1141–1150.
15. Brawn, R. J. (1970) *Int. J. Cancer* **7,** 245–249.
16. Dierlam, P., Anderson, N. G. & Coggin, J. H., Jr. (1971) in *Embryonic and Fetal Antigens in Cancer*, eds. Anderson, N. G. & Coggin, J. H., Jr. (U.S. Department of Commerce, Springfield, Va.), Vol. I, pp. 203–214.
17. Girardi, A. J. & Reppucci, P. (1972) in *Embryonic and Fetal Antigens in Cancer*, eds. Anderson, N. G. & Coggin, J. H., Jr. (U.S. Department of Commerce, Springfield, Va.), Vol. II, in press.
18. Ting, C. C., Lavrin, D. H., Shiu, G. & Herberman, R. B. (1972) *Proc. Nat. Acad. Sci. USA* **69,** 1664–1668.

Proc. Nat. Acad. Sci. USA
Vol. 70, No. 1, pp. 187–189, January 1973

A Frequency-Dependent Natural Selection Model for the Evolution of Social Cooperation Networks

(altruism/threshold effect/cooperative carnivore hunting behavior)

SCOTT A. BOORMAN* AND PAUL R. LEVITT†,‡

* Society of Fellows and Department of Sociology, Harvard University, Cambridge, Massachusetts 02138; † Department of Sociology, Harvard University and Courant Institute of Mathematical Sciences, New York University, New York, N.Y. 10012

Communicated by E. O. Wilson, November 14, 1972

ABSTRACT **A model is presented for the evolution of several aspects of sociality based on reciprocal ties of social cooperation, modeling especially cooperative hunting behavior in carnivores. This model captures the possibility of a critical threshold in gene frequency, which, if reached, will lead to an explosion toward fixation of the "social" trait. This threshold phenomenon might be restated as follows: the precondition for evolution favorable to the specific form of social behavior considered is hard to satisfy, but—once this condition is satisfied—the tendency toward sociality is effectively irreversible. The simple model proposed appears to be highly robust, with most realistic changes additionally favoring the social gene.**

There is growing evidence (surveyed in ref. 1) that formation of stable pair bonds between unrelated individuals other than mated pairs may be a behavioral basis for many vertebrate social adaptations, especially cooperative hunting behavior in carnivores (2) and the social structure of certain nonhuman primates (3). Looked at from the standpoint of its possible evolutionary origins, any predisposition for cooperative behavior cannot benefit a species member unless this individual happens to encounter and enter into a cooperative relation with another individual similarly adapted. The present note explores the problem of generating a critical mass of individuals with cooperative potential of this kind, assuming that such potential is genetically controlled. The process is developed from the standpoint of frequency-dependent selection in mathematical population genetics, and it is shown, as a consequence of this frequency-dependent structure (4, 5), that selection of social cooperation may have some interesting structural properties; more extensive mathematical developments will be published elsewhere. The concrete model proposed appears particularly suitable for study of the initial evolution of carnivore social behavior, though the applicability may extend quite generally throughout species where nonsexual pairbonding is identifiable and important. Moreover, insofar as the basic human adaptation may be more carnivore than primate (2), the model may be of interest for early human evolution.

The essence of our results is the prediction of a very fast increase in the frequency of an "altruist" allele once a certain critical threshold is exceeded. Specifically, consider a simple Mendelian dominant–recessive pair (B,b) with the following postulated selection mechanism. Interpret the bb recessives as having the capability for entering into a relation of cooperation with other bb individuals; a special case is what has been called (1) reciprocal altruism. Assume a population of highly mobile individuals that is randomly mixing within a generation (as is consistent with the predation behavior of many animal species), and suppose that each homozygous recessive individual in each generation makes $N \geq 1$ random contacts with other individuals of the species (for simplicity we assume N fixed and generations nonoverlapping); these contacts define a random graph or network in each generation. Certain of these contacts will, in general, be with individuals of the dominant (uncooperative or solitary) phenotype; if the frequency of the b allele is low and if N is small relative to the total population, then most or all of the contacts will be with dominants. Now, in the simplest model, assume that the bb phenotype is lethal if an individual of that phenotype fails to encounter (in the course of his random contacts with other species members) another individual who is also recessive; but assume that the bb phenotype has superior fitness should linkup occur (the phenomenology being that the contact with another recessive individual allows a cooperative relationship to develop that raises the fitness of both species members in question).

Running the process out in time, the following phenomenon occurs. There exists a critical density of the cooperative allele, β_{crit}, such that, if the starting frequency of the allele exceeds this value, then the frequency of the cooperative phenotype will explode, and the cooperative trait will eventually fixate in the population. If the starting frequency falls below β_{crit}, then the frequency of b will die away relatively slowly, and asymptotically the decay is algebraically slow like $1/n$, where n is the number of generations (this slow decay occurs for the standard reason that most of the remaining recessive alleles stay hidden in the heterozygotes: see ref. 6). This asymmetry of the rates of genetic change above and below β_{crit} is a very important conclusion that may be drawn from the present model. Crudely stated in qualitative terms, what this asymmetry entails is that, for β even slightly exceeding β_{crit}, the social trait will move on a turnpike to fixation that minor environmental fluctuations are unlikely to reverse; whereas if a population, for whatever reason, achieves a significant frequency $\beta = \beta_0 < \beta_{\text{crit}}$, a significant frequency of the cooperative trait will persist for a very long time, and any of a wide variety of random environmental fluctuations (7) could act on this frequency to push the process over the critical threshold.

Fig. 1 gives a diagrammatic illustration of the general

‡ Order of authorship is alphabetical.

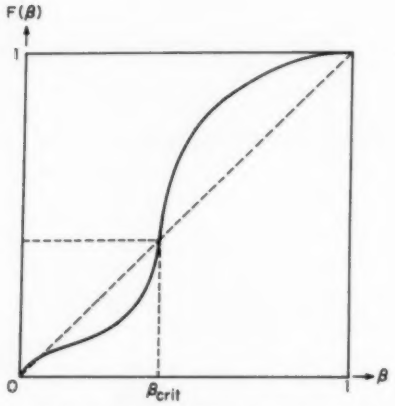

FIG. 1. Graph of intergenerational frequency change $\beta \rightarrow F(\beta)$. β_{crit} is the unique value of β between 0 and 1 that is a fixpoint of $F(\beta)$, i.e., for which $\beta_{crit} = F(\beta_{crit})$.

qualitative behavior of $F(\beta)$, defined to be the frequency of the recessive in the second generation given that this frequency is β in the first. One can give a particularly simple analytic form to $F(\beta)$ by making the following assumptions:

(1) The population is large and is in Hardy–Weinberg equilibrium with B having frequency $\alpha = 1 - \beta$ and b having frequency β.

(2) N is constant, uniform over individuals, and is small relative to the population size.

(3) The fitness of a recessive who links up with another recessive is 1; the fitness of all dominants is a constant σ, with $0 < \sigma < 1$, which may be interpreted as a survival probability per individual per generation; the fitness of a recessive that fails to link up is 0 (i.e., in this case the recessive phenotype is lethal).

(4) The contact network in each generation is random (random mixing).

(5) Mating is random, and is uncorrelated with the contact network.

Under these baseline assumptions, the probability that a given recessive will link up with some other recessive can be well approximated in the interesting β ranges (not too near 0 or 1) by the expression

$$f(\beta,N) = 1 - (1 - \beta^2)^N, \qquad [1]$$

which ignores sampling without replacement considerations and certain other statistical subtleties.

Then it can be shown that

$$F(\beta) = \left[\beta\left(\alpha + \beta\frac{f(\beta,N)}{\sigma}\right)\right] \Big/ \left[\alpha + \beta\left(\alpha + \beta\frac{f(\beta,N)}{\sigma}\right)\right] \qquad [2]$$

and the qualitative behavior of $F(\beta)$ in Fig. 1 may be deduced. The value β_{crit} is given by the unique internal fixed point of the mapping $\beta \rightarrow F(\beta)$; above β_{crit} the growth is essentially exponential, while for $\beta < \beta_{crit}$ the decay is asymptotically algebraic and $F(\beta)$ is tangent to the 45° line at the origin, so that at very low β values decay is very slow indeed.

In this simplest model, the effects of social cooperation networks have been developed as a special case of frequency-dependent invididual (Mendelian) selection, which as a pure concept is quite old, going back to studies by Wright (surveyed in ref. 8). As Levins (7) has pointed out, however, frequency-dependent selection as a concept has in general lacked motivation, and the main contribution of the present model from this standpoint lies in its use of network connectivity considerations in generating a concrete frequency-dependent *mechanism*. Moreover, most existing work on possible frequency-dependent selection effects stresses circumstances in which such effects lead to *stable* polymorphism, which is most relevant to a set of problems quite different from those involved in modeling social evolution (though see ref. 9). The utility of the present model lies in the fact that it is able to relate a threshold effect based on frequency-dependence to the possible evolution of a very specific and important form of sociality, namely, pairwise ties of social cooperation, i.e., to a primitive form of social networks.

It can be shown that the basic qualitative form of $F(\beta)$ displayed in Fig. 1 remains invariant for much more general $f(\beta,N)$ than that given by Eq. [1]. Specifically, the behavior shown in Fig. 1 is present if $f = f(\beta;\mathbf{p})$ where $f'(\beta) > 0$ (f is strictly monotone increasing) and $f(0) < \sigma < f(1)$, $\mathbf{p}$ being any fixed vector of parameters. In consequence, the basic mathematical behavior of the model is extremely robust, and the evolution of a wide variety of more complicated social network and group structures could be modeled along similar lines.

Moreover, it is important to stress that many perturbations of the null assumptions 1–5 actually help the recessive, essentially by pulling down the effective β_{crit}. Thus, in particular, if one considers nonrandom contacts owing to population viscosity, preferential mating (assortative between phenotypes), or positive correlation between the mating structure and the pattern of contacts between species members in a given generation—all of these assumptions being highly realistic—the result is a decreased value of β_{crit} and a general increase in the relative advantage of the recessives. In particular, in an island-like system consisting of a large number of small and weakly coupled populations that are internally panmictic (10, 11), if the *bb*s manage to take over even one local population, then eventual conquest of the whole metapopulation by diffusion outward from this secure base is essentially assured for appropriate migration rates, even though such conquest may take a long time. Further analysis of these qualitative statements involves interaction between sampling-with-replacement considerations necessary in the analysis of small local populations, stepping-stone models, drift effects, and comparison of relative time scales.

The present model has some resemblance to the models of Scudo and Karlin (12) dealing with the superior fertility of homogamous matings, which also may lead to thresholds of allele frequency, but has the crucial difference that these last models reduce or, in the limit, eliminate fertile interphenotype pairings, whereas the present model does not. One specific consequence of this asymmetry is that, in the Scudo–Karlin model, the dominant phenotype is in a symmetric position with the recessive one as far as the death of its alleles in cross-phenotype matings is concerned, and is, in this sense, likewise disadvantaged. The present model, by contrast, stresses the asymmetries between a solitary dominant and a social recessive.

At the same time that it is reasonable for social carnivores and certain other social vertebrates, it should be stressed that the whole thrust of the present network mechanism goes

strongly against much known data for social insects where pair bonding based on individual recognition plays a much smaller role (13, 14). As far as applications of the model are concerned, the main unsolved problem is differentiating the effects of a pairwise cooperation mechanism of the kind we have delineated from kin selection effects that are certainly present in most carnivore packs and social vertebrate groups in general (15). This differentiation remains largely an unsolved problem. It should be stressed, however, that the present model is like kin selection in that it postulates no group selection mechanism involving competition between intrinsically higher-order units such as colonies or populations (11, 16, 17). If higher-order units are involved in the present considerations, they should be thought of as networks, which are based on kin ties in kin selection and ties of cooperation in models along the lines of the present paper.

We are indebted for the comments of R. H. MacArthur, N. Howell, E. O. Wilson, T. W. Schoener, H. C. White, R. M. Solow, and S. Wright. Support for research on which the present work is based was obtained from NSF Grants GS-2689 (Principal Investigator: Harrison C. White) and GB-7734 (Principal Investigator: Edward O. Wilson).

1. Trivers, R. L. (1971) *Quart. Rev. Biol.* **46,** 35–57.
2. Schaller, G. B. & Lowther, G. R. (1969) *Southwest. J. Anthropol.* **25,** 307–341.
3. Struhsaker, T. T. (1969) *Folia Primat.* **11,** 80–118.
4. Wright, S. (1964) in *Evolution and the Genetics of Populations* (University of Chicago Press, Chicago), Vol. 2, p. 120.
5. Dobzhansky, Th. (1970) *Genetics of the Evolutionary Process* (Columbia Univ. Press, New York).
6. Crow, J. F. & Kimura, M. (1970) *An Introduction to Population Genetics Theory* (Harper and Row, New York).
7. Levins, R. (1968) *Evolution in Changing Environments* (Princeton Univ. Press, Princeton, N.J.)
8. Wright, S. (1955) *Cold Spring Harbor Symp. Quant. Biol.* **20,** 16–24.
9. Wright, S. (1949) in *Genetics, Paleontology, and Evolution,* eds. Jepson, G. L., Simpson, G. G. & Mayr, E. (Princeton Univ. Press, Princeton, N.J.), p. 377.
10. Wright, S. (1945) *Ecology* **26,** 415–419.
11. Levins, R. (1970) in *Some Mathematical Questions in Biology* (Lectures on Mathematics in the Life Sciences, American Mathematical Society, Providence, R.I.), Vol. 2, 75–108.
12. Scudo, F. M. & Karlin, S. (1969) *Genetics* **63,** 479–498.
13. Wilson, E. O. (1971) *The Insect Societies* (Harvard University Press, Cambridge, Mass.).
14. Grassé, P. P. (1959) *Insectes Soc.* **6,** 41–83.
15. Hamilton, W. D. (1964) *J. Theor. Biol.* **7,** 1–52.
16. Boorman, S. A. & Levitt, P. R. (1973) *Theor. Pop. Biol.,* in press; (1972) *Proc. Nat. Acad. Sci. USA* **69,** 2711–2713.
17. Wynne-Edwards, V. C. (1962) *Animal Dispersion in Relation to Social Behavior* (Hafner, New York).

Proc. Nat. Acad. Sci. USA
Vol. 70, No. 1, pp. 190–194, January 1973

Release of Infectious Epstein–Barr Virus by Transformed Marmoset Leukocytes

(human leukocytes/extracellular virus)

GEORGE MILLER*† AND MURIEL LIPMAN†

Departments of * Pediatrics, and † Epidemiology and Public Health, Yale University School of Medicine, New Haven, Connecticut 06510

Communicated by John F. Enders, November 2, 1972

ABSTRACT **Marmoset blood leukocytes transformed *in vitro* by Epstein–Barr virus regularly release extracellular infectious Epstein–Barr virus with high titers of transforming activity. By comparison, human umbilical cord leukocytes and adult human leukocytes transformed by Epstein–Barr virus release either no extracellular infectious virus or small amounts, irregularly.**

Human lymphoblastoid cells that contain Epstein–Barr virus (EBV) restrict replication of the virus. In some human lymphoblastoid lines no viral nucleocapsids are found, yet the viral genome is detectable by nucleic acid hybridization (1, 2). In other lines nucleocapsids or viral antigens detected by immunofluorescence (immunofluorescence antigens) are produced in only a few cells, although cloning experiments demonstrate that all cells contain the viral genome (3–5). Furthermore, not all lines in which nucleocapsids or immunofluorescence antigens are found give rise to biologically active virus detectable by transformation or superinfection assays (6, 7). The mechanisms of restriction of EBV by the host cell are unknown and present important practical and theoretical problems. The lack of a cell type that yields large amounts of virus has hindered study of the virus. The means of restriction of virus by the cell deserves study as an important example of the control of gene expression.

We recently reported that leukocytes from two species of new-world primates transform into continuous cell lines after exposure to EBV (8). Certain features of these cells suggested that simian leukocytes might produce more EB virions than transformed human leukocytes. A higher fraction of monkey cells than human cells demonstrated intracellular immunofluorescence antigen. In simian cell lines syncitia evolved that were the site of accumulation of immunofluorescence antigen, and the multinucleate giant cells contained intranuclear inclusions. Accordingly, supernatant fluids of EBV-converted monkey cells were tested for the presence of cell-free virus, which was readily demonstrated. This report is concerned with identification of the extracellular virus as EBV, a description of the virus' morphology and growth characteristics, and evidence that production of extracellular EBV is due to factors inherent in the transformed cell type rather than to a permanent change in the virus resulting from passage through simian cells.

METHODS

Virus. Two EBV strains were derived from patients with infectious mononucleosis: one (Hawley) from peripheral blood leukocytes, the other (Lederer) from a throat washing. The Hawley strain was maintained as a line of the patient's blood leukocytes (883L) or as a line of marmoset blood leukocytes (B95-8), which was established after exposure to an extract of line 883L. A virus stock from the B95-8 line consisted of culture fluids that had been centrifuged (400 × *g*); the supernatant had been frozen and thawed and passed through a 0.8-μm filter and stored at −70°. Virus of the Lederer strain was obtained by having the patient gargle 100 ml of medium RPMI 1640. Fetal bovine serum (final concentration 2%) was added to gargle fluids, which were frozen and thawed three times, then centrifuged at 400 × *g* for 10 min; the supernatant was filtered and stored at −70°. Transforming activity in extracts of lines 883L and B95-8, and in the Lederer throat washing, was neutralized by human sera with EBV antibody and unaffected by human sera free of EBV antibody (refs. 7, 8, and Miller, G. & Niederman, J. C., *N. Engl. J. Med.* in press).

Infectivity Assay. Transformation of umbilical cord leukocytes was the measure of EBV infectivity. Transformation was recognized by clumping, acid production, increase in cell numbers, and acquisition by the culture of the ability to be repeatedly subdivided. The terminal dilution method was used, four cultures per dilution, and titers were calculated by the Reed Muench formula. Cord leukocytes were used at 10^6/ml, and one cord yielded from 50–150 cultures. As far as possible a single umbilical cord served as the source of assay cells in comparable titrations; the infectivity titers presented in Tables 1 and 3 and Fig. 2 were obtained with one cord each. Included in each experiment were cultures consisting of leukocytes not exposed to EBV; no transformation occurred in these controls.

EBV Antigens and Neutralization Tests. Four reference human sera, two antibody-positive from mononucleosis patients and two antibody-free sera from healthy adults, were used to identify EBV antigens. EBV antigens detectable by complement-fixation were measured in cell extracts prepared from 5×10^7 cells per ml, and also in frozen and thawed supernatant fluids (8). The indirect method of Henle and Henle was used to enumerate the proportion of cells with EBV immunofluorescence antigen (9).

Infectious transforming virus released from marmoset cell cultures was identified through neutralization tests with the same two antibody-positive and two antibody-negative reference human sera. About 30 infectious units were mixed with 2-fold dilutions of serum, beginning at 1:2, and incubated for

Abbreviation: EBV, Epstein–Barr virus.

1 hr in a 37° water bath. The mixture was assayed for infectivity on umbilical cord leukocytes.

Ether and Chloroform Sensitivity of EBV. The effect of lipid solvents on the transforming capacity of virus released from marmoset cells was determined as follows: 2 ml of B95-8 virus stock was mixed with 1 ml of anhydrous ethyl ether and placed at 4° for 4 hr. For chloroform treatment, 2.7 ml of B95-8 virus stock was mixed with 0.3 ml of chloroform and placed at 4° for 1 hr. The organic layers were discarded, and air was bubbled through both mixtures for 2 min. Titrations of infectivity were done on untreated B95-8 stock virus and on the aqueous phase of chloroform-treated and ether-treated virus.

Examination of EBV Particles by Electronmicroscopy. Cells were sedimented from 200 ml of culture fluid at 400 × *g* for 20 min. The supernatant was centrifuged at 20,000 rpm in an SW25.2 rotor at 5°, and the resulting pellets were suspended in about 1/30 volume of Tris·HCl-buffered saline plus 1% bovine-serum albumin. This material was placed on top of a discontinuous gradient of 10 and 50% potassium tartrate in buffer (pH 7.4) composed of 1 M NaCl–0.1 M Tris·HCl–10 mM EDTA. An interphase with an opalescent band, which appeared after centrifugation at 25,000 rpm in an SW41 rotor at 5° for 2 hr, was collected. This interphase was then centrifuged in a linear 20–30% potassium tartrate gradient for 17 hr at 25,000 rpm in an SW41 rotor. An opalescent band in the bottom one-third of the tube was collected for electronmicroscopic examination and for density determination by weighing. Aliquots from the cell culture fluids after initial clarification, from the pellet after the first high-speed centrifugation, and from the interphase after centrifugation in the discontinuous gradient were also examined by electronmicroscopy. Samples were placed on Formvar carbon-coated grids, stained with 2% phosphotungstic acid (pH 6.0), and examined in a Phillips EM-200.

RESULTS

Transforming activity of extracellular virus from line B95-8 (marmoset cells) was neutralized by two human EBV-positive reference sera, and was unaffected by two EBV-negative human sera. Titrations of the antibody-positive sera demonstrate neutralizing activity at a 1:128 dilution or greater. When about 30,000 transforming units of extracellular virus from line B95-8 were mixed with ether or chloroform, all transforming activity was abolished.

Herpes virus nucleocapsids were seen in clarified supernatant fluid obtained 6 days after subculture of B95-8 cells. When the fluid was centrifuged at 48,000 × *g*, virions were found in the pellet. Similar viral particles were seen in the band between 10 and 50% potassium tartrate and in the band collected after overnight centrifugation. Debris was still present in the preparation after this step. The virions seen (Fig. 1) consisted of enveloped particles as well as naked nucleocapsids. The nucleocapsids were hexagonal and of uniform size (about 100 nm). A core could be seen in many of the particles. The density of the virus-containing band after centrifugation in the 20–30% potassium tartrate linear gradient was 1.186 g/ml. When line 883L was treated in an identical manner, only a rare naked nucleocapsid was identified in the banded material.

Time course of production of extracellular EBV

Extracellular virus increased in parallel with the exponential phase of cell growth (Fig. 2). The amount of infectious EBV

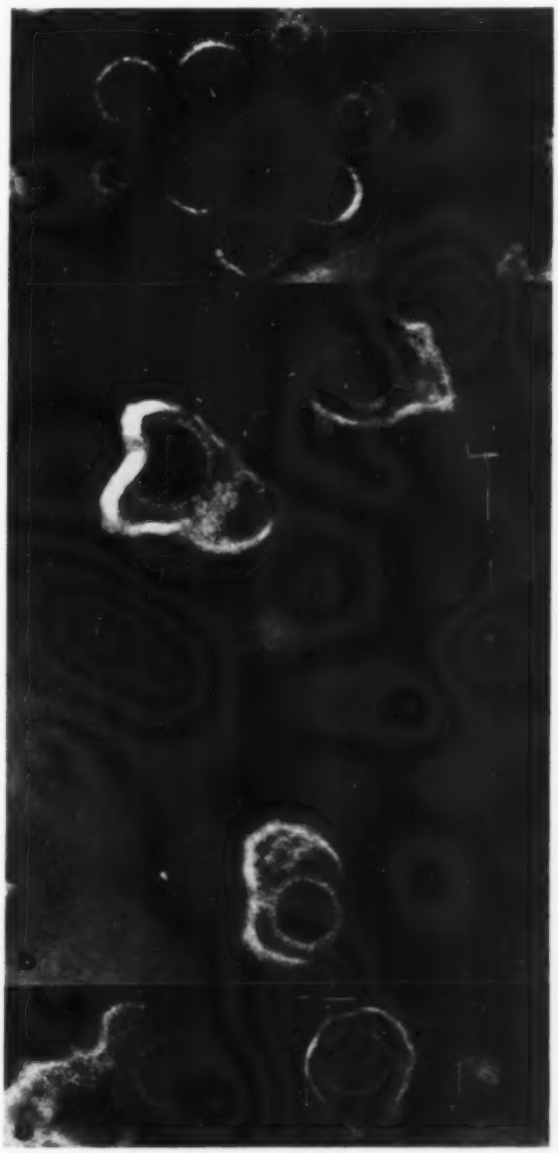

FIG. 1. Epstein–Barr virus (EBV) from infected marmoset leukocyte cell line B95-8. Tissue culture fluid was pelleted, resuspended in Tris·HCl-buffered saline, and centrifuged on a 10 and 50% potassium tartrate, noncontinuous gradient for 2 hr at 25,000 rpm. The band between the layers was collected, stained with 2% phosphotungstic acid, and examined by electron-microscopy (*a*). Group of nucleocapsids, three of which contain cores. Capsomeres are arranged in an orderly fashion and suggest the 5:3:2 axial symmetry of the herpes group of viruses. (*b*) Three enveloped particles were found in one field. Two have disrupted envelopes and the third a disintegrating nucleocapsid. (*c*) An intact enveloped EBV, which also contains a core, is accompanied by a nucleocapsid without an envelope. All micrographs were taken at the same magnification. *Bar* represents 100 nm.

TABLE 1. *Expression of EBV in a human and in two simian lines and in human cord cells transformed by virus derived from them*

Designation	Species	Method of transformation	Expression of EBV: CF antigen*	Expression of EBV: IF antigen†	Expression of EBV: Infectivity‡	Calc. yield§ of infectious EBV per 10^5 IF-positive cells
883L	Human (adult)	Spontaneous	4	2.8	0.3	36
B95-8	Marmoset	883L virus	16	12.5	3.8	25,000
B84-15	Squirrel monkey	883L virus	8	8.8	2.6	2,300
E46	Human (newborn)	883L virus	8	0	nil	0
E49-32	Human (newborn)	B95-8 virus	16	0	nil	0
E14	Human (newborn)	B84-15 virus	8	0	nil	0

Lines of transformed squirrel monkey and marmoset leukocytes were derived by exposure to EBV from line 883L (Hawley strain). EBV obtained from cell-free supernatant fluids of these three lines was used to transform cells from three umbilical cords. All six lines were carried in parallel for several months by subdividing 2:1 every 5–7 days. Cells and fluids were harvested for determination of antigen content and infectivity 1 week after last subdivision. At the time of harvest there were 10^6 viable cells per ml of each line.

* CF antigen, no. of complement fixing units per 25 μl of antigen prepared from an extract of 5×10^7 cells per ml.

† IF antigen, % cells demonstrating immunofluorescence in the indirect test, based on counts of 1000 cells.

‡ Infectivity, $\log_{10}$ 50% transforming units per 0.2 ml of supernatant fluid.

§ Yield of extracellular EBV = (no. of infectious units per ml/10^6 cells per ml × % IF-positive cells) × 10^5.

released exceeded the increase in cell numbers; the cell population increased 6-fold (from $10^{5.5}$/ml to $10^{6.3}$/ml), and the content of infectious EBV increased more than 300-fold (from $10^{3.2}$/ml to $10^{5.7}$/ml). A maximum yield of about 0.3 infectious units per cell was obtained 8 days after subculture. A rise in complement-fixing antigen present in culture supernatant fluids occurred in parallel with the rise in cell number and infectious virus. Complement-fixing activity was removed from supernatant fluids and recovered in the pellet when fluids from day 5 were centrifuged at 88,000 × *g* for 1 hr.

Comparison of expression of EBV in transformed human and monkey cells

A series of experiments were undertaken to determine whether the release of extracellular EBV by marmoset cells was due to a permanent change in the virus resulting from passage in marmoset cells ("adaptation") or to differences in the capacity of leukocytes from different sources to permit expression of infectivity of EBV.

First, a comparison was made of the content of EBV-specific antigens and of extracellular infectious virus in simian lines from two species and in the human line (883L) that was the original source of EBV used to transform the monkey cells (top half of Table 1). Simian lines contained higher titers of complement fixation antigen (2- to 4-fold) and immunofluorescence antigen (2- to 4-fold), and they released considerably more infectious virus (200- to 3000-fold) than the human line. A calculation related the yield of infectious virus

TABLE 2. *Expression of EBV in marmoset and human cells transformed by one stock of EBV derived from marmoset cells*

Species and designation	Expression of EBV*: CF antigen	IF antigen	Infectivity
Marmoset			
D39-32	16	5.7	3.7
D39-44	16	4.5	4.5
D39-14	16	12.5	4.5
D39-16	32	6.0	4.5
Human (newborn)			
E74	4	0	nil
E82	4	0	nil
E94	8	0.1	nil
E81	4	0	nil
Human (adult)			
F22-1	8	0.1	nil
F22-13	8	1.5	0.2
F22-25	16	1.2	nil
F22-37	8	0	nil

All cell lines were derived after exposure to about $10^{3.5}$ transforming doses of virus from line B95-8. Transformed cells were subdivided 2:1 every 5–7 days before assay for EBV antigens and infectivity.

* See footnotes for Table 1.

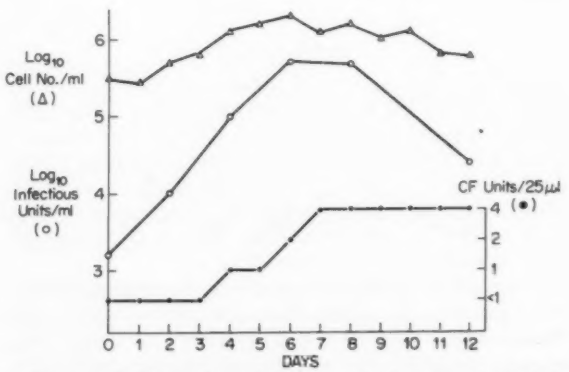

FIG. 2. EBV-transformed marmoset leukocytes (line B95-8) were diluted 1:4 in 50 ml of fresh medium to a concentration of 3×10^5 viable (trypan-blue excluding) cells per ml. An aliquot of 2 ml was removed daily. Daily cell counts were performed (Δ). Cells were sedimented by centrifugation (400 × *g* for 10 min); the supernatant fluids were frozen and thawed three times. Aliquots of supernatant fluids were assayed for infectivity by the capacity to transform human umbilical cord leukocytes into continuous cell lines (O). All the infectivity assays were performed in leukocytes from a single cord. The titer of complement-fixing (CF) antigen in the supernatant fluid was determined in a microtiter assay (●).

to the number of cells producing immunofluorescence antigen, on the assumption that the cells producing immunofluorescence antigens were the cells ultimately responsible for production of infectious virus. The results suggested that the greater amounts of infectious virus released by the monkey cells was due to an increased yield of infectious virus per virogenic cell. EBV from each of the three lines was used to transform leukocytes from three different human umbilical cord bloods. The transformed cord leukocytes were tested for expression of EBV antigens and infectious virus in parallel with the parent lines. The results (bottom half of Table 1) showed that cord cells transformed by the Hawley strain from three different cell types expressed only EBV complement fixation antigens and not immunofluorescence antigens. No transforming virus was detected in the supernatant fluids from the transformed human cord cells.

To verify that the phenomenon represented a general difference between transformed marmoset and human cells, we used a single stock prepared from extracellular EBV from line B95-8 to transform leukocytes from four marmosets, four additional human umbilical cords, and four EBV antibody-free adult humans. The transformants were studied for their content of EBV antigens and infectious EBV (Table 2). All lines of transformed marmoset cells contained both EBV antigens and also released infectious virus. By contrast, only one of four lines derived from human cells of newborns demonstrated a very low titer of immunofluorescence antigen, and none of the newborn lines released detectable infectious EBV. In adult human cells transformed by the same virus stock, complement fixation antigen was detected in all lines, low titers of immunofluorescence antigens were found in three of four lines, and extremely low titers of transforming activity were detected in culture fluids from one of four lines.

To establish whether these differences were peculiar to the Hawley strain of virus, which had undergone many passages in transformed human and marmoset cells, we performed further transformation studies with the Lederer strain, which was stored as a throat gargle from a patient (Table 3). Marmoset leukocytes transformed by the Lederer strain contained more than $10^{3.5}$ transforming units per 0.2 ml of both cell-associated and extracellular infectious EBV; human cord leukocytes transformed by the same strain demonstrated comparable titers of complement fixation antigen, but barely detectable levels of immunofluorescence antigen and infectious EBV.

TABLE 3. *Expression of EBV in human cord and marmoset cells transformed by a strain of EBV obtained from a throat washing from a patient with infectious mononucleosis*

Designation	Species	Expression of EBV*			
		CF antigen	IF antigen	Infectivity	
				Cells	Fluids
E49-3	Human (newborn)	4	<0.1	nil	<0.0
F26-11	Marmoset	4	3.6	3.5	4.3

Lines of human umbilical cord leukocytes and marmoset leukocytes were obtained after exposure to a throat washing. The transforming capacity of the throat washing was neutralized by EBV antibody and unaffected by EBV-free human sera. The cell lines were subdivided 2:1 every 3–5 days and tested for antigens and infectious EBV in supernatant fluids and extracts of 10^7 cells/ml.

* See footnotes of Table 1.

DISCUSSION

These experimental results indicate notable differences in the expression of EBV in transformants derived from different sources. Marmoset leukocytes yield considerable quantities of biologically active virus, adult human leukocytes yield minute quantities of virus, and human cord leukocytes rarely release biologically active EBV detectable by the transformation assay. At least two distinct processes are responsible for the increased yield of extracellular EBV by marmoset cells. First, a higher proportion of marmoset cells than human cells produce immunofluorescence antigens, i.e., a greater proportion of cells are activated to produce nucleocapsids. Second, on the basis of calculations made in Table 1 and similar calculations (not shown) for the data in Tables 2 and 3, those transformed marmoset cells that have been activated to produce immunofluorescence antigen yield much more infectious virus than comparable adult human cells. The yield is from 0.25–2.6 infectious units per marmoset cell with immunofluorescence antigen, while for those transformed adult human cells that yield infectious EBV one infectious unit is released per 200–3000 cells with immunofluorescence antigen.

The factors responsible for the higher yields of transforming virus per activated marmoset cell deserve further study. The most likely explanation is that envelopment of the virus proceeds more efficiently in marmoset cells. In keeping with this hypothesis, infectivity of virus from the B95-8 line was destroyed by ether and chloroform, and enveloped particles were seen by electronmicroscopy. By contrast, only a rare nucleocapsid, and no enveloped particles, were found in fluids of line 883L, which has a low titer of extracellular EBV. It is conceivable, therefore, that EB viral release from cells, in the absence of cellular degeneration, is facilitated by envelopment.

Activation of the viral genome of the transformed marmoset cells leading to release of infectious virus apparently occurs during the exponential phase of cell growth (Fig. 2), for there was no increase in infectious virus production once the cells reached stationary phase. The availability of a line that releases biologically active virus should permit close analysis of the events in the cell cycle in which viral activation proceeds. However, it is apparent that exponential cell growth *per se* is insufficient to activate the genome, for biologically active virus is not released at all by transformed cord cells. Some of the transformed cord cells have been tested for cell-associated virus; barely detectable transforming activity was found in an extract of one cord cell line and none in several others.

Finally, several biochemical, biophysical, and immunological experiments should be facilitated by the availability of a system that produces reasonably large quantities of cell-free virus that can be partially purified. One objective, now approachable, is to determine whether EBV associated with Burkitt lymphoma, nasopharyngeal carcinoma, and infectious mononucleosis is the same agent.

We are grateful for cheerful and excellent assistance from L. Andrews, M. Garrison, L. Heston, C. Shepard, D. Stitt, V. Thompson, and P. Utiger. Dr. J. F. Enders was a source of encouragement and advice. G. M. is an Investigator of the Howard Hughes Medical Institute. Supported by grants from the Jane

Coffin Childs Memorial Fund for Medical Research (JCC-257); the U.S. Public Health Service (AI-05577, CA12-05501A1); the American Cancer Society (VC-107); the Damon Runyon Memorial Fund (DRG-1147).

1. ZurHausen, H., Diehl, V., Wolf, H., Schulte-Holthausen, H. & Schneider, U. (1972) *Nature New Biol.* **237,** 189–190.
2. Nonoyama, M. & Pagano, J. (1971) *Nature* **233,** 103–106.
3. Miller, M. H., Stitt, D. & Miller, G. (1970) *J. Virol.* **6,** 699–701.
4. Maurer, B. A., Imamura, T. & Wilbert, S. M. (1970) *Cancer Res.* **30,** 2870–2875.
5. Zajac, B. A. & Kohn, G. (1970) *J. Nat. Cancer Inst.* **45,** 399–406.
6. Diehl, V., Henle, G., Henle, W. & Kohn, G. (1969) *In Vitro* **4,** 92–99.
7. Miller, G., Lisco, H., Kohn, H. L. & Stitt, D. (1971) *Proc. Soc. Exp. Biol. Med.* **137,** 1459–1465.
8. Miller, G., Shope, T., Lisco, H., Stitt, D. & Lipman, M. (1972) *Proc. Nat. Acad. Sci. USA* **69,** 383–387.
9. Henle, G. & Henle, W. (1966) *J. Bacteriol.* **91,** 1248–1256.

Proc. Nat. Acad. Sci. USA
Vol. 70, No. 1, pp. 195–199, January 1973

Inactivation System of the Mammalian X Chromosome

(Lyon hypothesis/heterochromatin/genetic regulation/sex chromatin)

SPENCER W. BROWN AND H. SHARAT CHANDRA

Department of Genetics, University of California, Berkeley, Calif. 94720; and Institute for Genetic Studies, Bangalore 27, India

Communicated by Curt Stern, November 13, 1972

ABSTRACT **In female mammals, one of the two X chromosomes present is inactivated during early development. In marsupials, the paternal X is inactivated; in eutherians, one of the two X chromosomes is inactivated at random. A mechanism is proposed to explain the cytogenetic data on inactivation and the derivation of the eutherian system from the marsupial system. In the marsupial system, a site on the X chromosome is sensitive to paternal origin: when the X chromosome is of maternal origin, this sensitive site is responsible for influencing an adjacent site, the receptor, to maintain the X in an active state; the paternal X becomes inactive. Transposition of the sensitive site to an autosome in eutherians would have two consequences. Since the receptor site of the X chromosome is no longer adjacent, the autosomal sensitive site of maternal origin would activate an X at random. The number of active X chromosomes would conform to the number of maternal sensitive sites and thus, generally, to the number of maternal sets of autosomes. The response of the sensitive site to its passage through the male may be designated as imprinting, a term used by Crouse to indicate that the behavior of *Sciara* chromosomes is determined by parental origin.**

The essential premise of the Lyon hypothesis (1), that in somatic cells of mammalian females one of the two X chromosomes normally present is genetically inactive, has been amply verified by a large body of biochemical, genetic, and cytological evidence (2). The focus of attention has, therefore, now shifted to the mechanism responsible for this remarkable situation in which an entire chromosome appears to be inactive and its homologue active or potentially active.

In cells of female eutherian mammals the inactive X can be either paternal or maternal in origin; the determination occurs independently in the several cells of the young embryo and, once made, is adhered to in all descendants of each cell. On the other hand, it has recently been found that among certain marsupial mammals, the kangaroos, it is always the paternal X that is inactive (3, 4). This somewhat unexpected finding, which may be a general characteristic of marsupials, has led Cooper (5) to propose that the random X inactivation of eutherian mammals has evolved from an ancestral condition still retained among the marsupials. He has further suggested that inactivation is brought about by the following mechanism: (*a*) among male marsupials, during meiosis or earlier, a controlling element is introduced into the X, probably by the Y, making the paternal X inactive in the next generation; (*b*) in eutherian mammals, the element is excised during early development and reinserted at random into one of the two X chromosomes, resulting in random inactivation. Cooper realized that, without further assumptions, his hypothesis could not account for several well-known facts of X chromosome behavior in man, mouse, and other mammals. Lyon (2, 6) has critically examined Cooper's model and those of others, and has pointed out (6) that it is advisable to start with the fewest assumptions and to develop a model that is both testable and consistent with currently available data. It may be added that the proposed mechanism for eutherian mammals should be capable of easy derivation from that of the marsupials, in which it is the paternal X that is always inactivated. A model satisfying these criteria is described here.

Abbreviations: Superscripts *m* and *p* indicate maternal and paternal origin, respectively; e.g., A^m is a set of autosomes derived from the mother; X^p, an X chromosome from the father.

PROPOSED CONTROL SYSTEM

On the basis of evidence to be discussed below, it is suggested that: (*a*) a locus (sensitive site) responsive to parental origin is located on an autosome in eutherians; (*b*) the paternal autosomal locus is presumed to be affected or influenced in a manner similar to that known for marsupials (3, 4), *Sciara* (7), and the coccids (8), while the maternal autosomal locus remains unaffected; the influence the paternal autosome undergoes during its passage through the male parent (see below, *Some General Considerations*) will be referred to as imprinting (9); (*c*) during early embryogeny, the unaffected sensitive site of the maternal autosome produces a single informational entity that attaches to a receptor site (10, 11) of one of the X chromosomes encountered at random; this X chromosome remains or becomes active; (*d*) at some later stage in development all other X chromosomes become inactive nonspecifically; that is, no special controlling elements are necessary to bring about the inactivation.

The control system is equally applicable to males. In normal XY and Klinefelter XXY males the presence of one maternal sensitive site would lead to one active X in each and one inactive X in Klinefelter males.

The eutherian system is presumed to have originated from the marsupial in an exceedingly simple fashion (Fig. 1). The marsupial X is sensitized by passage through the male parent, and becomes inactive during early female embryogenesis. All that is considered necessary is the transposition of the sensitive site, alone, to an autosome. The receptor site that controls activation versus inactivation remains on the X chromosome. The sensitive site in its new location on the maternal autosome is active and, since it is no longer coupled directly with an X chromosome, activates at random one of

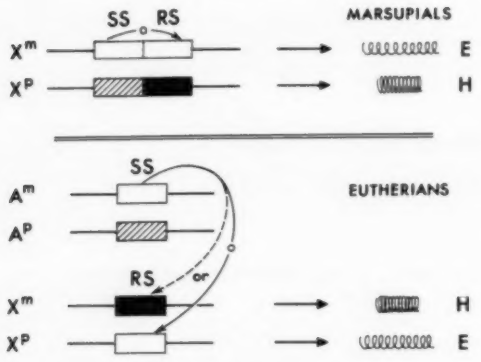

FIG. 1. *The marsupial system (above).* The sensitive site (*SS*) of the maternal X (X^m) produces an informational entity (*small circle*) that is transferred to the adjacent receptor site (*RS*). As a result, the maternal X remains euchromatic (*E*). The sensitive site of the paternal X (X^p) has been altered by its prior passage through the male phase of the life cycle: no informational entity is transferred to the adjacent receptor site. The paternal X becomes heterochromatic (*H*). (The paternal *RS* and *SS* regions have been marked for comparison with the eutherian system.) *The eutherian system (below).* Essentially the same as the marsupial system, except that the *SS* region has been inserted in an autosome. The *SS* of the paternally derived autosome (A^p) has been altered by prior passage through the male phase of the life cycle. The unaltered *SS* region of the maternal autosome (A^m) produces an informational entity that may attach to either X chromosome at random in each of the cells of the early embryo. The X chromosome receiving the entity remains euchromatic; the other becomes heterochromatic.

the X chromosomes present in the same nucleus. The sensitive site on the paternal autosome has been inactivated by its passage through the male and is, therefore, not capable of activating an X. This evolutionary step would be analogous to certain changes observed by McClintock (12) in gene-control systems in maize. In the Suppressor-mutator and Activator systems, one of the two essential components was not readily detected when both were close to the gene locus under control. A transposition of one component, the operator element, to a new location permitted identification of both it and the regulator element that had remained adjacent to the gene locus. Of special interest in the present context is McClintock's remark about one such case in which "A typical two-element system of control of gene action had evolved from an apparently one-element system."

The proposed evolutionary step would have the selective advantage of conferring on eutherian females a "mosaic heterozygosity" for the X, in contrast to the equivalent of a hemizygous X in marsupial females. For example, if the marsupial system were present in man, color blindness would be as common in females as in males; both would show the defect on receiving the mutant factor from the mother.

THE CYTOGENETIC EVIDENCE

Diploids

The expectation from the above scheme would be a strict concordance between the number of sets of maternal autosomes and the number of active X chromosomes. The parental origin of the X chromosomes themselves should have no bearing on their subsequent behavior. This is indeed what is observed (Table 1). In man, anomalous 46, X^mX^m males (13), who probably originate from XXY zygotes, show one sex chromatin body per diploid cell, and are in this respect indistinguishable from typical, diploid females (46, X^mX^p). Even in 49, XXXXY individuals, in whom all four X chromosomes were maternal in origin, all but one X appeared to be inactive (14, 15). It should be obvious that Cooper's hypothesis, as he himself was aware, cannot account for any of the observations cited in Table 1.

Although evidence from diploids effectively rules out the Cooper hypothesis, all examples have only one active X and can, therefore, be explained by the hypothesis of Grumbach, Morishima, and Taylor (10) that a single episome-like factor activates a single X.

Triploids

The concordance between the number of maternal sets of autosomes and the number of active X chromosomes is clearly better looked for in polyploid embryos, but the techniques that permit rapid identification of the chromosome sets in such embryos have only recently become available. However, even among those cases where the origin of the extra set is not known, a definite pattern emerges that is consistent with the scheme proposed here. Thus, in human 69,XXY triploids, one would expect two classes from the following gametic combinations: 2X2A ♀ + YA ♂ and XA ♀ + XY2A ♂, where each A denotes an autosomal set. On the basis of the control mechanism suggested here, the former class should be sex-chromatin negative and the latter class sex-chromatin positive, with a maximum of one sex-chromatin body per nucleus; XXY triploids of both classes have been observed (16, 17). Similarly, among 69,XXX triploids, two classes would be expected: some with only one sex chromatin body and others with a maximum of two bodies per cell; again both classes have been observed (16, 17). A minority of

TABLE 1. *Expected number of inactive X chromosomes (in parentheses), and, therefore, maximum number of sex chromatin bodies on a diploid autosomal background. All examples are human subjects reported in the literature**

Sex chromosome constitution (m = maternal, p = paternal)	Cooper model (5) No. of inactive X chromosomes = No. of paternal X chromosomes	Proposed model No. of inactive X chromosomes = No. of X chromosomes less No. of maternal sets of autosomes—here, one
X^mX^m (12, 36)	XX	X(X)
X^pO (33)	(X)O	XO
X^mX^mY (35)	XXY	X(X)Y
$X^mX^mX^p$ (36)†	XX(X)	X(XX)
$X^mX^mX^mY$ (36)	XXXY	X(XX)Y
$X^mX^mX^mX^m$ (34, 35)	XXXX	X(XXX)
$X^mX^mX^mX^mY$ (13, 14)	XXXXY	X(XXX)Y

* Only some of those genotypes that help differentiate between the two models and that are known to occur are listed here. See text for cases of typical diploidy and polyploidy.

† It is very likely that both $X^mX^mX^p$ and $X^mX^pX^p$ types occur, but it has not been possible to distinguish between them.

human XXX triploids have a maximum of two sex chromatin bodies per cell, whereas the majority have only one. According to the present interpretation, digyny would thus be the dominant mechanism in the origin of human triploidy. Edwards *et al.*, (17) have arrived at the same conclusion on the basis of other evidence.

Data on both the sex-chromatin status and parental origin of the extra set are available from one 69,XXY infant (17): his blood group data were more consistent with digyny than with diandry and the infant was sex-chromatin negative, as would be expected on the basis of the present hypothesis.

The most cogent evidence in favor of the hypothesis comes from the recent work of Bomsel–Helmreich (18), who induced triploidy in rabbit embryos by suppression of the second polar body. Triploidy was, therefore, always the result of digyny. XXX triploids had, like XX diploids, only one sex chromatin body, whereas XXY triploids were uniformly sex-chromatin negative. Assays of glucose-6-phosphate dehydrogenase, an enzyme believed to be X-linked in the rabbit (19), showed that enzymatic activity was consistently higher in triploid embryos as compared with diploid controls, indicating that more than one glucose-6-phosphate dehydrogenase locus was probably active among the triploid cells.

Although the triploid data do not permit a distinction to be made between the Cooper model and the one proposed here, they do rule out a single episome-like factor as an explanation of the number of active X chromosomes (10). An episome-like factor of extrachrómosomal origin would remain a possible explanation only if the further assumption is made that the number of such factors somehow conformed to the number of sets of maternal autosomes. However, this added assumption is unattractive, if only because it would be difficult to picture the derivation of such an extrachromosomal mechanism from the marsupial system of paternal X inactivation.

Tetraploids

Only two types of tetraploids are known, XXXX and XXYY. It seems very likely that these were derived from XX and XY zygotes in which early failure of cytokinesis led to a doubling of the chromosome complement (16). Two sex chromatin bodies have been observed in the XXXX tetraploids and none in the XXYY. These observations are comparable with those from tetraploid and higher endopolyploid cells occurring in normal XX and XY individuals (20) and offer no additional evidence bearing on our argument.

X-autosome translocations in mice

The mechanism responsible for inactivation of the X chromosome of mice has received much attention during the last decade. In all but one of the X-autosome translocations of mice, a "position-effect" type of variegation is induced for at least some of the genes of the autosome involved (2, 11, 21). The exceptional case is that of the Searle translocation (22); none of the genes on this autosome has been identified.

Considerable attention has been paid to the possibility that variegation patterns that have been observed may be the result of selection against cells in which inactivation has led to either (*a*) a modification of dosage, thus upsetting the normal dosage-compensation relationship, or (*b*) the equivalent of a homozygous deficiency. Inferences concerning the type of inactivation made from the observed variegation patterns thus become quite complex.

Nonetheless, there seems to be agreement among most mouse cytogeneticists that there is one major site on the X chromosome that is responsible for its inactivation (11, 21, 23). According to Russell and Montgomery (21), there is a single inactivation center on the X. Although Eicher (11) outlined a complex scheme that included two or more centers of inactivation, she believed that all were under the control of a single "empty" or unactivated receptor site on the X. The conclusions from analyses of inactivation in X-autosome translocations of mice are thus consistent with the main point made here, that there is a single, major controlling site on the X chromosome, regardless of secondary centers of inactivation.

Genetic and cytological evidence indicates that there are probably at least two inactivation centers on X chromosomes of mice, a primary center closely associated with the receptor site, and a secondary center elsewhere on the chromosome. The probability that the secondary center will induce inactivation is considerably lessened by complete physical separation from the primary center in typical, reciprocal translocations, and it may well be less effective in inducing inactivation in adjacent autosomal material. This concept reconciles some of the differences between the ideas of Russell (21) and those of Eicher (11); it is most like that of Eicher's defective memory system, even though objections may be raised in regard to the "memory" aspect of her system (2).

The Searle translocation is of special interest because the normal X is inactive in a large majority of cells and the translocation is correspondingly active. These data can be interpreted in several ways, including the obvious one of cell selection, but Lyon (2) has recognized that the autosome here may carry an activating center. In addition, it should be pointed out that the autosomal component of the Searle translocation is always of *maternal* origin, a requirement for activation in the system proposed here. Except for the Cattanach translocation, all other X-autosome translocations in mice induce male sterility; the chromosomes involved can be transmitted only by females. The autosome involved in the Searle translocation has recently been identified cytologically (24), and recognition of genetic markers on this chromosome would be of great value.

Deficient X chromosomes in man

Three different types of deficient X chromosome have been observed. The long arm may be missing (Xq-), and the short arm present singly or duplicated in an isochromosome (Xpi). Likewise, simple deficiencies of the short arm (Xp-) and isochromosomes of the long arm (Xqi) are also known. These two types are invariably inactive (25, 26). Because an inactivation of the normal chromosome would be equivalent to a gross homozygous deficiency in these cases, cell lineages of this sort would not be expected to survive. In the third type, that of the ring X, the positions of the breaks determine the size of the deficiency; the closer both breaks are to the ends of the chromosome, the smaller the deficiency. It is not surprising, therefore, that nearly all ring-X chromosomes are invariably inactive (25).

Since Xq-, Xpi, Xp-, and Xqi all become inactive (25, 26), it is obvious that there cannot be, as in mice, a single center of inactivation in human X chromosomes. The simplest

scheme, and one in agreement with that suggested for mice, is that there is a primary inactivation site—coupled with or acting as the receptor site—on one arm, and a secondary site on the other.

SOME GENERAL CONSIDERATIONS

If the proposed mechanism is basically valid, then the choice of which X becomes activated has to be made by a single entity in an embryonic diploid cell and, thus, it would appear that only one site on the chosen X can be "hit" to begin with; a subsequent, pervasive effect is therefore also necessary to involve the whole chromosome. The mechanism by which such a pervasive effect is obtained is much less clear in any of its aspects than the choice of the X to be activated. The overall problem of mammalian X chromosome inactivation can thus be approached at two separate levels: (*a*) the basic facultative determination of which X chromosome or chromosomes are to remain active, and (*b*) the mechanism by which the pervasive effect is achieved. We are concerned here primarily with the basic determination; more insight into the mechanism would increase our understanding of the translocation data.

Imprinting

Crouse (9) introduced the term imprinting to indicate a change of state of a chromosome that allowed it to be "recognized" as different from its homologue. In *Sciara*, the imprinting is believed to occur in maternal and paternal germ lines before fertilization, and to determine the later behavior of the X chromosomes and the autosomes. Once imprinted, the future behavior of the chromosome is apparently irrevocably determined. The heterochromatic L chromosomes, limited to the germ line, are not subject to imprinting (27). According to the scheme outlined here for mammals, the fate of the paternal X chromosome in marsupials would be irrevocably determined by an imprinting of the sensitive site in the male parent. In eutherian mammals, imprinting of the sensitive site of the paternal autosome would occur before the completion of fertilization. The same site on the maternal autosome, not so imprinted, would remain active and lead to a random determination of which X chromosome is to remain active; at this time the fates of the X chromosomes are irrevocably determined. Analysis of variegated phenotypes in adult eutherians would indicate the time in development when the fates of the X chromosomes are determined, not when inactivation occurs. Inactivation would be a realization of the prior determination and could occur either simultaneously or at a later stage of embryogenesis. A combined analysis of variegation in the adult and of heterochromatization and the action of specific genes during early development should eventually establish the correct chronology.

It should also be noted that the differentiation between maternal and paternal origin does not imply that the alteration that leads to subsequent differential behavior of homologues necessarily occurred in the body of the male parent. In a parthenogenetic scale insect, Nur (28) found that diploidy was restored by fusion of the first two cleavage nuclei; however, in some instances the chromosomes derived from one of these nuclei later became heterochromatic, and indistinguishable in this regard from the heterochromatization of the paternal chromosome set in early embryogeny of the males of related bisexual species. The observed differential behavior of the paternal X chromosome in marsupials and the proposed imprinting in an eutherian autosome could be the result of influences present after sperm emission, but before nuclear fusion completed fertilization. The term "male phase" may, therefore, be suggested as a comprehensive term to include, in addition to events occurring in the body of the male, the period between emission and completion of fertilization.

Activating entity

There is no information concerning the nature of the agent acting on the sensitive site, or that transfers information from there to the receptor site. The sensitive site might perhaps be sensitized to respond to minor influences in the male phase; there is no reason either to presume or to rule out specific informational macromolecules. On the other hand, the fact that only a single X-chromosome site is normally activated in a diploid indicates that a single specific macromolecule may well be involved in the transfer of information from the sensitive to the receptor site. It has been suggested that such specific macromolecules are episomes or episome-like entities (29, 30). In view of recent critical review of the use of the term episome (31), it seems best to use a noncommittal term such as informational entity to designate the agent responsible for the transfer of information by one or a few macromolecules.

Prediction of sex chromatin status

Published discussions of sex chromatin have often included a formula by Harnden (32) to predict the expected number of sex chromatin bodies under various genotypic conditions. It was soon discovered that the formula, $S = X - A/2$ (where S is the expected number of sex chromatin bodies, X is the number of X chromosomes, and A is the number of autosomal sets), could not account for the data from triploids. On the other hand, the control system proposed here, when reduced to $S = X - A^m$, where A^m is the number of maternal autosomal sets, is a satisfactory formulation for all situations thus far observed. Indeed, if exceptions to this rule should occur, such as among human abortuses trisomic or monosomic for autosomes, they could very well provide material for assigning the locus in question to a specific autosome.

H. S. C. acknowledges research grants from the Indian National Science Academy and the World Health Organization, and a travel award from the W.H.O., and also thanks Dr. David A. Hungerford and Dr. Timothy R. Talbot, Jr., who made available for part of this work a position as Visiting Scientist at The Institute for Cancer Research, Philadelphia, Pa. Thanks are also due for a grant to S. W. B., NSF GB-8196:2, from the National Science Foundation. This report is dedicated to Dr. Barbara McClintock on the occasion of her seventieth birthday.

1. Lyon, M. F. (1961) *Nature* **190,** 372–373.
2. Lyon, M. F. (1972) *Biol. Rev.* **47,** 1–35.
3. Cooper, D. W., VandeBerg, J. L., Sharman, G. B. & Poole, W. E. (1971) *Nature New Biol.* **230,** 155–157.
4. Sharman, G. B. (1971) *Nature* **230,** 231–232.
5. Cooper, D. W. (1971) *Nature* **230,** 292–294.
6. Lyon, M. F. (1971) *Nature New Biol.* **232,** 229–232.
7. Metz, C. (1938) *Amer. Natur.* **72,** 485–520.
8. Brown, S. W. & Nur, U. (1964) *Science* **145,** 130–136.
9. Crouse, H. V. (1960) *Genetics* **45,** 1429–1443.
10. Grumbach, M. M., Morishima, A. & Taylor, J. H. (1963) *Proc. Nat. Acad. Sci. USA* **49,** 581–589.
11. Eicher, E. M. (1970) *Advan. Genet.* **15,** 175–259.

12. McClintock, B. (1962) *Carnegie Inst. Wash. Yearb.* **61,** 448–461.
13. de la Chapelle, A. (1972) *Amer. J. Hum. Genet.* **24,** 71–105.
14. Lewis, F. J. W., Frøland, A., Sanger, R. & Race, R. R. (1964) *Lancet* **ii,** 589.
15. Von Murken, J.-D. & Scholz, W. (1968) *Blut* **16,** 164–168.
16. Carr, D. H. (1971) *J. Med. Genet.* **8,** 164–174.
17. Edwards, J., Yuncken, C., Rushton, D. I., Richards, S. & Mittwoch, U. (1967) *Cytogenetics* **6,** 81–104.
18. Bomsel-Helmreich, O. (1971) *Advan. Biosci.* **6,** 381–403.
19. Ohno, S. (1967) in *Sex chromosomes and sex linked genes* (Springer-Verlag, Berlin), pp. 46–73.
20. Mittwoch, U. (1964) *J. Med. Genet.* **1,** 50–76.
21. Russell, L. B. & Montgomery, C. S. (1970) *Genetics* **64,** 281–312.
22. Searle, A. G. (1962) *Heredity* **17,** 297.
23. Cattanach, B. M., Perez, J. M. & Pollard, C. E. (1970) *Genet. Res.* **15,** 183–195.
24. Eicher, E. M., Nesbitt, M. N. & Francke, U. (1972) *Genetics* **71,** 643–648.
25. Lindsten, J. (1963) *The Nature and Origin of X Chromosome Aberrations in Turner's Syndrome* (Almqvist and Wiksell, Stockholm), 167pp.
26. Polani, P. E., Angell, R., Gianelli, F., de la Chapelle, A. Race, R. R. & Sanger, R. (1970) *Nature* **227,** 613–616.
27. Crouse, H. V., Brown, A. & Mumford, B. C. (1971) *Chromosoma* **34,** 324–329.
28. Nur, U. (1963) *Chromosoma* **14,** 123–139.
29. Jacob, F. & Wollman, E. L. (1958) *Ct. R. H. Acad. Sci.* **247,** 154–156.
30. Campbell, A. M. (1969) in *Episomes* (Harper and Row, New York), pp. 161–164.
31. Hayes, W. (1969) in *Bacterial Episomes and Plasmids,* eds. G. E. W. Wolstenholme & O'Connor, M. (Little, Brown and Co., Boston), pp. 4–11.
32. Harnden, D. G. (1961) *Lancet* **ii,** 488.
33. Lindsten, J., Bowen, P., Lee, C. S. N., McKusick, V. A., Polani, P. E., Wingate, M., Edwards, J. H., Hamper, J., Tippett, P., Sanger, R. & Race, R. R. (1963) *Lancet* **i,** 558–559.
34. de Grouchy, J., Brissaud, H. E., Richardet, J. M., Repéssé, G., Sanger, R., Race, R. R., Salmon, C. & Salmon, D. (1968) *Ann. Genet.* **11,** 120–124.
35. Frøland, A., Sanger, R. & Race, R. R. (1968) *J. Med. Genet.* **5,** 161–164.
36. Race, R. R. & Sanger, R. (1969) *Brit. Med. Bull.* **25,** 99–103.

Proc. Nat. Acad. Sci. USA
Vol. 70, No. 1, pp. 200–204, January 1973

Cleavage of Adenovirus Type 2 DNA into Six Unique Fragments by Endonuclease R·RI

(restriction enzyme/electron microscopy/DNA gel electrophoresis/DNA sequence complexity)

ULF PETTERSSON, CAREL MULDER, HAJO DELIUS, AND PHILLIP A. SHARP

Cold Spring Harbor Laboratory, Cold Spring Harbor, New York 11724

Communicated by A. D. Hershey, November 8, 1972

ABSTRACT **The DNA of adenovirus type 2 was cleaved by restriction endonuclease R·RI into six fragments. These fragments were separated by electrophoresis on composite agarose–polyacrylamide gels. Their molecular weights ranged from 1.1×10^6 to 13.6×10^6, as measured by electron microscopy. Each fragment represented a unique segment of adenovirus type 2 DNA since: (*i*) the fragments were obtained in equimolar amounts; (*ii*) the sum of their molecular weights was equal to the molecular weight of complete adenovirus DNA; and (*iii*) each fragment exhibited a rate of renaturation that was inversely proportional to its size.**

Danna and Nathans (1) reported that a restriction endonuclease from *Hemophilus influenzae* Rd cleaves DNA of simian virus 40 (SV40) into 11 fragments. Such fragments are of great value for mapping of specific loci on the viral chromosome. In order to cleave the DNA of adenovirus type 2 (Ad2), we have used a restriction endonuclease from *Escherichia coli* carrying the drug resistance transfer factor RTF-1 (endonuclease R·RI). This endonuclease cuts circular SV40 DNA at one unique site (2, 3); it also cleaves duplex DNA by making single-stranded scissions in positions that are four base pairs apart, thereby generating cohesive ends (4, 5). Endonuclease R·RI has a molecular weight of about 80,000 and requires only magnesium as a cofactor (6).

Adenoviruses contain linear duplex DNA with a molecular weight of about 23×10^6 (7). Adenovirus DNA is not circularly permuted, but each of its strands contains complementary sequences at its ends that are inverted with respect to each other (8, 9). Adenovirus type 2, the most extensively studied serotype, belongs to the group of "nononcogenic" adenoviruses. These adenoviruses are capable of transforming cells *in vitro*, but are not known to cause tumors in animals (10). The adenoviruses are useful for investigation of cell transformation and for studies of regulatory mechanisms in eukaryotes since, during lytic adenovirus infection, host cell macromolecular synthesis is suppressed so that DNA, RNA, and protein synthesis is almost entirely controlled by the virus. Specific fragments of Ad2 DNA should be valuable for studying of gene functions expressed during the lytic cycle and in transformed cells.

MATERIALS AND METHODS

Virus and Cell Cultures. Adenovirus type 2, originally obtained from Dr. J. Rose, was propagated at an input multiplicity of about 1500 particles per cell in suspension cultures of KB-cells (11). The identity of the virus was established by immunodiffusion of antigens released from purified virus after treatment with 10% pyridine (12) against specific antisera. The virus was purified by the method of Green and Piña (13) as modified by Lonberg–Holm and Philipson (14), and the DNA was extracted from the virus as described by Pettersson and Sambrook (15). ^{32}P-labeled virus was obtained by including 10 μCi of [^{32}P]phosphoric acid/ml in a phosphate-free medium (Gibco "F13" without phosphate) from 6–40 hr after infection. The labeled DNA usually had a specific activity of about 5×10^5 cpm/μg. Although our virus stock had been grown at high multiplicities for many generations, the DNA was not heterogeneous when analyzed by electronmicroscopy after denaturation and renaturation (P. Sharp, unpublished results).

The Origin and Purification of Endonuclease R·RI was described by Mulder and Delius (3).

Enzyme Incubations. The standard incubation mixture contained 10 mM $MgCl_2$ and 90 mM Tris·HCl pH 7.9, 0.3 μg of protein per μg of DNA, and was incubated at 37° for 30 min. Digestion was stopped by addition of EDTA.

Rate Zonal Centrifugation. Samples (50–100 μl) were analyzed on linear gradients of 5–20% sucrose containing 50 mM Tris·HCl (pH 7.9)–1 M NaCl 1 mM EDTA in a Beckman/Spinco SW56 rotor. After 2 hr of centrifugation at 55,000 rpm and 20°, the gradients were fractionated by collection of drops from the bottom of the tube. Sedimentation coefficients were calculated in relation to that of intact adenovirus 2 DNA, which was assumed to be 31 S (16).

Agarose–Polyacrylamide Gel Electrophoresis. Samples were adjusted to 0.1 M NaCl, extracted with an equal volume of chloroform–isoamyl alcohol (24:1), and precipitated with 2 volumes of ethanol. The precipitate was dissolved in a 1:5 dilution of the electrophoresis buffer (see below). Composite gels containing 2.2% acrylamide (Bio-Rad), 0.11% *N',N'*-methylene-bis-acrylamide (Eastman Kodak), and 0.7% agarose (Sigma) were used essentially as described by Peacock and Dingman (17). The gels were polymerized in cylindrical glass tubes (0.6 cm internal diameter × 14 cm) by addition of 0.5 μl of *N,N,N',N'*-tetramethylethylenediamine and 5 μl of 10% ammonium persulfate per ml of agarose–acrylamide solution at 45°. The electrophoresis buffer contained 40 mM Tris·HCl–5 mM sodium acetate–1 mM EDTA (pH 7.8). After addition of sucrose to a concentration of about 10%, 100 μl of

Abbreviations: Ad2, Adenovirus type 2; SV40, Simian virus 40; SDS, sodium dodecyl sulfate: $P_T t_{1/2}$ the product of the DNA concentration P_T and the time taken for 50% of the DNA sequences to reassociate, expressed as mol of nucleotide × sec/liter.

sample was layered onto each gel. An initial voltage of 1 V/cm was applied for 30 min, after which the voltage was increased to 4 V/cm. The gels were removed from their tubes and cut into 1-mm slices with razors. The amount of radioactivity was measured as Čerenkov radiation in a liquid scintillation counter or in 4 ml of Aquasol (New England Nuclear). After counting, the DNA was recovered as follows: One or two slices were placed inside a glass tube (0.5 cm internal diameter × 5 cm) that had a constriction at one end. The constricted end was covered with dialysis tubing (1–2 cm). The tube was filled with electrophoresis buffer and placed in an apparatus for gel electrophoresis (Hoeffer Scientific Instruments). The constricted end was immersed in the buffer chamber with the anode, and a potential of 100 V was applied across the tube. After 2 hr of electrophoresis, 70–100% of the radioactivity was recovered from the buffer in the dialysis tubing.

Determination of the Rate of DNA Reassociation. Samples containing 200 μl of ^{32}P-labeled DNA were mixed with 50 μl of 1 M NaOH and boiled for 30 min to melt and fragment the DNA to uniform size. The size of the DNA after this treatment was about 500 nucleotides, as determined by sedimentation through alkaline sucrose gradients with marker fragments of SV40 DNA obtained by digestion with a restriction endonuclease from *H. influenzae* Rd (J. Sambrook, personal communication). The samples were neutralized by addition of 0.5 ml of 0.28 M phosphate buffer (pH 6.8) (containing equimolar amounts of Na_2HPO_4 and NaH_2PO_4) in 0.8% sodium dodecyl sulfate (SDS). The volume was then adjusted to 1 ml with water, and samples were overlayed with mineral oil before they were incubated at 68°. Aliquots (50–100 μl) were withdrawn at intervals and immediately diluted 10-fold with 0.14 M phosphate buffer containing 0.4% SDS. The amount of double-stranded DNA in each sample was determined by chromatography on hydroxyapatite (Biogel HTP) (18).

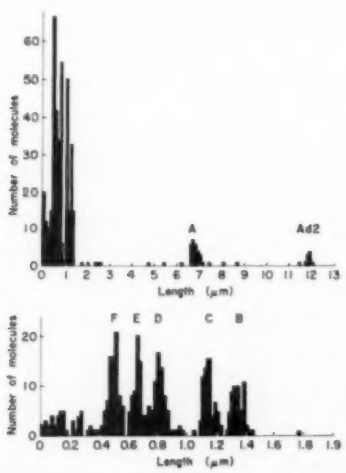

FIG. 1. Histograms of length measurements of Ad2 DNA fragments. Ad2 DNA was incubated with endonuclease R·RI under standard conditions. After digestion had been stopped by addition of EDTA to 0.05 M, Ad2 DNA was added as a marker. The mixture was spread for electronmicroscopic length measurement without further treatment. The absolute length was determined by calibration with 200 lines per diffraction grating. Small molecules were preferentially scored because some large molecules were entangled and, therefore, impossible to measure.

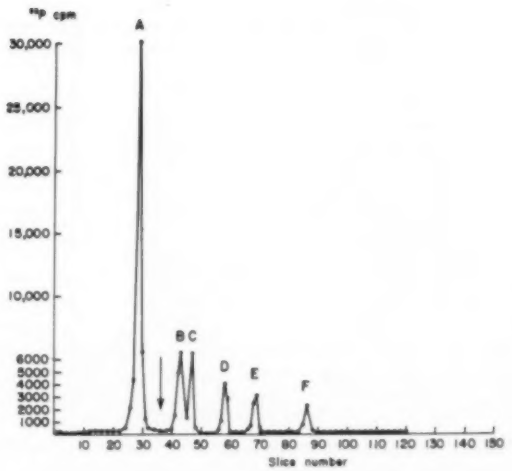

FIG. 2. Gel electrophoresis of ^{32}P-labeled fragments of Ad2 DNA. ^{32}P-labeled Ad2 DNA was incubated with endonuclease R·RI under standard conditions. The sample was extracted with chloroform–isoamyl alcohol; after ethanol precipitation, the digested DNA was subjected to electrophoresis on 2.2% acrylamide–0.7% agarose gels. After electrophoresis at 4 V/cm for 20 hr at 20°, the gels were cut into 1-mm slices. Radioactivity was measured as Čerenkov radiation. The anode is towards the *right*. Six peaks designated *A–F* were resolved. The *arrow* marks the position of linear SV40 DNA, as determined on a separate gel containing fragments *A–F*.

Electron Microscopy. DNA was mounted by the basic protein film technique for observations in an electron microscope (3, 19). Circular DNA from bacteriophage PM 2 (20) was sometimes added as an internal length standard.

RESULTS

Digestion of Ad2 DNA with Endonuclease R·RI. ^{32}P-labeled Ad2 DNA was digested with endonuclease R·RI and analyzed on neutral sucrose gradients with ^{3}H-labeled intact Ad2 DNA as a marker. The digested Ad2 DNA was resolved into three peaks: one major peak had a sedimentation coefficient of about 26 S and contained about 60% of the DNA; two minor, slower-sedimenting, broad peaks apparently contained DNA of various sizes (not shown). The digested Ad2 DNA was also examined by electron microscopy; no detectable amounts of intact DNA (<1%) remained after digestion. The lengths of the digested fragments were measured with intact Ad2 DNA as a standard; the digested DNA comprised six distinct size classes. The average length of the DNA in each of these classes, measured in relation to that of the marker DNA, was 0.57, 0.11, 0.10, 0.07, 0.06, and 0.04 (Fig. 1). A heterogeneous population of small DNA segments (0.004–0.03 of Ad2 DNA) was also observed (Fig. 1); as will be discussed below, we do not consider these to be cleavage products of Ad2 DNA.

Analysis of Digested Ad2 DNA by Gel Electrophoresis. ^{32}P-labeled Ad2 DNA, cleaved by endonuclease R·RI, was analyzed by electrophoresis on composite agarose–polyacrylamide

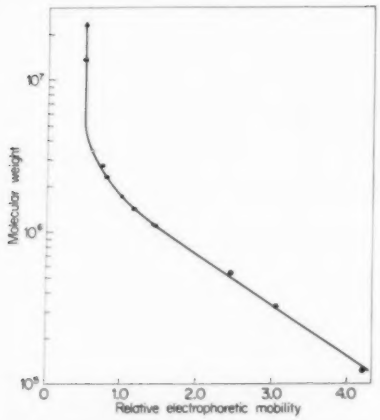

FIG. 3. Relationship between molecular weight and electrophoretic mobility of fragments *A–F*. Electrophoresis was done on 12-cm gels at 4 V/cm for 4, 20, and 25 hr. Relative electrophoretic mobility was defined as: (distance migrated by a fragment)/(distance migrated by fragment *D*). The following DNAs were used as markers: (▲) Intact Ad2 DNA (23×10^6), (○) linear SV40 DNA (3.6×10^6), and (•) fragments SV40-B (5.4×10^5), SV40-D (3.2×10^5), and SV40-H (1.2×10^6) obtained by treatment of SV40 DNA with a restriction endonuclease from *H. influenzae* Rd (1). Fragment *D* migrated with an electrophoretic mobility of 1.13×10^5 cm²/V × sec (17).

gels. All separations were performed at 20° to prevent joining of the cohesive ends that are generated by endonuclease R·RI (4, 5). Six peaks, designated *A–F*, were resolved by this method (Fig. 2). No radioactivity was recovered from the top of the gel, and more than 90% of the input radioactivity was recovered after electrophoresis. A separation time of 20 hr was required for good resolution. No additional peaks were observed when the electrophoresis time was decreased to 4 hr, which would allow a segment of DNA of molecular weight below 100,000 to remain on the gel (Fig. 3). For calibration of the gel system, marker DNAs were added to the digested samples before electrophoresis (Fig. 3). For this purpose we used intact Ad2 DNA (23×10^6), linear SV40 DNA (3.6×10^6), and fragments SV40-B (5.4×10^5), SV40-D (3.2×10^5), and SV40-H (1.2×10^5 daltons) obtained by digestion of SV40 DNA with a restriction endonuclease from *H. influenzae* Rd (1). All markers were resolved from the six fragments of Ad2 DNA, except intact Ad2 DNA, which migrated with fragment *A*. The mobilities of the five marker DNAs in relation to fragment *D* of adenovirus DNA were 0.5, 0.6, 2.5, 3.1, and 4.2 (Fig. 3).

In order to establish that digestion of Ad2 DNA was complete, we analyzed samples of ^{32}P-labeled Ad2 DNA that were digested for 5–120 min. The sum of the radioactivity in peaks *A–F* and the fraction of label recovered from each peak was determined. Analysis of samples after digestion for 5, 30, 60, and 120 min revealed no difference in distribution of radioactivity among the six peaks (Table 1).

Determination of Molecular Weight of Isolated Fragments. Ad2 fragments that migrated as peaks *A–F* were collected after electrophoresis and examined in an electron microscope with circular DNA from bacteriophage PM 2 as a standard. Each peak contained DNA of a unique size class as judged by the standard deviation in lengths (Table 2). If a molecular weight of 6.40×10^6 is assigned to PM 2 DNA, the molecular weights ($\times 10^{-6}$) of the fragments are: 13.6 (*A*), 2.7 (*B*), 2.3 (*C*), 1.7 (*D*), 1.4 (*E*), and 1.1 (*F*) (Table 2). The sum of the molecular weights of DNA fragments from peaks *A–F* ($22.8 \pm 0.8 \times 10^6$) was in good agreement with that of intact Ad2 DNA ($22.9 \pm 0.5 \times 10^6$) (Table 2); the experimental error did not exclude that one of the small peaks (*E* or *F*) contained two different segments of DNA of identical size. If all peaks contained segments of DNA of one kind there should be a correlation between the amount of DNA recovered in each peak and its molecular weight. Therefore, we determined the fraction of the total radioactivity that was recovered in peaks *A–F* after electrophoresis of seven separate samples of ^{32}P-labeled digested Ad2 DNA. As is shown in Table 2, there is a good correlation between the fraction of radioactivity and the fractional length of the DNA recovered from each of the six peaks.

Determination of the Complexity of DNA from Complete Ad2 DNA and Separated Fragments. To further establish that peaks *A–F* contained unique fragments of DNA, we examined the reassociation kinetics of each fragment and of complete Ad2 DNA (18). Before analysis, all DNAs were partially hydrolyzed to an average size of 500 nucleotides by being boiled in alkali (J. Sambrook, personal communication) to eliminate the effect of size on the rate of duplex formation (21). The time ($t_{1/2}$) required for 50% of the sequences to reassociate at a given DNA concentration (P_T) was calculated for fragments *A–F* and complete adenovirus DNA (Fig. 4; Table 2). The product ($P_T t_{1/2}$) for renaturation of two different DNAs will primarily depend upon their complexities, provided they have been degraded to identical size. Complexity is defined as the number of base pairs in nonrepeating sequences in a given DNA (21). DNA segments that do not contain reiterated sequences should have complexities that are proportional to their lengths (21, 22). Thus, the complexity of fragments *A–F* may be predicted from their molecular weights, provided each is unique. A 20% variation from this prediction must be allowed

TABLE 1. *Distribution of DNA in peaks A–F after incubation of Ad2 DNA with endonuclease R·RI for different periods of time*

Min of incubation	Distribution of ^{32}P (%)				
	A	*B* + *C*	*D*	*E*	*F*
5	58.4	23.5	7.3	5.8	5.1
30	59.2	21.1	7.5	6.8	5.4
60	59.8	22.7	7.3	6.2	4.0
120	59.4	19.8	7.8	6.1	6.7
Average of 4 separate 30-min digestions*	58.1 ± 1.1	22.6 ± 1.3	7.6 ± 0.3	6.6 ± 0.2	5.1 ± 0.3

Gels were sliced into 1-mm slices, and radioactivity was determined as Čerenkov radiation. Peaks *B* and *C* were not completely resolved on all electropherograms and, therefore, the number of counts in both peaks were added together. In all experiments, peaks *B* and *C* were of similar magnitude. The enzyme concentration was increased from 3 μg/ml to 6 μg/ml after 30 min and to 9 μg/ml after 60 min.

* ±SD.

TABLE 2. *Properties of fragments of Ad2 DNA after separation by gel electrophoresis*

Fragment	Length (μm)	Molecular weight ($\times 10^{-6}$)	Fractional length (%)	Distribution of radioactivity* (%)	$P_T t_{1/2}$ (mol × sec/liter) × 10^3
A	7.54 ± 0.10	13.6 ± 0.2	58.3	58.5 ± 1.1	10.7 ± 0.5
B	1.54 ± 0.05	2.7 ± 0.1	11.9	22.4 ± 1.5†	2.28 ± 0.14
C	1.28 ± 0.05	2.3 ± 0.1	9.9		2.64 ± 0.50
D	0.924 ± 0.05	1.7 ± 0.1	7.2	7.5 ± 0.3	1.46 ± 0.09
E	0.747 ± 0.03	1.4 ± 0.1	5.8	6.3 ± 0.4	1.73 ± 0.22
F	0.584 ± 0.03	1.1 ± 0.1	4.5	5.2 ± 0.8	1.14 ± 0.09
Intact Ad2 DNA	12.9 ± 0.3	22.9 ± 0.5	(100)	—	20.2 ± 0.2

Samples were mixed with nicked circular PM 2 DNA before electron microscopic analysis. The molecular weight of PM 2 DNA was calculated to be 6.40×10^6 from measurements that were standardized with T7 DNA (25.2×10^6; ref. 23). $P_T t_{1/2}$ was calculated as described in the legend to Fig. 4.

* Average of seven experiments. Background radioactivity was measured from fractions between peaks and was subtracted. Fragments *B* and *C* were not entirely resolved on all electropherograms and, therefore, the number of counts in both peaks were added together. In all experiments peaks *B* and *C* were of similar magnitude.

† For fragment *B* plus fragment *C*.

because of the effect of differences in base composition on the rate of renaturation (21). We found a good correlation between the complexity of each of the six fragments and its molecular weight, with a maximum deviation of 35% from the predicted value for $P_T t_{1/2}$ calculated from the results for complete Ad2 DNA (Table 2). From this we conclude that none of the fractions *A–F* contained more than one kind of DNA segment. The presence of two kinds of DNA segments in one peak would cause a 2-fold increase above the predicted value for $P_T t_{1/2}$.

Since fragment *A* was not resolved by gel electrophoresis from segments of DNA larger than 5×10^6 (Fig. 3), we wanted to ascertain that fragment *A* was not contaminated with large DNA fragments generated because of incomplete digestion. Such fragments could arise if Ad2 DNA was being modified by a contaminating methylase during digestion or if Ad2 DNA was heterogeneous with respect to cleavage sites for endonuclease R·RI. Electronmicroscopic length measurements of purified samples of fragment *A* showed that less than 1% of the molecules had a length corresponding to the sum of fragments *A* and *B* or *A* and *C* (data not shown). A significant contamination of molecules having a molecular weight of about 1×10^6 above the average could not be excluded however. Therefore, we estimated the amount of contaminating *D*, *E*, and *F* fragments in purified samples of fragment *A* by the following method: ^{32}P-labeled samples of fragments *D*, *E*, and *F* were mixed with a 200- to 1000-fold excess of either unlabeled fragment *A* or unlabeled intact Ad2 DNA. The samples were denatured and partially hydrolyzed, and the rate of renaturation was measured. Fig. 5 shows the results when 2 ng of ^{32}P-labeled fragment *F* was mixed with 1 μg of unlabeled fragment *A* or 1.7 μg of unlabeled Ad2 DNA. As expected, Ad2 DNA caused about a 40-fold increase in the rate of renaturation of the labeled DNA, whereas fragment *A* had an insignificant effect. Since contamination of 2 ng would have caused a 2-fold increase in the rate of renaturation, we conclude that purified samples of fragment *A* were contaminated with less than 0.2% by mass of fragment *F*. In a similar way, we determined that the corresponding amounts of contamination for fragments *E* and *D* were <0.3% and <0.8%, respectively.

DISCUSSION

We have identified, by gel electrophoresis, six fragments from Ad2 DNA after digestion with endonuclease R·RI. The cleavage was complete and the six fragments (fragments *A–F*) were demonstrated to be unique segments of the Ad2 DNA by the following observations: (*i*) The sum of the molecular weights of the six fragments equaled that of intact adenovirus type 2 DNA. (*ii*) All six fragments were generated in equimolar amounts. (*iii*) Each fragment had a renaturation

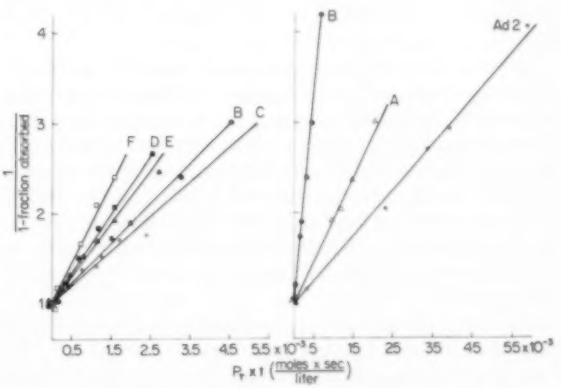

FIG. 4. Kinetics of reassociation of denatured ^{32}P-labeled samples of fragments *A–F* and complete Ad2 DNA. Samples in 0.14 M phosphate buffer (18) and 0.4% SDS were incubated at 68°. Aliquots (100–200 μl) were withdrawn at intervals and assayed by chromatography on hydroxylapatite. The time required for 50% of the sequences to renature ($t_{1/2}$) was calculated from $t_{1/2} = [t(1 - f_{DS})/f_{DS}]$; ($t$ = time of incubation; f_{DS} = fraction of double-stranded DNA in a sample at a given time, t, as determined by chromatography on hydroxylapatite). Each line represents the theoretical curve computed from the average $t_{1/2}$; in all cases, $t_{1/2}$ was calculated from three or more samples containing between 10 and 65% renatured DNA. The fraction of double-stranded DNA was calculated from the fraction of ^{32}P-counts that adsorbed to hydroxylapatite in 0.14 M phosphate buffer. No corrections were made for zero- or infinite-time renaturation.

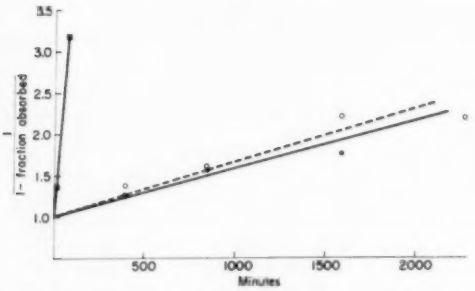

FIG. 5. Kinetics of reassociation of denatured ^{32}P-labeled fragment *F* in the presence of excessive amounts of unlabeled fragment *A* or Ad2 DNA. Reaction mixtures contained 2 ng of ^{32}P-labeled fragment *F* and 1 μg of fragment *A* (○) or 1.7 μg of Ad2 DNA (■) per ml. The rate of reassociation was also estimated for fragment *F* alone under identical conditions (●). The fraction of duplex DNA in the samples was estimated as described in the legend to Fig. 4, after different times of incubation at 68° in 0.14 M phosphate buffer (18) and 0.4% SDS.

complexity that is proportional to its molecular weight. (*iv*) The fraction of the total DNA migrating in each of the six peaks remained constant during prolonged digestion.

Electron microscopy showed, in addition, a heterogeneous population of fragments with molecular weights in the range 200,000–600,000 (Fig. 1). These fragments were apparently not derived from Ad2 DNA since (*i*) they were not present in equimolar amounts (Fig. 1) and (*ii*) gel electrophoresis of digested samples of ^{32}P-labeled Ad2 DNA containing 5×10^5 cpm (under conditions where DNA of molecular weight of 100,000 or less would be resolved) revealed no labeled material smaller than fragment *F*. Electron microscopy of our enzyme preparation showed some DNA-like material, and it is likely that this was the origin of the small fragments.

Electrophoresis on composite agarose–polyacrylamide gels (17) was a useful method for separation of the six fragments of Ad2 DNA. All fragments were clearly resolved from each other, although some of the fragments differ by as little as 15% in length. This method would not, however, resolve fragment *A* from DNA segments larger than 5×10^6 daltons (Fig. 3). The homogeneity of fragment *A* was therefore ascertained by electron microscopy and by estimates of the rate of DNA renaturation of fragments *D–F* in the presence of a vast excess of fragment *A*.

In view of its specificity, endonuclease R·RI should be of general importance for obtaining defined fragments of DNA from large mammalian DNA viruses. The fragments that were generated from Ad2 DNA with this enzyme should facilitate mapping of the adenovirus chromosome.

We thank Peter Jeppesen for *H. influenzae* Rd fragments of SV40 DNA and James Watson and Joe Sambrook for critical reading of the manuscript. Skillful technical assistance was provided by Elly Allet and Annelie Wilde. This work was supported by grants from the National Cancer Institute (CA 11432) and the American Cancer Society. U. P. was a recipient of a fellowship from the International Agency for Research on Cancer.

1. Danna, K. & Nathans, D. (1971) *Proc. Nat. Acad. Sci. USA* **68,** 2913–2917.
2. Morrow, J. F. & Berg, P. (1972) *Proc. Nat. Acad. Sci. USA* **69,** 3365–3369.
3. Mulder, C. & Delius, H. (1972) *Proc. Nat. Acad. Sci. USA* **69,** 3215–3219.
4. Mertz, J. E. & Davis, R. W. (1972) *Proc. Nat. Acad. Sci. USA* **69,** 3370–3374.
5. Hedgpeth, J., Goodman, H. M. & Boyer, H. (1972) *Proc. Nat. Acad. Sci. USA* **69,** 3448–3452.
6. Yoshimori, R. N. (1972) Ph.D. Dissertation, University of California, San Francisco Medical Center.
7. Green, M., Piña, M., Kimes, R., Wensink, P. D., MacHattie, L. A. & Thomas, C. A. (1967) *Proc. Nat. Acad. Sci. USA* **57,** 1302–1309.
8. Wolfson, J. & Dressler, D. (1972) *Proc. Nat. Acad. Sci. USA* **69,** 3054–3057.
9. Garon, C. F., Berry, K. W. & Rose, J. (1972) *Proc. Nat. Acad. Sci. USA* **69,** 2391–2395.
10. Freeman, A. E., Black, P. H., Vanderpool, A. E., Henry, P. H., Austin, J. B. & Heubner, R. J. (1967) *Proc. Nat. Acad. Sci. USA* **58,** 1205–1212.
11. Pettersson, U., Philipson, L. & Hoglund, S. (1967) *Virology* **33,** 575–590.
12. Page, L., Pettersson, U., Hoglund, S., Lonberg-Holm, K. & Philipson, L. (1970) *Virology* **42,** 341–358.
13. Green, M. & Pina, M. (1963) *Virology* **20,** 199–207.
14. Lonberg-Holm, K. & Philipson, L. (1969) *J. Virol.* **4,** 323–338.
15. Pettersson, U. & Sambrook, J. (1972) *J. Mol. Biol.* **72,** in press.
16. Doerfler, W. & Kleinschmidt, A. K. (1970) *J. Mol. Biol.* **50,** 579–593.
17. Peacock, A. C. & Dingman, C. W. (1968) *Biochemistry* **7,** 668–674.
18. Kohne, D. E. & Britten, R. J. (1971) in *Procedures in Nucleic Acid Research,* eds. Cantoni, F. L. & Davies, D. R. (Harper and Row, New York), Vol. 2, p. 500.
19. Davis, R. W., Simon, M. & Davidson, N. (1971) in "Nucleic Acids," *Methods in Enzymology,* eds. Colowick, J. P. & Kaplan, N. D., (Academic Press, New York) Vol. XXI, Part B, pp. 413–428.
20. Espejo, R. T., Canelo, E. S. & Sinsheimer, R. L. (1968) *Proc. Nat. Acad. Sci. USA* **63,** 1164–1168.
21. Wetmur, J. G. & Davidson, N. (1968) *J. Mol. Biol.* **31,** 349–390.
22. Marmur, J., Rownd, R. & Schildkraut, C. L. (1963) *Progress in Nucleic Acid Research,* eds. Davidson, J. N. & Cohn, W. E. (Academic Press, Inc., New York).
23. Freifelder, D. (1970) *J. Mol. Biol.* **54,** 567–577.

Proc. Nat. Acad. Sci. USA
Vol. 70, No. 1, pp. 205–209, January 1973

A Coat Protein of the Bacteriophage M13 Virion Participates in Membrane-Oriented Synthesis of DNA

(gene-3 protein/parental RF–gene-3 protein complex/cell inner membrane/φX174/fd and fl)

S. MICHAL JAZWINSKI, ROBERTO MARCO, AND ARTHUR KORNBERG

Department of Biochemistry, Stanford University School of Medicine, Stanford, California 94305

Contributed by Arthur Kornberg, November 13, 1972

ABSTRACT **Several molecules of a protein specified by gene 3 of M13 comprise a minor fraction of the phage coat and have been assigned a role in adsorption to the bacterial cell. We find that the gene-3 protein molecules of the virion are fully conserved in phage that have attached irreversibly to the host cell, and they form a complex with the phage DNA when it has been converted to a duplex replicative form. In cells infected at a restrictive temperature with a thermosensitive mutant in gene 3, there is no conversion of the phage DNA to the replicative form. Both the adsorbed phage and the complex of replicative form DNA with the gene-3 protein were isolated with the inner membrane fraction of the cell. We suggest that the gene-3 protein may perform an essential function in the synthesis of replicative form by linking the phage DNA to a cellular replicative system in or on the inner cell membrane.**

M13, a filamentous coliphage, is closely related to phages fl and fd (see ref. 1 for review). It is composed of a single-stranded, circular DNA molecule in a capsid of about 3000 molecules of a protein specified by gene 8 (5000 daltons), and a few molecules of a protein coded by gene 3 (70,000 daltons). Adsorption of the virion specifically to male cells has been attributed to the F-pilus structure (2). The gene-3 protein has been implicated in this initial step (3). Penetration of the phage and conversion of the single strand to RF I requires no synthesis of phage-specific proteins (4).

Our interest in the details of M13 DNA synthesis (5–7) has led us to inquire into how, and in what location, the phage template is made available to the host replicating machinery. There have been indications that uncoating of the phage depends on DNA replication (Forsheit, A. B. and Ray, D. S., personal communication), and that the DNA during its replication is associated with the cell-membrane fraction (8). We have exploited the unique labeling of the gene-3 protein with an amino acid that is missing from gene-8 protein (1, 9, 10). We show that the gene-3 protein remains with the phage after its irreversible adsorption, that it forms a complex with the RF, and that both attached phage and RF are associated with the inner cell membrane. Furthermore, we show that a phage mutant with a defective gene-3 protein fails to form RF.

MATERIALS AND METHODS

Chemicals were as follows: $H_3{}^{32}PO_4$ (carrier-free) from New England Nuclear, [^{3}H]thymine (17.5 Ci/mmol) from Schwarz/Mann, [^{3}H]histidine (51 Ci/mmol) from Amersham, chloramphenicol from Parke–Davis, and rifampicin from Calbiochem. [^{32}P]Phosphatidylglycerol (40 Ci/mmol) was prepared according to Scandella and Kornberg (11).

Growth of Cells and Phage. Bacterial and phage strains used were generously provided as follows: *Escherichia coli* K-12 5274 (*thy*$^-$, F$^+$) from the J. Lederberg collection, *E. coli* HfrC71 (*thy*$^-$, *endo* I$^-$, *met*$^-$, UVsens.) by Dr. H. Hoffman–Berling, *E. coli* K37 (su-1$^+$, F$^+$) by Dr. Dan Ray, M13 wild-type and mutant strains *am*2 and *am*5 (12), and M13 *ts*3 H-2 and H-8 (12, 13) by Dr. David Pratt.

The media used were: H-broth (14), Marvin medium (15), GCA medium (16), and a GCA medium for the preparation of histidine-labeled phage, in which the casamino acids in GCA were substituted by 20 μg/ml (each) of 19 L-amino acids found in protein, with histidine omitted.

Phage were purified by polyethyleneglycol precipitation (17), followed by sedimentation through a sucrose density gradient.

Labeling of Phage. For labeling of phage DNA, [^{32}P]phosphate (5 mCi/100-ml culture) or [^{3}H]thymine (2 mCi/100-ml culture) was added to the culture in GCA medium at the time of infection. For labeling of phage gene-3 protein, [^{3}H]-histidine (3 mCi/100-ml culture) was added to the culture. Specific activities (cpm/10^{10} PFU) were about: 4×10^4 for ^{32}P, 2×10^4 for [^{3}H]thymine, and 0.5×10^4 for [^{3}H]-histidine. After digestion of chloroform-treated phage with pancreatic deoxyribonuclease, more than 90% of the ^{32}P became acid-soluble. Similarly digestion of [^{3}H]histidine-labeled phage with Pronase rendered more than 95% of the ^{3}H acid-soluble. Protein from phage labeled with [^{3}H]-histidine and solubilized with 0.1 M NaOH–3% Na dodecyl sulfate displayed one peak of radioactivity on a dodecyl sulfate–acrylamide disc-gel (Fig. 1). This peak corresponds to a protein of about 70,000 daltons, as determined with protein standards, a value similar to that obtained for the gene-3 protein (10).

Cell Lysis. Cells were lysed with lysozyme–EDTA and Sarkosyl as described by Ray and Schekman (16). To measure the association of phage with the cell membranes, spheroplasts of infected cells were lysed (18) by osmotic shock.

Separation of DNA. M13 replicative forms were separated by velocity sedimentation. Samples (400 μl) were layered on 5–20% (w/v) linear sucrose gradients (12 ml) containing

Abbreviations: RF, (phage) double-stranded circular replicative form; RF I, (phage) covalently closed RF; RF II, (phage) RF with a discontinuity in at least one strand.

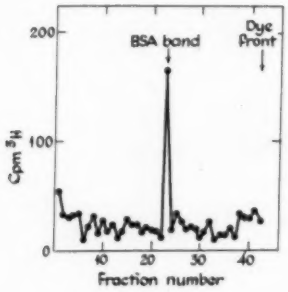

FIG. 1. Dodecyl sulfate–acrylamide disc-gel electrophoresis of [^{3}H]histidine-labeled phage protein. Labeled phage (wild-type) was incubated for 30 min at 37° with 0.1 M NaOH–3% dodecyl sulfate, applied to a 10% acrylamide gel containing 0.1% dodecyl sulfate, and electrophoresed in the discontinuous system of Jovin *et al.* (19). Dried gel slices were counted in a toluene-based scintillation fluid. *Arrows* represent the positions of a bovine-serum albumin (*BSA*) band on a parallel gel with protein standards and the front.

0.01 M Tris·HCl (pH 8.0)–1 M NaCl–1 mM EDTA in a nitrocellulose tube and sedimented for 16 hr at 26,000 rpm in a Spinco SW40 rotor at 5°. To separate the membrane-bound from freely-sedimenting phage DNA, samples (400 μl) were applied to two-step sucrose gradients (5–20 and 30–50%, w/v) (12 ml) [containing 0.01 M Tris·HCl (pH 7.5)–1 mM EDTA] in a nitrocellulose tube and sedimented for 3 hr at 40,000 rpm in a Spinco SW40 rotor at 5°. For sucrose-gradient equilibrium sedimentation, 30–70% (w/v) linear sucrose gradients containing 0.01 M Tris·HCl (pH 7.5)–5 mM EDTA

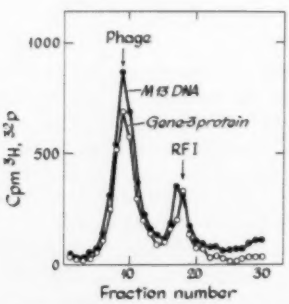

FIG. 2. Velocity sedimentation of Sarkosyl lysates of cells infected with phage labeled with ^{32}P and [^{3}H]histidine. *E. coli* 5274 cells were grown to 0.25 OD_{595} in GCA medium, pelleted at room temperature, resuspended in an equal volume of this medium (containing 200 μg/ml of chloramphenicol), and incubated for 10 min at 37°. The suspension was infected with wild-type phage (labeled with ^{32}P and [^{3}H]histidine) at MOI = 100 for 10 min at 37°. The suspension was then chilled to 0° and adjusted to 0.02 M NaCN. Cells were pelleted and washed three times with 10 mM Tris·HCl (pH 8.0)–1 mM EDTA–0.02 M NaCN, after which they contained 2–3 phage equivalents per cell. The cells were resuspended in Tris–EDTA–0.1 M NaCl and lysed by incubation with 400 μg/ml of lysozyme for 10 min at 37°, then with 0.5% Sarkosyl for 10 min at 37°, and were applied to a 5–20% sucrose velocity gradient, which was separated into 15-drop fractions. Direction of sedimentation is from *right* to *left*. Position of the phage peak was determined by sedimentation of marker phage and assays of infectivity. Position of the RF I peak was determined by its sedimentation relative to phage.

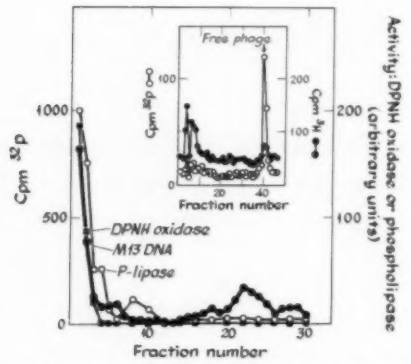

FIG. 3. Velocity sedimentation of gently lysed cells infected with ^{32}P-labeled phage. *E. coli* 5274 cells were grown to 0.25 OD_{595} in H-broth, pelleted at room temperature, resuspended in an equal volume of H-broth (containing 200 μg/ml of chloramphenicol), and incubated for 10 min at 37°. The suspension was infected with wild-type phage (^{32}P-labeled) at MOI = 100 for 10 min. The suspension was chilled to 0° and the cells were pelleted. The pellet was resuspended in 10% sucrose–0.01 M Tris·HCl (pH 7.5)–5 mM EDTA and lysed by incubation with 50 μg/ml of lysozyme for 30 min at 0° and the addition of 4 volumes of water, then was applied to a two-step gradient (*Methods*), which was separated into 15-drop fractions. Direction of sedimentation is from *right* to *left*. *Insert:* wild-type phage (^{32}P) added to cells infected with [^{3}H]thymine-labeled phage after lysis.

were formed (12 ml). Samples were applied and sedimented to equilibrium for 18 hr at 36,000 rpm in a Spinco SW40 rotor at 5°.

Other Methods. Phospholipase A assay was performed according to Scandella and Kornberg (11) and DPNH oxidase activity was measured essentially according to Osborn *et al.* (18).

RESULTS

Gene-3 Protein Remains with the Phage DNA. The fate of gene-3 protein upon infection was determined in chloramphenicol-treated cells; the phage was labeled with ^{32}P in the DNA and [^{3}H]histidine in the gene-3 protein. In a lysate, 10 min after infection, both the ^{32}P and ^{3}H labels were found, after velocity sedimentation, in two peaks (Fig. 2). The faster-sedimenting peak corresponds to phage (as determined by sedimentation of marker phage and by assay of infectivity across the gradient); the slower peak corresponds to RF I (from its position relative to the phage peak) (20). The ^{3}H/^{32}P ratio in the phage and RF I peaks were in the same range as that of the infecting phage (0.70 ± 0.10). Thus, the gene-3 protein remained associated with the phage after its adsorption, and with the phage DNA even after its conversion to RF.

Similar results were obtained when cells were grown in H-broth instead of GCA medium, and when cells were lysed somewhat later (15 min) after infection. In the absence of chloramphenicol, the sedimentation pattern was the same, except for the appearance of an RF II peak (40% of total RF), which contained a relatively smaller amount of the [^{3}H]histidine label; the ^{3}H/^{32}P ratio was about 0.2.

The Infecting Phage DNA and Gene-3 Protein Are Associated with the Inner Membrane. The phage DNA (adsorbed phage

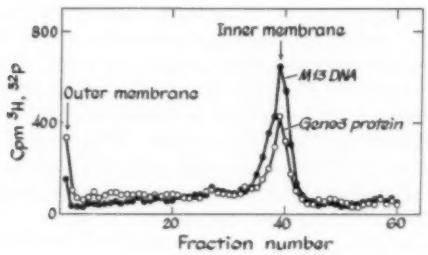

FIG. 4. Equilibrium sedimentation of gently lysed cells infected with phage labeled with ^{32}P and [^{3}H]histidine. Infection and lysis were performed as described in Fig. 3. A sucrose equilibrium gradient was separated into 6-drop fractions. Direction of sedimentation is from *right* to *left*.

and RF) was found in a fast-sedimenting form in lysates of infected cells (Fig. 3), cosedimenting with two membrane-bound enzymes, phospholipase A and DPNH oxidase (18). By contrast, free phage added to infected cells (Fig. 3, insert) or to uninfected cells after lysis were not recovered in a fast-sedimenting form. Thus, the association of the DNA of adsorbed phage and parental RF with the cell envelope fraction is probably not a simple artifact of secondary adsorption in the lysate. In contrast to wild-type phage DNA, which is associated with the cell envelope upon an infection at both 30° and 42°, *ts* 3 H-8 phage DNA was not associated at either temperature.*

When gently lysed cells (infected as in Fig. 2) were applied to a sucrose density gradient and centrifuged to equilibrium (Fig. 4), both labels cosedimented at the density of 45% sucrose, the position of the inner membrane, as determined by DPNH oxidase, a marker for the inner membrane (18). The outer membrane banded at 60–65% sucrose in this gradient (Fig. 4), as judged by phospholipase A, a marker for the outer membrane (Marco and Kornberg, unpublished results and ref. 18). Cell DNA banded in the region of outer membrane, with only a trace (1%) in the inner membrane region.

Association of infecting phage DNA with the inner cell membrane was observed with *E. coli* HfrC, as well as with *E. coli* 5274; results were the same in GCA medium as in H-broth.

Solubilization of the inner membrane fraction with Sarkosyl released both phage and RF, as determined by sucrose gradient sedimentation.

Growth of ts 3-Infected Cells at Nonpermissive Temperature. The growth curve of *ts* 3-infected cells (su$^-$) at 42° resembles the growth curve of uninfected and *am* 2-infected cells, in contrast to the growth curves for *am* 5- and wild-type-infected cells (Fig. 5). The *am* 2 phage are blocked early in the infectious process and, therefore, do not accumulate RF as do other amber mutants and wild-type phages (13). The fact that *ts* 3-infected cells display a growth curve similar to

* The inability to recover *ts*3 H-8 phage DNA with the cell envelope upon lysis of cells infected at 30° or 42° may be due to the lability of the association. In contrast, *ts*3 H-2 phage DNA was recovered with the cell envelope upon lysis of cells infected at 30°; upon infection at 42° this association was greatly reduced. (*ts*3 H-8 yields 10-fold lower titers at 30° than *ts*3 H-2 or M13 wild-type).

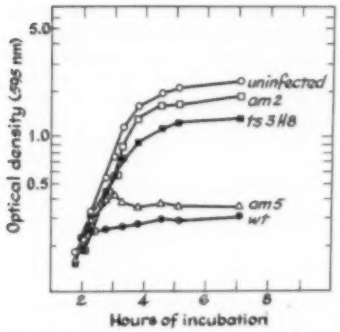

FIG. 5. Growth curves of phage-infected cells at 42°. *E. coli* HfrC cells were grown to 0.15 OD_{595} in Marvin medium and infected with wild-type and mutant M13 phage (MOI = 50) at 42°.

that of *am* 2-infected cells suggests that here too there is a block in an early event of infection. The nearly normal growth curve with *ts* 3 also indicates that this infection, unlike that of the wild-type phage, does not severely depress cell metabolism at 42°.

Complementation of ts3 and Amber Mutants. Can the *ts*3 phage adsorb to and penetrate the cell at the nonpermissive temperature? Complementation tests between *ts*3 and either *am* 2 or *am* 5 mutants indicate it can (Table 1). In su$^-$ cells at 42°, the *ts*3 complemented with both amber mutants as effectively as did the contrc' *am* 2 with *am* 5, which normally complement under these conditions.

TABLE 1. *Complementation of ts3 and amber mutants*

Type of infection	10^7 Infectious centers		% Complementation	
	Exp. I	Exp. II	Exp. I	Exp. II
*ts*3 H-2	<0.1	<1	—	—
*ts*3 H-8	<0.1	—	—	—
*am*2	<0.1	<1	—	—
*am*5	<0.1	<1	—	—
*ts*3 H-2 + *am*2	70.0	14	28.0	7.0
*ts*3 H-2 + *am*5	6.0	3	2.5	1.5
*ts*3 H-8 + *am*2	9.4	—	3.7	—
*ts*3 H-8 + *am*5	7.5	—	3.0	—
*am*2 + *am*5	3.7	13	1.8	6.5

E. coli HfrC were grown to 0.5 OD units at 595 nm in Marvin medium at 37° and concentrated 10-fold by pelleting and resuspension in this medium. Aliquots (0.1 ml) of this suspension were incubated at 42° for 10 min. 1–30 μl samples of phage dilutions (that had been incubated for 15 min at 42°) were added as designated in the table [multiplicity of infection (MOI) = 50 for each phage mutant and incubated for a further 10 min at 42°. The suspensions were then diluted 10^7-fold with Marvin medium (42°) and plated on *E. coli* HfrC at 42° (14, 16). Plaques were counted and infectious centers were thus determined. A mock infection was performed and the cell suspension was diluted 10^7-fold and plated directly (Exp. I: 250 × 10^7 cells per ml; Exp. II: 200 × 10^7 cells per ml). All steps were done at 42°. Percent complementation was calculated as:

[infectious centers/(250 × 10^7 or 200 × 10^7)] × 100.

TABLE 2. *Single-strand to RF conversion in ts 3 and wild-type infections at 30° and 42°*

Type of infection	30°		42°	
	Min	% RF	Min	% RF
*ts*3	0	0	0	0
	5	25	5	0
	10	33	15	0
Wild-type	0	0	0	0
	10	24	10	49
	30	59	30	60

E. coli 5274 cells were grown to 0.7 OD_{355} in Marvin medium at 37°, concentrated 3-fold by pelleting and resuspension in this medium, incubated for 10 min at either 30° or 42°, and infected with wild-type or *ts*3 H-8 phage (labeled in the DNA) at an MOI = 5 for the indicated times. Infection was stopped by addition of NaCN to 0.02 M and chilling to 0°. Cells were lysed and sedimented as described in Fig. 2. Percent RF was calculated from the gradients by summing up the counts in the phage and RF peaks; values of 4% or less were not detectable and were recorded as 0%.

The success of this complementation experiment argues that the *ts*3 phage adsorbs to and penetrates the cell at a nonpermissive temperature. It also argues that gene-3 protein produced by the amber mutant acted in a *trans* fashion in the conversion of the *ts*3 DNA to its RF, so that the RF would be enabled to express the gene functions defective in the amber mutants.

However, the complementation results do not measure effects of the gene-3 protein on the rates of adsorption and penetration. When adsorption was measured by sedimentation of ^{32}P-labeled phage with the cells, similar values were found for *ts*3 H-8 at 30° and 42°. At multiplicities of infection of 1–10 and at times of 0–15 min after mixture with the cells, the values for adsorption of wild-type phage at 30° and 42° were in the same range as for *ts*3 H-8.

Single-Strand to RF Conversion in ts3 Infection at 42°. Since *ts*3 phage penetrate the cell at 42°, it is possible to use this mutant to study the role of gene-3 protein in the conversion of single strands to RF. The conversion upon infection of cells with parental-labeled *ts*3 at 30° and 42° was determined at various times after infection by velocity sedimentation of cell lysates (Table 2); control determinations were made with wild-type phages. The single-strand to RF conversion of *ts*3 phage DNA was comparable to that of wild-type phage at 30°. At 42°, however, there was no conversion of *ts*3 phage DNA, while that of the wild-type phage remained at a high level. At 30°, the single-strand conversion to RF was inhibited by rifampicin but not by chloramphenicol in *ts*3 infections, just as in wild-type infections (5).

DISCUSSION

It had been accepted that the first stage in replication of the M13 phage, the conversion of the parental single strand to the duplex replicative form, required only the operation of host-cell proteins (1). Inasmuch as the infection progressed up to this point in the presence of high concentrations of chloramphenicol, it was clear that the new expression of host genes was not required. However, as the results to be discussed show, there is, nevertheless, an involvement of a viral gene product in this initial replicative event. It is a minor protein component of the phage, one coded by gene 3. The gene-3 protein, which appears to have a role in adsorption of the phage (3), enters the cell with the phage DNA and is fully conserved as part of a complex with the replicative form. Inasmuch as phage mutants with a defective gene-3 protein fail to form the replicative form, the functions of this protein in replication may be essential.

Relatively little is known at the molecular level about how M13 is adsorbed and decapsidated, and how its DNA penetrates the cell membrane. There have been indications that uncoating of the phage is coupled to DNA replication and that the phage single-strand never appears as a free intermediate (Forsheit, A. B. and Ray, D. S., personal communication). Our results support this view. In the presence of rifampicin, which blocks initiation of DNA replication (5), the phage are irreversibly attached to the cell, but there is no release of the DNA. There are 2–3 phages per cell, corresponding to the accepted number of F-pili and adsorption sites. Such attached phages have lost their infectivity (Jazwinski, Marco, and Kornberg, unpublished results) and have become susceptible to DNase, but their buoyant density has not been detectably altered. These phages, as well as the parental RF produced in the absence of rifampicin, retain the gene-3 protein molecules without loss (Fig. 2).

The significance of the gene-3 protein for DNA replication rests on three lines of evidence. To begin with, it is retained in cells in an amount stoichiometric with the phage DNA, and it persists as a complex with the parental RF. This behavior is unlike that of the gene-8 capsid protein, variable amounts of which remain in the cell membrane (21, 22). Secondly, a mutant that is temperature sensitive (*ts*) in gene 3 fails at an elevated temperature to produce RF, as judged by direct analysis (Table 2) and as may be inferred from the nearly normal growth rate of infected cells (Fig. 5). Finally, such *ts* mutants complement amber mutants in later functions (Table 1). The capacity of the *ts* gene-3 to exchange functions with *amber* gene-2 and gene-5 mutants in a mixed infection indicates not only that the *ts*-3 phage can adsorb to and penetrate the cells at a restrictive temperature, but that the gene-3 protein produced by the amber mutants acts in a *trans* fashion to permit the *ts*-3 replicative form to be made. These results do not necessarily conflict with earlier findings in which the involvement of the gene-3 protein in phage adsorption (1, 3) may have rested on kinetic factors.

An essential role for a viral protein in the first stage of replication of its chromosome may be of general significance. The findings described here for M13 resemble those reported for the small RNA phages, which also exploit the F-pilus for attachment and penetration. The maturation protein of MS2 enters infected cells (23, 24), and may be essential for the regulation of early events in the expression of the chromosome. We have extended our work to phage ϕX174, which relies on cell wall receptors for adsorption (ref. 25; Jazwinski, Marco, and Kornberg, unpublished results) and have found that the isolated parental RF has one or a few molecules of a unique phage coat protein associated with it (Jazwinski, Marco, and Kornberg, unpublished results). Should this prove to be a coat protein essential for infection, then the similarity with the M13 results would indeed be strong. One might speculate further that a diligent search for an analogous protein in all

bacterial and animal viruses would reveal a widespread need for such an element in the infective process.

Assuming that the gene-3 protein participates in the initial replication of phage DNA, what might its functions be? Our results on the association of the irreversibly adsorbed phage and the parental RF with the inner cell-membrane fraction of the cell (Figs. 3 and 4) (26) suggest that the gene-3 protein may link the phage DNA to a cellular replicative system in or near the membrane. Such a structural orientation or sequestration of the viral chromosome may, in fact, be essential if it is to compete successfully for a replicative system ordinarily reserved for host DNA elements. This role for the gene-3 protein, which is dispensable in soluble enzyme systems that replicate viral single strands (6, 7), may have to be sought at an earlier stage of phage uncoating at the cell membrane.

This work was supported in part by grants from the National Institutes of Health and the National Science Foundation. R. M. is an International Fellow of the National Institutes of Health, on leave of absence from Instituto de Enzimologia, Madrid, Spain.

1. Marvin, D. A. & Hohn, B. (1969) *Bacteriol. Rev.* **33,** 172–209.
2. Caro, L. G. & Schnös, M. (1966) *Proc. Nat. Acad. Sci. USA* **56,** 126–132.
3. Tzagoloff, H. & Pratt, D. (1964) *Virology* **24,** 372–380.
4. Pratt, D. & Erdahl, W. S. (1968) *J. Mol. Biol.* **37,** 181–200.
5. Brutlag, D., Schekman, R. & Kornberg, A. (1971) *Proc. Nat. Acad. Sci. USA* **68,** 2826–2829.
6. Wickner, W., Brutlag, D., Schekman, R. & Kornberg, A. (1972) *Proc. Nat. Acad. Sci. USA* **69,** 965–969.
7. Schekman, R., Wickner, W., Westergaard, O., Brutlag, D., Geider, K., Bertsch, L. L. & Kornberg, A. (1972) *Proc. Nat. Acad. Sci. USA* **69,** 2691–2695.
8. Forsheit, A. B. & Ray, D. S. (1971) *Virology* **43,** 647–664.
9. Asbeck, F., Beyreuther, K., Köhler, H., von Wettstein, G. & Braunitzer, G. (1969) *Hoppe-Seyler's Z. Physiol. Chem.* **350,** 1047–1066.
10. Henry, T. J. & Pratt, D. (1969) *Proc. Nat. Acad. Sci. USA* **62,** 800–807.
11. Scandella, C. J. & Kornberg, A. (1971) *Biochemistry* **10,** 4447–4456.
12. Pratt, D., Tzagoloff, H. & Erdahl, W. S. (1966) *Virology* **30,** 397–410.
13. Pratt, D., Tzagoloff, H. & Beaudoin, J. (1969) *Virology* **39,** 42–53.
14. Salivar, W. O., Tzagoloff, H. & Pratt, D. (1964) *Virology* **24,** 359–371.
15. Marvin, D. A. & Schaller, H. (1966) *J. Mol. Biol.* **15,** 1–7.
16. Ray, D. S. & Schekman, R. W. (1969) *Biochim. Biophys. Acta* **179,** 398–407.
17. Yamamoto, K. R., Alberts, B. M., Benzinger, R., Lawhorne, L. & Treiber, G. (1970) *Virology* **40,** 734–744.
18. Osborn, M. J., Gander, J. E., Parisi, E. & Carson, J. (1972) *J. Biol. Chem.* **247,** 3962–3972.
19. Jovin, T., Chrambach, A. & Naughton, M. A. (1964) *Anal. Biochem.* **9,** 351–369.
20. Tseng, B. Y. & Marvin, D. A. (1972) *J. Virol.* **10,** 371–383.
21. Trenkner, E., Bonhoeffer, F. & Gierer, A. (1967) *Biochem. Biophys. Res. Commun.* **28,** 932–939.
22. Henry, T. J. & Brinton, C. C. (1971) *Virology* **46,** 754–763.
23. Krahn, P. M., O'Callaghan, R. J. & Paranchych, W. (1972) *Virology* **47,** 628–637.
24. Kozak, M. & Nathans, D. (1971) *Nature* **236,** 209–211.
25. Newbold, J. E. & Sinsheimer, R. L. (1970) *J. Mol. Biol.* **49,** 49–66.
26. Griffith, J. & Kornberg, A. (1972) in *Membrane Research,* ed. Fox, C. F., (Academic Press, New York), pp. 281–292.

Proc. Nat. Acad. Sci. USA
Vol. 70, No. 1, pp. 210–214, January 1973

An Alteration in Glucose Metabolism Associated with a Defect in Ketone Body Metabolism

(skin fibroblasts/coenzyme A/transferase/pyruvate/Embden–Myerhof pathway)

J. TYSON TILDON

Departments of Biological Chemistry and Pediatrics, University of Maryland School of Medicine, Baltimore, Md. 21201

Communicated by Saul Roseman, November 10, 1972

ABSTRACT **Skin fibroblasts (CC-69) cultured from a patient with a unique syndrome of ketoacidosis associated with coenzyme A transferase (EC 2.8.3.5) deficiency showed an altered pattern of carbohydrate metabolism. These cells used glucose at a rate significantly less than controls (125 against 680 nmol/mg per hr). The oxidation of [6-^{14}C]-glucose to $^{14}CO_2$ by these cells was also significantly diminished (12 against 350 pmol/mg per hr), but [2-^{14}C]-pyruvate and [*1,4*-^{14}C]succinate oxidation by these cells did not differ from that by control cells. Measurements of glycolytic intermediates showed a reduction of several intermediates in the CC-69 cells that confirmed an inhibition of glycolysis between fructose-1,6-bisphosphate and pyruvate. The apparent inhibition in these cells could be reversed by an extended incubation of the cells in a buffered glucose solution. After 18 hr of incubation in 2.5 mM glucose, glucose uptake by the CC-69 cells increased 20-fold to 2560 nmol/mg per hr, whereas the rate for control cells remained constant at 640 ± 90. Concomitant with this increase, [6-^{14}C]glucose oxidation rose from 8 to 2261 pmol/mg per hr while controls remained constant at 428 ± 175. This change was not due to new enzyme formation because incubation with puromycin had no effect on the increased use of glucose. Mixing experiments demonstrated no transfer of a permeable inhibitor or activating substances. In view of the deficiency of coenzyme A transferase in these cells, the data suggest an indirect regulatory role for this enzyme in peripheral tissue glycolysis.**

Cultivation of human fibroblast cell strains provides a unique system for *in vitro* metabolic studies, and the use of explants from human skin biopsies has permitted the precise definition of several inborn errors of metabolism (1–3). Carbohydrate metabolism in cells in culture has been studied under various experimental conditions (4–7), and extensive reviews by Levintow and Eagle (8), Paul (9), and Cristofalo, Howard, and Kritchevsky (10) have documented that the metabolic processes of cells in tissue culture were consistently similar.

Investigations in this laboratory have described an alteration in the oxidation of labeled glucose in the tissue culture fibroblasts (CC-69) derived from a skin biopsy from an infant with an unknown form of ketoacidosis (11, 12). Subsequent reports have shown that the ketoacidosis in that infant was associated with a deficiency of Succinyl-CoA: 3-ketoacid CoA transferase (CoA transferase) (EC 2.8.3.5) (13, 14). The continued study of this cell strain offers a unique opportunity for the understanding of cellular metabolism.

It is the purpose of this report to further describe the alterations and irregularities in glucose metabolism in CC-69 cells and to contrast the metabolic processes in those cells with those in tissue culture fibroblast explants from normal controls. These data suggest an interrelationship between glucose metabolism and the oxidation of ketone bodies.

MATERIALS AND METHODS

Skin fibroblasts were grown from skin obtained by a punch biopsy from an infant with severe ketoacidosis who was shown to have a deficiency in CoA transferase (14). Control cell lines were derived from the foreskins and diagnostic skin biopsies of children with no evidence of ketoacidosis. All fibroblasts were maintained in culture in 8-oz bottles in Eagle's Minimal Essential Medium (Grand Island Biological Co., Grand Island, N.Y.) with added glutamine (1.8 mM), penicillin (56 μg/ml), streptomycin (90 μg/ml), and fetal-calf serum (10%). Periodic tests for contamination by bacteria and mycoplasma were negative.

For metabolic studies, cells were grown directly in 25-ml tissue culture reaction flasks (Kontes Glass Co., Vineland, N.J.), and were used 3–5 days after replating. After the medium was decanted and the adherent cell layer rinsed twice with warm Krebs–Ringer phosphate buffer (pH 7.4), 2 ml of the buffer containing labeled substrate was then added and each flask was capped with a soft rubber stopper with an attached plastic center well (Kontes) containing fluted filter papers (15). ^{14}C-Labeled substrates, 1.0 μCi per flask (New England Nuclear Corp., Boston, Mass.), were used without further purification. Except when otherwise noted, incubations were done at 37° in a Dubnoff metabolic shaker at a rate of 60 cycles/min for 2 hr.

At the end of the incubation period, 0.3 ml of 20% Cl_3CCOOH was injected into the flask by needle and syringe to kill the cells and to volatilize the CO_2, which was trapped in the center well containing 0.2 ml 5 N KOH. After 60 min of equilibration in the cold, the caps were removed. The center well, including its contents, was placed into 12 ml of dioxane base scintillation fluid for counting. Efficiencies, determined by the channels-ratio technique, ranged from 40 to 80%. Corrections for nonspecific or background radioactivity were obtained from flasks that had been autoclaved before the incubation or to which Cl_3CCOOH had been added before the substrate. Results were expressed as pmol of substrate converted to CO_2 per mg of protein per hr. In a series of experiments, the quenching effect of 0.2 ml of 5 N KOH was determined, as outlined above, and found to be constant. The results, when corrected for quenching, were consistent with experimental results obtained with hyamine hydroxide as the CO_2 absorbent.

In the system described above, $^{14}CO_2$ production was linear for a 6-fold range in protein concentration (0.06–0.36 mg of protein per flask) and for incubation periods of 2–4 hr. Although CC-69 cells required more time than control lines to reach confluency or a given protein concentration, the oxidation rates for a given substrate were similar for a given cell line on days 3, 4, and 5. Since relatively low substrate concentrations were used and no attempt was made to measure intracellular substrate pools, these results represented minimal values.

Glucose utilization experiments were performed in a similar manner, except that sterilized rubber stoppers were used to cap the flasks. Sterile glucose, 2.5 mM, in Krebs–Ringer phosphate buffer was added to each flask. At timed intervals, 0.2 ml of the supernatant reaction mixtures was removed and precipitated to prepare a Somogyi filtrate (16). Glucose was measured by a glucose oxidase method (17); lactate was measured enzymatically by dye reduction with diaphorase as a coupler (18). Protein concentrations were determined by the method of Lowry *et al.* (19) on the total reaction mixture after brief sonication to insure complete suspension of the cell protein. This allowed for the accurate protein determinations since no transfer of cells was necessary.

Glycolytic and Krebs cycle intermediates were measured by Dr. Oliver H. Lowry using fluorometric-enzymatic analysis with DPN or TPN indicator systems as described (20).

RESULTS

The results of oxidation of five different substrates to CO_2 by tissue culture cells are given in Table 1. The oxidation of pyruvate, succinate, and propionate was essentially the same in both CC-69 cells and controls. In contrast, the rate of $^{14}CO_2$ production from [6-^{14}C]glucose by the CC-69 cells was less than 5% of that of the control cells (Table 1). The rate of $^{14}CO_2$ production by CC-69 cells when [1-^{14}C]glucose was used, was about 50% that of the controls. These differences were independent of substrate concentration, which was varied from 0.1 to 2.5 mM.

These results suggested an inhibition of glucose oxidation via the Embden–Myerhof pathway between glucose and pyruvate in CC-69 cells. This conclusion was further supported by the inability of 2.5 mM unlabeled glucose to significantly reduce the pyruvate oxidation in the test cells (710 against 590 pmol/mg per hr) in contrast to a 4-fold reduction in control cells (940 against 210 pmol/mg per hr) (Table 1).

TABLE 1. *Substrate oxidation by tissue culture cells**

Substrate (mM)	CC-69 cells	Control cells
[1-^{14}C]Glucose (0.1)	670 ± 135	1420 ± 120†
[6-^{14}C]Glucose (0.1)	12 ± 4	350 ± 150†
[2-^{14}C]Pyruvate (0.13)	710 ± 158	940 ± 110
[2-^{14}C]Pyruvate (0.13) + glucose (2.5)	590 ± 200	210 ± 45†
[1-^{14}C]Propionate (0.05)	55 ± 8	65 ± 13
[1,4-^{14}C]Succinate (0.05)	73 ± 16	45 ± 8

* Values are expressed as pmol of substrate oxidized to CO_2 per hr per mg of protein. Each value is the average of six or more determinations ± SEM.

† Significant differences ($P < 0.05$) between the values for the test cells and controls.

TABLE 2. *Glycolytic intermediates* in tissue culture cells*

	Control	CC-69
Glucose-6-phosphate	0.32 ± 0.08	0.33 ± 0.05
Fructose 1,6-bisphosphate	0.31 ± 0.05	0.06 ± 0.01†
Dihydroxyacetone phosphate	0.14 ± 0.04	0.06 ± 0.01†
3-Phosphoglyceric acid	0.34 ± 0.06	0.03 ± 0.04†
Citrate	1.38 ± 0.18	0.52 ± 0.11†
Malate	0.91 ± 0.31	0.34 ± 0.09
Phosphocreatine	0.80 ± 0.12	0.65 ± 0.18
Adenosine triphosphate	4.12 ± 0.49	3.15 ± 0.40

For these experiments six flasks with subcultivated test and control cells (8–11 passages) were used. After 4 days, the growth media were removed, and cells were washed twice with Krebs–Ringer phosphate buffer. The cells were frozen within 30 sec in liquid nitrogen at −196°. Samples were stored at −80° until analysis. Extracts were prepared by addition of 200 μl of 3.3 M $HClO_4$ to each flask at −10°. After the ice had been dissolved, 10 μl of 10 mM EDTA was added followed by H_2O to a volume of 450 μl. The mixture was centrifuged, and 392 μl of supernate was neutralized with 310 μl of 2 M $KHCO_3$. For each analysis, 50–100 μl were used, equivalent to 5–10% of each sample.

* μmol/g wet weight of tissue ± SD.

† As in Table 1.

The concentration of six glycolytic intermediates, phosphocreatine, and ATP was measured in both CC-69 and control cells during proliferation. The concentration of glucose-6-phosphate per gram wet weight of cells was essentially the same in both CC-69 cells and the control cell populations. But the concentrations of fructose 1,6-bisphosphate, dihydroxyacetone phosphate, and 3-phosphoglyceric acid in CC-69 cells were significantly less than those in the control (Table 2). The concentrations of the two Krebs cycle intermediates, citrate and malate, were also significantly less in the test fibroblasts than in the controls. On the other hand, ATP and phosphocreatine concentrations were similar in extracts from control and test cells (Table 2). These results, in conjunction with the substrate-oxidation experiments, demonstrate that there is a definite alteration in glucose metabolism between the formation of glucose-6-phosphate and pyruvate in CC-69 cells.

Preliminary experiments reported earlier suggested a difference between the rate of glucose use by CC-69 cells and by control cells (12). The results diagrammed in Fig. 1 show that control cells used glucose at a constant rate when measured at 6- and 12-hr intervals for 24 hr. In contrast, there was a dramatic change in the rate of glucose use for the same period by the CC-69 fibroblasts. During the first 12 hr. CC-69 cells used 125 nmol of glucose per hr per mg of protein, which was less than 25% the rate of control cells (600 nmol/hr per mg). During the last 5-hr period (18–23 hr) the rate of use by CC-69 was almost four times that of the control (2200 against 580 nmol/hr per mg).

The concentration of lactate measured in the same incubation media decreased from 9.1 to 5.3 to 2.42 μmol/mg of protein at 12, 18, and 23 hr, respectively, in flasks with control cells. In the flasks with CC-69 cells, the concentrations that were consistently lower also showed a decrease from 2.9 to 0.9 to 0.0 μmol/mg of protein at the same time periods. The net lactate-production rates calculated from these data for

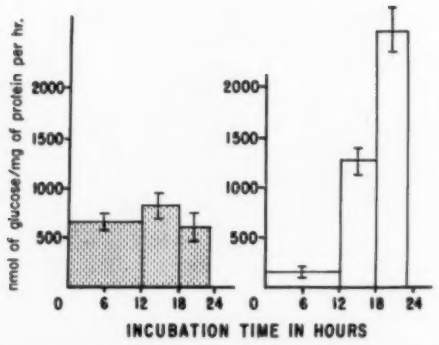

FIG. 1. The rate of glucose use by fibroblasts in culture. In these experiments, 1 to 3 × 10^5 monolayered cells in 25-ml flasks were incubated in 2.5 mM of sterile buffered glucose solution (pH 7.4) for 23 hr. Aliquots were taken at 12, 18, and 23 hr to measure glucose and lactate. The *open areas* represent the CC-69 cells, and the *shaded areas* represent the control cells. The results are expressed as the average nmol of glucose used per hr per mg of protein ± SEM.

the first 12 hr were 240 and 760 nmol/mg per hr for the CC-69 cells and control cells, respectively. This three-fold difference in the rate of lactate production for the CC-69 and control cells is similar to the difference in the rates of glucose use cited above. During the succeeding time intervals, there appeared to be a net lactate consumption by both types of cells, even when there was an increased use of glucose by the CC-69 cell line.

At least two possible mechanisms could be responsible for this striking change in the rate of glucose use in these cells. These include the induction of a critical enzyme or a possible decrease in the concentration of an inhibitor after extended incubation. The results in Fig. 2 show that the increasing rate of glucose use by CC-69 cells during a 24-hr incubation period was the same in the presence or absence of 1 mg/ml of puromycin. This would suggest that the increased rate of utilization was not the result of an induction *de novo* of enzyme.

In an experiment to determine whether the oxidation of [*6*-^{14}C]glucose to $^{14}CO_2$ by CC-69 cells could be correlated with the increased rate of glucose use, reaction flasks with equal amounts of cells were divided into two groups: those that were tested immediately after the removal of complete growth media and those that were tested for [*6*-^{14}C]-glucose oxidation after extended incubation in buffered glucose. The rate of [*6*-^{14}C]glucose oxidation by CC-69 cells immediately after their removal from growth media was essentially zero. In contrast, those cells that had been incubated in a medium with 2.5 mM glucose for 15–18 hr, oxidized [*6*-^{14}C]glucose to $^{14}CO_2$ at an average rate of more than 1900 nmol/hr per mg (Fig. 3). This represents more than a 100-fold increase in the rate of glucose oxidation by these cells. On the other hand, similar preincubation of control fibroblasts in glucose did not result in a significant change in the rate of oxidation by these cells.

The CC-69 cells were preincubated in glucose for 18 hr, then reincubated for another 6 hr in complete media. The rate of oxidation of [*6*-^{14}C]glucose was again essentially the same low rate as was observed in those cells that had not been preincubated in glucose (Fig. 4). Cells that had been preincubated in buffered glucose for 24 hr oxidized glucose at a rate similar to that of cells incubated for 18 hr. This result demonstrated that the decrease in oxidation was not the result of the additional 6-hr incubation.

The results of the use of glucose as well as the specific oxidation of [*6*-^{14}C]glucose suggest a reversible inhibition of glucose oxidation. The incubation of control cells with growth media from CC-69 cells for various periods up to 12 hr resulted in a significant decrease in the rate of [*6*-^{14}C]glucose oxidation by the control fibroblasts. In a similar experiment there was no change in the oxidation of [*6*-^{14}C]glucose by CC-69 cells that were incubated in growth media from control cells.

DISCUSSION

The rate of glucose use by control cell strains that is in the range of 400–700 nmol/hr per mg of protein as reported above, is in good agreement with results reported by other authors (4, 22) and reflects the metabolic similarity of many human fibroblasts in culture. In contrast, the glycolysis by CC-69 cells is strikingly different from that of control cells either as reported here or as compared to results from other human diploid fibroblasts in culture.

Despite the variability of cell culture techniques, the rate of glucose use by human fibroblasts appears to be similar for most cell lines. There have been several reports that have described some exceptions to this consistent pattern.

Barnes and Melnykovych, in a brief note, reported that prednisolone induced changes in glucose metabolism (21), and Condon *et al.* (23) have shown differences between the glucose metabolism of fetal and nonfetal human fibroblasts. Recently, Warshaw and Rosenthal (24) have also described changes in glucose oxidation that occur during the growth of embryonic heart cells in culture. Studies in this laboratory have demonstrated that there is no difference between the glucose metabolism in cell strains from explants of human foreskin and in cells derived from biopsies from infants who ranged from one day to six months of life (Tildon and Stevenson, unpublished data). Therefore, it can be concluded that the significant

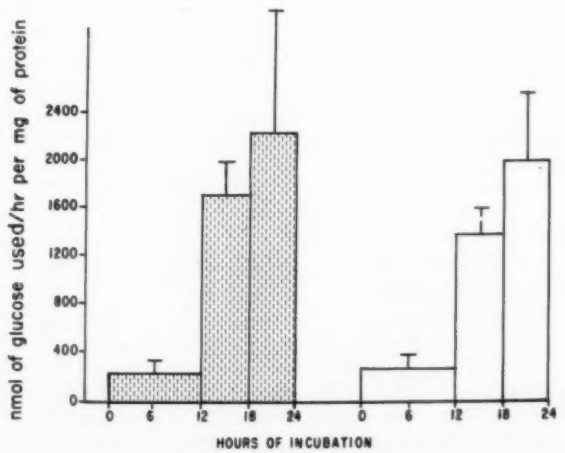

FIG. 2. Glucose use by CC-69 cells in the presence and absence of puromycin. The rate in the absence of puromycin is diagrammed by the *shaded areas*, and the rate in the incubation mixture containing 1 mg/ml of puromycin is represented by the *open areas*. The experimental methods are the same as those described in Fig. 1.

alteration in glucose metabolism observed in CC-69 cells represents a unique property of these fibroblast cells in culture.

The results described above indicate that glucose use and its subsequent oxidation via the Embden–Myerhof glycolytic pathway are both greatly reduced. The measurements of glycolytic intermediates indicate that the amount of glucose-6-phosphate in CC-69 cells is equivalent to the amount found in control cells. In contrast, the amounts of three other intermediates (fructose 1,6-bisphosphate, dihydroxyacetone phosphate, and 3-phosphoglyceric acid) were significantly reduced, as were citrate and malate. The use of labeled substrates supports the conclusion that there was a block in glycolysis in CC-69 fibroblasts. By use of [*1*-^{14}C]-glucose, the rate of labeled $^{14}CO_2$ produced by CC-69 cells was 45–50% that of control cells. In contrast, the rate of labeled CO_2 produced from [*6*-^{14}C]glucose by CC-69 cells was less than 5% of that of controls. The data also indicate a reduction in glucose use (Fig. 1), and it can be concluded that the reduced use of glucose by these cells was directly related to a block in glycolysis between G-6-P and pyruvate since labeled pyruvate was oxidized at a similar rate by both cell lines. However, this reduction seems not to be related to an alteration in glycolytic enzymes since other studies have shown that these enzymes were present in CC-69 cells in amounts similar to those found in control cells (14).

The block in glycolysis and consequent reduction in glucose use only occurred immediately after the cells were removed from growth media. Extended incubation of the cells in a buffered glucose solution consistently resulted in the reversal of the inhibition of glucose use. In addition, the increased use of glucose was correlated with an increase rate of [*6*-^{14}C]-glucose oxidation. The increased rate of use occurred even in the presence of added puromycin.

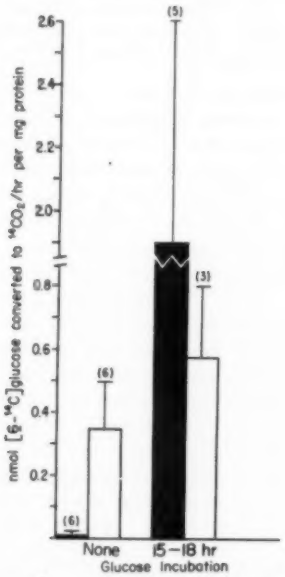

FIG. 3. Comparison of [*6*-^{14}C]glucose oxidation to CO_2 with and without prior incubation in buffered glucose. Growth media were decanted from CC-69 fibroblasts (■) and control fibroblasts (□) from normal males of similar ages. After two washes the cells were reincubated with either new media or buffered glucose for 15–18 hr. This solution was decanted, the cells were washed, and the rate of [*6*-^{14}C]glucose oxidation was measured by collection of $^{14}CO_2$ as described in the text. The apparent increase in oxidation by the control cells was not significant for the number of samples analyzed. The results are the average ± SEM. Numbers in parentheses are the number of individual sample flasks.

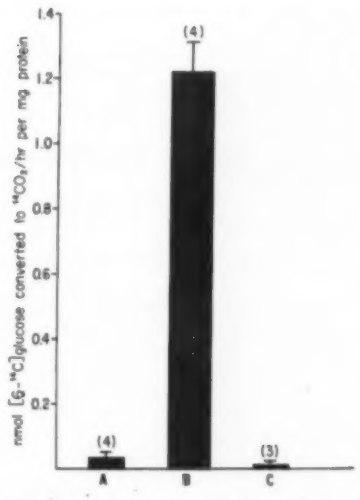

FIG. 4. The reversal of the increased [*6*-^{14}C]glucose oxidation by growth media. Growth media were decanted from CC-69 fibroblasts, which were then incubated with (*A*) new growth media; (*B*) buffered glucose for 24 hr; or (*C*) buffered glucose for 18 hr followed by new media for 6 hr. Oxidation of [*6*-^{14}C]glucose was measured simultaneously in all three groups by the method described in the text.

These data would suggest that a specific inhibitor of glycolysis accumulates only in the presence of total growth media, which include amino acids, vitamins, and serum. The specificity of the inhibitor is not immediately evident. However, since these cells were derived from a patient with CoA transferase deficiency and contained no CoA transferase activity, it seems reasonable to speculate that the inhibitor might be correlated with a deficiency of this ketone-using enzyme.

The results presented indicate that CC-69 cells do grow in minimal growth media even in the presence of an inhibited Embden–Myerhof pathway. Among alternate sources of energy for cell growth are the intact hexose monophosphate shunt and the oxidation of amino acids in the growth medium. The relatively consistent proliferation of these cells could be explained by the obligatory or preferential use of another substrate. One possible alternative is suggested by the work of Griffiths (22), who demonstrated that the growth yields of W138 cells (diploid human cells) for glutamine was about $^1/_3$ the growth yield for glucose. Two other reports (25, 26) suggest a unique metabolic role for glutamine. In one (26), more than 50% of this amino acid is converted to CO_2; Eagle *et al.* (27) have shown that glutamine is an essential metabolite for the growth of both HeLa cells and mouse L cells.

I thank Dr. Oliver Lowry for his willingness to analyze the fibroblasts for glycolytic intermediates and Dr. Marvin Cornblath for his valuable comments. The technical assistance of Joseph Stevenson is gratefully acknowledged. These studies were supported in part by research grants from the John A. Hartford Foundation and from the National Institutes of Child Health and Human Development (HD-03959-04 and HD-06291-01).

1. Hsia, Y. E., Scully, K. J. & Rosenberg, L. E. (1971) *J. Clin. Invest.* **50**, 127–130.
2. Okada, S. & O'Brien, J. S. (1969) *Science* **165**, 698–700.
3. Morrow, G., Mellman, W. J., Barness, L. A. & Dimitrow, N. V. (1969) *Pediat. Res.* **3**, 217–219.
4. Kruse, P. F. & Miedema, E. (1965) *Proc. Soc. Exp. Biol. Med.* **119**, 1110–1112.
5. Cristofalo, V. J. & Kritchevsky, D. (1965) *Proc. Soc. Exp. Biol. Med.* **118**, 1109–1113.
6. Moulder, J. W. (1970) *J. Bacteriol.* **104**, 1189–1196.
7. Cristofalo, V. J. & Kritchevsky, D. (1966) *J. Cell. Physiol.* **67**, 125–132.
8. Levintow, L. & Eagle, H. (1961) *Annu. Rev. Biochem.* **30**, 605–640.
9. Paul, J. (1965) "Carbohydrate and Energy Metabolism" in *Cells and Tissues in Culture*, ed. Willmer, E. N. (Academic Press, New York), Vol. 1, pp. 239–276.
10. Cristofalo, V. J., Howard, B. V. & Kritchevsky, D. (1970) *Res. Progr. Org. Biol. Med. Chem.* **2**, 95–146.
11. Tildon, J. T., Cornblath, M. & Stevenson, J. (1971) *Fed. Proc.* **30**, Abstr. 207.
12. Tildon, J. T., Leffler, A. T., Cornblath, M. & Stevenson, J. (1971) *Pediat. Res.* **5**, 518–522.
13. Cornblath, M., Gingell, R. L., Fleming, G. A., Tildon, J. T., Leffler, A. T. & Wapnir, R. A. (1971) *J. Pediat.* **79**, 413–418.
14. Tildon, J. T. & Cornblath, M. (1972) *J. Clin. Invest.* **51**, 493–498.
15. Umbreit, W. W. (1964) "The absorption of carbon dioxide," in *Manometric Techniques*, ed. Umbreit, W. W., Burris, R. H. & Stauffer, J. F. (Burgess Publishing Co., Minneapolis), 4th ed., p 12.
16. Somogyi, M. (1945) *J. Biol. Chem.* **160**, 69–73.
17. Marks, V. (1959) *Clin. Chem. Acta* **4**, 395–400.
18. Friedland, I. M. & Dietrich, L. S. (1961) *Anal. Biochem.* **2**, 390–392.
19. Lowry, O. H., Rosebrough, N. J., Farr, H. L. & Randall, R. J. (1951) *J. Biol. Chem.* **193**, 265–275.
20. Lowry, O. H., Carter, J., Ward, J. B. & Glaser, L. (1971) *J. Biol. Chem.* **246**, 6511–6521.
21. Barnes, P. R. & Melnykovych, G. (1970) *In Vitro* **6**, 240.
22. Griffiths, J. B. (1970) *J. Cell Sci.* **6**, 739–749.
23. Condon, A., Oski, F. A., Dimauro, S. & Mellman, W. J. (1971) *Nature New Biol.* **229**, 214–215.
24. Warshaw, J. B. & Rosenthal, M. D. (1972) *J. Cell Biol.* **52**, 283–291.
25. Cavender, F. L. (1971) *In Vitro* **6**, 383.
26. Stoner, G. D. & Merchant, D. J. (1971) *In Vitro* **6**, 383–384.
27. Eagle, H., Oyama, V. I., Levy, M., Horton, C. L. & Fleischman, R. (1956) *J. Biol. Chem.* **218**, 607–616.

Proc. Nat. Acad. Sci. USA
Vol. 70. No. 1, pp. 215–219, January 1973

Self-Complementarity of Terminal Sequences Within Plus or Minus Strands of Adenovirus-Associated Virus DNA*

(circular DNA/electron microscopy/length measurements/exonuclease III)

FRANK J. KOCZOT, BARRIE J. CARTER, CLAUDE F. GARON, AND JAMES A. ROSE

Laboratory of Biology of Viruses, National Institute of Allergy and Infectious Diseases, National Institutes of Health, Bethesda, Maryland 20014

Communicated by Robert W. Berliner, November 16, 1972

ABSTRACT **At least 70% of plus or minus strands of adenovirus-associated virus DNA contain self-complementary sequences at or near their termini. Self-annealing of these sequences generates circular molecules that are closed by duplex, hydrogen-bonded segments. The self-annealed segments are sensitive to exonuclease III and have a thermal stability comparable to that of double-stranded DNA molecules. Length measurements of double-stranded adenovirus-associated virus DNA molecules show a bimodal distribution, with the larger component being 10% shorter than SV40 DNA.**

The presence of self-complementary terminal sequences in single-stranded molecules of viral DNA has been observed previously only with DNA from adenoviruses. It is thus especially notable that adenovirus-associated virus replication is unconditionally dependent on a helper adenovirus. A possible role for terminal self-complementary sequences in viral DNA replication is suggested.

On the basis of hydroxyapatite chromatography data and their resistance to degradation by nuclease S_1, we recently concluded that minus strands of adenovirus-associated virus (AAV) DNA contain self-complementary nucleotide sequences (1). These studies suggested that over 50% of the strands contained self-annealed regions, estimated to represent up to 20–25% of the total DNA sequences. Although plus strands were not similarly studied, they also would be expected to contain self-complementary sequences.

In this report the presence of self-complementary sequences in both plus and minus strands of AAV DNA is confirmed by electron microscopy. After denaturation, plus or minus strands rapidly form stable, hydrogen-bonded circles. These circular structures indicate that the complementary sequences are located at or near the ends of the DNA strand. Depending on the method used to extract DNA from virions, the percentage of self-annealed molecules in minus or plus strand preparations ranged from 50 to 70%.

MATERIALS AND METHODS

Viral DNA. The preparation of ^{3}H-labeled, bromodeoxyuridine (BrdU)-substituted AAV type 2 (AAV-2) DNA and separation of the plus and minus strands of AAV DNA in CsCl gradients has been described (2). For extraction of DNA from virions, prolonged incubations with papain (12 hr) and trypsin (3 hr) have been used (3). To avoid possible breakage of DNA during these incubations, an alternative extraction procedure was used. DNA was efficiently released when purified virions were centrifuged into alkaline sucrose gradients. Fractions containing DNA were pooled and dialyzed against 0.2 M Tris·HCl (pH 8.5)–0.01 M EDTA at 4°. Comparison of alkaline sucrose sedimentation profiles of AAV-2 DNA extracted with NaOH (Fig. 1*A*) or with proteolytic enzyme (Fig. 1*B*) demonstrates that the latter technique produces considerable strand breakage.

DNA was digested with *Escherichia coli* exonuclease III (free of endonuclease activity) as before (4), except that the incubation temperature was increased to 45° (5, 6).

Electron Microscopy. Samples of DNA were mounted by either the formamide or aqueous techniques described by Davis *et al.* (7). Thermal denaturation of DNA was performed in the presence of 12% formaldehyde essentially as

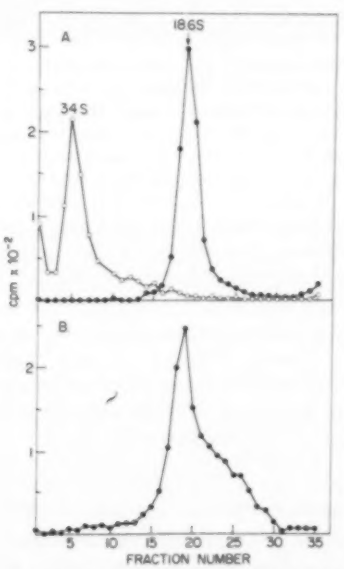

FIG. 1. Sedimentation of [^{3}H]BrdU-labeled DNA from AAV through 5–20% alkaline sucrose gradients. Gradients contained 0.3 N NaOH, 0.7 M NaCl, 1 mM EDTA, and 0.15% Sarkosyl. Centrifugation was for 3 hr at 42,000 rpm and 20° in a Spinco model 50.1 rotor. (*A*) Alkali-extracted DNA. (*B*) Enzyme-extracted DNA. (○) ^{32}P-labeled adenovirus type-2 DNA marker. BrdU-substituted AAV DNA sediments more rapidly than AAV DNA without BrdU (2).

Abbreviation: AAV, adenovirus-associated virus.

* Paper no. X in the series, "Adenovirus-Associated Virus Multiplication." Paper no. IX is ref. 1.

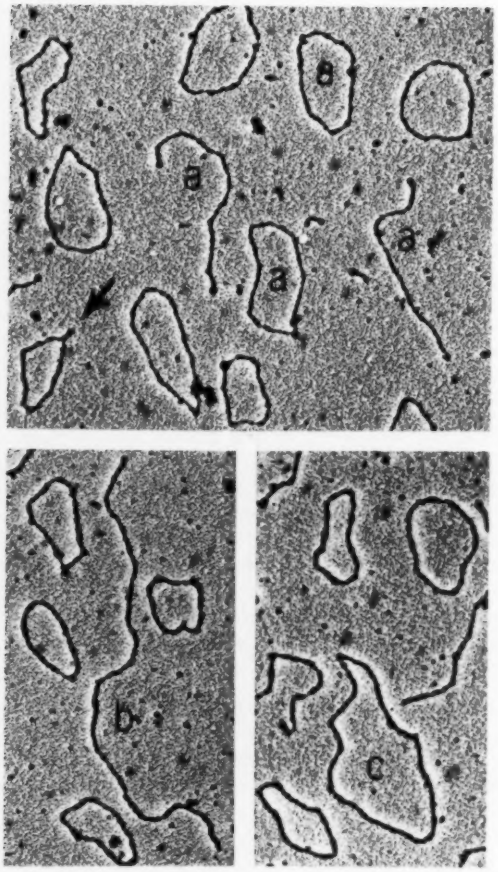

FIG. 2. Minus strand DNA. After preparative purification in CsCl, minus strands were dialyzed into 0.01 M Tris·HCl (pH 8.5)–1 mM EDTA and mounted for electron microscopy by the formamide technique, which permits visualization of extended single-stranded molecules. DNA concentration, 5 μg/ml. (*a*) Circular and linear monomers, (*b*) linear dimer, and (*c*) circular dimer. *Arrow* indicates projection. Magnification ×43,000. When DNA from the same preparation was mounted under conditions that promote collapse of single-stranded DNA (aqueous technique), linear or circular structures were not observed.

described by Doerfler and Kleinschmidt (8). Grids were examined in a Siemens Elmiskop 101 and photographed as described (4). Contour lengths of molecules were measured with a Rand Tablet and PDP-10 computer (Digital Equipment Corporation, Maynard, Mass.).

RESULTS

Electron microscopy of minus and plus strands

The apparent extent of minus strand self-annealing (1), which readily occurs during preparative separation in CsCl gradients, would be expected to produce distinctive structures that could be identified by electron microscopy. When molecules from minus strand preparations are mounted for electron microscopy by the formamide technique, both linear and circular structures are observed (Fig. 2). Identical results are also obtained with plus strand preparations. However, since minus strands are more easily purified than plus strands (2), studies were performed mainly with minus strands. DNA preparations shown in Fig. 2 were extracted from virions in 0.3 N NaOH, and the proportion of circular molecules is relatively high (70–75%). When DNA was extracted with proteolytic enzymes, the proportions of circular molecules was diminished (50–55%). This difference is probably due to less strand breakage during alkali extraction (Fig. 1*A* and *B*). It is notable that with minus strands prepared from enzyme-extracted DNA, the fraction of strands containing self-annealed sequences based on hydroxyapatite chromatography (1) is similar to that found to be circular by electron microscopy. The circular molecules present in plus or minus strand preparations thus appear to be generated by *intramolecular* annealing of complementary sequences located at or near each end of the DNA strand.

If minus or plus strands contain self-complementary terminal sequences, they should also be capable of producing specific structures as a result of *intermolecular* annealing reactions. As shown in Fig. 2, both linear and circular dimers can be seen. It must be noted, however, that linear and circular molecules either smaller or larger than those taken to represent the predominant monomeric species are also present in these preparations. This size variation may be due to technical factors, to the presence of true subspecies, or to both. The significance of the small projections (shown by the arrow in Fig. 2) seen on some linear and circular molecules is not clear. We have observed similar projections on single-stranded linear and circular SV40 DNA molecules spread under identical conditions, a result that suggests that these projections may represent preparational artifacts. Neither the size nor frequency of the projections was altered with higher concentrations of formamide.

Since the formation of circular molecules apparently results from self-annealing during strand purification in CsCl, it should be possible to open circles by alkali denaturation and to subsequently reform them under conditions of renaturation. Furthermore, the ability to efficiently denature circular molecules would indicate that covalently closed strands are absent. The experiment shown in Fig. 3 demonstrates that circular molecules are completely denaturable and that they are rapidly and efficiently reformed during renaturation (50% reformation within 10 min). In addition, the initial fraction of circles did not significantly increase during incubation under annealing conditions, suggesting that maximal self-annealing is achieved during preparative separation of the strand species.

The above data indicate that circular molecules are closed by a duplex, hydrogen-bonded segment. As further evidence for this mechanism of closure, it was observed that circular molecules were converted to linear forms when they were

TABLE 1. *Treatment of minus strand circles with exonuclease III*

Incubation time (min)	% Circular molecules*	
	+Enzyme	−Enzyme
0	67	67
2	37	63
4	29	66

* 200 Molecules were scored in each sample.

treated with exonuclease III (Table 1), which specifically cleaves nucleotides from the 3′ ends of polynucleotide chains in duplex molecules (5). There was a 57% reduction in circular molecules after 4 min of incubation. The use of exonuclease III in confirming the duplex, hydrogen-bonded closure of circular, single-stranded adenovirus DNA molecules has been described in detail (4, 6).

The stability of the hydrogen-bonded closure of single-stranded AAV DNA circles was tested by thermal denaturation in 12% formaldehyde. Temperatures that produced a 50% or greater denaturation of double-stranded AAV DNA molecules that contained BrdU (54° and 56°) were required to convert single-stranded circles to linear forms (conversions of 53 and 96%, respectively). This finding is consistent with a highly ordered base-pairing between sequences involved in cyclization of DNA strands.

Electron microscopy of double-stranded AAV DNA

Double-stranded AAV DNA is formed by an annealing of plus and minus strands after their release from virions (9). When these preparations of extracted DNA are mounted for electron microscopy by either the aqueous or formamide procedures, aggregated masses of DNA strands, branched and unbranched molecules, and occasional circular structures are observed. However, denaturation and reannealing of this DNA, as described in Fig. 4, prevents molecular aggregations and produces about equivalent proportions of single- and double-stranded molecules. An electron micrograph of reannealed DNA, mounted by the aqueous procedure, is shown in Fig. 4. Since, as previously noted, only duplex molecules remain extended during aqueous mounting, the circular molecules seen must be double-stranded. Double-stranded circles could be found in all preparations of reannealed DNA mounted by the aqueous technique, and accounted for 5–15% of the total molecules. The presence of covalently closed, double-stranded circular molecules in extracted AAV DNA is argued against by the absence of a fast-sedimenting component in alkaline sucrose gradients (J. A. Rose *et al.*, unpublished experiments). Therefore, it seems likely that the observed double-stranded circles arise from annealing of intact strands with either strands missing some or all of their terminal sequences, or with a subpopulation of permuted strands.

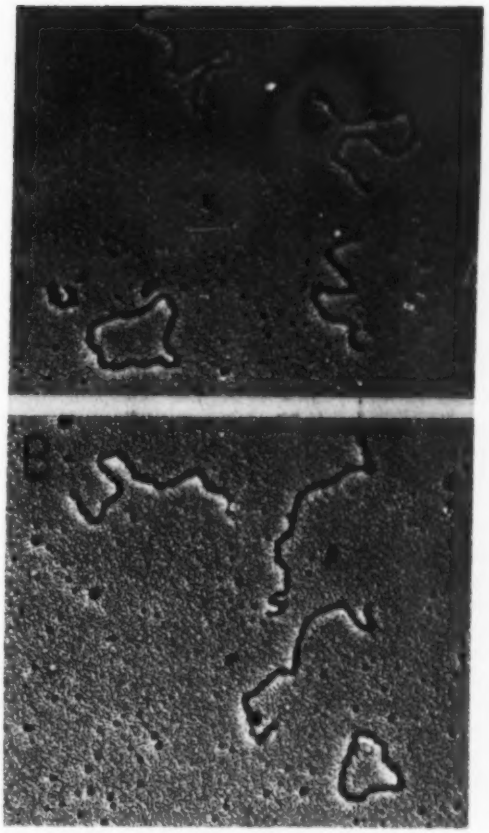

FIG. 4. Double-stranded AAV DNA. DNA was extracted from virions with NaOH. Conditions for denaturation and renaturation of DNA (5 μg/ml) as in Fig. 3. Renaturation was done for 30 min, and DNA was mounted by the aqueous technique. Small circular molecules (panel *B*) were infrequent. Magnification ×38,000.

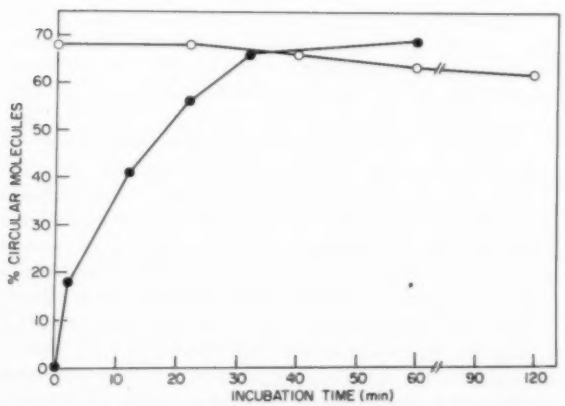

FIG. 3. Reformation of single-stranded circles after denaturation. Minus strands were denatured with alkali and renatured in 50% formamide according to conditions described by Davis *et al.* (7). DNA was mounted by the formamide technique at the indicated times. The "zero time" was obtained by neutralization of a denatured DNA sample at 4° before spreading. (O) Incubated, nondenatured strands. 200 Molecules were scored in each sample.

Lengths of duplex AAV DNA molecules mounted by the aqueous technique were measured in samples that also contained added SV40 component-II DNA. The length distributions of both AAV and SV40 DNA molecules are shown in Fig. 5. The SV40 DNA molecules (Fig. 5*B*) were 97% circular, with a mean contour length of 1.55 ± 0.04 μm. This value agrees well with data published by others (10). SV40 DNA molecules are readily resolved from AAV DNA molecules (Fig. 5*A* and *B*), which are shorter. A bimodal distribution of the lengths of AAV molecules (components with means of 1.25 and 1.39 μm) is seen, and the few AAV circular forms (5% of total molecules) have lengths in the range of the larger linear component (Fig. 5*A* and *B*). Also, smaller circular structures were occasionally found in these DNA preparations (Fig. 4*B*).

DISCUSSION

We conclude that a self-annealing of complementary sequences at or near the ends of plus or minus strands of AAV DNA generates the observed single-stranded circular molecules (Fig. 2). On the basis of nuclease S_1 data (1), the self-annealed region appears to contain 400–500 base-pairs. Two possible arrangements of the terminal complementary sequences in plus or minus strands are shown diagrammatically in Fig. 6. In model *A*, self-annealed strands would be closed by an "in-line" duplex segment, whereas strand closure in model *B* produces a duplex projection or "panhandle." The terminal sequence arrangement depicted in model *A* must be considered highly unlikely (though not completely excluded), because self-annealing would result in a base-paired, *parallel* structure that is not known to occur. However, if the self-annealed region contains 400–500 base-pairs, then the panhandles predicted by model *B* should be visible. Alternatively, it may be that the length of self-annealed sequences has been over-estimated and that panhandles are simply too small to be seen. Although small projections can be seen on occasional single-stranded molecules (Fig. 2), their significance is not clear.

Thus far, only one other virus species has been found that contains DNA with self-complementary terminal sequences within its strands. Their presence in single-stranded molecules of adenovirus DNA was reported by this laboratory (4, 11), and subsequently confirmed by others (6). Denatured adenovirus DNA can also self-anneal to form single-stranded circles. These circles are closed by duplex segments, which may be similar in size (4) to those that close plus and minus AAV circles. As is the case with AAV circles, the structure of the self-annealed region of adenovirus circles has not been determined definitively.

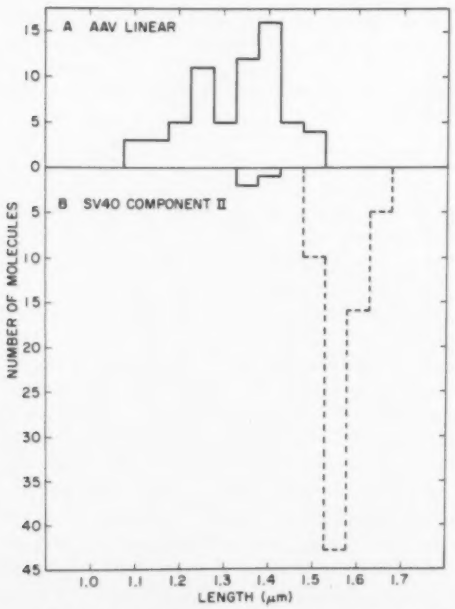

FIG. 5. Length distributions of double-stranded AAV DNA molecules and SV40 component II DNA molecules. Double-stranded AAV DNA molecules were prepared as described in Fig. 4. The *solid line* in *B* represents double-stranded AAV circles.

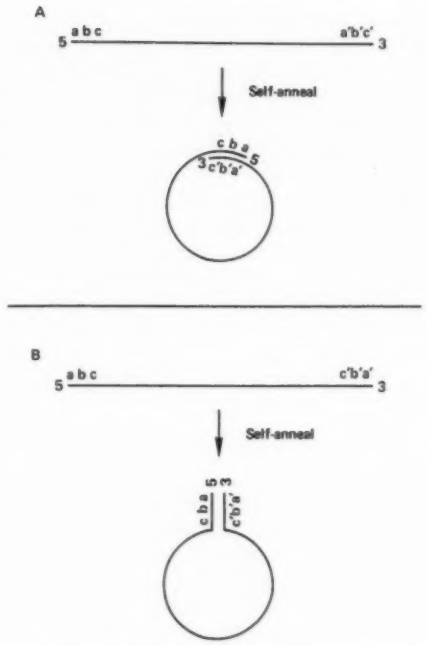

FIG. 6. Two possible models for the arrangement of terminal sequences in plus or minus strands of AAV DNA. (*A*) Self-annealing results in an in-line duplex segment. (*B*) Self-annealing produces a duplex panhandle. The model depicted in (*A*) must be considered highly unlikely (see text).

The occurrence of self-complementary terminal sequences in both AAV and adenovirus DNA strands is of great interest in view of the fact that AAV replication is unconditionally dependent on a helper adenovirus (12), and that adenoviruses appear to provide a factor(s) necessary for AAV DNA synthesis (13). That these self-complementary sequences may play a role in DNA replication is suggested by recent evidence that adenovirus DNA is replicated from an end of the template molecule (14), as well as by data that indicate that the self-complementary sequences in AAV DNA are not transcribed *in vivo* (1). Furthermore, if we assume the existence of a duplex replicative form of AAV DNA, it is interesting that the most likely order of terminal sequences (model *B*) would yield double-stranded AAV molecules having identical ends. The same conclusion also holds true for adenovirus duplexes (4, 6). This circumstance might provide a structural basis for initiating DNA replication from either end of the parent molecule. It would not be surprising if a bidirectional mechanism was involved in the synthesis of plus or minus strands of AAV DNA. For instance, if AAV plus or minus strands are synthesized separately by strand displacement from a linear duplex molecule, then a bidirectional replication mechanism would seem necessary. However, whether or not the terminal sequences in AAV or adenovirus DNA play a role in DNA replication, there is a good probability that they have some function in common.

We thank G. Fareed for *E. coli* exonuclease III and B. Hoyer for critical review of this manuscript. We are indebted to Karen Berry for technical assistance.

1. Carter, B. J., Khoury, G. & Rose, J. A. (1972) "Adenovirus-Associated Virus Multiplication IX. The Extent of Transcription of the Viral Genome *In Vivo*," *J. Virol.* **10**, 1118–1125.
2. Berns, K. I. & Rose, J. A. (1970) "Evidence for a Single-Stranded Adenovirus-Associated Virus Genome: Isolation and Separation of Complementary Single Strands," *J. Virol.* **5**, 693–699.
3. Rose, J. A., Hoggan, M. D. & Shatkin, A. J. (1966) "Nucleic Acid from an Adeno-Associated Virus: Chemical and Physical Studies," *Proc. Nat. Acad. Sci. USA* **56**, 86–92.
4. Garon, C. F., Berry, K. W. & Rose, J. A. (1972) "A Unique Form of Terminal Redundancy in Adenovirus DNA Molecules," *Proc. Nat. Acad. Sci. USA* **69**, 2391–2395.
5. Richardson, C. C., Lehman, I. R. & Kornberg, A. (1964) "A Deoxyribonucleic Acid Phosphatase-Exonuclease from *Escherichia coli*," *J. Biol. Chem.* **239**, 251–258.
6. Wolfson, J. & Dressler, D. (1972) "Adenovirus-2 DNA Contains an Inverted Terminal Repetition," *Proc. Nat. Acad. Sci. USA* **69**, 3054–3057.
7. Davis, R. W., Simon, M. & Davidson, N.(1971) in *Methods in Enzymology*, eds. Grossman, L. & Moldave K. (Academic Press, New York), Vol. XXI, pp. 413–528.
8. Doerfler, W. & Kleinschmidt, A. K. (1970) "Denaturation Pattern of the DNA of Adenovirus Type 2 as Determined by Electron Microscopy," *J. Mol. Biol.* **50**, 579–593.
9. Rose, J. A., Berns, K. I., Hoggan, M.D. & Koczot, F. J. (1969) "Evidence for a Single-Stranded Adenovirus-Associated Virus Genome: Formation of a DNA Density Hybrid on Release of Viral DNA," *Prod. Nat. Acad. Sci. USA* **64**, 863–869.
10. Sebring, E. D., Kelly, T. J., Jr., Thoren, M. M. & Salzman, N. P. (1971) "Structure of Replicating Simian Virus 40 Deoxyribonucleic Acid Molecules," *J. Virol.* **8**, 478–490.
11. Garon, C. F., Berry, K. W. & Rose, J. A. (1972) "Terminally Repeated Sequences in Adenovirus DNA Molecules," Abstracts: *72nd Meeting American Society for Microbiology* **84**, 199.
12. Atchison, R. W., Casto, B. C. & Hammon, W. McD. (1965) "Adenovirus-Associated Defective Virus Particles," *Science* **149**, 754–756.
13. Rose, J. A. & Koczot, F. (1972) "Adenovirus-Associated Virus Multiplication VII. Helper Requirement for Viral Deoxyribonucleic Acid and Ribonucleic Acid Synthesis," *J. Virol.* **10**, 1–8.
14. Sussenbach, J. S., van der Vliet, P. C., Ellens, D. J. & Jansz, J. S. (1972) "Linear Intermediates in the Replication of Adenovirus DNA," *Nature New Biol.* **239**, 47–49.

Proc. Nat. Acad. Sci. USA
Vol. 70, No. 1, pp. 220–224, January 1973

Qualitative Differences in the *N*-Acetyl-D-galactosaminyltransferases Produced by Human A^1 and A^2 Genes

(blood group A/serum glycosyltransferases/glycoprotein biosynthesis/milk oligosaccharides)

H. SCHACHTER*, M. A. MICHAELS*, CHRISTINE A. TILLEY†, MARIE C. CROOKSTON‡, AND J. H. CROOKSTON‡

* Department of Biochemistry, University of Toronto; † Department of Hematology, Toronto General Hospital, and ‡ Departments of Pathology and Medicine, University of Toronto, Toronto, Canada

Communicated by Saul Roseman, November 2, 1972

ABSTRACT **This study describes the kinetic properties of *N*-acetyl-D-galactosaminyltransferase in serum from subjects with blood groups A_1 and A_2. When the A^1 and A^2 enzymes were compared, with lacto-*N*-fucopentaose I and 2′-fucosyllactose as acceptors, the enzymes differed in their cation requirements, pH optima, and K_m values. The two acceptors competed for the same transferase. Mixing experiments showed that the lower activity of the A^2 enzyme could not be attributed to a modifier or inhibitor in serum. It was concluded that the A^1 and A^2 enzymes differ qualitatively.**

The *N*-acetyl-D-galactosaminyltransferase determined by the blood group *A* gene has been found in soluble form in human milk (1, 2) and membrane-bound in human submaxillary gland (3), human gastric mucosa (4, 5), hog submaxillary gland (6, 7), and hog gastric mucosa (8–10). This transferase has been found recently in human ovarian cyst linings and fluids (11). Various soluble glycosyltransferases involved in the synthesis of the prosthetic groups of plasma glycoproteins have been found in the serum of humans (12, 13), rats (12, 14), and pigs (15–17).

There have been several recent reports that the serum of human subjects with the blood group *A* gene contains a soluble glycosyltransferase, which can transfer *N*-acetyl-D-galactosamine (GalNAc) from UDP-GalNAc to suitable exogenous acceptors (18–21). When enzyme assays were performed at pH 5.5, the activity of serum from subjects with blood group A_1 was 5- to 10-times higher than that from subjects with blood group A_2 (20). The present communication describes the kinetic properties of *N*-acetyl-D-galactosaminyltransferase in the serum of A_1 and A_2 subjects. These studies indicate that the A^1 and A^2 transferases are different enzymes. A preliminary report of this work has appeared (22).

MATERIALS AND METHODS

Oligosaccharide Acceptors. Lacto-*N*-fucopentaose I (LNF-I) and 2′-fucosyllactose (2′-FL) were prepared from the milk of a group O, Le(a-b-) secretor, as described by Kobata *et al.* (23, 24). LNF-I was readily identified, since it is a major oligosaccharide component of milk from O, Le(a-b-) secretors (24). 2′-FL was identified by chromatographic comparison in solvent system I (see below) with a sample of 2′-FL prepared by Dr. Adeline Gauhe. LNF-I and 2′-FL each showed a single spot after descending chromatography in solvent systems I, II, and III (see below). The concentrations of 2′-FL and LNF-I were determined by the reducing sugar method, with glucose as the standard (25).

Paper Chromatography. Descending chromatography was performed with Whatman 3 MM paper for preparative purposes and Whatman 1 paper for analytic studies. The following solvent systems were used: (I) ethyl acetate–pyridine–water (120:50:40); (II) *n*-butanol–pyridine–water (6:4:1); (III) ethyl acetate–pyridine–acetic acid–water (5:5:3:1). Monosaccharides were chromatographed for 24 hr, and oligosaccharides for 3–5 days. Radioactive compounds were detected with a Packard model 7201 radioscanner and measured with a liquid scintillation counter (26). Nonradioactive saccharides were detected with a silver nitrate dip (27).

Nucleotide-Sugar. Uridine diphosphate-*N*-acetyl-D-[1-^{14}C]-galactosamine (UDP-[1-^{14}C]GalNAc), 50 Ci/mol, New England Nuclear Corp., was diluted to a specific activity of 2×10^7 cpm/μmol with nonradioactive UDP-GalNAc prepared as described (28).

Preparation of Enzyme from Human Serum. Serum was obtained from healthy subjects whose ABO phenotype had been determined by standard techniques (29). The genotype of some subjects was deduced from the phenotypes of their parents or children (30). In kinetic comparisons of A^1 and A^2 enzymes, subjects of genotype A^1O or A^1B were used as a source of A^1 enzyme, to avoid the presence of A^2 enzyme in A_1 subjects of genotype A^1A^2. Since A_2 subjects cannot carry the A^1 gene, it was not essential to know the genotype of the A_2 serum donors.

Enzyme was partially purified by ammonium sulfate fractionation at 4°. Saturated ammonium sulfate was added to fresh serum (5 ml) to a concentration of 35% ammonium sulfate; the mixture was centrifuged (17,000 × *g* for 30 min) and the precipitate was discarded. The supernatant was adjusted to a concentration of 55% ammonium sulfate, centrifuged as above, and the precipitate was dissolved in 0.25 ml of 5 mM TES (*N*-tris[hydroxymethyl]-methyl-2-aminoethanesulfonate) at pH 7.4. The resulting solution was dialyzed against 5 mM TES at pH 7.4 for 4 hr and stored at −20° until used for enzyme studies. The final protein concentration was usually between 50 and 70 mg/ml.

Abbreviations: LNF-I, lacto-*N*-fucopentaose I, 2-*O*-α-L-fucosyl-3-*O*-β-D-galactosyl-3-*O*-β-*N*-acetyl-D-glucosaminyl-4-*O*-β-D-galactosyl-D-glucose; 2′-FL, 2′-fucosyllactose, 2-*O*-α-L-fucosyl-4-*O*-β-D-galactosyl-D-glucose; GalNAc, *N*-acetyl-D-galactosamine.

TABLE 1. *Cation requirements for N-acetyl-D-galactosaminyltransferases from human serum*

Incubation mixture	Enzyme activity: A^1O serum fraction* (cpm/mg of protein per 3 hr)	Enzyme activity: A^2 serum fraction* (cpm/mg of protein per 3 hr)
Complete system†	7,710	2,500
−acceptor	120	80
$-Mn^{++}$	860	180
$+2.0\ \mu mol\ Mn^{++}$	13,770	2,160
$-Mn^{++}, +0.5\ \mu mol\ Mg^{++}$	8,480	60
$-Mn^{++}, +2.5\ \mu mol\ Mg^{++}$	6,950	0

* The 35–55% ammonium sulfate fractions were dialyzed at 4° against 10 mM EDTA–5 mM TES at pH 7.4 (4 hr) followed by dialysis against 5 mM TES at pH 7.4 (overnight).

† Complete incubation mixture contained the following components in a final volume of 45 μl: 2′-FL (0.09 μmol); TES, pH 7.4 (1.25 μmol); $MnSO_4$ (0.5 μmol); UDP-[*1*-^{14}C]GalNAc (0.01 μmol, 2×10^5 cpm); and ammonium sulfate fraction of serum (15 μl and 20 μl). The pH of the incubation mixture was 7.2.

Enzyme Assay. Conditions for glycosyltransferase assay are given in Tables 1 and 3. After incubation at 37° for 3 hr, the reaction was stopped by addition of 0.25 M EDTA–2% sodium tetraborate (20 μl). Aliquots (50 μl) of the resulting solution were subjected to high voltage (3000 V) electrophoresis in 1% sodium tetraborate (pH 9) on Whatman 3 MM paper for 40 min, in order to remove excess radioactive nucleotide–sugar from the origin. After drying, the papers were washed overnight by descending chromatography with 80% ethanol, to remove any free radioactive GalNAc from the origin. Oligosaccharide products moved 2–3 inches from the origin, and were measured by subjection of appropriate areas of the paper to liquid scintillation counting (26).

All assays were performed with and without exogenous acceptor. The endogenous acceptor activity was found to be proportional to enzyme volume and was the same for both A_1 and A_2 serum (100–250 cpm/10 μl of the 35–55% ammonium sulfate fraction, per 3 hr). The endogenous acceptor activity was always subtracted from the values obtained with exogenous acceptor.

In competition studies of LNF-I and 2′-FL for enzyme, incubations were at 37° for 5 hr, with LNF-I and 2′-FL separately, and with both acceptors together in the same incubation mixture. The reaction was stopped by freezing (no EDTA–tetraborate solution was added). The entire sample was subjected to high voltage electrophoresis in pyridine acetate at pH 6.5 (31) on Whatman 3 MM paper. The papers were dried, and the origins were removed and sewn onto another sheet of Whatman 3 MM paper, for descending chromatography in solvent system I for 72 hr. The products of the enzyme reaction were located with the radioscanner and measured in a liquid scintillation counter (26).

Product Identification. The following mixtures were prepared in final volumes of 0.40 ml:

(*a*) LNF-I (0.37 μmol); MES(2-[*N*-morpholino]ethanesulfonate), pH 5.5 (12.5 μmol); $MnSO_4$ (5 μmol); UDP-[*1*-^{14}C]GalNAc (10^6 cpm, 0.05 μmol); 35–55% ammonium sulfate fraction of serum from an A^1O donor (0.2 ml).

(*b*) Same as (*a*) but LNF-I replaced by 2′-FL (0.45 μmol).

(*c*) LNF-I (0.37 μmol); piperazine-*N*,*N*′-bis(2-ethanesulfonate), pH 7.0 (12.5 μmol); $MnSO_4$ (5 μmol); UDP-[*1*-^{14}C]GalNAc (10^6 cpm, 0.05 μmol); 35–55% ammonium sulfate fraction of serum from an A_2 donor (0.25 ml).

(*d*) Same as (*c*) but LNF-I replaced by 2′-FL (0.45 μmol).

The mixtures were incubated at 37° for 16 hr. Salt was removed by passage through small columns (Pasteur pipets with glass wool plugs) of AG 1-X2, 100–200 mesh, in bicarbonate form, followed by passage through Dowex 50W-X8, 100–200 mesh, in hydrogen-ion form. The effluents were adjusted to 70% ethanol and centrifuged (12,000 × *g* for 20 min). The supernatants were flash-evaporated at 37°, reconstituted in 0.4 ml of 70% ethanol, and subjected to descending chromatography in solvent system I on Whatman 3 MM paper for 5 days.

Only one radioactive peak was detected on each paper; each peak was eluted by descending chromatography with water for 2 days, and the eluates were flash-evaporated at 37° and reconstituted in 0.5 ml of water. The yields of radioactive material were as follows: (*a*) 1.2×10^6 cpm; (*b*) 1.9×10^6 cpm; (*c*) 0.2×10^5 cpm; (*d*) 0.6×10^5 cpm. 50-μl Aliquots of the solutions were subjected to descending chromatography

TABLE 2. *Michaelis constants for the oligosaccharide acceptors of N-acetyl-D-galactosamine*

	A_1 serum fraction*				A_2 serum fraction*			
			K_m (mM)				K_m (mM)	
pH	Donor	Genotype	LNF-1	2′-FL	Donor	Genotype	LNF-1	2′-FL
7.2	C.Ti	A^1O	0.43	0.03	C.Hu	†	4.7	4.6
(TES)	D.Cr	A^1O	0.87	0.12	T.Bo	†	7.5	2.7
	I.Cr	A^1O	0.62	0.16	L.Cu	A^1O	5.2	3.4
	W.Pr	A^1B	0.87	0.11	C.Me	†	5.1	3.6
5.8	C.Ti	A^1O	4.5	0.8	C.Hu	†	‡	‡
(MES)	L.Ae	A^1B	2.7	1.5				

* 35–55% ammonium sulfate fractions, assayed as described in *Methods*.

† Genotype not determined.

‡ The enzyme activity at pH 5.8 (MES) was too low to permit accurate determination of the Michaelis constants.

TABLE 3. *N-acetyl-D-galactosaminyltransferase activity in enzyme mixtures*

Enzyme preparation (μl)		Enzyme activity* (cpm/3 hr)		
A^1	A^2	TES pH 7.2	MES pH 5.8	Glycyl-glycine pH 5.6
10	—	4030	5730	5610
—	10	950	370	380
10	10	5100	6220	6360

* Incubation mixtures contained the following components in a final volume of 45 μl: LNF-1 (0.07 μmol); $MnSO_4$ (0.5 μmol); UDP-(*1*-^{14}C)GalNAc (0.01 μmol, 2×10^5 cpm); buffer (1.25 μmol); and enzyme preparation (35–55% ammonium sulfate fractions, from serum of A^1O and A_2 donors).

in solvent systems I, II, and III on Whatman 1 paper for 72 hr. Other aliquots (0.2 ml) were hydrolyzed with 1 N HCl at 100° for 1 hr; acid was removed by flash-evaporation at 37°, and the hydrolyzates were subjected to descending chromatography in solvent system I on Whatman 1 paper for 24 hr. Other aliquots (10 μl) of the radioactive products were incubated at 37° for 3 hr with 1.25 μmol of TES (pH 7.4), 0.5 μmol of $MnSO_4$, and 5, 10, and 20 μl of the 35–55% ammonium sulfate fractions of A_1 and A_2 serum in a final volume of 45 μl. The incubations were subjected to the standard assay procedure for the determination of radioactive product.

Protein was measured by the method of Lowry *et al.* (32) with bovine-serum albumin as standard.

RESULTS

Properties of Enzyme Preparation. The distribution of enzyme activity in ammonium sulfate fractions was similar for both A_1 and A_2 sera, namely, 0–35% fraction: 10–15% activity; 35–55% fraction: over 80% activity; supernatant from 55% ammonium sulfate fraction: no activity. The total recovery of A^1 enzyme after ammonium sulfate fractionation of A_1 serum was about 50%; recovery could not be accurately estimated for A^2 enzyme because the rate of product formation when whole A_2 serum is used is not proportional to serum volume (20), and the amount of enzyme in whole A_2 serum cannot therefore be accurately measured.

The 35–55% ammonium sulfate fractions were stable during storage at −20° or −70° for at least a week. As reported (20), the enzymes required an exogenous acceptor and Mn^{++}. With the 35–55% ammonium sulfate fractions from both A_1 and A_2 sera, the rate of product formation was proportional to enzyme volume up to 20 μl (Fig. 1), and was constant with time for at least 5 hr at 37°.

Qualitative Differences Between A^1 *and* A^2 *Glycosyltransferases.* Table 1 shows that the transferases differ in their cation requirements. Thus, when Mg^{++} is substituted for Mn^{++}, the A^1 transferase shows appreciable activity with 2′-FL but the A^2 transferase is inactive. Fig. 2 shows that the A^1 transferase has a pH optimum of about 5.6, while the A^2 transferase has a broad pH optimum between 7 and 8. When Michaelis constants (K_m) were determined at pH 7.2 for several A^1 and A^2 enzyme preparations, the K_m values for the A^1 enzyme were an order of magnitude smaller than those for the A^2 enzyme, with either LNF-I or 2′-FL as acceptor (Table 2). At pH 5.8, the activity of the A^2 enzyme preparation was too low to permit accurate determination of K_m values. There was no consistent difference between A^1 and A^2 enzyme preparations in the K_m values for UDP-GalNAc (average values were 0.06 mM with LNF-I and 0.09 mM with 2′-FL).

Mixing Experiments. Table 3 shows that the A^1 *N*-acetyl-D-

TABLE 4. *Competition studies*

Enzyme source	Acceptor concentration (mM)		Transferase activity* (cpm/mg of protein per 5 hr)		Calculated activity† (cpm/mg of protein per 5 hr)	
	LNF-1	2′-FL	Product I	Product II	Product I	Product II
D.Cr (A^1O)	0.8	—	12,200	250		
	—	1.0	0	15,000		
	0.8	1.0	3,350	10,700		
	0.8	1.0	3,390	10,900	2,330	13,600
L.Cu (A^1O)‡	1.6	—	2,290	130		
	—	1.0	0	3,260		
	1.6	1.0	2,020	3,000		
	1.6	1.0	1,870	2,920	1,870	2,620
C.Hu (A_2)	9.3	—	8,570	0		
	—	5.6	0	9,380		
	9.3	5.6	4,660	6,850		
	9.3	5.6	4,760	6,810	6,100	5,000

* Ammonium sulfate fractions of A_1 and A_2 serum were assayed at pH 7.2 (TES) with LNF-1 or 2′-FL alone, and with both LNF-1 and 2′-FL together in the same incubation mixture (see *Methods*). Product I is the hexaose formed with LNF-1 as acceptor, and Product II is the tetraose formed with 2′-FL as acceptor.

† Calculated on the assumption that both LNF-1 and 2′-FL compete for a single enzyme; the following formulas were used (33): Rate of incorporation into Product I = $V_1(S_1/K_1)/(1 + S_1/K_1 + S_2/K_2)$; rate of incorporation into Product II = $V_2(S_2/K_2)/(1 + S_1/K_1 + S_2/K_2)$, where V_1,S_1,K_1, and V_2,S_2,K_2 are, respectively: the maximum velocity, substrate concentration, and Michaelis constant for LNF-1 and 2′-FL. The values of K_1 and K_2 are listed in Table 2. The values of V_1 and V_2 are, respectively: 25,100 and 16,800 for D.Cr; 9,560 and 14,500 for L.Cu; and 12,900 and 17,100 for C.Hu.

‡ For the A^2 transferase, competition was not appreciable at acceptor concentrations that were effective for the A^1 transferase; however, with a 5-fold increase in acceptor concentrations, competition was readily demonstrated (see C. Hu).

galactosaminyltransferase activity was not affected by the presence of the A^2 enzyme. Similar results were obtained in mixing experiments with whole serum.

Competition Experiments. Competition between LNF-I and 2′-FL for serum *N*-acetyl-D-galactosaminyltransferase was assessed by comparision of enzyme activity when either LNF-I or 2′-FL was present alone, with activity when both acceptors were present in the incubation mixture. Table 4 shows that, with either the A^1 or A^2 enzyme preparation, LNF-I and 2′-FL compete for the same transferase.

Product Identification. When the products of four incubation mixtures (see *Methods*) were compared, each product showed a single radioactive peak after chromatography in three different solvent systems. Table 5 shows the $R_{lactose}$ value of each product. The mobility of each product was always slightly slower than that of the corresponding oligosaccharide substrate, a fact consistent with the hypothesis that the product is a larger oligosaccharide than its corresponding substrate (2). Furthermore, when acid hydrolyzates of the four products were chromatographed (see *Methods*), in every instance radioscanning detected only a single radioactive peak that cochromatographed with galactosamine and was well separated from glucosamine, galactose, glucose, mannose, and fucose. These findings, and the fact that the glycosyltransferase is present only in the serum of subjects with an *A* gene, indicate that the products of the reactions of the serum enzymes with LNF-I and 2′-FL are identical, respectively, to the hexaose and tetraose products obtained by Kobata and Ginsburg (2) using group A human milk as a source of *N*-acetyl-D-galactosaminyltransferase. Treatment of either product with A^1 or A^2 enzyme preparation under the conditions for transferase assay resulted in 88–95% recovery of undegraded product.

DISCUSSION

The above evidence indicates that serum *N*-acetyl-D-galactosaminyltransferases produced by the A^1 and A^2 genes are qualitatively different enzymes. The differences are: (*i*) Cation requirements: Mg^{++} can replace Mn^{++} in assays for the A^1 transferase, but not for the A^2 transferase. (*ii*) pH: the A^1 enzyme has a lower and narrower pH optimum than the A^2 enzyme. (*iii*) K_m: the A^1 enzyme has an appreciably lower K_m value than the A^2 enzyme, with either LNF-I or 2′-FL.

Since these studies were performed with only partially purified enzyme preparations, two explanations are possible: (*a*) the A^1 and A^2 genes each code for a different *N*-acetyl-D-galactosaminyltransferase, or (*b*) the A^1 and A^2 genes produce the same transferase, but either A_1 or A_2 subjects produce a modifier that alters the behavior of this transferase. The

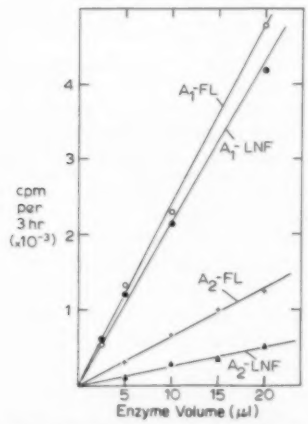

FIG. 1. The effect of enzyme volume on the activity of serum *N*-acetyl-D-galactosaminyltransferase. Ammonium sulfate fractions of A_1 and A_2 serum were assayed as described in *Methods* and Table 1.

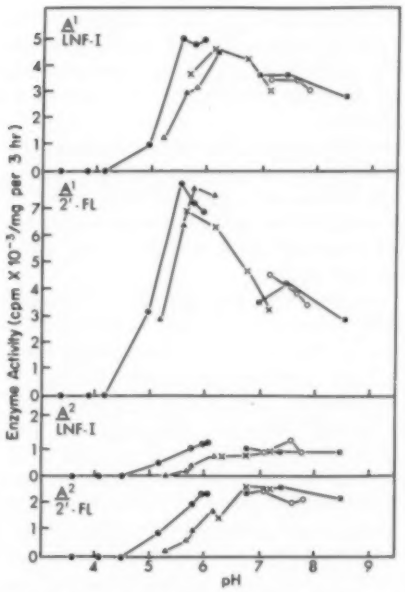

FIG. 2. The effect of pH on the activity of serum *N*-acetyl-D-galactosaminyltransferase. Ammonium sulfate fractions of A_1 and A_2 serum were assayed at several different pH values as described in *Methods* and Table 1. The following buffers were used: glycylglycine, ●——●; MES, ▲——▲; piperazine-*N*,*N*′-bis(2-ethanesulfonate), ×——×; TES, ○——○; glycine, ■——■. The pH values refer to the incubation mixtures and not to the stock buffer solutions.

TABLE 5. *Chromatographic mobilities of enzyme products*

Compound*	$R_{lactose}$ values†		
	Solvent system I	Solvent system II	Solvent system III
LNF-1	0.29	0.16	0.13
Product I with A^1 enzyme	0.22	0.09	0.07
Product I with A^2 enzyme	0.24	0.09	0.09
2′-FL	0.77	0.74	0.74
Product II with A^1 enzyme	0.50	0.27	0.43
Product II with A^2 enzyme	0.52	0.41	0.42

* Radioactive products were prepared as described in *Methods*. Product I was obtained with LNF-1 as acceptor, and Product II was obtained with 2′-FL as acceptor.

† Conditions of descending chromatography are described in *Methods*. The mobility of lactose was: system I, 40.1 cm; system II, 11.0 cm; and system III, 28.9 cm.

mixing experiments shown in Table 3 appear to exclude the presence of such a modifier. Further, there was no destruction of product by either A^1 or A^2 enzyme preparation, indicating the absence in these preparations of *N*-acetyl-D-galactosaminidase activity.

Kobata and Ginsburg (2) have reported that there were no apparent differences between the A^1 and A^2 transferases purified from human milk. In preliminary experiments with ammonium sulfate fractions, we have found that the enzyme preparations from milk of A_1 and A_2 donors differ in their K_m values and pH optima.

It has been suggested (34) that the structural basis for the difference between the A_1 and A_2 antigens depends on whether the A determinant, *N*-acetyl-D-galactosamine, is linked to a Type 1 oligosaccharide side chain [galactosyl-(β, 1→3)-*N*-acetylglucosamine] or to a Type 2 chain [galactosyl-(β,1→4)-*N*-acetylglucosamine]. The A_1 antigen is believed to contain GalNAc linked to both Type 1 and Type 2 chains on a single branched molecule, whereas the A_2 antigen may contain GalNAc linked only to Type 2 chains. However, it has been shown in our experiments, and by others (35, 36), that the A^2 *N*-acetyl-D-galactosaminyltransferase acts on both LNF-I (a Type 1 chain analogue) and 2′-FL (a Type 2 chain analogue). Our competition studies show that both of these oligosaccharide acceptors compete for the same enzyme sites. However, the *N*-acetyl-D-galactosaminyltransferases may not show the same specificity towards the macromolecular H substance as they do towards these oligosaccharide analogues.

We thank Miss Judith Shindman for technical assistance, and Drs. E. J. McGuire and A. Gauhe for a sample of 2′-fucosyllactose. This work was supported by grants from the Medical Research Council of Canada (Grants MT-3285 and MT-696) and the Bickell Foundation.

1. Kobata, A., Grollman, E. F. & Ginsburg, V. (1968) *Arch. Biochem. Biophys.* **124,** 609–612.
2. Kobata, A. & Ginsburg, V. (1970) *J. Biol. Chem.* **245,** 1484–1490.
3. Hearn, V. M., Smith, Z. G. & Watkins, W. M. (1968) *Biochem. J.* **109,** 315–317.
4. Tuppy, H. & Schenkel-Brunner, H. (1969) *Vox Sang.* **17,** 139–142.
5. Schenkel-Brunner, H. & Tuppy, H. (1970) *Eur. J. Biochem.* **17,** 218–222.
6. Carlson, D. M. (1968) in *Biochemistry of Glycoproteins and Related Substances, Proc. 4th Intl. Conf. Cystic Fibrosis of the Pancreas,* ed. Rossi, E. & Stoll, E. (S. Karger, New York), Part II, pp. 304–307.
7. McGuire, E. J. (1970) in *Blood and Tissue Antigens,* ed. Aminoff, D. (Academic Press, New York), pp. 461–478.
8. Tuppy, H. & Staudenbauer, W. L. (1966) *Nature* **210,** 316–317.
9. Schenkel-Brunner, H. & Tuppy, H. (1969) *Nature* **223,** 1272–1273.
10. Tuppy, H. & Schenkel-Brunner, H. (1969) *Eur. J. Biochem.* **10,** 152–157.
11. Hearn, V. M., Race, C. & Watkins, W. M. (1972) *Biochem. Biophys. Res. Commun.* **46,** 948–956.
12. Mookerjea, S., Chow, A. & Hudgin, R. L. (1971) *Can. J. Biochem.* **49,** 297–299.
13. Kim, Y. S., Perdomo, J., Bella, A. & Nordberg, J. (1971) *Biochim. Biophys. Acta* **244,** 505–512.
14. Wagner, R. R. & Cynkin, M. A. (1971) *Biochem. Biophys. Res. Commun.* **45,** 57–62.
15. Hudgin, R. L. & Schachter, H. (1971) *Can. J. Biochem.* **49,** 829–837.
16. Hudgin, R. L. & Schachter, H. (1971) *Can. J. Biochem.* **49,** 838–846.
17. Hudgin, R. L. & Schachter, H. (1971) *Can. J. Biochem.* **49,** 847–852.
18. Kim, Y. S., Perdomo, J., Bella, A. & Nordberg, J. (1971) *Proc. Nat. Acad. Sci. USA* **68,** 1753–1756.
19. Sawicka, T. (1971) *FEBS Lett.* **16,** 346–348.
20. Schachter, H., Michaels, M. A., Crookston, M. C., Tilley, C. A. & Crookston, J. H. (1971) *Biochem. Biophys. Res. Commun.* **45,** 1011–1018.
21. Ko, G. K. W. & Raghupathy, E. (1972) *Biochem. Biophys. Res. Commun.* **46,** 1704–1712.
22. Schachter, H., Michaels, M. A., Tilley, C. A., Crookston, M. C. & Crookston, J. H. (1972) *Proc. Can. Fed. Biol. Soc.* **15,** 656.
23. Kobata, A., Tsuda, M. & Ginsburg, V. (1969) *Arch. Biochem. Biophys.* **130,** 509–513.
24. Grollman, E. F., Kobata, A. & Ginsburg, V. (1969) *J. Clin. Invest.* **48,** 1489–1494.
25. Dubois, M., Gilles, K. A., Hamilton, J. K., Rebers, P. A. & Smith, F. (1956) *Anal. Chem.* **28,** 350–356.
26. Schachter, H., Jabbal, I., Hudgin, R. L., Pinteric, L., McGuire, E. J. & Roseman, S. (1970) *J. Biol. Chem.* **245,** 1090–1100.
27. Smith, I. (1960) in *Chromatographic and Electrophoretic Techniques,* ed. Smith, I. (W. Heinemann, London), Vol. I, p. 252.
28. Carlson, D. M., Swanson, A. L. & Roseman, S. (1964) *Biochemistry* **3,** 402–405.
29. Mollison, P. L. (1972) *Blood Transfusion in Clinical Medicine,* (F. A. Davis, Philadelphia), 5th ed., pp. 392–396.
30. Race, R. R. & Sanger, R. (1968) *Blood Groups in Man,* (F. A. Davis, Philadelphia), 5th ed., pp. 9–13.
31. Efron, M. (1960) in *Chromatographic and Electrophoretic Techniques,* ed. Smith, I. (W. Heinemann, London), Vol. II, p. 170.
32. Lowry, O. H., Rosebrough, N. J., Farr, A. L. & Randall, R. J. (1951) *J. Biol. Chem.* **193,** 265–275.
33. Dixon, M. & Webb, E. C. (1964) in *Enzymes* (Longmans, London), 2nd ed., pp. 84–87.
34. Moreno, C., Lundblad, A. and Kabat, E. A. (1971) *J. Exp. Med.* **134,** 439–457.
35. Watkins, W. M. (1970) in *Blood and Tissue Antigens,* ed. Aminoff, D. (Academic Press, New York), p. 200.
36. Kobata, A., Ginsburg, V. & Kabat, E. A. (1971) Unpublished observations cited in *Glycoproteins of Blood Cells and Plasma,* eds. Jamieson, G. A. & Greenwalt, T. J. (J. B. Lippincott, Philadelphia), pp. 122–123.

Proc. Nat. Acad. Sci. USA
Vol. 70, No. 1, pp. 225–229, January 1973

Double-Stranded RNA as an Inhibitor of Protein Synthesis and as a Substrate for a Nuclease in Extracts of Krebs II Ascites Cells

(encephalomyocarditis virus/messenger RNA/ribonuclease)

HUGH D. ROBERTSON* AND MICHAEL B. MATHEWS†

M.R.C. Laboratory of Molecular Biology, Hills Road, Cambridge, CB2 2QH, England

Communicated by F. H. C. Crick, October 27, 1972

ABSTRACT **Concentrations of double-stranded RNA above about 0.1 μg/ml inhibit translation of encephalomyocarditis viral RNA and mouse globin messenger RNA in extracts of Krebs II ascites cells. Protein synthesis initially proceeds at the control rate, then abruptly shuts off in a manner similar to that observed in reticulocyte lysates [Hunt, T. & Ehrenfeld, E. (1971) *Nature New Biol.* 230, 91–94]. Substantially higher concentrations of double-stranded RNA are required to give this effect in ascites extracts.**

Subcellular fractions of Krebs II ascites cells contain a nucleolytic activity capable of digesting several natural and synthetic double-stranded RNAs. This nuclease is most active under conditions of protein synthesis, and part of the activity remains associated with ribosomes upon sedimentation. It is probably because of digestion of double-stranded RNA by this nuclease that higher concentrations of double-stranded RNA are required for inhibition of protein synthesis in Krebs cell extracts than in reticulocyte lysates.

Double-stranded RNA (dsRNA) is involved in several biological processes in animal cells. In particular, dsRNA induces the production of interferon (1–3), can cause tumor regression (4, 5), and has been implicated in the shut-off of protein synthesis in cells infected with poliovirus (6, 7). Several recent reports have demonstrated the binding and uptake of dsRNA by cells in tissue culture (8, 9), and dsRNA has been found in normal rat liver (10) and in nuclei of sea urchin embryos (11).

One of the most striking effects of dsRNA is the ability of very small amounts to inhibit the initiation of globin synthesis in reticulocyte lysates (6, 7, 12, 13). Another cell-free extract that can translate various mammalian mRNAs faithfully is that prepared from Krebs II ascites cells (14). This system has the advantage that it can translate efficiently exogenous RNA of both viral and cellular origin (15). We report here the effect of dsRNA on the translation of encephalomyocarditis (EMC) viral RNA and mouse globin mRNA in Krebs cell extracts. Our results demonstrate that protein synthesis is inhibited by dsRNA in a manner qualitatively similar to that reported for globin synthesis in extracts of rabbit reticulocytes (6, 7, 12), but that substantially higher concentrations of dsRNA are required. During these investigations, we detected a nuclease in extracts of ascites cells that digests dsRNA, and we believe that such an activity accounts for the lower sensitivity of this extract to dsRNA.

Abbreviations: dsRNA, double-stranded RNA; ssRNA, single-stranded RNA; EMC, encephalomyocarditis virus.

* Present Address: The Rockefeller University, New York, N.Y. 10021.

† Present Address: University of California, School of Medicine, San Francisco, Calif. 94122.

MATERIALS AND METHODS

Procedures for handling Krebs II ascites cells and S-30 extracts for protein synthesis have been described (15, 16). Protein synthesis reactions contained, in 25 μl, 7.5 μl of incubated S-30 extracts, 2.5 mM Mg^{++}, and 0.1 M KCl. [^{14}C]Phenylalanine or [^{14}C]aminoacid mixture (475 Ci/mol and 45 Ci/atom, respectively) were obtained from the Radiochemical Centre, Amersham, England; other components of the reactions were as specified (15, 16). EMC viral RNA was prepared as before (15), mouse globin mRNA was a gift from Dr. J. B. Lingrel, College of Medicine, Cincinnati, Ohio, and f2 single-stranded (ss)RNA was prepared from f2 bacteriophage. S-30 extracts were fractionated into ribosomes and S-150 supernatant by centrifugation at 48,000 rpm for 2.5 hr in a 50Ti rotor in a Beckman ultracentrifuge.

The dsRNAs tested as inhibitors of protein synthesis were obtained as follows: reovirus RNA was the gift of Dr. R. T. Hunt, Cambridge University; dsRNA from a virus of *Penicillium chrysogenum* was the gift of Dr. D. Planterose, Beecham Research Laboratories, Betchworth, Surrey, England; phage f2 replicative ensemble, the derivative of the replicating complex from phage f2-infected cells that contains dsRNA, was prepared and purified as described (17). The preparation used here was badly degraded after several years of storage at 4°, and contained dsRNA fragments no larger than 8 S, rather than the original 14S or greater dsRNA.

dsRNAs tested as substrates for nuclease activities were prepared as follows: the homopolymer pair poly(G·C) containing [^{3}H]GMP (1.8×10^{6} dpm/μg) was synthesized as before (18) by use of poly(C) and *Escherichia coli* RNA polymerase, kindly provided by Dr. J. Roberts of this laboratory. ^{32}P-labeled phage f2 dsRNA and ssRNA were prepared and purified from phage-infected cells as described (19), and were used at a specific activity of 3 to 6×10^{5} dpm/μg. ^{32}P-labeled phage f1 ssRNA and dsRNA (specific activity about 1×10^{6} cpm/μg) were synthesized *in vitro* with [^{32}P]CTP (The Radiochemical Centre, Amersham), and purified as described (20).

E. coli ribonuclease III (21, 18) was purified (18) from strain MRE 600 with several modifications of the earlier procedure (Robertson, H. D. & Hunter, A. R., in preparation). The enzyme had an activity of about 5000 units/ml, where one unit solubilizes 1 nmol of poly(AU) nucleotides/hr (18).

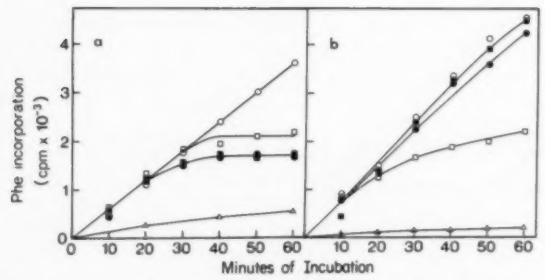

FIG. 1. (*a*) Effect of different concentrations of dsRNA on rate of protein synthesis. 10-μl Samples were removed from 75-μl protein synthesis reactions containing 25 μg/ml of EMC RNA (see *Methods*) for determination of incorporation into hot Cl_3CCOOH-insoluble material. Control, (○——○); with 0.17 (□——□), with 0.4 (■——■), or with 1 (●——●) μg/ml of dsRNA from *P. chrysogenum;* without EMC RNA (△——△). (*b*) Abolition of inhibitory activity of dsRNA by prior incubation with RNase III. dsRNA from *P. chrysogenum* (2 μl of an 880 μg/ml solution) was incubated for 90 min at 37° with 10 μl of RNase III or TM buffer, then for a further 90 min after addition of another 10 μl of RNase III or TM buffer. The incubated dsRNA was diluted 1:40 with water and 9 μl was added to 75 μl of protein synthesis reactions, which were assayed as in Fig. 1*a*. Control (○——○); with dsRNA from *P. chrysogenum* incubated in TM buffer, (□——□); with dsRNA from *P. chrysogenum* incubated with RNase III, (■——■); with an identical amount of fresh RNase III, (●——●); with no EMC RNA, (△——△).

Digestion of dsRNA in ascites subcellular fractions was assayed in a volume of 0.1 ml; the assay mixture contained 75 μl of TM buffer [0.02 M Tris·HCl (pH 7.6)–0.01 M magnesium acetate–0.2 M NH_4Cl–5% sucrose]. Incubations were at 37°, and samples were withdrawn periodically for determination of cold 5% Cl_3CCOOH-precipitable radioactivity (18). When reaction mixtures contained a substantial proportion of an ascites subcellular fraction in the salts of medium K [25 mM Tris·HCl–(pH 7.5)–125 mM KCl–5 mM magnesium acetate–6 mM 2-mercaptoethanol] (15), control incubations were performed with an equal amount of these salts.

RESULTS

dsRNA and protein synthesis

The effect of added dsRNA on the rate of EMC RNA translation by the ascites cell-free system is shown in Fig. 1*a*. The inhibition is similar to that observed in the reticulocyte system (6, 7, 12): after a period during which protein synthesis proceeds at the control rate, there is an abrupt and almost complete cessation of protein synthesis. This shutoff occurs at about 30 min with 0.17 μg/ml of dsRNA, and somewhat earlier (at about 20 min) with higher concentrations (0.4 μg/ml). A further increase in the concentration of dsRNA did not bring about any decrease in the time required to block incorporation.

Fig. 1*b* shows that prior incubation of the inhibitory dsRNA with RNase III, an *E. coli* nuclease specific for dsRNA (21, 18), abolished its action on protein synthesis. It is also apparent that RNase III itself has only a slight effect on protein synthesis at this concentration, though higher activities of this nuclease are highly inhibitory (data not shown).

The effects of various concentrations of dsRNA on translation in the ascites system were also examined. Fig. 2*b* shows that phage f2 dsRNA inhibited the translation of EMC viral RNA by up to 75%. It is evident that about 1–10 μg/ml of partially degraded f2 dsRNA is required to obtain inhibition of EMC translation under these conditions. Using *P. chrysogenum* and reovirus dsRNAs, which are much larger than the f2 dsRNA fragments, we found that substantially lower concentrations (about 0.05–0.1 μg/ml) are sufficient to inhibit translation (Fig. 2*a*, *e*, *f*). In no case have we found inhibition by any dsRNA at a concentration lower than 0.02 μg/ml in the ascites system. This result contrasts with the findings of Hunter *et al.* (12), who detected inhibition with concentrations of dsRNA below 0.5 ng/ml in reticulocyte lysates.

It is evident (Fig. 2*a*) that a certain proportion of the incorporation in the ascites system is resistant to inhibition, even at high dsRNA concentrations. Furthermore, the highest dsRNA concentrations tested did not relieve this inhibition, in contrast to the results obtained with rabbit reticulocyte lysates (7, 12). Fig. 2 also shows that the endogenous incorporation of this system is inhibited by dsRNA. Comparable concentrations of ssRNA from phage f2 do not inhibit translation in this system (Fig. 2*c*). In fact, a small stimulation is reproducibly obtained at high concentrations of f2 RNA, both in the presence and in the absence of added mammalian mRNA. Preliminary indications suggest that this stimulation

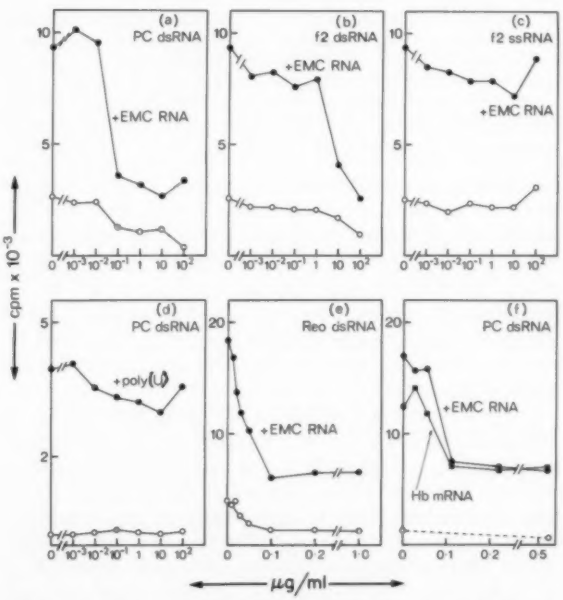

FIG. 2. Effect of several types of dsRNA on translation of various mRNAs. 25-μl reaction mixtures containing [^{14}C]-phenylalanine (*a*–*d*) or [^{14}C]aminoacid mixture (*e*, *f*) were incubated for 60 min. The Mg^{++} concentration was raised to 5 mM in (*d*). Messenger RNAs that were present in reactions denoted by (●——●) or (■——■), were added at the following concentrations: EMC RNA, 20 μg/ml; mouse globin mRNA, 20 μg/ml; poly(U), 100 μg/ml; reactions with no added mRNA, (○——○). In each case, the potential inhibitory nucleic acid (indicated in the upper right-hand corner of each panel) was present in the concentrations indicated in the abscissa (note log scales in *a*–*d*, linear scales in *e* and *f*). The ordinate scales refer to the incorporation of ^{14}C into hot Cl_3CCOOH-insoluble material. *PC, P. chrysogenum; Hb,* hemoglobin; *Reo,* reovirus.

is the result of low levels of translation of the f2 RNA under these conditions.

Fig. 2*f* shows that translation of globin mRNA and EMC RNA were inhibited in a similar manner. To discover whether the inhibitory action of dsRNA extends to the incorporation directed by synthetic polynucleotide messengers that lack an initiator codon, we used poly(U). This messenger requires a somewhat higher Mg^{++} concentration for optimal translation. Fig. 2*d* shows that under these conditions protein synthesis was markedly less sensitive to dsRNA.

A nuclease that digests dsRNA in ascites cell extracts

One way to explain the lower sensitivity of the ascites extract to dsRNA relative to the reticulocyte lysate would be to postulate the existence in the ascites extract of a nuclease capable of degrading dsRNA. Hunter *et al.* (12) have already reported the absence of such an activity from reticulocyte extracts. In contrast, the ascites S-30 fraction solubilizes the dsRNA purified from *E. coli* infected with bacteriophage f2 (Fig. 3.)

Using the substrate poly(G·C), we assayed a series of fractions obtained during the preparation of S-30 from ascitic fluid. Table 1 shows that no activity occurs in the ascitic fluid itself or in the final wash of the cells before lysis. This result is important, since Stern (22) has reported the existence in animal sera of a nuclease capable of digesting poly(I·C). Activity against poly(G·C) is observed after homogenization of the ascites cells, and much of this activity remains in the S-30 supernatant. A similar pattern of intracellular localization was obtained for *E. coli* RNase III (18).

Having established that we are dealing with an intracellular activity, we investigated its properties in S-30 extracts in more detail. An extract was separated into ribosomal and S-150 fractions, as described in *Methods*, and activity against equal amounts of phage f1 dsRNA or ssRNA of identical specific activity was measured. In the S-30 fraction, 72% of the dsRNA or 35% of the ssRNA was solubilized in 24 min, and a similar 100% difference in rate was observed with the S-150 supernatant fraction. However, with resuspended ribosomes, 70% of the dsRNA, but only 12% of the ssRNA, was solubilized in this interval. Similar results were obtained with ssRNA or dsRNA prepared from phage f2. In each case, solubilization of dsRNA is inhibited by 50 mM EDTA. These

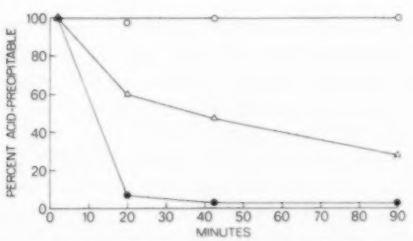

FIG. 3. Digestion of f2 dsRNA by ascites S-30 extracts. ^{32}P-Labeled f2 dsRNA was prepared as described in *Methods*. Each assay included, in a volume of 100 μl: 70 ng of f2 dsRNA (about 20,000 cpm); 25 μl of ascites S-30 or medium K; and 75 μl of TM buffer. 20-μl Samples were withdrawn at the times indicated for determination of cold Cl_3CCOOH-precipitable radioactivity. Control incubation, with no added nuclease, (○——○); reaction containing 10 units of *E. coli* RNase III, (●——●); reaction containing 25 μl of ascites S-30, (△——△).

TABLE 1. *Digestion of dsRNA by ascites-cell fractions*

Additions	pmol of poly(G·C) digested
None	0
Media RS and K	0
RNase III	16.4
RNase III + media RS and K	14.6
Ascitic fluid	0
Supernatant from eighth wash of ascites cells	0
Ascites cell homogenate	24.6
30,000 × *g* pellet	20.3
30,000 × *g* supernatant (S-30)	22.1

The dsRNA substrate, poly(G·C), is described in *Methods* Ascites cells were washed by repeated sedimentation and suspension in medium RS (5.2 mM KCl-130 mM NaCl-7.4 mM $MgCl_2$) and were homogenized and fractionated as described (15). All samples were adjusted to equal volumes before assay. Reactions contained in 50 μl: 10 ng (30 pmol) of poly([^{3}H]G·C), and 5 μl of a buffer containing 0.5 M Tris·HCl (pH 7.6)–0.20 M magnesium acetate–1.0 M NH_4Cl–40% sucrose. Additions were as follows: Medium RS and medium K, 5 μl each; *E. coli* RNase III, 0.2 unit in 10 μl of TM buffer; ascites cellular fractions, 10 μl each. Incubation was at 37° for 30 min, and digestion was assayed as described in *Methods*.

results suggest that a nuclease with preference for dsRNA is located in the cytoplasm of ascites tumor cells, perhaps in association with ribosomes.

Effects of prior incubation with dsRNA

Hunter *et al.* (12) showed that prior incubation of dsRNA with reticulocyte lysates resulted in a potentiation of the inhibitory effect. It might have been anticipated that observation of this phenomenon in the ascites extract would be obstructed by the nuclease described above. However, as shown in Table 2, prior incubation of the ascites S-30 fraction together with dsRNA indeed led to an increase in the inhibitory action. Addition of dsRNA at the same time as the mRNA inhibited protein synthesis directed by EMC RNA by about 50%, regardless of whether the S-30 itself was preincubated or not. When the S-30 was first incubated for 5 or 15 min with an identical

TABLE 2. *Effect of prior incubation with dsRNA on protein synthesis*

EMC RNA	dsRNA addition	[^{14}C]Phe incorporation (cpm × 10^{-3}) *Prior incubation (min)* 0	5	15
+	—	15.2	15.3	13.7
+	After incubation	7.9	7.7	7.4
+	Before incubation	8.5	3.2	2.9
+	Both	4.9	3.2	2.8
−	—	2.2	1.6	0.9

The components of 25 μl of protein-synthesis reactions were incubated for the times shown in a volume of 17.5 μl. dsRNA from *P. chrysogenum* (2.5 ng) was added before or after this incubation, or at both times. EMC RNA (30 μg/ml) was then added, the volume was adjusted to 25 μl, and the reaction mixtures were further incubated for 60 min at 37°.

amount of dsRNA, the inhibition of EMC RNA translation increased to 85–90%. Addition of more dsRNA to an extract that had been incubated with dsRNA produced no further inhibition. This result suggests that the plateau level corresponding to the maximal inhibition is rapidly obtained with lower dsRNA concentrations as a consequence of prior incubation.

This potentiation was observed with prior incubation times as short as 1 min, or as long as 40 min. This result suggests that dsRNA rapidly binds to some component of the protein synthetic machinery, and that this interaction protects the bound portion of the inhibitor from the action of the dsRNA-digesting nuclease. A similar situation was created artificially in the reticulocyte lysate when *E. coli* RNase III was added after incubation of the system with radioactive dsRNA (H. D. Robertson, R. J. Jackson, R. T. Hunt, and A. R. Hunter, unpublished experiments). Under these conditions, the nuclease solubilized up to 90% of the dsRNA without reversing the increased inhibitory effect.

DISCUSSION

Effect of dsRNA on protein synthesis in ascites and reticulocyte cell-free extracts

We have shown that dsRNA inhibits the translation of two natural mRNAs in an ascites cell-free system. This effect resembles that previously observed in reticulocyte lysates (6, 7, 12) in the following respects: (*a*) the rate of protein synthesis in the presence of dsRNA shows a sharp cutoff after an initial period of synthesis at the control rate (Fig. 1*a*). (*b*) Translation of poly(U) is inhibited to a much smaller extent than that of natural mRNA (Fig. 2*d*). (*c*) Single-stranded RNA does not inhibit the ascites system (Fig. 2*c*). (*d*) Prior incubation of an ascites S-30 fraction with dsRNA potentiates the inhibitory activity of dsRNA (Table 2). (*e*) At no tested concentration of dsRNA is the inhibition of translation in the ascites extract complete (Fig. 2). Therefore, this sort of inhibition by dsRNA may be a general property of numerous cell types.

In contrast to these similarities in the response to dsRNA of the ascites and reticulocyte extracts, there are several differences: (*a*) Whereas high concentrations of dsRNA (over 10 μg/ml) do not inhibit translation in reticulocyte lysates (7, 12), dsRNA concentrations up to 100 μg/ml do not relieve inhibition in the ascites system. It is, of course, still possible that even higher dsRNA concentrations might have this effect. (*b*) The proportion of ascites translation that is resistant to dsRNA inhibition (Fig. 2) is significantly higher than that reported for reticulocyte lysates (12). This finding is also reflected by the absence of a progressively earlier shutoff of incorporation in the ascites system as the concentration of dsRNA is raised above a certain limit (Fig. 1*a*). Moreover, a significant proportion of ascites translation continues to be resistant to inhibition even after prior incubation with dsRNA (Table 2), whereas such treatment of reticulocyte lysates virtually abolishes their activity (12). (*c*) The minimum dsRNA concentration at which inhibition can be observed in the ascites system is at least 40-fold higher than that observed with reticulocyte extracts (12). Furthermore, the ascites system displays a greater sensitivity to large dsRNA molecules than to small fragments, while the rabbit reticulocyte system was almost equally sensitive to all dsRNA inhibitors used in these experiments (R. J. Jackson, personal communication).

Properties of cell-free extracts that could account for different effects of dsRNA

These differences could be explained in several ways, especially as the reticulocyte is a differentiated cell that synthesizes a small number of proteins, whereas the ascites cell is a tumor cell that makes numerous proteins. Moreover, the incubated ascites S-30 fraction is largely dependent upon added mRNA (15, 16), whereas the reticulocyte system efficiently reinitiates translation of its endogenous mRNA (23). Several of our observations suggest that the explanation for the higher dsRNA concentrations required to inhibit the ascites system is the dsRNA-digesting nuclease present in ascites extracts. First, ascites S-30 fractions can solubilize dsRNA at a concentration of up to 0.1 μg/ml under conditions of protein synthesis; this is also the dsRNA concentration below which little inhibition of protein synthesis is observed. Second, this explanation is also consistent with the fact that large dsRNA molecules inhibit the ascites system (but not the reticulocyte system) better than small ones (see Fig. 2*a* and *b*). Finally, in an experiment performed in collaboration with Dr. R. J. Jackson, Cambridge University, we found that prior incubation of dsRNA from *P. chrysogenum* (0.2–1 μg/ml) with ascites cell S-30 diminished by over 80% the ability of that dsRNA to inhibit the more sensitive reticulocyte system.

Digestion of dsRNA by a nuclease in ascites extracts

The experiments in Fig. 3 and Table 1 establish the presence of a nucleolytic activity capable of digesting dsRNA in ascites extracts. There have been several earlier reports of enzymes that use helical RNA as substrate. Activities in *E. coli* RNase III cleave large, regular helical RNA molecules (in either dsRNA (21, 18) or DNA:RNA hybrids (24, 20), reducing them to sizes between 10 and 20 base-pairs (ref. 25 and H. D. R., unpublished observations). In eukaryotic systems, in addition to the activity against dsRNA in serum (22), an activity that digests dsRNA in a frog virus has been reported (26). Also, there have been several reports of enzymes, termed RNase H, that digest the RNA of DNA·RNA hybrids with high specificity (27). These enzymes are incapable of digesting RNA·RNA duplexes, and have been found in calf-thymus nuclei (27) and RNA tumor viruses (28). These earlier findings and our observations here demonstrate that higher cells contain nucleases that can metabolize both of the major types of helical RNA.

Possible roles for the recognition of dsRNA in translation

These findings may help to clarify our view of virus-induced shutoff of host-cell protein synthesis, and to suggest some properties of protein synthesis in eukaryotic cells. Our finding (Fig. 2*f*) that globin mRNA and EMC mRNA translation are inhibited about equally by dsRNA does not support the idea that dsRNA may inhibit translation of cellular, but not viral, mRNAs (6, 7). Thus, translation of EMC RNA and globin mRNA may not be initiated by radically different mechanisms. However, this negative result cannot be considered a definitive disproof of this hypothesis, since more subtle aspects of cellular control processes may not be fully effective *in vitro*.

The findings reported here show that two eukaryotic cell extracts display a qualitatively similar response to dsRNA. In addition, it has been recently reported that translation of reovirus mRNA in extracts of mouse L cells is partially

inhibited by dsRNA (29). The experiment shown in Fig. 2*d*, in which translation of poly(U) is not inhibited by dsRNA, suggests that this inhibitory effect of dsRNA may be confined to the proper translation of natural mRNAs.

Recent studies with reticulocyte lysates (13) have indicated that dsRNA specifically inhibited an early step in the initiation of protein synthesis. In light of the numerous similarities between the two systems in their response to dsRNA, it seems reasonable to suppose that initiation is also the step inhibited in the ascites system, although this has not been proved. Inhibition of protein synthesis by dsRNA could be due to a fortuitous recognition of this nucleic acid by some component of the translation machinery whose normal function does not involve recognition of, or binding to, helical RNA. On the other hand, it may become necessary to postulate a step involving recognition of regular helical RNA as part of the initiation process in higher cells.

Hunter *et al.* (12) have proposed that recognition of a length of dsRNA by a cellular component, such as an initiation factor, could be necessary for translation. This helical region would have to be greater than about 20 base-pairs long and quite stable, since prior treatment of dsRNA with RNase III abolishes inhibition (ref. 12 and Fig. 1*b*). It is possible that the recognition of stable dsRNA in protein initiation may be one way in which mammalian and bacterial processes are differentiated. We have been unable to demonstrate any effect of added natural dsRNA upon the translation of phage f2 RNA by *E. coli* S-30 fractions.

The existence of such dsRNA recognition in higher systems might be part of a pathway in which a nuclease of the sort described here could regulate the extent and rate of translation, either by cleaving the mRNA itself or by removing dsRNA of nonmessenger origin.

We thank Drs. F. Sanger and J. D. Smith, in whose laboratories this work was performed. H. D. R. was a Helen Hay Whitney Foundation Fellow. M. B. M. was a Beit Memorial Research Fellow.

1. Lampson, G. P., Tytell, A. A., Field, A. K., Nemes, M. N. & Hilleman, M. R. (1967) *Proc. Nat. Acad. Sci. USA* **58**, 782–789.
2. Tytell, A. A., Lampson, G. P., Field, A. K. & Hilleman, M. R. (1967) *Proc. Nat. Acad. Sci. USA* **58**, 1719–1722.
3. Colby, C., Stollar, B. D. & Simon, M. I. (1971) *Nature New Biol.* **229**, 172–174.
4. Levy, H. B., Law, W. & Rabson, A. S. (1969) *Proc. Nat. Acad. Sci. USA* **62**, 357–361.
5. Cordell-Stewart, B. & Taylor, M. W. (1971) *Proc. Nat. Acad. Sci. USA* **68**, 1326–1330.
6. Hunt, R. T. & Ehrenfeld, E. (1971) *Nature New Biol.* **230**, 91–94.
7. Ehrenfeld, E. & Hunt, R. T. (1971) *Proc. Nat. Acad. Sci. USA* **68**, 1075–1078.
8. Colby, C. & Chamberlin, M. J. (1969) *Proc. Nat. Acad. Sci. USA* **63**, 160–167.
9. Schell, P. L. (1971) *Biochim. Biophys. Acta* **240**, 472–484.
10. Harel, L. & Montagnier, L. (1971) *Nature New Biol.* **229**, 106–108.
11. Kronenberg, L. H. & Humphreys, T. (1972) *Biochemistry* **11**, 2020–2026.
12. Hunter, A. R., Hunt, R. T., Jackson, R. J. & Robertson, H. D. (1972) in *Synthese, Struktur und Funktion des Hämoglobins*, eds. Martin & Nowicki (J. F. Lehmanns Verlag, München, Germany), pp. 133–145.
13. Darnbrough, C., Hunt, T. & Jackson, R. J. (1972) *Biochem. Biophys. Res. Commun.* **48**, 1556–1564.
14. Mathews, M. B., Osborn, M. & Lingrel, J. B. (1971) *Nature New Biol.* **233**, 206–209.
15. Mathews, M. B. & Korner, A. (1970) *Eur. J. Biochem.* **17**, 328–338.
16. Mathews, M. B. (1972) *Biochim. Biophys. Acta* **272**, 108–118.
17. Engelhardt, D. L., Robertson, H. D. & Zinder, N. D. (1968) *Proc. Nat. Acad. Sci. USA* **59**, 972–979.
18. Robertson, H. D., Webster, R. E. & Zinder, N. D. (1968) *J. Biol. Chem.* **243**, 82–91.
19. Robertson, H. D. & Zinder, N. D. (1969) *J. Biol. Chem.* **244**, 5790–5800.
20. Robertson, H. D. (1971) *Nature New Biol.* **229**, 169–172.
21. Robertson, H. D., Webster, R. E. & Zinder, N. D. (1967) *Virology* **32**, 718–719.
22. Stern, R. (1970) *Biochem. Biophys. Res. Commun.* **41**, 608–614.
23. Lamfrom, H. & Knopf, P. M. (1964) *J. Mol. Biol.* **9**, 558–575.
24. Robertson, H. D. & Zinder, N. D. (1968) *Fed. Proc.* **27**, 296.
25. Schweitz, H. & Ebel, J. (1971) *Biochimie* **53**, 585–593.
26. Palese, P. & Koch, G. (1972) *Proc. Nat. Acad. Sci. USA* **69**, 698–701.
27. Hausen, P. & Stein, H. (1970) *Eur. J. Biochem.* **14**, 278–283.
28. Mölling, K., Bolognesi, D. P., Bauer, H., Büsen, W., Plassmann, H. W. & Hausen, P. (1971) *Nature New Biol.* **234**, 240–243.
29. Graziadei, W. D., III & Lengyel, P. (1972) *Biochem. Biophys. Res. Commun.* **46**, 1816–1823.

Proc. Nat. Acad. Sci. USA
Vol. 70, No. 1, pp. 230–234, January 1973

A Single Subunit from Avian Myeloblastosis Virus with Both RNA-Directed DNA Polymerase and Ribonuclease H Activity

(RNA virus/polyacrylamide gel electrophoresis)

DUANE P. GRANDGENETT, GARY F. GERARD, AND MAURICE GREEN

Institute for Molecular Virology, St. Louis University School of Medicine, 3681 Park Ave., St. Louis, Missouri 63110

Communicated by Robert J. Huebner, November 7, 1972

ABSTRACT **Two structurally distinct forms of RNA-directed DNA polymerase from avian myeloblastosis virus were resolved by chromatography on phosphocellulose and purified. In addition to RNA-directed DNA polymerase activity, both enzymes had ribonuclease H (RNase H) activity, which degraded the RNA moiety of RNA·DNA hybrids. As determined by sodium dodecyl sulfate–polyacrylamide disc-gel electrophoresis, one form had two subunits, alpha (α) and beta (β), with molecular weights of 65,000 and 105,000, respectively. The other had a single subunit, α, with a molecular weight of 65,000. The sedimentation coefficients of $\alpha\beta$ and α, determined by glycerol gradient centrifugation in 0.35 M KCl, were 7.8 S and 5.2 S, respectively. Both enzymes had similar antigenic determinants and could not be distinguished by a differential response to several different RNA and DNA templates. We suggest that α, which contains both RNA-directed DNA polymerase and RNase H activity, is derived by dissociation of $\alpha\beta$; the function of the β subunit is unknown.**

The discovery of an enzyme activity closely associated with RNA-directed DNA polymerase from avian myeloblastosis virus (AMV) (1), ribonuclease H (RNase H), has provided stimulus for the structural identification of specific enzyme activities that may be involved in viral DNA synthesis. RNase H specifically degrades the RNA moiety of RNA·DNA hybrids and is present in 10 different RNA tumor viruses (2).

A major and a minor peak of DNA polymerase activity have been noted in lysates of AMV after phosphocellulose chromatography (3). The structure (4) and properties (3, 4) of only the protein with the major enzyme activity have been studied. In this report we present results of studies on the structure and catalytic properties of the proteins containing both enzyme activities. Our results show that both RNase H and DNA polymerase activity reside on a single polypeptide subunit.

MATERIALS AND METHODS

Virus Purification and Nucleic Acid Isolation. Avian myeloblastosis virus, BAI strain A, was purified as described (5) from frozen virus preparations generously supplied by Dr. J. W. Beard, Duke University. AMV 70S RNA (6), adenovirus type 2 and 7 DNA (7), and SV-40 Form 1 DNA (8) were isolated by published procedures.

Preparation of RNA·DNA Hybrids. Calf-thymus [^{3}H]-RNA·DNA (2 nmol/ml of RNA nucleotides, 2800 cpm/pmol) and the synthetic homopolymer hybrid, [^{3}H]poly(A)·poly(dT) [100 μM [^{3}H]poly(A), 10 cpm/pmol; 400 μM poly(dT)], were prepared as described (2).

Abbreviations: AMV, avian myeloblastosis virus; SDS, sodium dodecyl sulfate.

Enzyme Assays. Poly(A)·oligo(dT)-directed DNA polymerase activity was assayed at 37° in the following reaction mixture (0.09 ml): 50 mM Tris·HCl (pH 8.3), 50 mM NaCl, 3 mM dithiothreitol, 5 mM $MgCl_2$, and 0.1 mM [^{3}H]TTP (500 cpm/pmol) with oligo(dT)$_{12-18}$ and poly(A) at 10 μg/ml each. AMV 70S RNA-directed DNA polymerase activity was assayed in a reaction mixture (0.09 ml) containing 50 mM Tris·HCl (pH 8.3), 50μ mM NaCl, 3 mM dithiothreitol, 5 mM $MgCl_2$, 1 mM $MnCl_2$, 0.1 mM each of dGTP, dCTP, and dATP, 3 μM [^{3}H]TTP (1.6×10^4 cpm/pmol), and 10 μg/ml of AMV 70S RNA. With calf-thymus DNA (30 μg/ml) as template, the reaction mixture was identical except that AMV 70S RNA and $MnCl_2$ were omitted. Reactions were terminated by addition of 10 μl of 0.2 M EDTA (pH 7.4). The amount of polymer product formed was determined by assay on Whatman DEAE–cellulose (DE-81) paper discs (9).

The reaction mixture (0.1 ml) for assay of RNase H activity (1) contained 30 mM Tris·HCl (pH 7.8), 5 mM dithiothreitol, 100 mM $(NH_4)_2SO_4$, 2 mM $MnCl_2$, and either calf-thymus [^{3}H]RNA·DNA (1 to 2×10^4 cpm) or [^{3}H]poly(A)·poly(dT) (4×10^3 cpm). The reaction was terminated after 10 min of incubation at 37° by addition of cold 10% trichloroacetic acid (90 μl) and calf-thymus DNA (30 μg) as carrier. Radioactivity of acid-soluble material in the supernatant was determined after centrifugation at $12,000 \times g$ for 15 min.

The assay for single-stranded nuclease was identical to the assay for RNase H except that 3 μM [^{3}H]poly(U) (35 cpm/pmol) was used as substrate.

DEAE–Cellulose and Phosphocellulose Chromatography. These and subsequent purification steps were done at 4° unless otherwise specified. Just before enzyme purification, purified virus containing 500 mg of protein was dialyzed against 10% glycerol–10 mM potassium phosphate (pH 8.0)–2 mM dithiothreitol–0.1 mM EDTA for 2–4 hr. This buffer was used throughout the purification with changes in the glycerol and potassium phosphate concentrations as indicated. The virus suspension was adjusted to a protein concentration of 1 mg/ml in the above buffer, lysed with Nonidet P-40 (NP-40) at a final concentration of 2%, stirred for 10 min at 25°, and centrifuged at $12,000 \times g$ for 8 min to remove debris. Less than 1% of the total enzyme activity was in the pellet. The supernate was applied to a 2.5×25 cm DEAE–cellulose (Whatman DE-52) column equilibrated with phosphate buffer. The column was washed with three column volumes of phosphate buffer and developed with a 700-ml linear gradient of 0.01–0.5 M potassium phosphate. The salt concentration was determined conductimetrically. The fractions in the single peak containing both DNA poly-

merase and RNase H activity were pooled; protein was precipitated by addition of solid ammonium sulfate to give 60% saturation. The precipitate was collected by centrifugation, dissolved in a minimum volume of 0.2 M potassium phosphate buffer, and dialyzed overnight against the same buffer.

The dialyzed DEAE-cellulose eluate was diluted 10-fold with 10 mM phosphate buffer and adsorbed to a 1 × 25 cm phosphocellulose (Whatman P-11) column. After a wash with four column volumes of phosphate buffer, the column was developed with a 200-ml linear gradient of 0.01–0.5 M potassium phosphate. The peaks of DNA polymerase activity were pooled and concentrated by cyclic dialysis against 50 and 10% glycerol in 0.2 M phosphate buffer. Each cycle required 24 hr to complete and reduced the sample volume by 50–60%. The dialysis bag was tied after each cycle to maintain the reduced volume. The last dialysis was with 50% glycerol, and the enzyme was stored at −20°.

Glycerol Gradient Centrifugation. Before centrifugation the enzyme preparations were either diluted or dialyzed for 2 hr with 10% glycerol in the appropriate high and low salt buffers described below. Enzyme preparations purified on phosphocellulose were centrifuged in 4.8-ml gradients of 20–40% glycerol containing 0.35 M KCl, 50 mM Tris·HCl (pH 8.0), 0.2% NP-40, 3 mM dithiothreitol, and 0.1 mM EDTA (high salt). In the low salt gradient, KCl was omitted. Centrifugation was for 24 hr at 2° at 46,000 rpm in an SW50.1 rotor. Fractions of 0.2 ml were collected from the bottom of the tubes and assayed. The peak fractions were pooled and concentrated by cyclic dialysis as described above against 0.2 M KCl–50 mM Tris·HCl (pH 8.0)–3 mM dithiothreitol–0.1 mM EDTA in 10 and 50% glycerol.

Nondissociating Polyacrylamide Disc-Gel Electrophoresis. Nondissociating polyacrylamide gels were prepared and run by the procedure of Brown (10), except 4% acrylamide was used in the absence of calf-thymus DNA. Enzyme preparations were diluted before electrophoresis with 0.1 M potassium phosphate (pH 7.5)–50 mM glycine–15 mM dithiothreitol. Gels (0.6 × 6.0 cm) were run at 10 mA per gel at 4° for 4–8 hr. The gels were cut into 2-mm slices and eluted with 0.2 ml of 0.1 M potassium phosphate (pH 7.5)–10 mM dithiothreitol–10% glycerol.

Gel fractions to be examined by sodium dodecyl sulfate (SDS)–polyacrylamide gel electrophoresis were further eluted by addition of SDS to a final concentration of 1% and incubation overnight at 25°. The gel fragments were removed by centrifugation, and the protein in the supernatant was precipitated with cold 10% trichloroacetic acid. The precipitate was collected by centrifugation and dissolved in denaturing solution (see next section). After addition of bromophenol blue to 0.1%, the pH was adjusted to 7 by addition of NaOH (2 N).

SDS–Polyacrylamide Disc-Gel Electrophoresis. SDS–polyacrylamide gels were prepared and run by the procedure of Maizel (11). Electrophoresis was performed with 0.5 × 11 cm gels of 6% acrylamide at 8 mA per gel at 25° for 6 hr. Proteins were denatured for 10 min at 100° with 1% 2-mercaptoethanol, 1% SDS, 10 mM sodium phosphate (pH 7.1), and 10% glycerol (denaturing solution). Gels were stained with 0.05% Coomassie blue in methanol–acetic acid–water (5:1:5, v/v) for 2 hr at 37° and were destained with 10% methanol in 7.5% acetic acid for 48 hr.

Enzyme Inactivation by Antibody. Gammaglobulin, purified from antisera prepared against purified AMV polymerase that contained two subunits with molecular weights of 110,000 and 69,000 (4), was a gift from Drs. K. Watson and S. Spiegelman. Phosphocellulose peak I (0.06 μg) or peak II (0.03 μg) was mixed with this gammaglobulin suspended in 10 mM Tris·HCl (pH 8.3), 5 mM $MgCl_2$, 0.15 M NaCl, 20% glycerol, and 50 μg of bovine-serum albumin in 60 μl. After 5 min at 37°, DNA synthesis was initiated by addition of 0.3 nmol of [^{3}H]TTP (1.6×10^4 cpm/pmol) and poly(A)·oligo(dT) (1:1, 1 μg of each) to give a final volume of 100 μl. The amount of DNA product formed in 30 min was assayed.

RESULTS

Purification of AMV Enzymes by DEAE-Cellulose and Phosphocellulose Chromatography. RNA-directed DNA polymerase, RNase H, and single-stranded ribonuclease activities were routinely followed throughout purification. All the detectable DNA polymerase and RNase H activities in detergent-lysed AMV adsorbed to a DEAE-cellulose column. A single coincident peak of DNA polymerase and RNase H activity eluted from DEAE-cellulose at 0.09 M potassium phosphate. Single-stranded nuclease activity eluted as a single peak at 0.08 M potassium phosphate. A 15- to 20-fold purification of DNA polymerase was achieved on DEAE-cellulose with recoveries of 30–50%. Precipitation of the protein in the peak of enzyme activity with ammonium sulfate gave an additional 4-fold purification with no loss in total activity.

Chromatography on phosphocellulose gave two peaks of DNA polymerase activity (Fig. 1*A*). The first phosphocellulose peak (peak PCI) represented 10–15% of the total

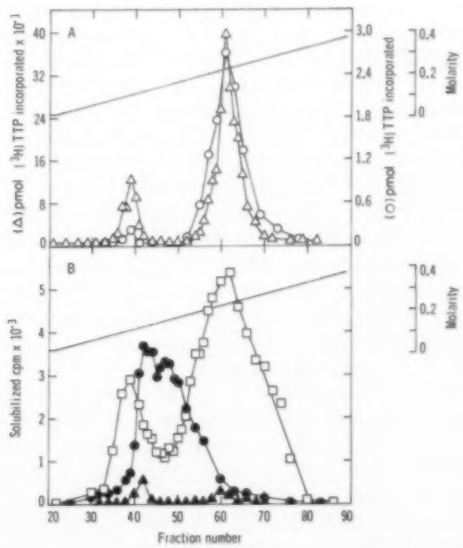

Fig. 1. Chromatography of AMV enzymes, purified on DEAE-cellulose, on phosphocellulose. Aliquots (2 μl) of 2-ml fractions were assayed for: (*A*) DNA polymerase with poly(A)·oligo(dT) (△) and AMV 70S RNA (○); (*B*) RNase H with native calf-thymus hybrid (□) and denatured hybrid (▲); and (*B*) single-stranded nuclease with [^{3}H]poly(U) (●).

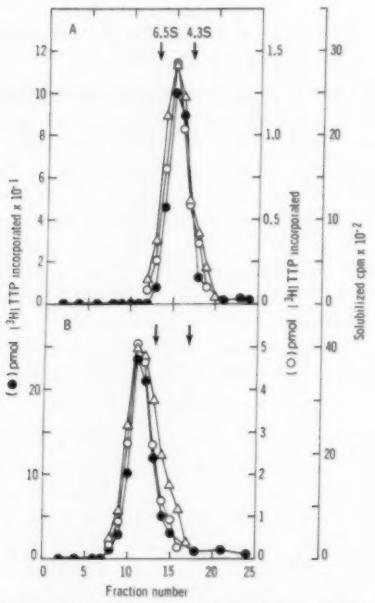

FIG. 2. Glycerol gradient centrifugation of peaks PCI and PCII. Total protein applied to the gradients in *A* and *B* were 500 and 300 μg of PCI and PCII, respectively. Fractions were assayed for DNA polymerase with poly(A)·oligo(dT) (●) and AMV 70S RNA (○), and for RNase H with native calf-thymus hybrid (△). Aliquots of 5 and 2 μl were used in the 70S RNA assay and in the other two assays, respectively. Hemoglobin (4.3 S) and [¹²⁵I]gammaglobulin (6.5 S) were run in separate tubes as sedimentation markers.

recovered activity and eluted at 0.11 M potassium phosphate; the second peak (peak PCII), representing the remainder of the activity, eluted at 0.22 M potassium phosphate. Total recovery of enzyme activity was 50–70%. A major and a minor peak of DNA polymerase activity on phosphocellulose have been noted by Hurwitz and Leis (3) with AMV and by Faras *et al.* (12) with RSV. Peak PCI chromatographed again on phosphocellulose as a single peak of activity eluting at 0.11 M potassium phosphate. If peak PCII was again chromatographed on phosphocellulose, two peaks of activity were again obtained in about the same ratio as initially shown, eluting at 0.11 and 0.22 M potassium phosphate. The poor response of peak PCI relative to peak PCII to exogenous AMV 70S RNA was due to single-stranded nuclease that eluted from 0.10–0.20 M potassium phosphate (Fig. 1*B*), almost completely overlapping peak PCI and only partially overlapping peak PCII.

RNase H cochromatographed with DNA polymerase activity in both peaks PCI and PCII (Fig. 1*A* and *B*). The ratio of RNase H to DNA polymerase activity appears to be greater in peak PCI than in peak PCII due to the limiting amount of calf-thymus [³H]RNA·DNA used in screening for RNase H activity. It was necessary to use a denaturable hybrid such as calf-thymus RNA·DNA to demonstrate the specificity of the assay for RNase H (13). With [³H]poly(A)·poly(dT) at a saturating concentration, as substrate for RNase H, identical elution profiles for the two enzyme activities were obtained (data not shown). The ratio of RNase H to DNA polymerase activity across the two peaks was constant and equal.

Glycerol Gradient Centrifugation. The centrifugation of phosphocellulose peaks I and II in high salt (0.35 M KCl) glycerol gradients is illustrated in Fig. 2. Peaks PCI and PCII sedimented as single components with sedimentation coefficients ($s_{20,w}$) of 5.2 S and 7.8 S, respectively, based on a 4.3S value for hemoglobin (14). Based on these S values, the molecular weights of peaks PCI and PCII are about 90,000 and 160,000, respectively, from the equation $SW_1/SW_2 = (MW_1/MW_2)^{2/3}$ (15) (hemoglobin standard = 66,000). For both peaks PCI and PCII, the profiles of DNA polymerase activity with poly(A)·oligo(dT) and AMV 70S RNA were coincident. RNase H cosedimented with DNA polymerase from both peaks PCI and PCII. Single-stranded nuclease activity sedimented as a single component at 4.3 S in both enzyme preparations (data not shown). The recoveries of DNA polymerase activity were 70–80% in the presence of 0.2% NP-40, but 10–20% in its absence.

The sedimentation properties and stability of peak PCI in glycerol gradients was not affected by ionic strength. Peak PCII, however, aggregated in the absence of KCl, and recovery of DNA polymerase activity after glycerol gradient centrifugation in the absence of KCl was only 10–15%.

Properties of Purified Peaks PCI and PCII. The response of peaks PCI and PCII purified on glycerol gradients to several RNA and DNA polymers is shown in Table 1. The ratio of the specific enzyme activities with all templates tested was essentially constant.

The DNA endo- and exonuclease activity in both enzyme preparations purified on phosphocellulose was determined. We assayed DNA endonuclease activity by exposing adenovirus type 2 and 7 [¹⁴C]DNA or SV-40 Form 1 [¹⁴C]DNA to enzyme under conditions for DNA synthesis, and then examining the sedimentation profiles of the DNA in alkaline sucrose gradients (16). Incubation of adenovirus type 2 and 7 DNA or SV-40 Form 1 DNA for 2 hr with either peak PCI

TABLE 1. *Template specificities of enzyme peak PCI and peak PCII*

Templates*	pmol [³H]TTP incorporated/10 min per μg of protein		Activity ratio (PCII/PCI)
	Peak PCI	Peak PCII	
Poly(A)·oligo(dT)	42.0	155	3.7
Poly(A)·poly(dT)	46.0	144	3.2
AMV 70S RNA	0.44	1.40	3.1
Activated calf-thymus DNA†	6.20	19.5	3.1
Native calf-thymus DNA	2.20	7.10	3.2
Denatured calf-thymus DNA‡	3.20	10.0	3.1

* Various polymers were used to assay peak PCI and peak PCII purified on glycerol gradients. The polymer concentrations were: activated, native, or denatured calf-thymus DNA, 30 μg/ml; AMV 70S RNA, 20 μg/ml; poly(A), 21 μg/ml; poly(dT), 30 μg/ml; and oligo(dT)$_{12-18}$, 30 μg/ml. Peak PCI was at 0.6 and PCII at 0.3 μg/ml. The time course of enzyme activity was linear with each template for at least 20 min.

† Calf-thymus DNA was activated by treatment with DNase I (23).

‡ Calf-thymus DNA was denatured by heating at 100° for 10 min.

(3 μg/ml) or peak PCII (5 μg/ml) did not alter the sedimentation profiles of the DNA in alkaline sucrose gradients. DNA exonuclease activity was monitored by measurement of the release of trichloroacetic acid-soluble counts from [^{3}H]-poly(dAT), SV-40 Form 2 [^{14}C]DNA, or whole cell [^{14}C]DNA from monkey kidney cells. Neither peak PCI (1.4 μg/ml) nor peak PCII (1.0 μg/ml) solubilized detectable amounts of these DNAs during a 2-hr incubation.

Subunit Structures of Peaks PCI and PCII. The subunit structures of peaks PCI and PCII purified on glycerol gradients were examined by SDS–polyacrylamide disc-gel electrophoresis. Peak PCI contained one major subunit (Fig. 3, gel *2*), which we call alpha (α). Several minor contaminating bands that can be removed by gel electrophoresis were also present after glycerol gradient centrifugation. Two subunits were resolved in peak PCII (Fig. 3, gel *4*), designated α and beta (β) in order of decreasing mobility. Peaks PCI and PCII were mixed and examined by SDS–polyacrylamide gel electrophoresis (data not shown). The α subunits of PCI and PCII had identical mobilities. For comparison, SDS–polyacrylamide gels of phosphocellulose peak I (gel *1*) and peak II (gel *3*) are also shown in Fig. 3. Gel patterns identical to those in Fig. 3 were obtained with proteins treated with iodoacetamide (17) before gel analysis.

The molecular weights of AMV DNA polymerase subunits were determined from a standard curve (data not shown) that related the logarithm of the molecular weight to the distance of migration of polypeptides on SDS–polyacrylamide gels. The molecular weight markers used were: adenovirus hexon, bovine-serum albumin, gammaglobulin, ovalbumin, chymotrypsinogen, and cytochrome *c*. The molecular weights of α and β were estimated to be 65,000 and 105,000, respectively.

The amount of β relative to α in peak PCII was determined by measurement of the area under each subunit peak in densitometric tracings of SDS–polyacrylamide gels stained by Coomassie blue of peak PCII purified on glycerol gradients. The ratio of the amount of β relative to α determined by this method was 1.7; the ratio of the molecular weight of β relative to α was also 1.7. Therefore, the relative molar concentration of α and β was 1.0. The subunit structural formulas for peaks PCI and PCII were, therefore, α and αβ, respectively, or an integral multiple thereof. The 90,000 molecular weight estimated from density gradient analysis for peak PCI could be consistent with either α or α_2. The molecular weight of peak PCII estimated by density gradient analysis was 160,000. Thus, the subunit structural formula for peak PCII was αβ with a molecular weight of 170,000.

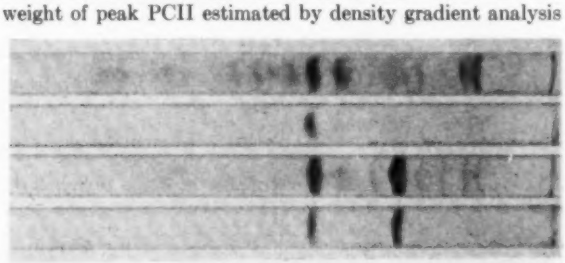

FIG. 3. SDS–polyacrylamide disc-gel electrophoresis of peaks PCI and PCII before and after glycerol gradient purification. From *top* to *bottom*, the amount of protein applied to each gel was (*1*) 16 μg of peak PCI, (*2*) 2 μg of peak PCI purified on a glycerol gradient, (*3*) 10 μg of peak PCII, and (*4*) 3 μg of peak PCII purified on a glycerol gradient. Gels were stained with Coomassie blue.

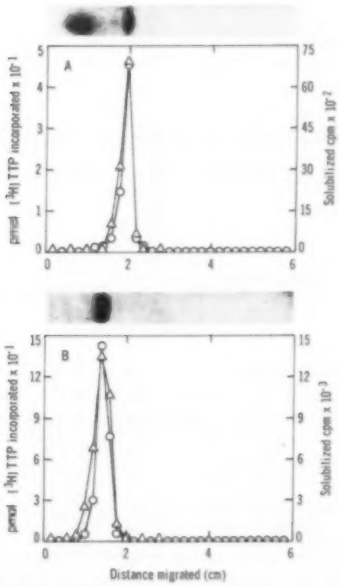

FIG. 4. Nondissociating polyacrylamide disc-gel electrophoresis of phosphocellulose peak I(*A*) and peak II(*B*). The total time of electrophoresis was 4.5 hr. For measurement of enzyme activities, 10 μg of protein of peak PCI or 11 μg of peak PCII was applied to a gel. Each gel was cut and eluted; 20-μl aliquots of various fractions were assayed for DNA polymerase with poly(A)·oligo(dT) (○) and for RNase H with native calf-thymus hybrid (△). Gels run in parallel for staining with Coomassie blue contained 7 μg of peak PCI or 7 μg of peak PCII protein. The enzyme activity profiles of fractionated gels and the photographs of stained gels of peaks PCI and PCII are shown.

The Antigenic Relationship of Peak PCI and PCII. Antibody directed against Peak PCII inactivated the DNA polymerase activity of both Peak PCI and Peak PCII. In the presence of 6, 12, and 18 μg/ml of anti-AMV DNA polymerase gammaglobulin, equivalent amounts of DNA polymerase activity of Peaks PCI and PCII were inhibited by 80, 90, and 96% and 54, 69, and 71%, respectively. This result demonstrates that α in both enzymes has similar antigenic determinants.

Both DNA Polymerase and RNase H Reside on Alpha: Purification on Nondissociating Polyacrylamide Gels and Analysis by SDS–Polyacrylamide Gel Electrophoresis. To definitely establish that α possesses both DNA polymerase and RNase H activity, peak PCI was subjected to further purification on nondissociating polyacrylamide gels under conditions where DNA polymerase and RNase H activities were stable and could be eluted from the gels. For comparison, peak PCII was also examined. Typical results are shown in Fig. 4. Peak PCI migrated 7.5 mm farther than peak PCII after 4.5 hr of electrophoresis. Doubling the time of electrophoresis doubled the separation achieved. Analysis of DNA polymerase and RNase H eluted from gels of peak PCI (Fig. 4*A*) and peak PCII (Fig. 4*B*) showed that for each, both enzyme activities comigrated. In addition, AMV 70S RNA-directed DNA polymerase activity comigrated with the above two activities in gels from both enzymes (data not shown).

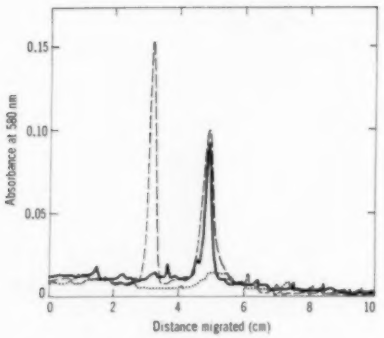

FIG. 5. Densitometric tracings of SDS–polyacrylamide gels of peaks PCI and PCII purified by nondissociating polyacrylamide gel electrophoresis. Phosphocellulose peaks I and II were subjected to electrophoresis on nondissociating polyacrylamide gels (see Fig. 4) for 7.5 hr. Three sets of three gels each were run simultaneously, one set for peak PCI containing 11 μg of protein per gel, one set for peak PCII containing 20 μg of protein per gel, and one set with no protein. Gels of peaks PCI and PCII were fractionated, eluted, and assayed for DNA polymerase activity. The six fractions from each set of three gels containing the highest DNA polymerase activity were combined. The protein was precipitated and analyzed by SDS–polyacrylamide gel electrophoresis. Six appropriate fractions from the blank gels were treated and analyzed in a similar manner. The SDS gels were stained with Coomassie blue, and densitometric tracings at 580 nm of peak PCI (——), peak PCII (– – –), and the blank (· · ·) were made with a Beckman Acta V equipped with a linear transport.

Usually 60–80% of input DNA polymerase activity could be recovered from the gel.

The subunit structure of peaks PCI and PCII after nondissociating polyacrylamide gel electrophoresis was determined by extraction of the protein in the two gel fractions with the highest DNA polymerase activity and analysis of the protein on SDS–polyacrylamide gels. Superimposed densitometric tracings of SDS gels of peak PCI, peak PCII, and a blank are shown in Fig. 5. Only α was present in PCI, while both α and β were present in PCII. These results were highly reproducible with several different enzyme preparations. Thus, both DNA polymerase and RNase H activity reside on α in peak PCI.

DISCUSSION

Two structurally different forms of RNA-directed DNA polymerase having RNase H activity, α and $\alpha\beta$, were purified from AMV. Chromatography on phosphocellulose separated the two enzymes with α (peak PCI) eluting at 0.11 M and $\alpha\beta$ (peak PCII) at 0.22 M potassium phosphate. Both forms of the enzyme were also physically separable by glycerol gradient centrifugation and nondissociating polyacrylamide gel electrophoresis.

Based on SDS–polyacrylamide gel electrophoresis of $\alpha\beta$, α and β had molecular weights of 65,000 and 105,000, respectively. The AMV DNA polymerase isolated by Kacian *et al.* (4) had subunits of 69,000 and 110,000, and is probably identical to $\alpha\beta$. We estimated the molecular weight of $\alpha\beta$ to be 160,000 by density gradient centrifugation, in agreement with the results of Hurwitz and Leis (3).

Chromatography of peak PCII a second time on phosphocellulose gave both peaks PCII and PCI. The α subunits of α and $\alpha\beta$ had identical molecular weights and common antigenic determinants. These results strongly indicate that the α subunits are identical, and suggest that the source of α is $\alpha\beta$. The possibility exists that α and $\alpha\beta$ are unique to different virus types (18), but this seems unlikely because of the identity in molecular weight and antigenic relatedness of α in α and $\alpha\beta$.

DNA polymerase and RNase H activity in AMV are located on α in peak PCI, and probably on the α subunit of $\alpha\beta$. The biological function of β in peak PCII has not been determined. The origin of the β subunit in peak PCII is also open to question. It is interesting that only avian RNA tumor viruses appear to have the β subunit associated with RNA-directed DNA polymerase (2–4, 12, 19, 20). Perhaps $\alpha\beta$ in AMV is analogous to purified Qβ replicase, which is composed of both a viral and several host-specific polypeptide subunits (21, 22).

We thank Drs. H. Raskas and R. Roeder for critical reading of the manuscript. This work was supported by Contract PH43-67-692 within the Special Virus-Cancer Program of the National Cancer Institute, National Institutes of Health, Public Health Service, Bethesda, Md. M. G. is a Research Career Awardee of the National Institutes of Health (5K6-AI-4739), and D. P. G. is a postdoctoral fellow of the American Cancer Society.

1. Mölling, K., Bolognesi, D. P., Bauer, H., Büsen, W., Plassmann, H. W. & Hausen, P. (1971) *Nature New Biol.* **234,** 240–243.
2. Grandgenett, D. P., Gerard, G. F. & Green, M. (1972) *J. Virol.* **10,** 1136–1142.
3. Hurwitz, J. & Leis, J. P. (1972) *J. Virol.* **9,** 116–129.
4. Kacian, D. L., Watson, K. F., Burny, A. & Spiegelman, S. (1971) *Biochim. Biophys. Acta* **246,** 365–383.
5. Green, M., Rokutanda, M., Fujinaga, K., Ray, R. K., Rokutanda, H. & Gurgo, C. (1970) *Proc. Nat. Acad. Sci. USA* **67,** 385–393.
6. Duesberg, P. H. & Robinson, N. S. (1966) *Proc. Nat. Acad. Sci. USA* **55,** 219–227.
7. Landgraf–Leurs, M. & Green, M. (1971) *J. Mol. Biol.* **60,** 185–202.
8. Hirt, B. (1967) *J. Mol. Biol.* **26,** 365–366.
9. Blatti, S. P., Ingles, C. J., Lindell, T. J., Morris, P. W., Weaver, R. F., Weinberg, F. & Rutter, W. J. (1970) *Cold Spring Harbor Symp. Quant. Biol.* **35,** 649–657.
10. Brown, I. R. (1969) *Biochim. Biophys. Acta* **191,** 731–734.
11. Maizel, J. V., Jr. (1969) in *Fundamental Techniques in Virology* (New York, Academic Press), pp. 334–362.
12. Faras, A. J., Taylor, J. M., McDonnell, J. P., Levinson, W. E. & Bishop, J. M. (1972) *Biochemistry* **12,** 2334–2341.
13. Hausen, P. & Stein, H. (1970) *Eur. J. Biochem.* **14,** 278–283.
14. Svedberg, T. & Pederson, K. O. (1940) *The Ultracentrifuge* (Oxford University Press, London).
15. Schachman, H. K. (1959) *Ultracentrifugation in Biochemistry* (Academic Press, New York).
16. Sambrook, J. & Shatkin, A. J. (1969) *J. Virol.* **4,** 719–726.
17. Roblin, R., Harle, E. & Dulbecco, R. (1971) *Virology* **45,** 555–566.
18. Moscovici, C. & Vogt, P. K. (1968) *Virology* **35,** 487–497.
19. Ross, J., Scolnick, E. M., Todaro, G. J. & Aaronson, S. A. (1971) *Nature New Biol.* **231,** 163–169.
20. Duesberg, P., Helm, K. V. D. & Canaani, E. (1971) *Proc. Nat. Acad. Sci. USA* **68,** 757–762.
21. Kondo, M., Gallerani, R. & Weissmann, C. (1970) *Nature* **228,** 525–527.
22. Kamen, R. (1970) *Nature* **228,** 527–529.
23. Aposhian, H. V. & Kornberg, A. (1962) *J. Biol. Chem.* **237,** 519–525.

Proc. Nat. Acad. Sci. USA
Vol. 70, No. 1, pp. 235–239, January 1973

Immunochemical Analysis of the Cross-Reacting Idiotypes of Mouse Myeloma Proteins with Anti-Dextran Activity and Normal Anti-Dextran Antibody

(radioimmunoassay/hapten/light and heavy chains/mice)

DENNIS CARSON AND MARTIN WEIGERT

The Salk Institute for Biological Studies, San Diego, California 92112; and University of California, San Diego, School of Medicine, Department of Medicine, La Jolla, Calif. 92037

Communicated by Henry G. Kunkel, November 13, 1972

ABSTRACT **The idiotype of the mouse myeloma protein with anti-α-1,3 dextran activity, J558, has been characterized by a solid-phase radioimmunoassay. The idiotype of the J558 protein depends on a specific light and heavy chain interaction and is altered in the presence of the hapten, nigerose. Cross-reacting idiotypes were found on another mouse myeloma protein with α-1,3 dextran specificity, normal anti-dextran antibody, and certain reconstructed myeloma proteins composed of the J558 heavy chain and heterologous light chains.**

The immune response to α-1,3-linked dextrans in mice is controlled by an autosomal dominant locus linked to the genes of the constant region of the heavy chain. This locus determines the level of the response to dextrans containing α-1,3 glucosyl linkages, as well as the structure of the antibody. Certain strains that respond well to this antigen produce anti-dextran antibody restricted to the λ class. Most or all anti-dextran antibodies share an antigenic determinant(s) (idiotype) that occurs on a γAλ BALB/c myeloma immunoglobulin with specificity for α-1,3-linked dextrans. Thus, this idiotype provides a marker for the antibody variable region that is coded for by the locus controlling the dextran response (1).

In this study, we show that this idiotype is dependent on variable regions of both heavy and light chains; and that the idiotype of the antibodies to the dextrans is related to their specificity, as demonstrated by studies on the influence of hapten, and the effect of amino-acid differences in the complementarity-determining regions of anti-dextran antibodies on the idiotype.

MATERIALS AND METHODS

Dextran B-1355S (35% α-1,3 linkages) (2) was a gift from Dr. Allene Jeanes, Northern Regional Research Laboratory, U.S. Department of Agriculture, Peoria, Ill. The α-1,3-linked disaccharide, nigerose, was provided by Dr. I. R. Johnson, University College, London, England. Isomaltose was obtained from Pierce Chemical Co., Rockford, Ill. The source of the plasmacytomas and certain properties of the myeloma proteins used are shown in Table 1. The BALB/c mice were obtained from the breeding colony of the Salk Institute; all other strains were obtained from the Jackson Laboratory, Bar Harbor, Me. ^{125}I (NEZ-033H) and [^{3}H]iodoacetic acid (NET-147) were obtained from New England Nuclear Corp., Boston, Mass. SJL, anti-MOPC104E serum was a gift from Dr. Rose Lieberman (NIH).

The proteins produced by plasmacytomas MOPC104E, J558, and W3129 were purified on dextran B1355S–polyacrylamide gel columns (3). The concentration of dextran was 3.3 mg/ml of polymerized gel. The other myeloma proteins and light chains were isolated as discussed (4). Partial reduction and alkylations were performed by the method described by Bridges and Little (5), except for J558. In this case the protein was labeled with [^{3}H]iodoacetic acid according to the method of Edelman and Gottlieb (6) before separation of heavy and light chains.

To produce anti-idiotypic antisera A/HeJ mice were immunized with purified J558 or W3129 proteins by the method of Potter and Lieberman (7). Animals were bled 6 weeks after the first injection and the antisera were pooled. Anti-idiotypic sera were passed over Sepharose columns to which BALB/c serum was bound by the method of Wofsy and Burr (8). (BALB/c x C57/BL6)F1 mice were bled 12 days after immunization and the serum was pooled.

The idiotypic determinant was investigated by the solid-phase radioimmunoassay of Askenase and Leonard (9). 10 × 75 mm polystyrene tubes (Falcon Plastics) were incubated for 4 hr with 1 ml of a 1:500 dilution of anti-idiotypic anti-

TABLE 1. *Properties of myeloma proteins used in this study*

Tumor	Heavy chain class	Light chain class*	Specificity
J558	A	λ_3	α-1,3 dextran
MOPC104E†	M	λ_6	α-1,3 dextran
W3159	A	λ_6	Unknown
XS104	—	λ_6	—
S176	A	λ_1	5-AU and α-1,3 dextran
RPC20†	—	λ_1	—
H2020	A	λ_2	Unknown
S178	—	λ_3	—
W3129	A	κ	α-1,6 dextran

* The subscript refers to the sequence of the λ chain: λ_6 is the prototype sequence; λ_1, λ_2, and λ_3 differ from the λ_6 sequence by 1, 2, or 3 amino acids, respectively (4).

† Tumors obtained from Dr. Michael Potter. All other tumors were induced and characterized in Dr. Melvin Cohn's laboratory (Hirst, J. W., Jones, G., Weigert, M., and Cohn, M., unpublished).

Abbreviations: L and H, light and heavy (chains), respectively; V and C, variable and constant (regions), respectively.

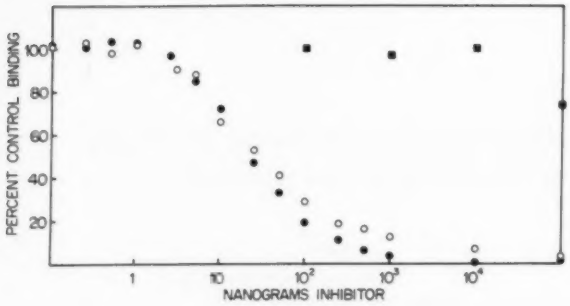

FIG. 1. Inhibition of [^{125}I]J558 and [^{125}I]W3129 binding to their respective anti-idiotypic sera. ○, Inhibition of [^{125}I]J558 binding to anti-J558 by J558: ●, inhibition of [^{125}I]W3129 binding to anti-W3129 by W3129: ■, inhibition of [^{125}I]W3129 binding to anti-W3129 by J558. Percent control binding = (cpm bound in the presence of inhibitor/cpm bound without inhibitor) × 100. Each point represents the average of three determinations. Protein concentrations were determined by the absorbance of undiluted purified protein solutions at 280 nm with an extinction coefficient of 1.40 per mg per ml, 1-cm light path. The specific activity of the [^{125}I]myeloma proteins was about 5000 cpm/ng and 4000 cpm/ng for J558 and W3129, respectively.

serum in phosphate-buffered saline, pH 7.4 (PO_4-saline). Tubes were washed with PO_4-saline and incubated for 30 min in a 1% bovine-serum albumin solution in PO_4-saline. The albumin solution was removed and each tube received 1.1 ml of 1% albumin–0.1% normal rabbit serum in PO_4-saline containing about 25,000 cpm of [^{125}I]myeloma protein and various amounts of unlabeled protein. Iodinations were performed by the chloramine T method of Greenwood, Hunter, and Glover (10). Tubes were incubated for 18 hr at 37° and washed three times with PO_4-saline. The radioactivity bound to the tubes was measured in a Packard auto-gamma counter. Nonspecific binding to albumin-coated tubes was less than 0.1% of the added counts and was subtracted. Inhibition curves obtained by this method were sigmoidal on linear coordinates. For convenience in calculation of the relative inhibitory power of the various proteins, data were plotted on a semi-logarithmic scale, and gave approximately linear plots for a large range of concentrations.

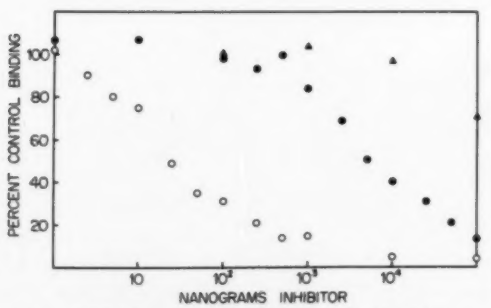

FIG. 2. Inhibition of [^{125}I]MOPC104E binding to anti-MOPC104E idiotypic serum. ○, inhibition of [^{125}I]MOPC104E binding by MOPC104E; ●, inhibition of [^{125}I]MOPC104E binding by J558; ▲, inhibition of [^{125}I]MOPC104E binding by W3129. Each point represents the average of four determinations. The percent control binding and protein concentrations were determined as described in Fig. 1. The specific activity of the [^{125}I]MOPC104E was about 7000 cpm/ng.

TABLE 2. *Binding to dextran* of [^{3}H]558 heavy chain combined with heterologous light chains*

Heavy chain	Light chain	% Bound
J558	—	0
J558	W3129 (κ)	0
J558	J558 (λ_0)	63, 65
J558	XS104 (λ_0)	58, 60
J558	MOPC104E (λ_0)†	60, 61
J558	J2020 (λ_3)	53, 63
J558	RPC-20 (λ_1)	72, 78
J558	S176 (λ_1)	60, 65
J558	S178 (λ_3)	34, 28

* Aliquots of the reconstructed mixtures were passed over columns containing 1–2 ml of dextran B1355S–polyacrylamide. Columns were washed with PO_4-saline to remove unbound protein. Bound protein was eluted with 0.2 M glycine·HCl buffer (pH 2.2). % bound = [(cpm eluted, pH 2.2)/(total cpm recovered)] × 100. In all cases recoveries were greater than 85% of input counts.

† The MOPC104E light chain used in this reconstruction was isolated from the urine of mice bearing the MOPC104E tumor.

The heavy and light chains of partially alkylated proteins were separated, and proteins were reconstructed from separated heavy (H) and light (L) chains according to the methods described by Bridges and Little (5), except that light chains were used in 4-fold molar excess over [^{3}H]iodoacetic acid-labeled J558H chain.

RESULTS

Specificity of anti-idiotypic antibodies

It has been shown that immunization of certain strains of mice with BALB/c myeloma proteins elicits highly specific antibodies (7). For example, strain A/He mice immunized with J558 myeloma protein produce antibody that showed no detectable crossreaction with either normal BALB/c serum or 60 different BALB/c myeloma proteins, including MOPC-104E, in precipitation tests in double-diffusion agar-gel plates (Weigert, unpublished). An analogous result has been obtained by immunization of SJL mice with MOPC104E

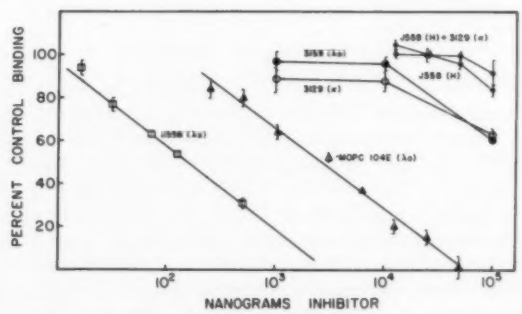

FIG. 3. Inhibition of [^{125}I]J558 binding to anti-J558 serum by various myeloma proteins and subunits. Each point represents the mean of five determinations; brackets represent the standard error of the mean. Protein concentrations were determined as in Fig. 1. The specific activity of the [^{125}I]J558 was about 250 cpm/ng.

(Rose Lieberman, unpublished). The specificity of these anti-idiotypic antibodies and anti-W3129 antibody produced in A/He mice were tested by the solid-phase radioimmunoassay. By this assay no significant crossreaction could be demonstrated in any of these three cases (Figs. 1, 2, and 3; Table 3).

Crossreactions have been shown between anti-idiotypic antisera directed against a BALB/c myeloma protein with phosphorylcholine specificity and other myeloma proteins also in the γAλ class with a similar specificity, suggesting the possibility of sequence similarity between these independently induced myeloma proteins (11). Since both MOPC104E and J558 have specificity for α-1,3-linked oligosaccharides (12, 13), it was of particular interest to test MOPC104E for crossreaction with the J558 idiotype by the radioimmunoassay. As shown in Fig. 3, MOPC104E significantly inhibits the binding of [^{125}I]J558 to anti-J558 as compared to either normal BALB/c serum or other myeloma proteins; however, it is not as effective an inhibitor as J558 (Table 3). Likewise, J558 can inhibit the binding of [^{125}I]MOPC104E to anti-MOPC104E idiotypic antiserum prepared in SJL mice, however not as effectively as MOPC104E (Fig. 2). To eliminate any differences in inhibition resulting from the degree of polymerization of the two proteins, the monomeric form of partially reduced and alkylated MOPC104E was used in these experiments.

J558 (13) and MOPC104E (12), while demonstrating specificity for α-1,3-linked oligosaccharides, are different as shown by the analysis of inhibition of dextran binding of these proteins by various nigerosyl derivatives. One explanation for the idiotypic difference between these proteins could be that they share certain idiotypic determinants in common, while differing in others. However, as shown in Fig. 3, though the relative inhibitory power of MOPC104E is less than that of J558, the [^{125}I]J558 binding to anti-J558 can be completely inhibited by MOPC104E. Though the relative inhibitory power of J558 is less than that of MOPC104E, the [^{125}I]-MOPC104E binding to anti-MOPC104E can be almost completely inhibited by J558 (Fig. 2). These results indicate that both proteins share a similar, but not identical, determinant(s). Since the light chains of J558 and MOPC104E are identical (14), the binding site and the idiotype of MOPC-104E and J558 must differ because of differences in heavy chain sequence.

TABLE 3. *Relative inhibitory power* of various immunoglobulins and immunoglobulin subunits of the binding of [^{125}I]J558 protein to anti-J558 idiotypic serum*

Protein	Relative inhibitory power
J558	1.0
J558H chain–xS104 λ_a	1.0
J558H chain–MOPC104E λ_a	1.0
J558H chain–J2020 λ_2	1.0
J558H chain–S176 λ_1	1.0
J558H chain–RPC20 λ_1	1.0
J558H chain–S178 λ_3	0.150
MOPC104E	0.050
J558†	0.005
W3159	<0.001
W3129	<0.001
J558H chain–W3129α	<0.001
J558H	<0.001
λ_a	<0.001

* Relative inhibitory power is the ratio of nanograms of inhibitor giving 50% inhibition of [^{125}I]J558 binding to anti-J558/nanograms of control giving 50% inhibition of [^{125}I]J558 binding to anti-J558. For reconstructed molecules, the control is J558 reconstructed from separated J558H and λ_a; in all other cases, the control is partially reduced and alkylated J558.

† Relative inhibitory power of the [^{125}I]MOPC104E binding to anti-MOPC104E.

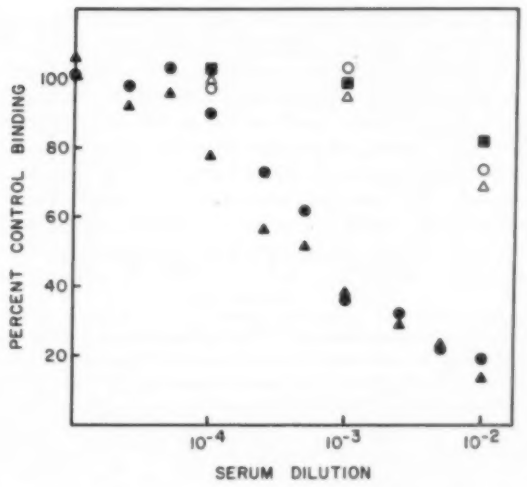

FIG. 4. Inhibition of [^{125}I]myeloma protein binding to anti-idiotypic sera by serum from normal mice and from mice immunized by dextran B1355S. Inhibition of [^{125}I]J558 binding to anti-J558 by serum from immunized mice, ●; by serum from unimmunized mice, ○. Inhibition of [^{125}I]MOPC104E binding to anti-MOPC104E by serum from unimmunized mice, △; by serum from immunized mice, ▲. ■, Inhibition of [^{125}I]W3129 binding to anti-W3129 by serum from immunized mice. Each point represents the average of three determinations. The specific activities of the [^{125}I]myeloma proteins were the same as in the experiments described in Figs. 1 and 2.

As has been shown previously, immunization of certain strains of mice such as BALB/c with dextran B1355S elicits an anti-dextran antibody that only reacts with dextrans containing α-1,3 glucosyl linkages. Furthermore, this antibody appears to share the J558 idiotype (1). As shown in Fig. 4, pooled serum from (BALB/c x C57BL6)F1 mice immunized with dextran B1355S can specifically inhibit the [^{125}I]MOPC104E binding to anti-MOPC104E and [^{125}I]-J558 binding to anti-J558. The relative inhibitory power of the normal anti-dextran antibody, which in this serum is all of the γM class (Carson and Riblet, unpublished), is about the same for J558 and MOPC104E binding. Since the inhibitory power of either J558 or MOPC104E differs markedly when compared to the inhibitory power of either protein of its own idiotype binding (Table 3), the normal anti-dextran must either be of a unique idiotype that crossreacts equally well with either idiotype or a mixture of idiotypes.

Heavy- and light-chain contribution to the J558 idiotype

The subunits of J558 have been tested for their contribution to the idiotype. As shown in Fig. 3 and Table 3 neither J558H

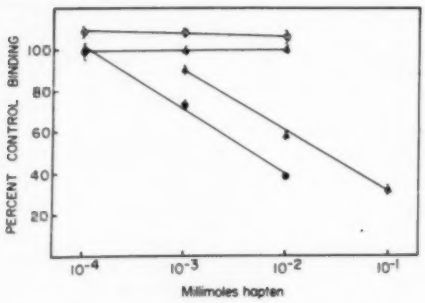

FIG. 5. Effect of hapten on idiotype expression. Percent control binding = (cpm bound in the presence of hapten/cpm bound without hapten) × 100. Each point represents the mean of three determinations and the brackets indicate the standard error of the mean. Inhibition of [^{125}I]J558 binding to anti-J558 by isomaltose, ○; by nigerose, ●. Inhibition of [^{125}I]W3129 binding to anti-W3129 by nigerose, △; by isomaltose, ▲. The specific activity of [^{125}I]J558 was about 250 cpm/ng, of [^{125}I]W3129 about 4000 cpm/ng.

chain nor λ_0 (J558L chain for example), at various concentrations, significantly inhibits the binding of [^{125}I]J558 to anti-J558. As shown in Figs. 5 and 6, the idiotype is restored by reconstruction of J558 from separated J558 subunits. In order to test whether the idiotype might be restored to a J558L or H chain in combination with a heterologous subunit, both reconstructed molecules of J558H chain–3129 L chain (κ) and native W3159 (a IgAλ_0 myeloma protein without anti-dextran activity) were tested for the J558 idiotype. As shown in Fig. 3 neither protein inhibits [^{125}I]J558 binding. Conditions for reconstruction were used under which the efficiency of reconstruction of proteins the size of the original myeloma protein has been shown to be high (5). These results suggest that the J558 idiotype is formed by the specific interaction of heavy- and light-chain variable regions. A similar requirement is found for the dextran-binding capacity of J558. As shown in Table 2 neither J558H nor J558H chain–W3129 (κ) chain reconstructed protein bind to dextran, whereas dextran binding is restored to the protein reconstructed from J558 chain and λ_0 chain.

The idiotype of heterologous chain mixtures

As shown above, the J558 idiotype depends on a specific H and L chain interaction. For example, J558H and a heterologous L chain of the κ class, W3129, lack the idiotype. The effect of subtle differences in sequence on the degree of specificity was determined by analysis of the idiotype of J558H in combination with λ chains possessing various amino-acid substitutions (λ_1,λ_2, and λ_3; Table 1). Fig. 6 and Table 3 show the results of inhibition of binding of [^{125}I]J558 to various J558-λ chain combinations. As expected, reconstruction of J558 with λ_0 chains resulted in an idiotype identical to that of J558. λ_1 (serine to asparagine at residue 25), λ_1 (isoleucine to leucine at residue 50), and λ_2 (serine to threonine at residue 25 and serine to glycine at residue 32) have no detectable effect on the idiotype. The λ_3 (serine to asparagine at residue 25, glycine to asparagine at residue 52, and histidine to arginine at residue 97) significantly alters the idiotype (Table 3). This result cannot be attributed to differences in the efficiency of reconstruction of λ_0 and λ_3 with J558H chain. As shown in Table 2, binding to dextran is restored in all cases to approximately the same extent except for J558H chain–λ_3. If the percent bound reflects the minimum efficiency of reconstruction of J558 chain–λ_3 relative to J558H chain–λ_0, the relative inhibitory power of the J558H–λ_3 idiotype would be 0.30. If the efficiency of reconstruction is the same for λ_0 and λ_3, the difference in dextran binding of J558–λ_3 as compared to J558H–λ_0 might reflect a lower affinity for dextran. By this explanation the relative inhibitory power of J558H chain–λ_3 is 0.150.

Effect of hapten on the J558 idiotype

J558 binds to α-1,3-linked dextrans and is inhibitable by the α-1,3-linked disaccharide, nigerose (13). Fig. 5 shows the effect of nigerose on the binding of [^{125}I]J558 to anti-J558. Under the conditions used in this assay (J558 concentrations of 100 ng/1.1 ml), the binding was 60% inhibitable at a 10 mM concentration of nigerose. No inhibition can be observed at the same concentration of the α-1,6-linked disaccharide, isomaltose. Further evidence for the specificity of inhibition comes from the reciprocal experiment with W3129, a γAκ that binds α-1,6-linked dextrans. In this case, isomaltose inhibits the binding of [^{125}I]W3129 to anti-W3129, whereas nigerose does not, precluding a nonspecific effect of nigerose.

DISCUSSION

These studies show that the idiotype of J558 a γAλ anti-dextran myeloma is dependent on a specific H-chain and L-chain interaction. A crossreacting determinant is found on at least 90% of the anti-dextran antibody of mouse strains that respond well to this antigen. The idiotype is absent from the anti-dextran antibody of strains that respond poorly. Both the level of the response and the idiotype of the antibody are controlled by the dextran-response locus, which is inherited as an autosomal dominant locus. Because the idiotype is controlled by a V_H (heavy chain variable region) and a V_λ (λ chain variable region) gene, the inability of certain strains such as C56BL/6 to respond in this manner could be due to differences in one or both of these V genes. The idiotypes of rabbit antibodies to streptococcal carbohydrates are also inherited (15). The heavy and light chains of these antibodies,

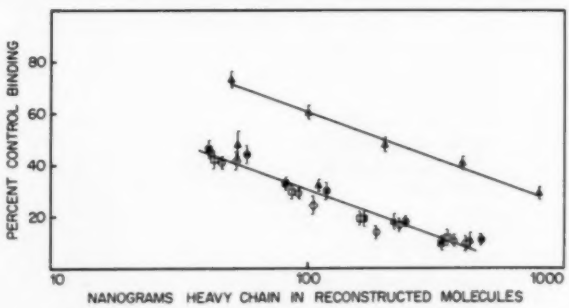

FIG. 6. Inhibition of [^{125}I]J558 binding to anti-J558 by reconstructed antibodies. Each point represents the mean of 5 determinations; brackets represent the SEM. Heavy chain concentrations were determined as in Fig. 1. Values were not corrected for the efficiency of reconstruction as determined by binding to dextran of the reconstructed proteins (Table 2). The following symbols are used for the light chains in combination with J558H: ◇, J558; ■, S104; ○, MOPC104E; ●, RPC20; □, J2020; ▲, S176; △, S178. The specific activity of [^{125}I]J558 was about 250 cpm/ng.

however, have separate idiotypic determinants that are inherited independently. In this case, only the gene controlling V_H appears to be linked to C_H (heavy chain constant region) genes. That dextran response is controlled by a locus linked to the genes controlling C_H structure (1) only suggests that the variance is in V_H, because the possibility remains that in mice both V_H and V_λ genes are linked to the C_H genes.

The effect of hapten on the idiotype of rabbit anti-*p*-azobenzoate antibodies shown by Brient and Nisonoff (16) has suggested a relationship of idiotypic determinants to antibody specificity. Our results suggest that the idiotype of the anti-dextran antibody is also due to determinants related to the specificity of the antibody, since the α-1,3-linked disaccharide, nigerose, inhibits at least 60% of the binding of J558 to the anti-idiotypic serum.

Kunkel and coworkers have shown crossreacting idiotypes among cold agglutinins (17) and antigammaglobulins (18) in human populations. Such evidence for the relationship of idiotype to specificity is also illustrated here by the comparison of myeloma antibodies J558 (13) to MOPC104E (12) that have specificities for various nigerosyl derivatives. We have shown that the hapten-inhibitable idiotype of J558 is similar, but not identical, to the idiotype of the anti-dextran myeloma antibody, MOPC104E. Since the λ_3 chains of both are identical, this difference must be due to amino-acid sequence differences in the V_H regions of these antibodies that might also modulate the specificity for α-1,3-linked saccharides. Additional support for this notion comes from comparisons of the idiotype of anti-dextran antibodies with altered L-chains. Certain amino-acid differences in what are believed to be the complementarity determining regions of L-chains have no detectable effect on the idiotype. Hence, even with the sensitive assay used here, idiotypic identity is not an argument for sequence identity. In one case (three amino-acid differences), however, the idiotype is significantly altered. In this case all differences are confined to what have been proposed to be the L-chain complementarity-determining regions (19), and may, if the binding site and idiotype of these antibodies are synonomous, directly affect the idiotypic determinant. Sequence variation in the binding site may, however, affect other regions of antibody structure that, in addition, are subject to conformational changes resulting from antibody–hapten interaction.

The normal anti-dextran antibody may represent a heterogeneous population with similar, but not identical, idiotypes, as indicated by the comparison of the relative inhibitory power of normal anti-dextran antibody of the [^{125}I]MOPC104E binding to anti-MOPC104E and [^{125}I]J558 binding to anti-J558. This comparison demonstrates at least two idiotypes for anti-dextran antibodies, and from the studies with reconstructed anti-dextran antibodies it is conceivable that the idiotype, as defined by this assay, could include a large number of antibodies with different sequences. Since antibodies with different sequences are known to bind dextran, certain variants of a germ-line antibody may have new specificities while retaining specificity for dextran. The normal anti-dextran antibody, therefore, could consist mainly, if not exclusively, of antibodies at early stages of diversification.

We are indebted to Dr. Rose Lieberman, who developed the methods for preparing anti-MOPC104E idiotypic antiserum, and permitted us to study the antiserum made in her laboratory. Aided by a grant from the National Institutes of Health, no. GM 18263, to M. W., and Research Grant A105875 and Training Grant A100430 from the National Institute of Allergy and Infectious Diseases to Dr. Melvin Cohn. M. W. is a recipient of an American Cancer Society Faculty Research Award PRA-59.

1. Blomberg, B., Geckeler, W. & Weigert, M. G. (1972) *Science* **177**, 178–180.
2. William, C. A., Alexander, B. H. & Jeanes, A. (1955) *Arch. Biochem. Biophys.* **59**, 61–75.
3. Carrel, S. & Barandun, S. (1971) *Immunochemistry* **8**, 39–48.
4. Weigert, M. G., Cesari, I. M., Yonkovich, S. J. & Cohn, M. (1970) *Nature* **228**, 1045–1047.
5. Bridges, S. H. & Little, J. R. (1971) *Biochemistry* **10**, 2525–2530.
6. Edelman, G. M. & Gottlieb, P. D. (1970) *Proc. Nat. Acad. Sci. USA* **67**, 1192–1199.
7. Potter, M. & Lieberman, R. (1967) *Advan. Immunol.* **7**, 91–145.
8. Wofsy, L. & Burr, B. J. (1969) *J. Immunology* **103**, 380–382.
9. Askenase, P. W. & Leonard, E. J. (1970) *Immunochemistry* **7**, 29–42.
10. Greenwood, F. C., Hunter, W. M. & Glover, J. S. (1963) *Biochem. J.* **89**, 114–123.
11. Potter, M. & Lieberman, R. (1970) *J. Exp. Med.* **132**, 737–751.
12. Young, N. M., Jocius, I. B. & Leon, M. A. (1971) *Biochemistry* **10**, 3457–3460.
13. Lundblad, A., Stellar, R., Kabat, E. A., Hirst, J. W., Weigert, M. & Cohn, M. (1972) *Immunochemistry* **9**, 535–543.
14. Cesari, I. M. & Weigert, M. in press.
15. Eichmann, K. & Kindt, T. J. (1971) *J. Exp. Med.* **134**, 532–552.
16. Brient, B. W. & Nisonoff, A. (1970) *J. Exp. Med.* **132**, 951–962.
17. Kunkel, H. G. (1970) *Fed. Proc.* **29**, 55–58.
18. Agnello, U., Joslin, F. G. & Kunkel, H. G. (1972) *Scand. J. Immunol.* **1**, 283–290.
19. Wu, T. T. & Kabat, E. A. (1970) *J. Exp. Med.* **132**, 211–250.

Proc. Nat. Acad. Sci. USA
Vol. 70, No. 1, pp. 240–244, January 1973

Weaver Mutant Mouse Cerebellum: Defective Neuronal Migration Secondary to Abnormality of Bergmann Glia

(cerebellar development/neuron-glial cell interaction/neurological mutant mice)

P. RAKIC AND R. L. SIDMAN

Department of Neuropathology, Harvard Medical School and Department of Neuroscience, Children's Hospital Medical Center, Boston 02115

Communicated by Francis O. Schmitt, October 30, 1972

ABSTRACT **Previous work showed that in cerebella of mice homozygous for the autosomal mutation weaver, *wv*, most postmitotic granule cell neurons die during the first 2 weeks after birth close to their site of genesis in the external granular layer. Analysis of the less severely affected heterozygotes by electron microscopy and autoradiography indicates that granule cell death occurs several days after cell genesis and is secondary to failure of their somas to migrate across the molecular layer to the granular layer. This migration defect in turn appears secondary to a hitherto unrecognized disorder of Bergmann glial cells, the cells that normally guide the young neurons in their migration. In +/*wv* cerebella, Bergmann glial processes are enlarged and irregular in caliber, electronlucent, and often vacuolated; in *wv*/*wv*, Bergmann cell processes are almost absent. The primary genetic abnormality remains undefined, but the gene dosage effect, here recognized at a cellular level for the first time in a mammalian neurological mutant, suggests that even though neuronal death serves as the most prominent and clinically relevant phenotypic expression, the Bergmann glial abnormality may actually be closer to the primary cellular target of the *wv* genetic locus.**

The cerebellar cortex has been the most intensively analyzed region of adult brains (1–3), and it receives comparable special emphasis during development (4). In the immature cerebellum, precursors of granule cell neurons proliferate on the external surface. The postmitotic daughter cell then undergoes a highly ordered series of transformations in shape as its soma migrates inward to the granular layer, while a T-shaped axon remains behind in the molecular layer where it contacts the growing dendrites of earlier-formed Purkinje cells (5–7). These cell relationships are essentially identical in mice (8, 9), rats (10), rhesus monkeys (6, 7), and man (11).

Recent electronmicroscopic analysis of monkey cerebellum has demonstrated that, during their entire translocation across the molecular layer during late developmental stages, young granule cell neurons are directly apposed to rectilinear, vertically oriented Bergmann glial fibers that span the entire width of the layer (6). The newly generated granule cell contacts the distal part of the Bergmann glial fiber soon after its final division or earlier; then the vertical part of the axon maintains the contact even after the granule cell soma has passed deep to the Bergmann and Purkinje cell somas and into the granular layer. (The term "contact" is used to designate side by side apposition, with the electron dense components of the surface membranes of the two cells separated by an about 180-Å space usually seen in epithelia; no other cellular processes intervene.)

Several observations suggest that this cell interrelationship is necessary for the granule cell to attain its normal position and establish its synaptic contacts (6). First, if numerous sections through a migrating granule cell are examined, the neuron–glial contact is always seen. Second, the young granule cell establishes no such relationship with any of the myriad other processes that it encounters during its passage across the complex developing molecular layer. Third, a similar relationship is seen at late stages of cerebral development in fetal monkeys, when young neurons migrating outward from their sites of genesis near the ventricular wall to the distant cortical plate are apposed during their entire migration to radially-arranged glial fiber guides (12, 13).

In both cerebellum and cerebrum these oriented glial fibers perhaps impose radial constraints and provide guidelines facilitating migration of young neurons, especially at late developmental stages when the migration route is densely packed with cell processes, many of which have already established synaptic connections (6).

Weaver (*wv*), a mutant mouse with an abnormal cerebellum, provides a critical test of the possible developmental significance of this neuron–glia relationship. The mutation occurred in and is maintained in the C57BL/6J strain. It is expressed as an autosomal recessive by the behavioral criteria of severe ataxia, hypotonia, and fine tremor (14, 15). Homozygous affected mice rarely survive more than 1 month after birth. Heterozygous mice are often slightly smaller in body size than normal, but do not show abnormal behavior (16).

Cerebella of 3-week-old or older *wv*/*wv* mice are drastically reduced in size. The most dramatic histological abnormality is virtual absence of the granule cell population (15). In addition, the molecular layer is attenuated, and the Purkinje cells are crowded, somewhat irregularly oriented, and moderately reduced in volume. The deficit of granule cells is accounted for by cell death in the external granular layer during the first 2 weeks after birth.

Rezai and Yoon (16) established that cerebellar development is partially affected in weaver heterozygotes, both on the inbred genetic background and where the gene was outcrossed to other backgrounds. The major defect is an abnormality of postmitotic granule cell migration. By autoradiography after injection of [^{3}H]thymidine, they found that in the heterozygote, external granule cells proliferate normally but the daughter cells move more slowly than normal across the molecular layer, some of them never reaching the granular layer. They confirmed earlier observations that extensive cell death occurs in the external granular layer of homozygous weavers (15) and suggested, by extrapolation from their findings in heterozygotes, that cell death is a consequence of migration failure rather than the reverse.

The present study was undertaken to seek evidence for a possible abnormal developmental interaction between granule cell neurons and Bergmann glia that might underlie the migration disorder. C57BL/6J-+/*wv* mice were mated and pro-

duced wild-type, heterozygous, and homozygous affected offspring in the expected 1:2:1 Mendelian ratios. Since the homozygous mutants die by about 3 weeks of age on the inbred genetic background, one older *wv/wv* male from a cross with noninbred mice was studied. In another series, the ovaries from a *wv/wv* female were transplanted to a normal histocompatible recipient, who was mated to a wild-type (+/+) male and produced a litter of 100% +/*wv* offspring. In both series, mice were killed and the brains were fixed by cardiac perfusion for 15–25 min with a formaldehyde–glutaraldehyde mixture in phosphate buffer (6, 7). Brains were examined at intervals between 3 and 21 days after birth, when cerebellar granule cells are forming and migrating, and at 3 months of age. Each brain was removed and bisected in the midsagittal plane. Three to four sagittal slices across one side of the cerebellum were processed for electronmicroscopic analysis; the other half of the brain was impregnated by a modification of the rapid Golgi method (6, 7). In a third series, progeny from several additional matings of C57BL/6J-+/*wv* mice were injected once each with 5 μCi/g of [^{3}H]-thymidine between 3 and 21 days after birth and were killed 1 hr and either 1, 2, 5, or 10 days later; sections of cerebellum were processed for autoradiography (17).

Up to the third day after birth animals show no differences in cerebellar size, gross morphology, or cytoarchitectonic organization. As noted previously (16), the differences between normal, heterozygous, and homozygous animals appear at the fourth day, the age when granule cells begin to migrate inward from the external granular layer. Specimens taken at 10 days, when granule cell proliferation and migration reaches a peak (8), demonstrate the developmental defect vividly (Fig. 1). The cerebellar cortex in homozygous wild-type (+/+) animals (Fig. 1*A*) shows granule cells descending through the molecular layer along straight, vertically oriented Bergmann glial fibers and undergoing the same complex morphogenetic transformations that were reconstructed three-dimensionally for developing monkey cerebellar cortex (6). In 10-day old heterozygous (+/*wv*) littermates the gross size of the cerebellum is reduced by 5–10%. Cytologically it is clearly distinguishable from normal (Fig. 1*B*). The external granular layer is somewhat disarranged and occasionally wider than in control specimens. Purkinje cells are less strictly aligned, the granular layer is much thinner than in the control, and the molecular layer is narrower but contains about a 3-fold excess of cell bodies per unit volume (Fig. 1*B*). Electronmicroscopic examination establishes that these cell bodies belong to young granule cells, although the oval or round shape of many of them is a departure from the usual bipolar form of cell bodies that are in transit across the developing molecular layer. Those cells that do show typical somas appear to be properly aligned with normal Bergmann glial fibers (Fig. 2*A*). However, many of the cells that have anomalous shapes lie contiguous with abnormal glial processes. Others appear to have lost their direct contact with a glial cell and are in various stages of degeneration (Fig. 1*B*). The increased number of granule cell somas and the rounded, rather than bipolar, shapes are consistent with a delay in translocation across the molecular layer, as found by Rezai and Yoon (16).

A dramatic finding in +/*wv* mice is an alteration in many Bergmann glial cells. The cell bodies and proximal segments of the cytoplasmic processes in the molecular layer appear normal, but the distal half of the Bergmann fibers are often 2- to 4-times larger in diameter than normal and show varicose, irregular contours (Figs. 1*B* and 2*B*). The enlarged

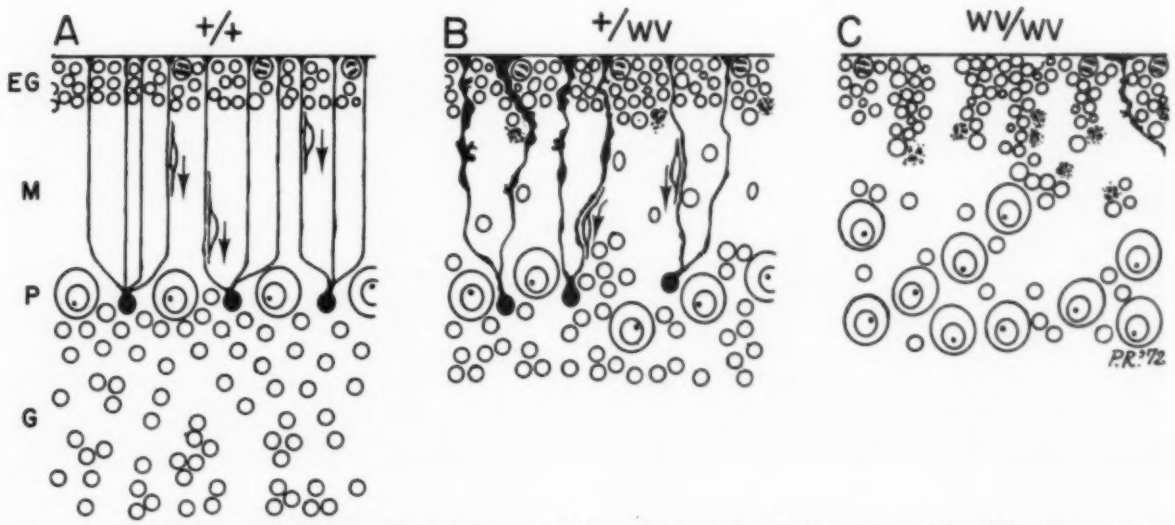

FIG. 1. Schematic drawing of the developing cerebellar cortex in 10-day-old wild-type (*A*), heterozygous (*B*), and homozygous weaver (*C*) littermates. To highlight the main effects of the *wv* allele, the drawing has been grossly simplified by omitting dendrites and axons of Purkinje and granule cell neurons, and omitting entirely the other cell classes and afferent axons of the cerebellar cortex. (*A*) In normal mice, cells migrate (*arrows*) from the external granular layer (*EG*) to the granular layer (*G*) along straight, radially oriented Bergmann glia (*black cells*) whose cytoplasmic processes span the entire thickness of the molecular layer (*M*). (*B*) In heterozygous mice, a smaller than normal number of granule cell somas becomes successfully translocated. Many are oval or round and lie in contact with thickened and irregular Bergmann glial fibers; some of these granule cells remain permanently in the molecular layer or degenerate (*fragmented cells*). (*C*) In homozygous affected weavers, almost no granule cells descend deep to the Purkinje cell bodies and, instead, most of them degenerate at the border between the external granular layer and the molecular layer.

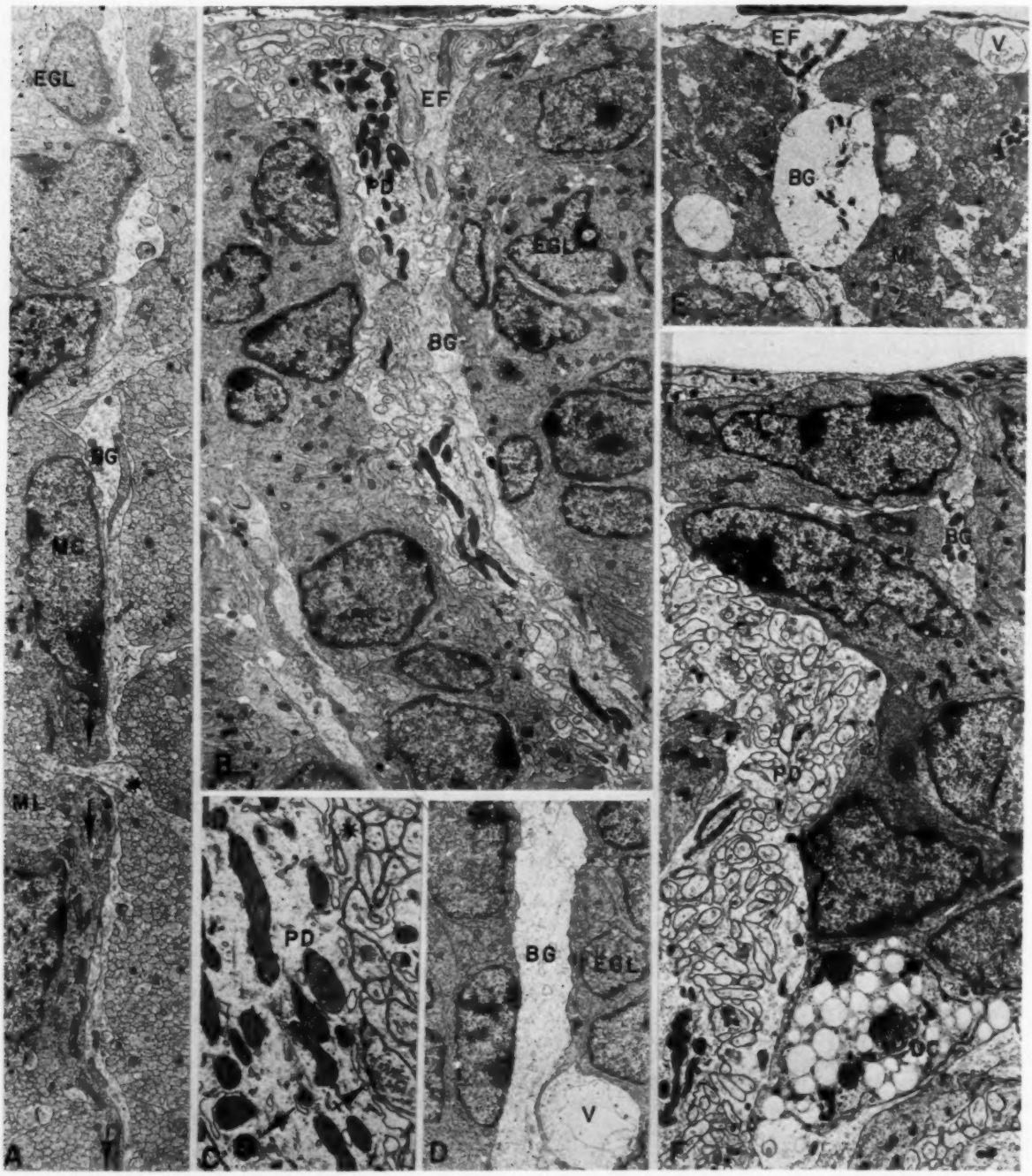

FIG. 2. Electronmicrographs of comparable regions of cerebellar cortex from weaver heterozygotes (+/*wv*) (*A–E*) and homozygotes (*wv/wv*) (*F*) at various ages. (*A*) Bipolar-shaped part of a migrating cell (*MC*) passing inward (*arrows*) from the external granular layer (*EGL*) across the molecular layer (*ML*); through the whole length of the picture this young granule cell neuron is closely apposed to a Bergmann glial process (*BG*) and appears to ignore the other cell processes that cross its path (*asterisks*); 10-day-old heterozygous mouse. (*B*) Purkinje cell dendrite (*PD*) penetrates the external granular layer (*EGL*), although they never do so in normal specimens; the dendrite lies adjacent to an enlarged Bergmann glial fiber (*BG*) and terminates among glial endfeet (*EF*). Attenuated glial cytoplasmic processes separate the Purkinje and other cell processes from the external surface; 11-day-old heterozygous animal. (*C*) Abnormally positioned Purkinje dendrites (*PD*) in a heterozygous animal are identified by several normal features, such as multivesicular bodies (*arrow*), synapses on dendritic shafts (*crossed arrow*), and dendritic spines (*asterisk*); however, in areas such as this where granule cell axons are missing, the dendritic spines are devoid of synaptic contacts. (*D*) Many of the Bergmann glial fibers (*BG*) in heterozygous animals are enlarged and are composed of unusually electronlucent cytoplasm with numerous empty vacuoles (*V*). (*E*) The vacuolization (*V*) is more severe in

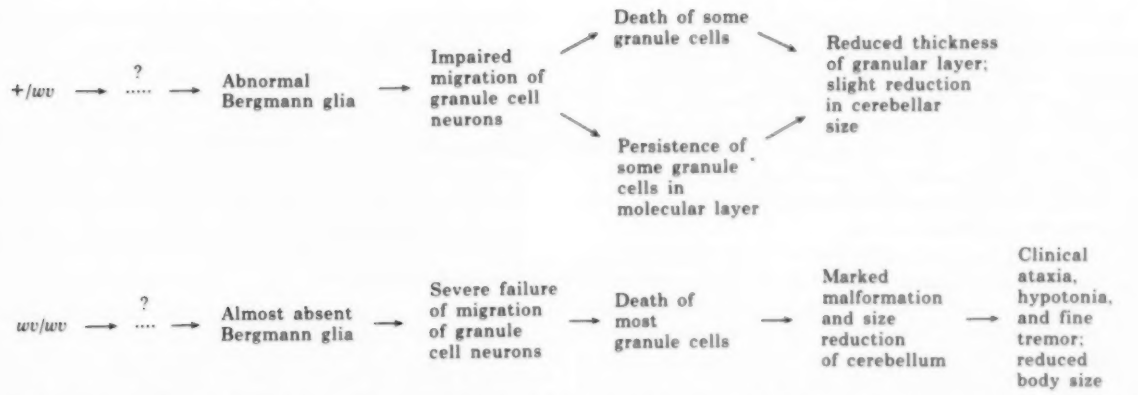
+/wv
?
Abnormal Bergmann glia
Impaired migration of granule cell neurons
Death of some granule cells
Reduced thickness of granular layer; slight reduction in cerebellar size
Persistence of some granule cells in molecular layer
wv/wv
?
Almost absent Bergmann glia
Severe failure of migration of granule cell neurons
Death of most granule cells
Marked malformation and size reduction of cerebellum
Clinical ataxia, hypotonia, and fine tremor; reduced body size

FIG. 3. Diagram suggesting a likely causal sequence in the main phenotypic expressions of the weaver mutation. The *dotted lines* and *question marks* at the left indicate lack of information on the primary action and target cell of the *wv* genetic locus.

profiles are electronlucent and contain numerous empty vacuoles of various sizes (Fig. 2*D*). Purkinje cell dendrites are closely entwined with some of these altered glial fibers and penetrate the full thickness of the external granular layer (Fig. 2*B*,*C*). The Purkinje cells develop numerous dendritic spines despite the lack of contact with granule cell axons. Dendritic spines not only form in the absence of the usual presynaptic element, but they are then maintained indefinitely in the absence of any direct synaptic input.

Cerebella of 10-day-old *wv*/*wv* littermates are about one-quarter to one-third the normal size, i.e., about the size of normal 3-day cerebella. Cytoarchitecturally they are very abnormal. The external granular layer is indistinct. Postmitotic granule cells are concentrated in irregular vertical stacks in which many cells, particularly the deeper ones, are degenerating (Figs. 1*C* and 2*F*). Purkinje cells form a layer several rows thick, and there are virtually no granule cells in the usual zone below them (Fig. 1*C*). Radial Bergmann glial fibers are very rare, though not absent. Whereas in the normal cerebellum at this age the endfeet of Bergmann fibers form an almost continuous sheet at the external surface, the reduced number of Bergmann fibers in the homozygous affected weavers leaves large areas without an external glial coat. The radial alignment of migrating granule cells along glial fibers, an intercellular relationship so frequently encountered in ultrathin sagittal sections of the developing +/+ or +/*wv* specimens, has not been observed in extensive sampling of the medial parts of the *wv*/*wv* cerebellum.

At subsequent developmental stages, cerebellar cytoarchitecture in the heterozygotes somewhat improves. Many of the granule cells do eventually succeed in crossing the molecular layer and reach the granular layer. However, some granule cells remain permanently in the molecular layer, and the granular layer never attains normal thickness. In homozygous affected mice, abnormalities become even more severe at later developmental stages. Most of the postmitotic granule cells that accumulate just below the proliferating cells in the external granular layer degenerate and completely disappear. Only a few granule cells, particularly in the most lateral parts of the cerebellar hemispheres, descend among the multilayered Purkinje cell somas. Those granule cells that do survive in the heterozygous and homozygous mutants form morphologically normal synaptic connections with mossy fibers, Golgi II neurons, and spines of Purkinje cell dendrites.

Our autoradiographic studies, confirming and amplifying those of Rezai and Yoon (16), illustrate further the dramatic disturbance of cell migration. One hour after [^{3}H]thymidine injection on P9 (Postnatal day 9) or P13, the labeling index (% labeled cells) in the external granular layer is normal or increased in +/*wv* and *wv*/*wv*. (The apparently increased labeling index in the homozygous weaver probably reflects increased death of unlabeled cells.) 2 Days after injection on P10, somas of heavily labeled cells are in transit across the molecular layer in +/+ animals, but lie predominantly in the deepest zone of the external granular layer in *wv*/*wv* mice. 5 Days after labeling on P9 or P10, most of the heavily labeled cell bodies in the normal cerebellum have entered the granular layer as described earlier (8); in the heterozygote, by contrast, about half or more still lie in the molecular layer, whereas in the *wv*/*wv* cerebellum, only rare labeled cells have left the external granular layer. At 10–12 days after injection on P10 to P12, labeled cells again lie mainly in the granular layer in the +/+ cerebellum and are in the molecular and granular layers in +/*wv*, while few labeled cells persist in the *wv*/*wv* specimen. Heterozygotes at 10 and 11 days after injection show a lower percentage of their labeled cells in the granular layer than wild-type animals at 5 days after injection.

The interval between cell generation and cell death was estimated by recording the percentage of pyknotic nuclei labeled in +/*wv* and *wv*/*wv* specimens killed at various times after a single injection of [^{3}H]thymidine on P9, 10, 11, or 12.

---

some areas and is accompanied by degeneration of the Bergmann fiber shafts (*BG*) in the molecular layer (*ML*) and endfeet (*EF*) spreading at the external surface of the cerebellum; 3-week heterozygous mouse. (*F*) Completely disarranged external granular layer in 10-day-old homozygous animal. This field shows one of the few Bergmann glial fibers (*BG*) present in the homozygous weaver cerebellum and also illustrates a representative Purkinje dendrite (*PD*) abnormally penetrating the markedly reduced external granular layer. Superimposed on the dendrite section are numerous profiles of dendritic spines lacking synaptic inputs. Degenerating cells (*DC*) are usually concentrated, as here, at the inner border of the external granular layer, where postmitotic granule cells have become stacked up through failure of their somas to translocate across the molecular layer.

1 Hr, 1 day, and 2 days after injection pyknotic nuclei are unlabeled, whereas 5 days after injection up to 10% of the pyknotic nuclei in both +/*wv* and *wv*/*wv* specimens are labeled; at 10–12 days almost all pyknotic nuclei again are unlabeled. Thus, cell death occurs in the mutant several days after cell genesis on the average, i.e., at a time when cell migration is already completed in normal mice. The failure of migration, then, precedes cell death and, as already suggested (16), may be a causal antecedent.

It is more difficult to establish whether the neuron migration disorder is traceable to the Bergmann glial defect or vice versa. The two are clearly proportional, in that (*i*) granule cell migration is slowed along abnormal glial fibers in heterozygotes and fails completely where Bergmann fibers are absent in homozygotes, and (*ii*) the defects parallel each other regionally within a given cerebellum.

We would argue from principles of pathology that the glial change is the cause of neuronal death rather than the reverse. If the Bergmann glial fibers were enlarging in response to granule cell death, one would expect them to contain the increased concentration of cytoplasmic fibrils characteristic of reactive glial cells (18), but instead they appear electronlucent and vacuolated (Fig. 2). Also, reactive glial cells persist indefinitely whereas many of the Bergmann cells in the mutant cerebellum die. A further argument against a nonspecific glial reaction is that other mutants, staggerer and reeler, on the C57BL background show increased death of young granule cells but do not display the weaver-type of Bergmann glial abnormality (ref. 19, and unpublished observations). Our speculations on the probable causal sequences in phenotypic expression are summarized in Fig. 3.

Comparison with other mutants also gives insight into a possible reason why the nonmigrating granule cells die instead of merely persisting near their site of genesis in the external granular layer. In staggerer, the granule cell–Bergmann glial relationship appears normal and migration proceeds properly, but the Purkinje cells fail to form dendritic spines, the granule cells fail to make synapses on Purkinje cells (though they do synapse on their other usual targets), and the granule cells secondarily die (Landis and Sidman, in preparation). In reeler, many populations of neurons are malpositioned, but only cerebellar granule cells are significantly reduced in number (14, 15); this reduction results in part from a decrease in granule cell genesis, but it appears in addition that those granule cells die that fail to contact Purkinje cells (Rakic and Sidman, unpublished observations). In another mutant, nervous, Purkinje cells die several weeks after birth, and in lateral areas of the cerebellum where the Purkinje loss is most severe, granule cells disappear secondarily (20). These data and our present findings in weaver, while clearly incomplete, are consistent with the view that young granule cells may be unusual among neurons in depending for their very survival upon establishment of effective contacts with Purkinje cells.

The causal chain suggested in Fig. 3 is deliberately ambiguous at the left side. The primary action and target cell of the *wv* gene are unknown. The gene dosage effect, i.e., the early expression of a Bergmann glial abnormality in heterozygotes and the near absence of these cells in homozygotes, implies that this phenotypic expression is likely to be reasonably close to the direct action of the *wv* genetic locus. Weaver is the first mammalian neurological mutant to show a dosage effect at the cellular level.

This study was supported by U. S. Public Health Service Grant NS 08359. We are grateful to Mrs. P. Lane, Jackson Laboratory, Bar Harbor, Maine for mice produced with the support of National Science Foundation Grant GB 27487. The origin of the *wv* mutation was described by Lane (1964) in *Mouse News Letter* **30**, 32 (personal communication).

1. Eccles, J. C., Ito, M. & Szentagothai, J. (1967) *The Cerebellum as a Neuronal Machine* (Springer–Verlag, New York), 355pp.
2. Mugnaini, E. (1972) in *The Comparative Anatomy and Histology of the Cerebellum: The Human Cerebellum, Cerebellar Connections, and Cerebellar Cortex*, eds. Larsell, O. & Jansen, J. (The Univ. of Minnesota Press, Minneapolis, Minn.), pp. 201–264.
3. Chan-Palay, V. & Palay, S. L. (1972) *Z. Anat. Entwicklungsgesch.* **136**, 224–248.
4. Sidman, R. L. (1973) in *The Neurosciences, Third Study Program*, eds. Schmitt, F. O. & Worden, F. G. (M.I.T. press, Cambridge, Mass.), in press.
5. Ramon y Cajal, S. (1960) *Studies on Vertebrate Neurogenesis*, translator, Guth, L. (C. C Thomas, Springfield, Ill.), pp. 253–301.
6. Rakic, P. (1971) *J. Comp. Neurol.* **141**, 283–312.
7. Rakic, P. (1972) *J. Comp. Neurol.* **146**, 335–354.
8. Miale, I. & Sidman, R. L. (1961) *Exp. Neurol.* **4**, 277–296.
9. Fujita, S. (1967) *J. Cell Biol.* **32**, 277–288.
10. Altman, J. (1969) *J. Comp. Neurol.* **136**, 269–294.
11. Rakic, P. & Sidman, R. L. (1970) *J. Comp. Neurol.* **139**, 473–500.
12. Rakic, P. (1971) *Brain Res.* **33**, 471–476.
13. Rakic, P. (1972) *J. Comp. Neurol.* **145**, 61–84.
14. Sidman, R. L., Green, M. C. & Appel, S. H. (1965) *Catalog of the Neurological Mutants of the Mouse* (Harvard Univ. Press, Cambridge, Mass.), pp. 66–67.
15. Sidman, R. L. (1968) in *Physiological and Biochemical Aspects of Nervous Integration*, ed. Carlson, F. D. (Prentice-Hall, Englewood Cliffs, N.J.), pp. 163–193.
16. Rezai, Z. & Yoon, C. H. (1972) *Develop. Biol.* **29**, 17–26.
17. Sidman, R. L. (1970) in *Contemporary Research Methods in Neuroanatomy*, eds., Nauta, W. J. H. & Ebbesson, S. O. E. (Springer–Verlag, New York), pp. 252–274.
18. Maxwell, D. S. & Kruger, L. (1965) *J. Cell Biol.* **25**, 141–157.
19. Sidman, R. L. (1972) in *Cell Interactions*, ed. Silvestri, L. G. (North Holland Publishing Co., Amsterdam), pp. 1–13.
20. Sidman, R. L. & Green, M. C. (1970) in *Les mutants pathologiques chez l'animal. Leur interet pour la recherche biomedicale*, ed. Sabourdy, M. (CNRS, Paris, France), pp. 69–79.

Proc. Nat. Acad. Sci. USA
Vol. 70, No. 1, pp. 245–249, January 1973

Mutagenic DNA Polymerase in Human Leukemic Cells

(tumor progression/leukemia/lymphocytes)

CLARK F. SPRINGGATE AND LAWRENCE A. LOEB

The Institute for Cancer Research, Fox Chase, Philadelphia, Pennsylvania 19111

Communicated by Daniel Mazia, November 6, 1972

ABSTRACT **Evidence is presented that DNA polymerases from human leukemic cells are mutagenic. Nucleic acid-free extracts of acute lymphoblastic leukemic cells polymerized about 10-times more dCTP using poly(dA-dT)·poly(dA-dT) as a template than did extracts from normal lymphocytes. Mutagenic DNA polymerases could perhaps play an important role in tumor progression.**

We have started to inquire whether DNA synthesis in malignant cells is less exact than in normal cells. Some of the characteristics of tumor progression (1), namely, (*a*) continuing evolution of new cell variants, (*b*) uncontrolled cellular proliferation, and (*c*) increasing number of chromosomal aberrations, suggest that as malignant cells become progressively anaplastic there is an accumulation of errors in genetic information.

For study of the fidelity of *in vitro* DNA synthesis, human lymphocytes offer several advantages. Leukemic lymphocytes of the acute "blastic" type have considerable DNA polymerase activity. DNA polymerase activity in normal lymphocytes can be increased 30- to 200-fold by stimulating them with phytohemagglutinin (2). This increase parallels the ability of these lymphocytes to incorporate thymidine into DNA, suggesting that the polymerase measured *in vitro* functions in chromosomal replication. Thus, there is sufficient polymerase activity in normal stimulated lymphocytes and their malignant counterparts to analyze and compare the exactness of DNA synthesis. The exceptionally low deoxyribonuclease activity in these cells facilitates meaningful experiments with partially purified enzymes (2). We have chosen to investigate the fidelity of DNA synthesis using peripheral blood lymphocytes rather than cells from long-term tissue culture in order to relate our findings more directly to the biology of the disease state. In these initial experiments we measured the ability of "nucleic acid-free extracts" of stimulated normal and leukemic lymphocytes to exactly copy the base sequences of the synthetic homopolymers poly(dA-dT)·poly(dA-dT) and poly(dG)·poly(dC).

METHODS

Enzymes. Lymphocytes from normal donors and from patients with acute lymphatic leukemia were purified as described (2). Leukemic lymphocytes were obtained from untreated patients with white blood cell counts greater than 40,000 cells per mm^3. Even though acute leukemic lymphocytes are probably not stimulated by phytohemagglutinin, both the normal and leukemic cells were cultured with phytohemagglutinin for 3 days (3). Cell-free extracts were obtained by disruption of the cells with repeated freeze-thawing, elimination of DNA by phase extraction (4, 5), and exhaustive dialysis against 20 mM Tris·HCl (pH 7.8) containing 4 mM 2-mercaptoethanol–1 mM EDTA–20% glycerol. Samples could be stored at −70°C with negligible loss of polymerase activity for at least 1 week. Homogeneous *Escherichia coli* DNA polymerase I was prepared by the method of Jovin *et al.* (6). Homogeneous T4 phage DNA polymerase was the generous gift of Dr. Paul Englund. Protein was determined by the method of Lowry *et al.* (7).

Polynucleotides. Poly(dG)·poly(dC) was purchased from Collaborative Research. Poly(dA-dT)·poly(dA-dT) was synthesized by the *de novo* reaction of *E. coli* polymerase I.

DNA Polymerase Activity. To measure the fidelity with which poly(dA-dT)·poly(dA-dT) is copied in lymphocyte extracts, we measured the incorporation of correct nucleotides (dATP and dTTP) and incorrect nucleotides (dGTP or dCTP) in separate assays using the same enzyme preparations. For determination of total synthesis, a standard reaction mixture was used containing in a total volume of 0.2 ml: 13.0 μM [^{3}H]dTTP (1500 dpm/pmol), 12.5 μM dATP, 20 μM dCTP, 1 mM $MgCl_2$, 100 mM Tris·HCl (pH 7.8), and 92 μM phosphorus of poly(dA-dT)·poly(dA-dT). The concentration of metal ion and template used gave maximum incorporation with both normal and leukemic extracts. Assays were initiated with 0.10 ml of enzyme and incubated at 37° for 6 hr, the maximum incubation period during which linear incorporation was observed. For measurement of dCTP incorporation, identical reaction mixtures were used except that they contained unlabeled dATP and dTTP and 20 μM [^{3}H]dCTP (28,030 dpm/pmol). Incorporation was stopped by addition of 400 μl of 0.1 N perchloric acid containing 0.05 M $Na_2P_2O_7$ (Acid Stop Solution). The mixture was incubated for 2 min; 100 μl of 0.2 M NaOH–50 mM $Na_2P_2O_7$ was added followed by 100 μl of carrier DNA (1 mg/ml of denatured calf-thymus DNA) and then 600 μl of Acid Stop Solution. To aid in washing the assays, 100 μl of unlabeled 0.05 mM carrier dCTP was also added. Samples were centrifuged at 5000 × *g* for 10 min, and the supernatant was discarded. The precipitated DNA was solubilized with 0.2 M NaOH–50 mM $Na_2P_2O_7$ and then precipitated with acid. This procedure was repeated three times. Finally, the DNA was washed onto a Whatman GF/C filter disc with aliquots of cold H_2O and 20 ml of cold Acid Stop Solution, followed by 10 ml of ethanol. This disc was then placed in a scintillation counting solution [Toluene–2,5-diphenyloxazole(PPO)] for determination of radioactivity. Determinations were done in triplicate or quadruplicate, and the results given are the average after subtraction of controls without added poly(dA-dT)·poly(dA-dT)

TABLE 1. *Incorporation of dCTP with poly(dA-dT)·poly(dA-dT)*

Enzyme source	Correct nucleotide incorporation (pmol)	Incorrect nucleotide incorporation (pmol)	Level of infidelity
Normal lymphocytes			
Donor 1	439	0.092	1/4800
2	51	0.025	1/1990
3	221	0.064	1/3460
4	335	0.056	1/5980
5	309	<0.01	<1/30,900
6	382	0.091	1/4200
Acute lymphatic leukemic			
Patent 1	53	0.11	1/480
2	108	0.43	1/250
3	189	0.35	1/540
4	58	0.069	1/850
E. coli DNA polymerase I	1843	<0.01	<1/184,300
T4 phage DNA polymerase	5509	0.48	1/11,500

template. For dGTP incorporation, conditions similar to those described above were used except for the presence of 20 μM dGTP in incorporation experiments for correct nucleotide and 20 μM [^{3}H]dGTP (26,360 dpm/pmol) in incorporation experiments for incorrect nucleotide.

In assays with homogeneous *E. coli* polymerase I, incorporation of correct and incorrect nucleotides into poly(dA-dT)·poly(dA-dT) was measured as described above except for the presence of 40.2 μM [^{3}H]dTTP (147,790 dpm/mmol), 40 μM dATP, 20 μM dCTP, 5 mM $MgCl_2$, and 219 μM phosphorus of poly(dA-dT)·poly(dA-dT). Reactions were initiated with 2.5 units of enzyme and incubated for 10 min at 37°. With T4 phage DNA polymerase, conditions were similar to those for *E. coli* except for the presence of 10 mM 2-mercaptoethanol, 10 mM ammonium sulfate, 2 mM $MgCl_2$, 100 mM Tris·HCl (pH 8.6), and correct nucleotides at concentrations of 100 μM each. The mixtures were incubated for 45 min at 30°, and each contained 10 units of enzyme.

Hydrolysis of the DNA Product. The DNA product was digested to 5′-mononucleotides by the combined action of pancreatic DNase and snake venom phosphodiesterase (8). The 5′-mononucleotides were separated by thin-layer chromatography (9).

RESULTS

Fidelity of poly(dA-dT)·poly(dA-dT) replication

Cell-free extracts were prepared from acute leukemic lymphocytes and from normal lymphocytes grown with phytohemagglutinin. The cells were disrupted by repeated freezing and thawing, and the DNA was removed by phase extraction (4, 5). For measurement of the exactness of DNA replication, experiments were performed with poly(dA-dT)·poly(dA-dT) as template in the presence of highly radioactive dGTP or dCTP and unlabeled dATP and dTTP. Both the normal and leukemic extracts catalyzed the incorporation of incorrect bases into poly(dA-dT)·poly(dA-dT) (Table 1). Replication with leukemic extracts, however, appeared to be less exact than replication with normal extracts. For dCTP incorporation, this result is indicated by an average level of infidelity about 10-fold greater for leukemic preparations (1/250–1/850) as compared to that of the normal lymphocyte enzymes (1/1990–<1/30,000). The observed differences in the exactness of poly(dA-dT)·poly(dA-dT) synthesis does not appear to be due to nonspecific factors—activators or inhibitors present in excess in either the normal or leukemic preparations. We demonstrated this hypothesis by mixing the normal and leukemic enzymes and subsequently observing that the level of infidelity of the combined preparation was intermediate to the value obtained with the individual extracts (Table 2). Preliminary experiments were also done that measured the incorporation of dGTP into the poly(dA-dT)·poly(dA-dT) template. The data we obtained so far with this nucleotide do not permit any conclusions to be drawn as to the relative levels of infidelity.

Fidelity of poly(dG)·poly(dC) replication

In experiments with poly(dG)·poly(dC) as template, dATP and dTTP were labeled with tritium while dGTP and dCTP were not labeled. The major feature of polymerization of poly(dG)·poly(dC) was that far fewer incorrect nucleotides were incorporated with either the normal or leukemic extracts as compared with polymerization with poly(dA-dT)·poly(dA-dT). The level of infidelity with dTTP and dATP by both normal and leukemic extracts was generally less than 1 in 50,000, the lower limit of detection in these assays.

Control experiments

To discount the possibility that the "errors in DNA synthesis" we observed with lymphocyte extracts were actually only a consequence of chemical contamination of either the templates or labeled nucleotide, the fidelity of homogeneous preparations of *E. coli* polymerase I and T4 phage DNA polymerase was tested with the same reagents. With poly(dA-dT)·poly(dA-dT) as template, the *E. coli* enzyme made less than 1 error in 100,000 nucleotides polymerized (Table 1). T4 phage DNA polymerase replicated the homopolymers with less precision. Polymerization of poly(dA-dT)·poly(dA-dT) appeared to have about 1 incorrect base incorporated for 10,000 correct bases polymerized, in agreement with the results of Hall and Lehman (10). Thus, contamination of reagents was not responsible for the errors that we observed with the various enzymes. This conclusion is further sup-

TABLE 2. *Fidelity of copying poly(dA-dT)·poly(dA-dT) with a mixture of normal and acute leukemic extracts*

Enzyme source*	Units of polymerase†	Level of infidelity (% total incorporation)	
		dGTP	dCTP
Normal	110	0.025	0.049
Acute leukemic	110	0.52	0.21
Normal + acute leukemic	55 + 55	0.18	0.11

* DNA polymerase extracts. Normal, donor 1; acute leukemic, patient 2.

† One unit of enzyme is that which polymerized 1 pmol of nucleotide in 6 hr.

ported by the finding that a decrease in the specific activity of labeled dCTP and dTTP 5-fold by addition of appropriate unlabeled nucleotide led to a 4- to 6-fold decrease in the ^3H counts incorporated. In order to show that the incorrectly incorporated nucleotide was actually deoxycytidylic acid, we degraded the product of the reaction to deoxyribonucleoside 5′-monophosphates by hydrolysis with pancreatic DNase and snake venom phosphodiesterase. Subsequent chromatography identified over 80% of the incorporated ^3H label as dCMP.

In order to determine if dCTP was indeed incorporated into poly(dA-dT)·poly(dA-dT), we studied the requirements for incorporation of both correct and incorrect nucleotides (Table 3) and characterized the product of the reaction. Table 3 shows that the requirements for correct and incorrect base incorporation are similar and typical for DNA polymerases. Without an added metal cofactor (Mg^{2+}) or with heated extracts there was no detectable incorporation of either the correct or incorrect deoxynucleotides. Without the added polynucleotide templates, incorporation of incorrect nucleotides was less than 20% of the values observed with the complete reaction mixtures. Correct nucleotide incorporation in the absence of poly(dA-dT)·poly(dA-dT) was less than 0.05% of that obtained with the complete reaction mixture. Thus, any native DNA that might be a contaminant is not the template for polymerization of either correct or incorrect deoxynucleotides. As would be expected if the added poly(dA-dT)·poly(dA-dT) serves as template, equal amounts of [^3H]dATP and [α-^{32}P]dTTP were incorporated into the DNA product in each extract.

Supporting evidence that dCTP was polymerized into the added poly(dA-dT)·poly(dA-dT) template was provided by analysis of the product of the reaction by cesium chloride density gradient centrifugation (Fig. 1). The product of the reaction banded at a density expected for that of poly(dA-dT)·poly(dA-dT), indicating that both the correct nucleotide ([α-^{32}P]dTTP) and the incorrect nucleotide ([^3H]dCTP) are indeed incorporated into this polynucleotide. Neither correct nor incorrect nucleotides were incorporated into DNA in incubation mixture lacking the poly(dA-dT)·poly(dA-dT) template (Fig. 1*C*).

In order to determine the position of the incorrect bases in the polynucleotide product, we studied the relations between correct and incorrect base incorporation. Polymerization of both correct and incorrect bases were proportional to time and to protein concentration for all of the enzyme preparations. Representative data with a normal lymphocyte extract is shown in Fig. 2. Moreover, variation in protein concentration did not significantly alter the misincorporation ratio of incorrect bases into the poly(dA-dT)·poly(dA-dT) product (Fig. 2, *inset*). Since the extent of incorrect base incorporation closely paralleled incorporation of the correct bases, the observed infidelity does not appear to indicate solely the addition of a few bases to the end of polynucleotide chains. If incorporation of dCTP into poly(dA-dT)·poly(dA-dT) was merely a result of terminal labeling, the omission of correct nucleotide would not be expected to have grossly affected the extent of incorrect nucleotide incorporation. On the other hand, if the incorrect bases were polymerized into the poly(dA-dT)·poly(dA-dT) template in concert with the correct base, omission of dATP and dTTP should severely limit incorrect nucleotide incorporation. We found that dCTP incorporation without dATP and dTTP was only 0–28% of the incorporation observed in assays containing the correct nucleotides (Table 3). These correlated

TABLE 3. *Reaction requirements for correct and incorrect nucleotide incorporation with poly(dA-dT)·poly(dA-dT)*

Reaction mixture	Normal (% incorporation)		Acute leukemic (% incorporation)	
	dTTP	dCTP	dTTP	dCTP
Complete	100 (330 pmol)	100 (0.06 pmol)	100 (150 pmol)	100 (0.30 pmol)
Minus enzyme	0	0	0	0
Minus poly(dA-dT)·poly(dA-dT)	<0.05	16 ± 7	<0.05	20 ± 4
Minus Mg^{++}	0	0	0	0
Minus dATP and dTTP	—	13 ± 11	—	12
Heated enzyme	0	0	0	0

Results given as mean ± SEM.

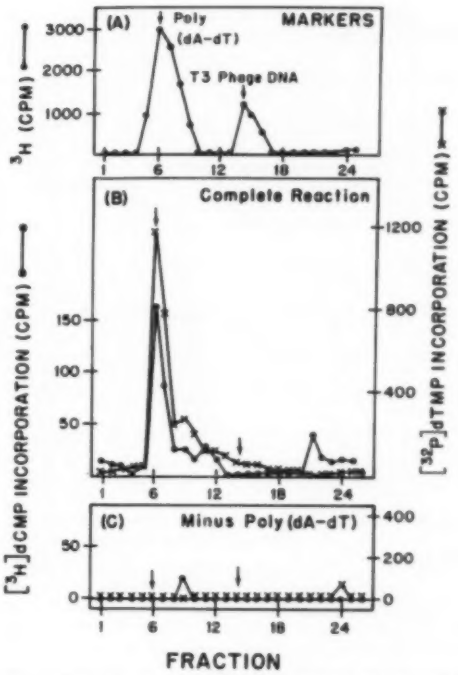

FIG. 1. Neutral cesium chloride density gradient centrifugation of the product of the reaction with DNA polymerase from patient 4. Five standard assays with [α-^{32}P]dTTP (25 dpm/pmol) and [^3H]dCTP (9300 dpm/pmol) were combined. The polynucleotide product was precipitated five times, after which it was suspended in 0.1 M Tris·HCl (pH 7.3) containing 0.1 mM EDTA and cesium chloride (final density, 1.700) in a final volume of 4.0 ml. The solution was centrifuged for 80 hr at 35,000 rpm (147,000 × *g*) at 20°. About 0.1-ml fractions were collected from the top of the tube, and the radioactivity was determined. Separate gradients contained: (*A*) marker DNA consisting of ^3H-labeled poly(dA-dT)·poly(dA-dT) and ^3H-labeled T3 phage DNA (50% G+C); (*B*) complete reaction mixture; (*C*) reaction mixture without added poly(dA-dT)·poly(dA-dT).

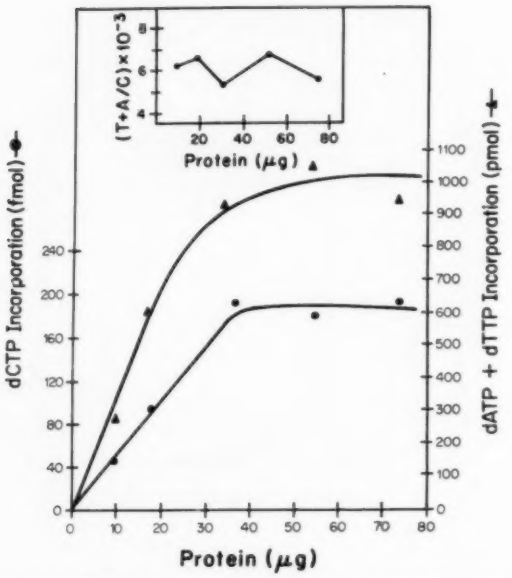

FIG. 2. Effect of protein concentration on correct and incorrect nucleotide incorporation. Normal human lymphocyte polymerase from donor 1 was used. The assay procedure was identical to that in Table 1 except that all reaction components were present in 2-fold greater quantity. *Inset* presents the ratio of correct nucleotides incorporated (dATP and dTTP) to incorrect nucleotide (dCTP) incorporated plotted against protein concentration.

results suggest that terminal labeling was not responsible for incorrect nucleotide incorporation. In another kind of experiment, the DNA product was labeled with [α-^{32}P]dTTP and [^{3}H]dCTP and hydrolyzed sequentially from the 3′-terminus with snake venom phosphodiesterase. Fig. 3 shows that the time release of correct (dTMP) and incorrect (dCMP) nucleotides closely paralleled each other, indicating that dCMP was distributed evenly throughout the entire product.

DISCUSSION

If hydrogen bonding between bases alone was responsible for the fidelity of DNA synthesis it would not be reasonable to expect differences in the exactness with which normal and leukemic polymerases copy poly(dA-dT)·poly(dA-dT). Rather, it would seem more likely that the precision of DNA synthesis would be similar for all polymerases, regardless of source. Theoretical considerations predict that precise DNA synthesis requires base-pairing specificity of greater energy than that provided by hydrogen bonding alone. For example, the ionization and spontaneous tautomerization of bases are capable of promoting transitions in one out of every hundred base pairs (11) during replication of DNA. Moreover, it has recently been demonstrated (12) that mononucleotides exhibit a degree of hydrogen bonding specificity that cannot account for the fidelity of DNA synthesis with several prokaryotic polymerases (10, 13) or for the results reported in this paper.

Two distinct mechanisms by which DNA replication enzymes could participate in guaranteeing the genetic code have been proposed. These are: (*i*) base selection during polymerization (14, 15) and (*ii*) editing the errors after polymerization by nuclease activity (15). Nuclease activity of prokaryotic DNA polymerase has a role in fidelity of DNA synthesis. *E. coli* polymerase I and T4 phage polymerase, for example, excise mismatched bases (16, 17). T4 phage containing anti-mutator genes that decrease spontaneous mutation rates have enhanced nuclease–polymerase activity (18). These data are interpreted as suggesting that the fidelity of *in vivo* replication in T4 phage is dependent on the relative rates of insertion and removal of nucleotides during polymerization. However, exonuclease activity does not appear to be invariably associated with prokaryotic DNA polymerases and has not been reported to be a prominent constituent of animal DNA polymerases. Other repair enzymes may be operative in eukaryotic cells. The data presented here do not allow us to choose between the possibilities of deficits in base selection or decreased editing of errors as an explanation of the observed increased infidelity with the leukemic extracts. Even with homogeneous enzymes this distinction may be difficult if a polymerase enzyme has both activities.

We envision that the major consequences of base pairing errors during DNA replication in leukemic cells, and perhaps in other types of cancer, would be that of promoting an increased mutation frequency. It seems probable that these random genetic changes would result in cellular alterations, some of which would have selective value for proliferation in the host. Lethal and neutral mutations, of course, would also occur. The lethal mutants will perish and, therefore, are only of minor significance. Those cells with neutral mutations will survive and be capable of undergoing subsequent genotypic changes, the nature of which will determine their importance in tumor progress. A central correlate of this hypothesis is that malignant cells, even from a single type of neoplasia, will eventually develop a wide range of variation. Many reports indicate that most tumor cell populations show marked variation with continuing proliferation (1, 19, 20).

The most direct explanations for the differences in the precision of homopolymer replication between normal and leu-

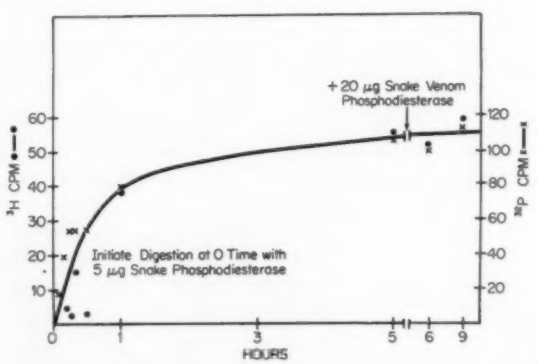
+20 μg Snake Venom Phosphodiesterase
Initiate Digestion at 0 Time with 5 μg Snake Phosphodiesterase
³H CPM
³²P CPM
HOURS

FIG. 3. Digestion of the DNA product of DNA polymerase from patient 4 with snake venom phosphodiesterase. Five standard assays with [α-^{32}P]dTTP (25 dpm/pmol) and [^{3}H]dCTP (28,030 dpm/pmol) were combined. The acid-insoluble products were washed as in *Methods*, except that after 3 successive precipitations, they were dissolved in 2.5 ml of 0.1 M Tris·HCl (pH 7.5) containing 5 mM $MgCl_2$ and 5 μg of 3′-snake venom phosphodiesterase. At intervals, 250-μl aliquots were removed, and the acid-soluble radioactivity was determined.

kemic extracts are (i) the presence of a viral DNA polymerase in leukemic cells or (ii) the presence of an altered cellular polymerase that is faulty in base selection. It is now important to determine the precision of homopolymer replication with RNA-directed DNA polymerases from animal tumor viruses. A conclusive demonstration that any cellular DNA polymerases are actually modified awaits extensive purification of these enzymes.

We thank Dr. S. Sorof for frequent stimulating discussions and Gita Seal for expert technical assistance. We also thank Drs. A. Rubin, E. Hersh, C. Treat, and F. Saunders for obtaining samples of blood. This work was supported by grants from The National Institutes of Health (CA-11524, CA-11835, and CA-12818) and The National Science Foundation (GB-18419), by grants to this Institute from the NIH (CA-06927, RR-05539), and an appropriation from the Commonwealth of Pennsylvania. C. F. S. is a fellow of the Leukemia Society of America.

1. Foulds, L. (1964) in *Cellular Control Mechanisms and Cancer*, ed. Emmelot, P. & Muhlblock, O. (Elsemer Publishing Co., New York), pp. 242–259.
2. Loeb, L. A., Agarwal, S. W. & Woodside, A. M. (1968) *Proc. Nat. Acad. Sci. USA* **61**, 827–834.
3. Agarwal, S. S., Bugbee, S. J. & Loeb, L. A. (1970) *Nature* **226**, 448–449.
4. Albertsson, P. (1962) *Arch. Biochem. Biophys.* **98**, 264–269.
5. Loeb, L. A. (1969) *J. Biol. Chem.* **244**, 1672–1681.
6. Jovin, T. M., England, Paul T. & Bertsch, L. L. (1969) *J. Biol. Chem.* **244**, 2996–3008.
7. Lowry, O. H., Rosebrough, N. J., Fan. A. L. & Randall, R. J. (1951) *J. Biol. Chem.* **193**, 2651–2655.
8. Miyazawa, Y. & Thomas, C. A. (1965) *J. Mol. Biol.* **11**, 223–228.
9. Ranm, K. (1964) *Biochim. Biophys. Acta* **76**, 622–623.
10. Hall, W. & Lehman, I. R. (1968) *J. Mol. Biol.* **36**, 321–333.
11. Koch, A. L. & Miller, C. (1965) *J. Theor. Biol.* **8**, 71–80.
12. Raszka, M. & Kaplan, N. (1972) *Proc. Nat. Acad. Sci. USA* **69**, 2025–2029.
13. Trautner, T. A., Swartz, M. N. & Kornberg, A. (1962) *Proc. Nat. Acad. Sci. USA* **48**, 449–455.
14. Speyer, J. F. (1965) *Biochem. Biophys. Res. Commun.* **21**, 6–8.
15. Drake, J. W. & Allen, E. F. (1968) *Cold Spring Harbor Symp. Quant. Biol.* **33**, 339–344.
16. Brutlag, D. & Kornberg, A. (1972) *J. Biol. Chem.* **247**, 241–248.
17. Hershfeld, M. S. & Nassal, N. G. (1972) *J. Biol. Chem.* **247**, 3393–3404.
18. Bessman, M. J., Mazyczka, N. & Poland, R. J. (1972) *Fed. Proc.* **31**, 444.
19. Sandberg, A. A., Ishihara, T., Miwa, T. & Hauschka, T. S. (1961) *Cancer Res.* **21**, 678–689.
20. Harris, M. (1964) *Cell Culture and Somatic Variation* (Holt, Rinehart, and Winston, New York), pp. 33–67.

Proc. Nat. Acad. Sci. USA
Vol. 70, No. 1, pp. 250–254, January 1973

A Cellular Basis for Genetically Controlled Immunologic Unresponsiveness in Mice: Tolerance Induction in T-Cells

(histocompatibility genes/memory cells)

RICHARD K. GERSHON*, PAUL H. MAURER†, AND CARMEN F. MERRYMAN†

* Department of Pathology, Yale University School of Medicine, New Haven, Connecticut 06510; and
† Department of Biochemistry, Jefferson Medical College of Thomas Jefferson University, Philadelphia, Pennsylvania 19107

Communicated by Edward A. Adelberg, October 10, 1972

ABSTRACT **$H\text{-}2^q$ mice (DBA/1) do not make an antibody response to a synthetic aminoacid polymer, (Glu, Ala,Tyr_{10}), after an immunizing regimen that produces a good antibody response in mouse strains with other H-2 alleles. Their thymocytes, however, show evidence of recognizing this antigen since they synthesize DNA when they meet the antigen in the spleen. This recognition event does not lead to memory production, as it does in genetic responders, since the thymocytes fail to respond to a second immunization with (Glu,Ala,Tyr_{10}). Nonresponder mice do make antibody to (Glu,Ala,Tyr_{10}) when they are immunized with it complexed to an immunogenic carrier, but previous treatment with free polymer can temporarily abolish this response. Thus, we suggest that the basis for the unresponsiveness of these mice is that their T-cells (thymus-processed lymphocytes) have an inordinate propensity to become (or to induce other cells to become) immunologically tolerant.**

The immune response to several synthetic polymers of amino acids is genetically controlled. The gene loci that regulate the antibody response to these polymers have, so far, been inseparable from those that code for the major histocompatibility antigens (1, 2). Although the cellular basis for the poor responsiveness of certain strains of mice and guinea pigs has not been completely clarified, several possibilities have been excluded. Since the deficit in nonresponder animals can be overcome by linking the antigens to immunogenic carriers, one may assume that the deficit is not due to an absence of a clone of antibody-forming cells (B-cells) with specificity for the antigens (3). Also, the macrophages of nonresponder animals appear to handle antigen normally (4, 5). Thus, by exclusion it would appear that the cellular basis for unresponsiveness of nonresponder mice lies in thymus-processed lymphocytes (T-cells). Recent evidence indirectly supports this view (6–8).

We have attempted to examine the interaction of T-cells from nonresponder mice with antigen directly, using a recently established technique for measuring T-cell DNA synthesis (9). Thymocytes incorporate very little [^{125}I]dU into DNA after injection into lethally irradiated syngeneic mice unless they are stimulated with antigens that elicit a thymus-dependent immune response (9, 10). Thus, antigens such as polyvinylpyrrolidone and pneumococcal polysaccharide fail to stimulate a significant DNA synthetic response.

Abbreviations: T-cells, thymus-processed lymphocytes; B-cells, bone marrow-derived cells that are the precursors of the cells that make antibodies; (Glu,Ala,Tyr), a synthetic linear copolymer of glutamic acid, alanine, and tyrosine.

Our results show that thymocytes of nonresponder mice synthesize significant amounts of DNA when they meet the antigen in the spleen. Thus, we suggest the genetic deficit of these mice lies distal to the T-cell–antigen recognition event.

MATERIALS AND METHODS

Antigens. The antigen studied was a random linear copolymer of glutamic acid, alanine, and tyrosine, Glu (60%), Ala (30%), Tyr (10%) (Glu,Ala,Tyr_{10}). It was prepared by base-initiated polymerization of *N*-carboxy anhydrides of the specific amino acids (11). The polymer was purified by dialysis and stored frozen until used.

Sheep erythrocytes were maintained in refrigerated Alsever's solution and washed three times before use. They were inoculated as a 20% suspension, intraperitoneally.

Bovine-serum albumin was methylated for 24 hr at 5° with 0.1 N methanolic HCl and then exhaustively dialyzed. The resultant methylated bovine-serum albumin at a concentration of 5 mg/ml was added by drops, with stirring, to a solution (Glu,Ala,Tyr_{10}) (1 mg/ml H_2O) containing trace amounts of (Glu,Ala,Tyr_{10}) labeled with ^{125}I. When maximum flocculation and aggregate formation had occurred, the precipitate was centrifuged at 4°C and washed 3–4 times with 0.15 M NaCl, until the washings were free of radioactivity.

Experimental Animals. All mice were from Jackson Laboratories, Bar Harbor, Me. After arrival, they were kept in our colony for at least 1 week before use. DBA/2 ($H\text{-}2^d$) and C57B1/6 ($H\text{-}2^d$) were used as responder strains and DBA/1 ($H\text{-}2^q$) as nonresponder (12). Recipients of thymocytes and mice used for antibody studies were 7- to 8-week-old male mice. Thymocyte donors were 5-week-old males.

Cell Suspensions. Donor mice were killed by cervical dislocation and thymuses were carefully dissected out under sterile conditions. They were then gently squeezed between two sterile glass slides. The cell suspension thus obtained was filtered through three layers of gauze and washed twice in ice-cold sterile medium M-199 (Grand Island Biological Co., Grand Island, N.Y.) with 100 units/ml each of penicillin, streptomycin, and kanamycin and 10 units/ml of heparin. Viable cell counts were made with a hemocytometer by the trypan blue dye-exclusion method.

Irradiation. A Siemens 250-kV machine with a 2-mm aluminum filter was used for irradiation of recipients. They

were placed in a Plexiglass chamber on a rotating platform and received 900 R at a dose rate of 85 R/min.

Cell Inoculations were given intravenously by tail vein, in a volume of 0.2 ml.

Method of Immunization. In the studies of thymocyte DNA synthesis,. antigen was inoculated in sterile pyrogen-free saline intraperitoneally. In studies on antibody formation the (Glu,Ala,Tyr_{10})–methylated bovine-serum albumin complex was emulsified, 1:1, in complete Freund's adjuvant and 10 μg of antigen was inoculated in the rear food pad in a final volume of 0.1 ml. 3 Weeks later mice were boosted intraperitoneally with 10 μg of (Glu,Ala,Tyr_{10})–methylated bovine-serum albumin in saline. Serum was collected from individual mice 1 week later.

Measurement of Antibodies. The antibody response was measured by a modification of Herzenberg's (13) antigen-binding assay with iodinated polypeptides as follows: 50 μl of phosphate-buffered saline (110 mM NaCl–40 mM Na phosphate, pH 7.2) containing 300 μg of nitrogen as [^{121}I]polymer and 1% bovine-serum albumin were added to 25 μl of 1:2 dilutions of mouse antiserum. After 1 hr at 37°, 500 μl of the appropriate dilution of a polyvalent antibody to mouse gamma-globulin, prepared in sheep, was added. A second 2-hr period of incubation at 37° was followed by a 30-min centrifugation at 3000 rpm (1000 × *g*). An aliquot (200 μl) of the supernatant was counted in a well-type gamma scintillation counter (Nuclear Chicago Corp., Des Plaines, Ill.). The results are presented as the percent antigen bound by 25 μl of the 1:2 dilution of mouse antiserum. Controls included normal mouse serum that bound 0–6% (Glu,Ala,Tyr_{10}) and both rabbit and mouse antisera containing antibody against (Glu,Ala,Tyr_{10}) that bound 80–90% (Glu,Ala,Tyr_{10}).

Measurement of T-Cell DNA Synthesis. The technique used for measuring the response of thymus cells to antigen has been described (9). Briefly, lethally irradiated recipient mice were inoculated intravenously with 3–5 × 10^7 syngeneic thymocytes and immunized with test or control materials intraperitoneally on the same day. At intervals thereafter, they were given 2 μCi of [^{125}I]dU (specific activity, 4 Ci/g; New England Nuclear Corp.). Essentially all of this thymidine analogue that is not intimately associated with DNA is excreted within 12 hr (9). Thus, 24 hr after isotope injection, mice were killed and their spleens were counted for 5 min in a Nuclear Chicago gamma counter. The number of counts minus the background divided by the number of counts emitted by 2 μCi of isotope (% uptake) was taken to represent the amount of DNA synthesized by the inoculated cells on the day of isotope injection. In the experiments reported, 1% of isotope uptake yielded 8400–8600 counts per min (cpm) at the settings used. Background was less than 10 cpm. All results presented are mean observations from four individual mice.

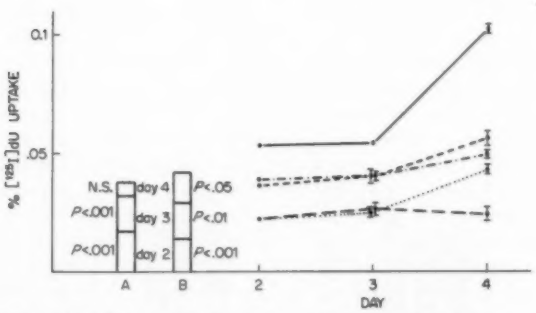

FIG. 1. DNA synthetic response (±SE) of DBA/1 (nonresponder) thymocytes to stimulation with test and control materials in the spleens of lethally irradiated recipients. The *bars* show the response to the test materials minus the saline controls on the 3 days of study. *A*, (Glu,Ala,Tyr_4); *B*, (Glu,Ala,Tyr_{10}). (——) sheep erythrocytes; (— — —) (Glu_{60},Tyr_{10}); (– – –) (Glu, Ala,Tyr_{10}); (–·–) (Glu,Ala,Tyr_4); (· · · ·) NaCl.

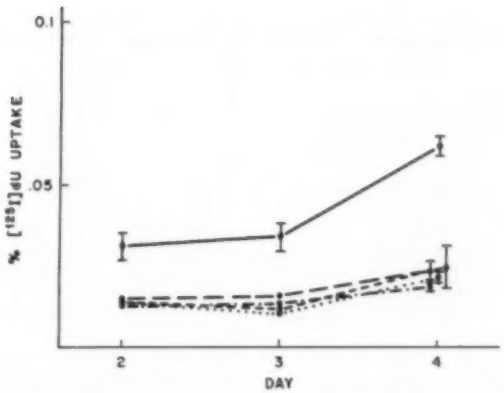

FIG. 2. DNA synthetic response (±SE) of DBA/2 (responder) thymocytes to stimulation with test and control materials in the spleens of lethally irradiated recipients. See legend to Fig. 1 for symbols.

RESULTS

DNA synthetic response of thymocytes to a primary challenge with (Glu,Ala,Tyr)

Nonresponder Mice. Spleen-localizing thymocytes from nonresponder mice (DBA/1) synthesized significant amounts of DNA in response to challenge with 100 μg of (Glu,Ala, Tyr) containing two different mol percents of tyrosine [(Glu,Ala,Tyr_{10}) and (Glu,Ala,Tyr_4)] (Fig. 1). The increase in isotope uptake produced by (Glu,Ala,Tyr_{10}) immunization (versus saline controls) was statistically significant on all assay days, and that produced by (Glu,Ala,Tyr_4) immunization was significant on days 2 and 3. We used a copolymer of glutamic acid and tyrosine (Glu_{60},Tyr_{10}) as one negative control since it is nonimmunogenic in mice (14). Another control, (Glu,Ala, Tyr_{10}) polymer made of only D-amino acids, which is also nonimmunogenic at normal concentrations (15), was included in other experiments (data not shown), and did not produce a DNA synthetic response. The response of the thymocytes to a positive control (0.2 ml of a 20% suspension of sheep erythrocytes is also presented.

Responder Mice. A similar experiment was performed with responder mice (DBA/2). The DNA synthetic response of their thymocytes to stimulation with all three polymers was indistinguishable from the saline controls, although the positive control, sheep erythrocytes, elicited a significant response (Fig. 2).

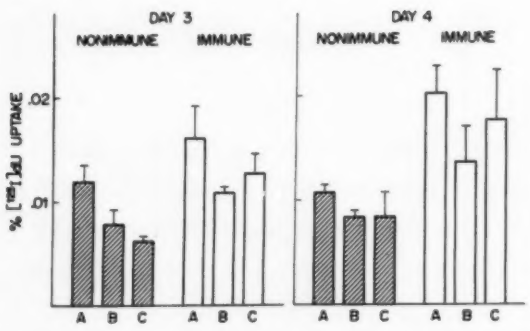

FIG. 3. DNA synthetic response (±SE) of DBA/1 (nonresponder) thymocytes that had been passed through spleens to stimulation with test and control materials. The passaged cells had been immunized either with 100 μg of (Glu,Ala,Tyr_{10}) (*open bars*) or with saline (*hatched bars*) in the spleens of lethally irradiated donor mice. *A*, sheep erythrocytes; *B*, (Glu,Ala,Tyr_{10}); *C*, saline.

DNA synthetic response of thymocytes to a second challenge with (Glu,Ala,Tyr)

A seeming paradox exists; thymocytes from nonresponder mice respond to antigen while those from responder mice do not. Since thymocytes can synthesize significant amounts of DNA during tolerance induction (16), we investigated the possibility that tolerance was being induced in the thymus cells in the spleens of nonresponder mice. We inoculated syngeneic thymocytes into lethally irradiated recipients and injected half with 100 μg of (Glu,Ala,Tyr_{10}) and half with saline. 8 Days later we harvested the spleens and inoculated the recovered cells (on a one spleen–one recipient basis) into another group of syngeneic lethally irradiated mice, and measured the DNA synthetic response to antigen of these cells that had been passed through spleens.

Nonresponder Mice. Immunized thymocytes from nonresponder mice failed to respond to a second challenge with (Glu,Ala,Tyr_{10}) (Fig. 3); indeed their response was poorer than the saline controls (reminiscent of the negative response produced by (Glu,Tyr) in normal thymocytes) (see Fig. 1), although the diminution was not statistically significant. The nonimmunized thymocytes that had been passed through spleens did not make a significant response to (Glu,Ala,Tyr_{10}) either. The difference between these results and those obtained with nonpassaged thymocytes can be a function of cell dose; a significant loss of cells occurs. This loss is also exemplified by the small response ($P < 0.05$) in both immune and nonimmune cells to sheep erythrocytes (see Fig. 1). Of interest was the considerable increase in background DNA synthesis produced by the initial immunization with (Glu,-Ala,Tyr_{10}). (The saline controls of (Glu,Ala,Tyr_{10}) "educated" cells against the saline controls of "uneducated" cells; $P < 0.02$). This increase apparently was due to the increased DNA synthesis that occurred during the initial immunization (see Fig. 1), and that continued after cell transfer.

Responder Mice. Responder thymocytes that had been passed through spleens and immunized against (Glu,Ala,Tyr_{10}) made a striking response to a second immunization with (Gly,Ala,Tyr_{10}) ($P < 0.01$) (Fig. 4). Their response to (Glu,Ala,Tyr_{10}) was much greater than the response to sheep erythrocytes ($P < 0.02$) (see Figs. 1–3). Also, in contrast to nonresponder mice, primary immunization with (Glu,Ala,Tyr_{10}) did not result in an increase in background DNA synthesis, pointing up again the difference in the responses of responder and nonresponder mice to a primary confrontation with antigen.

Effect of (Glu,Ala,Tyr) immunization on the antibody response to (Glu,Ala,Tyr)-methylated bovine-serum albumin)

These results are compatible with the notion that both nonresponder and responder thymus cells recognize (Glu,Ala,-Tyr_{10}), but that the recognition event leads to paralysis in the nonresponders and to immunity in responders.

We tested this possibility in the following manner. We gave normal responder (DBA/2 and C57B1/6) mice and nonresponder (DBA/1) mice an intraperitoneal inoculation of 100 μg of (Glu,Ala,Tyr_{10}) in aqueous solution 5 or 10 days before immunizing them with 10 μg of (Glu,Ala,Tyr_{10}) coupled to an immunogenic carrier, methylated bovine-serum albumin. We have found (Glu,Ala,Tyr_{10})–methylated bovine-serum albumin to be immunogenic in both responder and nonresponder mice (Merryman and Maurer, unpublished). 10 μg of noncoupled (Glu,Ala,Tyr_{10}) was inoculated intraperitoneally at the time of immunization with (Glu,Ala,Tyr_{10})–methylated bovine-serum albumin to prevent a breakage of tolerance, which is produced by altered antigens (17, 18). The breakage can be prevented by simultaneous inoculation of unaltered antigen (19). The results (Table 1) show that treatment with 100 μg of (Glu,Ala,Tyr_{10}) 5 days before immunization abolished the antibody response of nonresponders against (Glu,Ala,Tyr_{10}), but not that of responder mice. Interestingly, the abolition was only temporary. By 10 days after the treatment, the mice that had received (Glu,Ala,Tyr_{10}) polymer in saline made more antibody after immunization with (Glu,Ala,Tyr_{10})–methylated bovine-serum albumin than did controls ($P < 0.001$).

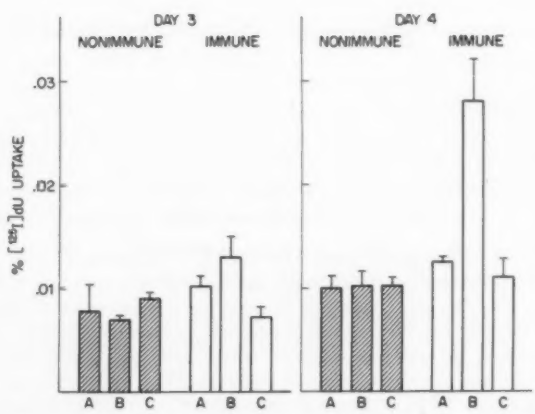

FIG. 4. DNA synthetic response (±SE) of DBA/2 (responder) thymocytes that had been passed through spleens to stimulation with test and control materials. The passaged cells had been immunized either with 100 μg of (Glu,Ala,Tyr_{10}) (*open bars*) or with saline (*hatched bars*) in the spleens of lethally irradiated donor mice. *A*, sheep erythrocytes; *B*, (Glu,Ala,Tyr_{10}); *C*, saline.

DISCUSSION

Immunologically competent T-cells characteristically respond to antigen with a wave of DNA synthesis (9, 10, 20). The technique we have used to study the DNA synthetic response of T-cells after antigenic stimulation yields results parallel to those from studies of mitosis of chromosomally marked cells (10). Thus, both studies give the same hierarchy of stimulation between antigens, and both have shown that antigens without a T-cell component in the immune response they elicit are nonstimulatory. It is therefore reasonable to assume, should an antigen stimulate DNA synthesis in T-cells, that an event of immunologic recognition has transpired. Since thymocytes of mice that are genetically incapable of making a significant antibody response to Glu,Ala,Tyr_{10} synthesize DNA after confronting the antigen in the spleen, we assume that a recognition event took place. This conclusion is strengthened by the fact that nonimmunogenic substances such as (Glu, Tyr) and the (Glu,Ala,Tyr_{10}) polymer made of D-amino acids were nonstimulatory. Indeed, the amount of DNA synthesis produced by immunization with (Glu,Ala,Tyr) was suprisingly high; about half as much as produced by immunization with sheep erythrocytes. Bovine-serum albumin, which is clearly recognized by T-cells (21), is significantly less stimulatory (10).

The fact that the polymer did not stimulate a detectable DNA synthetic response in T-cells of mice that are genetically capable of making an antibody response to it is interesting, but its meaning is less clear, as negative results always are. The amount of T-cell DNA synthesis an antigen will stimulate depends on a number of factors such as antigen dose, number of T-cells present, ratio of cortisone-resistant to cortisone-sensitive cells in the thymocyte population, and strain of mouse (9, 10, 22). Thus, a highly stimulatory substance may yield negative results under nonoptimal conditions, and we cannot conclude from the present data that (Glu,Ala,Tyr) cannot stimulate DNA synthesis in T-cells of responder mice. That responder T-cells recognized the antigen in spite of their lack of DNA synthesis was demonstrated by their striking secondary response. The acquisition of memory in the absence of significant DNA synthesis has been previously noted (16, 23).

The striking secondary response of these cells points up all the more clearly the absence of such a response in the nonresponders. Thus, although a clear-cut response occurred the first time the T-cells of nonresponders saw the antigen, they not only did not acquire an increased capacity, but rather tended to make a negative secondary response. These results suggest that the T-cells of the nonresponder strain of mice may have been made tolerant by the initial contact with antigen. The occurrence of significant amounts of DNA synthesis by T-cells during tolerance induction to sheep erythrocytes has recently been demonstrated (16). Tolerance induction in the T-cells [or other cells with which they may communicate (24, 25)] by (Glu,Ala,Tyr_{10}) immunization of nonresponder mice would explain the ability of prior treatment with the free polymer to suppress the antibody response to the polymer on an immunogenic carrier.

It is interesting that the suppressive effect of prior antigen treatment was short-lived; although the antibody response was suppressed 5 days after prior treatment, at 10 days after it was enhanced. These results parallel a recent study of induction of tolerance to sheep erythrocytes in T-cell populations (16). In that study, T-cells were noted to be completely unresponsive to sheep erythrocytes after previous treatment with a large dose of antigen, even though they had previously synthesized considerable amounts of DNA. The unresponsive period of the T-cells was short-lived and passed into a phase of hyper-responsiveness, as did the antibody response of nonresponder mice previously treated with (Glu,Ala,Tyr_{10}).

TABLE 1. *Effect of prior treatment with (Glu,Ala,Tyr_{10}) on the antibody response of different mice to (Glu,Ala,Tyr_{10}) conjugated to methylated bovine-serum albumin*

Prior treatment	Antibody titer (±SE)
Nonresponder (DBA/1)	
(Glu,Ala,Tyr) day-5	0
(Glu,Ala,Tyr) day-10	42 ± 4.2
0	18 ± 2.4
Responder (DBA/2)	
(Glu,Ala,Tyr_{10}) day-5	45 ± 19
0	58 ± 19
Responder (C57B1/6)	
(Glu,Ala,Tyr_{10}) day-5	73 ± 10
0	77 ± 11

Thus, our results both with the effects of (Glu,Ala,Tyr_{10}) on the antibody response to (Glu,Ala,Tyr_{10})–methylated bovine-serum albumin and on T-cell DNA synthesis are consistent with the notion that this polymer has an inordinate propensity to induce tolerance in certain strains of mice. Parish has recently suggested that the affinity of antigen for cell receptors is of crucial importance in determining whether immunity or tolerance results (26). We suggest that the gene products of the H-2 locus on the T-cell membrane may contribute to the affinity of binding of the antigen with the membrane-bound receptor and, through this contribution, regulate immunological responsiveness.

Whatever the explanation, our results clearly demonstrate, at least with one system of genetically controlled immunologic unresponsiveness linked to *H-2*, that the deficit in nonresponder mice lies in their T-cells, but distal to the event of antigenic recognition.

We thank Margalit Mokyr for her expert technical assistance. This work was supported by National Institutes of Health Research Grants, AI 07825, AI 10497, and CA 08593, and American Cancer Society Grant T-452. R. K. G. is a recipient of Career Development Award (CA 10,316) from the National Cancer Institute.

1. McDevitt, H. O. & Benacerraf, B. (1969) "Genetic control of specific immune responses," *Advan. Immunol.* **11**, 31–74.
2. Benacerraf, B. & McDevitt, H. O. (1972) "Histocompatibility-linked immune response genes," *Science* **175**, 273–279.
3. Green, I., Paul, W. E. & Benacerraf, B. (1966) "The behavior of hapten-poly-L-lysine conjugates as complete antigens in genetic responder and as haptens in nonresponder guinea pigs," *J. Exp. Med.* **123**, 859–879.
4. Levine, B. B. & Benacerraf, B. (1964) "Studies on antigenicity. The relationship between *in vivo* and *in vitro* enzymatic degradability of hapten-polylysine conjugates and their antigenicities in guinea pigs," *J. Exp. Med.* **120**, 955–965.
5. Smyth, R. D. & Maurer, P. H. (1972) "*In vitro* formation of polypeptide-RNA complexes," *Ann. N.Y. Acad. of Sci.*, in press.
6. McDevitt, H. O., Bechtol, K. B., Grumet, F. C., Mitchell, G. F. & Wegmann, T. G. "Genetic control of the immune re-

sponse to branched synthetic polypeptide antigens in inbred mice," in *Progress in Immunology*, ed. Amos, B. (Academic Press, New York), pp. 495–508.
7. Tyan, M. L. (1972) "Genetically determined immune responses: *In vitro* studies," *J. Immunol.* **108**, 65–72.
8. Katz, D. H., Davie, J. M., Paul, W. E. & Benacerraf, B. (1971) "Carrier function in anti-hapten antibody responses. IV. Experimental conditions for the induction of hapten-specific tolerance or for the stimulation of anti-hapten anamnestic responses by "nonimmunogenic" hapten-polypeptide conjugates," *J. Exp. Med.* **134**, 201–223.
9. Gershon, R. K. & Hencin, R. S. (1971) "The DNA synthetic response of adoptively transferred thymocytes in the spleens of lethally irradiated mice," *J. Immunol.* **107**, 1723–1728.
10. Krüger, J. & Gershon, R. K. (1972) "DNA synthetic response of thymocytes to a variety of antigens," *J. Immunol.* **108**, 581–585.
11. Katchalski, E. & Sela, M. (1958) "Synthesis and chemical properties of poly-L-amino acids," *Advan. Protein Chem.* **13**, 243–492.
12. Merryman, C. F. & Maurer, P. H. (1972) Genetic control of immune response to glutamic acid, alanine, tyrosine copolymers in mice," *J. Immunol.* **108**, 135–141.
13. Herzenberg, L. A., Warner, N. L. & Herzenberg, L. A. (1965). "Immunoglobulin isoantigens (allotypes) in the mouse. I. Genetics and cross-reactions of the $7S_{\gamma 2A}$-isoantigens controlled by alleles at the Ig-1 locus," *J. Exp. Med.* **121**, 415–438.
14. Pinchuck, P. & Maurer, P. H. (1965) "Antigenicity of polypeptides (poly alpha amino acids). XV. Studies on the immunogenicity of synthetic polypeptides in mice," *J. Exp. Med.* **122**, 665–671.
15. Maurer, P. H. (1963) "Antigenicity of polypeptides (poly alpha amino acids). X. Studies with polymers of D-amino acids," *Proc. Soc. Exp. Biol. Med.* **113**, 553–557.
16. Spiesel, S. Z. & Gershon, R. K. (1972) "Production and temporary suppression of memory cells during tolerance induction of T-cells," *Nature New Biol.* **238**, 271–273.
17. Weigle, W. O. (1962) "Termination of acquired immunological tolerance to protein antigens following immunization with altered protein antigens," *J. Exp. Med.* **116**, 913–928.
18. Cinader, B. & Dubert, J. M. (1955) "Acquired immune tolerance to human albumin and the response to subsequent injection of diazo human albumin," *Brit. J. Exp. Pathol.* **36**, 515–529.
19. Weigle, W. O. (1964) "Studies on the termination of acquired tolerance to serum protein antigens following the injection of serologically related antigens," *Immunology* **7**, 239–247.
20. Davies, A. J. S., Leuchars, E., Wallis, V. & Koller, P. C. (1966) "The mitotic response of thymus-derived cells to antigenic stimulus," *Transplantation* **4**, 438–451.
21. Taylor, R. B. (1969) "Cellular cooperation in the antibody response of mice to two serum albumins: Specific function of thymus cells," *Transplant. Rev.* **1**, 114–149.
22. Gershon, R. K., Cohen, P., Hencin, R. & Liebhaber, S. A. (1972) "Suppressor T-cells," *J. Immunol.* **108**, 586–590.
23. Byfield, P. & Sercarz, E. (1969) "The X-Y-Z scheme of immunocyte maturation. VII. Cell division and the establishment of short-term IgM memory," *J. Exp. Med.* **129**, 897–907.
24. Gershon, R. K. & Kondo, K. (1970) "Cell interactions in the induction of tolerance: The role of thymic lymphocytes," *Immunology* **18**, 723–737.
25. Gershon, R. K. & Kondo, K. (1971) "Infectious immunological tolerance," *Immunology* **21**, 903–914.
26. Parish, C. R. (1971) "Immune response to chemically modified flagellin. I. Induction of antibody tolerance to flagellin by acetoacetylated derivatives of the protein," *J. Exp. Med.* **134**, 1–20.

Proc. Nat. Acad. Sci. USA
Vol. 70, No. 1, pp. 255–259, January 1973

Experimental Differential Light-Scattering Correction to the Circular Dichroism of Bacteriophage T2

(light-detection geometry/C-form DNA/ordered asymmetry)

BURTON P. DORMAN* AND MARCOS F. MAESTRE†

* Department of Chemistry and † Space Sciences Laboratory, University of California, Berkeley, Calif. 94720

Communicated by Paul Doty, November 13, 1972

ABSTRACT **Experimental techniques are presented that can be used to assay and correct for differential light scattering effects in circular dichroism spectra of biological macrostructures. The assay is based upon use of variable detector geometries that collect light over large solid angles. Disrupted T2 virus suspensions and purified T2 phage DNA exhibit geometry-independent spectra; the spectrum of intact T2 virus is highly sensitive to detection geometry. On the basis of spectra obtained after light-scattering correction, the structure of T2 DNA in the phage particle is assigned to the C form. We conclude that: (*i*) The measured circular dichroism of a light-scattering specimen may be highly sensitive to light-detection geometry of the instrument. This effect is indicative of differential scattering intensity for left and right circularly polarized light. (*ii*) Some optically active particles, although they scatter light intensely, exhibit circular dichroism that is independent of detection geometry and, therefore, apparently uninfluenced by differential light scattering. We infer that whether differential light scattering arises may depend upon the presence or absence of ordered asymmetry in the organization of the scattering particle. (*iii*) The circular dichroism of any light-scattering specimen should be measured again in apparatus designed for differential light-scattering correction as a prerequisite to meaningful structural conclusions. (*iv*) Differential scattering effects in circular dichroism may be potentially useful as a probe for large-order organization of the scattering particle.**

Circular dichroism (CD) studies, although at one time devoted to simple molecules (1, 2), have recently been focused upon a variety of complex biological macrostructures. Much promising CD work has been contributed on the molecular conformation of DNA in chromosomes (3), chromatin (4–12), and related material, such as reconstituted nucleohistone (13–19) or other model systems for DNA–protein interactions (20–23). The structure of virus particles has been studied with CD in this laboratory (24). The conformation of membrane-incorporated proteins has recently motivated considerable CD effort (25–34).

Due to their large size and particulate nature, biological macrostructures tend to form intensely light scattering suspensions. The effect, if any, of light scattering on CD measurements has not been well understood, although it has been discussed (25–33, 35–39). Several possible artifacts of CD measurement have been identified: absorption flattening (25–27, 29, 30, 32, 33, 35), other concentration-obscuring effects (30, 32, 33), and differential light scattering (25, 26, 29, 31–33). It is the last of these with which we are concerned.

Abbreviations: CD, circular dichroism; PMT, photomultiplier tube.

Space Sciences Laboratory Series 13, Issue 41.

Differential light scattering occurs when left and right circularly polarized light is scattered with different efficiency out of the measuring beam of a CD spectropolar-meter. The result is to modify the differential absorption measurement that constitutes normal CD. This result necessarily complicates the interpretation of CD data from scattering specimens and the comparison with spectra from molecularly dispersed samples of the same chemical compound. Several theoretical treatments of differential light scattering (35–39) have appeared, and some experimental work has been presented (25, 26, 29, 31, 32) or proposed (37, 38) for particular applications.

We now report a quite general experimental approach to assay the presence of differential light scattering and to correct for its effects on measurements in a circular dichrograph. The proposed assay involves determination of whether the observed CD spectrum varies with changes in the light-collection geometry of the spectropolarimeter. The collection geometry may be described in terms of the position, size, and shape of the light-detection element relative to the incident measuring beam and the sample cell.

As a basis for later discussion, we consider first the measurement of normal, unpolarized light absorption spectra. For a photomultiplier tube (PMT) detector located on the optical axis, and with a sufficiently collimated measuring beam, the absorption spectrum recorded for a nonscattering sample should be independent of the distance from sample cell to detector. In the presence of a scattering sample, on the other hand, some of the incident beam may be deviated from the beam axis through an angle great enough to miss the detector. Such scattered light will appear to have been absorbed and produce anomalously high optical densities.

Experimental remedies have frequently involved an increase of the solid angle of detection to enable capture of scattered photons missed by normal instruments. This may be done most simply by increasing the size of the detector, decreasing the distance from sample cell to detector, or both. Clearly, the scattered photons must penetrate the sample cell to reach a downbeam detector. When detected, the scattered photons are counted as if they were transmitted photons. Although considerable uncertainty may exist about the effective optical path through a light-scattering sample, it has been found, from work with mixtures of scattering and absorbing particles, that far more accurate absorption spectra result from detection of the scattered light and counting it as transmitted than from counting it as absorbed (*Methods in Enzymology*, in press*). The preceding generalization is not necessarily applicable to all samples or circumstances, e.g., absorption measurements on highly fluorescent specimens.

When large-angle detection is acceptable, one of the most convenient contemporary instrumental techniques involves the use of an end-window photomultiplier tube detector with a large area photocathode. In the Cary Instruments (model 1462) scattered transmission accessory, for example, a 2-inch (5.1-cm) diameter PMT may be translated along the optical axis over a range of several inches to a closest position just behind the sample cuvettes. A series of spectra recorded at various tube positions successively closer to the sample cell display a monotonic reduction, and even elimination, of spectral features due to scattering, such as the long-wavelength extinction tails extending outside the absorption band. Optical densities inside the band are also reduced. For coliphage, OD_{280} measurements are about 10% lower with scattered light correction in the model 1462 than in the standard Cary 14 or Cary 15 (40).

In principle, the large-angle detection approach should be equally applicable to CD. Ideally at least, the CD photomultiplier tube detector measures only the light intensity and is insensitive to its polarization. Therefore, if left and right circularly polarized light are scattered with equal efficiency, and if the scattered light from each polarization is equally distributed in space around an optically active sample, the scattered light contribution will subtract out from recorded CD spectra regardless of the solid angle of detection. But if the spectra should change with a modification in the solid angle of detection, the spectral change must imply that one circular polarization or the other is contributing more scattered intensity to the region of space that is accessible to the larger-angle geometry but inaccessible to the smaller. The difference between two such spectra provides a direct measure of the "differential light scattering" into that region of space where measuring photons are detectable in one case but not detectable in the other.

There is nothing in the preceding argument that limits its application to instruments using end-window photomultiplier tubes or other planar detectors. One device capable of larger solid-angle detection is the fluorescent scattering (fluorscat) cell (*Methods in Enzymology*, in press*). The use of the fluorscat scattering cell, as well as a movable, end-window photomultiplier, to assay for differential light scattering from T2 phage and to study the secondary conformation of T2 DNA *in vivo* forms the subject of this paper.

Materials and Methods. The three principal instrumental configurations used are:

(*i*) Unmodified Cary 6001, 6003, or 61 CD spectropolarimeters, whose data are termed "conventional spectra."

(*ii*) A modified Cary 6001 instrument containing a movable end-window photomultiplier with 2-inch (5.1-cm) diameter photocathode, whose data are termed "large-angle planar detector spectra."

(*iii*) A Cary 6001, either modified or unmodified, used in conjunction with special fluorescence cells that enlarge the collection angle beyond that obtained with a planar detector (*Methods in Enzymology*, in press*). Data from these fluorescent scattering cells are termed "fluorscat spectra."

The Cary 6001 modifications were as follows:

(*i*) The ORD modulator, focusing lens, side-window photomultiplier, and the light mask separating the sample elevator and ORD modulator compartments were removed. The opening between these two compartments was widened by 1 inch (2.54 cm). The photomultiplier preamplifier was remounted to the underside of the top plate of the elevator.

(*ii*) A Dumont no. KM2703 photomultiplier was installed on a variable-position roller-bearing mount in the ORD modulator compartment. The mount is supported by a plate that can be translated horizontally and that rests, in turn, on a facsimile of the ORD modulator's adjustable-height kinematic leveling table.

(*iii*) A positioning rod extending outside the instrument by way of a light lock allows the photomultiplier to be moved along the optical axis to locations 0.04–5.0 inches (0.10–12.7 cm) from the sample cell. The leveling provisions described above enable alignment such that the photocathode remains normal to the measuring beam and centered on the optical axis. The positioning rod is grooved at 1.5-inch (3.8-cm) intervals to allow several photomultiplier positions to be located reproducibly with negligible error. Whenever the photomultiplier extends into the sample space, the sample elevator is automatically locked in place to preclude tube damage or misalignment.

(*iv*) Shielded wiring connects the cathode, anode, and final dynode pin positions of the PMT socket to the preamplifier. The photomultiplier is magnetically shielded, and electrically shielded at cathode potential.

All sample cells were 1-cm path length. The zero ellipticity line in all spectrograms was obtained from solvent baselines, and no instrumental adjustments were made between solvent and sample runs. All spectra were run without multipots, but with the 14-Å spectral bandwidth automatic slit program, unless otherwise noted. Data were acquired with an instrumental time constant of 1 sec and digitally recorded by an on-line computer with available pen-averaging, baseline subtracting, and data smoothing programs (41). Subsequent processing to obtain difference curves and plotted output was also done on a CDC 6400 computer. Extinction per mol of phosphate at 260 nm was assumed to be 6440 for T2 DNA and 10,206 for intact T2 virus (24).

All CD instruments were calibrated with d-10 camphor sulfonic acid (Eastman Organic, 1 mg/ml in H_2O). Calibration readings of 0.304 ± 0.004 degrees ellipticity at 290 nm were obtained and checked periodically during several weeks of experimentation. Agreement between the various instruments was within 1.5%.

Calibration tests were also performed on optically inactive samples providing extinction due to: (*i*) Absorption: potassium dichromate solution (Mallinckrodt Chem.), 6 mg/liter in 0.01 N KOH; (*ii*) scattering: alumina suspensions (Vitro Labs.) of nearly spherical particles in the range of 0.01–0.2 μm diameter in 0.01 N KOH. All instruments gave readings, so-called inactive sample artifacts, of no greater than 1 millidegree/OD for the above samples. These readings varied from one instrument to another, but observed magnitudes were nearly independent of tube position in the modified Cary 6001. Inactive sample artifacts for the fluorescent cells were consistently lower than those observed with standard cuvettes.

T2 phage and T2 phage DNA preparation, purification, and all subsequent handling was by reported techniques (24). In particular, virus was purified by hydroxyapatite column chromatography, then dialyzed exhaustively against 0.5 M NaCl–1 mM $MgSO_4$–1 mM Tris·HCl (pH 6.8). Phage were disrupted by freeze-thawing, leading to release of DNA into

the surrounding solvent. Viral DNA was extracted with phenol and dialyzed extensively against 0.1 M NaCl–10 mM Na-phosphate (pH 7.2).

RESULTS

Conventional CD spectra of intact T2 bacteriophage, disrupted T2 bacteriophage, and T2 DNA have been reported (24). Above 250 nm, the observed CD of a disrupted phage suspension is essentially that of T2 DNA. The CD of T2 DNA exhibits a positive maximum at 280 nm ($\Delta\epsilon$ = 1.99), is zero at 265 nm, and exhibits a negative minimum at 250 nm ($\Delta\epsilon$ = −5.01). The spectrum of a shocked suspension, due to the presence of the protein phage coats, begins to diverge from that of DNA at 245 nm and below. The coats scatter sufficient light to register OD_{310} = 0.04 per OD_{260} in a Cary 14 absorption spectrophotometer (Dorman & Maestre, unpublished data). Such scattering leads to no detectable signal outside the absorption band when conventional CD spectra are measured.

The conventional CD spectrum of intact T2 phage differs from that of T2 DNA in several respects (24): the positive maximum is red-shifted to 286 nm and reduced in magnitude to $\Delta\epsilon$ = 1.6, crossover is shifted to 276.5 nm, the negative minimum is slightly red-shifted and enhanced to $\Delta\epsilon$ = −6.9. Below 240 nm, the intact T2 CD spectrum is intermediate between that of shocked T2 and purified T2 DNA. The intact virus scatters light at OD_{310} = 0.07 per OD_{260} in a Cary 14 (Dorman & Maestre, unpublished data) and exhibits a positive tail at long wavelength extending well into the visible spectrum. This tail admits no theoretical explanation in terms of a DNA structural modification. However, a nonzero CD signal outside the absorption band might conceivably be due to differential light scattering from a highly compacted DNA organization inside the phage head. To investigate this possibility, and the extent to which other features of the intact T2 CD spectrum might derive from differential light scattering, we performed the following experiments.

The large-angle CD spectrum of intact T2 phage was measured in a Cary 6001 spectropolarimeter modified to accommodate an end-window PMT with 2-inch (5.1-cm) diameter photocathode. The PMT may be positioned on the optical axis of the instrument at various distances from the sample cell. The spectra obtained from distant, intermediate, and close PMT positions may be compared with conventional Cary 60 data in Fig. 1. For the most part, the conventional T2 spectrum exhibits values that are intermediate between the large-angle data. However, as the solid angle is increased by moving the large-angle detector to the intermediate and close positions, the 286-nm peak and the long-wavelength tail are reduced. Indeed, the tail is no longer evident in the close PMT spectrum.

The shape of the differential light-scattering contribution detected with the large-angle modified Cary 6001 geometry was obtained by subtraction of the close PMT spectrum from the distant PMT spectrum. Such difference spectra are presented in Fig. 2 for intact T2 phage, disrupted T2 phage, and purified T2 DNA. The intact phage difference spectrum displays a long-wavelength tail, has a maximum at 290 nm, goes to zero at 265 nm, and has a larger maximum at 220 nm. In contrast, the T2 DNA and the disrupted phage suspension spectra exhibit essentially no dependence on PMT position down to 220 nm. Because these latter specimens

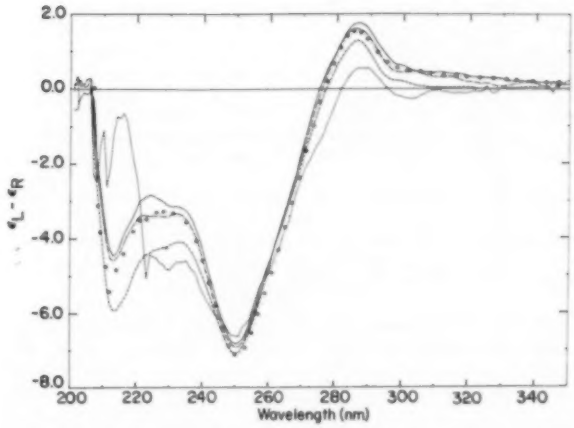

FIG. 1. Intact T2 phage CD spectra with four large-angle plus conventional detection geometries. Three curves represent large-angle planar detector data recorded in modified Cary 6001 CD spectropolarimeter with 2-inch (5.1-cm) diameter end-window photomultiplier (PMT) at distant (——), intermediate (— —), and close (– – –) positions relative to sample cuvette. Nominal clearance (inches) between cuvette and PMT was 5.00, 3.04, and 0.04, respectively (12.7, 7.72, and 0.10 cm). Solid angle of detection increases as PMT is moved closer to cuvette. The lowest curve (------) was recorded in unmodified Cary 6001 with a fluorescent scattering (fluorscat) cell that offers a larger solid detection angle than the close PMT geometry. Fluorscat spectrum represents the computer average of three runs with monochrometer slits set at 2.4 mm. The conventional spectrum (⊙·····⊙) was obtained with a standard cuvette in an unmodified Cary 6003 CD instrument.

produce spectra that do not change with the solid angle of detection, we may conclude that differential light-scattering contributions, if any, are beneath the sensitivity level of the present measurements. Moreover, this result demonstrates the absence of a systematic position dependence to the large-angle planar detector CD spectra, even in the presence of a light-scattering specimen such as the disrupted phage.

The fluorescent scattering (fluorscat) cell CD spectrum of intact T2 was measured in an unmodified Cary 6001 (lowest curve of Fig. 1). The fluorscat spectrum is zero above 330 nm, assumes small negative values between 330 and 310 nm, and exhibits a negative minimum at 303 nm ($\Delta\epsilon$ = −0.27). The positive maximum, slightly red-shifted, is further reduced to about half the value obtained in the close PMT spectrum. Inasmuch as the fluorscat cell is capable of detecting light scattering through angles even larger than 90 degrees, the reported data demonstrate that the more scattered light detected, the greater is the depression of the positive 286-nm ellipticity band in the intact T2 phage spectrum. It may be concluded that differential light scattering is contributing significantly to the magnitude of this band observed in the conventional CD spectrum of intact T2.

DISCUSSION

T2 DNA conformation *in vivo*

The CD spectrum of DNA in aqueous solution at low salt concentration has been discussed above. In comparison, DNA spectra obtained in the presence of high salt (42), methanol (Maestre, unpublished results), ethylene glycol (43, 44),

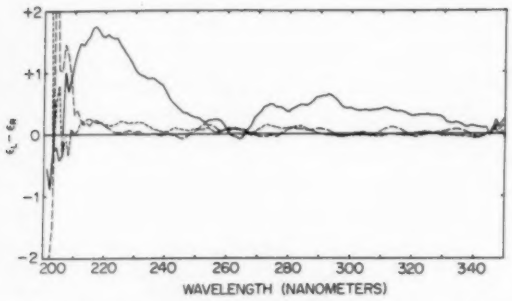

FIG. 2. CD difference spectra computed for large-angle planar detector data by subtracting close PMT spectrum from distant PMT spectrum of intact T2 bacteriophage (——), disrupted T2 bacteriophage (— —), and purified T2 DNA (– – –). Only the intact virus exhibits a nonzero difference spectrum indicative of differential light scattering. Values obtained at wavelengths below 210 nm are believed to be artifacts due to high sample absorbance and the resultant instrumental noise level.

and in Li-DNA films at low ($\leq 75\%$) relative humidity (42) exhibit depression of the positive ellipticity band with little or no effect on the adjacent negative band. X-ray structures determined for Li-DNA fibers formed at salt and humidity conditions thought to be comparable to those used for the cited Li-DNA film studies indicate that under such conditions DNA exists in the C conformation (45). We note the conclusion of Nelson and Johnson (43) that C-form DNA possesses the minimum specific volume of the DNA structures characterized to date by x-ray. Thus, a C-form helix might be a favorable conformation for DNA that is tightly compacted into a phage coat.

The CD spectrum of purified T2 phage DNA, the fluorscat spectrum of intact T2 phage, and the low-humidity (C-form) Li-DNA film spectrum for calf-thymus DNA are shown in Fig. 3. Comparison of the T2 DNA spectrum with the fluorscat, scatter-corrected phage spectrum reveals that compaction of the DNA into the T2 phage coat leads to substantial depression and red shift of the 280-nm DNA band in the manner characteristic of a transition to C-form geometry. The extensively glucosylated T2 DNA exhibits a solution-form CD that is highly nonconservative and whose prominent spectral features (e.g., extrema and crossover) are red-shifted about 5 nm relative to calf-thymus DNA (24). When allowances are made for these intrinsic differences, however, the correspondence of the CD spectrum for intact T2 virus and for low-humidity Li-salt DNA films is quite striking (Fig. 3). With decreasing wavelength, both spectra exhibit a perceptible negative tail, a small trough, a slightly larger positive maximum, crossover in the vicinity of 280 nm, a shoulder at about 270 nm, and a large negative trough between 240 and 250 nm. On the basis of this correspondence, and the related x-ray fiber structure, we conclude the secondary conformation of T2 DNA *in vivo* may be assigned to the C-form, or to a similar geometry.

General conclusions

The present work clearly demonstrates that CD spectra of a light-scattering suspension may be very sensitive to instrumental light-detection geometry. If scattered light were generated in equal intensities for both circular polarizations, we would expect the resultant spectra to be invariant with changes in the solid angle of detection. Thus, we interpret geometry-sensitive spectra as an indication that differential light scattering is present. Differential light scattering may be a general property of biological macrostructures in suspension. Where it is present, the observed CD of such suspensions will vary with the experimental geometry used, the optical path length, and the relative dimensions of beam cross section, cell diameter, and the position and size of the light-detection apparatus. Under these circumstances, structural conclusions based upon CD data obtained from particulate suspensions in conventional CD spectropolarimeters may be unreliable or meaningless.

It is important to emphasize from our work with disrupted phage suspensions that all particulate suspensions need not exhibit geometry-dependent CD spectra. Although the disrupted T2 samples contain essentially intact phage coats after the DNA is released (46), no significant spectral changes are observed upon going from conventional to large-angle planar to fluorscat detection geometries. Thus, if the phage coats do generate differential light scattering, the effect apparently is not large enough to influence conventional measurements. For practical purposes, we must conclude that differential light scattering will influence the CD of some, not all, particulate suspensions of optically active particles. Whether or not differential light scattering arises may depend then on the specific organization of the aggregated chromophores. We infer that where differential light scattering exists, the organization must exhibit ordered asymmetry. [Wrigglesworth and Packer (47) have made a related suggestion.] For intact T2 virus, we attribute the observed differential light scattering to asymmetry in the DNA packing organization.

Other plausible sources of differential light scattering have been proposed. In the treatment of Gordon (35), differential light scattering arises as a specific consequence of the par-

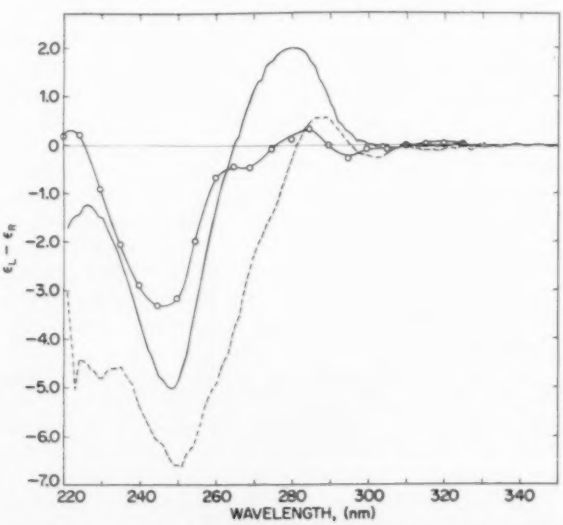

FIG. 3. CD spectra of T2 DNA recorded in a conventional Cary 6003 with a standard cuvette (——), and of intact T2 phage measured in an unmodified Cary 6001 with a fluorscat cell (– – –). The spectrum of a Li-salt DNA film at 75% relative humidity (O——O) is reproduced from earlier work (42).

ticulateness of the specimen rather than the organization of the particle. Using Mie theory for spherical particles and the optical properties of molecularly dispersed sample solutions, Gordon (35) and Gordon and Holzwarth (26) have obtained impressive agreement between the calculated and experimental CD spectra for two particulate suspensions—poly(L-glutamic acid) spheres and erythrocyte ghosts. Large spherical particles in suspension might conceivably represent a class of specimens that will yield to existing theory by the use of known scattering spatial distribution functions. However, such theory is presently limited to treatment of highly symmetric scattering arrays. It remains to be demonstrated that a similar approach can be applied to numerous important, but asymmetric, biological structures, e.g., coliphage. For asymmetric structures in particular, a generally applicable experimental approach is especially desirable. The large-angle detection techniques reported here promise to be useful. (But absorption flattening artifacts intrinsic to particulate suspensions should be independent of detection geometry, and will remain uncorrected by these large-angle techniques.)

Our work suggests that the CD spectra of any scattering specimen ought to be determined again under conditions permitting empirical analysis of possible differential light-scattering contributions. The data presented reveal a large light-scattering effect on the CD of intact T2 virus. We anticipate differential scattering contributions may be influencing the conventional CD of other viruses, chromosomes, chromatin, and membrane structures.

If the observed differential light scattering is in fact produced by an ordered asymmetry at the scattering center, which we believe to be the case, it is conceivable the shape of the scattering contribution curves may be used to assess details of the relevant ordered structure. As such, the differential light-scattering phenomenon might constitute a uniquely powerful probe for molecular organization at the level of tertiary or quaternary conformation.

* *Note Added in Proof.* A more detailed description of the fluorscat cell and related large-angle light detection techniques has been written; see Chap. 30 in *Enzyme Structure*, Vol. 27D of *Methods in Enzymology*, eds. Hirs, C. H. W. & Timasheff, S. N. (Academic Press, New York).

We thank Prof. John E. Hearst for his interest and support throughout this study. We are indebted to Dr. K. D. Philipson and Profs. K. Sauer and I. Tinoco, Jr. for use of essential instrumentation. We also thank Mrs. K. Sieux for isolation and purification of T2 virus. This research was supported by NASA Grant 05-003-020 and by NIH Grants AI-08427-04 and GM-11180.

1. Yang, J. T. & Samejima, T. (1969) in *Progress in Nucleic Acid Research and Molecular Biology*, eds. Davidson, J. N. & Cohn, W. E. (Academic Press, New York), Vol. 9, pp. 224–300.
2. Brahms, J. & Brahms, S. (1970) in *Fine Structure of Proteins and Nucleic Acids*, eds. Fasman, G. D. & Timasheff, S. N. (Dekker, New York, N. Y.), Vol. 4, pp. 191–270.
3. Cantor, K. P. & Hearst, J. E. (1969) *J. Mol. Biol.* **49**, 213–229.
4. Fric, I. & Sponar, J. (1971) *Biolpolymers* **10**, 1525–1531.
5. Matsuyama, A., Tagashira, Y. & Nagata, C. (1971) *Biochim. Biophys. Acta* **240**, 184–190.
6. Wagner, T. E. & Snelsberg, T. C. (1971) *Biochemistry* **10**, 2599–2605.
7. Henson, P. & Walker, I. O. (1970) *Eur. J. Biochem.* **16**, 524–531.
8. Permogorov, V. I., Debabov, V. G., Sladkova, I. A. & Rebentish, B. A. (1970) *Biochim. Biophys. Acta* **199**, 556–558.
9. Ramm, E. I., Vorob'ev, V. I., Birshtein, T. M., Bolotina, I. A. & Volkenshtein, M. V. (1972) *Eur. J. Biochem.* **25**, 245–253.
10. Shih, T. Y. & Fasman, G. D. (1970) *J. Mol. Biol.* **52**, 125–129.
11. Simpson, R. T. & Sober, H. A. (1970) *Biochemistry* **9**, 3103–3109.
12. Wilhelm, F. X., Champagne, M. H. & Duane, M. P. (1970) *Eur. J. Biochem.*, **15**, 321–330.
13. Adler, A. J., Schaffhausen, B., Langan, T. A. & Fasman, G. D. (1971) *Biochemistry* **10**, 909–913.
14. Fasman, G. D., Valenzuela, M. S. & Adler, A. J. (1971) *Biochemistry* **10**, 3795–3801.
15. Olins, D. E. & Olins, A. L. (1971) *J. Mol. Biol.* **57**, 437–455.
16. Shih, T. Y. & Fasman, G. D. (1971) *Biochemistry* **10**, 1675–1683.
17. Fasman, G. D., Schaffhausen, B., Goldsmith, L. & Adler, A. (1970) *Biochemistry* **9**, 2814–2822.
18. Slayter, H. S., Shih, T. Y., Adler, A. J. & Fasman, G. D. (1972) *Biochemistry* **11**, 3044–3054.
19. Olins, D. E. (1969) *J. Mol. Biol.* **43**, 439–460.
20. Carroll, D. (1972) *Biochemistry* **11**, 421–426; 426–433.
21. Davidson, B. & Fasman, G. D. (1971) *Arch. Biochem. Biophys.* **144**, 650–656.
22. Shapiro, J. T., Leng, M. & Felsenfeld, G. (1969) *Biochemistry* **8**, 3219–3232.
23. Haynes, M., Garrett, R. A. & Gratzer, W. B. (1970) *Biochemistry* **9**, 4410–4416.
24. Maestre, M. F., Gray, D. M. & Cook, R. B. (1971) *Biopolymers* **10**, 2537–2553.
25. Glaser, M. & Singer, S. J. (1971) *Biochemistry* **10**, 1780–1787.
26. Gordon, D. J. & Holzwarth, G. (1971) *Proc. Nat. Acad. Sci. USA* **68**, 2365–2369.
27. Gordon, D. J. & Holzwarth, G. (1971) *Arch. Biochem. Biophys.* **142**, 481–488.
28. Glaser, M., Simpkins, H., Singer, S. J., Sheetz, M. & Chan, S. I. (1970) *Proc. Nat. Acad. Sci. USA* **65**, 721–728.
29. Schneider, A. S., Schneider, M.-J. T. & Rosenheck, K. (1970) *Proc. Nat. Acad. Sci. USA* **66**, 793–798.
30. Urry, D. W., Hinners, T. A. & Masotti, L. (1970) *Arch Biochem. Biophys.* **137**, 214–221.
31. Urry, D. W. & Krivacic, J. (1970) *Proc. Nat. Acad. Sci. USA* **65**, 845–852.
32. Ji, T. H. & Urry, D. W. (1969) *Biochem. Biophys. Res. Commun.* **34**, 404–411.
33. Urry, D. W. & Ji. T. H. (1968) *Arch. Biochem. Biophys.* **128**, 802–807.
34. Lenard, J. & Singer, S. J. (1966) *Biochemistry* **56**, 1828–1835.
35. Gordon, D. J. (1972) *Biochemistry* **11**, 413–420.
36. Schneider, A. S. (1971) *Chem. Phys. Lett.* **8**, 604–608.
37. Barron, L. D. & Buckingham, A. D. (1971) *Mol. Phys.* **20**, 1111–1119.
38. Blum, L. & Frisch, H. L. (1971), *J. Chem. Phys.* **55**, 1188–1196: (1970) *J. Chem. Phys.* **52**, 4379–4384.
39. Ottaway, C. A. & Wetlaufer, D. B. (1970) *Arch. Biochem. Biophys.* **139**, 257–264.
40. Maestre, M. F. & Tinoco, I., Jr. (1967) *J. Mol. Biol.* **23**, 323–335.
41. Tomlinson, B. L. (1968) Ph. D. Thesis, University of California, Berkeley.
42. Tunis-Schneider, M. J. B. & Maestre, M. F. (1970) *J. Mol. Biol.* **52**, 521–541.
43. Nelson, R. G. & Johnson, W. C., Jr. (1970) *Biochem. Biophys. Res. Commun.* **41**, 211–216.
44. Green, G. & Mahler, H. R. (1971) *Biochemistry* **10**, 2200–2216.
45. Marvin, D. A., Spencer, M., Wilkins, M. H. F. & Hamilton, L. D. (1961) *J. Mol. Biol.* **3**, 547–565.
46. Herriott, R. M. & Barlow, J. L. (1957) *J. Gen. Physiol.* **40**, 809–825.
47. Wrigglesworth, J. M. & Packer, L. (1968) *Arch. Biochem. Biophys.* **128**, 790–801.

Proc. Nat. Acad. Sci. USA
Vol. 70, No. 1, pp. 260–264, January 1973

In Vitro Assembly of Bacteriophage Lambda Heads

(morphogenesis/DNA condensation/*in vitro* complementation)

DALE KAISER AND TERRIE MASUDA

Department of Biochemistry, Stanford University School of Medicine, Stanford, California 94305

Contributed by Dale Kaiser, October 30, 1972

ABSTRACT **The assembly of plaque-forming particles in cell-free extracts of induced lambda lysogens was observed two ways. (*i*) DNA isolated from a λ-related phage, 434 for example, is added to an extract of an induced λ lysogen, and plaque-formers with the genotype of the added DNA are detected. (*ii*) One extract from an induced λ lysogen that carries an amber mutation in one of the head genes (*A*, *B*, *C*, *D*, or *E*) is mixed with one carrying an amber mutation in a different head gene; an increase in the number of λ plaque-formers is found over that in either extract alone. These plaque-forming particles have the properties of normal phage particles. They are resistant to DNase, although DNase added to an extract before addition of DNA prevents their appearance; they have a sensitivity to neutralizing antibody and a specificity of adsorption to bacteria characteristic of the source of the extract, but they have the genotype of the added DNA; and they have about the same bouyant density as phage particles.**

Mutants in genes *B*, *C*, or *D* can donate DNA to the phage formed by complementation between extracts of different mutants, but mutants in genes *A* or *E* cannot. Complementation occurs between a pair of extracts only if one (or both) is a DNA donor. This observation suggests a tentative pathway for head assembly: that the products of genes *A* and *E* act before those of *B*, *C*, and *D*.

After the germinal discovery of Edgar and Wood (1) that bacteriophage T4 heads, tails, and tail fibers can join together *in vitro*, many steps in bacterial virus assembly were worked out. But the problem of how DNA-containing phage heads are assembled has remained unsolved. How is DNA cut, condensed, and packaged inside a protein coat? Phage λ may be a good subject for experimental exploration of this problem because its isometric head contains relatively few proteins, six perhaps (2), its head genes cluster and saturate the left end of the phage chromosome (3, 4), and several assembly reactions *in vitro* have already been demonstrated (5–7).

Eight proteins are required for λ head assembly: the protein products of seven phage genes, *A*, *W*, *B*, *C*, *D*, *E*, and *F*, (8) and the product of the bacterial *gro E* gene (9, 10). DNA molecules isolated from phage particles have two short, single-stranded ends of unique sequence (11). The precursor to this DNA is a polymer of more than two phage-sized units that lacks cohesive ends (12, 13). Two of the eight required proteins, the *F* and *W* proteins, act after DNA is cut and packaged, because W^- and F^- mutants accumulate morphologically normal heads that contain cohesive-ended monomers (7). These heads, however, cannot join to tails. Mutants in any of the other six genes, *A*, *B*, *C*, *D*, *E*, or *gro E*, accumulate precursor or precursor-like DNA (14–16, 9), as if DNA cutting depended on prior functioning of the products of all these genes. A challenging problem in head assembly is to explain how cutting and packing of DNA is coupled to aggregation of head protein subunits. As an initial experimental step toward the solution of this problem, we wish to report evidence for the *in vitro* assembly of λ heads.

Abbreviation: PFU, plaque-forming units.

MATERIALS AND METHODS

Bacteria, Phage, and DNA. All bacterial strains used for preparation of extracts were derived from the Su^- prototrophic *Escherichia coli* K12 strain W3101 (17). A series of heat-inducible lysogens were prepared by infection of W3101 with each of the following strains of phage: λ *c*Its857 *S*am7, λ *A*am11 *c*Its857 *S*am7, λ *A*am32 *c*Its857 *S*am7, λ *B*am10 *c*Its857 *S*am7, λ *B*am427 *c*Its857 *S*am7, λ *C*am42 *c*Its857 *S*am7, λ *D*am15 *c*Its857 *S*am7, and λ *E*am4 *c*Its857 *S*am7. DNA was extracted with water-saturated phenol from λ*imm* 434 *c*Its56 *S*am7, φ80(19), and λ*imm*21 (21 hy 1 of ref. 20).

Preparation of Extracts. The procedure is an adaptation of that used by Wickner *et al.* (18) to prepare extracts active in DNA synthesis. Lysogenic bacteria were grown in H broth (containing per liter: 8 g of nutrient broth, 5 g of Bactopeptone, 1 g of glucose, 5 g of NaCl) to a density of 8×10^7 bacteria per ml. Then they were heat-induced by warming to 46° for 15 min, with aeration. Bacteriophage were allowed to develop for 40 additional minutes at 37°, by which time, determined by experiment to be the period of most rapid completion of phage particles, the bacterial mass had tripled. The culture was chilled on ice, and the bacteria were collected by centrifugation at 10,000 × *g* for 15 min at 5°. The bacterial pellet was immediately suspended in 10% sucrose–50 mM Tris·HCl (pH 7.4) (200 ml of culture in 0.4 ml of sucrose–Tris). Aliquots of 0.1–0.6 ml were then quick-frozen and stored in liquid nitrogen. These frozen bacteria were stable for at least 1 month.

Frozen bacteria were thawed rapidly at 35°, cooled to 0°, and, for each 0.1 ml of bacteria, 5 μl of egg-white lysozyme [1 mg/ml in 0.25 M Tris·HCl (pH 7.4)] were added. The thawed bacteria were lysed by exposure to lysozyme for 30 min at 0° and addition of 10 μl of the following mixture: 6 mM Tris·HCl (pH 7.4), 15 mM ATP, 18 mM $MgCl_2$, 60 mM spermidine–HCl, 30 mM 2-mercaptoethanol. The lysed suspension was sedimented at 40,000 × *g* for 20 min at 5°, and a resulting amber-colored, slightly opalescent supernatant was removed with a micropipet. Because of its instability, the supernatant, called "the extract," was kept at 0° and was used within 30 min.

In Vitro Assembly. In a typical experiment, 100 μl of extract was mixed with 10 μl of DNA [in 10 mM Tris·HCl (pH 7.4)–670 mM NaCl] and incubated at 35° for 80 min. The reaction was terminated by addition of 25 μl of pancreatic DNase I [Worthington, 200 μg/ml in 10 mM Tris·HCl (pH 7.4)–100 mM $MgCl_2$]. At this point, 100 μl of T broth (10 g/liter of Bacto-tryptone, 5 g/liter of NaCl) were added, and the mixture was plated with appropriate indicator bacteria as described with each experiment on T agar (T broth containing 1% agar) plates.

RESULTS

Head Assembly with Exogenous DNA. If DNA isolated from λ *imm* 434 phage particles is added to a concentrated cell-free extract of an induced λ lysogen, then plaque-forming particles carrying 434 DNA are produced (Table 1). The extracts are prepared from a λ lysogen 40 min after thermal induction, at which time the bacteria are producing complete phage particles at maximum rate. The extracts contain about 10^9 complete λ per ml, but 434 DNA-containing particles are specifically assayed by plating the incubation mixture for plaques on a λ lysogen. Because of the specificity of the λ repressor present in these bacteria, this assay has the capacity to detect one 434 particle against a background of more than 10^9 λ particles.

The data presented in Table 1 also show that the number of 434 plaque-forming units (PFU) increases with amount of 434 DNA added, at a rate of about one plaque per 10^8 DNA molecules. Pancreatic DNase added before phage DNA destroys the plaque-forming activity. Six-times the amount of DNase used in the experiment reported in Table 1 is routinely added at the end of the incubation of extract with DNA. Therefore, the extract converts the plaque-forming capacity of 434 DNA from a DNase-sensitive to a DNase-resistant state. The reaction is stimulated by ATP and is dependent upon addition of spermidine. Spermidine may help DNA condense (23), and it is required for φX174 DNA synthesis in similar extracts (24). In another experiment, 434 DNA was added to an extract of (mock-) induced nonlysogenic bacteria, but no 434 PFU were observed. Thus, some phage-specific product(s) must be present in the extract, a property that distinguishes these experiments from reports of λ multiplication *in vitro* (25, 26).

The bouyant density of the 434 PFU was measured in an equilibrium density gradient (*upper panel*, Fig. 1). Complete λ phage particles present in the extract before addition of 434 DNA serve as a density reference, but as confirmation that these λ had not been altered in some way as a result of the extraction procedure, λ cI^+S^+ phage was added to the assembly mixture in CsCl just before centrifugation. These phage form turbid plaques at 40° on Su^- bacteria and can, therefore, be distinguished from endogenous λ *c*Its857 *S*am 7, which cannot plate on Su^- bacteria and which form clear plaques on $Su3^+$ bacteria at 40°. The ratio of turbid to clear plaque-formers was about constant across the λ peak, showing that endogenous λ had normal bouyant density.

λ *imm* 434 phage form a band with its mode four fractions up-gradient from that of λ phage (*bottom panel*, Fig. 1). This occurs because *imm*434 DNA is 2% shorter than λ DNA but is enclosed in the same amount of protein as λ (27). The 434 PFU from an assembly mixture (Fig. 1, *top panel*) band more broadly than *imm*434 phage and have a mode 11 fractions up-gradient from λ, indicating an average 1% lower density than *imm*434 phage particles. Because, as will be shown below, the PFU contain an entire molecule of added DNA, their lowered density can be explained by the presence of 4% more than the normal phage content of protein. Perhaps a small but variable amount of protein is trapped inside a head as it forms in an extract.

TABLE 1. *Requirements for production of plaque-forming particles*

Components added	Plaques
Complete	3334
Complete minus ATP	1334
Complete minus spermidine	1
Complete plus DNase*	0
Complete, ½ × DNA	710
Complete, 3 × DNA	8932

Complete contains 0.5 mM Tris·HCl (pH 7.4), 1.6 mM $MgCl_2$, 3 mM 2-mercaptoethanol, 67 mM NaCl, 1.5 mM ATP, 6 mM spermidine–HCl, extract of 1.3 × 10^9 bacteria, and 0.23 μg of λ *imm*434 DNA. The total incubation mixture of 55 μl was plated.

* Pancreatic DNase (9 μg/ml) added before DNA.

Additional evidence that exogenous DNA can be encapsulated by extracts is presented in Table 2. Phage φ80, though related to λ, differs from it antigenically and in host range (28). Antibodies, raised in rabbits by inoculating them with purified λ, neutralize λ but not φ80. Lambda adsorbs well to phage T1-resistant strains of K12, symbolized K12/T1, but φ80 adsorbs poorly. DNA extracted from purified particles of phage φ80 was mixed with an extract of induced Su^- (λ *c*Its857 *S*am7) bacteria, and φ80 plaque-formers were generated. As shown in Table 2, PFU from the assembly reaction were inactivated by antiserum against λ at about the same rate as the endogenous λ present in the same mixture and many times faster than φ80 phage. The φ80 PFU proved to adsorb faster to K12/T1 than to K12, as did λ, whereas φ80 phage adsorbed more slowly to K12/T1 than to K12. Subsequently, the φ80 PFU were propagated on K12 $Su3^+$ bacteria and, as shown by the last line of Table 2, as a result they regained the antiserum resistance and adsorption properties of φ80 phage. Therefore, the φ80 PFU generated in an assembly mixture behave like φ80 DNA encapsulated in λ head and tail proteins provided by the extract. After propagation these phage regained φ80 adsorption and antibody specificity because they possessed φ80 genes.

Head Assembly with Endogenous DNA. If extracts of induced lysogens for amber mutants in head genes *A*, *B*, *C*, *D*, or *E* are mixed by pairs, then complementation between mutants in different genes can be observed. As shown in Table 3, the mixtures yield more plaque-forming particles than either of the component extracts alone. Only the A^- plus E^- mixture does not exceed its background, while the most efficient mixtures rise 80-times higher than their background. The ability to complement does not seem to depend on the particular amber mutants chosen: *A*am11 and *A*am19 have the same complementation pattern. So do *B*am10 and *B*am427 (data not shown).

As expected, these plaque-forming particles have the immunity specificity of λ: they form plaques on nonlysogenic

Su3$^+$ bacteria, on *Su3*$^+$(434), but not on *Su3*$^+$(λ). No exogenous DNA has been added; as shown by their immunity specificity, the plaque-formers arise from DNA endogenous to the extracts. To determine the bouyant density of the plaque-formers, they were sedimented to equilibrium in CsCl solution. Comparison of the middle and bottom panels of Fig. 1 shows that the λ plaque-formers generated by the mixed extracts have the same average bouyant density, measured relative to added *imm*434 phage particles, as complete λ phage particles. Though the A^- and C^- extracts contain some λ plaque-formers before mixing, these are less than 10% of the total. In the experiment shown in the middle panel of Fig. 1, more than 50% of the λ plaque-formers added to the CsCl solution were recovered, and all of them were in the single λ peak shown. Therefore, at least 80% of the plaque-formers in that peak were generated by complementation.

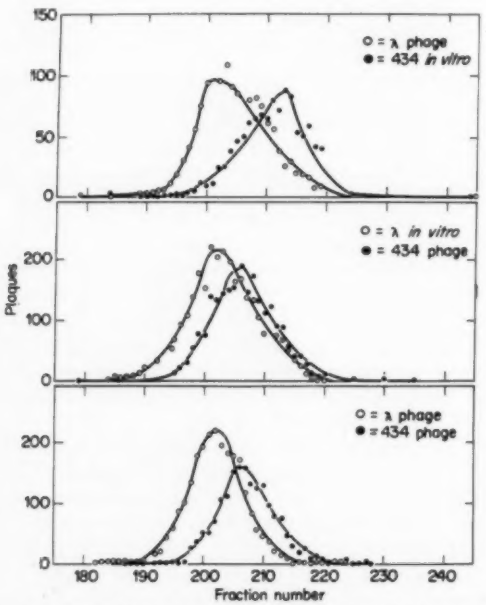

FIG. 1. Equilibrium density gradient sedimentation of phage assembled in extracts. To 600 μl of an assembly mixture was added sufficient CsCl solution to bring the total volume to 5.25 ml and the bouyant density to $\rho = 1.46$ g/ml. The solutions were sedimented at 32,000 rpm at 5° in an SW39 rotor for 72 hr. Single-drop fractions of 0.01 ml were collected through the bottom of the tube into 1 ml of T broth. Aliquots of these broth solutions, referred to below as the "fractions," were assayed for λ or 434 plaque-forming units by plating them on K12 *Su3*$^+$ (434) or K12 *Su3*$^+$ (λ) indicators. (*Top panel*) The assembly mixture contained 434 DNA and an extract of *Su*$^-$ (λ *cI*857 *S*am7). The extract, before it was mixed with DNA, contained 2.5×10^8 λ *cI*857 *S*am7 phage particles per ml. These λ phage serve as a bouyant density reference for alignment with λ phage in the lower panel. The peak 434 fraction contained 147 plaque-formers per ml, and a total of 0.6 ml of each fraction were plated. The peak λ fraction contained 1.1×10^8 phage per ml and 30 μl of a 10^{-3} dilution were plated. The λ plaque counts were divided by 10 to put them on the same scale with the 434 plaques. (*Middle panel*) The assembly mixture contained 300 μl of an extract of induced *Su*$^-$ (λ *A*am11 *cIts*857 *S*am7) and 300 μl of an extract of induced *Su*$^-$ (λ *B*am427 *cIts*857 *S*am7). Phage λ *imm*434 *cIts*56 *S*am7 was added to the mixture in CsCl at a final concentration of 10^4 phage per ml, to serve as a density reference for alignment with 434 phage in the lower panel. The peak fraction of plaque-formers with λ specificity contained 2.2×10^3 PFU per ml, and three platings of 0.1 ml were made. The peak fraction of 434 phage contained 950 phage per ml, and two platings of 0.1 ml were made. (*Bottom panel*) A reconstruction was prepared by mixing λ *cIts*857 *S*am7 phage and λ *imm* 434*cIts*56 *S*am7 phage, with an extract of nonlysogenic *Su*$^-$ bacteria, prepared in the standard way. The peak fraction of λ phage contained 2.2×10^3 phage per ml and the peak fraction of 434 phage, 1.6×10^3 phage per ml; 0.1 ml of each fraction was plated.

Although both members of each pair of complementing extracts contain phage DNA, usually only one of them donates DNA to the phage particles formed by complementation. In the A^- plus B^- extract complementation, for example, all 75 of the progeny phage tested had a B^- genotype, indicating that DNA was contributed by the B^- extract to the phage formed by complementation. In general, extracts of B^-, C^-, and D^- serve as DNA donors; extracts of A^- and E^- do not. A^- or E^- particles found in the complementation mixtures can be accounted for by the background plaque-forming activity of unmixed extracts.

Exogenous DNA can also be encapsulated by mixed extracts. As shown in Table 3, plaque-forming particles with 434 immunity specificity are formed from added *imm*434 DNA. The encapsulation of exogenous DNA is strongly correlated with the *in vitro* encapsulation of endogenous DNA: those pairs of extracts that complement for endogenous DNA encapsulate added *imm*434, with the possible exception of B^- plus E^-.

To test whether genetic recombination occurs between exogenous and endogenous DNA, we added λ*imm*21 DNA to a mixture of an extract of a λ *A*am11 *cIts*857 *S*am7 lysogen with an extract of a λ *C*am42 *cIts*857 *S*am7 lysogen. The assembly mixture was plated on *Su3*$^+$ bacteria at 42°, and the turbid plaque-formers were picked and purified on *Su3*$^+$ bacteria. Finally, they were tested for immunity specificity and for their ability to form plaques on *Su*$^-$ bacteria. All 100 independent plaques tested proved to be λ*imm*21 *A*am$^+$ *C*am$^+$ *S*am$^+$. These genes span 95% of the λ genome, suggesting that the added *imm*21 DNA molecules were encapsulated intact.

DISCUSSION

The experiments reported here can be explained by the *in vitro* assembly of phage heads. To what extent can they be explained in other ways? For example, might the plaque-forming particles be DNA molecules adventitiously coated with protein from the concentrated extract? Probably not. The properties of these particles—their DNase resistance, bouyant density, sensitivity to neutralizing antibodies, and capacity to adsorb to certain bacteria—are those of phage particles. Assuming, then, that the reaction products are phage particles, might they be arising in the extract from surviving bacteria or spheroplasts infected with the added DNA or with DNA from a complementing extract? Probably not, for two reasons. First, bacteria and spheroplasts should have been removed by the centrifugation at 40,000 × *g* that precedes the use of the extracts. Second, the pattern of complementation differs from that observed in cells. Whereas in cells any pair of mutants in different genes complement each other (3), in extracts A^- fails to complement E^-. Whereas mixedly infected cells yield a mixture of both in-

fecting genotypes, in extracts complementation of A^- or E^- with B^-, C^-, or D^- yields only B^-, C^-, or D^- offspring. (A few A^- or E^- particles are formed, but these are accounted for by the background activity of the A^- or E^- extracts.)

If it be granted that phage heads are being assembled *in vitro*, then the pattern of complementation suggests a pathway for head assembly. As a rule, the more steps required to complete an assembly process *in vitro*, the less efficient is that process. For example, gene *F* controls the last step in λ head assembly and gene *W* controls the next to last (7). Under the same *in vitro* conditions, the conversion of W^- heads to complete phage particles is two to three orders of magnitude less efficient than conversion of F^- heads to complete phage (7). For this reason the failure of A^- or E^- extracts to donate DNA to the phage particules formed by complementation suggests that the reactions governed by the products of *A* and *E* occur before those governed by *B*, *C*, and *D*.

There is evidence that the *A* and *E* proteins interact directly with λ DNA. Brody (submitted to *Virology*) has recently described a soluble form of *E* protein that binds DNA. *E* protein eventually makes up 75% of the mass of protein in the complete head (29, 30). Gene *A* appears to specify an enzyme that cleaves polymeric head precursor DNA into cohesive-ended monomers. Extracts of induced lysogens for mutants in genes *B*, *C*, *D*, or *E* contain, but mutants in gene *A* lack, an activity that, in crude extracts, produces molecules with cohesive ends from a mixture of dimeric and monomeric, covalently-closed λ DNA circles (31). The cohesive ends have a unique specific sequence (11), and the *A* protein must recognize that sequence, presumably by binding to it. However, if *A* protein cuts the cohesive ends, then there is a paradox, because, as indicated in Table 3, *A* gene function is required to assemble phage particles from exogenous DNA that already has cohesive ends. To resolve this paradox, we would like to suggest that *A* protein binds DNA at the cohesive end sequence as one of the initial steps in head assembly, but that it does not cleave the DNA until the entire head is formed. This notion might also help to explain why cohesive-ended monomers do not accumulate in bacteria infected with the head mutants A^-, B^-, C^-, D^-, or E^- (12, 14–16), how a DNA end is correctly positioned in the head to pass through the tail, and how the sequence of the cohesive end can influence phage particle assembly (32).

TABLE 2. *Antigenic and adsorption specificity of plaque-formers assembled in vitro*

	Fraction not neutralized by antiserum against λ	Adsorption rate × 10^{-10} (bacteria per ml)$^{-1}$ min^{-1}	
		to K12	to K12/T1
φ80 PFU	0.03	0.12	0.60
λ phage	0.01	0.16	1.0
φ80 phage	0.75	0.28	0.06
φ80 PFU after propagation	0.77	0.36	0.04

30 μl of φ80 DNA, $A_{260} = 5.2$, were mixed with 100 μl of extract of *Su*$^-$ (λ *cI*ts857 *S*am7) and processed as described in *Methods*. After treatment with DNase, the mixture contained 1.6×10^3 φ80 PFU assayed on *Su*3$^+$ (λ) and 3.7×10^8 λ assayed on *Su*3$^+$ bacteria. To one aliquot of this mixture, antiserum from rabbit against λ was added at a final dilution of 1/200. After 20 min at 25°, the mixture was assayed for the number of surviving λ and φ80. Control φ80 phage was treated separately. φ80 PFU were purified and propagated through single plaque growth on *Su*3$^+$ bacteria. To a second aliquot of the mixture, K12*Su*3$^+$ bacteria were added, and to a third, K12*Su*3$^+$/T1 bacteria. After these mixtures were incubated for 15 min at 35°, the bacteria were sedimented to a pellet (at 5°), and the unadsorbed phage remaining in the supernatant fluid were assayed. From the fraction of unadsorbed phage, the (pseudo-) first order rate of adsorption was calculated.

TABLE 3. *Complementation between extracts of induced lysogens for λ head mutants*

Extracts mixed	Plaques	Genotype (%)	Number tested	*imm*434 plaques
$A^- + B^-$	816	100 B^-	75	500
$A^- + C^-$	816	97 C^- 3 A^-	75	1520
$A^- + D^-$	11,820	100 D^-	75	855
$A^- + E^-$	100	88 E^- 8 A^- 4 S^-	25	4
$B^- + C^-$	1,670	38 B^- 6 C^- 56 S^-	66	152
$B^- + D^-$	5,550	56 D^- 13 B^- 31 S^-	75	2100
$B^- + E^-$	1,770	50 B^- 50 S^-	50	2
$C^- + D^-$	12,950	88 D^- 12 C^-	72	3200
$C^- + E^-$	4,030	96 C^- 4 E^-	50	2200
$D^- + E^-$	8,150	100 D^-	50	724
A^- —	10	88 A^- 12 S^-	50	0
B^- —	468	100 B^-	50	24
C^- —	100	100 C^-	50	24
D^- —	46	98 D^- 2 S^-	51	0
E^- —	99	96 E^- 4 S^-	25	0

Lysogens carrying mutations in different head genes were grown, induced, and extracted. 50 μl of the extracts were mixed and then incubated for 80 min at 35°. DNase, then 100 μl T broth were added. Finally 100 μl of each mixture (about half the total volume) was plated on the *Su*3$^+$ bacterial strain, Ymel. The number of plaques observed is given in the second column. The particular mutant alleles used were *A*am11, *B*am427, *C*am42, *D*am15, and *E*am4. Plaques were picked; the phage were purified on *Su*3$^+$ bacteria and tested for genotype by plating on a series of *Su*$^-$ (λdg *imm*434) strains (22). S^- phage are able to form plaques on the dg lysogen that lacks the entire head region. To each of a similar set of mixtures of extracts, 0.11 μg of *imm*434 DNA was added. After incubation and DNase treatment, the entire volume of each complementation mixture was plated on *Su*2$^+$ (λ). The number of plaques observed are recorded in the last column. The mutant alleles used were *A*am32, *B*am10, *C*am42, *D*am15, and *E*am4. For purposes of comparison, the same amount of *imm*434 DNA added to an extract of a lysogen for λ *cI*857 *S*am 7 would have given 10^4 plaques.

This work was supported by a grant from the National Institute of Allergy and Infectious Diseases (AI-04509).

1. Edgar, R. S. & Wood, W. B. (1966) *Proc. Nat. Acad. Sci. USA* **55**, 498–505.
2. Casjens, S. R. (1972) *Morphogenesis of the Bacteriophage Lambda Head*, Thesis, Stanford University, Stanford, Calif.
3. Campbell, A. (1961) *Virology* **14**, 22–32.
4. Parkinson, J. S. & Davis, R. W. (1971) *J. Mol. Biol.* **56**, 425–428.
5. Weigle, J. (1968) *J. Mol. Biol.* **33**, 483–489.
6. Parkinson, J. S. (1968) *Genetics* **59**, 311–325.

7. Casjens, S., Hohn, T. & Kaiser, A. D. (1972) *J. Mol. Biol.* **64,** 551–563.
8. Kellenberger, E. & Edgar, R. S. (1971) in *The Bacteriophage Lambda*, ed. Hershey, A. D. (Cold Spring Harbor Laboratory, Cold Spring Harbor, N.Y.), pp. 271–295.
9. Georgopoulos, C. P., Hendrix, R. W., Casjens, S. R. & Kaiser, A. D. (1973) *J. Mol. Biol.*, in press.
10. Sternberg, N. (1973) *J. Mol. Biol.*, in press.
11. Wu, R. & Taylor, E. (1971) *J. Mol. Biol.* **57,** 491–511.
12. Skalka, A., Poonian, M. & Bartl, P. (1972) *J. Mol. Biol.* **64,** 541–550.
13. Wake, R. G., Kaiser, A. D. & Inman, R. B. (1972) *J. Mol. Biol.* **64,** 519–540.
14. Dove, W. F. (1966) *J. Mol. Biol.* **19,** 187–201.
15. Mackinlay, A. G. & Kaiser, A. D. (1969) *J. Mol. Biol.* **39,** 679–683.
16. Yarmolinsky, M. B. (1971) in *The Bacteriophage Lambda*, ed. Hershey, A. D. (Cold Spring Harbor Laboratory, Cold Spring Harbor, N.Y.), pp. 97–111.
17. Lederberg, E. M. (1960) *Symp. Soc. Gen. Microbiol.* **10,** 115–131.
18. Wickner, W., Brutlag, D., Schekman, R. & Kornberg, A. (1972) *Proc. Nat. Acad. Sci. USA* **69,** 965–969.
19. Wu, R. & Kaiser, A. D. (1967) *Proc. Nat. Acad. Sci. USA* **57,** 170–177.
20. Liedke-Kulké, M. & Kaiser, A. D. (1967) *Virology* **32,** 465–474.
21. Goldberg, A. R. & Howe, M. (1969) *Virology* **38,** 200–202.
22. Campbell, A. (1963) *Genetics* **48,** 409–421.
23. Kaiser, D., Tabor, H. & Tabor, C. W. (1963) *J. Mol. Biol.* **6,** 141–147.
24. Schekman, R., Wickner, W., Westergaard, O., Brutlag, D., Geider, K., Bertsch, L. L. & Kornberg, A. (1972) *Proc. Nat. Acad. Sci. USA* **69,** 2691–2695.
25. Mackal, R. P., Werninghaus, B. & Evans, E. A. (1964) *Proc. Nat. Acad. Sci. USA* **51,** 1172–1178.
26. Zgaga, V. (1967) *Virology* **31,** 559–562.
27. Davidson, N. & Szybalski, W. (1971) in *The Bacteriophage Lambda*, ed. Hershey, A. D. (Cold Spring Harbor Laboratory, Cold Spring Harbor, N.Y.), pp. 45–82.
28. Hershey, A. D. & Dove, W. (1971) in *The Bacteriophage Lambda*, ed. Hershey, A. D. (Cold Spring Harbor Laboratory, Cold Spring Harbor, N.Y.), pp. 3–11.
29. Casjens, S., Hohn, T. & Kaiser, A. D. (1970) *Virology* **42,** 496–507.
30. Buchwald, M., Murialdo, H. & Siminovitch, L. (1970) *Virology* **42,** 390–400.
31. Wang, J. C. & Kaiser, A. D. (1973) *Nature*, in press.
32. Little, J. W. & Gottesman, M. (1971) in *The Bacteriophage Lambda*, ed. Hershey, A. D. (Cold Spring Harbor Laboratory, Cold Spring Harbor, N.Y.), pp. 371–394.

Proc. Nat. Acad. Sci. USA
Vol. 70, No. 1, pp. 265–269, January 1973

Squalene and Sterol Carrier Protein: Structural Properties, Lipid-Binding, and Function in Cholesterol Biosynthesis

(liver/microsomal enzymes/phospholipids/fatty acids)

MARY C. RITTER AND MARY E. DEMPSEY*

Department of Biochemistry, University of Minnesota, Minneapolis, Minn. 55455

Communicated by William D. McElroy, October 31, 1972

ABSTRACT **Squalene and sterol carrier protein of liver plays a general role as a vehicle for cholesterol and its water-insoluble precursors; the carrier protein is essential for enzymic cholesterol synthesis. Liver microsomal enzymes contain a small amount of endogenous carrier protein, which is readily removed by washing or purification of the enzyme. Enzymic conversion to products of a cholesterol precursor·carrier protein complex is markedly faster than that for initially unbound sterol. The protomer form of the carrier protein has a molecular weight of 16,000; during sodium dodecyl sulfate gel electrophoresis one band is observed. Phospholipid facilitates the aggregation of the protomer to the oligomer form (>150,000 daltons; purified 720-fold) accompanied by the binding of cholesterol precursors to the oligomer. The carrier protein binds fatty acids as well as cholesterol precursors, suggesting that it may more generally be a *lipid carrier protein* with "squalene and sterol carrier protein" describing the functional aspects of the lipid carrier in cholesterol biosynthesis. Studies with several steroids and related compounds revealed that the binding sites of lipid carrier protein must contain highly specific hydrophobic and polar regions.**

Earlier we reported that squalene and sterol carrier protein (SCP), a heat-stable protein found in the soluble fraction of liver homogenates, is essential for optimum conversion of water-insoluble precursors to cholesterol by microsomal enzymes (1–8). Aspects of these findings were confirmed by other laboratories, (e.g., refs. 9 and 10). In the two previous articles of this series (5, 6), we also presented evidence that: (*i*) SCP specifically binds squalene and sterol intermediates, (*ii*) a noncovalent squalene or sterol·SCP complex (oligomer, >150,000 daltons) appears to form part of the active site of each microsomal enzyme in cholesterol biosynthesis, and (*iii*) an SCP-like molecule is a component of the high-density lipoprotein fraction of serum. More recently we demonstrated the occurrence of an SCP-like molecule in adrenal preparations catalyzing the initial steps of cholesterol metabolism to steroid hormones (11). Accordingly, we proposed that SCP functions uniquely as a vehicle for water-insoluble precursors during cholesterol biosynthesis and that SCP or a structurally similar protein participates in the transport and metabolism of cholesterol (5, 11).

In this communication we describe the absolute requirement for SCP by microsomal enzymes, effects on conversion rates of the interaction of a sterol·SCP complex with microsomal enzymes, properties of the protomer (16,000 daltons) of SCP, optimum conditions for purification of SCP by aggregation of its protomer in the presence of lipid, binding of biologically important lipids other than sterols to SCP, and structural features of the lipid-binding site(s) of SCP. Our evidence suggests SCP should more generally be named a *lipid carrier protein* with "squalene and sterol carrier protein" describing the functional aspects of lipid carrier protein in sterol biosynthesis, metabolism, and transport.

Addreviations: SCP, squalene and sterolcarrier protein; SDS, sodium dodecyl sulfate.

* To whom requests for reprints should be addressed.

This paper is no. III of a series. The previous papers are refs. 5 and 6.

METHODS AND MATERIALS

Unpurified SCP (i.e., the soluble or upper half of the 105,000 × *g* supernatant fractions, previously designated Fraction A), Fraction C (microsomes washed once), and Fraction D (Fraction C, purified by solubilization, salt fractionation, and gel filtration) were prepared from rat-liver homogenates as detailed elsewhere (4). Complexes of sterols and other lipids with the oligomer of SCP were made under the conditions of Fig. 1A of ref. 6 and Table 5 of this report. The protomer of SCP was isolated from unpurified SCP by heat treatment (100°, 5 min) in the presence of 5% (w/v) $(NH_4)_2SO_4$ and gel filtration (4–8). SCP of highest purity was obtained by aggregation of protomer-SCP in the presence of sterol and phospholipid, followed by isolation of the oligomer (lipid·SCP complex) with a column of Sephadex G-75 (see conditions of Table 3). Formation of cholesta-5,7-dienol from cholest-7-enol by Δ^7-sterol-Δ^5-dehydrogenase (EC 1.3.3.x) was assayed by ultraviolet spectral analysis or the epiperoxide derivative procedure; the amount of cholesterol synthesized from cholesterol precursors was determined by passage of sterols through the dibromide derivative (4). For some experiments (e.g., Table 2) isotopically labeled sterols were separated on silicic acid–Super Cel columns with benzene as eluting agent (12). Organic and phospholipid phosphorus was measured by the method of Bartlett (13). Gel electrophoresis of SCP preparations was done in 0.1% sodium dodecyl sulfate (SDS) on 10% acrylamide as described by Weber and Osborn (14). Sterol substrates were dissolved in propylene glycol, steroyl esters in dioxane, and fatty acids (sodium salts) in water. Lecithin was microdispersed in 30 mM Tris·HCl buffer (pH 8.5) by sonication (15).

Labeled sterols ([2,4-^{3}H]cholest-7-enol, [4-^{14}C]cholesta-5,7-dienol, and [4-^{14}C]cholesteryl-acetate) were synthesized and characterized as described (1–4, 7). [4-^{14}C]Cholesterol was purchased from Schwarz-Mann Research Laboratories, NAD from Calbiochem, lecithin (egg yolk) from Cyclo Chemi-

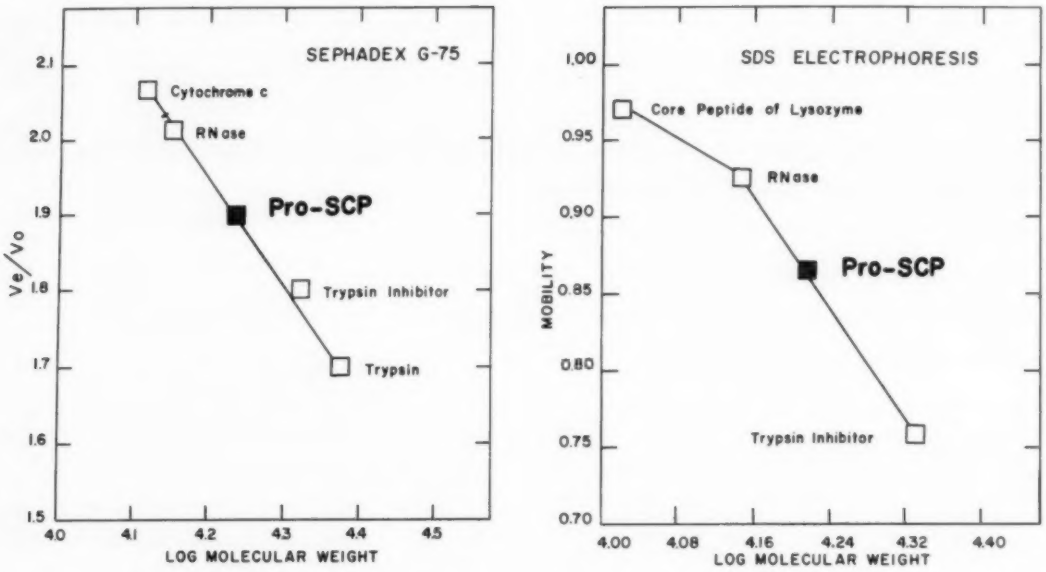

FIG. 1. Migration during gel filtration (*left*) and SDS gel electrophoresis (*right*) of protomer-SCP relative to proteins of known molecular weight. Average electrophoretic mobilities and standard errors were protomer-SCP, 0.86 ± 0.04 (10 determinations); trypsin inhibitor, 0.76 ± 0.04 (4 determinations); ribonuclease, 0.93 ± 0.02 (4 determinations); core peptide of lysozyme [reduced cyanogen bromide cleavage product, residues 13–105 (16)], 0.97 ± 0.01 (3 determinations). The molecular weight of protomer-SCP determined by both techniques was 16,000.

TABLE 1. *Removal of endogenous SCP from microsomal enzyme preparations*

Exp.	Enzyme preparation	Washes*	Δ⁵-Dehydrogenase activity, μM/mg protein: SCP + enzyme	Δ⁵-Dehydrogenase activity, μM/mg protein: Enzyme	Activation by SCP of microsomal Δ⁵-dehydrogenase (-fold)
1†	Microsomes	1	8.0	2.0	4.0
	Purified microsomes	1	13.8	0.9	15.3
2‡	Microsomes	1	8.0	2.0	4.0
		2	7.5	1.4	5.4
		3	7.2	0.8	9.0
	Purified microsomes	3	17.6	0.0	∞

* Preparations were washed with 0.1 M phosphate (pH 7.4) by centrifugation at 105,000 × *g* for 60 min.

† Unpurified SCP (16.3 mg of protein, 21.7 mg/ml), when present, was incubated in 0.1 M phosphate (pH 7.4) with 62 μM cholest-7-enol, 120 nM AY-9944, 1 mM NAD, and 2.2 mg (8.9 mg/ml) of microsomal protein washed once (Fraction C) or 0.9 mg (3.6 mg/ml) of purified microsomal protein (Fraction D) (total incubation volume, 1.2 ml) for 30 min at 37° under oxygen (4).

‡ Unpurified SCP, when present, was incubated with 2.3 mg (9.2 mg/ml) of microsomal protein washed once, or 2.2 mg (8.8 mg/ml) of the protein washed twice, or 2.9 mg (11.6 mg/ml) of the protein washed three times, or 0.7 mg (2.8 mg/ml) of purified microsomal protein prepared from microsomes washed three times; other conditions were as given for Exp. 1.

cal, and crystalline proteins of known molecular weight from Sigma Chemical Co. All other chemicals were reagent or anayltical grade.

RESULTS AND DISCUSSION

Absolute Requirement for SCP by Microsomal Enzymes. In previous reports we showed that conversion of water-insoluble precursors to cholesterol by microsomal enzymes is stimulated at least 4-fold by SCP, i.e., a small amount of enzymic activity is usually detected in the absence of SCP (1–8) (see also Table 2). It was important to establish whether or not the activity in the absence of SCP was due to incomplete removal of residual SCP during preparation of the enzymes. The results of Table 1 (obtained with a preparation of Δ⁷-sterol Δ⁵-dehydrogenase) demonstrate that endogenous SCP was gradually removed by repeated washing or by purification of the microsomal enzyme (Exp. 1 and 2), resulting in increased activation by added SCP. Complete removal of residual SCP and infinite activation of Δ⁵-dehydrogenase by added SCP required repeated washings of the enzyme followed by purification (Exp. 2, Table 1). In some enzyme preparations, residual SCP was not detectable (see dihydrolanosterol, Table 2) or was totally removed by the purification procedure, and extra washings were not required (see Table 4). These findings (Table 1) are typical of those obtained with other microsomal enzymes of cholesterol biosynthesis; they demonstrate the absolute requirement for SCP by these enzymes. Furthermore, similar experiments with purified SCP showed that effects described in Table 1 are specific for SCP and not caused by other components in unpurified SCP.

Effects of Interaction of Sterol·SCP Complex with Microsomal Enzymes. We demonstrated previously that all water-insoluble

TABLE 2. *Increased conversion rate to products of a cholesterol precursor·SCP complex over that of initially unbound cholesterol precursor and SCP*

Cholesterol precursor[a]	Total sterol synthesized (μM) during 30-min incubation
[*24,25*-^{3}H]Dihydrolanosterol (C-30)	
Dihydro·SCP	0.8[b]
Dihydro + SCP	0.1[c]
Dihydro; no SCP	0.0
[3α-^{3}H]Cholesta-7,24-dienol (C-27)	
$\Delta^{7,24}$·SCP	1.6[d]
$\Delta^{7,24}$ + SCP	0.7[e]
$\Delta^{7,24}$; no SCP	0.2[e]
[*2,4*-^{3}H]Cholest-7-enol (C-27)	
Δ^{7}·SCP	0.9[f]
Δ^{7} + SCP	0.4[f]
Δ^{7}; no SCP	0.1[f]
[*4*-^{14}C]Cholesta-5,7-dienol (C-27)	
$\Delta^{5,7}$·SCP	1.4[g]
$\Delta^{5,7}$ + SCP	0.5[g]
$\Delta^{5,7}$; no SCP	0.2[g]

[a] Cholesterol precursors were bound to SCP (oligomer form) as given with Table 3 and in ref 6. Incubations (total volume, 1.9 ml) contained 8.4 mg of SCP protein (6.0 mg/ml, when present), 3.4 mg of microsomal protein (8.5 mg/ml) (Fraction C), and initially unbound or bound precursor: 1 μM [*24,25*-^{3}H]-dihydrolanosterol; or 2.2 μM [3α-^{3}H]cholesta-7,24-dienol; or 1 μM [*2,4*-^{3}H]cholest-7-enol and 120 nM AY-9944; or 1.0 μM [*4*-^{14}C]cholesta-5,7-dienol. All incubations were done for 30 min. Other conditions were as described (4); see also Table 1 and *Methods*.

[b] Hydroxylated C-29 and C-28 compounds and cholest-7-enol.

[c] Hydroxylated C-29 and C-28 compounds.

[d] Cholesta-5,7,24-trienol, cholest-7-enol, and cholesterol.

[e] Cholesta-5,7,24-trienol and cholest-7 enol.

[f] Cholesta-5,7-dienol.

[g] Cholesterol.

precursors of cholesterol are capable of complexing with SCP (5–8). The data of Table 2 (obtained with four representative cholesterol precursors) further show that conversion to products by microsomal enzymes of a sterol present in a sterol·SCP complex (oligomer form of SCP) is markedly faster than conversion of initially unbound sterol. Results

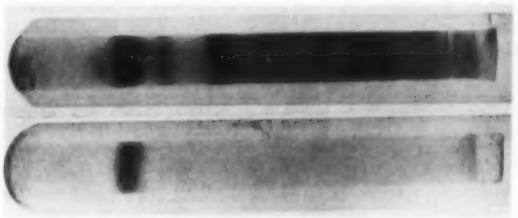

FIG. 2. SDS gel electrophoretic patterns of unpurified SCP (*top*) and protomer-SCP (*bottom*).

of similar studies with various other cholesterol precursors established that in all cases the conversion of a precursor·SCP complex to cholesterol or other sterols is increased 2-fold or more over that of initially unbound precursor. In this regard, the absolute dependency on SCP for detectable enzymic activity was just described (e.g., Table 1). The probable explanation for the increased conversion rate to products of a precursor·SCP complex is given by data obtained with a cholest-7-enol·SCP complex. The apparent K_m for the enzymic conversion of cholest-7-enol·SCP to cholesta-5,7-dienol·SCP was 10 μM at a ratio of SCP protein to enzyme protein of 10.2/1 (the optimum ratio for this reaction); at a suboptimal protein ratio (5.1/1), the apparent K_m for substrate was 30 μM. At both ratios of SCP to enzyme protein, the maximum rate of the reaction was not markedly changed. These results indicate that the microsomal enzymes have a high affinity for a preformed sterol·SCP complex (the oligomer) that participates at the active site of each enzyme.

Properties of the Protomer of SCP. Heat treatment at high ionic strength causes dissociation of the oligomer of SCP to a low molecular weight protein (protomer-SCP) and loss of associated sterol (5–8). As indicated in Fig. 1, the apparent molecular weight of protomer-SCP determined by gel filtration and SDS gel electrophoresis is 16,000. Protomer-SCP migrates as a single band during SDS gel electrophoresis; a protein with the same mobility as protomer-SCP is present in unpurified SCP (Fig. 2). During preparation of protomer-SCP, we observe small amounts of aggregates (30,000–60,000 daltons) of protomer-SCP (see Fig. 1B of ref. 6). These aggregates do not contain bound sterols and are most probably the SCP preparations obtained in the absence of heat treatment at high ionic strength by Scallen *et al.* (17).

Spectral analysis of protomer-SCP revealed no measurable absorbance in the visible region (350–500 nm); in the

TABLE 3. *Influence of phospholipid on formation of aggregated SCP and binding of cholest-7-enol*

Addition of phospholipid	Formation of aggregated SCP*		Cholest-7-enol bound to aggregated SCP		Organic phosphorus bound to aggregated SCP	
	μg	% of protomer-SCP†	nmol	% of initial†	μmol	% of initial†
−	1335	2.9	18	17.3	0.8	5.3
+	5250	11.7	81	77.9	2.3	13.7

* Aggregated SCP (oligomer form) was obtained by incubation in 0.3 M Tris·HCl buffer, pH 7.4, of 45 mg of protomer-SCP (containing 15 μmol of organic phosphorus) with 104 nmol of [*2,4*-^{3}H]cholest-7-enol and, when present, 46 μmol of lecithin (equivalent to 1.8 μmol of organic phosphorus) for 30 min at 37° under nitrogen, followed by separation of the protomer and oligomer on Sephadex G-75 (6) with the Tris·HCl buffer as eluant.

† Expressed as the percentage of total initial protomer-SCP protein, cholest-7-enol, or organic phosphorus applied to the gel column that emerged with the oligomer of SCP and lipid.

TABLE 4. *Purification of aggregated SCP*

SCP preparation	Total SCP protein (mg)	Total activity†	Specific activity‡ (μM/mg)	Purification (-fold)	Yield (%)
Unpurified SCP	2100	21	0.01	1	100
Aggregated SCP*	1.8	13	7.2	720	62

* The oligomer, sterol·SCP complex, was formed from protomer-SCP in the presence of lecithin and [2,4-^{3}H]cholest-7-enol (see conditions of Table 3).

† SCP activation ability was measured by incubation (total volume, 1.04 ml) of 5.5 μM [2,4-^{3}H]cholest-7-enol, either initially unbound to 14 mg of unpurified SCP or bound to 200 μg of aggregated SCP protein, and 1.3 mg of purified microsomal Δ^5-dehydrogenase protein (Fraction D). Other conditions were as given with Table 1.

‡ Specific activity is expressed as μM [2,4-^{3}H]cholesta-5,7-dienol synthesized in 30 min per mg of unpurified or aggregated SCP protein; no formation of [2,4-^{3}H]cholesta-5,7-dienol was detected in the absence of SCP.

ultraviolet region, protomer-SCP has a characteristic A_{280}/A_{260} of 0.68. The relatively high absorbance of protomer-SCP at 260 nm may be due to nucleotide contamination, e.g., we reported previously that SCP binds pyridine nucleotide as well as sterols (6). Nucleotide contamination may also contribute to the amount of organic phosphorus (100–300 nmol/mg protein) present in protomer-SCP preparations (Table 3). A typical unpurified SCP preparation contains 1.2 μmol of organic phosphorus per mg of protein. The organic phosphorus present in protomer-SCP may also reflect some bound phospholipid.

Influence of Phospholipid on Aggregation and Purification of SCP. The functional similarities of one of the human plasma lipoprotein peptides and human liver-SCP are now well characterized (6, 18). These findings led us to investigate possible additional similarities between plasma lipoproteins and SCP, in particular the interaction of SCP with phospholipids. During these studies we made the striking observation that phospholipid facilitated aggregation of protomer-SCP and sterol binding. The presence of lecithin resulted in a 4-fold increase in oligomer formation accompanied by a similar increase in bound sterol and organic phosphorus (Table 3). It is probable that some of the organic phosphorus present in the sterol·SCP complex formed in the presence of lecithin represents bound lecithin; at present this point has not been rigorously established. The influence of phospholipid on aggregation and sterol binding of protomer-SCP was used to obtain a 720-fold purification of the sterol·SCP complex in 62% yield, based on activation of microsomal Δ^5-dehydrogenase (Table 4). The latter preparation of SCP may be of ultimate purity, i.e., the sterol·SCP complex elutes in the void volume of a Sephadex G-75 column and is thus widely separated from protomer-SCP (see Fig. 1C of ref. 6).

Binding of Biologically Important Lipids Other Than Sterols to SCP. We reported previously that cholesterol, its water-insoluble precursors, β-sitosterol, and hydroxy-derivatives of cholestane (in particular, 3β, 5α, 6β-cholestanetriol) bind to SCP; bile acids, steroid hormones, cholestane, and keto-derivatives of cholestane (not cholesterol precursors) are not bound or poorly bound to SCP (5–8). Additional studies (Table 5) were undertaken to define further structural requirements for lipid-binding to SCP. Esterification of cholesterol and another representative sterol (cholesta-5,7,22-trienol) results in markedly decreased sterol-binding to SCP (Table 5). Also, the chain length and saturation of the esterified fatty acid appear to influence the observed amount of binding. In contrast, free fatty acids longer than six carbon atoms are bound to SCP regardless of the degree of their saturation.

Structural Features of the Lipid Binding Site(s) of SCP. The binding studies just described and our earlier work demonstrate that SCP not only forms high molecular weight complexes with water-insoluble cholesterol precursors [Table 2 and (6–8)], but also with fatty acids (Table 5) and probably phospholipids (Table 3). These results suggest that a more appropriate name for SCP is lipid carrier protein with "squalene and sterol carrier protein", describing the function of lipid carrier protein in cholesterol biosynthesis, metabolism, and transport.

Regarding structural features of the lipid-binding site(s), it is apparent that SCP (lipid carrier protein) must contain: (*i*) a hydrophobic region to accommodate the sterol nucleus and its side chain or the long hydrocarbon chains of fatty acids and (*ii*) a hydrophilic region for the binding of hydroxyl groups and other polar sites (e.g., areas of unsaturation) in the lipid molecules. It is possible that SCP contains a thin cleft in its tertiary structure; the flat steroid molecule would reside within the hydrophobic interior of the cleft with the

TABLE 5. *Binding of cholesterol, cholesteroyl esters, fatty acids, and related compounds to aggregated SCP*

Compound	Binding* (%)
Cholesterol, cholesteroyl esters, and related compounds	
[4-^{14}C]Cholesterol	90
[4-^{14}C]Cholesteroyl-acetate	35
[7α-^{3}H]Cholesteroyl-palmitate	10
[4-^{14}C]Cholesteroyl-stearate	7
[1-^{14}C]Cholesteroyl-oleate	39
[4-^{14}C]Cholesta-5,7,22-trienol	90
[4-^{14}C]Cholesta-5,7,22-trienyl-acetate	62
Fatty acids	
[1-^{14}C]Caproic acid (C-6)	78
[1-^{14}C]Myristic acid (C-14)	100
[1-^{14}C]Palmitic acid (C-16)	100
[1-^{14}C]Stearic acid (C-18)	100
[1-^{14}C]Oleic acid (C-18; 1ω9)	100
[1-^{14}C]Linoleic acid (C-18; 2ω6)	100

* Binding assays were performed by heat treatment of unpurified SCP (100°, 1 min), removal of coagulated protein by centrifugation, incubation (37°, 15 min) of the supernatant fraction with the compound (25 μg), followed by $(NH_4)_2SO_4$ precipitation (40–80% saturation), and finally by gel filtration (Sephadex G-25) (6, 7). Binding is expressed as the percentage of the total radioactivity applied to the gel column that emerged with the SCP complex (oligomer form).

hydroxyl group(s) at or near the surface of the protein. A cleft is present at the functional centers of myoglobin (19), lysozyme (20), and ribonuclease (21); a cleft may also be present in the recently discovered retinol-binding protein (22). Upon specific interaction of a cholesterol precursor·SCP complex with a microsomal enzyme a conformational change would occur, followed by the catalytic step and transfer of the sterol·SCP complex to the next microsomal enzyme. This hypothesis is in accord with our findings that a sterol present in a sterol·SCP complex is more readily available to the catalytic site of a microsomal enzyme (Table 2) and that inhibitors of specific steps in cholesterol biosynthesis block formation of the activated conformation of a sterol·SCP·enzyme complex (e.g., refs. 7 and 23).

We gratefully acknowledge the following gifts: cholesteroyl esters from Dr. R. St. Clair, Bowman-Gray School of Medicine; cholesta-5,7,22-trienol and cholesta-5,7,22-trienyl-acetate from Dr. R. Conner, Bryn Mawr College; fatty acids from Dr. R. Johnson, University of Minnesota and Dr. R. Holman, Hormel Institute; dihydrolanosterol from Dr. E. Grossi Paoletti, University of Milan; and cholesta-7,24-dienol from Dr. I. D. Frantz, Jr., University of Minnesota; core peptide (residues 13–105) of lysozyme from Dr. D. Wetlaufer, University of Minnesota. The work was supported by USPHS Grants HE-8634 and HE-6314 and predoctoral Fellowship (GM42265) to M. C. Ritter.

1. Dempsey, M. E., Seaton, J. D., Schroepfer, G. J., Jr. & Trockman, R. W. (1964) *J. Biol. Chem.* **239,** 1381.
2. Dempsey, M. E. (1965) *J. Biol. Chem.* **240,** 4176.
3. Dempsey, M. E. (1968) *Ann. N.Y. Acad. Sci.* **148,** 631.
4. Dempsey, M. E. (1969) in *Methods in Enzymology*, ed. Clayton, R. B. (Academic Press, New York), Vol. XV, pp. 505.
5. Ritter, M. C. & Dempsey, M. E. (1970) *Biochem. Biophys. Res. Commun.* **38,** 921.
6. Ritter, M. C. & Dempsey, M. E. (1971) *J. Biol. Chem.* **246,** 1536.
7. Ritter, M. C. (1971) *Ph.D. Thesis*, University of Minnesota.
8. Dempsey, M. E. (1971) in *The Chemistry of Brain Development*, eds. Paoletti, R. & Davison, A. N. (Plenum Press, New York), pp. 31.
9. Scallen, T. J., Schuster, M. E. & Dhar, A. K. (1971) *J. Biol. Chem.* **246,** 224.
10. Rilling, H. C. (1972) *Biochem. Biophys. Res. Commun.* **46,** 470.
11. Kan, K. W., Ritter, M. C., Ungar, F. & Dempsey, M. E. (1972) *Biochem. Biophys. Res. Commun.* **48,** 423.
12. Frantz, I. D., Jr. (1963) *J. Lipid Res.* **4,** 176.
13. Bartlett, G. R. (1959) *J. Biol. Chem.* **234,** 466.
14. Weber, K. & Osborn, M. (1969) *J. Biol. Chem.* **244,** 4406.
15. Fleischer, S. & Fleisher, B. (1967) in *Methods in Enzymology*, eds. Estabrook, R. W. & Pullman, M. E. (Academic Press, New York), Vol. X, pp. 406.
16. Bonavida, B., Miller, A. & Sercarz, E. E. (1969) *Biochemistry* **8,** 968.
17. Scallen, T. J., Srikantaiah, M. V., Skrdlant, H. B. & Hansbury, E. (1972) *Fed. Proc.* **31,** 429.
18. Dempsey, M. E., Ritter, M. C. & Lux, S. E. (1972) *Fed. Proc.* **31,** 430.
19. Kendrew, J. C. (1963) *Science* **139,** 1259.
20. Blake, C. C. F., Johnson, L. N., Mair, G. A., North, C. T., Phillips, D. C. & Sarma, V. R. (1967) *Proc. Roy. Soc. Ser. B.* **167,** 378.
21. Kartha, G., Bello, J. & Harker, D. (1967) *Nature* **213,** 862.
22. Kanai, M., Raz, A. & Goodman, D. S. (1968) *J. Clin. Invest.* **47,** 2025.
23. Witiak, D. T., Parker, R. A., Brann, D. R., Dempsey, M. E., Ritter, M. C., Connor, W. E. & Brahmankar, D. M. (1971) *J. Med. Chem.* **14,** 216.

Proc. Nat. Acad. Sci. USA
Vol. 70, No. 1, pp. 270–274, January 1973

Development of Acetylcholine Receptor Clusters on Cultured Muscle Cells

(α-bungarotoxin/autoradiography/synapses)

A. J. SYTKOWSKI, Z. VOGEL, AND M. W. NIRENBERG

Laboratory of Biochemical Genetics, National Heart and Lung Institute, National Institutes of Health, Bethesda, Maryland 20014

Contributed by M. W. Nirenberg, November 14, 1972

ABSTRACT **Clusters of acetylcholine receptors were formed in the absence of neurons during the development of cultured chick-embryo skeletal muscle cells. The average concentration of receptors in clusters was estimated to be 9000 per μm^2. At other regions of the cell, receptor concentration was 900 per μm^2. The possibility that receptor clusters may participate in synapse formation is suggested.**

[^{125}I]α-Bungarotoxin and related toxins bind to acetylcholine receptors of skeletal muscle grown *in vitro* (1–3). Since the toxins interact with receptors with specificity and relatively high affinity, they have been used to assay both receptor concentration and synapses (1–11). Dividing myoblasts have few, if any, acetylcholine receptors (12). The cells fuse, thereby forming nondividing, multinucleated myotubes with acetylcholine receptors distributed over the entire muscle cell. Upon innervation, active acetylcholine receptors disappear from all parts of the muscle except that portion participating in the synapse (13, 14). Denervation results in the appearance of active acetylcholine receptors over the entire surface of the muscle, starting from the synapse and proceeding towards the cell extremities (15, 16); hence, restriction of receptor location is a reversible process. Similarly, Kuffler, Dennis, and Harris (17) have shown that frog parasympathetic ganglion neurons are highly sensitive to acetylcholine only at the synapse on the cell body, whereas after the incoming axons are cut, the entire surface of the neuron becomes sensitive to acetylcholine.

Acetylcholine receptors may be distributed nonuniformly on cells that have not formed synapses. For example, acetylcholine receptors are restricted to various sites on some mouse neuroblastoma cells (18). Cohen and Fischbach (19) have shown by electrophysiologic methods that muscle cells cultured in the absence of neurons have small areas that are 3- to 6-fold more sensitive to acetylcholine than adjacent areas. Similarly, we have reported that cultured muscle cells have discrete clusters of acetylcholine receptors that bind labeled α-bungarotoxin (3).

In this report, the development and distribution of acetylcholine receptor clusters on muscle cells cultured in the absence of neurons is described, and the formation of receptor clusters is proposed as a normal step in synapse formation.

METHODS AND MATERIALS

Chick-Embryo Muscle Cultures. Cells dissociated from the legs of chick embryos that were 10 days of age were grown *in vitro* by a modification (3) of the method of Konigsberg (20). 50×10^3 Cells were added into each collagen-coated 50-mm petri dish (Falcon Plastics) containing 2.5 ml of growth medium [85% F-14 medium (3); 10% fetal-calf serum (Colorado Serum); 5% chick-embryo extract (Microbiological Ass.)]; 33% of the medium was conditioned, as described by White and Hauschka (21). Cultures were incubated at 37° in a humidified atmosphere of 90% air–10% CO_2; the medium was changed every 3–4 days.

[^{125}I]α-Bungarotoxin Binding Assay. [^{125}I]Diiodo-α-bungarotoxin was prepared (2.7×10^5 Ci/mol) by use of a $^{127}I/^{125}I$ ratio of 11.5/1 in the reaction mixture. The diiodotoxin was separated from the monoiodotoxin as described (3). On the assumption that the isotope ratio of the iodinated toxin was the same as that of the reaction mixture, about 2% of the diiodo-α-bungarotoxin molecules were labeled with two ^{125}I atoms; 12% with one ^{125}I and one ^{127}I; and 86% with two ^{127}I atoms.

Before incubation of cells with labeled α-bungarotoxin, the medium was removed from each petri dish and replaced with 1.5 ml of solution A [the Dulbecco-Vogt modification of Eagle's medium (22) (GIBCO) containing 20 mM HEPES buffer (*N*-2-hydroxyethylpiperazine-*N'*-2-ethane-sulfonic acid), pH 7.4, in place of $NaHCO_3$, and 2 mg of crystalline bovine-serum albumin (Armour Pharm. Co.) per ml of medium]. Cultures were incubated at 37° for 20 min in air, then [^{125}I]diiodo-α-bungarotoxin was added (3.3 mM final concentration) and cultures were incubated for an additional 60 min. The medium was removed and each culture was washed three times with 3-ml portions of solution A and three times with 3-ml portions of solution A without albumin. Cells with bound toxin were removed and radioactivity was determined (3).

Autoradiography. Cells incubated and washed as described above were fixed for 1 hr in a solution containing 2.5% glutaraldehyde and 0.1 M sodium phosphate buffer, pH 7.4 (2 ml per culture) at 24°; then each culture was washed six times with 2 ml of 0.1 M sodium phosphate buffer, pH 7.4 (10 min per wash) and dehydrated by adding in succession 3 ml of 35, 50, 75, 95, and 100% ethanol (5 min per step). Dishes were dried in air, coated with Kodak NTB-2 emulsion diluted 1:1 with H_2O, and incubated at 4° for 4 days in a light-proof box containing a desiccant. Autoradiographs were developed for 4 min with Kodak D-19 developer at 26° and fixed with Kodak Fixer.

RESULTS

The rate of appearance of acetylcholine receptors on cultured chick-embryo muscle cells is shown in Fig. 1. Cells divided rapidly during the early stages of culture. Myoblast fusion was first observed on the third day of incubation, resulting

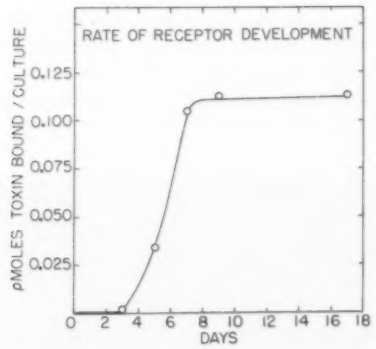

FIG. 1. Binding of [^{125}I]diiodo-α-bungarotoxin to chick-embryo skeletal muscle grown *in vitro* for different periods. Cells were incubated with 3.3 nM [^{125}I]diiodo-α-bungarotoxin, as described in *Methods*. Each point represents the average value found with duplicate 50-mm petri dishes (each dish, 20-cm^2 surface area). Sister cultures were subjected to autoradiography (shown in the following figures).

in the formation of nondividing, multinucleated myotubes and, concomitantly, a marked increase in acetylcholine receptors was observed. The maximum number of receptors per culture was achieved by the eighth day of incubation, and the number of receptors per culture remained constant thereafter.

During the course of this experiment, replicate cultures were subjected to autoradiography. A phase-contrast view of cells cultured for 3 days is shown in Fig. 2, panel *A*, and the corresponding autoradiograph is shown in panel *B*. Multinucleated myotubes formed by cell fusion were labeled with α-bungarotoxin, whereas mononucleated cells, such as myoblasts and fibroblasts, were not labeled (panels *C* and *D*). An occasional mononucleated cell bound α-bungarotoxin, but such cells usually were not heavily labeled (panels *E* and *F*). In Fig. 3, panels *A* and *B*, are shown phase-contrast and bright-field views of muscle cells cultured for 5 days and subjected to autoradiography. Many myotubes were present, and all were labeled with α-bungarotoxin. Acetylcholine receptors were distributed rather uniformly over the entire surface of each myotube; however, some myotubes contained more receptors than others. No unlabeled myotubes were found in this or other experiments.

After 7 days of incubation, discrete clusters of acetylcholine receptors were present on about 1% of the myotubes (Fig. 4, panels *A*, *B*, and *C*). In Fig. 5 autoradiographs are shown of cells cultured for 9 days (panel *A*) and 11 days (panels *B* and *C*). Cells cultured for 9 days had more receptor clusters than younger cultures, and by the 11th day in culture, more than 80% of the myotubes had receptor clusters. Some myotubes had as many as 20 clusters. The size of receptor clusters varied considerably; the average cluster was 125 μm^2. They were found predominantly along cell margins and were frequently ovoid in shape, the long axis of the cluster being parallel to the long axis of the cell, and boundaries were defined rather sharply. Regions of cells that were richest in receptors had larger and more frequent clusters; however, they were also found on myotubes that were labeled relatively lightly with α-bungarotoxin (see bottom of panel *B*). Occasionally, receptor clusters were found on structures that resembled partially retracted processes. The clusters

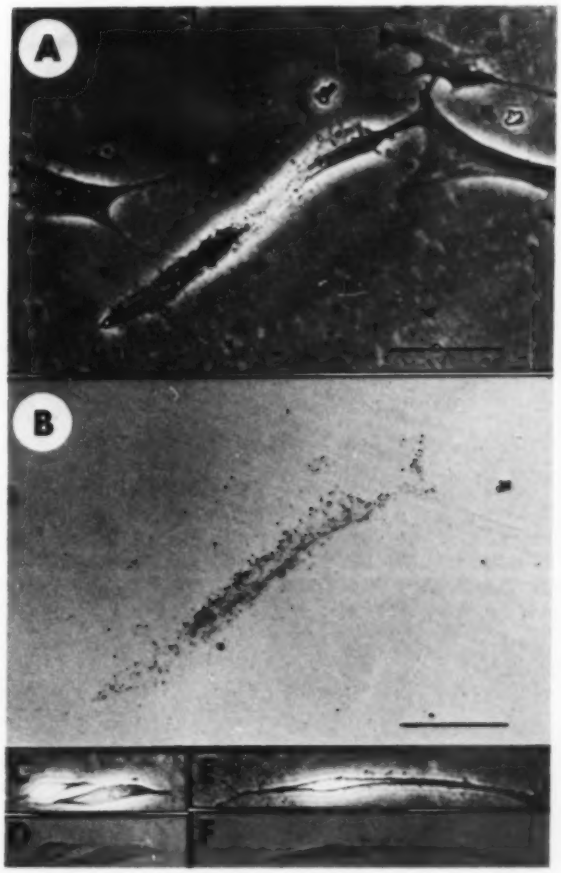

FIG. 2. Autoradiographs of chick-embryo muscle cells cultured for 3 days and then labeled with [^{125}I]diiodo-α-bungarotoxin (see Fig. 1). Panels *A*, *C*, and *E* are phase-contrast views to show cell detail; panels *B*, *D*, and *F* are the corresponding autoradiographs viewed with bright-field optics to show silver grains. The *bar* represents 50 μm and the scale applies to all panels.

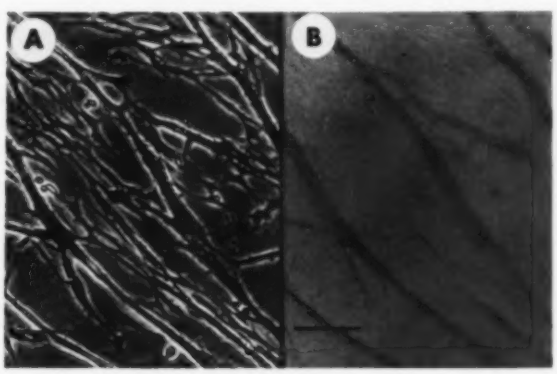

FIG. 3. Autoradiographs of muscle cells cultured for 5 days and then labeled with [^{125}I]diiodo-α-bungarotoxin (see Fig. 1). Panel *A* is a phase-contrast view and panel *B* the corresponding autoradiograph. The *bar* in each panel represents 100 μm.

were not consistently associated with a cell organelle when viewed with phase-contrast optics. Similar results were obtained in preliminary electron microscopic studies.

The clusters, as well as diffuse labeling of myotubes, were also found when cells were incubated in F-14 growth medium or with [^{125}I]monoiodo- instead of [^{125}I]diiodo-α-bungarotoxin (3). Similar results were obtained when other methods of fixation were used, such as (*a*) 100% methanol; (*b*) 2.5%

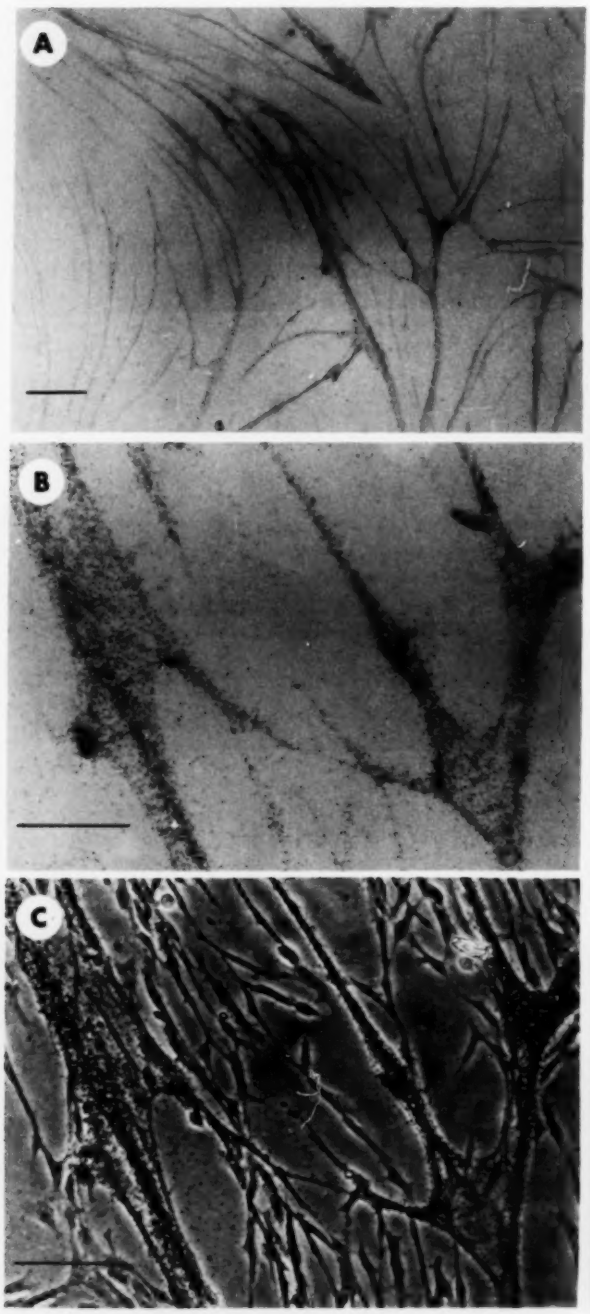

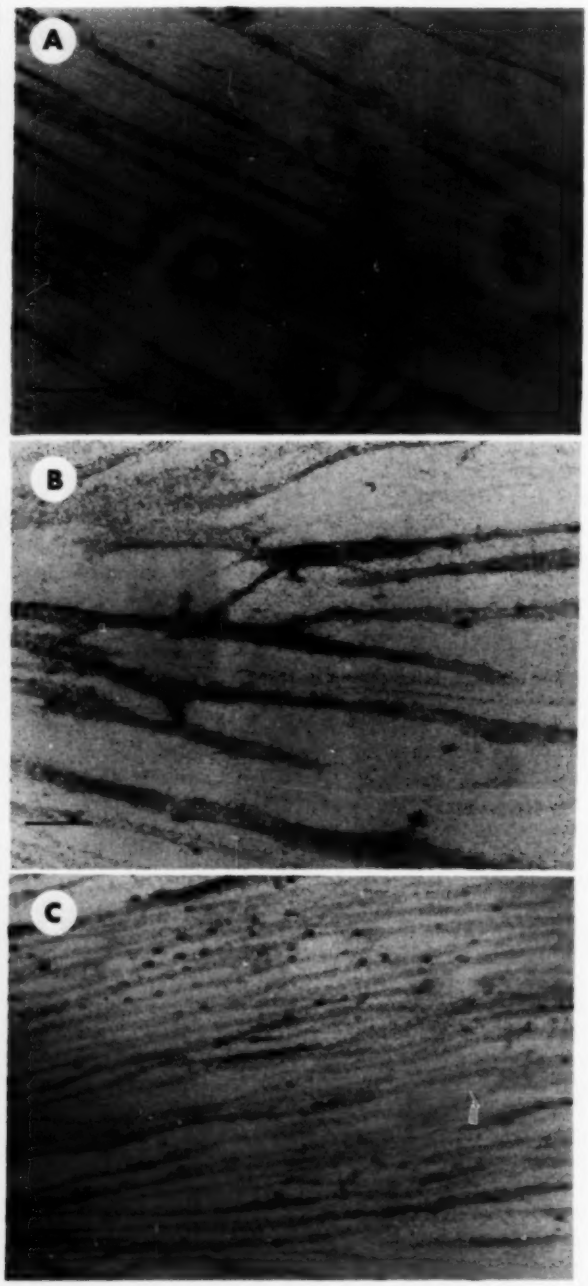

FIG. 4 (*left*). Autoradiographs of muscle cells cultured for 7 days and labeled with [^{125}I]diiodo-α-bungarotoxin (see Fig. 1). In panels *A* and *B*, photomicrographs obtained with bright-field optics are shown at low and high magnification, respectively. The *bars* in panels *A* and *B* represent 200 and 100 μm, respectively. In panel *C*, a phase-contrast view of the field corresponding to panel *B* is shown; the *bar* represents 100 μm.

FIG. 5 (*right*). Autoradiographs of muscle cells labeled with [^{125}I]diiodo-α-bungarotoxin (see Fig. 1). Panel *A* is a bright-field view of cells cultured for 9 days. Panels *B* and *C* are bright-field views of cells cultured for 11 days. The *bar* in each panel represents 100 μm.

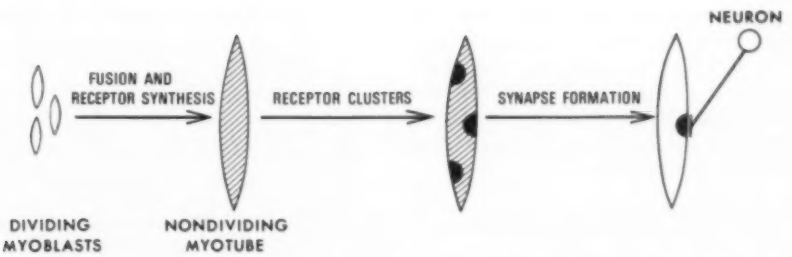

FIG. 6. Formation of acetylcholine receptor clusters, a possible step in synapse formation. Dividing myoblasts fuse and form nondividing multinucleated myotubes with acetylcholine receptors uniformly distributed over the surface of the cell (step 1). Synapse-like clusters of acetylcholine receptors then form in the absence of neurons (step 2). Acetylcholine receptors or molecules associated with them may interact with appropriate molecules on the innervating neuron, and thus may specify synapse formation. Synapse formation is accompanied by the disappearance of active acetylcholine receptors from the noninnervated portion of the muscle cell surface, thereby converting the muscle cell from a permissive to a nonpermissive state with respect to establishing functional synapses with other neurons.

glutaraldehyde–0.1 M sodium cacodylate (pH 7.4)–2 mM $CaCl_2$; or (*c*) 10% formaldehyde in Dulbecco's phosphate-buffered saline (pH 7.4) (23). Cells fixed for 45 min in a solution containing 10% formaldehyde in Dulbecco's phosphate-buffered saline before incubation with labeled α-bungarotoxin bound 80% of the amount of toxin bound to unfixed cells, and no change was observed in diffuse or clustered receptor distribution.

Cells were subjected to autoradiography, embedded in Epon 812, sectioned, and examined with an electron microscope. The results showed that the NTB-2 emulsion was distributed in a uniform thickness over the myotubes and remained in contact with the cell membrane. The distribution of acetylcholine receptors on the cell surface in contact with the petri dish was examined as follows: after incubation cells were fixed with glutaraldehyde and embedded in Epon 812 while still attached to the petri dish. Each dish was removed, and NTB-2 emulsion was applied to the surface of the Epon formerly attached to the dish. Autoradiographs revealed that uniformly distributed and clustered receptors were present on the bottom surface of the cells.

In other experiments fewer cells were added to each petri dish to obtain well-isolated muscle colonies. All myotubes in the 101 colonies examined bound α-bungarotoxin, and every colony cultured 11 days or longer had receptor clusters.

In other experiments autoradiographs were exposed for only 20 hr in order to determine the number of silver grains per cluster. From the specific activity of the labeled α-bungarotoxin, and on the assumation that one molecule of toxin binds to one acetylcholine receptor, the average receptor concentrations of the diffusely labeled and cluster regions of the cell were estimated to be 900 and 9000 receptors per μm^2, respectively.

DISCUSSION

The results show that clusters of acetylcholine receptors form during the development of chick-embryo skeletal muscle cells cultured in the absence of neurons. On the assumption that one molecule of α-bungarotoxin binds to one acetylcholine receptor, the concentration of receptors in the clusters was about 9000 per μm^2, similar to that found at the neuromuscular and the electroplax synapse (7, 8, 10, 24, 25). The average receptor concentration in other regions of the cell was 900 μm^2.

It is unlikely that the receptor clusters are artifacts of fixation, since no apparent relation was found between the abundance of clusters and the method of fixation, and such clusters were not observed on chick-embryo sympathetic ganglion neurons grown *in vitro* that were assayed in the same way (L. Greene *et al.*, manuscript in preparation). In addition, Cohen and Fischbach examined living muscle cells grown *in vitro* by electrophysiological techniques and found small areas of cells 3- to 6-fold more sensitive to acetylcholine than adjacent areas (19).

The data suggest that some receptor clusters result from retraction of cell processes. It should be noted that because of the close apposition of the lower and upper cell membranes, the grain concentration at the cell margin may be twice that found towards the cell center. However, the concentration of silver grains in receptor clusters was considerably more than twice that of neighboring regions. No ultrastructural specialization of surface membranes or cell organelles were associated with these regions.

Formation of receptor clusters may be due to interactions between acetylcholine receptors and other molecules. Acetylcholine receptors of electroplax apparently interact either with each other or with other molecules to form more complex structures (6, 26–28).

A possible relation between receptor clusters and synapse formation is shown schematically in Fig. 6. Dividing myoblasts have few, if any, active acetylcholine receptors, whereas nondividing, multinucleated myotubes have many receptors distributed over the entire cell surface. Regions of relatively high acetylcholine receptor concentration appear on muscle grown *in vitro*. Synapse formation *in vivo* is accompanied by a loss of active acetylcholine receptors from the noninnervated portion of a muscle cell, thereby converting the muscle cell from a permissive to a nonpermissive state with respect to establishing functional synapses with the neurons (16, 29, 30).

It seems likely that molecules attached to the tip of an exploring axon interact with complementary molecules attached to the surface of another cell and thereby select sites for synapse formation. Obviously a cell receiving information across a chemical synapse must have an appropriate species of receptor and other components of the neurotransmitter translation apparatus. Such molecules or molecules that interact with them may be part of a synaptic recognition

code. Stable interaction between two cells most surely depends upon many molecular interactions. It is possible that acetylcholine receptors or molecules associated with them function as determinants of synapse recognition, and that receptor cluster formation may be a normal step in synapse formation. Further work is needed to determine whether such clusters are required for synapse formation.

We thank Mrs. Theresa Caryk for invaluable assistance and Dr. Mathew Daniels for the electron microscope studies.

1. Hartzell, H. C. & Fambrough, D. M. (197) *Soc. for Neuroscience First Annual Meeting—Abstracts*, p 161.
2. Patrick, J., Heinemann, S. F., Lindstrom J., Schubert, D. & Steinbach, J. H. (1972) *Proc. Nat. Acad. Sci. USA* **69**, 2762–2766.
3. Vogel, Z., Sytkowski, A. J. & Nirenberg, M. W. (1972) *Proc. Nat. Acad. Sci. USA* **69**, 3180–3184.
4. Lee, C. Y., Tseng, L. F. & Chiu, T. H. (1967) *Nature* **215**, 1177–1178.
5. Changeux, J.-P., Kasai, M. & Lee, C.-Y. 1970) *Proc. Nat. Acad. Sci. USA* **67**, 1241–1247.
6. Miledi, R., Molinoff, P. & Potter, L. T. (971) *Nature* **229**, 554–557.
7. Miledi, R. & Potter, L. T. (1971) *Nature* **2. 3**, 599–603.
8. Barnard, E. A., Wieckowski, J. & Chiu, T. H. (1971) *Nature* **234**, 207–209.
9. Berg, D. K., Kelly, R. B., Sargent, P. B., Williamson, P. & Hall, Z. W. (1972) *Proc. Nat. Acad. Sci. USA* **69**, 147–151.
10. Fambrough, D. M. & Hartzell, H. C. (1972) *Science* **176**, 189–191.
11. Bosmann, H. B. (1972) *J. Biol. Chem.* **247**, 130–145.
12. Fambrough, D. & Rash, J. E. (1971) *Develop. Biol.* **26**, 55–68.
13. Ginetzinsky, A. G. & Shamarina, N. M. (1942) *Usp. Sovrem. Biol.* **15**, 283–294.
14. Diamond, J. & Miledi, R. (1962) *J. Physiol.* **162**, 393–408.
15. Axelsson, J. & Thesleff, S. (1959) *J. Physiol.* **149**, 179–193.
16. Miledi, R. (1960) *J. Physiol.* **151**, 1–23.
17. Kuffler, S. W., Dennis, M. J. & Harris, A. J. (1971) *Proc. Roy. Soc. Ser. B* **177**, 555–563.
18. Harris, A. J. & Dennis, M. J. (1970) *Science* **167**, 1253–1255.
19. Cohen, S. & Fischbach, G. (1971) *Soc. for Neuroscience First Annual Meeting–Abstracts*, p. 162.
20. Konigsberg, I. R. (1971) *Develop. Biol.* **26**, 133–152.
21. White, N. K. & Hauschka, S. D. (1971) *Exp. Cell Res.*, **67**, 479–482.
22. Vogt, M. & Dulbecco, R. (1960) *Proc. Nat. Acad. Sci. USA* **46**, 365–370.
23. Dulbecco, R. & Vogt, M. (1954) *J. Exp. Med.* **99**, 167–182.
24. Waser, P. G. (1970) in *Molecular Properties of Drug Receptors*, eds. Porter, R. & O'Connor, M. (J. & A. Churchill, London), pp. 59–75.
25. Bourgeois, J. P., Ryter, A., Menez, A., Fromageot, P., Boquet, P. & Changeux, J. P. (1972) *FEBS Lett.* **25**, 127–133.
26. Meunier, J. C., Olsen, R., Menez, A., Morgat, J. L., Fromageot, P., Ronserray, A. M., Boquet, P. & Changeux, J. P. (1971) *C. R. H. Acad. Sci.* **273**, 595–598.
27. Fulpius, B., Cha, S., Klett, R. & Reich, E. (1972) *FEBS Lett.* **24**, 323–326.
28. Raferty, M. A., Schmidt, J. & Clark, D. G. (1972) *Arch. Biochem. Biophys.* **152**, 882–886.
29. Miledi, R. (1963) *Nature* **199**, 1191–1192.
30. Katz, B. & Miledi, R. (1964) *J. Physiol.* **170**, 389–396.

Proc. Nat. Acad. Sci. USA
Vol. 70, No. 1, pp. 275–278, January 1973

A Model for Active Transport of Sodium and Potassium Ions as Mediated by a Tetrameric Enzyme*

(cell membranes/adenosine triphosphatase/transport kinetics/cation pumping/protein conformation changes)

W. D. STEIN, W. R. LIEB†, S. J. D. KARLISH, AND Y. EILAM

Institute of Life Sciences, The Hebrew University, Jerusalem, Israel

Communicated by David E. Green, October 20, 1972

ABSTRACT **A new model is proposed for the system that actively transports sodium and potassium ions across animal-cell membranes. The model is based on the physical and chemical properties of transport-associated adenosine triphosphatase (EC 3.6.1.3) and on the kinetics of ion movements mediated by the system. Transport is postulated to occur by internal transfer of cations across a protein tetramer embedded in the cell membrane. The protein tetramer can exist in either of two forms of identical energy; transport occurs as a result of the sequential "flipping" from one conformation to the other. The conformation change results in the interchanging of the affinities of cation-binding sites associated with different subunits of the tetramer, with a concomitant splitting of adenosine triphosphate.**

Models for the mechanism of action of the system that actively transports sodium (Na^+) and potassium (K^+) ions across cell membranes have often involved diffusible carriers or proteins undergoing conformational changes (1). We recently put forward a model for glucose transport in human erythrocytes, involving conformational changes within a protein tetramer embedded in the cell membrane (2–4). Similarities in the kinetics of cation and of glucose transport hinted that a similar type of model might explain transport in these two systems. We thus developed a tentative model for Na^+ and K^+ transport, based on accumulated experimental data concerning the behavior of the system as a cation transporter (5–11), as a (Na + K)-activated ATPase (12–20), and as a K-activated phosphatase (12, 21). Much of the data is indirect, and our model cannot yet account for all the experimental data. Nevertheless, we propose it now because it is an essentially new model and it suggests, therefore, several interesting new experiments.

Physical approach toward the new model

That a tetramer is involved in glucose transport in human erythrocytes was inferred from purely kinetic data (2, 3). The components of the cation active transport system have been isolated. [We assume that in its fundamental features the active transport system for Na^+ and K^+ is the same in all animal tissues and is identical with (Na + K)-activated ATPase (20), ATP phosphohydrolase (EC 3.6.1.3).]

Kyte (13, 14) purified (Na + K)-activated ATPase, which contains two polypeptide chains in equimolar quantities. Tentatively, the protein is of the form $\alpha_n\beta_n$, where α and β are different polypeptide chains and n is a small integer that we proceed to estimate. Only one of the chains can be covalently labeled with phosphate from ATP (14); we call this the α chain. Kyte (13, 14) reports the molecular weights of the α and β chains to be 84,000 and 57,000, respectively. Kyte's results are consistent with those of Uesugi *et al.* (15), who found the two most prominent chains to have apparent molecular weights of 94,000 and 53,000. Thus, the molecular weight of the functional ATPase is about 140,000 n. To determine n, we need the molecular weight of the functional enzyme. Kepner and Macey (12) obtained an average molecular weight for the functional (Na + K)-activated ATPase of about 250,000. Nakao *et al.* (17) had obtained a value of 500,000, but Kepner and Macey (12) considered that Nakao *et al.* had overestimated the molecular weight. These results suggest that the value of n in $\alpha_n\beta_n$ is certainly greater than unity, with $n = 2$ being the most likely value. Thus, these physical studies are consistent with the tetrameric nature of the cation pump.

Chemical approach toward the new model

We shall draw an analogy between the results of chemical binding studies and the phenomenon of "half of the sites reactivity." Consider alkaline phosphatase (EC 3.1.3.1) from *Escherichia coli*, an α_2 dimer, both chains of which are disposed symmetrically in crystals (22). The binding sites on the two subunits appear identical in the unbound form of the dimer. Nevertheless, one molecule of phosphate binds with high affinity, while a second molecule binds with much reduced affinity, (23). Furthermore, while alkaline phosphatase can bind two molecules of phosphate or ATP per dimer, only one molecule of phosphate from ATP can be retained covalently under physiological conditions (23). Levitzki *et al.* (24) have pointed out that "a significant number of enzymes have now been shown to exhibit the paradox of half-of-the-sites reactivity, in which only one of two apparently identical subunits is expressed in a given reaction." This finding is apparently due to negative cooperativity: binding of substrate at one subunit of an α_2 dimer reduces the affinity at the second subunit.

Consider now the study of Hegyvary and Post (18), who measured the binding of ATP to membranes. Let R be the ratio of the moles of ATP found bound ionically under nonphosphorylating conditions (i.e., in the absence of Mg) to the

* This paper is dedicated to the memory of our beloved mentor, colleague, and friend, Aharon Katchalsky, Foreign Associate, National Academy of Sciences, who lost his life in the tragedy at Lod Airport, 30 May 1972.

† MRC Biophysics Unit, King's College, London W.C.2.

moles of terminal phosphate incorporated covalently from ATP under standard phosphorylating conditions. With neither Na^+ nor K^+ present, $R = 1$ for ionic binding at a high-affinity site, with the hint of an additional binding at a lower-affinity site. With K^+ added, $R = 2$ for ionic binding at what appeared to be a single population of low-affinity sites, with no binding at sites of high affinity. Thus, twice as many ionic binding sites are expressed under one condition as under another. Further, twice as many ATP molecules can bind ionically to this membrane preparation as can donate at any one time a terminal phosphate group to be stably linked to the enzyme at physiological pH. This result is reminiscent of the behavior of the "half-of-the-sites-reactive" enzymes.

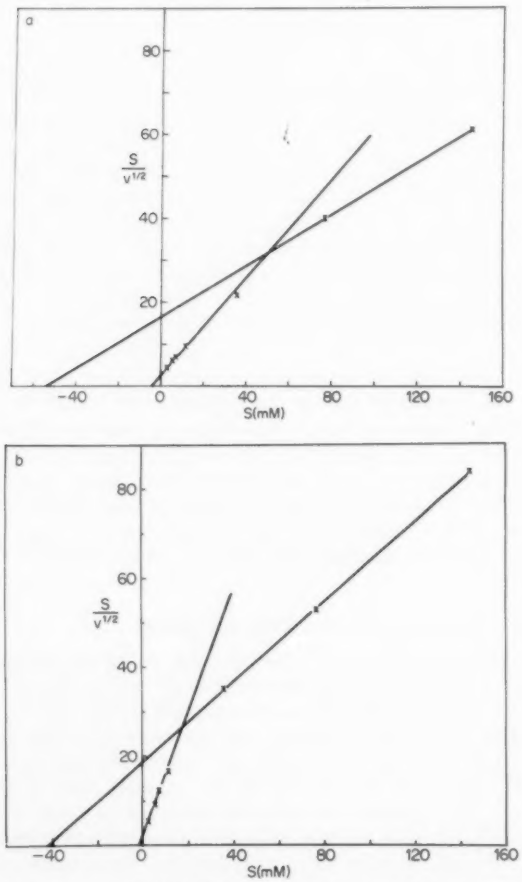

FIG. 1. A plot of the Na^+-Na^+ exchange data from Fig. 5 of ref. 9. Cells loaded with various concentrations of labeled Na^+ were suspended in a high concentration of Na^+ with no K^+. v is efflux (mmol/l erythrocyte per hr) of labeled Na^+; S is intracellular concentration (mM) of Na^+, assuming 70% cell water. Since Na^+ binding is cooperative, we plot data according to $v = [S/(S + K)]^2 V$, where K is the intrinsic dissociation constant of a single binding site and V is the maximum velocity. Concentration K_m (half-saturation constant) at which velocity is half-maximal is then $K_m = 2.42\ K$. Intercept on abscissa is $-K$, intercept on ordinate is $K/V^{1/2}$. (*a*) Ouabain absent. K_m = 12 mM and V = 3.2 mmol per erythrocyte per hr (transport on inner high-affinity site); K_m = 130 and V = 7.5 (inner low-affinity site). (*b*) Ouabain at 0.1 mM. K_m = 5 and V = 1 (inner high-affinity site); K_m = 110 and V = 4.1 (inner low-affinity site).

(Na + K)-activated ATPase can function also as a K-activated phosphatase (21), a smaller portion of the enzyme being necessary for activity than for ATPase activity (12). We suggest that the phosphatase activity resides in the α_2 dimer portion of an $\alpha_2\beta_2$ cation pump tetramer. Although all α chains have the intrinsic ability to bind ATP, we postulate that only one chain of a pair can retain terminal phosphate from ATP in a covalent form under physiological conditions. A simple calculation from the data of Uesugi *et al.* (15) shows that the (Na + K)-activated ATPase preparation contains from 0.4 to 0.6 mol of covalently bound phosphate from ATP for every mol of α chain. Thus, the results of chemical binding studies present an interesting analogy to the properties of other enzymes showing "half-of-the-sites reactivity," and are consistent with the view that the cation transport protein is an $\alpha_2\beta_2$ tetramer.

The transport approach

Most models of active transport assume that during physiological operation of the pump there appear sequentially a high-affinity site for Na^+ on the inside face of the membrane and low-affinity site on the outside. However, recent transport studies performed under nonpumping conditions (i.e., in the absence of external K^+) indicate that high- and low-affinity sites for Na^+ can coexist simultaneously at each face of the membrane. (A high-affinity site for Na^+ has a half-saturation constant, K_m, of about 10 mM; a low-affinity site, a K_m of about 100 mM.)

The properties of the Na^+-binding sites that can appear at the inside face of the membrane can be inferred from Sachs' experiment with human erythrocytes (Fig. 1). Although the dependence of Na^+ efflux on internal Na^+ concentration is greater than first-order, we take this cooperativity into account by plotting, not S/v against S, as for a conventional saturation curve, but $S/v^{1/2}$ against S. The resulting plot (Fig. 1) is fitted best by two straight lines, indicative of the presence of two classes of binding sites, with different affinities for Na^+. Each class of sites binds more than one Na^+ ion in a cooperative fashion. (If $S/v^{1/3}$ is plotted against S, the same two classes of binding sites are observed.) The analysis in Fig. 1 suggests that, both in the presence and absence of the transport inhibitor ouabain, efflux of labeled Na^+ involves both a high- and a low-affinity site for Na^+ at the inward face of the membrane.

Similarly, the properties of the Na^+-binding sites at the outward face of the membrane can be inferred from an experiment by Garrahan and Glynn (5). Fresh erythrocytes were suspended in K^+-free solutions of various Na^+ concentrations. The results of the influx measurement (5) demonstrate the existence of both a high- and low-affinity site for Na^+ at the outer face of the membrane. That the low-affinity site is not merely a simple diffusive leak is shown by the fact that the flux occurring on it was reduced considerably by ouabain. In the efflux measurement (5), as the Na^+ concentration in the external solution was raised from zero, the Na^+ efflux at first dropped to a minimum at about 5 mM and then slowly rose in accordance with a half-saturation constant for a low-affinity site.

Thus, the experiment of Sachs indicates the presence of both a high- and a low-affinity site for Na^+ on the inner face of the membrane, while the experiment of Garrahan and Glynn suggests a similar situation at the outer face. The evidence

indicates the presence of at least four cation binding units per enzyme, consistent with a tetrameric protein.

The tetramer model

An extension of our previous tetramer model (2, 3) to the Na^+ and K^+ transport system can be arrived at as follows: In both systems, tranport is postulated to occur by internal transfer of substrate across a protein tetramer embedded in the membrane. For glucose transport (Fig. 2*a*), each subunit of the tetramer retains its binding affinity for substrate throughout the transport process, while for active transport (Fig. 2*b*) we now suggest the affinities are switched during each conformation change. The conformation change that alters the position of the binding sites is termed a *transposition;* a change in the nature or affinity of the binding sites is termed a *transformation*. Thus, facilitated glucose transport involves only a succession of transpositions (Fig. 2*a*), while active cation transport would involve a succession of concerted transposition and transformation events (Fig. 2*b*).

The cation transport enzyme (Fig. 3) is postulated to be an $\alpha_2\beta_2$ tetrameric protein, asymmetrically disposed in the membrane. The active centers of the α subunits (and perhaps, although not necessarily, the entire α subunits) reside in that half of the membrane that faces the cell interior; those of the β subunits are in the outer half of the membrane. Each subunit has the potential to exist in either a high- or a low-affinity state for the binding of Na^+; in the physiological operation of the pump (Fig. 3) each subunit assumes successively such high- and low-affinity states. High affinity for Na^+ (an H_α or H_β site) implies low affinity for K^+, while low affinity for Na^+ (an L_α or L_β site) implies high affinity for K^+. The two conformations A and A' are functionally and energetically equivalent. Sequential flipping from one conformation to the other is sufficient to allow active transport to occur.

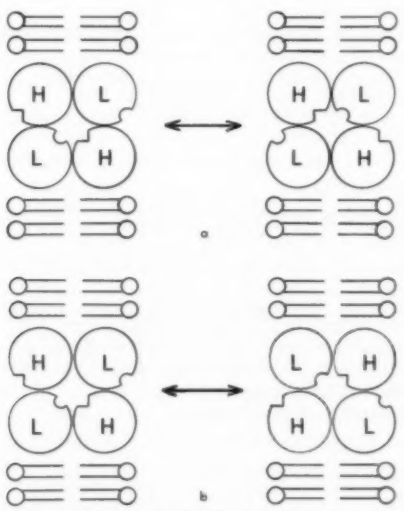

FIG. 2. Molecular events during transport according to the tetramer model. (*a*) A transposition. (*b*) Simultaneous transposition and transformation. *H*, subunit in high-affinity binding state; *L*, low-affinity state. Transport occurs as follows: (*i*) Substrate molecules bind to sites directed outwards from the tetramer; (*ii*) they enter the internal cavity after a conformational change; (*iii*) within the internal cavity substrate molecules redistribute themselves according to the binding affinities; and (*iv*) after a change back to the original conformation, the substrate molecules emerge into the bathing solutions.

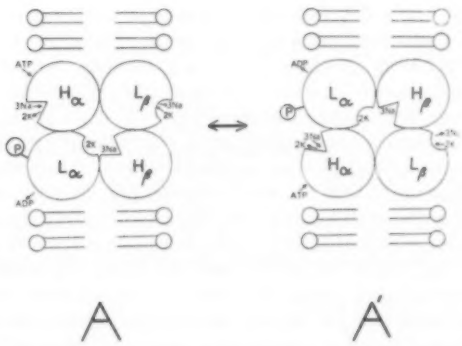

FIG. 3. Model for active transport of Na^+ and K^+ ions as mediated by an $\alpha_2\beta_2$ tetrameric enzyme. *H*, subunit having a high affinity for Na and low affinity for K; L, the converse situation. Each binding site can, intrinsically, be either *H* or *L*. (For simplicity, release of inorganic phosphate from *H* is not shown.) Active transport results from the sequential flipping between the isoenergetic conformations *A* and *A'*.

The postulated sequence of events involved in normal transport is as follows. Consider first cation movements on the upper two subunits. (*a*) In conformation *A*, Na^+ binds at the H_α subunit and K^+ at L_β. (*b*) The tetramer flips to state *A'*; this involves both a transposition and a transformation. (*c*) In conformation *A'*, ions brought into the internal cavity formed by the upper two subunits will now redistribute and Na^+ and K^+ will bind at the H_β and L_α subunits, respectively. (*d*) The tetramer flips back to state *A*, causing Na^+ to be expelled into the external medium, K^+ into the cell interior. (*e*) The process repeats from step (*a*). Cation movements on the lower two subunits proceed in an entirely equivalent manner, but 180° out of phase.

The simultaneous changes in the phosphorylation status of the α subunits, which cause the above affinity changes, can be considered in an exactly parallel fashion. Consider first the upper α subunit. (*a*) In conformation *A*, ATP binds to H_α. (*b*) With Na^+ (and Mg^{++}, assumed always present), this subunit is phosphorylated, and simultaneously the tetramer flips to state *A'*, the upper α subunit transforming from H_α to L_α. The K^+ brought into the internal cavity binds to the upper α subunit. (*d*) With these K^+ ions as cofactors, this upper α subunit dephosphorylates, and simultaneously the tetramer flips back to state *A*. (*e*) The process repeats from step (*a*). Events on the lower α subunit proceed in an entirely equivalent manner, but 180° out of phase. It is important that phosphorylation of one α subunit and dephosphorylation of the other is a concerted process, accounting for the "half-of-the-sites reactivity" finding that under physiological conditions only one phosphate from ATP can be retained covalently by the tetramer at any one time.

Thus, under pumping conditions (Fig. 3), cellular Na^+ ions serve as cofactors for phosphorylation of the α subunit by ATP, whereas K^+ ions in the internal cavity act as cofactors for the transfer of covalently-bound phosphate to water. We suggest that if, in the internal cavity Na^+ rather than K^+ binds to the L_α subunit, then Na^+ will serve instead as a cofactor for the transfer of covalently-bound phosphate to ADP, if this is present. This presumably occurs during the reversal

of the pump (7), with the concomitant synthesis of ATP. Such a postulate would account for the finding (19) that low concentrations (8 mM) of Na^+ are sufficient for complete phosphorylation of (Na + K)-activated ATPase by ATP, whereas much higher concentrations (160 mM) are required for subsequent dephosphorylation by deoxy-ADP. On the tetramer model, dephosphorylation by ADP requires Na^+ in the internal cavity to bind to the L_α site. This binding will occur only if sufficient Na^+ ions are present within the cavity to bind to both H_β and L_α sites. But to have this number of Na^+ ions inside the cavity, both the high- and low-affinity sites must have carried Na^+ into the cavity. Thus, dephosphorylation by ADP requires use of the low-affinity subunits.

During transport under nonpumping conditions, transformations of the binding sites may not occur, even though transpositions of the tetramer continue (Fig. 2). These transpositions would cause the appearance of binding states that are not seen during active transport; thus the L_α and H_β sites, which under pumping conditions are occluded within the internal cavity (Fig. 3), may be revealed (e.g., Fig. 1).

Several important effects of ouabain are understandable if we postulate that ouabain binds to a β subunit in its L_β binding state, preventing the movement of cations on this subunit. Thus, ouabain inhibits cation pumping only if applied extracellularly; influx of labeled Na^+ on low-affinity sites (i.e., on L_β) is inhibited by ouabain (5), as is stimulation of Na^+ efflux by high concentrations of external Na^+ (5); of the cation fluxes inhibited by ouabain, the influx of K^+ (on L_β) is perhaps that most severely affected (6, 8); K-activated phosphatase activity of the system (K entering the internal cavity by L_β) is abolished by oubain.

Immediately testable predictions of our model are: (*a*) transport experiments in K^+-free and in Na^+-free systems will display kinetic anomalies like those found for glucose transport in human erythrocytes (4); (*b*) many additional parallels will be found between properties of the cation pump enzyme and other "half-of-the-sites reactive" enzymes (24); (*c*) a method might be developed capable of detecting the occlusion of cations (19) within the internal cavity of the tetramer; (*d*) the β subunit will combine with cardiac glycosides and derivatives that are site-directed irreversible inhibitors (16); (*e*) if some residual ATPase or phosphatase activity can be found in α_2 dimers free of β chains, it will be insensitive to ouabain.

From the model (Fig. 3), the two conformations of the protein involved in the energy-transducing process are exactly isoenergetic, which may be important for at least two reasons. For rapid rates of energy transduction, the conformations of the protein must not differ much in free energy lest the protein be trapped in the more stable conformation and the number of transitions decrease. For efficient energy transduction, none of the hydrolysis energy of the high-energy phosphate bond need be stored in the conformation of a stable intermediate, presumably a wasteful process. Indeed, with isoenergetic conformations, the hydrolysis free energy can be directly converted to cation pumping, with minimal losses.

W. R. L. thanks Prof. M. H. F. Wilkins for encouragement and support and Dr. C. W. F. McClare for helpful discussions. S.J.D.K. and Y.E. hold Prof. Philip Stein Fellowships, sponsored by the Sagov Industrial Management Co. Ltd. of South Africa. W. R. L. acknowledges receipt of an EMBO short-term travel fellowship.

1. Caldwell, P. C. (1970) in *Membranes and Ion Transport*, ed. Bittar, E. E. (John Wiley & Sons, London), Vol. I, pp. 433–461.
2. Lieb, W. R. & Stein, W. D. (1970) *Biophys. J.* **10,** 585–609.
3. Lieb, W. R. & Stein, W. D. (1971) *Nature New Biol.* **230,** 108–109.
4. Lieb, W. R. & Stein, W. D. (1972) *Biochem. Biophys. Acta* **265,** 187–201.
5. Garrahan, P. J. & Glynn, I. M. (1967) *J. Physiol.* **192,** 159–174.
6. Garrahan, P. J. & Glynn, I. M. (1967) *J. Physiol.* **192,** 189–216.
7. Garrahan, P. J. & Glynn, I. M. (1967) *J. Physiol.* **192,** 237–256.
8. Glynn, I. M., Lew, V. L. & Lüthi, U. (1970) *J. Physiol.* **207,** 371–391.
9. Sachs, J. R. (1970) *J. Gen. Physiol.* **56,** 322–341.
10. Sachs, J. R. (1971) *J. Gen. Physiol.* **57,** 259–282.
11. Caldwell, P. C. & Keynes, R. D. (1959) *J. Physiol.* **148,** 8P.
12. Kepner, G. R. & Macey, R. I. (1968) *Biochem. Biophys. Acta* **163,** 188–203.
13. Kyte, J. (1971) *J. Biol. Chem.* **246,** 4157–4165.
14. Kyte, J. (1971) *Biochem. Biophys. Res. Commun.* **43,** 1259–1265.
15. Uesugi, S., Dulak, N., Dixon, J. F., Hexum, T. D., Dahl, J. L., Perdue, J. F. & Hokin, L. E. (1971) *J. Biol. Chem.* **246,** 531–543.
16. Hokin, L. E. (1969) *J. Gen. Physiol.* **54,** 327S–342S.
17. Nakao, H., Nagano, K., Nakao, T., Mizuno, Y., Tashida, Y., Fujita, M., Maeda, H. & Matsudaira, H. (1967) *Biochem. Biophys. Res. Commun.* **29,** 588–592.
18. Hegyvary, C. & Post, R. L. (1971) *J. Biol. Chem.* **246,** 5234–5240.
19. Post, R. L. & Kume, S. (1971) *Proc. Int. Union Physiol. Sci.* **8,** 84–85.
20. Bonting, S. L. (1970) in *Membranes and Ion Transport*, ed. Bittar, E. E. (John Wiley & Sons, London), Vol. I, pp. 257–363.
21. Rega, A. F., Pouchan, M. I. & Garrahan, P. J. (1970) *Science* **167,** 55–56.
22. Hanson, A., Applebury, M. L., Coleman, J. E. & Wyckoff, H. W. (1970) *J. Biol. Chem.* **245,** 4975–4976.
23. Lazdunski, M., Pettitclerc, C., Chappelet, D. & Lazdunski, C. (1971) *Eur. J. Biochem.* **20,** 124–139.
24. Levitzki, A., Stallcup, W. B. & Koshland, D. E., Jr. (1971) *Biochemistry* **10,** 3371–3378.

Proc. Nat. Acad. Sci. USA
Vol. 70, No. 1, pp. 279–283, January 1973

The Crystal Structures of 2,5-Piperazinediones Having Epipolysulfide Bridges Between C3 and C6: The Structures of *N,N'*-Dimethyl-3,6-Epitetrathio-2,5-Piperazinedione

(x-ray structures/cyclic dipeptides/active site of sporidesmin G/viral inhibitors/cytotoxins/*Pythomyces chartarum*)

BETTY R. DAVIS AND IVAN BERNAL*

Department of Chemistry, Brookhaven National Laboratory, Upton, Long Island, New York 11973

Communicated by H. A. Scheraga, November 8, 1972

ABSTRACT **The crystal and molecular structure of *N,N'*-dimethyl-3,6-epitetrathio-2,5-piperazinedione ($C_6H_8O_2N_2S_4$) has been determined from three-dimensional x-ray diffraction data collected by counter techniques. The substance crystallizes in the orthorhombic space group Fdd2, with a = 15.352(5), b = 20.432(7), and c = 6.635(2) Å; V = 2081.2(8) Å³, D(meas) = 1.72(2) g/cm³, and z = 8 molecules per unit cell. The molecule lies on a crystallographic 2-fold axis, the piperazinedione ring is in the boat conformation, and the deviation from planarity is 18°. The bonds of the tetrasulfide chain alternate in length so that the S–S distances are 2.0244(9), 2.076(1), and 2.0244(9) Å. The structural data were refined by least-squares methods to an R(F) of 2.5% by use of the 1089 independent reflections ($2\theta \leq 71°$; MoKα) for which $F_o^2 \geq 3\sigma(F_o^2)$. Since this molecule is chemically identical with the active center of the recently isolated natural product sporidesmin G, our structural study constitutes a description of the epitetrathio-2,5-piperazinedione fragment of that molecule.**

The therapeutic value (1) and biological interest in cyclic dipeptides have made these substances the object of many studies (2–11) aimed at determining the relationship between their conformation and other physical properties. Disulfide linkages are ubiquitous in nature, and the combination of a 2,5-piperazinedione and a disulfide bridge across the 3,6-positions (3,6-epidithio-2,5-piperazinediones) constitute the active fragment of such biologically interesting substances as gliotoxin, (12, 13*a*), virus-inhibiting antibiotics of the aranotin type (14), sporidesmins (13*b*, 15), and cancerostatic antibiotics of the chaetocin type (16).

Until recently, all biologically active materials of this type isolated from natural sources were thought to contain *epidithio* bridges only. However, Taylor and associates demonstrated in 1967 (17) that an *epitrithio* derivative could be isolated from *Pythomyces chartarum*. In 1970, Taylor *et al.* (18) showed that epitrithio and epitetrathio derivatives (made synthetically from the natural epidithio compound and H_2S_2) had biological activity comparable with that of the naturally occurring epidithio derivative. Finally, in 1972, Taylor *et al.* (19) isolated sporidesmin G, which is a naturally occurring 3,6-epitetrathio-2,5-piperazinedione. This substance and bis-(3-oxoundecyl)tetrasulfide, isolated from the Hawaiian algae *Dictyopteris* by Moore (20), constitute the only two known natural products containing a tetrasulfide chain. Efforts to understand the chemistry associated with the syntheses of these substances, and their stereochemistry, have been underway for some time (12–22). In this report, we describe the stereochemistry of the title compound, which was prepared by Poisel and Schmidt (21). Extensive comparisons are made with the bonding details of other substances containing tetrasulfide chains (23–25) and with other studies of the stereochemistry of cyclic dipeptides (4, 9–11).

* To whom correspondence should be addressed.

EXPERIMENTAL

Crystal Data. $C_6H_8O_2N_2S_4$, M = 268.40, orthorhombic, a = 15.352(5), b = 20.432(7), c = 6.635(2) Å, D_m = 1.72(2) (by flotation), Z = 8, D_c = 1.71. Space group Fdd2 (26*a*); MoK$\bar{\alpha}$ radiation, λ = 0.71069 Å; μ (MoK$\bar{\alpha}$) = 8.710 cm^{-1} [estimated from mass absorption coefficients (26*b*)].

Crystallographic Measurements. Precession photographs taken with MoK$\bar{\alpha}$ radiation showed the crystals to be orthorhombic; the space group (Fdd2) was deduced from these photographs. The cell constants and their standard deviations were determined by a least-squares refinement of 30 reflections that were automatically centered on a Picker diffractometer equipped with a graphite monochromator; a take-off angle of 2.0° was used. The crystal selected for data collection contained 18 faces; 8 of the form {111}, 6 of the form {100}, and 4 of the form {110}. The crystal was 0.471 × 0.251 × 0.385 mm along the [100], [010], and [001] directions, respectively. Data were collected with a Picker diffractometer controlled by the Brookhaven Multiple Spectrometer Control System. The scintillation counter system included a pulse-height analyzer and pulse-shape discriminator, and was set to accept about 90% of the diffracted intensity. The take-off angle was set to 2.5°, which gave 80% of the maximum intensity observed in a plot of intensity against take-off angle. Data were collected by the θ–2θ scan technique, and a reflection was scanned in steps of $\Delta(2\theta)$ = 0.02°, with a counting time of 2 sec for each step. The total scan range of 1.6 (1.0 + 1.0 tanθ) was centered about the Bragg angle, which corresponds to the unweighted average wavelength of 0.7114 Å for MoKα_1 and MoKα_2 radiation. The intensities of 2856 reflections with $2\theta \leq 71°$, comprising two asymmetric forms (hk*l* and $\bar{h}$k*l*), were measured. Two standard reflections were monitored every 30 reflections, but no significant variation of intensity was found during the entire period of data collection.

The values of I and σ(I) were corrected for Lorentz-polarization effects, but not for absorption. An absorption correction was not applied due to the complex shape of the crystal and

TABLE 1.

	Fractional coordinates			Thermal parameters*,†						Root-mean-square amplitudes of vibration along the three principal axes of the thermal ellipsoid (Å)		
	x	y	z	β_{11} or B	β_{22}	β_{33}	β_{12}	β_{13}	β_{23}	Axis 1	Axis 2	Axis 3
S1	0.06737(4)	0.00432(3)	0.0	532(3)	317(2)	1498(9)	−118(2)	283(4)	−143(3)	0.165	0.217	0.299
S2	0.09220(3)	0.08238(2)	0.17894(12)	407(2)	185(1)	1865(9)	−88(1)	73 (4)	110(2)	0.158	0.214	0.243
O	0.06120(9)	−0.12154(6)	0.48401(29)	371(5)	127(2)	2585(36)	57(3)	208(12)	93(8)	0.152	0.199	0.257
N	0.08914(8)	−0.01298(6)	0.47662(22)	213(4)	136(2)	1430(24)	31(2)	−45(7)	−13(6)	0.148	0.174	0.185
C1	0.18208(11)	−0.02382(10)	0.50838(38)	238(5)	199(4)	2326(44)	49(3)	−80(13)	−61(11)	0.157	0.206	0.235
C2	0.03567(9)	−0.06497(6)	0.46496(22)	250(4)	125(2)	1259(26)	27(2)	85(8)	19(6)	0.151	0.161	0.188
C3	0.06072(9)	0.05239(6)	0.43440(26)	235(4)	120(2)	1429(24)	1(2)	−58(9)	−42(7)	0.154	0.165	0.185
H1	0.188(4)	−0.058(3)	0.569(12)	6.0(1.2)								
H2	0.205(3)	0.010(3)	0.554(11)	6.4(1.2)								
H3	0.207(3)	−0.035(2)	0.381(9)	4.4(1.0)								
H4	0.093(2)	0.078(1)	0.541(5)	2.0(0.5)								

* The anisotropic thermal parameters are of the form $\exp[-(\beta_{11}h^2 + \beta_{22}k^2 + \beta_{33}l^2 + 2\beta_{12}hk + 2\beta_{13}hl + 2\beta_{23}kl)]$.
† The values of S2 in this category have been multiplied by 10^4.

the low value of the absorption coefficient. Equivalent forms were averaged and this procedure gave 1089 reflections for which $F_o^2 \geq 3\sigma(F_o^2)$, with $\sigma(F_o^2) = 1/\mathrm{Lp}\,[(I+B) + (0.04I)^2]^{1/2}$, where Lp is the Lorentz-polarization factor, I is the total integrated peak, and B is the time-scaled background (27).

SOLUTION AND REFINEMENT

The function minimized in the least-squares refinement was $\sum w(|Fo| - |Fc|)^2$, where the weight w is $4F_o^2/\sigma^2(F_o^2)$. For all calculations of Fc, the atomic scattering factors were taken from the tables of Cromer (28). The effect of anomalous dispersion for the sulfur atoms was included in the calculation of Fc (28).

Since the molecule lies on a crystallographic 2-fold axis of symmetry, there are only eleven independent atoms for the structural analysis. The sulfur atoms were located by means of a Patterson function. This process was followed by a difference Fourier synthesis, which yielded approximate coordinates of the three carbons, nitrogen, and oxygen atoms. This synthesis was followed by several cycles of refinement in which the positional and isotropic thermal parameters of these seven atoms were varied; by this procedure, the hydrogen atoms were located. The position of the hydrogen atom attached to C3 was calculated and the methyl hydrogen atoms were located from a difference Fourier synthesis, calculated perpendicular to the (methyl carbon)–(nitrogen) vector. These were then idealized to have a C–H distance of 0.98 Å.

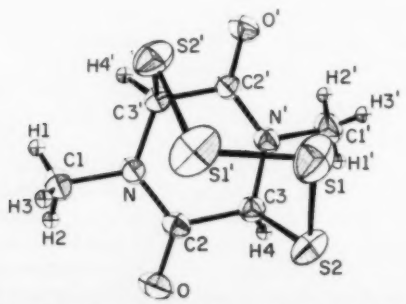

FIG. 1. The configuration of the molecules and the labeling system used during the crystallographic study.

In the final stages of refinement the positional and anisotropic thermal parameters of the sulfur, carbon, nitrogen, and oxygen atoms were varied and the positional and isotropic thermal parameters of the hydrogen atoms were also varied. Such a refinement converged at values of $R_1 = 2.5$ and $R_2 = 3.5$, where $R_1 = \sum(|Fo| - |Fc|)/\sum|Fo|$ and $R_2 = \{\sum w(|Fo| - |Fc|)^2/\sum F_o^2\}^{1/2}$. For the 79 variables and 1089 observations, the error in an observation of unit weight was 1.40 electrons.

The positional and thermal parameters derived from the last cycle of refinement are presented in Table 1, along with associated standard deviations in these parameters as estimated from the inverse of the normal equations matrix. The root-mean-square amplitudes of vibration along the three principal axes of the thermal ellipsoid (Å) are also listed in Table 1. The following programs were used: PROCH (initial processing of data; DATAPH (Lorentz-polarization corrections); ECSORTH (sorting and averaging of data);

TABLE 2. *Molecular geometry*

	Bond distances (Å)		
S1–S2	2.0244(9)	C2–O	1.227(2)
S1–S1′	2.076(1)	N–C1	1.459(1)
S2–C3	1.866(2)	C3–H4	1.01(3)
C3–N′	1.433(2)	C1–H1	0.81(7)
C3–C2	1.515(2)	C1–H2	0.83(6)
C2–N	1.345(2)	C1–H3	0.95(5)
	Bond angles (deg)		
S1′–S1–S2	104.76(4)	N–C2–C3	118.0(1)
S1–S2–C3	103.02(5)	N–C2–O	122.9(1)
S2–C3–N′	113.9(1)	C3–C2–O	119.0(1)
S2–C3–C2	108.6(1)	C1–N–C2	119.0(1)
N′–C3–C2	115.4(1)	C1–N–C3	117.9(1)
		C2–N–C3′	112.6(1)

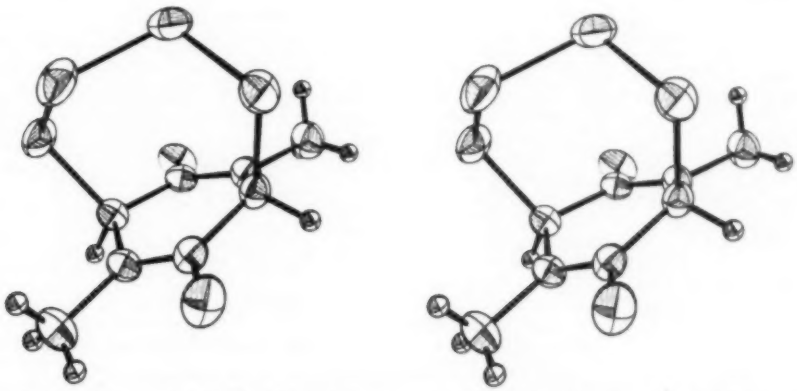

FIG. 2. A stereoscopic view of the molecule. The thermal parameters of the hydrogen atoms were made of a uniform, isotropic, size for representational convenience, while those of the heavy atoms are shown as 50% probability envelopes.

JIMDAP (local version of the Zalkin Fourier summation program); LINUS (Modification of the Busing, Martin, and Levy ORFLS least-squares program) (29); ORFFE (function and error) (30); PLANET (least-squares planes) (31); and ORTEP (molecular plotting) (32).

DISCUSSION

A view of the molecule looking nearly down the 2-fold crystallographic axis is shown in Fig. 1, where the numbering system used in the crystallographic study is also given. In Fig. 2, a stereo view of the molecule is depicted in an orientation chosen to emphasize the nonplanarity of the piperazinedione ring, and also the three-dimensional nature of the epitetrasulfide chain. Fig. 3 shows the packing of the molecules in an orthorhombic unit cell. A selection of bond distances and angles is presented in Table 2. The equations of least-squares planes passing through interesting groups of atoms in the molecule are given in Table 3; in Table 4 are listed the torsional angles about the interatomic vectors of the molecule. There are no unusual intra- or intermolecular contacts in the structural analysis. The bond distances and bond angles associated with the 2,5-piperazinedione ring are quite normal and in the range found in other 2,5-piperazinedione derivatives, as may be seen by examination of those listed in Table 3. Our results are in excellent agreement with those given by Sletten (4), and reinforce his conclusion that the results of Benedetti *et al.* (9–11) are incorrect. As may be seen from Fig. 2, the piperazinedione ring is nonplanar at positions C3 and C3′. The dihedral angle between planes defined by atoms C2,-N,N′,C2′ and by atoms C2′,C3,N is 18.08°. In 2,5-piperazinedione (34) and in *trans*-3,6-dimethyl-2,5-piperazinedione (10), the rings are planar, while in *cis*-3,6-dimethyl-2,5-piperazinedione, deviation from planarity is 8°. An interesting feature of our compound, and of others listed in Table 3, is the length of the C–S bond. The distances listed range from 1.87 to 1.91 Å, and are considerably longer than the C–S bonds found in

TABLE 3. *Planes*

Equations of planes and distances (Å) of selected atoms from these planes

(*a*) Plane containing C2, C2′, N, and N′

$$0.0x + 0.0y - 1.0z = -3.125$$

C2	0.040
N	−0.037
C3	0.243

(*b*) Plane containing N, C2, and C3

$$-0.175x - 0.256y - 0.951z = -3.177$$

(*c*) Plane containing N, C1, C2, and C3

$$0.173x - 0.110y - 0.979z = -2.792$$

N	−0.037	C2	0.014
C1	0.029	C3	0.015

Angles (deg) between normals to planes a–b 18.08

TABLE 4. *Torsional angles in degrees**

				Distances between (Å)				
A	B	C	D	A–B	B–C	C–D	A–D	[Angle]
S1	S1′	S2	C3′	2.076	2.024	1.866	3.676	68.63
S1	S2	C3	N	2.024	1.866	1.433	3.200	42.81
S1	S2	C3	C2′	2.024	1.866	1.515	3.682	−87.29
S2	S1	S1′	S2′	2.024	2.076	2.024	4.398	−105.33
S2	C3	N	C1	1.866	1.433	1.459	3.375	71.13
S2	C3	N	C2	1.866	1.433	1.345	3.663	−101.00
S2	C3	C2′	O′	1.866	1.515	1.227	3.207	−69.68
S2	C3	C2′	N′	1.866	1.515	1.345	3.696	112.48
O	C2	N	C1	1.227	1.345	1.459	2.731	1.54
O	C2	N	C3	1.227	1.345	1.433	3.569	173.58
O	C2	C3′	N′	1.227	1.515	1.433	3.589	161.07
N	C2	C3′	N′	1.345	1.515	1.433	2.788	−16.77
C1	N	C2	C3′	1.459	1.345	1.515	3.805	179.29
C1	N	C3	C2′	1.459	1.433	1.515	3.814	−162.26
C2	N	C3	C2′	1.345	1.433	1.515	2.872	25.61
C3	N	C2	C3′	1.433	1.345	1.515	2.839	−8.67

* The convention used is that of the IUPAC–IUB Commission (38).

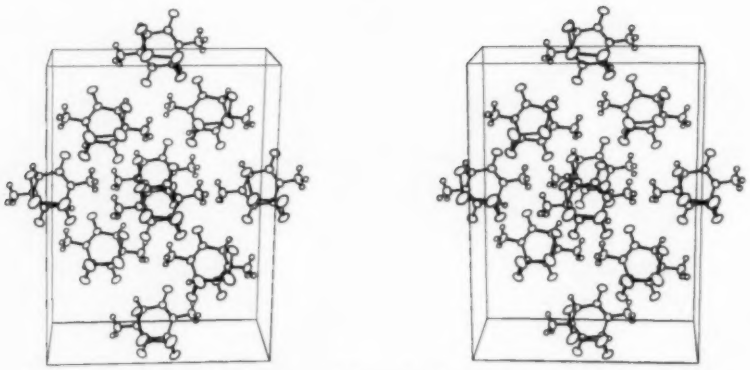

FIG. 3. A stereo packing diagram of the molecules in the orthorhombic unit cell.

aromatic systems, where these bonds range in length between 1.78 and 1.82 Å (23, 35). The longest C–S bonds we have found in the literature were reported by Lemmer *et al.* (36) for 1,2,3,-6,7,8-hexathiecane [1.859(4) Å] and by Lee and Bryant (37) in dicinnamyl sulfide [1.88(3) Å], both of which contain aliphatic carbon–sulfur bonds similar to ours. Thus, the statement made previously (13–17) that the change in dihedral angle at the disulfide sulfur of epidithiopiperazinediones from the normal value of 90° was responsible for the lengthening of this bond is probably exaggerated. In our system, the dihedral angle at the sulfur is 68.63° (see Table 3) and the length of the C–S bond is 1.866(2) Å. In LL-S88α (33), these values are about 17° and 1.882 Å; in gliotoxin (13*a*), there are two independent molecules and, therefore, two values of the C–S–S–C dihedral angle, namely 8.8 and 15.8°, while the C–S bonds average 1.88(3) and 1.89(3) Å, respectively. Similar comparisons can be made with the other values listed in Table 5. The outcome of such comparisons is that the difference between extremely low values of the dihedral angle (8°) reported for gliotoxin (13*a*) and the 68.63° observed in our system lead to relatively minor changes in the C–S bonds. This observation is reinforced by the results Feher *et al.* (24) reported for 1,2,3,4-tetrathiadecalin, which is a fully aliphatic system containing a tetrasulfide chain very similar to ours. In this system, the dihedral angles at the four sulfurs average 67.8°, while the average C–S distance is only 1.802(20) Å. Comparison between our results and those of Feher *et al.* (38) indicate that the relationship between dihedral angles and the C–S bond length is not as simple as has been thought. Furthermore, since the values of our dihedral angle and that in tetrathiadecalin (24) are essentially identical while the C–S bond lengths differ by about 0.07 Å it is clear that the dihedral angle alone cannot account for the length of the C–S bonds in the epipolythiopiperazinediones.

The S–S bond lengths alternate in the manner short–long–short, the distances being 2.0244(9) and 2.076(1) Å. A similar bond length alternation was observed in $C_{20}H_{24}O_4S_8$, where the average value of four short S–S distances was 2.028(2) Å and the average value of the two long bond lengths was 2.066(2) Å (23*a*). This phenomenon of bond length alternation was also observed in $C_{14}H_{12}N_2S_4$, where the three independent S–S bond lengths were 2.031(3), 2.088(4), and 2.026(3) Å (25). In $(C_5H_5)_2WS_4$ the alternation was in the reverse order (23*b*) (long–short–long), and the distances were 2.103(5), 2.017(6), and 2.099(6) Å. Such alternation indicates delocalization of electron density across the tetrasulphide chain, a process that need not occur when this chain is connected to saturated groups, as in $C_6H_{10}S_4$ where no alternation is observed (24), and where the average S–S bond distance was 2.057(7) Å.

CONCLUSIONS

(*i*) Our structural parameters for the diketopiperazine ring are in close agreement with those of Sletten (4), and indicate that the abnormal results reported by Benedetti *et al.* (9–11) are incorrect. (*ii*) The addition of an epitetrathio bridge across the 3,6-positions of the diketopiperazine effects only dihedral angles in the cyclic dipeptide and not the bond lengths. (*iii*)

TABLE 5.

Compound	N–C3′	C2–C3	N–C2	C2–O	C3–S	N–C2–O	C3–C2–O	C3′–N–C2	C2–C3–N′	Refs.
N-N′-Dimethyl-3,6-Epitetrathio-2,5-piperazinedione	1.433(2)	1.515(2)	1.345(2)	1.227(2)	1.866(2)	122.9(1)	119.0(1)	122.6(1)	115.4(1)	This work
Gliotoxin ($C_{13}H_{14}O_4N_2S_2$)	1.46	1.51	1.35	1.23	1.88	125.5	120.7	117.5	110.0	13*a*
Sporidesmin ($C_{19}H_{21}O_6N_3S_5Cl\cdot CH_2Br_2$)	1.46 1.35	1.52 1.59	1.39 1.35	1.20 1.27	1.90 1.91	122.8 124.7	123.2 125.4	115.1 121.7	110.5 114.0	13*b*
LL-S88α ($C_{22}H_{30}N_4O_8S_2$)	1.446	1.537	1.346	1.216	1.882	127.0	122.0	119 0	–	33
2,5-Piperazinedione	1.449	1.499	1.325	1.239		122.6	118.5	126.0	115.1	34
trans-3,6-Dimethyl-2,5-piperazinedione	1.462	1.470	1.325	1.240		122.9	117.8	127.9	112.8	10
cis-3,6-Dimethyl-2,5-piperazinedione	1.462 1.457	1.534 1.512	1.323 1.344	1.218 1.244		122.0 124.8	120.1 120.4	126.3 127.1	112.0 109.9	11

Aside from changes in dihedral angles imposed on the tetrasulfide chain by spanning across the cyclic dipeptide, its bond lengths and angles are normal. (*iv*) The structural parameters of our molecule should provide an accurate description of the active site of sporidesmin G; minor variations in bond lengths and angles will result from the constraints imposed by the peripheral rings in the molecule, but these will not change conformational details very much.

We thank Prof. Ulrich Schmidt for his gift of the crystals and Mr. John Smith, a member of the Brookhaven Semester Program, for his technical assistance. This research was done under the auspices of the U.S. Atomic Energy Commission.

1. Michalsky, J., Ctvrtink, J., Horakova, A. & Bydzovsky, V. (1962) *Experientia* **18,** 217.
2. Kopple K. D. & Marr, D. H. (1967) *J. Amer. Chem. Soc.* **89,** 6193.
3. Kobble, K. D. & Ohnishi, M. (1969) *J. Amer. Chem. Soc.* **91,** 962.
4. Sletten, E. (1970) *J. Amer. Chem. Soc.* **92,** 172.
5. Gawne, G., Kenner, G. W., Rogers, N. H., Sheppard, R. C. & Titlestad, K. (1968) *Peptides* **1968**, ed. Bricas, E. (John Wiley & Sons, New York), pp. 28.
6. Blaha, K. & Fric, D. (1968) in *Peptides 1968*, ed. Bricas, E. (John Wiley & Sons, New York), pp. 40.
7. Schellman, J. A. & Nielsen, B. E. (1967) in *Conformation of Biopolymers*, (ed.) Ramachandran, G. N. (Academic Press, New York), pp. 109.
8. Caillet, J., Pullman, B. & Maigret, B. (1971) *Biopolymers* **10,** 221.
9. Benedetti, E., Corradini, P. & Pedone, C. (1969) *Biopolymers* **7,** 751.
10. Benedetti, E., Corradini, P. & Pedone, C. (1969) *J. Phys. Chem.* **73,** 2891.
11. Benedetti, E., Corradini, P., Goodman, M. & Pedone, C. (1969) *Proc. Nat. Acad. Sci. USA* **62,** 650–652.
12. Bell, M. R., Johnson, J. R., Wildi, B. S. & Woodward, R. B. (1958) *J. Amer. Chem. Soc.* **80,** 1001.
13. (*a*) Fridrichsons, W. J. & Mathieson, A. McL. (1967) *Acta Crystallogr.* **23,** 439; (*b*) (1965) *Acta Crystallogr.* **18,** 1043.
14. Nagarajan, R., Neuss, N. & Marsh, M. M. (1968) *Amer. Chem. Soc.* **90,** 6518.
15. Synge, R. L. M. & White, E. P. (1959) *Chem. Ind. (London)* 1546.
16. Auser, D. H., Wiber, H. P. & Sigg, H. P. (1970) *Helv. Chim. Acta* **53,** 1061.
17. Rahman, R., Safe, S. & Taylor, A. (1969) *J. Chem. Soc. C,* 1665.
18. Safe, S. & Taylor, A., (1970), *J. Chem. Soc. C,* 432.
19. Francis, E., Rahman, R., Safe, S. & Taylor, A. (1972) *J. Chem. Soc.* (Perkin I), 470.
20. Moore, R. E. (1971) *Chem. Commun.* 1168.
21. Davis, B. R., Bernal, I. & Schmidt, U. (1972) *Angew. Chem., Int. Ed. Engl.* **11,** 632.
22. Poisel, H. & Schmidt, U. (1971) *Chem. Ber.* **104,** 1714.
23. (*a*) Ricci, J. S. & Bernal, I. (1971) *J. Chem. Soc. B,* 1928; (*b*) Davis, B. R., Bernal, I. & Köpf, H. (1971) *Angew. Chem. Int. Ed. Engl.* **10,** 921.
24. Feher, V. F., Klaeren, A. & Linke, K. H. (1972) *Acta Crystallogr. Sect. B* **28,** 534.
25. Barrick, J. C., Calvo, C. & Olsen, F. P. (1971) *Chem. Commun.* 1043.
26. *International Tables for X-Ray Crystallography* (Kynoch Press, Birmingham), (*a*) (1952) Vol. I, p. 129; (*b*) (1968) Vol. III, p. 166.
27. Corfield, P. W. R., Doedens, R. J. & Ibers, J. A. (1967) *Inorg. Chem.* **6,** 197.
28. Cromer, D. T. (1970) to be published in the new edition of the *International Tables for X-Ray Crystallography.*
29. Busing, W. R., Martin, K. O. & Levy, H. (1962) *ORFLS, A Fortran Crystallographic Least-Squares Program, Report ORNL TM 305* (Oak Ridge National Laboratory, Tenn.).
30. Busing, W. R., Martin, K. O. & Levy, H. (1964) *ORFFE, A Fortran Crystallographic Function and Error Program Report ORNL TM 306* (Oak Ridge National Laboratory, Tenn.).
31. Smith, D. L. (1962) Ph.D. Thesis, University of Wisconsin.
32. Johnson, C. K. (1965) *A Fortran Thermal Ellipsoid Plot Program For Crystal Structure Illustrations, Report ORNL 3794* (Oak Ridge National Laboratory, Tenn.), revised.
33. Cosulich, D. B., Nelson, N. R. & vanden Herde, J. H. (1968) *J. Amer. Chem. Soc.* **90,** 6519.
34. Degeilh, R. & Narsh, R. E. (1959) *Acta Crystallogr.* **12,** 1007.
35. Davis, B. R. & Bernal, I (1971) *J. Chem. Soc. B,* 2307.
36. Lemmer, F., Feher, F., Green, A., Hechtsfischer, S. & Hoppe, W. (1970) *Angew. Chem. Int. Ed. Engl.* **9,** 313.
37. Lee, J. D. & Bryant, M. W. R. (1971) *Acta Crystallogr.* **B27,** 2325.
38. IUPAC-IUB Commission on Biological Nomenclature (1970) *J. Mol. Biol.* **52,** 1.

Correction. In the article "Computation of Large Molecules with the Hartree–Fock Model," by Clementi, E., which appeared in the October 1972 issue of *Proc. Nat. Acad. Sci. USA* **69,** 2942–2944, all the pronouns "we" and "our" were subjected to an editorial change whereby these pronouns were transformed into "I" and "my", respectively, when the original manuscript was submitted to the Proceedings.

Correction. In the article "The Spectrum of Cobalt Bovine Procarboxypeptidase A, an Index of Catalytic Function," by Behnke, W. D. & Vallee, B. L., which appeared in the September 1972 issue of *Proc. Nat. Acad. Sci. USA* **69,** 2442–2445, the following correction should be made in column 3, Table 1, p. 2443: the number 13 should read 3.

Correction. In the article "Sequence of Spontaneous Epstein–Barr Activation and Selective DNA Synthesis in Activated Cells in the Presence of Hydroxyurea," by Hampar, B., Derge, J. G., Martos, L. M., Tagamets, M. A. & Burroughs, M. A., which appeared in the September 1972 issue of *Proc. Nat. Acad. Sci. USA* **69,** 2589–2593, in the legend for Fig. 2 (p. 2590, 3rd line from bottom) and Fig. 4 (p. 2592, 2nd line from bottom), the symbol "% $FA^+/^3H^+$" should read: % FA^+ cells that are $^3H^+$. In the legend for Fig. 2, the symbol, 2nd line from bottom "% $^3H^+/FA^+$" should read: % $^3H^+$ cells that are FA^+.

Correction. In the article "Biosynthesis of Acetylcholine in Turtle Photoreceptors," by Lam, D. M. K., which appeared in the July 1972 issue of *Proc. Nat. Acad. Sci.* **69,** 1987–1991, the following should be added to the acknowledgments.

"I would like to thank Dr. David S. Barkley, Department of Neuropathology, Harvard Medical School, for communicating prior to publication the technique used in this paper for preparing a cell suspension suitable for velocity sedimentation."

Correction. In the article "Modulation of Cell Behavior *In Vitro* by the Substratum in Fibroblastic and Leukemic Mouse Cell Lines," by Macieira-Coelho, A. & Avrameas, S., which appeared in the September 1972 issue of *Proc. Nat. Acad. Sci. USA* **69,** 2469–2473, the following correction should be made. On page 2469, right-hand column, under *Measurement of DNA Synthesis*, the first two sentences should read: ^{3}H-labeled thymidine ([^{3}H]dT; 15 Ci/mmol) was added to the cultures at a final concentration of 0.5 μCi/ml. After 30 min the cultures were suspended in the PBS solution supplemented with trypsin and. . .."

Correction. In the article "Endogenous RNA-directed DNA Polymerase Activity in Uninfected Chicken Embryos," by Kang, C.-Y. & Temin, H. M., which appeared in the June 1972 issue of *Proc. Nat. Acad. Sci. USA* **69,** 1550–1554, in the asterisked footnote to Table 1 (p. 1551), ". . . contained 10 nM dATP, 10 nM dCTP, 10 nM dGTP, 7.5 nM ATP . . . (about 0.2 nM) [^{3}H]TTP" should read: ". . . contained 10 nmol dATP, 10 nmol dCTP, 10 nmol dGTP, 7.5 nmol ATP . . . (about 0.2 nmol) [^{3}H]TTP."

Announcing...

the Third Edition of

Specifications and Criteria for Biochemical Compounds

prepared by the Committee on Specifications and Criteria for Biochemical Compounds of the NRC Division of Chemistry and Chemical Technology

Specifications and Criteria for Biochemical Compounds, Third Edition, contains the best information available to date for each class of compounds described, including amino acids, carbohydrates, carotenoids, coenzymes, enzymes, lipids, nucleotides, and porphyrins. The 216-page volume not only provides revised and updated information on the 392 biochemical compounds listed in earlier editions, but it also describes 129 compounds previously unlisted. A section on radioactive compounds appears for the first time in this edition, providing some general comments concerning the use of these materials in biochemical research. A comprehensive, cross-reference index lists both common names and systematic names for each compound described in the volume. If you are concerned with evaluating the quality of biochemical compounds used for research purposes, *Specifications and Criteria for Biochemical Compounds,* Third Edition, is an essential addition to your professional library.

ISBN 0-309-01917-6; 1972, xxi + 216 pages, clothbound, $15.25

NATIONAL ACADEMY OF SCIENCES
Printing and Publishing Office
2101 Constitution Avenue
Washington, D.C. 20418

Complete Catalog Available Upon Request

Abelson, J. 179
Acs, G. 41
Alberte, R. S. 134
Apirion, D. 156
Attardi, G. 115
Avrameas, S. 284
Babior, B. M. 98
Baglioni, C. 173
Barnhart, F. E. 15
Behnke, W. D. 284
Bernal, I. 279
Bick, M. D. 138
Bishop, J. M. 164
Bodley, J. W. 147
Boorman, S. A. 187
Brody, S. S. 50
Brown, S. W. 195
Burroughs, M. A. 284
Canonico, P. G. 66
Carson, D. 235
Carter, B. J. 215
Caspary, W. J. 66
Cerdonio, M. 161
Chandra, H. S. 195
Chapman, F. 27
Chen, Y-D. 62
Clementi, E. 284
Coggin, J. H., Jr. 183
Cormier, M. J. 120
Cosloy, S. D. 84
Cozzarelli, N. R. 103
Creagan, S. 98
Crookston, J. H. 220
Crookston, M. C. 220
Csanady, G. T. 93
Dalldorf, G. 15
Daniel, V. 76
Davidson, E. A. 54
Davidson, R. L. 138
Davies, J. N. P. 15
Davis, B. R. 279
Dawidowicz, K. 111
DeAngelo, A. B. 18
Debreceni, N. 31
Delius, H. 200
Delovitch, T. L. 173
Dempsey, M. E. 265
Derge, J. G. 284
Dierlam, P. 183
Diggs, J. 169
Dole, V. P. 10
Dorman, B. P. 255
Duff, R. 54
Eilam, Y. 275
Emery, K. O. 93
Faras, A. 164
Fujimoto, G. I. 18
Gabelman, N. 11
Ganoza, M. C. 31
Garon, C. F. 215
Gass, K. B. 103
Gerard, G. F. 230
Gershon, R. K. 250
Gibson, Q. H. 1
Giordano, R. 46
Girardi, A. J. 183
Goldberg, I. H. 22
Gordon, J. 147
Grandgenett, D. P. 230
Granger, G. A. 27
Gray, H. B. 161
Green, M. 230
Greenblatt, M. 46
Gustafsson, T. 80
Hammel, H. T. 124
Hampar, B. 284
Hanawalt, P. C. 129
Hasenbank, R. 147
Hehlmann, R. 5
Highland, J. H. 147
Hill, T. L. 62
Hirschhorn, K. 11
Hori, K. 120
Ikeya, Y. 71
Ingbar, S. H. 98
Jackson, J. 164
Jaworska, H. 80
Jazwinski, S. M. 205
Kaiser, D. 260
Kang, C.-Y. 284
Kaplan, H. S. 36
Kaplan, J. 66
Kappen, L. S. 22
Karlish, S. J. D. 275
Kipnes, R. S. 98
Klein, M. P. 143
Koczot, F. J. 215
Kolb, W. P. 27
Kornberg, A. 205
Kreek, M. J. 10
Kufe, D. 5
Kyner, D. 41
Lam, D. M. K. 284
Lamfrom, H. 179
Laserna, E. C. 27
Levin, D. H. 41
Levinson, W. 164
Levinthal, C. 57
Levitt, P. R. 187
Lieb, W. R. 275
Lima-De-Faria, A. 80
Lipman, M. 190
Litwack, G. 76
Loeb, L. A. 245
Lopresti, V. 57
Low, R. L. 103
Macagno, E. R. 57
Macieira-Coelho, A. 284
Maestre, M. F. 255
Mahler, H. R. 111
Marco, R. 205
Marsh, R. C. 151
Martos, L. M. 284
Masker, W. E. 129
Masuda, T. 260
Mathews, M. B. 225
Matzinger, D. F. 108
Maurer, P. H. 250
di Mayorca, G. 46
McPhee, J. 50
Merryman, C. F. 250
Meyhack, B. 156
Meyhack, I. 156
Michaels, M. A. 220
Miller, G. 190
Mulder, C. 200
Murphy, W. 115
Naylor, A. W. 134
Nierlich, D. P. 179
Nirenberg, M. W. 270
Oishi, M. 84
Okazaki, R. 88
Parmeggiani, A. 151
Pettersson, U. 200
Phillips, S. L. 31
Price, P. M. 11
Rakic, P. 240
Rapp, F. 54
Reppucci, P. 183
Ritter, M. C. 265
Robertson, H. D. 225
Root, C. A. 161
Rose, J. A. 215
Rosenberg, R. C. 161
Rosso, P. 169
Rutala, W. 183
Sarabhai, A. 179
Satoh, C. 54
Schachter, H. 220
Scholander, P. F. 124
Sharp, P. A. 200
Sidman, R. L. 240
Soller, A. 46
Sparling, P. F. 71
Spiegelman, S. 5
Springgate, C. F. 245
Stein, W. D. 275
Stewart, A. 15
Stoffler, G. 147
Sugino, A. 88
Suzuki, H. 22
Sytkowski, A. J. 270
Tagamets, M. A. 284
Temin, H. M. 284
Thornber, J. P. 134
Tildon, J. T. 210
Tilley, C. A. 220
Tomkiewics, M. 143
Tomkins, G. M. 76
Trauthen, T. 46
Vallee, B. L. 284
Vandermeer, J. 31
Vogel, Z. 270
Wang, R-H. 161
Waxman, S. 11
Weigert, M. 235
Weissman, I. L. 36
Wernsman, E. A. 108
Winick, M. 169
Witte, O. N. 36
Woodson, B. 164
Zimmermann, R. A. 71

Selected New and Recent Titles from

NATIONAL ACADEMY OF SCIENCES
NATIONAL ACADEMY OF ENGINEERING
NATIONAL RESEARCH COUNCIL

Asbestos: The Need for and Feasibility of Air Pollution Controls, Committee on Biologic Effects of Atmospheric Pollutants
ISBN 0-309-01927-3; 1971, vii + 40 pp., paper, $1.75
This monograph discusses the pathogenicity of asbestos in man and animals, human nonoccupational exposure to asbestos, and health risks associated with various degrees and types of exposure. It also identifies sources of environmental contamination by asbestos and indicates high-priority areas where research is needed.

An Assessment of Industrial Activity in the Field of Biomedical Engineering, Committee on the Interplay of Engineering with Biology and Medicine
ISBN 0-309-01925-7; 1971, xvi + 146 pp., paper, $5.25
Current attitudes and activities in the biomedical engineering industry are analyzed in this report, which also offers a profile of the industry, identifies major areas that have an effect on industrial contributions to the health care system, and recommends action to meet current and future needs in health care.

Evaluating the Safety of Food Chemicals, Food Protection Committee
ISBN 0-309-01859-5; 1970, v + 55 pp., paper, $2.50
This report directs attention to recently proposed or adopted procedures for evaluation of the safety of food chemicals and considers the new methods against a background of experience with conventional procedures.

Fluorides, Committee on Biologic Effects of Atmospheric Pollutants
ISBN 0-309-01922-2; 1971, xi + 295 pp., paper, $6.50
For those concerned with the biologic effects of atmospheric pollutants, this volume evaluates the world literature on fluorides and summarizes the best scientific knowledge available on their biologic effects. Topics discussed include environmental sources and forms of fluorides and their relative hazards to plants, animals, and humans, with particular emphasis on the susceptibility of special population groups.

Jamaica Bay and Kennedy Airport: A Multidisciplinary Environmental Study, Environmental Studies Board
ISBN 0-309-01874-4; 1971, 178 pp. in 2 volumes + 13 foldout 3-color maps, paper, $8.95 per set
This report identifies and evaluates the effects of various plans for expansion of New York's Kennedy Airport on the physical environment and on human ecology in the Jamaica Bay area, suggests alternative courses of action, and examines their implications.

Immunoglobulins: Biologic Aspects and Clinical Uses, Ed. by Ezio Merler, Division of Medical Sciences
ISBN 0-309-01850-1; 1971, xii + 404 pp., illus., cloth, $9.50
The papers presented in this volume review the fundamental, technological, and clinical aspects of immunoglobulins and suggest lines of investigation that may further increase their value in preventing and alleviating human disease.

Reference Methods for the Microbiological Examination of Foods, Food Protection Committee
ISBN 0-309-01863-3; 1971, 40 pp., paper, $2.25
In an effort to simplify laboratory practice and minimize variability of results, this report suggests reference methods for establishing microbiological criteria for classes of foods susceptible to microbiological contamination.

NATIONAL ACADEMY OF SCIENCES
Printing and Publishing Office
2101 Constitution Avenue
Washington, D.C. 20418

Complete Catalog Available Upon Request

Contents *(Continued from inside back cover)*

	An alteration in glucose metabolism associated with a defect in ketone body metabolism *(skin fibroblasts/coenzyme A/transferase/pyruvate/Embden–Myerhof pathway)* ... *J. Tyson Tildon*	210–214
GENETICS	Inactivation system of the mammalian X chromosome *(Lyon hypothesis/heterochromatin/genetic regulation/sex chromatin)* ... *Spencer W. Brown and H. Sharat Chandra*	195–199
	Genetic transformation in *Escherichia coli* K12 *(DNA/$CaCl_2$/recombination/genetic linkage)* ... *Sharon D. Cosloy and Michio Oishi*	84–87
	Bromodeoxyuridine dependence—a new mutation in mammalian cells *(hamster cells/drug dependence/DNA)* ... *Richard L. Davidson and Michael D. Bick*	138–142
	Release of amplified ribosomal DNA from the chromomeres of *Acheta (RNA cistrons/hybridization/oocytes/pachytene/meiosis)* ... *A. Lima-De-Faria, Halina Jaworska, and T. Gustafsson*	80–83
	In situ hybridization of RD114-virus RNA with human metaphase chromosomes *(density gradient centrifugation/karyotype/RNA-dependent DNA polymerase)* ... *Peter M. Price, Kurt Hirschhorn, Norman Gabelman, and Samuel Waxman*	11–14
IMMUNOLOGY	Immunochemical analysis of the cross-reacting idiotypes of mouse myeloma proteins with anti-dextran activity and normal anti-dextran antibody *(radioimmunoassay/hapten/light and heavy chains/mice)* ... *Dennis Carson and Martin Weigert*	235–239
	Estimation of light-chain gene reiteration of mouse immunoglobulin by DNA–RNA hybridization *(12S RNA/myeloma/protein synthesis/variable region)* ... *T. L. Delovitch and C. Baglioni*	173–178
	A cellular basis for genetically controlled immunologic unresponsiveness in mice: tolerance induction in T-cells *(histocompatibility genes/memory cells)* ... *Richard K. Gershon, Paul H. Maurer, and Carmen F. Merryman*	250–254
	Prevention of simian virus 40 tumors by hamster fetal tissue: influence of parity status of donor females on immunogenicity of fetal tissue and on immune cell cytotoxicity *(primiparous and multiparous hamsters/lymph node cells/peritoneal exudate cells)* ... *Anthony J. Girardi, Phyllis Reppucci, Peggy Dierlam, William Rutala, and Joseph H. Coggin, Jr.*	183–186
	Human lymphotoxin: purification and some properties *(phytohemagglutinin/human lymphocytes)* ... *G. A. Granger, E. C. Laserna, W. P. Kolb, and F. Chapman*	27–30
MEDICAL SCIENCES	Methadone plasma level: sustained by a reservoir of drug in tissue *(heroin/humans/opiate/maintenance treatment/addiction)* ... *Vincent P. Dole and Mary Jeanne Kreek*	10
	RNA related to that of a murine leukemia virus in Burkitt's tumors and nasopharyngeal carcinomas ... *D. Kufe, R. Hehlmann, and S. Spiegelman*	5–9
	Malignant lymphomas of African children *(lymphoblastic leukemia/Burkitt lymphoma/malaria/Epstein–Barr virus/cancer survey)* ... *Alice Stewart, J. N. P. Davies, Gilbert Dalldorf, and Frances E. Barnhart*	15–17
MICROBIOLOGY	Sequence of spontaneous Epstein–Barr activation and selective DNA synthesis in activated cells in the presence of hydroxyurea (Correction) ... *B. Hampar, J. G. Derge, L. M. Martos, M. A. Tagamets, and M. A. Burroughs*	284
	Inhibition of RNA-dependent DNA polymerase of Rous sarcoma virus by thiosemicarbazones and several cations *(RNA tumor viruses/DNA synthesis/viral inactivation/chelation)* ... *Warren Levinson, Anthony Faras, Bruce Woodson, Jean Jackson, and J. Michael Bishop*	164–168
	Release of infectious Epstein–Barr virus by transformed marmoset leukocytes *(human leukocytes/extracellular virus)* ... *George Miller and Muriel Lipman*	190–194
	Structural characteristics of some murine RNA tumor viruses studied by lactoperoxidase iodination *(radiation leukemia virus/Moloney leukemia virus/mouse mammary tumor virus/gel electrophoresis)* ... *Owen N. Witte, Irving L. Weissman, and Henry S. Kaplan*	36–40
PHYSIOLOGY	On the theory of ion transport across the nerve membranes, VII. Cooperativity between channels of a large square lattice *(computer simulation/Ising kinetics/Adam model/correlation functions/phase transition)* ... *Yi-der Chen and Terrell L. Hill*	62–65
	Biosynthesis of acetylcholine in turtle photoreceptors (Correction) ... *D. M. K. Lam*	284
ZOOLOGY	A frequency-dependent natural selection model for the evolution of social cooperation networks *(altruism/threshold effect/cooperative carnivore hunting behavior)* ... *Scott A. Boorman and Paul R. Levitt*	187–189

Corrections

CHEMISTRY	Computation of large molecules with the Hartree–Fock model ... *E. Clementi*	284
CELL BIOLOGY	The spectrum of cobalt bovine procarboxypeptidase A, an index of catalytic function ... *W. D. Behnke and B. L. Vallee*	284
	Endogenous RNA-directed DNA polymerase activity in uninfected chicken embryos ... *C. -Y. Kang and H. M. Temin*	284
	Modulation of cell behavior *in vitro* by the substratum in fibroblastic and leukemic mouse cell lines ... *A. Macieira-Coelho and S. Avrameas*	284
MICROBIOLOGY	Sequence of spontaneous Epstein–Barr activation and selective DNA synthesis in activated cells in the presence of hydroxyurea ... *B. Hampar, J. G. Derge, L. M. Martos, M. A. Tagamets, and M. A. Burroughs*	284
PHYSIOLOGY	Biosynthesis of acetylcholine in turtle photoreceptors ... *D. M. K. Lam*	284

Contents (Continued from outside back cover)

Ultraviolet-stimulated DNA synthesis in toluenized *Escherichia coli* deficient in DNA polymerase I *(temperature-sensitive mutants/nonconservative/dnaE/repair synthesis)*
Warren E. Masker and Philip C. Hanawalt 129–133

Colicin E3: a unique endoribonuclease *(ribosomes/16S rRNA/gel electrophoresis/RNase-less mutants)*
Bernd Meyhack, Irene Meyhack, and David Apirion 156–160

Stability of cytoplasmic messenger RNA in HeLa cells *(actinomycin D/benzoylated-DEAE/cellulose/poly-(T)-cellulose/nucleoside triphosphate pools/cold chase)*
William Murphy and Guiseppe Attardi 115–119

Transfer RNA synthesis *in vitro (T4 DNA/RNA transcription/RNA processing/sequence analysis)*
Donald P. Nierlich, Hildegard Lamfrom, Anand Sarabhai, and John Abelson 179–182

Cleavage of adenovirus type 2 DNA into six unique fragments by endonuclease R·RI *(restriction enzyme/electron microscopy/DNA gel electrophoresis/DNA sequence complexity)*
Ulf Pettersson, Carel Mulder, Hajo Delius, and Phillip A. Sharp 200–204

Squalene and sterol carrier protein. Structural properties, lipid-binding, and function in cholesterol biosynthesis *(liver/microsomal enzymes/phospholipids/fatty acids)*
Mary C. Ritter and Mary E. Dempsey 265–269

Double-stranded RNA as an inhibitor of protein synthesis and as a substrate for a nuclease in extracts of Krebs II ascites cells *(encephalomyocarditis virus/messenger RNA/ribonuclease)*
Hugh D. Robertson and Michael B. Mathews 225–229

Production of mucopolysaccharides by normal and transformed cells *(hyaluronic acid/transformed cells/hamster-embryo cultures)*
C. Satoh, R. Duff, F. Rapp, and E. A. Davidson 54–56

Qualitative differences in the *N*-acetyl-D-galactosaminyltransferases produced by human A^1 and A^2 genes *(blood group A/serum glycosyltransferases/glycoprotein biosynthesis/milk oligosaccharides)*
H. Schachter, M. A. Michaels, Christine A. Tilley, Marie C. Crookston, and J. H. Crookston 220–224

Mutagenic DNA polymerase in human leukemic cells *(tumor progression/leukemia/lymphocytes)*
Clark F. Springgate and Laurence A. Loeb 245–249

A model for active transport of sodium and potassium ions as mediated by a tetrameric enzyme *(cell membranes/adenosine triphosphatase/transport kinetics/cation pumping/protein conformation changes)*
W. D. Stein, W. R. Lieb, S. J. D. Karlish, and Y. Eilam 275–278

Development of acetylcholine receptor clusters on cultured muscle cells *(α-bungarotoxin/autoradiography/synapses)*
A. J. Sytkowski, Z. Vogel, and M. W. Nirenberg 270–274

RNA-linked DNA fragments *in vitro (E. coli/toluene-treated cells/DNA synthesis/discontinuous replication/RNA synthesis/nucleotide sequence)*
Akio Sugino and Reiji Okazaki 88–92

Photooxidation of chlorophyll *b* by quinones studied by chemically-induced dynamic nuclear polarization *(NMR/excited states/radical pairs)*
Micha Tomkiewicz and Melvin P. Klein 143–146

Alteration of ribosomal protein S4 by mutation linked to kasugamycin-resistance in *Escherichia coli (ribosomal proteins/ribosomal RNA/reconstitution/phosphocellulose chromatography)*
Robert A. Zimmermann, Yoshiko Ikeya, and P. Frederick Sparling 71–75

BOTANY

Biosynthesis of the photosystem I chlorophyll–protein complex in greening leaves of higher plants *(photosystem I/chloroplast development/lamellar proteins/P700)*
Randall S. Alberte, J. Philip Thornber, and Aubrey W. Naylor 134–137

CELL BIOLOGY

The spectrum of cobalt bovine procarboxypeptidase A, an index of catalytic function (Correction)
W. D. Behnke and B. L. Vallee 284

Endogeneous RNA-directed DNA polymerase activity in uninfested chicken embryos (Correction)
C. Y. Kang and H. M. Temin 284

Electron spin resonance studies of spin-labeled mammalian cells by detection of surface-membrane signals *(lipid-soluble labels/living nucleated cells/erythrocytes/potassium ferricyanide)*
Joseph Kaplan, Peter G. Canonico, and William J. Caspary 66–70

Structure and development of neuronal connections in isogenic organisms: variations and similarities in the optic system of *Daphnia magna (neuronal specificity/serial section reconstruction/crustacea)*
E. R. Macagno, V. Lopresti, and C. Levinthal 57–61

Modulation of cell behavior *in vitro* by the substratum in fibroblastic and leukemic mouse cell lines (Correction)
A. Macieira-Coelho and S. Avrameas 284

Autonomy of mitochondria in *Saccharomyces cerevisiae* in their production of messenger RNA *(RNA synthesis/polysomes/inhibition/ethidium bromide/mitochondrial genome)*
Henry R. Mahler and Karl Dawidowicz 111–114

Photophosphorylation by monomolecular films at an air-water interface *(surface chemistry/chlorophyll/photosynthesis/coupling factor I/lipid membranes)*
J. McPhee and S. S. Brody 50–53

Malignant transformation of BHK_{21} clone 13 cells *in vitro* by nitrosamines—a conditional state *(in vitro chemical carcinogenesis/transformed phenotype conditioned by high temperature)*
Giampiero di Mayorca, Melvin Greenblatt, Thomas Trauthen, Arthur Soller, and Roberto Giordano 46–49

Weaver mutant mouse cerebellum: defective neuronal migration secondary to abnormality of Bergmann glia *(cerebellar development/neuron-glial cell interaction/neurological mutant mice)*
P. Rakic and R. L. Sidman 240–244

Changes in alkaline ribonuclease activity during compensatory renal growth
Pedro Rosso, James Diggs, and Myron Winick 169–172

(Continued on page 288)

INFORMATION TO CONTRIBUTORS ..... i–iv

Physical Sciences

CHEMISTRY
Computation of large molecules with the Hartree–Fock model (Correction) ..... *E. Clementi* 284
The nature of the ground states of cobalt(II) and nickel(II) carboxypeptidase A *(metallocarboxypeptidase A/magnetic susceptibility/coordination geometry/spectra)* ..... *Robert C. Rosenberg, Charles A. Root, Run-Han Wang, Massimo Cerdonio, and Harry B. Gray* 161–163

GEOPHYSICS
Surface circulation of lakes and nearly land-locked seas *(marginal seas/wind drive/water movements)* ..... *K. O. Emery and G. T. Csanady* 93–97

PHYSICS
Thermal motion and forced migration of colloidal particles generate hydrostatic pressure in solvent *(osmotic pressure/ferrofluid)* ..... *H. T. Hammel and P. F. Scholander* 124–128

Biological Sciences

APPLIED BIOLOGY
Extranuclear temperature-sensitive lethality in *Nicotiana tabacum* L. *(cytoplasmic inheritance/genetics/tobacco)* ..... *D. F. Matzinger and E. A. Wernsman* 108–110

BIOCHEMISTRY
Stimulation of mitochondrial adenosine diphosphate uptake by thyroid hormones *(mitochondrial O_2 uptake/mitochondrial respiratory control/atractyloside/2,4-dinitrophenol)* ..... *Bernard M. Babior, Susan Creagan, Sidney H. Ingbar, and Ruby S. Kipnes* 98–102
Induction of cytolysis of cultured lymphoma cells by adenosine 3′:5′-cyclic monophosphate and the isolation of resistant variants *(cytoplasmic receptor molecules/protein kinase)* ..... *Violet Daniel, Gerald Litwack, and Gordon M. Tomkins* 76–79
The crystal structures of 2,5-piperazinediones having epipolysulfide bridges between C3 and C6: the structures of *N,N′*-dimethyl-3,6-epitetrathio-2,5′-piperazinedione *(x-ray structures/cyclic dipeptides/active site of sporidesmin G/viral inhibitors/cytotoxins/Pythomyces chartarum)* ..... *Betty R. Davis and Ivan Bernal* 279–283
Translational control of specific uterine protein synthesis after estrogen induction *(rat/gel electrophoresis/actinomycin D/17β-estradiol)* ..... *Anthony B. DeAngelo and George I. Fujimoto* 18–21
Experimental differential light-scattering correction to the circular dichroism of bacteriophage T2 *(light-detection geometry/C-form DNA/ordered asymmetry)* ..... *Burton P. Dorman and Marcos F. Maestre* 255–259
Mechanism of protein chain termination: further characterization of a mutant defective in a new protein synthesis factor *(ribosomes/f2 bacteriophage/coding/peptidyl-tRNA/thermolabile proteins)* ..... *M. C. Ganoza, J. Vandermeer, N. Debreceni, and S. L. Phillips* 31–35
Inhibition of a DNA polymerase from *Bacillus subtilis* by hydroxyphenylazopyrimidines *(base-pairing/antimicrobials/DNA replication)* ..... *Kenneth B. Gass, Robert L. Lou, and Nicholas R. Cozzarelli* 103–107
The contribution of the α and β chains to the kinetics of oxygen binding to and dissociation from hemoblogin *(heme proteins/ligand binding/protein chemistry)* ..... *Quentin H. Gibson* 1–4
A single subunit from avian myeloblastosis virus with both RNA-directed DNA polymerase and ribonuclease H activity *(RNA virus/polyacrylamide gel electrophoresis)* ..... *Duane P. Grandgenett, Gary F. Gerard, and Maurice Green* 230–234
Identity of the ribosomal proteins involved in the interaction with elongation factor G *(E. coli/ribosomal protein antibodies/translocation/GTP/fusidic acid)* ..... *Joseph H. Highland, James W. Bodley, Julian Gordon, Renate Hasenbank, and Georg Stoffler* 147–150
Structure and chemical synthesis of a biologically active form of *Renilla* (Sea Pansy) luciferin *(bioluminescence/pyrazine derivative/coelenterates)* ..... *Kazuo Hori and Milton J. Cormier* 120–123
A coat protein of the bacteriophage M13 virion participates in membrane-oriented synthesis of DNA *(gene-3 protein/parental RF-gene-3-protein complex/cell inner membrane/φX174/fd and fl)* ..... *S. Michal Jazwinski, Roberto Marco, and Arthur Kornberg* 205–209
In vitro assembly of bacteriophage lambda heads *(morphogenesis/DNA condensation/in vitro complementation)* ..... *Dale Kaiser and Terrie Masuda* 260–264
Inhibition of reticulocyte peptide-chain initiation by pactamycin: accumulation of inactive ribosomal initiation complexes *(methionyl-puromycin/methionyl-$tRNA_f$/initiation factors/Mg^{2+} concentration)* ..... *Lizzy S. Kappen, Hideo Suzuki, and Irving H. Goldberg* 22–26
Self-complementarity of terminal sequences within plus or minus strands of adenovirus-associated virus DNA *(circular DNA/electron microscopy/length measurements/exonuclease III)* ..... *Frank J. Koczot, Barrie J. Carter, Claude F. Garon, and James A. Rose* 215–219
Protein initiation in eukaryotes: formation and function of a ternary complex composed of a partially purified ribosomal factor, methionyl transfer RNA_f, and guanosine triphosphate *(binding assay/L-cells/ribosome subunits/protein inhibitors)* ..... *Daniel H. Levin, David Kyner, and George Acs* 41–45
Requirement of proteins S5 and S9 from 30S subunits for the ribosome-dependent GTPase activity of elongation factor G *(CsCl 30S core/ribosomal split protein/30S reconstitution/30S–50S association)* ..... *Robert C. Marsh and Andrea Parmeggiani* 151–155

(Continued on inside back cover)